UNIVERSITY OF SOUTHAMPTON

CLAY INFLUENCE ON THE THRESHOLD OF MOVEMENT AND PHYSICAL PARAMETERS OF SAND-MUD DEPOSITS

By

IOANNIS POLYKARPOS PANAGIOTOPOULOS

Thesis submitted in fulfilment of the requirements for the degree of

Doctor of Philosophy

DEPARTMENT OF OCEANOGRAPHY

FACULTY OF SCIENCE

APRIL 1996

UNIVERSITY OF SOUTHAMPTON

ABSTRACT

FACULTY OF SCIENCE
OCEANOGRAPHY

Doctor of Philosophy

CLAY INFLUENCE ON THE THRESHOLD OF MOVEMENT AND PHYSICAL PARAMETERS OF SAND-MUD DEPOSITS

By
Ioannis Polykarpos Panagiotopoulos

The erosion of mixed sediment deposits is described, under the action of unidirectional steady currents and (simulated) waves, separately, and in combination. The experiments were undertaken using a rectangular recirculating flume, incorporating an oscillating tray. The mixtures consisted of angular fine-grained quartz sands (D_{50}=152.5 μm and 215 μm) combined with a very cohesive estuarine mud.

Time-averaged erosion threshold current speeds, during the unidirectional and combined flow experiments, were measured. In addition, pore (water) pressure measurements, during the oscillatory and combined flow experiments, have been monitored.

The results obtained under the action of currents show that there is an incremental increase, with clay content, in critical erosion shear stress. This increase is small for clay percentages lower than 11% (dry weight); it is larger for clay contents in excess of 11-14%. The quantity and cohesive nature of the clay fraction are suggested as the mechanisms to explain the bi-modal pattern of sediment erodibility. When the mixtures were subjected to different pre-threshold current speeds, together with various time-periods of flow, the critical erosion shear stress was higher than the original. In this process, current velocity is more important than flow duration.

Data obtained under the influence of simulated wave action show that, for clay contents $\leq$ 11%, sediment erodibility is unaffected by the increasing clay concentrations. However, with clay contents in excess of 11-14%, a positive linear function may describe the variation in erosion threshold with clay content.

Results obtained under the co-linear combined action of waves and currents demonstrate a significant and positive linear relation between erosion threshold and the cohesive additive. Furthermore, waves protect the sediment/water interface from the eroding competence of the steady currents. The resistance to erosion increases with a decrease in wave period (from 10 s to 6 s).

The pore pressure response in the bed indicates a dramatic reduction in the magnitude of pore water pressure fluctuation; this occurs within the upper 20 mm of the sediment deposit, when the clay content exceeds a crucial value of 11-14%. The different rheology of the muddier sediments may explain this phenomenon.

Finally, the shear strength of the sediments, determined through liquid limit and rheological (yield stress) measurements, is also increaced significantly when the percentage of clay material is higher than the value defined above (11-14%).

To my beloved Sofia

LIST OF CONTENTS

LIST OF FIGURES	i
LIST OF PLATES	xix
LIST OF TABLES	xx
ACKNOWLEDGEMENTS	xxx
NOTATION	xxxi
CHAPTER 1. INTRODUCTION	1
1.1. The Present Study	3
CHAPTER 2. THEORETICAL BACKGROUND	8
2.1. Introduction	8
2.2. Unidirectional (Steady) Current Flow Characteristics	8
2.1.1. Boundary Layer Development	8
2.2.2. Turbulent Boundary Layer	10
2.3. Threshold of Sediment Motion Under Steady Flow	18
2.3.1. Non-Cohesive Sediments	18
2.3.2. Cohesive Sediments	28
2.3.3. Turbulent Bursting Related to Sediment Motion	35
2.4. Waves	37
2.4.1. Types	37
2.4.2. Wave Theory	38
2.4.3. Oscillatory Boundary Layer	42
2.4.4. Permeable Beds	47
2.5. Initial Motion Under the Action of Waves	49
2.5.1. Non-Cohesive Sediments	49
2.5.2. Cohesive Sediments	56
2.6. Unsteady Flow Combined With Currents	57
2.6.1. Transitional Stage	57
2.6.2. Laminar Flow	58
2.6.3. Turbulent Flow	58
2.7. Threshold Studies of Erosion Under Combined Flow	59
CHAPTER 3. EXPERIMENTAL EQUIPMENT AND TESTED MATERIAL	72
3.1 Introduction	72
3.2. Hydrodynamic Apparatus	72
3.2.1. The Recirculating Flume	72
3.2.2. Oscillating Plate	73
3.2.3. Plate Positioning System	77
3.3. Laser Doppler Anemometer (LDA)	77
3.4. Pressure Transducers	80
3.5. Equipment for Threshold Observation	81
3.6. Computer and Data Acquisition Card	81
3.7. Samples Examined	82

CHAPTER 4. METHODOLOGY 99
4.1. Introduction 99
4.2. Scientific Objectives 100
4.3. Experimental Design 100
4.4. Erosion Threshold Criteria 102
4.4.1. Unidirectional Flow 103
4.4.2. Oscillatory Flow 104
4.4.3. Combined Flow 104
4.5. Experimental Procedure 104
4.6. Experimental Investigations 107
4.6.1. Erosion Threshold Determinations 107
4.6.2. Effect of Pre-threshold Conditions on the Threshold of Sediment Movement (Unidirectional Flow) 109
4.6.3. Pore Pressure Measurements 111
4.6.4. Liquid Limit and Yield Stress Measurements 112
4.7. Experimental Process 112
4.7.1. Erosion Threshold Experiments 112
4.7.2. Pore Pressure Determination 118
4.7.3. Liquid Limit and Rheological Measurements 122

CHAPTER 5. BOUNDARY LAYER RESEARCH 152
5.1. Introduction 152
5.2. Unidirectional Flow Rates 152
5.2.1. Experimental Approach 153
5.2.2. Series 1 Velocity Profiles: Results and Discussion 156
5.2.3. Series 2 Velocity Profiles 158
5.2.4. The Derivation of Bed Shear Stress Related to the Threshold Experiments 161
5.3. Oscillatory Flow 162
5.3.1. Shear Stress Calculation 164
5.4. Combined Flow Regime 164
5.4.1. Shear Stress Calculation 166

CHAPTER 6. RESULTS AND DISCUSSION: UNIDIRECTIONAL FLOW 184
6.1. Erosion Threshold Determinations 184
6.2. Data Collected 186
6.3. Discussion 189
6.3.1. Set 1 Experimental Data 189
6.3.2. Stress History (Set 2 Experiments) 195

CHAPTER 7. RESULTS AND DISCUSSION: OSCILLATORY FLOW 237
7.1. Erodibility Experiments 237
7.1.1. Threshold Determinations 237
7.1.2. Data Collected 239
7.1.3. Discussion 242
7.2. Pore Pressure Response 248
7.2.1. Introduction 248
7.2.2. Data Collected and Discussion 249

CHAPTER 8. RESULTS AND DISCUSSION: COMBINED FLOW 348
8.1. Erosion Tests 348
8.1.1. Threshold Determinations 348
8.1.2. Data Collected 348
8.1.3. Discussion 353
8.2. Pore Pressure Measures 358

CHAPTER 9. RESULTS AND DISCUSSION: LIQUID LIMIT AND RHEOLOGY 404
9.1. Liquid Limit Determination 404
9.1.1. Introduction 404
9.1.2. Measurements 404
9.2. Rheology 407
9.2.1. Introduction 407
9.2.2. Rheological Curves and Yield Stress Definition 408

CHAPTER 10. CONCLUSIONS AND PROPOSALS FOR FUTURE RESEARCH 427
10.1. Conclusions 427
10.2. Proposals for Future Research 429
10.2.1. Experimental Apparatus Improvements 429
10.2.2. Proposed Experiments 432

REFERENCES

APPENDIX: WRITER'S SCIENTIFIC PAPER

LIST OF FIGURES

Fig. No	Caption	Page No
2.1	Transition from laminar flow to turbulent flow, in the boundary layer developed adjacent to a flat plate retained parallel to the flow (after Middleton & Southard, 1984).	62
2.2	Diagrammatic representation of the velocity profiles for (A) Smooth turbulent flow, and (B) Rough turbulent flow. The thickness of the layers is not to scale (from Dyer, 1986).	62
2.3	Roughness function B_s plotted against grain Reynolds number: Curve 1, Equation 2.11; Curve 2, Equation 2.12; and Solid line, observed values (from Dyer, 1986).	63
2.4	Forces acting on a static grain resting on a grain boundary (after Dyer, 1986). For explanation of terms, see text.	63
2.5	Shields threshold curve (solid line), compared with the results of White (1970, dashed line) and those of Grass (1970, dotted line) (from Dyer, 1986).	64
2.6	Curve of the observed values of the threshold of motion, on a flat bed (from Dyer, 1986).	64
2.7	Forces acting on a sediment grain at the surface of a cohesive bed subjected to unidirectional flow (after Mehta & Lee, 1994). For details, see text.	65
2.8	Force diagram at incipient grain transport (after Mehta & Lee, 1994). For details, see text.	65
2.9	Threshold curve for muddy sediments. The dashed line is only approximate, since the actual threshold for mud depends upon mineralogy, concentration etc (from Dyer, 1986).	66
2.10	Diagrammatic sequence of suspension caused by a burst. Shaded area is a zone of low velocity fluid (from Dyer, 1986).	66
2.11	Definition sketch for progressive waves (from Sleath, 1984).	67

2.12	Water particle velocities in a progressive wave (from Dean & Dalrymple, 1992).	67
2.13	Hydrostatic and dynamic pressure components at, various phase positions in a progressive water wave (from Dean & Dalrymple, 1992).	68
2.14	(a) Water surface displacement associated with a standing water wave, and (b) distribution of water particle velocities in a standing water wave (from Dean & Dalrymple, 1992).	68
2.15	Comparison of critical values of $U_{o(max)}$ predicted by various initial motion formulae, for 0.8 mm sand in fresh water at 20°C (after Sleath, 1984).	69
2.16	Comparison of critical values of $U_{o(max)}$ predicted by various initial motion formulae, for 0.2 mm sand in fresh water at 20°C (after Sleath, 1984).	69
2.17	Variation in $U_{o(max)}$ with the critical value of U_c under combined steady and oscillatory flow (after Hammond & Collins, 1979).	70
2.18	Critical velocity combinations (solid line: 6 s, dashed line: 10 s) for the threshold of gravel movement: thick error bars—wave period of 6 s; thin error bars—wave period of 10 s (from Panagiotopoulos *et al.*, 1994).	71
3.1	General arrangement of the flume used in the present study (after Tomlinson, 1993).	84
3.2	Water particle trajectories in progressive water waves of different relative depths (from Dean & Dalrymple, 1992).	85
3.3	Cross section, demonstrating the mechanism of the oscillating plate (from Tomlinson, 1993).	86
3.4	Schematic representation of the geometric motion of the oscillating plate (after Tomlinson, 1993).	87
3.5	Laser Doppler Anemometer arrangement (From Tomlinson, 1993).	88
3.6	Calibration formulae for the channel of the data acquisition system to which, the Laser Doppler Anemometer (LDA) was connected.	89
3.7	Pore pressure transducer.	90

3.8	Calibration of the channels of the data acquisition card to which (a) the LDA and (b) the pressure sensors were connected.	91
3.9	Grain size distribution of the mud fraction of the sand-mud deposits.	92
4.1	Cross section of the flume, showing the circular test section containing the sample and the location of the pore pressure sensor (schematic).	125
4.2	Observational consistency in defining the threshold of sediment movement, for a 152.5 μm monosized sample.	126
4.3	Schematic representation of the experimental set up during the hydrodynamic tests, under a combined flow regime.	127
4.4	Cross section of the flume, displaying the experimental arrangement of the video camera, Laser Doppler Anemometer (LDA) and pore pressure transducer.	127
4.5	Initial calibration of the pressure sensor, located within the test section and beneath the sediment/water interface.	128
4.6	Calibration of the pressure sensor located at the surface of the oscillating plate.	128
4.7	Re-calibration of the pressure sensor situated beneath the sediment/water interface, following the introduction of a new power supply (see text).	128
4.8	Pressure signals obtained during Study B. Key: Pressure 1 obtained from the sensor located at the top of the oscillating plate; pressure 2 obtained from the sensor located in the test section.	129
4.9	Pressure signals obtained during Study B. Key: Pressure 1 obtained from the sensor located at the top of the oscillating plate; pressure 2 obtained from the sensor located in the test section.	130
4.10	Pressure signals obtained during Study B. Key: Pressure 1 obtained from the sensor located at the top of the oscillating plate; pressure 2 obtained from the sensor located in the test section.	131

4.11 Pressure signals obtained during Study B. Key: Pressure 1 obtained from the sensor located at the top of the oscillating plate; pressure 2 obtained from the sensor located in the test section. 132

4.12 Liquid limit test results for mixtures containing the 152.5 μm sands together with: (a) 10% mud; (b) 20% mud; (c) 30% mud; (d) 40% mud; and (e) 50% mud. 133

4.13 Liquid limit test results for mixtures containing the 215 μm sands together with: (a) 10% mud; (b) 20% mud; (c) 30% mud; (d) 40% mud; and (e) 50% mud. 134

5.1 Boundary layer modifications along the flume channel (schematic). Key: BL1, BL2, BL3, BL4—boundary layers; $\delta 1$, $\delta 2$, $\delta 3$, $\delta 4$—thickness of boundary layers; U_1, U_2, U_3, U_4—flow velocity within boundary layers; and U_s—free stream velocity. 170

5.2 Determination of shear velocity (U_*) above the sediment/water interface, for sand of 152.5 μm or 215 μm in size, associated with a *slow* flow rate, using the 'Law of the Wall' for (a,c) smooth and (b,d) rough boundaries (solid lines—simulated velocity profiles, x—measured velocity profile in the flume). The apparent boundaries of the constant stress layer (c.s.l.) and viscous sub-layer have been drawn in accordance with the definitions presented by Middleton & Southard (1984). 171

5.3 Determination of shear velocity (U_*) above the sediment/water interface, for sand of 152.5 μm or 215 μm in size, associated with a *medium* flow rate, using the 'Law of the Wall' for (a,c) smooth and (b,d) rough boundaries (solid lines—simulated velocity profiles, x—measured velocity profile in the flume). The apparent boundaries of the constant stress layer (c.s.l.) and viscous sub-layer have been drawn in accordance with the definitions presented by Middleton & Southard (1984). 172

5.4 Determination of shear velocity (U_*) above the sediment/water interface, for sand of 152.5 μm or 215 μm in size, associated with a *fast* flow rate, using the 'Law of the Wall' for (a,c) smooth and (b,d) rough boundaries (solid lines—simulated velocity profiles, x—measured velocity profile in the flume). The apparent boundaries of the constant stress layer (c.s.l.) and viscous sub-layer have been drawn in accordance with the definitions presented by Middleton & Southard (1984). 173

5.5 Boundary layer conditions under the action of (simulated) waves, during the erodibility experiments, according to the definitions of: Li, 1954 (solid line); Kajiura, 1968 (small-stroke dashed line); and Sleath, 1974 (large-stroke dashed line). Key: x, mixtures containing 152.5 μm sands; and □, mixtures containing 215 μm sands. 174

5.6 Wave friction factor design diagram (from Kamphuis, 1975). 175

5.7 Flow regime definition of the oscillatory component, during the erodibility experiments under combined flow [Li, 1954 (solid line); Kajiura, 1968 (small-stroke dashed line); and Sleath, 1974 (large-stroke dashed line)]. Key: x, wave periods of 10 s; □, wave periods of 6 s. 176

6.1. Variation in the mean threshold current speed, with mud content, for mixed sediments under unidirectional flow. The mean and standard error of the mean are shown (Key: Solid line —mixtures containing the 152.5 μm sands; and dashed line—mixtures containing the 215 μm sands). 200

6.2. Variation in the bulk density with mud content, for the various sediments under investigation: (a) 152.5 μm sand mixtures; and (b) 215 μm sand mixtures. 201

6.3 The influence of stress history on the original threshold current speed (dashed line) of the mixtures containing the 152.5 μm sands and mud contents of 0%, 5%, 10% and 20%, respectively (Note: Values close to the edges of the solid lines represent unidirectional flow durations). 202

6.4 The influence of stress history on the original threshold current speed (dashed line) of the mixtures containing the 152.5 μm sands and mud contents of 30%, 40% and 50%, respectively (Note: Values close to the edges of the solid lines represent unidirectional flow durations). 203

6.5 The influence of stress history on the original threshold current speed (dashed line) of the mixtures containing the 215 μm sands and mud contents of 0%, 5%, 10% and 20%, respectively (Note: Values close to the edges of the solid lines represent unidirectional flow durations). 204

6.6 The influence of stress history on the original threshold current speed (dashed line) of the mixtures containing the 215 μm sands and mud contents of 30%, 40% and 50%, respectively (Note: Values close to the edges of the solid lines represent unidirectional flow durations). 205

6.7 Incipient motion, for various sand-mud admixtures, determined by the laboratory studies of Smerdon & Beasley (1961); Smerdon, (1964); Peirce *et al.* (1970); and Kamphuis & Hall (1983). 206

6.8 Incipient motion determined for different types of cohesive additive (clay minerals) (Key: □, kaolinite; ▵, smectite) (after Torfs, 1994). 207

6.9 Comparison of the results of the present study (x, □) with those of the Nalluri & Alvarez (1992) investigation (◇, +) and the Miller *et al.* (1977) envelope (solid lines). Key: x, mixtures of 152.5 μm sand; □, mixtures of 215 μm sand; ◇, mixtures of 500 μm sand; and +, mixtures of 2000 μm sand. 208

6.10 Variation in the critical erosion shear stress with mud content, for mixtures containing 152.5 μm sands, under different pre-threshold current speeds (70%, 80% and 90% of the original critical value) and flow durations of: (a) 5 min; (b) 10 min; and (c) 20 min (Note: The small-stroke dashed lines represent sediment beds without any stress history). 209

6.11 Variation in the critical erosion shear stress with mud content, for mixtures containing 215 μm sands, under different pre-threshold current speeds (70%, 80% and 90% of the original critical value) and flow durations of: (a) 5 min; (b) 10 min; and (c) 20 min (Note: The small-stroke dashed lines represents sediment beds without any stress history). 210

7.1 Simultaneous water velocity (upper plot) and pressure (lower plot) measurements, demonstrating the existence of a standing wave in the flume during the oscillatory hydraulic experiments (strokes of 0.283 m and 0.378 m; and period of 3.20 s). 255

7.2 Simultaneous water velocity (upper plot) and pressure (lower plot) measurements, demonstrating the existence of a standing wave in the flume during the oscillatory hydraulic experiments (strokes of 0.468 m and 0.568 m; and period of 3.20 s). 256

7.3 Simultaneous water velocity (upper plot) and pressure (lower plot) measurements, demonstrating the existence of a standing wave in the flume during the oscillatory hydraulic experiments (strokes of 0.283 m and 0.378 m; and period of 9.20 s). 257

7.4 Simultaneous water velocity (upper plot) and pressure (lower plot) measurements, demonstrating the existence of a standing wave in the flume during the oscillatory hydraulic experiments (strokes of 0.468 m and 0.568 m; and period of 9.20 s). 258

7.5 Variation in critical maximum plate (wave) velocity, with the mud content of sediments containing 152.5 μm sands and under the action of simulated waves, for strokes of: (a) 0.283 m; (b) 0.378 m; (c) 0.468 m; and (d) 0.568 m (Note: The mean and the standard error of the mean are displayed). 259

7.6 Variation in critical maximum plate (wave) velocity, with the mud content of sediments containing 215 μm sands and under the action of simulated waves, for strokes of: (a) 0.283 m; (b) 0.378 m; (c) 0.468 m; and (d) 0.568 m (Note: The mean and the standard error of the mean are displayed). 260

7.7 The threshold conditions under oscillatory flow, for various sand-mud admixtures, compared with the Komar & Miller expression (solid line). 261

7.8 The threshold conditions under oscillatory flow, for various sand-mud admixtures, compared with the Komar & Miller expression (solid line). 262

7.9	The threshold conditions under oscillatory flow, for various sand-mud admixtures, compared with the Komar & Miller expression (solid line).	263
7.10	The threshold conditions under oscillatory flow, for various sand-mud admixtures, compared with the Komar & Miller expression (solid line).	264
7.11	Pore water pressure measurements obtained at 2 cm below the sediment/water interface, for the sediment bed containing only sand of 152.5 μm size, under a wave stroke of 0.283 m.	265
7.12	Pore water pressure measurements obtained at 2 cm below the sediment/water interface, for the sediment beds containing the 152.5 μm sand fraction and mud contents of 5% and 10% respectively, under a wave stroke of 0.283 m.	266
7.13	Pore water pressure measurements obtained at 2 cm below the sediment/water interface, for the sediment beds containing the 152.5 μm sand fraction and mud contents of 20% and 30% respectively, under a wave stroke of 0.283 m.	267
7.14	Pore water pressure measurements obtained at 2 cm below the sediment/water interface, for the sediment beds containing the 152.5 μm sand fraction and mud contents of 40% and 50% respectively, under a wave stroke of 0.283 m.	268
7.15	Pore water pressure measurements obtained at 2 cm below the sediment/water interface, for the sediment bed containing only sand of 152.5 μm size, under a wave stroke of 0.378 m.	269
7.16	Pore water pressure measurements obtained at 2 cm below the sediment/water interface, for the sediment beds containing the 152.5 μm sand fraction and mud contents of 5% and 10% respectively, under a wave stroke of 0.378 m.	270
7.17	Pore water pressure measurements obtained at 2 cm below the sediment/water interface, for the sediment beds containing the 152.5 μm sand fraction and mud contents of 20% and 30% respectively, under a wave stroke of 0.378 m.	271

7.18	Pore water pressure measurements obtained at 2 cm below the sediment/water interface, for the sediment beds containing the 152.5 μm sand fraction and mud contents of 40% and 50% respectively, under a wave stroke of 0.378 m.	272
7.19	Pore water pressure measurements obtained at 2 cm below the sediment/water interface, for the sediment bed containing only sand of 152.5 μm size, under a wave stroke of 0.468 m.	273
7.20	Pore water pressure measurements obtained at 2 cm below the sediment/water interface, for the sediment beds containing the 152.5 μm sand fraction and mud contents of 5% and 10% respectively, under a wave stroke of 0.468 m.	274
7.21	Pore water pressure measurements obtained at 2 cm below the sediment/water interface, for the sediment beds containing the 152.5 μm sand fraction and mud contents of 20% and 30% respectively, under a wave stroke of 0.468 m.	275
7.22	Pore water pressure measurements obtained at 2 cm below the sediment/water interface, for the sediment beds containing the 152.5 μm sand fraction and mud contents of 40% and 50% respectively, under a wave stroke of 0.468 m.	276
7.23	Pore water pressure measurements obtained at 2 cm below the sediment/water interface, for the sediment bed containing only sand of 152.5 μm size, under a wave stroke of 0.568 m.	277
7.24	Pore water pressure measurements obtained at 2 cm below the sediment/water interface, for the sediment beds containing the 152.5 μm sand fraction and mud contents of 5% and 10% respectively, under a wave stroke of 0.568 m.	278
7.25	Pore water pressure measurements obtained at 2 cm below the sediment/water interface, for the sediment beds containing the 152.5 μm sand fraction and mud contents of 20% and 30% respectively, under a wave stroke of 0.568 m.	279

7.26 Pore water pressure measurements obtained at 2 cm below the sediment/water interface, for the sediment beds containing the 152.5 μm sand fraction and mud contents of 40% and 50% respectively, under a wave stroke of 0.568 m. 280

7.27 Pore water pressure measurements obtained at 2 cm below the sediment/water interface, for the sediment bed containing only sand of 215 μm size, under a wave stroke of 0.283 m. 281

7.28 Pore water pressure measurements obtained at 2 cm below the sediment/water interface, for the sediment beds containing the 215 μm sand fraction and mud contents of 5% and 10% respectively, under a wave stroke of 0.283 m. 282

7.29 Pore water pressure measurements obtained at 2 cm below the sediment/water interface, for the sediment beds containing the 215 μm sand fraction and mud contents of 20% and 30% respectively, under a wave stroke of 0.283 m. 283

7.30 Pore water pressure measurements obtained at 2 cm below the sediment/water interface, for the sediment beds containing the 215 μm sand fraction and mud contents of 40% and 50% respectively, under a wave stroke of 0.283 m. 284

7.31 Variation in pore pressure fluctuation (dashed line) with mud content, for the 152.5 μm sand admixtures, under a wave stroke of 0.283 m and wave (oscillation) period ranges of: (a) 4.43-4.76 s; (b) 3.90-4.25 s; and (c) 3.58-3.81 s (Key: Solid line—amplitude of pressure head transmitted into the bed). 285

7.32 Variation in pore pressure fluctuation (dashed line) with mud content, for the 152.5 μm sand admixtures, under a wave stroke of 0.378 m and wave (oscillation) period ranges of: (a) 5.15-5.49 s; (b) 4.53-4.89 s; and (c) 4.26-4.45 s (Key: Solid line—amplitude of pressure head transmitted into the bed). 286

7.33	Variation in pore pressure fluctuation (dashed line) with mud content, for the 152.5 μm sand admixtures, under a wave stroke of 0.468 m and wave (oscillation) period ranges of: (a) 6.22-6.55 s; (b) 5.45-5.79 s; and (c) 5.00-5.39 s (Key: Solid line—amplitude of pressure head transmitted into the bed).	287
7.34	Variation in pore pressure fluctuation (dashed line) with mud content, for the 152.5 μm sand admixtures, under a wave stroke of 0.568 m and wave (oscillation) period ranges of: (a) 7.27-7.61 s; (b) 6.70-6.99 s; and (c) 6.18-6.49 s (Key: Solid line—amplitude of pressure head transmitted into the bed).	288
7.35	Variation in pore pressure fluctuation (dashed line) with mud content, for the 215 μm sand admixtures, under a wave stroke of 0.283 m and wave (oscillation) period ranges of: (a) 5.04-5.22 s; (b) 4.55-4.69 s; and (c) 3.85-4.10 s (Key: Solid line—amplitude of pressure head transmitted into the bed).	289
7.36	Variation in pore pressure fluctuation (dashed line) with mud content, for the 215 μm sand admixtures, under a wave stroke of 0.378 m and wave (oscillation) period ranges of: (a) 5.35-5.71 s; (b) 4.80-5.09 s; and (c) 4.53-4.62 s (Key: Solid line—amplitude of pressure head transmitted into the bed).	290
7.37	Variation in pore pressure fluctuation (dashed line) with mud content, for the 215 μm sand admixtures, under a wave stroke of 0.468 m and wave (oscillation) period ranges of: (a) 7.02-7.34 s; (b) 6.20-6.55 s; and (c) 5.54-5.90 s (Key: Solid line—amplitude of pressure head transmitted into the bed).	291
7.38	Variation in pore pressure fluctuation (dashed line) with mud content, for the 215 μm sand admixtures, under a wave stroke of 0.568 m and wave (oscillation) period ranges of: (a) 7.68-8.01 s; (b) 6.90-7.17 s; and (c) 6.44-6.79 s (Key: Solid line—amplitude of pressure head transmitted into the bed).	292

7.39 Pore pressure record in relation to the amplitude of the pressure head (solid lines) transmitted into the sediment bed containing only the 152.5 μm sand, under a wave stroke of 0.283 m and period of 3.58 s. 293

7.40 Pore pressure records in relation to the amplitude of the pressure head (solid lines) transmitted into the 152.5 μm sand admixtures containing 5% and 10% of mud respectively, under a wave stroke of 0.283 m and periods of 3.77 s and 3.64 s, respectively. 294

7.41 Pore pressure records in relation to the amplitude of the pressure head (solid lines) transmitted into the 152.5 μm sand admixtures containing 20% and 30% of mud respectively, under a wave stroke of 0.283 m and periods of 3.81 s and 3.63 s, respectively. 295

7.42 Pore pressure records in relation to the amplitude of the pressure head (solid lines) transmitted into the 152.5 μm sand admixtures containing 40% and 50% of mud respectively, under a wave stroke of 0.283 m and periods of 3.59 s and 3.79 s, respectively. 296

7.43 Pore pressure record in relation to the amplitude of the pressure head (solid lines) transmitted into the sediment bed containing only the 215 μm sand, under a wave stroke of 0.468 m and period of 6.30 s. 297

7.44 Pore pressure records in relation to the amplitude of the pressure head (solid lines) transmitted into the 215 μm sand admixtures containing 5% and 10% of mud respectively, under a wave stroke of 0.468 m and periods of 6.45 s and 6.20 s, respectively. 298

7.45 Pore pressure records in relation to the amplitude of the pressure head (solid lines) transmitted into the 215 μm sand admixtures containing 20% and 30% of mud respectively, under a wave stroke of 0.468 m and periods of 6.35 s and 6.28 s, respectively. 299

7.46 Pore pressure records in relation to the amplitude of the pressure head (solid lines) transmitted into the 215 μm sand admixtures containing 40% and 50% of mud respectively, under a wave stroke of 0.468 m and periods of 6.20 s and 6.55 s, respectively. 300

7.47 Variation in the attenuation of the pressure head transmitted into the 152.5 μm sediment admixtures containing 40% and 50% of mud respectively, as threshold is approached (Note: Values close to the edges of the curves represent particular wave strokes). 301

7.48 Variation in the attenuation of the pressure head transmitted into the 215 μm sediment admixtures containing 40% and 50% of mud respectively, as threshold is approached (Note: Values close to the edges of the curves represent particular wave strokes). 302

7.49 Pore pressure records as threshold is approached in relation to the amplitude of the pressure head (solid lines) transmitted into the 152.5 μm sand admixture containing 50% of mud, under a wave stroke of 0.283 m (wave periods of 3.79 s and 3.32 s). 303

7.50 Pore pressure records as threshold is approached in relation to the amplitude of the pressure head (solid lines) transmitted into the 152.5 μm sand admixture containing 50% of mud, under a wave stroke of 0.283 m (wave periods of 2.94 s and 2.47 s). 304

7.51 Pore pressure record at threshold in relation to the amplitude of the pressure head (solid lines) transmitted into the 152.5 μm sand admixture containing 50% of mud, under a wave stroke of 0.283 m (wave period of 1.96 s). 305

7.52 Pore pressure records as threshold is approached in relation to the amplitude of the pressure head (solid lines) transmitted into the 152.5 μm sand admixture containing 50% of mud, under a wave stroke of 0.468 m (wave periods of 6.22 s and 5.73 s). 306

7.53 Pore pressure records as threshold is approached in relation to the amplitude of the pressure head (solid lines) transmitted into the 152.5 μm sand admixture containing 50% of mud, under a wave stroke of 0.468 m (wave periods of 5.21 s and 4.71 s). 307

7.54 Pore pressure record at threshold in relation to the amplitude of the pressure head (solid lines) transmitted into the 152.5 μm sand admixture containing 50% of mud, under a wave stroke of 0.468 m (wave period of 4.34 s). 308

7.55	Pore pressure records as threshold is approached in relation to the amplitude of the pressure head (solid lines) transmitted into the 215 μm sand admixture containing 40% of mud, under a wave stroke of 0.378 m (wave periods of 5.42 s and 5.02 s).	309
7.56	Pore pressure records as threshold is approached in relation to the amplitude of the pressure head (solid lines) transmitted into the 215 μm sand admixture containing 40% of mud, under a wave stroke of 0.378 m (wave periods of 4.57 s and 4.07 s).	310
7.57	Pore pressure record at threshold in relation to the amplitude of the pressure head (solid lines) transmitted into the 215 μm sand admixture containing 40% of mud, under a wave stroke of 0.378 m (wave period of 3.53 s).	311
7.58	Pore pressure records as threshold is approached in relation to the amplitude of the pressure head (solid lines) transmitted into the 215 μm sand admixture containing 50% of mud, under a wave stroke of 0.283 m (wave periods of 5.22 s and 4.69 s).	312
7.59	Pore pressure records as threshold is approached in relation to the amplitude of the pressure head (solid lines) transmitted into the 215 μm sand admixture containing 50% of mud, under a wave stroke of 0.283 m (wave periods of 4.24 s and 3.85 s).	313
7.60	Pore pressure record at threshold in relation to the amplitude of the pressure head (solid lines) transmitted into the 215 μm sand admixture containing 50% of mud, under a wave stroke of 0.283 m (wave period of 3.38 s).	314
8.1	Combined flow results associated with the 152.5 μm sand admixtures, for various wave strokes and periods of (a) 10 s and (b) 6 s (Key: The mean and the standard error of the mean are displayed).	361
8.2	Combined flow results associated with the 215 μm sand admixtures, for various wave strokes and periods of (a) 10 s and (b) 6 s (Key: The mean and the standard error of the mean are displayed).	362

8.3 Regression analysis for the mean threshold speeds of the current component related to the 152.5 μm sand admixtures, for near-bed wave amplitudes of 0.283 m, 0.378 m, 0.468 m and 0.568 m and periods of (a) 10 s and (b) 6 s. 363

8.4 Regression analysis for the mean threshold speeds of the current component related to the 215 μm sand admixtures, for near-bed wave amplitudes of 0.283 m, 0.378 m, 0.468 m and 0.568 m and periods of (a) 10 s and (b) 6 s. 364

8.5 Best-fit lines describing the variation in combined critical bed shear stress with mud content, for mixtures associated with the 152.5 μm sands, under wave strokes of 0.283 m, 0.378 m, 0.468 m and 0.568 m and periods of (a) 10 s and (b) 6 s. 365

8.6 Best-fit lines describing the variation in combined critical bed shear stress with mud content, for mixtures associated with the 215 μm sands, under wave strokes of 0.283 m, 0.378 m, 0.468 m and 0.568 m and periods of (a) 10 s and (b) 6 s. 366

8.7 Critical velocity combinations for the 152.5 μm sand admixtures containing 0%, 5%, 10% and 20% mud, respectively (Key: Large-stroke dashed line, 6 s period; small-stroke dashed line, 10 s period). 367

8.8 Critical velocity combinations for the 152.5 μm sand admixtures containing 30%, 40% and 50% mud, respectively (Key: Large-stroke dashed line, 6 s period; small-stroke dashed line, 10 s period). 368

8.9 Critical velocity combinations for the 215 μm sand admixtures containing 0%, 5%, 10% and 20% mud, respectively (Key: Large-stroke dashed line, 6 s period; small-stroke dashed line, 10 s period). 369

8.10 Critical velocity combinations for the 215 μm sand admixtures containing 30%, 40% and 50% mud, respectively (Key: Large-stroke dashed line, 6 s period; small-stroke dashed line, 10 s period). 370

8.11 Velocity combinations at threshold, under combined flow, for the Voulgaris *et al.* (1995) data sets. Each of the envelopes presented enclose 8 curves, derived from separate samples within the mean grain size range of 320-400 μm. 371

8.12 Velocity combinations at threshold, under combined flow, for each grain size in the Hammond & Collins (1979) data set. Hollow circles represent 5 s period waves, filled circles represent 15 s period waves. 372

8.13 Velocity combinations at threshold, under combined flow, for each grain size in the Tomlinson (1993) data set. Hollow circles represent 5 s period waves, filled circles represent 15 s period waves. 373

8.14 Pore pressure records, under combined flow, with reference to the amplitude of the pressure head (solid lines) transmitted into the sediment bed containing the 152.5 μm sand fraction and 40% of mud. Data relate to wave strokes of 0.283 m and 0.378 m and a period of 6 s. 374

8.15 Pore pressure record, under combined flow, with reference to the amplitude of the pressure head (solid lines) transmitted into the sediment bed containing the 152.5 μm sand fraction and 40% of mud. Data relate to a wave stroke of 0.468 m and period of 6 s. 375

8.16 Pore pressure records, under combined flow, with reference to the amplitude of the pressure head (solid lines) transmitted into the sediment bed containing the 152.5 μm sand fraction and 50% of mud. Data relate to wave strokes of 0.283 m and 0.378 m and a period of 6 s. 376

8.17 Pore pressure record, under combined flow, with reference to the amplitude of the pressure head (solid lines) transmitted into the sediment bed containing the 152.5 μm sand fraction and 50% of mud. Data relate to a wave stroke of 0.468 m and period of 6 s. 377

8.18 Pore pressure records, under combined flow, with reference to the amplitude of the pressure head (solid lines) transmitted into the sediment bed containing the 215 μm sand fraction and 40% of mud. Data relate to wave strokes of 0.283 m and 0.378 m and a period of 6 s. 378

8.19 Pore pressure record, under combined flow, with reference to the amplitude of the pressure head (solid lines) transmitted into the sediment bed containing the 215 μm sand fraction and 40% of mud. Data relate to a wave stroke of 0.468 m and period of 6 s. 379

8.20 Pore pressure records, under combined flow, with reference to the amplitude of the pressure head (solid lines) transmitted into the sediment bed containing the 215 μm sand fraction and 50% of mud. Data relate to wave strokes of 0.283 m and 0.378 m and a period of 6 s. 380

8.21 Pore pressure record, under combined flow, with reference to the amplitude of the pressure head (solid lines) transmitted into the sediment bed containing the 215 μm sand fraction and 50% of mud. Data relate to a wave stroke of 0.468 m and period of 6 s. 381

8.22 Variation in pore pressure fluctuation (dashed line) with mud content and under combined flow conditions for the 152.5 μm sand admixtures. Data shown for various wave strokes and periods of (a) 10 s and (b) 6 s. Key: Solid line—amplitude of pressure head transmitted into the bed. 382

8.23 Variation in pore pressure fluctuation (dashed line) with mud content and under combined flow conditions for the 215 μm sand admixtures. Data shown for various wave strokes and periods of (a) 10 s and (b) 6 s. Key: Solid line—amplitude of pressure head transmitted into the bed. 383

9.1 Liquid limit variation with mud content, for sediments investigated for erodibility in the flume. Key: Solid line, 'linear mixture law' proposed by Tan *et al.* (1994); ▵, liquid limit of the mud; □, mixtures of 215 μm sand; and x, mixtures of 152.5 μm sand. 412

9.2 Correlation between (a) critical current-induced shear stresses and (b) maximum critical wave-induced shear stresses (each data point corresponds to the mean critical wave-induced shear stress of the 4 used wave strokes), with the liquid limit of the mixtures. Key: □, mixtures of 215 μm sand; and x, mixtures of 152.5 μm sand. 413

9.3 Rheological models for flow behaviour (from Dade & Nowell, 1991). Key: A—Curve representative of Newtonian viscous flow. B—Curve which typifies shear-thinning, or pseudoplastic behaviour. C—Curve representative of shear thickening, or dilatant behaviour. D—Curve which typifies a shear-thinning material with true yield stress τ_y. E—Curve which illustrates an ideal Bingham behaviour. 414

9.4 Rheological curves for the 152.5 μm sand admixtures, containing 10% of mud. 415

9.5 Rheological curves for the 152.5 μm sand admixtures, containing 20% of mud. 416

9.6 Rheological curves for the 152.5 μm sand admixtures, containing 30% of mud. 417

9.7 Rheological curves for the 152.5 μm sand admixtures, containing 40% of mud. 418

9.8 Rheological curves for the 152.5 μm sand admixtures, containing 50% of mud. 419

9.9 Rheological curves for the 215 μm sand admixtures, containing 20% of mud. 420

9.10 Rheological curves for the 215 μm sand admixtures, containing 30% of mud. 421

9.11 Rheological curves for the 215 μm sand admixtures, containing 40% of mud. 422

9.12 Rheological curves for the 215 μm sand admixtures, containing 50% of mud. 423

9.13 Yield stress variation, with mud content, for sediments investigated for erodibility in the flume. Key: □, mixtures of 215 μm sand; and x, mixtures of 152.5 μm sand. 424

9.14 Correlation between (a) critical current-induced shear stresses and (b) maximum critical wave-induced shear stresses, with the yield stress of the mixtures. Wave-induced stress represents the mean value of the (4) wave strokes used, whilst yield stress represents the mean value of 5 tests. Key: □, mixtures of 215 μm sands; and x, mixtures of 152.5 μm sands. 425

LIST OF PLATES

Plate No	Caption	Page No
3.1	Laser Doppler Anemometer and video camera arrangement.	93
4.1	General plan view of the oscillating bed, incorporating the circular test area and surrounding sand-covered rubber mat.	135

LIST OF TABLES

Table No	Heading	Page No
3.1	Derivation of the original calibration formula for the LDA (for details, see text).	94
3.2	Derivation of a new calibration formula for the LDA (for details, see text).	94
3.3	Calibration of the channel of the data acquisition card, to which the Laser Doppler Anemometer (LDA) was connected.	95
3.4	Calibration of the channel of the data acquisition card to which the pressure transducer, located beneath the sediment/ water interface, was connected.	96
3.5	Calibration of the channel of the data acquisition card to which the pressure transducer, located at the surface of the oscillating plate, was connected.	96
3.6	Grain size analysis of the mud fraction of the sediment mixtures.	97
3.7	Estimation of the mean size of the artificially-produced mixtures.	98
4.1	Observer consistency in defining the threshold of movement for a uniform sediment bed, with a median grain size of 152.5 μm.	136
4.2	Data used for the derivation of the calibration formula for the pressure transducer located beneath the sediment/ water interface.	137
4.3	Water pressure measurements for different periods of oscillation, in the absence of sediment. Wave stroke of 0.283 m.	138
4.4	Water pressure measurements for different periods of oscillation, in the absence of sediment. Wave stroke of 0.378 m.	139
4.5	Water pressure measurements for different periods of oscillation, in the absence of sediment. Wave stroke of 0.468 m.	140

4.6	Water pressure measurements for different periods of oscillation, in the absence of sediment. Wave stroke of 0.568 m.	141
4.7	Data used in the derivation of the calibration formula for the pressure transducer located at the surface of the oscillating plate.	142
4.8	Data used in the derivation of the new calibration formula for the pressure transducer located beneath the surface of the sediment deposit.	142
4.9	Water pressure measurements for different periods of oscillation, in the absence of sediment. Wave stroke of 0.283 m (Note: Pressure 1 is obtained from the sensor situated at the top of the trolley, whilst pressure 2 relates to the sensor located within the test section).	143
4.10	Water pressure measurements for different periods of oscillation, in the absence of sediment. Wave stroke of 0.378 m (Note: Pressure 1 is obtained from the sensor situated at the top of the trolley, whilst pressure 2 relates to the sensor located within the test section).	144
4.11	Water pressure measurements for different periods of oscillation, in the absence of sediment. Wave stroke of 0.468 m (Note: Pressure 1 is obtained from the sensor situated at the top of the trolley, whilst pressure 2 relates to the sensor located within the test section).	145
4.12	Water pressure measurements for different periods of oscillation, in the absence of sediment. Wave stroke of 0.568 m (Note: Pressure 1 is obtained from the sensor situated at the top of the trolley, whilst pressure 2 relates to the sensor located within the test section).	146
4.13	Liquid limit (cone penetrometer) measurements for the sediment mixture containing the 152.5 micron sand and 10% mud (LL=29.2%).	147
4.14	Liquid limit (cone penetrometer) measurements for the sediment mixture containing the 152.5 micron sand and 20% mud (LL=28.5%).	147

4.15	Liquid limit (cone penetrometer) measurements for the sediment mixture containing the 152.5 micron sand and 30% mud (LL=29.4%).	148
4.16	Liquid limit (cone penetrometer) measurements for the sediment mixture containing the 152.5 micron sand and 40% mud (LL=29.6%).	148
4.17	Liquid limit (cone penetrometer) measurements for the sediment mixture containing the 152.5 micron sand and 50% mud (LL=43.5%).	149
4.18	Liquid limit (cone penetrometer) measurements for the sediment mixture containing the 215 micron sand and 10% mud (LL=26.3%).	149
4.19	Liquid limit (cone penetrometer) measurements for the sediment mixture containing the 215 micron sand and 20% mud (LL=26.6%).	150
4.20	Liquid limit (cone penetrometer) measurements for the sediment mixture containing the 215 micron sand and 30% mud (LL=27.4%).	150
4.21	Liquid limit (cone penetrometer) measurements for the sediment mixture containing the 215 micron sand and 40% mud (LL=37.7%).	151
4.22	Liquid limit (cone penetrometer) measurements for the sediment mixture containing the 215 micron sand and 50% mud (LL=44.0%).	151
5.1	Velocity measurements defining the overall structure of the unidirectional flow within the experimental flume channel (for explanation, see text).	177
5.2	Measured vertical velocity profile above the sediment water/interface containing only sand of 152.5 microns size, for a *slow* unidirectional flow rate.	178
5.3	Measured vertical velocity profile above the sediment water/interface containing only sand of 152.5 microns size, for a *medium* unidirectional flow rate.	179
5.4	Measured vertical velocity profile above the sediment water/interface containing only sand of 152.5 microns size, for a *fast* unidirectional flow rate.	180
5.5	Measured vertical velocity profile above the sediment water/interface containing only sand of 215 microns size, for a *slow* unidirectional flow rate.	181

5.6	Measured vertical velocity profile above the sediment water/interface containing only sand of 215 microns size, for a *medium* unidirectional flow rate.	182
5.7	Measured vertical velocity profile above the sediment water/interface containing only sand of 215 microns size, for a *fast* unidirectional flow rate.	183
6.1	Experimental results obtained under unidirectional flow, for sediments containing a sand component of 152.5 microns size (in the absence of any stress history of the bed).	211
6.2	Experimental results obtained under unidirectional flow, for sediments containing a sand component of 215 microns size (in the absence of any stress history of the bed).	212
6.3	Derived mean critical current speeds and shear stresses under unidirectional flow rates, for sediment beds without any stress history.	213
6.4	The moisture content for each of the mixtures tested (containing the 152.5 micron sand component) *before* the threshold experiment (2nd column) and *after* the threshold experiment (3rd column).	214
6.5	The moisture content for each of the mixtures tested (containing the 215 micron sand component) *before* the threshold experiment (2nd column) and *after* the threshold experiment (3rd column).	215
6.6	Experimental results, under unidirectional flow, with a stress history of the bed containing only sand of 152.5 microns in size.	216
6.7	Experimental results, under unidirectional flow, with a stress history of the bed containing sand of 152.5 microns in size and with 5% mud.	217
6.8	Experimental results, under unidirectional flow, with a stress history of the bed containing sand of 152.5 microns in size and with 10% mud.	218
6.9	Experimental results, under unidirectional flow, with a stress history of the bed containing sand of 152.5 microns in size and with 20% mud.	219
6.10	Experimental results, under unidirectional flow, with a stress history of the bed containing sand of 152.5 microns in size and with 30% mud.	220

6.11 Experimental results, under unidirectional flow, with a stress history of the bed containing sand of 152.5 microns in size and with 40% mud. 221

6.12 Experimental results, under unidirectional flow, with a stress history of the bed containing sand of 152.5 microns in size and with 50% mud. 222

6.13 Experimental results, under unidirectional flow, with a stress history of the bed containing only sand of 215 microns in size. 223

6.14 Experimental results, under unidirectional flow, with a stress history of the bed containing sand of 215 microns in size and with 5% mud. 224

6.15 Experimental results, under unidirectional flow, with a stress history of the bed containing sand of 215 microns in size and with 10% mud. 225

6.16 Experimental results, under unidirectional flow, with a stress history of the bed containing sand of 215 microns in size and with 20% mud. 226

6.17 Experimental results, under unidirectional flow, with a stress history of the bed containing sand of 215 microns in size and with 30% mud. 227

6.18 Experimental results, under unidirectional flow, with a stress history of the bed containing sand of 215 microns in size and with 40% mud. 228

6.19 Experimental results, under unidirectional flow, with a stress history of the bed containing sand of 215 microns in size and with 50% mud. 229

6.20 The derived mean values of the critical parameters studied in the stress history experiments (sand size, 152.5 microns; 0% mud). 230

6.21 The derived mean values of the critical parameters studied in the stress history experiments (sand size, 152.5 microns; 5% mud). 230

6.22 The derived mean values of the critical parameters studied in the stress history experiments (sand size, 152.5 microns; 10% mud). 231

6.23 The derived mean values of the critical parameters studied in the stress history experiments (sand size, 152.5 microns; 20% mud). 231

6.24 The derived mean values of the critical parameters studied in the stress history experiments (sand size, 152.5 microns; 30% mud). 232

6.25	The derived mean values of the critical parameters studied in the stress history experiments (sand size, 152.5 microns; 40% mud).	232
6.26	The derived mean values of the critical parameters studied in the stress history experiments (sand size, 152.5 microns; 50% mud).	233
6.27	The derived mean values of the critical parameters studied in the stress history experiments (sand size, 215 microns; 0% mud).	233
6.28	The derived mean values of the critical parameters studied in the stress history experiments (sand size, 215 microns; 5% mud).	234
6.29	The derived mean values of the critical parameters studied in the stress history experiments (sand size, 215 microns; 10% mud).	234
6.30	The derived mean values of the critical parameters studied, in the stress history experiments (sand size, 215 microns; 20% mud).	235
6.31	The derived mean values of the critical parameters studied in the stress history experiments (sand size, 215 microns; 30% mud).	235
6.32	The derived mean values of the critical parameters studied in the stress history experiments (sand size, 215 microns; 40% mud).	236
6.33	The derived mean values of the critical parameters studied in the stress history experiments (sand size, 215 microns; 50% mud).	236
7.1	Resonance phenomena and their significance to the modification of the critical erosion conditions. Note: The values of $U_{o,sw}$ have been calculated taking into account that the threshold of movement was observed to start approximately 45° before the oscillating plate reached the mid-stroke position.	315
7.2	Experimental results obtained under oscillatory flow (sand size, 152.5 microns; 0% mud).	316
7.3	Experimental results obtained under oscillatory flow (sand size, 152.5 microns; 5% mud).	317
7.4	Experimental results obtained under oscillatory flow (sand size, 152.5 microns; 10% mud).	318
7.5	Experimental results obtained under oscillatory flow (sand size, 152.5 microns; 20% mud).	319

7.6	Experimental results obtained under oscillatory flow (sand size, 152.5 microns; 30% mud).	320
7.7	Experimental results obtained under oscillatory flow (sand size, 152.5 microns; 40% mud).	321
7.8	Experimental results obtained under oscillatory flow (sand size, 152.5 microns; 50% mud).	322
7.9	Experimental results obtained under oscillatory flow (sand size, 215 microns; 0% mud). Key: X, transducer not functioning.	323
7.10	Experimental results obtained under oscillatory flow (sand size, 215 microns; 5% mud). Key: X, transducer not functioning.	324
7.11	Experimental results obtained under oscillatory flow (sand size, 215 microns; 10% mud). Key: X, transducer not functioning.	325
7.12	Experimental results obtained under oscillatory flow (sand size, 215 microns; 20% mud). Key: X, transducer not functioning.	326
7.13	Experimental results obtained under oscillatory flow (sand size, 215 microns; 30% mud). Key: X, transducer not functioning.	327
7.14	Experimental results obtained under oscillatory flow (sand size, 215 microns; 40% mud). Key: X, transducer not functioning.	328
7.15	Experimental results obtained under oscillatory flow (sand size, 215 microns; 50% mud). Key: X, transducer not functioning.	329
7.16	Critical shear stresses related to simulated wave action, for a plate displacement of 0.283 m.	330
7.17	Critical shear stresses related to simulated wave action, for a plate displacement of 0.378 m.	331
7.18	Critical shear stresses related to simulated wave action, for a plate displacement of 0.468 m.	332
7.19	Critical shear stresses related to simulated wave action, for a plate displacement of 0.568 m.	333

7.20 Pore pressure measurements obtained under oscillatory flow (sand size, 152.5 μm; 0% mud). The values marked with an asterisk were obtained during the threshold of sediment motion. 334

7.21 Pore pressure measurements obtained under oscillatory flow (sand size, 152.5 μm; 5% mud). The values marked with an asterisk were obtained during the threshold of sediment motion. 335

7.22 Pore pressure measurements obtained under oscillatory flow (sand size, 152.5 μm; 10% mud). The values marked with an asterisk were obtained during the threshold of sediment motion. 336

7.23 Pore pressure measurements obtained under oscillatory flow (sand size, 152.5 μm; 20% mud). The values marked with an asterisk were obtained during the threshold of sediment motion. 337

7.24 Pore pressure measurements obtained under oscillatory flow (sand size, 152.5 μm; 30% mud). The values marked with an asterisk were obtained during the threshold of sediment motion. 338

7.25 Pore pressure measurements obtained under oscillatory flow (sand size, 152.5 μm; 40% mud). The values marked with an asterisk were obtained during the threshold of sediment motion. 339

7.26 Pore pressure measurements obtained under oscillatory flow (sand size, 152.5 μm; 50% mud). The values marked with an asterisk were obtained during the threshold of sediment motion. 340

7.27 Pore pressure measurements obtained under oscillatory flow (sand size, 215 μm; 0% mud). The values marked with an asterisk were obtained during the threshold of sediment motion. 341

7.28 Pore pressure measurements obtained under oscillatory flow (sand size, 215 μm; 5% mud). The values marked with an asterisk were obtained during the threshold of sediment motion. 342

7.29	Pore pressure measurements obtained under oscillatory flow (sand size, 215 μm; 10% mud). The values marked with an asterisk were obtained during the threshold of sediment motion.	343
7.30	Pore pressure measurements obtained under oscillatory flow (sand size, 215 μm; 20% mud). The values marked with an asterisk were obtained during the threshold of sediment motion.	344
7.31	Pore pressure measurements obtained under oscillatory flow (sand size, 215 μm; 30% mud). The values marked with an asterisk were obtained during the threshold of sediment motion.	345
7.32	Pore pressure measurements obtained under oscillatory flow (sand size, 215 μm; 40% mud). The values marked with an asterisk were obtained during the threshold of sediment motion.	346
7.33	Pore pressure measurements obtained under oscillatory flow (sand size, 215 μm; 50% mud). The values marked with an asterisk were obtained during the threshold of sediment motion.	347
8.1	Experimental results obtained under combined flow conditions: Sand size, 152.5 μm; 0% mud.	384
8.2	Experimental results obtained under combined flow conditions: Sand size, 152.5 μm; 5% mud.	385
8.3	Experimental results obtained under combined flow conditions: Sand size, 152.5 μm; 10% mud.	386
8.4	Experimental results obtained under combined flow conditions: Sand size, 152.5 μm; 20% mud.	387
8.5	Experimental results obtained under combined flow conditions: Sand size, 152.5 μm; 30% mud.	388
8.6	Experimental results obtained under combined flow conditions: Sand size, 152.5 μm; 40% mud.	389
8.7	Experimental results obtained under combined flow conditions: Sand size, 152.5 μm; 50% mud.	390
8.8	Experimental results obtained under combined flow conditions: Sand size, 215 μm; 0% mud.	391
8.9	Experimental results obtained under combined flow conditions: Sand size, 215 μm; 5% mud.	392

8.10 Experimental results obtained under combined flow conditions: Sand size, 215 μm; 10% mud. 393

8.11 Experimental results obtained under combined flow conditions: Sand size, 215 μm; 20% mud. 394

8.12 Experimental results obtained under combined flow conditions: Sand size, 215 μm; 30% mud. 395

8.13 Experimental results obtained under combined flow conditions: Sand size, 215 μm; 40% mud. 396

8.14 Experimental results obtained under combined flow conditions: Sand size, 215 μm; 50% mud. 397

8.15 Critical shear stresses due to the co-linear combined action of waves and currents, for a plate displacement of 0.283 m and wave period of 10 s. 398

8.16 Critical shear stresses due to the co-linear combined action of waves and currents, for a plate displacement of 0.378 m and wave period of 10 s. 399

8.17 Critical shear stresses due to the co-linear combined action of waves and currents, for a plate displacement of 0.468 m and wave period of 10 s. 400

8.18 Critical shear stresses due to the co-linear combined action of waves and currents, for a plate displacement of 0.568 m and wave period of 10 s. 401

8.19 Critical shear stresses due to the co-linear combined action of waves and currents, for a plate displacement of 0.283 m and wave period of 6 s. 402

8.20 Critical shear stresses due to the co-linear combined action of waves and currents, for a plate displacement of 0.378 m and wave period of 6 s. 403

8.21 Critical shear stresses due to the co-linear combined action of waves and currents, for a plate displacement of 0.468 m and wave period of 6 s. 403

9.1 Yield stress (τ_y) values obtained from the rheometer tests (for details, see text). 426

ACKNOWLEDGEMENTS

The writer is much obliged for the precious scientific advice, criticism and moral support given by his supervisor Prof. Mike Collins. Many thanks are due also to Dr G.C. Sills, of the Department of Enginneering Science, University of Oxford, for her contribution in the pore (water) pressure investigation.

Also the writer is grateful for the invaluable technical assistance provided by Mr John Davis.

The assistance of Dr A.E. James, from UMIST, in the performance of rheological measurements is appreciated greatly.

Dr G. Voulgaris, Dr S. Gao and Mr M. Wilkin are thanked sincerely for their help with experiments and advice in scientific matters.

Last, but most deeply, the writer is indebted to Emmanuil Oikonomou, for his companionship and support during the last stage of writing up the thesis.

This investigation was supported through the EU MAST (Human Capital and Mobility) programme (Grant No: B/MAST/923023).

NOTATION

a'	angle of dynamic friction
a_δ	near-bed wave amplitude
A	area
A_o	amplitude of the horizontal displacement of the moving plate
$c_{D'}$	drag coefficient
c_L	lift coefficient
C	phase wave speed
d	mean depth of water
d_1	bed thickness
D	grain diameter
D_{gm}	geometric mean grain diameter
D_{50}	median grain diameter
D_{90}	grain size exceeded by 10% by weight of a sample of a sediment
D'	drag force
f	unknown function
f_c	current friction factor
f_w	wave friction factor
f_{wc}	combined wave-current friction factor
F_C	active cohesive force
F_R	reactive shear force
F_d	frequency difference
g	gravitational acceleration (9.81 cm/s^2)
G	shear modulus of the sediment
H, h	wave height
k	Von Karman's constant (≈0.4 for the clear water
K	wave number
K'	specific permeability
K''	elasticity modulus
K_s	roughness length of the bed
$K_{P(z)}$	pressure response factor
l	mixing length of turbulent eddies
L	lift force, wave length

$n_{x,t}$	water surface elevation
P	pressure
P_o	amplitude of P
r^2	correlation coefficient of the regression analysis
Re	Reynolds number, $U_s d/\nu$ or $U_s X/\nu$
Re_*	grain Reynolds number, $U_* K_s/\nu$
RE	wave Reynolds number, $U_{o(max)} A_o/\nu$
t	time
T	wave period
u	horizontal component of velocity
u′	fluctuating component of u in a turbulent flow
U	time-averaged flow speed
U_c	time-averaged critical current speed
$U_{c(0.4\ cm)}$	time-averaged critical current speed 0.4 cm above the sediment/water interface
$U_{100,c}$	critical flow velocity 100 cm above the bed surface
U_{da}	depth-averaged mean water speed
U_s	time-averaged free-stream velocity
U_y, U_{y1}, U_{y2}	time-averaged flow speed at a specific height above the bed surface
U_o	horizontal component of velocity just outside the wave boundary layer
$U_{o(max)}$	amplitude of U_o
$U_{o(max),c}$	critical maximum wave velocity
$U_{w(max)}$	maximum wave-induced near-bed current velocity
$U_{o,sw}$	horizontal component of velocity at the bed due to the standing wave
U_*	time-averaged shear velocity
$U_{*,c}$	critical shear velocity
$U_{*w(max)}$	maximum shear velocity due to waves
U^+	dimensionless parameter, U/U_*
v	vertical component of velocity

v'	fluctuating component of v in a turbulent flow
w	water (moisture) content
W	immersed weight of a grain of sediment
X, x	distance measured in the horizontal direction
y	vertical distance from the bed surface
y^+	dimensionless distance from the boundary, U_*y/ν
y_o	physical roughness parameter ($K_s/30$, for flat beds)
y_{oa}	apparent roughness length due to both wave boundary layer and y_o
z	vertical coordinate direction
β	Stokes parameter
γ	specific grain weight, shear rate
δ	thickness of boundary layer
δ_w	thickness of wave boundary layer
δ_1	thickness of wave boundary layer when $\omega t=0$
δ_*	thickness of viscous sub-layer
δ_*	displacement thickness
ε	eddy viscosity
ϵ	dimensionless function of Shields threshold parameter (θ_c) and grain Reynolds number (Re_*)
θ_c	Shields threshold parameter, $\tau_c/(\rho_s-\rho)gD$
λ	wavelength of laser light
μ	dynamic viscosity
μ_B	Bingham dynamic viscosity
ν	kinematic viscosity
π	constant (3.1416)
ρ	fluid density
ρ_s	grain density
σ	standard deviation
τ	time-mean shear stress
τ_R	Reynolds stress
τ_c	critical bed shear stress due to currents

τ_o	bed shear stress
$\tau_{w(max)}$	maximum bed shear stress due to waves
τ_{wc}	combined near-bed shear stress due to waves and currents
τ_B	Bingham yield stress
τ_y	yield stress
φ	velocity potential
ϕ	angle of repose of the grains
$\vec{\omega}$	angular velocity

CHAPTER 1

INTRODUCTION

1. INTRODUCTION

Although sand and mud deposits have different physical properties, they are found together in homogeneous, patchy or laminated forms. Characteristic examples of such deposits are described below.

(a) In the North Sea, sand-mud beds are subjected to a reworking process by a strong tidal current regime, resulting in well mixed deposits. In general, there is an abundance of sand, with mud contents not exceeding 30% (Williamson, 1991).

(b) The shelf sediments of the Santa Monica Basin (USA) are mostly fine- to medium-grained sands, with some pockets of mud (Malouta *et al.*, 1981).

(c) In the Suwannee River Estuary (USA), four main areas of cohesive sedimentation are present, with mud contents in excess of 50%. A region containing sediments with a high percentage of sand is present between these zones containing cohesive sediments (Leadon, 1985).

(d) Vertical stratification consisting of sand and mud layers (between 0.5 cm and 2 cm thickness) has been observed along the northern side of the Humber Estuary (UK). In contrast, the southern coastline consists of well mixed sandy-muddy sediments (with mud contents < 17%) (Williamson, op. cit.).

(e) The lower Severn Estuary (UK) has found to contain sediments comprised of silty clays, with fine sand lenses and layers interbedded within the clay matrix (Kirby & Parker, 1983).

(f) Finally, the inter-tidal flat deposits of western Europe are associated with bed characteristics containing different types of mud and sand interlaminations. This pattern may be attributed to highly variable hydrodynamic conditions, in space and time, associated with local morphology (De Raaf & Boersma, 1971).

In order to investigate the transport behaviour of such sediments, it is necessary to understand the erosional and depositional properties of various combinations of sand and mud. In addition, in field situations, it is necessary to consider: (i) the effects of the internal structure; (ii) the consolidation history; and (iii) biological activity associated with the sediment deposits.

Sand-mud mixtures contribute to a wide range of sedimentological design, maintenance and management problems in estuarine and coastal areas. For example, the accumulation of sand-mud mixtures in navigation channels and berths (e.g. Poole Harbour (UK)) results often in the need for expensive dredging operations (incorporating hydrographic and bathymetric surveys, together with geotechnical investigations). Likewise, inshore developments (e.g. sea walls, groynes, breakwaters, revetments, artificial offshore islands) can cause significant changes in the water flow structure (West *et al.*, 1984) and, subsequently, in the transport pathways of sediment mixtures. Thus, prediction of these changes, by using mathematical models which usually incorporate critical erosion values, is necessary before any engineering project can proceed. In addition, the presence of sand-mud mixtures in sewers (Crabtree, 1988) can cause a loss of hydraulic capacity; this leads eventually to various operational problems such as surcharging, surface flooding and premature operation of overflows with a consequent increase in the pollution of watercourses. Further, many pollutants are absorbed preferentially onto the fine-grained cohesive fraction (Lindsay *et al.* 1996) of any sediment mixture. Thus, environmentally, it is important to improve the predictive capability of contaminant transport models requiring erosion threshold values (Westrich, 1989; and

Onishi *et al.*, 1993); this may be achieved by evaluating the condition of critical motion for such mixtures.

Extensive sedimentological investigations, concerning the erosion threshold of estuarine and coastal deposits, have been undertaken independently into: (a) cohesive muds (Raudkivi, 1990; Dade *et al.*, 1992; Mehta, 1993); or (b) non-cohesive sands (Miller *et al.*, 1977; Sleath, 1984; Dyer, 1986;). However, only limited studies have addressed the two sediment types in combination.

Most of these latter investigations are preliminary in character and have been performed mainly in the laboratory. The empirical results obtained have been useful in providing some basis for the qualitative prediction of sediment movement. However, the laboratory tests undertaken were not performed to any standard procedure; therefore it is very difficult to derive any generalisations. The effects of all the factors associated with the erosion, transport, deposition and consolidation processes need to be understood, if the quantitative predictions of the behaviour of sediment mixtures are to be accomplished.

1.1. THE PRESENT STUDY

The present contribution describes a laboratory approach to: (i) the understanding of the erosional behaviour, under steady and unsteady flow conditions (separately and in combination), of quartz fine-grained angular sand mixed with various proportions of (naturally deposited) estuarine mud; and (ii) the examination of such mixed sediments pore water pressure response, under unsteady and combined overlying flow conditions.

The basic objectives of the study may be defined in terms

of: (a) to establish the critical erosion velocity, in terms of near-bed current speed/maximum wave velocity and bed shear stress necessary to erode each sediment mixture; (b) to define the (shear) strength of the sediment structure, on the basis of liquid limit and yield stress measurements; (c) to investigate the generation of pore pressure within the sediment deposits; and (d) to examine the influence of clay (mud) content on the various physical parameters.

It should be noted here that the term 'clay content' is used normally to describe the size fraction less than 2 μm, since, sediment particles contained within this size range consist generally of clay minerals. However, non-clay minerals can be present at diameters less than 2 μm; likewise clay minerals can be present as large as 5 μm (Chiou *et al.*, 1991).

In order to define the critical moment at which sediment movement commences is somewhat difficult, as a high level of subjectivity is inherent in these types of experiments. The concept of critical motion (threshold) can be determined, generally, as the interface between 'no movement' and 'some form of initial movement'. Various threshold criteria have been suggested elsewhere; most of these incorporate different levels of sediment transport, depending upon the observational capability of each investigator. Thus, comparison between the results of the various studies is limited.

Threshold conditions vary in relation to fluid properties, flow regime characteristics and the type of sediments. Hence, an extensive methodology has been used to examine the inter-relationships between parameters, at threshold; these have been tested then on the basis of various series of laboratory investigations. Further, it

is worth noting here the analyses put forward by Lavelle & Mojfeld (1987). These authors, based upon the studies undertaken by Paintal (1971), Taylor & Vanoni (1972) and Graf & Pazis (1977), argue against the use of threshold criteria in terms of the investigation of sediment motion. Rather, these investigators consider that there is no 'non-zero' fluid velocity at which 'no motion' is observed.

In spite of the limitations outlined above, it is important to be able to define the threshold of motion for a variety of sediments; this requires correlation with the physical properties of the deposited material. The information derived could contribute considerably to an improvement in the accuracy of the results produced by numerical models associated with the prediction of (bed and suspended load) sediment transport pathways i.e. rates and directions. Finally, within the context of coastal engineering, it is useful to be able to establish and predict the range of (current and wave) conditions over which the bed sediments become mobile.

Within the context of the present study, hydraulic experiments were performed in a recirculating laboratory flume; this was used to represent a unidirectional (tidal or river) current. Installed in the flume was an oscillating plate, which simulated wave action on the sediment bed. Measurements of the unidirectional current speed were undertaken using a Laser Doppler Anemometer (LDA). Wave conditions were defined through use of a formula describing the sinusoidal motion of the oscillating plate. Finally, pressure measurements within the water column and sediment bed were obtained using (Druck) transducers.

A review of the published scientific literature related

to the present understanding of the threshold of movement of non-cohesive and cohesive sediments is presented in Chapter 2. This particular Chapter presents also the appropriate background theory related to sediment characteristics, and fluid and flow properties associated with threshold conditions.

The instrumentation used in the hydrodynamic investigation is presented in Chapter 3. This particular Chapter incorporates a description of the principles of operation of the equipment and an appraisal of the mechanisms of operation of each item.

Chapter 4 describes the sequence in which the various experiments were carried out and, in detail, the various experimental procedures.

The results of the boundary layer flow investigations, within the flume are presented in Chapter 5. These investigations were concerned with testing the feasibility of the flume to simulate natural (flow) conditions and establishing an understanding of the flow structure above the sediment/water interface, at threshold. These investigations were limited to unidirectional flows, due to the inability of the LDA to monitor oscillatory flow conditions.

Chapters 6, 7 and 8 describe and discuss the results obtained on the threshold of sediment movement under unidirectional, oscillatory and combined flow conditions. In addition, results from the investigation of pore pressure generation are presented in Chapters 7 and 8.

Chapter 9 incorporates a discussion of the geotechnical information derived on the basis of liquid limit and yield stress measurements.

Chapter 10 summarises the basic conclusions derived from the study and incorporates suggestions: for (i) the improvement of the experimental equipment; and (ii) for future research.

Finally, a scientific paper written by the candidate, published in 1994 in *Sedimentology*, is appended to the thesis. This paper is concerned with an investigation into the erosion (threshold) of gravel-sized particles under the combined action of waves and currents. Although not applicable directly to the present investigation, the experimental technique and analysis applied were similar to those adopted for the investigation of mud-sand mixtures. The study of gravel threshold formed part of a South Coast Sea Bed Mobility Study (Axe & Collins, 1993).

CHAPTER 2

THEORETICAL BACKGROUND

2. THEORETICAL BACKGROUND

2.1. INTRODUCTION

This Chapter describes various aspects of the boundary layer at the sediment/water interface and the complex interaction between fluid motion and movement of bed sediment: the dissipation of energy and the transport of sediment. In order to undertake such a review, it is necessary to utilise results for the fluid velocities and pressures.

The Chapter summarises briefly the state of knowledge in these particular areas of research. Such investigations are described already in a large number of existing written sources. Therefore, the derivations and discussions are retained as brief as possible in the present section.

2.2. UNIDIRECTIONAL (STEADY) CURRENT FLOW CHARACTERISTICS

2.2.1. Boundary Layer Development

Consider a laminar free stream, $(du/dy)=0$, approaching a flat plate with a speed of U_s (Fig. 2.1). The plate itself is stationary and, consequently, the fluid lying immediately adjacent to it is also stationary. Away from the plate, the flow speed increases gradually, until it reaches the value (U_s) of the free stream. The region in which the speed differs from U_s is referred to as the boundary layer. The fluid speed approaches the free stream value gradually, therefore, the edge of the boundary layer is indefinitely described. For convenience, the edge is taken usually as the point at which the fluid velocity reaches 99% of U_s.

Boundary layers are not initiated only from interaction of flow with flat plates. Any change in bed roughness or flow conditions can generate a new boundary layer.

The thickness of the boundary layer (Fig. 2.1) increases with distance downstream of the edge of the plate immersed in the fluid. Hence, the velocity distribution within the boundary layer changes with distance. If the depth of flow is infinite, there may come a point at which the boundary layer fills the whole of the flow. After some initial adjustment, there will be no further change with downstream distance, provided conditions remain unchanged and the flow is fully developed. For free surface flows, it is accepted usually that if X is the distance downstream of the point at which the boundary was initiated, the flow is fully developed if X>100d.

Transition to turbulence

It is common to distinguish a Reynolds number (Re_a) above which small disturbances within the laminar flow are amplified; below another (Re_b), the turbulence is damped out. For fully developed two-dimensional free surface flow, Re_a=890 and Re_b=5,000 (Sleath, 1984) where the Reynolds number is defined as:

$$\frac{U_s d}{\nu} \qquad (2.1)$$

For a growing boundary layer at constant pressure, Re_a=420 and Re_b is unknown (Sleath, op. cit.), where the Reynolds number is:

$$\int_0^d \frac{U_s - U}{\nu} dy \qquad (2.2)$$

For the same conditions, the Reynolds number is quoted also as:

$$\frac{U_s X}{\nu} \qquad (2.3)$$

The transition condition is: $(U_s X)/\nu = 5 \times 10^5$ to 3×10^6 (Sleath, 1984). This value is influenced strongly by the intensity of turbulence in the free stream and by bottom roughness.

2.2.2. Turbulent Boundary Layer

(a) Velocity distribution

It is convenient to divide the flow within a turbulent boundary layer into the following three regions: inner layer; overlap or logarithmic layer; and outer layer The structure related to smooth turbulent or rough turbulent flows is summarised schematically on Fig. 2.2.

Inner layer

For smooth beds, the inner layer is referred to also as the *viscous sub-layer*. In the immediate vicinity of the bed, turbulent eddies are inhibited by the presence of the solid boundary and viscous stresses dominate the motion. However, flow within this layer is far from steady, since the fluid is constantly being buffeted by turbulent eddies from the overlying flow. Hence, shear in the viscous sub-layer, as characterised by the rate of change of average fluid velocity away from the wall, is very high; this is because the fast-moving fluid is mixed right down to the top of the viscous sub-layer by turbulent diffusion.

The thickness of the viscous sub-layer depends upon the characteristics of a particular flow and fluid; it is typically within the range of a fraction of a millimetre

to many millimetres. Molecular transport of fluid momentum dominates over the turbulent transport of momentum near the boundary. Therefore, fluctuations in velocity very close to the boundary must be largely parallel to it. Thus, fluctuations in shear stress at and near the boundary, caused by the velocity fluctuations, can be substantial; these must have an important bearing on sediment transport processes. Velocity fluctuations normal to the boundary, within the viscous sub-layer can, likewise, be important in the diffusion of sediment towards or away from the boundary even though they are unimportant in the diffusion of the fluid momentum. The turbulent fluctuations in velocity in the viscous sub-layer are the result of advection of eddies from regions further away from the wall; these eddies are damped out by viscous shear stresses in the sub-layer.

The region of the viscous sub-layer closest to the bed which extends to a height of $y^+=5$ is sometimes referred to as the linear sub-layer. Above this layer, there is a zone which exceeds the upper limit of the viscous sub-layer ($y^+=11.6$); this reaches a height of $y^+=30-70$. This region is termed the buffer layer and the gradient of time-averaged velocity is still very high and the flow is strongly turbulent. The outstanding characteristic of this particular zone is that both viscous shear stresses and turbulent shear stresses are too important to be ignored. Very energetic small-scale turbulence is generated here, by instability of the strongly sheared flow. There is a sharp peak in the conversion of mean-flow kinetic energy to turbulent kinetic energy and in the dissipation of this energy. For this reason, the buffer layer is often referred to as the 'turbulence generation layer'. The buffer layer is relatively thin, but is thicker than the viscous sub-layer.

The mean velocity distribution within the inner (viscous) layer is given by

$$U = \frac{yU_*^2}{\nu} \qquad (2.4)$$

whilst its thickness is taken usually to be (Middleton & Southard, 1984):

$$\delta_\nu = \frac{11.6\nu}{U_*} \qquad (2.5)$$

When the bed is rough, no single relationship can be established for the velocity distribution. There remains a region in which the viscous stress dominates, but this is restricted to the troughs between the bed roughness elements. The local velocity will depend clearly upon the shape and arrangement of the roughness elements on the bed.

Overlap layer (constant stress layer)

This layer derives its name from the fact that it is a region of overlap between the wall layer and a defect layer. In the wall layer, the flow is determined mainly by the shear stress at the bed and, hence, on the basis of dimensional analysis:

$$\frac{U}{U_*} = f\left(\frac{U_* y}{\nu}\right) \qquad (2.6)$$

Equation 2.4 satisfies this relationship.

In the defect layer, the difference between the local time-averaged speed (U) and the speed within the free stream (U_s) (i.e. the velocity defect) is unaffected by viscosity. Consequently, dimensional analysis shows that:

$$\frac{U_s - U}{U_*} = f\left(\frac{y}{\delta}\right) \qquad (2.7)$$

If the wall and defect layers overlap, Equations 2.6 and 2.7 must be satisfied; this can be undertaken only by an expression of the form:

$$\frac{U}{U_*} = \frac{1}{k}\ln\left(\frac{y}{y_o}\right) \qquad (2.8)$$

The above Equation is the well-known Prandtl-Von Karman expression. The constant y_o must be determined experimentally; its magnitude depends upon the size of the bed roughness (K_s), compared with the thickness (δ_v) of the viscous sub-layer. Using Equation 2.5, it may be demonstrated that the controlling parameter is the grain Reynolds number:

$$Re_* = \frac{U_* K_s}{\nu} \qquad (2.9)$$

Differentiation of Equation 2.8 and then, integration between the lower and upper boundary of the overlap layer (the constant stress layer), yields:

$$\frac{U}{U_*} = U^+ = \frac{1}{k}\ln\left(\frac{y}{K_s}\right) + B_s \qquad (2.10)$$

Hydraulically smooth beds ($Re_*<5$)

Here, the height of the bed roughness K_s is small compared with the thickness of the viscous sub-layer. Nikuradse (1933), who investigated flow through pipes covered uniformly with a single layer of monosized sand grains, attempted to correlate B_s with K_s (where $B_s=(1/k)\ln(Re_*)+C_{smooth}$, and $C_{smooth}=5.5$ (Fig 2.3)). Hence, Equation 2.10 becomes the 'Universal Law of the Wall',

for a smooth boundary:

$$\frac{U}{U_*}=U^+=\frac{1}{k}\ln\left(\frac{yU_*}{\nu}\right)+5.5 \qquad \textbf{(2.11)}$$

Hydraulically rough beds (Re_*>70)

Within this system, the roughness height (K_s) is now much larger than the thickness of the viscous sub-layer. Consequently, y_o should be proportional to K_s; from experimental studies, it has been found that $y_o=K_s/30$ (Sleath, 1984). Nikuradse (1933) derived a value of 8.5 for B_s. Thus, replacing this value into Equation 2.10, the 'Universal Law of the Wall' for a rough boundary becomes:

$$\frac{U}{U_*}=U^+=\frac{1}{k}\ln\left(\frac{y}{K_s}\right)+8.5 \qquad \textbf{(2.12)}$$

In the above formula, the origin of y for plane beds of sand is taken usually the plane passing through the tops of the grains (Middleton & Southard, 1984), or $0.3D_{90}$ below the mean level of the grain crests (Sleath, 1984).

Transitional stage

In the transition region, y_o is a function of both the viscous sub-layer thickness and the bed roughness size.

Outer layer

This particular component is the part of the defect layer which does not overlap the wall layer; it is called also the 'wake region'. The velocity profile can be represented here by the velocity defect law

$$\frac{U_s-U}{U_*}=-\frac{1}{k}\ln\left(\frac{y}{d}\right)+const. \qquad \textbf{(2.13)}$$

where the constant is dependent upon the concentration of sediment in suspension (Coleman, 1981).

The outer layer occupies most of the flow depth, from the free surface down to near the boundary. Here, the turbulent shear stresses are predominant and the viscous shear stresses can be neglected. Turbulence within this zone is on a much larger scale than nearer the boundary. Because of their large size, the turbulent eddies here are more efficient at transporting momentum normal to the flow direction than are the much smaller eddies nearer to boundary. This property is why the mean velocity profile is much more gently sloping in this region, than nearer the bottom. However, the eddies contain much less kinetic energy (per unit volume of fluid) than in the buffer layer.

(b) Other relationships for turbulent boundary layers and free surface flows

Velocity profile method

This approach makes use of the Prandtl-Von Karman velocity profile Equation (Sternberg, 1972). By changing the logarithmic expressions from *ln* to *log*, then assuming that k=0.4 (for clear water) the following expression is derived:

$$\tau_o=\rho\left(\frac{U_{y2}-U_{y1}}{5.75(logy_2-logy_1)}\right)^2 \qquad \textbf{(2.14)}$$

This approach requires a minimum of two simultaneous velocity measurements within 1.5 m of the sea bed (Sternberg, op. cit.).

Quadratic stress law

Experimental evidence has demonstrated that the boundary shear stress in a turbulent flow is proportional to the fluid density and the square of the mean velocity. Introducing a drag coefficient ($c_{D'}$), the following formula is obtained:

$$\tau_o = c_{D'} \rho U_y^2 \qquad \textbf{(2.15)}$$

The early laboratory investigations of Nikuradse (1933), together with the field measurements undertaken by Sternberg (1968), suggest that $c_{D'}$ in fully rough turbulent flows does not vary with height above the bed; it assumes a constant value, related to bed configuration. Equation 2.15 enables the bed shear stress to be evaluated from a single measurement of current speed, obtained usually at 1 m above the bed.

Seventh power law

Some researchers (Dyer, 1986) prefer to adopt a single power law expression, with the most frequently used being:

$$\frac{U}{U_s} = \left(\frac{y}{\delta}\right)^{\frac{1}{7}} \qquad \textbf{(2.16)}$$

The formula may be regarded only as an approximation, since the exponent has been found to vary within the range 1/3 to 1/10.

(c) Shear stress

One of the principal difficulties encountered in describing turbulent flows is to obtain a satisfactory relationship between shear stress and the time-mean velocity. One approach is to assume that the mean flow is

the same as that as in laminar flow, except that the kinematic viscosity (ν) is replaced by an eddy viscosity (ε). For mean flow parallel to the bed:

$$\frac{\tau}{\rho} = \varepsilon \frac{du}{dy} \qquad (2.17)$$

Clauser (1956) has suggested that, for a smooth bed, ε varies as follows:

(i) inner layer

$$\varepsilon = \nu \qquad (2.18)$$

(ii) overlap layer

$$\varepsilon = kU_* y \qquad (2.19)$$

(iii) outer layer

$$\varepsilon = 0.018 U_s \delta_* \qquad (2.20)$$

where δ_* is the displacement thickness defined as:

$$\delta_* = \int_0^\infty (1 - \frac{U}{U_s})\, dy \qquad (2.21)$$

An alternative approach is to use the mixing length hypothesis of Prandtl (1952) and Von Karman (1952). If the velocity is divided into time-averaged and fluctuating components, then a time-mean is taken of the formulae of motion. The resulting formulae are the same as for a steady flow, except for an additional stress

$$\tau_R = -\rho \overline{u'v'} \qquad (2.22)$$

where u′, v′ are the fluctuating components of velocity in the x and y directions, respectively. This particular variable is referred to as the Reynolds stress. Prandtl (1952) has suggested that turbulent eddies travel a distance (l), before giving up their momentum to the surrounding fluid. In this case, the fluctuation u′ should be equal to the difference between the horizontal

component of velocity at the level from which the eddy originated and that at a distance l above that at which it terminated. Using Taylor's theorem (Stephenson, 1973):

$$u' \approx -l \frac{\partial u}{\partial y} \qquad (2.23)$$

Assuming that v′ ∝ u′ and in combination with Equation 2.22, we obtain:

$$\tau_R = \rho l^2 \left|\frac{\partial u}{\partial y}\right| \frac{\partial u}{\partial y} \qquad (2.24)$$

Von Karman (1952) derived the same relationship on the basis of dimensional analysis. To make use of this Equation, it is necessary to adopt an expression for the mixing length (l). The most obvious assumption here is that:

$$l = ky \qquad (2.25)$$

Outside the viscous sub-layer, the Reynolds stress (τ_R) due to the turbulence is much larger than the viscous stress. Also, within the wall layer, the shear stress is virtually constant. Thus, within the overlap layer:

$$U_* = \left(\frac{\tau_R}{\rho}\right)^{\frac{1}{2}} \qquad (2.26)$$

A combination of Equations 2.24, 2.25 and 2.26 leads to the expression listed as Equation 2.8.

2.3. THRESHOLD OF SEDIMENT MOTION UNDER STEADY FLOW

2.3.1. Non-Cohesive Sediments

(a) Nature of the sediment

The physical nature of non-cohesive grains can be expressed in terms of their size, shape, density, angle

of repose, fall velocity and their particle size distribution.

Since the shapes of naturally-occuring grains vary considerably, the use of the particle diameter (D) is not a unique classification. Some of the various definitions available are: (i) sieve diameter; and (ii) the diameter of an equivalent sphere, having the same settling velocity. The size of a grain can be determined on the basis of sieving (Folk, 1974), although this technique does not account for the hydraulic properties of the grain. However, there is a difference in the projected area of grains having the same volume, but different shapes (Jonasz, 1987). The hydraulic properties can be determined on the basis of settling velocity analysis. In the literature, the diameter (D) of a particle of sand or gravel is referred to usually as that established from the results of sieve analysis. In contrast, settling velocity analysis is restricted normally to silt and clay (mud) particles (although sand is increasingly subjected to this particular approach).

The concepts governing the shape of particles are sphericity and roundness. The sphericity of a particle measures the degree to which the grain approaches a spherical shape. This concept was developed by Wadell (1932), who defined it as the ratio between the diameter of the sphere with the same volume as the particle and the diameter of the circumscribed sphere. Methods of quantifying sphericity include the expression of Wadell (1932) and the classification diagram of Sneed & Folk (1958).

Grain roundness is referred to the sharpness of the corners and edges of the particle; this was quantified by Wentworth (1919), whose definition was modified by Wadell

(1932). Wadell's definition (which Blatt *et al.*(1980) present as the most 'universally accepted') defines roundness as the ratio of the average radius of curvature of the corners, to the radius of the largest inscribed circle. One of the more widely-used determinations of roundness is that of Powers (1953), where the shape of the particle is compared with that of standard images of known roundness; subsequently, a roundness value is assigned to it.

The density of a particle is expressed often in terms of its specific weight, γ ($=\rho_s g$).

Another fundamental property of cohesionless grains is the angle of their repose (ϕ) (also called the friction angle (see, Li & Komar, 1986; Kirchner *et al.*, 1990)). This angle is determined usually using methods similar to that suggested by Chepil (1959). This investigator placed a layer of uniform grains on to a flat surface covered with a single fixed layer of particles; these were identical to the grains being investigated. The surface was then tilted until the grains rolled or slid over the surface and the angle ϕ measured.

The settling velocity of a particle is reached when the drag of the fluid is exactly equal to the force due to gravity. The viscosity of the fluid tending to resist motion produces positive and negative pressures below and above the grain, respectively. Settling velocity measurements are particularly useful in the investigation of the hydraulic properties of particles (Collins & Rigler, 1982).

Finally, the erodibility of cohesionless particles depend not only upon their shape and size, but also on the overall size distribution i.e. the relative position of a

grain, in relation to those surrounding it. Any naturally-occuring sediment consists of grains of different sizes, shapes and densities. Quartz is the most commonly-occurring mineral in non-cohesive sediments. Thus, the specific gravity of sands lies normally close to 2.65.

In comparing the results of natural processes and laboratory experiments, on sediments of different size distributions, various attempts have been made to classify the samples by means of a single size characteristic (representative of the whole sample). Such classifications have included: (i) median grain size (D_{50}); and (ii) geometric mean, which is defined as $D_{gm} = 1/3\ (\Phi_{16} + \Phi_{50} + \Phi_{84})$. Each of the Φ values is derived from a probability plot, of percentage occurrence against grain size. Often, the distribution of grain sizes is log-normally distributed and, for example, a normal distribution yields a straight line on the probability plot.

(b) Nature of the fluid

The properties of a fluid relevant to sediment erosion threshold are density (ρ) and kinematic viscosity (ν). Density is important, since it determines the submerged weight of the grain [$W \propto (\rho_s - \rho) g D^3$], whilst viscosity ($\nu$) is important in its relationship to the stress applied by the fluid (to the bed). Over the time span of a single erosion threshold experiment, under freshwater flow conditions, both ρ and ν will remain essentially constant. These parameters change only in response to considerable temperature changes. However, in the natural environment where the temperature ranges are large, these fluid properties may vary considerably. Further, dissolved salts and suspended material can also cause a

significant change in the fluid characteristics.

(c) Forces acting on the grains

A sediment particle resting on a grain boundary will experience a drag force when exposed to a flowing fluid. This force can be represented by a drag coefficient, using the following expression:

$$D' = \frac{1}{2}\rho C_{D'} A U^2 \qquad (2.27)$$

Even though a particle may not be fully exposed to the flow, the projected area (A) is assumed to be equal to $\pi D^2/4$. Moreover, the grain resting on the rough or smooth boundary will disturb the flow, with streamlines being deflected over the top of the grain. Because of this distortion, the fluid accelerates over the top of the grain and causes a lowering in pressure. Consequently, there will be a difference in pressure vertically across the grain; this will cause a lift force, similar to that induced by flow over an aerofoil and providing a tendency for the grain to rise. The lift force may be considered in a similar way to the drag force:

$$L = \frac{1}{2}\rho C_L A U^2 \qquad (2.28)$$

Chepil (1961) has showed that the lift force is 0.75 of the drag force for a grain, on a boundary of similar grains and in air. Likewise, that the lift decreased rapidly as the grain was raised above the bed, reaching a zero value at one or two grain diameters above the mean surface.

(d) Initiation of grain movement

When water flows over a bed of loose grains, there will be a certain speed (velocity) at which the combined drag

and lift forces on the uppermost particles will be sufficient to dislodge them from their equilibrium positions. This flow is referred to as the critical or threshold velocity; this is associated with an equivalent critical or threshold shear stress. If the flow speed is increased in small increments, motion will firstly occur for a few exposed grains; it will reduce with time, as they come to rest in new equilibrium positions. With increasing speed, the movement will become more general and prolonged. The threshold of motion is, consequently, difficult to define: much of the scatter in the experimental results is because observers have used different numbers of grains, moving per unit area per unit time, as their threshold criterion. For example, Kramer (1935) has used 'weak movement', Chepil (1959) the 'moment when the first downward movement of individual grains became perceptible', Neil (1967) the 'conditions for a single stone to be first displaced', Rathbun & Guy (1967) the 'scattered particle movement' and Collins & Rigler (1982) 'intermittent motion'. Alternatively, first motion criteria have been proposed based upon a more specific quantitative criterion; these are, for example, the Yalin criterion (Neil & Yalin, 1969; see below) and Vanoni's (1964) 'sediment movement bursts'. The direction of 'easiest' movement (threshold) will vary from grain to grain, depending upon the local packing and degree of 'exposure' of the grain to flow. Fluid forces will vary from particle to particle, being highest on the more exposed grains: they fluctuate with time, even for steady flow, because of the turbulent motions observed within the viscous sub-layer (Section 2.2.2). Hence, the determination of the initiation of motion can be regarded only as a stochastic process.

A simple model of the forces on spherical grains developed by Chepil (1959), will now be considered. The

exposed grains rest upon others, but with their centres lying in the plane corresponding to the direction of the flow. There will be a gravitational force acting on the particles, equal to their own immersed weight; this will act through the centre (b) of the sphere (Fig. 2.4):

$$W=\frac{\pi}{6}(\rho_s-\rho)gD^3 \qquad (2.29)$$

The drag and lift forces, however, need not necessarily act through b (Fig. 2.4) because flow around the sphere will be influenced by the configuration of the surrounding grain surface. When the grain is at the point of movement, the resultant of the three forces must act through the point of contact (c) between the grains. With a further increase in the drag, there will be a couple which will rotate the grain (about c) and dislodge it. If the angle between bc and the vertical is small, then the grain will tend to roll over the other; if it is larger, then the grain will be forced to 'hop out' of its resting place. Chepil (1959) has shown also that the drag acts some way above the centre of the sphere i.e. 0.29 of a grain diameter below the top of the grain. This configuration provides a value for a′ of 24°. The angle a′ is the angle of dynamic friction; it contrasts with the angle of static friction (ϕ), which is equal to the angle of repose of the grains. When the point of movement arises, the resultant of the forces will act along the line ac (Fig. 2.4). Then,

$$D'=(W-L)\tan a' \qquad (2.30)$$

(e) Shield's study of the threshold of sediment motion

Shields (1936) investigated the following relationship

$$\theta_c = \frac{\tau_c}{(\rho_s - \rho) g D} = f(Re_*) \qquad (2.31)$$

and produced the threshold curve presented as Fig. 2.5. The dimensionless grouping on the left hand side of Equation 2.31 effectively compares the critical shear stress, with the immersed weight of a unit grain thickness layer of the bed; it is referred to as, the 'Shields entrainment function (θ)', with a threshold value of θ_c. The curve shown on Fig. 2.5 is divided into three distinct zones, whose limits correspond to the following boundary layer flow regimes:
(i) up to Re_*=3, smooth boundary flow exists and the particles are embedded in the viscous sub-layer—Shields assumed that the threshold shear in this zone was independent of grain diameter and, in that case, the curve should have a slope of -45° and $\theta_c \propto Re_*^{-1}$;
(ii) for 3<Re_*<200, there is a transitional region where the grain size is the same order of thickness as the viscous sub-layer—there is a minimum value of θ_c, of about 0.03; and
(iii) for Re_*>200, the flow regime becomes rough turbulent and θ_c has a constant value of between 0.03-0.06.

There have been few studies of threshold characteristics within the low grain Reynolds numbers regime. Likewise, this section of the Shields original curve was not confirmed at the time of the original investigation, because of the lack of experimental data. However, White (1970) has studied more recently the threshold of natural quartz grains and of glass ballotini, down to a $Re_* \approx 0.05$; this corresponds to a grain size of about 20 μm. The results may be expressed in terms of the curve $\theta_c = 0.06\ Re_*^{-0.5}$ (Fig 2.5). This expression does not show, however, an independent relationship between threshold

and grain diameter, as Shields proposed originally. A possible reason for this is that the bed cannot be formed in a completely smooth manner and the height of the small piles of grains is sufficient to be compared with the viscous sub-layer thickness. Also there are significant bursting events (see below, Section 2.3.3) occurring in the viscous sub-layer, which are likely to cause movement of any exposed grains.

The effect of turbulent fluctuations on the viscous sub-layer and grain motion have been investigated by Grass (1970). This investigator considered both the distribution of the available shear stress and that of the threshold stresses (in statistical terms, each with a mean and a standard deviation) required by the potentially mobile grains. When the mean stress is low, it is only the occasional large fluctuations that move the most unstable grains. At higher stresses, grain movement is almost general over the bed. Consequently, the degree of grain movement will be a measure of the overlap of the two distributions. Thus,

$$\tau + n\sigma_\tau = \tau_t - n\sigma_t \qquad (2.32)$$

where n determines the degree of overlap of the ambient shear stress (τ) and of the stress required to move the uppermost grains (τ_t), whose standard deviations are σ_τ and σ_t respectively. The threshold results of Grass (1970) lie slightly higher than those of White (1970, Fig 2.5). This discrepancy may be due to the use of different threshold criteria by these investigators.

There have been many studies of the threshold of sand and, despite the large scatter in the data points, the general reduction to about θ_c=0.03, at a Re_* of about 10, is fairly well established. However, the threshold shear stress increases gradually with grain size.

There have been fewer studies of threshold at Re* greater than about 1000 and, correspondingly, there are relatively large discrepancies between the results obtained. Some of the discrepancies are due to the relative protrusion of the grains above the surrounding bed (Fenton & Abbott, 1977; Carling, 1983; Panagiotopoulos *et al.*, 1994).

Much of the scatter in the observed threshold values, for any particular grain size, may be the result of using different criteria for the relative intensity of transport. Several criteria have been developed as was mentioned previously. The most-widely used threshold criterion is that of Neil & Yalin (1969). These investigators proposed that the number of grains (N) moving over an area (A) during a time interval (t) should be defined as

$$\frac{N}{At}=\epsilon\left(\frac{\rho D^5}{(\rho_s-\rho)g}\right)^{-\frac{1}{2}} \qquad \textbf{(2.33)}$$

where ϵ is an unknown function of θ_c and Re*. However, experiments can be compared using a standard value of ϵ (10^{-6} has been proposed).

The Shields curve is useful, in that it allows direct comparison of results obtained for different grain densities and fluid viscosities. However, since U* and D appear in both ordinate and absicca, the relationship between the variables is not immediately apparent. Curves, such those presented in Fig. 2.6, are of more direct use to investigators. Such representations are derived mainly from Miller *et al.* (1977), who compiled most of the available data for flat beds. Useful threshold curves were presented of: θ_c plotted against Re*; $U_{*,c}$ against D; and τ_c and $U_{100,c}$ versus D.

2.3.2. Cohesive Sediments

(a) Nature of the sediment

A characteristic feature of many cohesive sediment deposits is that they form a coherent mass, not just a collection of individual particles in contact with each other. Such coherent deposits are said to be cohesive, a term like 'climate' which is used to describe the combined effect of complex interactions of many factors but cannot be defined.

Cohesive sediments contain significant amounts of clay minerals, which assume control of the properties of the material. The cohesive properties arise from electrochemical forces in the clay-water medium. The clay particles are plate-like with a diameter less than 2 μm; this is typically of the order of 10 times the particle thickness. The most common minerals are two- or three-layer clays; these are bonded units of silica tetrahedral (T) and alumina octahedral (O) sheets. The most inert clay is two-layer O-T, bonded together by hydrogen bonds, with strong attraction between O and T and with little isomorphous substitution within the lattice structures. These sediments, kaolinites, are relatively inactive and show little or no ability to absorb water within the lattice; this can cause swelling. Three-layer clays, T-O-T, that show such surface activity due to large-scale isomorphous substitution and great abilities to absorb water within the lattice, are montmorillonites. Illites are of the same form as montmorillonites but, because of the large potassium ion present between the T and O sheets, strong bonding occurs and the swelling potential is greatly reduced.

On the face of each clay mineral, there is normally a

negative charge due to the exposed oxygen atoms in the broken bonds of the crystal lattice. In addition, negative charges will result from isomorphic substitution of positively-charged cations of low valency, within the lattice, with principal structural cations of a higher valency. At the clay-particle edge, however, the charge is positive; this relates to the broken bonds of the silica tetrahedra. The overall particle charge is usually negative for clay minerals; its magnitude can be calculated by measuring the electrophoretic mobility of the particle, and speed within a known electric field.

In a saline fluid, the free ions in the water interact with the charges on the clay-particle. The positive ions are attracted to the clay-face and the negative ones to the clay-edges. A closely-held layer of cations (such as sodium (Na^+), potassium (K^+) and magnesium (Mg^{++})) will be formed on the clay-face, by the action of the most negative residual ions. There will also be a more diffuse layer of hydrated cations neutralising some of the remaining negative charge. These diffuse ions can be exchanged with the surrounding fluid, depending upon the concentration and valency of the ions in the fluid. The total effect of this electrical double layer (Helmholtz) is to reduce the magnitude of the negative charge on the particle. If the charge on the face of the clay particle were the only factor, then the clay-plates, being similarly charged, would continually repel one another. The electrostatic (coulombic) force would be repulsive, decreasing exponentially with distance. However, there is also a molecular attractive force, known as the London-van der Waals force. This force varies and is inversely proportional to the square of the distance of separation; it tends to largely counteract the repulsive force under certain conditions.

Within river waters, when the double layer is not significant, the electrostatic repulsive forces are large and generally dominate; these tend to prevent the particles flocculating. Nevertheless, there is a possibility of the positively-charged edges meeting the negatively charged faces; thus, a very open 'house-of-cards' structure is formed. This arrangement is likely to be a very weak bonding, which could easily be broken by turbulent shearing. In saline waters, the presence of the double layer reduces the surface charge and the attractive van der Waals dominate. Consequently, the particles have a greater tendency to flocculate.

(b) Incipient transport

Consider the forces acting on a grain at the surface of a horizontal bed, which is subjected to unidirectional turbulent flow (Fig 2.7). Within the cohesive size range, such material will be considered to consist of a series of flocs. The physics of floc transport is complicated, on the basis of interaction between the ambient flow and the floc properties. For example, flocs which are exposed partially at the bed surface tend to deform plastically under shear flow; this leads consequentially to a reduction in the interfacial drag (Gust, 1976). Here, we will assume the grain to be non-deformable, and to possess a physically-recognizable identity (either at rest or in motion).

In a cohesive bed, each grain is retained by cohesive forces, which bind the grain to its neighbours at discrete points of contact. Grain-grain contact can be broken, therefore, by shear or normal forces. Clay cohesion, which arises from electrochemical effects, is often significantly modulated in marine muds by biochemical factors. Here, however, cohesion is

considered be similar to electromagnetic attraction. Thus, for rupturing the intergranular bond, a normal tensile force (e.g. due to lift) is required as an agency opposing cohesive attraction. Shearing (due to drag) is opposed by resistance due to cohesion, friction and interlocking.

By reference to Fig. 2.7, the prevailing hydrodynamic forces include the lift (L) and the drag (D′), whilst the active cohesive force (F_C, which is added to the immersed weight (W) of the grain), will oppose the lift force. F_R is the reactive shear force, equal in magnitude and opposite in direction to D′. The spatial-mean bed plane passes through point a, which lies above the centre of mass of the grain at point b (Christensen, 1975). Consequently, whilst D′ and F_R pass through a, L and W act through b. Thus, since all the forces do not pass through a single point, an evaluation of the condition for grain motion must consider both the forces and the moments. The active moment of interest here is D′ab, which can enhance entrainment of the grain, by causing it to roll into the fluid. For simplicity, D′ is assumed to act through point b i.e. ignoring the typically small couple arm, ab.

The condition for incipient transport, in terms of the active forces corresponding to those shown on Fig. 2.7, is shown on Fig. 2.8. This condition indicates, that with this particular physical condition of the grain, the resultant of the drag force (D′) and the net downward force $W+F_C+L$ must subtend an angle ϕ; this is equal to the angle of repose. By definition, therefore, the resultant passes through c; this is the point of intergranular contact. The angle of repose has a clear physical meaning for cohesionless sediments, but for cohesive sediments it becomes a coefficient that embodies shear resistance (Lambe & Whitman, 1969). From Fig. 2.8, the well-known

condition for incipient transport is defined by (Mehta & Lee, 1994):

$$\tan\phi = \frac{D'}{W + F_C - L} \qquad \textbf{(2.34)}$$

(c) Previous erosion studies concerning cohesive sediments

The published literature on the erosion of cohesive sediments reflects, by its diversity, the embryonic state of knowledge in this field. Erosion characteristics have been described almost exclusively with the aid of parameters used in soil mechanics which, themselves are bulk characteristics and not definable in terms of the parameters of soil physics or chemistry. The common parameters used in such analyses are: grain size, dispersion ratio, clay content, Atterberg limits (plasticity index and liquid limit), shear and tensile strength, moisture content of the soil, and cation exchange capacity; and the salt content, temperature and sodium absorption ratio of the pore water and eroding (ambient) fluid.

The grain size of non-cohesive soils (sediments) has a dominant influence on erosion, since the weight is proportional to the cube of the diameter. In cohesive soils, by contrast, grain size (if it can be defined) and weight are likely to be insignificant controls, in comparison to the prevailing electrochemical forces.

The US Bureau of Reclamation has used the dispersion ratio as the basis for the prediction of the erodibility of cohesive soils; at best, however, it only indicates trends. The ratio used is that between the percentage finer than clay-sized particles, of the non-dispersed and

dispersed cohesive soils.

The general influence of clay content has been emphasised in previous investigations (cf. Raudkivi, 1990). With an increase in clay content, the sediment bed deposits become more plastic: the swelling, shrinkage and compressibility increase, whilst the associated permeability and angle of internal friction decrease (Raudkivi, op. cit.). Approximately 5-10% of clay, by dry weight, is considered to be sufficient for the clay to assume complete control of the soil (sediment) properties (Dyer, 1986; Raudkivi, op. cit.) and generally increase the resistance of the sediment to erosion.

The Atterberg limits have been used also to predict the erodibility of soils. For example, flume experiments performed by Smerdon & Beasley (1961), using 11 different natural soils, showed that the critical erosion shear stress correlated best with the plasticity index of the soil. Similar experiments carried out by Lyle & Smerdon (1965), testing 7 different natural soils, have demonstrated that the plasticity index and voids ratio correlated well with the critical erosion shear stress. Finally, Kamphuis & Hall (1983) have demonstrated that the capability of a cohesive soil to resist erosion increases with the plasticity index. However, the majority of the attempts to relate the erosion stress to these fundamental sediment physical parameters (Atterberg limits) has not been fully successful (Institution of Civil Engineers, 1985).

Elsewhere, the shear and the tensile strength of a cohesive soil have been used to correlate with critical erosion shear stress. Most of the results obtained by investigators (Dunn, 1959; Flaxman, 1963; Mirtsukhulava, 1966; Migniot, 1977) show positive correlation, but

there is an absence of any single relationship between shear strength and the critical erosion shear stress.

The trends shown in the experimental data, in terms of variation in moisture content with critical erosion shear stress, have indicated that the latter decreases with increasing moisture content (Postma, 1967). This relationship is consistent with the concept that the inner particle bonding of a fine-grained cohesive soil decreases with increasing particle spacing.

Investigations into cation exchange capacity have not derived any unique trends concerning sediment erodibility. Montmorillonite, with a relatively high-ion exchange capacity, can have both very low and very high erodibility (Raudkivi, 1990).

The addition of salts to pore waters have been demonstrated to lead to a reduction in the thickness of the Helmholtz double layer and, as a consequence, to a reduction in the repulsive force between the particles. Hence, an increase in erosion resistance could be expected with increasing salt concentration in the pore waters. Such a trend has been demonstrated by Sargunam *et al.* (1973) and Arulanandan *et al.* (1975).

The cohesive sediment erodibility is also a function of pore water temperature. In general, the erosion rate increases with temperature, although the bed shear stress decreases through decreasing viscosity. The dependence of the erodibility with temperature has been studied by Rao (1971) for halloysite and Raudkivi & Hutchison (1974) for kaolinite.

Finally, the erodibility of cohesive material in terms of the sodium absorption ratio (SAR) has been studied by

various researchers (cf. Raudkivi, 1990). The SAR (i.e. a measure of the relative abundance of Na^{+}, to the Ca^{++} and Mg^{++} cations) is determined by the chemical analysis of a sample of pore water. Generally, low SAR values are associated with interparticle attraction. In contrast, high values of SAR cause the particles to repel each other and dispersion. As a consequence, addition of salts increases erosion resistance markedly at low values of SAR; it has no effect at high SAR-values (Raudkivi, op. cit.).

In summary, a number of authors have attempted to incorporate the results of experiments on the threshold of movement of cohesive sediments into a 'Shields type curve'. Hjulstrom (1935) produced a series of early results; these were restated by Inman (1949) and are shown diagrammatically as Fig. 2.9. Generally, the threshold velocity increases with decreasing grain size, below about 200 microns. Subsequently, Postma (1967) and various other authors have pointed out that deviation from the curve, for non-cohesive sediments, varies in relation to the moisture content. Well consolidated mud thresholds lie farthest from the Shields curve. However, although density correlates with moisture content, there is not a clear relationship between density and grain size. Consequently, the use of such a threshold curve for cohesive sediments is not to be recommended (Dyer, 1986).

2.3.3. Turbulent Bursting Related to Sediment Motion

The study undertaken by Sutherland (1967) appears to be the first to have reported that an essential characteristic of sediment transport is the tendency of grains to move in intermittent bursts. It was identified that, near to threshold conditions on a flat bed, motion was restricted to isolated locations; a small number of

grains moved briefly, by only a few centimetres. Bursts of motion occurred at one location, then another. This investigator connected the intermittent movement, to penetration of eddies into the viscous sub-layer. The mechanism was illustrated by experiments with vortex rings impinging on the bed. It was concluded that the particle is lifted into suspension by the velocity vectors, inclined at an angle to the horizontal within the centre of the vortex.

The vortex model of Sutherland (1967) has most of the essential features of the bursting sequence (the entire cycle of events is shown schematically on Fig. 2.10.) and is summarised below.
(i) A high velocity eddy moves towards the boundary and interacts with low velocity fluid, located near the boundary itself. This inrush, known as a 'sweep', causes acceleration, increase in shear and the development of small scale-turbulence.
(ii) The accelerated fluid is lifted then from the boundary as a turbulent burst, into a region of flow further away from the boundary.
(iii) Finally, the break-up of any signs of coherency in the physical representation of the events takes place.

It may be anticipated, therefore, that sweep motions would be relatively more effective at moving bedload, whilst the ejections in the promotion of suspension events (Heathersaw, 1974). Outward interactions, the part of the fluid motion having a high longitudinal fluctuation coupled with a vertical one, may be even more effective in causing suspension; however, they are relatively fewer in number than the ejections. If these suppositions are correct, there must be a level, presumably near the mean level of the upper part of the trajectory of saltating particles, where sweeps give way

to ejections as the prime events causing sediment movement.

Vanoni (1964) has recognised the importance of bursting to the erosion process, defining a threshold criterion based upon the burst frequency. Burst frequency has also been investigated in the sea by Heathershaw (1974). The results showed that bursts appeared for a period of between 5 and 10 s, during which there was a relatively calm intermittent period of around 20-200 s. Further, studies on sediment particle motions have been carried out by Sumer & Oguz (1978) and Sumer & Deigaard (1981); these have been interpreted in terms of the turbulent bursting process, as visualised by Offen & Kline (1975). Sumer & Oguz (op. cit.) measured particle trajectories over a smooth bed, proposing that particle lift from the bed is the result of the temporary local adverse pressure gradient created by the burst passing over the particle. The lifted particle is then carried into the body of the flow by the ejection and, as this structure gradually breaks up, the particle settles towards the wall, only to be incorporated into the next burst.

2.4. WAVES

2.4.1. Types

The waves of greatest importance, as far as the dynamics of the sea bed are concerned, are the gravity waves formed by wind action on the water surface. In relatively deep water, these surface waves are progressive. However, near a boundary, standing waves caused by reflection of the incident progressive waves, may be significant. Edge waves, both progressive and standing, may also be important in regions adjacent to the coastline. All of these wave types are periodic and, because they arrive in

groups of steady wave trains, it is possible to identify a period of oscillation. In an ideal fluid the only non-periodic wave of permanent form is the solitary wave. In deep water these waves, also called tsunamis, are caused mainly by movements of the earth's crust.

The density of sea water varies by only a small amount, in general terms, from one location to another. Any variation which does occur has a negligible effect on the dynamics of the surface waves. However, density variations do have a very significant effect on internal waves. Such waves are seldom of great importance as far as flow near the sea bed is concerned, apart from their interaction with (for example) the continental slope and the initiation of nepheloid layers (Gardner, 1989; Durrieu de Madron *et al.*, 1990)

2.4.2. Wave Theory

Because the free-surface boundary condition is non-linear, most of the available solutions for the velocities and pressures produced by wave action are based upon approximations; these are valid only over a restricted range of conditions. The various solutions available presently may be grouped as follows:
(i) small-amplitude theory—the first approximation is referred to often as Airy waves and higher approximations are Stokes waves;
(ii) shallow water theory (cnoidal waves, solitary waves);
(iii) rotational wave theory (trochoidal waves); and
(iv) numerical methods—these include the exact solution of Cokelet (1977) and the non-exact, but somewhat more manageable, 'stream function' and 'vocoidal theories' of Dean (1974) and Swart (1976).

Of the existing wave theories, the first approximation of the small-amplitude theory is used most generally (Hedges, 1986).

(a) Small-amplitude wave theory (first approximation)

Consider the case of a steady train of waves of constant height, as shown in Fig. 2.11. The following assumptions must be taken into account when the small-amplitude wave theory is applied:

1) the bed is horizontal and impermeable and no current is present;
2) the flow is two-dimensional, incompressible and irrotational; and
3) the wave height is small, compared with the wavelength and water depth.

Progressive waves (Fig 2.12)

The first order solution (Airy waves) which satisfies the boundary conditions is:

$$\varphi = -\frac{Hg\cosh(K(d+z))\sin(Kx-\omega t)}{2\omega\cosh(Kd)} \qquad \textbf{(2.35)}$$

The velocity components under the wave are given in terms of the velocity potential (φ) as:

$$u = -\frac{\partial\varphi}{\partial x} \qquad \textbf{(2.36)}$$

$$v = -\frac{\partial\varphi}{\partial z} \qquad \textbf{(2.37)}$$

The water surface elevation is described by:

$$n_{x,t} = \frac{H}{2}\cos(Kx-\omega t) \qquad \textbf{(2.38)}$$

The pressure is obtained from the unsteady Bernoulli

Equation as

$$P=\frac{\rho gH\cosh(K(d+z))\cos(Kx-\omega t)}{2\cosh(Kd)}-\rho gz \qquad (2.39)$$

or

$$P=-\rho gz+\rho gnK_{P(z)} \qquad (2.40)$$

The first term on the right hand side of Equation 2.40 is the hydrostatic term, whilst the second is the dynamic pressure. The term $K_{P(z)}$ is referred to as the pressure response factor; below the mean water surface, this is always less than unity. The dynamic pressure is the result of two contributions; the first and most obvious is the surcharge of pressure, due to the presence of free surface displacement. If the pressure response factor ($K_{P(z)}$) were unity, then the pressure contribution from the free surface displacement would be purely hydrostatic. However, associated with the wave motion is the vertical acceleration, which is 180° out of phase with the free surface displacement. This contribution modifies the pressure from the purely hydrostatic case. On Fig. 2.13, the effect of the dynamic pressure in modifying the hydrostatic is shown. The pressure response factor has a maximum of unity at (z=0) and a minimum of 1/cosh(Kd) (at the bed surface).

The horizontal component of velocity at the bed (just outside the wave boundary layer) is

$$U_o=U_{o(\max)}\cos(\omega t-Kx) \qquad (2.41)$$

where

$$U_{o(\max)}=\frac{\omega H}{2\sinh(Kd)} \qquad (2.42)$$

The relationship between wavelength and period is given by

$$L=\frac{gT^2}{2\pi}\tanh\left(\frac{2\pi d}{L}\right) \qquad (2.43)$$

and the phase wave speed by:

$$C=\frac{L}{T}=\frac{gT}{2\pi}\tanh\left(\frac{2\pi d}{L}\right) \qquad (2.44)$$

Standing waves (Fig 2.14)

Standing waves may be considered, at least as far as a first order solution is concerned, as the sum of two progressive wave trains of equal wavelength and frequency travelling in opposite directions. Thus, the first order solution for the velocity potential is

$$\varphi=\frac{gH'\cosh(K(d+z))}{2\omega\cosh(Kd)}\sin(\omega t)\cos(Kx) \qquad (2.45)$$

where H′ = 2H.

The velocity components under the wave are still given by the Equations 2.36 and 2.37, so that the horizontal component of velocity at the bed is

$$U_o=U_{o(\max)}\sin(\omega t)\sin(Kx) \qquad (2.46)$$

where

$$U_{o(\max)}=\frac{\omega H'}{2\sinh(Kd)} \qquad (2.47)$$

The wave profile can be described by:

$$n_{x,t}=\frac{H'}{2}\cos(Kx)\cos(\omega t) \qquad (2.48)$$

Similarly, the first order solution for the pressure is

$$P=\frac{\rho gH'\cosh(K(d+z))}{2\cosh(Kd)}\cos(\omega t)\cos(Kx)-\rho gz \qquad (2.49)$$

or

$$P=-\rho gz+\rho gnK_{P(z)} \qquad (2.50)$$

It should be noted that, under the nodes, the pressure is solely hydrostatic. Once again, however, the dynamic pressure is in phase with the water surface elevation and, as in the case of progressive waves, the combined result of the local water surface displacement and the vertical accelerations of the overlying water particles.

2.4.3. Oscillatory Boundary Layer

(a) Transition from laminar to turbulent flow

One of the most important factors determining the velocity distribution under a wave is whether or not the flow is laminar or turbulent. Not surprisingly, there have been many investigations undertaken into the conditions under which the transition, from one to the other, takes place.

Considering firstly a smooth bed, the results of Hino *et al.* (1976) are particularly interesting. This study observed that at values of RE significantly higher than $1.6\text{x}10^5$ (Li, 1954), the flow is not turbulent throughout the complete wave cycle. Turbulence sets in soon after the velocity passes its maximum; it disappears when the flow reverses. Likewise, Hino *et al.* (1976) found that at values of RE lower than $1.6\text{x}10^5$, the flow showed signs of 'unsteadiness'. However, this unsteadiness was of very small amplitude and did not significantly perturb the flow. Similar results were obtained by Merkli & Thomman (1975) and Tromans (1978). Generally, the value for transition to turbulence proposed by Li (op. cit.) is considered satisfactory (Sleath, 1984) and is in a reasonable agreement with one of $RE=10^5$ recommended by Jonsson (1980), for design purposes.

For flat beds of sand or gravel, the gradual increase of the flow intensity causes the following sequence of events: (i) at very low Reynolds numbers, the flow follows the contours of the bed roughness and there is no sign of turbulence; and (ii) when the RE exceeds a certain limit, jets of fluid start to be thrown up from the bed when the flow reverses at the end of each half cycle. The jets of fluid have been observed by Vincent (1957), Lhermitte (1958), George & Sleath (1978); they are caused by the ejection, as the flow reverses, of the vortices which are formed around the bed roughness elements. Strictly speaking, this formation and ejection of vortices is not turbulence i.e. 'actual' turbulence probably sets in soon after this condition. Consequently, for most practical purposes, the appearance of these jets of fluid may be taken as the start of a transitional phase.

Kalkanis (1964) has suggested that Manohar's expression (1955), which is very similar to that of Kajiura's (1968), should be used for all flat beds of sand or gravel:

$$RE=104\left(\frac{A_o}{D}\right) \qquad \textbf{(2.51)}$$

Also, Kajiura (1968) has suggested that Equation 2.51 is only the start of the transition process and the fully developed turbulence is not obtained until:

$$RE=1000\left(\frac{A_o}{D}\right) \qquad \textbf{(2.52)}$$

Sleath (1988) suggests that the above formula should be used only as a rough estimate and that a revised expression for the onset of fully-developed turbulence is the most appropriate:

$$RE=5770\left(\frac{A_o}{D}\right)^{0.45} \qquad \textbf{(2.53)}$$

(b) Velocity distribution inside a laminar oscillatory boundary layer (flat beds)

Variation in the horizontal component of water orbital velocity for a specific vertical distance from the bottom (y) is described by

$$U_o=U_{o(max)}\left[\cos(\omega t-Kx)-e^{-\beta y}\cos(\omega t-Kx-\beta y)\right] \qquad \textbf{(2.54)}$$

where the Stokes parameter is given by:

$$\beta=\left(\frac{\omega}{2\nu}\right)^{\frac{1}{2}} \qquad \textbf{(2.55)}$$

The phase of the maximum velocity at the bed is 45° ahead of that in the free stream (Sleath, 1984; Dyer, 1986). Likewise, the thickness of the boundary layer is proportional to $1/\beta$.

(c) Velocity distribution inside a turbulent oscillatory boundary layer (flat beds)[1]

There are not any analytical solutions proposed for turbulent flow, but several different models have been put forward. Agnew (1965), Jonsson (1966, 1980), Kajiura (1968), Bakker (1974), Johns (1975, 1977), and Brevik (1980) have all proposed theoretical models, based upon assumptions which have been found to provide good results for unidirectional flows. It follows a brief description of Kajiura's (op. cit.) and Jonsson's (1980) models, which are considered the most consistent and detailed

[1]Note: The term 'flat' includes both completely smooth beds and plane beds consisting of sand or gravel.

oscillatory boundary layer theories.

Kajiura's model

The shear stress is expressed in terms of an eddy viscosity:

$$\tau = \rho \varepsilon \frac{\partial u}{\partial y} \qquad (2.56)$$

Kajiura splits the flow into inner, overlap and outer layer in which eddy viscosity (ε) varies as follows:
(i) smooth beds

$$0 < y < \frac{12\nu}{U_{*w(\max)}} \qquad \varepsilon = \nu \qquad (2.57)$$

$$9\frac{12\nu}{U_{*w(\max)}} < y < \Delta \qquad \varepsilon = kU_{*w(\max)} y \qquad (2.58)$$

$$y > \Delta \qquad \varepsilon = kU_{*w(\max)} \Delta \qquad (2.59)$$

where

$$\Delta = 0.05\frac{U_{*w(\max)}}{\omega} \qquad (2.60)$$

and represents the thickness of the wall layer.
(ii) rough beds

$$0 < y < \frac{K_s}{2} \qquad \varepsilon = 0.185 kU_{*w(\max)} K_s \qquad (2.61)$$

$$\frac{K_s}{2} < y < \Delta \qquad \varepsilon = kU_{*w(\max)} y \qquad (2.62)$$

$$y > \Delta \qquad \varepsilon = kU_{*w(\max)} \Delta \qquad (2.63)$$

Jonsson's model

Jonsson (1980) starts from the concept that, for fully

developed turbulent oscillatory flow, there is (as in steady flow): (a) a wall region, in which the velocity distribution is determined by local conditions; and (b) a defect layer, in which the velocities are independent of viscosity. Thus, by dimensional analysis, for the wall layer and assuming the bed to be rough

$$\frac{U_o}{U_{*w(max)}} = f\left(\frac{y}{K_s}\right) \qquad \textbf{(2.64)}$$

and, for the defect layer:

$$\frac{U_o - U_{o(max)}}{U_{*w(max)}} = f\left(\frac{y}{\delta}\right) \qquad \textbf{(2.65)}$$

If there is an overlap between the wall layer and the defect layer it follows, in the same way as for steady flow, that provided the variation in phase within the boundary layer is not great then Equations 2.64 and 2.65 can be satisfied only simultaneously in the form

$$\frac{U_o}{U_{*w(max)}} = \frac{1}{k}\ln\left(\frac{y}{y_o}\right)\cos(\omega t + \varphi_o) \qquad \textbf{(2.66)}$$

where φ_o varies with A_o/K_s. Jonsson (1980) suggests φ_o=25° when A_o/K_s=100 and φ_o=11°, when A_o/K_s=1000. The constant y_o is equal to $K_s/30$ for a steady flow. Also, Jonsson (op. cit.) developed an expression for the thickness (δ) of the boundary layer, assuming that velocity is logarithmic over the whole boundary layer i.e. not just in the overlap layer. Taking δ_1 to be the value of δ when ωt=0,

$$\frac{30\delta_1}{K_s}\log\left(\frac{30\delta_1}{K_s}\right) = 1.2\frac{A_o}{K_s} \qquad \textbf{(2.67)}$$

Some measurements undertaken by Hino *et al.* (1983) have shown that the logarithmic profile extends over only a limited part of the velocity profile, not over the whole of the boundary layer as Jonsson assumed.

(d) Shear stress

Laminar wave boundary layer

The bottom shear stress leads $U_{o(max)}$ in phase by $\pi/4$ and is given by

$$\tau_{w(max)} = \frac{1}{2} f_w \rho U_{o(max)}^2 \qquad \textbf{(2.68)}$$

where f_w is the wave friction factor and is determined by

$$f_w = \frac{2}{\sqrt{RE}} \qquad \textbf{(2.69)}$$

Turbulent wave boundary layer

The peak bed shear stress is given by Equation 2.68, whilst the wave friction factor (f_w) can be defined using the diagrams of Jonsson (1966) and Kamphuis (1975). Similarly, Dyer (1986) has estimated that, within a turbulent boundary layer, the lead of the shear stress over the maximum free stream orbital velocity is less than $\pi/4$ (found in laminar flow) by a factor of 2. Jonsson (1963) found the lead to be 25°.

2.4.4. Permeable Beds

The flow produced under wave action in permeable beds has been studied by Reid & Kajiura (1957), Murray (1965), Sleath (1970), Yamamoto *et al.* (1978), Madsen (1978), Puri (1980) and others. Most investigators have assumed that the flow obeys Darcy's Law:

$$u=-\frac{K'}{\mu}\frac{\partial P}{\partial x} \qquad (2.70)$$

$$v=-\frac{K'}{\mu}\frac{\partial P}{\partial y} \qquad (2.71)$$

The coefficient K' is referred to usually as the specific permeability.

If the fluid, grains, and the grain skeleton are incompressible then,

$$\frac{\partial u}{\partial x}+\frac{\partial v}{\partial y}=0 \qquad (2.72)$$

Thus, the pressure obeys Laplace's Equation:

$$\nabla^2 P=0 \qquad (2.73)$$

Percolation into and out of the bed will cause the waves to lose energy and, consequently, to attenuate as they propagate in toward the shore. However, such attenuation is usually slow enough for pressure fluctuations at the bed surface to be assumed periodic, at least as a first approximation.

It has been suggested (e.g. Nakamura *et al.*, 1973; Prevost *et al.*, 1975) that the much larger waves found *in situ* could produce deformation of the grain skeleton, or even of the pore fluid. Yamamoto *et al.* (1978) have pointed out that when air is trapped in the bed, significant modifications to the fluctuating component of pressure may be observed with small waves. These investigators assume that both the water and air in the pores, the grains and the grain skeleton deform elastically.

When no air is trapped in the pores of the sediment bed, the compressibility of the pore water is very much less

than the compressibility of the grain skeleton. The solution for the fluctuating component of the pressure in the bed, in this case, is:

$$P=P_o e^{Ky}\cos(\omega t-Kx) \qquad (2.74)$$

The above Equation is for an infinitely deep bed of sediment. The corresponding expression for a bed of depth d_1, is obtained by replacing e^{Ky} by:

$$\frac{\cosh(K(y+d_1))}{\cosh(Kd_1)} \qquad (2.75)$$

Although the pressure distribution is the same as for a rigid bed, the fact that the grain skeleton is not rigid means that there must be movement of the bed in response to fluctuations in pressure (Sleath, 1984).

Now, when air is trapped within the pores, the compressibility of the air-water mixture may be much greater than that of the grain skeleton. Under such conditions, the modulus of elasticity K'' of the air-water mixture may be small compared with the shear modulus (G) of the sediment. As a result of this relationship, the pressure will fall off much faster than predicted by Equation 2.74; this could have significant implications for the erodibility of the sediment, or any structure resting on the bed (Sleath, 1984). Although the pressure falls off much faster when air is trapped in the pores, the bed displacements and effective stresses are not affected in the same way (Sleath, op. cit.).

2.5. INITIAL MOTION UNDER THE ACTION OF WAVES

2.5.1. Non-Cohesive Sediments

Suppose an infinite flat bed of sediment exists, acted upon by a steady train of small-amplitude waves of

constant height, then the fluid velocity just above the boundary layer at the bed will be approximately simple harmonic. Many problems of engineering importance are, of course, more complicated than this simple concept. Once the solution is known for the case of a flat bed, however, it is possible to estimate the solution for more complex situations. Because of the importance of this problem, there have been many attempted solutions. Some of the formulae which have been suggested are summarised in the succeeding text.

(i) Bagnold (1946) (in SI units):

$$\frac{U_{o(max)c}}{\left(\frac{\rho_s-\rho}{\rho}\right)^{\frac{2}{3}} D^{0.433} T^{\frac{1}{3}}} = 2.38 \qquad \textbf{(2.76)}$$

Bagnold (op. cit.) used a flume with an oscillating bed and increased the oscillatory velocity until grain movement began (on the basis of an undefined visual assessment). The material examined included quartz sand (0.009-0.33 cm in diameter), coal (0.036-0.8 cm in diameter) and steel (0.06 cm in diameter). This investigator postulated that a factor containing viscosity should also be present in the derived formula (Eq. 2.76).

(ii) Manohar (1955) (in SI units):
(a) initial motion in laminar boundary layer

$$\frac{U_{o(max)c}\nu^{\frac{1}{2}}}{\left(\frac{\rho_s-\rho}{\rho}\right) gDT^{\frac{1}{2}} \tan\phi} = 0.025 \qquad \textbf{(2.77)}$$

(b) initial motion in turbulent boundary layer

$$\frac{U_{o(max)c}}{\left(\frac{\rho_s-\rho}{\rho}\right)^{0.4} g^{0.4}\nu^{0.2}D^{0.2}}=7.45 \qquad \textbf{(2.79)}$$

Manohar (1955) used an oscillating bed flume and decreased progressively the period of oscillation, until point of threshold reached i.e. until a few particles in the upper layer of an horizontally smoothed bed were dislodged from their positions of rest. The material investigated consisted of glass beads (0.0235-0.061 cm in diameter), sand (0.028-0.1981 cm in diameter), PVC (0.317 cm in diameter), and polystyrene pellets (0.317 cm in diameter).

(iii) Komar & Miller (1973, 1974) (in SI units):

$$for \quad \left(\frac{\rho_s-\rho}{\rho}\frac{g}{\nu^2}\right)^{\frac{1}{3}}D \leq 12.5 \qquad \textbf{(2.79)}$$

$$\frac{U_{o(max)c}}{\left(\frac{\rho_s-\rho}{\rho}\right)^{\frac{2}{3}} g^{\frac{2}{3}}D^{\frac{1}{3}}T^{\frac{1}{3}}}=0.24 \qquad \textbf{(2.80)}$$

$$for \quad \left(\frac{\rho_s-\rho}{\rho}\frac{g}{\nu^2}\right)^{\frac{1}{3}}D > 12.5 \qquad \textbf{(2.81)}$$

$$\frac{U_{o(max)c}}{\left(\frac{\rho_s-\rho}{\rho}\right)^{\frac{4}{7}} g^{\frac{4}{7}}D^{\frac{3}{7}}T^{\frac{1}{7}}}=1.05 \qquad \textbf{(2.82)}$$

Komar & Miller (1973, 1974) have reviewed the data of Bagnold (1946), Manohar (1955) and Rance & Warren (1968) and derived the above two threshold expressions. The first expression has been proposed for laminar flow conditions which, according to Komar & Miller (op. cit.),

corresponds to a grain diameter < 0.05 cm. Kinematic viscosity (ν) is absent because it was considered to have a negligible effect on threshold conditions. The second formula has been suggested for turbulent flow conditions which, according to Komar & Miller (1973, 1974) corresponds to a grain diameter > 0.05 cm.

Other formulae have been developed by Sato & Kishi (1954), Kurihara *et al.* (1956), Larras (1956), Vincent (1957), Eagleson & Dean (1959), Goddet (1960), Ishihara & Sawaragi (1962), Sato *et al.* (1962), Bonnefille & Pernecker (1966), Horikawa & Watanabe (1967), Carstens *et al.* (1969), Silvester & Mogridge (1970), Chan *et al.* (1972), Dingler (1975), Hallermeier (1980) and Lenhoff (1982).

In addition to these explicit formulae, essentially graphical criteria for initial motion have been proposed by Kajiura (1968), Rance & Warren (1968), Madsen & Grant (1976) and Sleath (1978).

Rance & Warren (op. cit.) carried out experiments in a pulsating water tunnel and decreased progressively the wave period, until the point of threshold was reached i.e. a visual determination of critical erosion conditions, in agreement with calculated values of threshold using standard deviation plots of probability curves (corresponding to the dislodgement of one or two particles). These researchers studied the movement of limestone chips (0.41-2.52 cm in diameter), coal (0.70-4.52 cm in diameter), glass spheres (0.59-11.86 cm in diameter) and sand (0.024-0.082 cm in diameter). The dimensionless expression derived by the above investigators is of the form:

$$\frac{\rho U_{o(max)c}}{(\rho_s-\rho)gT} = f\left(\frac{2A_o}{D}\right) \qquad \textbf{(2.83)}$$

Madsen & Grant (1976) have reviewed the data of Bagnold (1946), Manohar (1955), Vincent (1957), Horikawa & Watanabe (1967) and Rance & Warren (1968) and presented a modified Shields diagram of θ_c against S_*, where S_* is a dimensionless parameter of the form $S_*=D/4\nu[(s-1)gD]^{0.5}$. These authors concluded that the Shields curve adequately describes the erosion threshold under oscillatory flow providing that θ_c is calculated using the curves of Jonsson (1966).

All the above established formulae commence with a consideration of the balance of forces on a grain of sediment, which is just at the limit of equilibrium. The fluid forces tend to drag the grain from the bed, whereas gravity tends to retain it. It has been shown by Shields (1936), for steady flow, that this limiting condition could be expressed as:

$$\frac{\tau_c}{(\rho_s-\rho)gD} = f\left(\frac{U_* D}{\nu}\right) \qquad \textbf{(2.84)}$$

In steady flow, τ_c is the critical value of the shear stress (τ_o) on the bed, at which the grains begin to move. However, in oscillatory flow, this value should be taken as the total horizontal force (per unit area) acting upon the bed, rather than just the shear stress. The reason for this difference is that, in oscillatory flow, a major contribution to the force on the grains of sediment comes from the horizontal pressure gradient within the fluid. In steady flow, this pressure gradient is not usually important. When allowance is made for this modification, Equation 2.84 might be expected to apply in oscillatory flow if: either the lift force on the grain of sediment

were negligible; or if there were a similar relationship between lift and drag, as for steady flow.

Figs 2.15, 2.16 show the critical values of $U_{o(max)}$ predicted by the above formulae for two grades of sand, in fresh water at 20°C. Where relevant, $\tan\phi$ has been taken as being equal to 1. Most of the curves in Figs 2.15 and 2.16 show $U_{o(max)}$ increasing at a rate equal or very close to $T^{1/2}$. All of the curves represented on Figs 2.15 and 2.16 are based, at least in part, on actual measurements. Thus, there is some range of experimental conditions for which each one of these curves could be shown to provide the best results. The large difference between the predicted values of $U_{o(max)}$, shown in Figs 2.15 and 2.16, illustrates the problem of extrapolating empirical curves beyond the experimental range for which they were established. One reason for the divergence of these curves is the experimental difficulty in estimating the initial motion condition i.e. different observers have different ideas about what constitutes 'initial motion'.

Another important source of error is that the function *f*, in Equation 2.84, is not a constant. Komar & Miller (1974) and Madsen & Grant (1976) have suggested, independently, that the function *f* in Equation 2.84 could be obtained from Shield's well-known curve for steady flow. Also, that the maximum wave-induced shear stress [$\tau_{w(max)}$] should be calculated using Jonsson's curves (1966). However, Hallermeier (1980) has shown that slightly better agreement between theory and experiment is obtained if Kamphuis' curves (1975) are used instead. Good agreement between oscillatory and steady flow results was found by Ishihara & Sawaragi (1962). On the other hand, Sleath (1978) has suggested that unsteady and steady flows may differ fundamentally and that different

curves ought to be used in the two cases. It was suggested also that new curves could incorporate some of the effects of lift force, which are neglected if use is made of Jonsson's or Kamphuis' curves. At the present time, the best approach appears to be to use the Shields curve, together with Kamphuis' curves for the definition of friction factor (Sleath, 1984).

Effect of bed permeability

When a bed is permeable, the fluctuation in pressure induced by the waves will cause flow into and out of the bed. This seepage has two effects: firstly, the seepage will modify the flow inside the boundary layer, which will change the shear stress exerted by the flow on the bed; and, in general, seepage out of the bed reduces the shear stress whilst seepage into the bed increases it. However, these effects may be reversed if the boundary is near the laminar-turbulent transition, since seepage into the bed may retain the flow as laminar and *vice-versa*. In addition, seepage exerts a vertical force on the sediment-grains. Martin & Aral (1971) have demonstrated that the seepage force on a grain on the surface is only 50% of that on an embedded grain but, even allowing for this, it is clear that upward seepage will reduce the stability of surface grains: in contrast, downward seepage will increase it.

The above effects counteract each other. For example, Martin (1970) and Watters & Rao (1971) have carried out experiments under steady flow and concluded that seepage did not affect significantly the initial motion condition for values of $(1/\rho g)dP/dy$, ranging from +1 down almost to the point at which fluidisation of the bed occurred i.e. the condition for bed fluidisation is $(1/\rho g)dP/dy=-(\rho_1-\rho)/\rho$, where ρ_1 is the density of the saturated bed

material (if the specific gravity of the dry sediments were 2.65 and the voids ratio 0.35, the critical condition would be $(1/\rho g)dP/dy=-1.07$). However, Oldenziel & Brink (1974) found, also for steady flow, that seepage into the bed decreased the rate of sediment transport whilst seepage out of the bed increased it. An opposite result to that identified by Oldenziel & Brink (op. cit.) was obtained by Willetts & Drossos (1975). Such a discrepancy may be caused by the somewhat coarser sediment used by the latter investigators, or possibly the limited area over which suction was applied to the bed in their experiments.

Kruijt (1976) carried out experiments under oscillatory flow and concluded that, for values of $(1/\rho g)dP/dy$ ranging from +1 down almost to the point at which fluidisation occurred, bed seepage had no observable effect on the initial motion condition.

Madsen (1974) has showed elsewhere that failure of the bed could be caused also by the horizontal pressure gradient becoming too large. The critical condition for this type of failure is

$$\frac{1}{\rho g}\frac{\partial P}{\partial x}=\left(\frac{\rho_1-\rho}{\rho}\right)\tan\phi \qquad \textbf{(2.85)}$$

where ρ_1 is the density of the saturated bed material. For relatively loose sands in seawater, the right-hand side of Equation 2.85 would be about 0.6. This critical value could be surpassed under the steep forward slope of a breaking wave.

2.5.2. Cohesive Sediments

Because cohesive sediment particles are so small, the critical shear stress for initial motion will be the same

for wave-induced motion and steady flow i.e at such small grain Reynolds numbers, acceleration effects are negligible. Thus, it is satisfactory to utilise formulae obtained under steady flow conditions.

2.6. UNSTEADY FLOW COMBINED WITH CURRENTS

2.6.1. Transitional Stage

Sarpkaya (1966) has studied combined flow in a straight pipe of diameter d'. This investigator concluded that when the oscillatory velocity $U_{o(max)}$ is very small, compared with the steady current U_s, the critical Reynolds number is around 2200. As $U_{o(max)}$ increases, the critical Reynolds number rises initially and then, for any given value of the parameter δd', falls steadily.

It is possible that waves have a stabilising effect on the flow, such that the critical value of the Reynolds number ($U_s d/\nu$) may be higher than 890 (Sleath, 1984); this is the lower critical value for steady flow, in a wide open channel. However, it is clear that in most situations of practical importance the steady current would have to be extremely weak for the flow to remain laminar within the main body of the fluid.

In an early investigation, Collins (1964) carried out experiments on combined flow in a laboratory wave channel and showed that the flow within the oscillatory boundary layer remained laminar, even though flow in the overlying fluid was turbulent. Similarly, Ramaprian & Tu (1980) showed that in the initial stages of transition, inside the wave boundary layer, the flow regime varies throughout the cycle of oscillation. Turbulent flow forces predominated during one part of the cycle, with laminar flow forces predominating during the other part.

Also, Kemp & Simons (1982) have observed that the wave boundary layer flow was laminar during the accelerating phase of the oscillating cycle and turbulent during the decelerating phase.

2.6.2. Laminar Flow

Combined steady and oscillatory flows over a flat bed have been studied by Lighthill (1954). This study demonstrated that, if the frequency of oscillation is high enough, a reasonable first approximation to the velocity distribution is provided by the assumption that the oscillatory and steady currents are unaffected by each other. Within this context, a high frequency is one that produces an oscillatory boundary layer which is thin compared with the steady flow length scale. Under the combined influence of wave and currents, the oscillatory boundary layer is only a few millimetres thick: in comparison, the length scale of the steady flow is the depth of water column. Consequently, the condition required by Lighthill (1954) is very well satisfied (Sleath, 1984).

The conclusion outlined above is confirmed by the work of Cebeci (1977), who obtained a numerical solution for the problem of combined steady and oscillatory laminar flow over a flat bed.

2.6.3. Turbulent Flow

When the combined flow regime is turbulent, there must be interaction between the steady and oscillatory components. The turbulence generated by one component will affect the velocity distribution of the other, and *vice-versa*.

Kemp & Simons (1982), in studying the interaction between laminar gravity waves and turbulent currents, found the maximum shear stress measured in the wave-dominated viscous sub-layer was about twice as high as that measured in the logarithmic layer. These authors found also that calculating the maximum bed shear stress, by adding numerically the separately calculated stresses due to currents and waves, it was possible to obtain a value only 10-20% different from that defined through measurements within the viscous-dominated region.

Most of the available mathematical models assume that the flow can be divided into two layers. The lower layer is dominated by wave action; this is extremely thin relative to the upper layer, which is dominated by the steady current. The model of Bijker (1966) considers that waves and currents can be treated separately, then superimposed non-linearly. On the other hand, the Grant & Madsen (1979) model considers that waves and currents cannot be treated separately; it assumes that the wave boundary layer acts as an additional roughness element to the steady current. Elsewhere, Christoffersen & Jonsson (1985) have presented two simple, two-layer eddy viscosity models, in order to describe the velocity field and the associated shear stress under the combined action of waves and currents. Finally, Sleath (1991) has reanalysed turbulence measurements obtained in oscillatory flow and has derived an expression for the eddy viscosity; this avoids the need for the division of the flow into a wave boundary layer and a current boundary layer.

2.7. THRESHOLD STUDIES OF EROSION UNDER COMBINED FLOWS

There have been very few studies undertaken into initial motion conditions under combined steady and oscillating

flows. These studies have been concerned with the critical erodibility of non-cohesive sediments only and, to the writer's knowledge, no investigations exist into the entrainment of sediments containing cohesive material, such as pure muds or sand-mud mixtures.

Fig. 2.17 presents an example of the results obtained by Hammond & Collins (1979), for flat beds of sediment (sand) oscillated with simple harmonic motion in a steady flow. During these measurements the simulated wave propagation is in the direction of the unidirectional current. The critical motion of the grains in these particular experiments was defined using the Neil & Yalin criterion (1969). The speed (U_c) shown in Fig. 2.17 is the time-averaged critical current velocity, measured at 2 cm above the bed. For the better understanding of these results it is helpful to consider the extreme situations outlined below.

(1) If the frequency of the oscillation is very low, the oscillatory flow may be treated as if it were steady. Thus, motion of the sediment particles takes place when the sum of the steady and oscillatory components of velocity in the vicinity of the grains reaches the critical value for a steady current alone. This condition would correspond to a straight line on Fig. 2.17, between the value of $U_{o(max)}$ at which $U_c=0$ and the value of U_c for $U_{o(max)}=0$. Hammond & Collins' (op. cit.) measurements, suggest that, for (wave) periods of oscillation equal to 15 s the results approach this 'straight line' condition.

(2) If the frequency of the oscillatory flow is high, the wave-induced boundary layer will be very thin, compared with that of steady flow; hence, the wave-induced and steady motions will be uncoupled. In the extreme case, the condition for initial motion would be either $U_{o(max)}$ or U_c to exceed the critical values corresponding, respectively, to 'no current' and 'no wave oscillation'.

On Fig. 2.17, the results for a 5 s period wave appear to approach this condition.

In another study Natarajan (1969) has carried out experiments (using sand fractions) with currents at right angles to the direction of the wave-induced oscillation. Periods of oscillation did not exceed 1.7 s and $U_c/U_{o(max)}$ was less than 0.28. Under such conditions, the steady current appeared to have little effect on the initial motion condition.

Katori *et al.* (1984) performed also experiments with currents and waves directed at right angles to one another (using rippled sand beds). It was concluded that there is clear correlation between the rates of sediment transport and the unidirectional current component of the flow.

Lee-Young & Sleath (1988) have studied the incipient motion of non-cohesive sediment (sand), under combined flow at right angles, using Kramer's criterion of 'weak motion' to define threshold. These investigators concluded that the Shields curve (1936) may be used to predict the initial motion of sediment under combined flow conditions. The total shear stress was calculated on the assumption that there is no non-linear interaction between the steady and the oscillatory flows.

Finally, Panagiotopoulos *et al.* (1994) have examined the threshold of movement of gravel-sized particles under the co-linear combined action of simulated waves and currents. These investigators found that, for low values of wave-induced near-bed current velocities, the resistance to erosion increased when the wave period decreased (Fig 2.18).

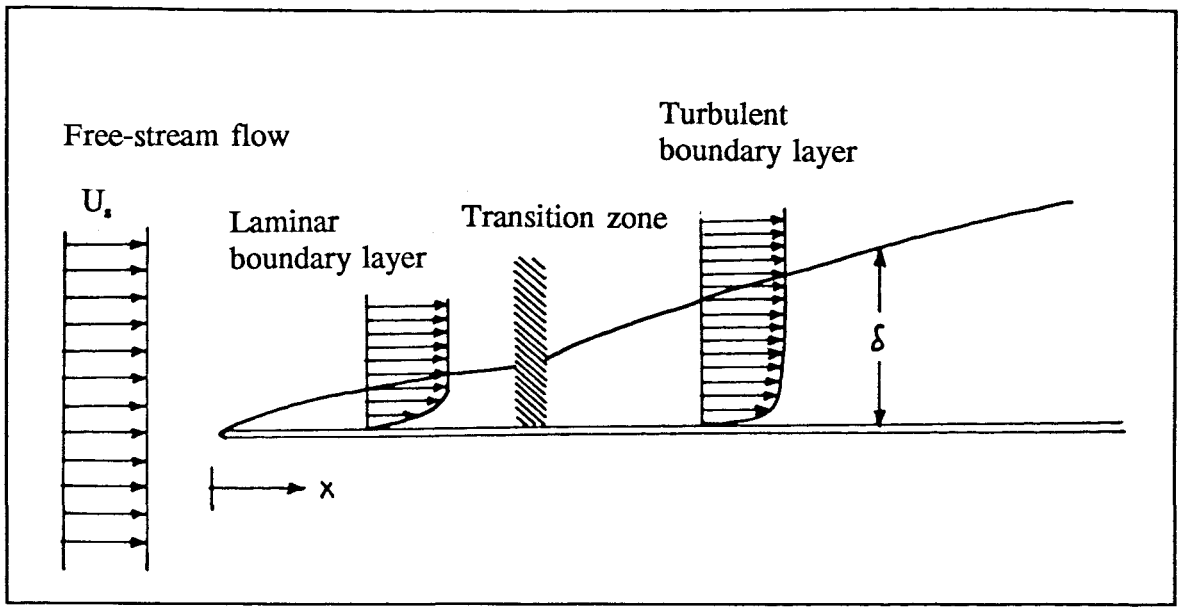

Fig. 2.1. Transition from laminar flow to turbulent flow, in the boundary layer developed adjacent to a flat plate retained parallel to the flow (after Middleton & Southard, 1984).

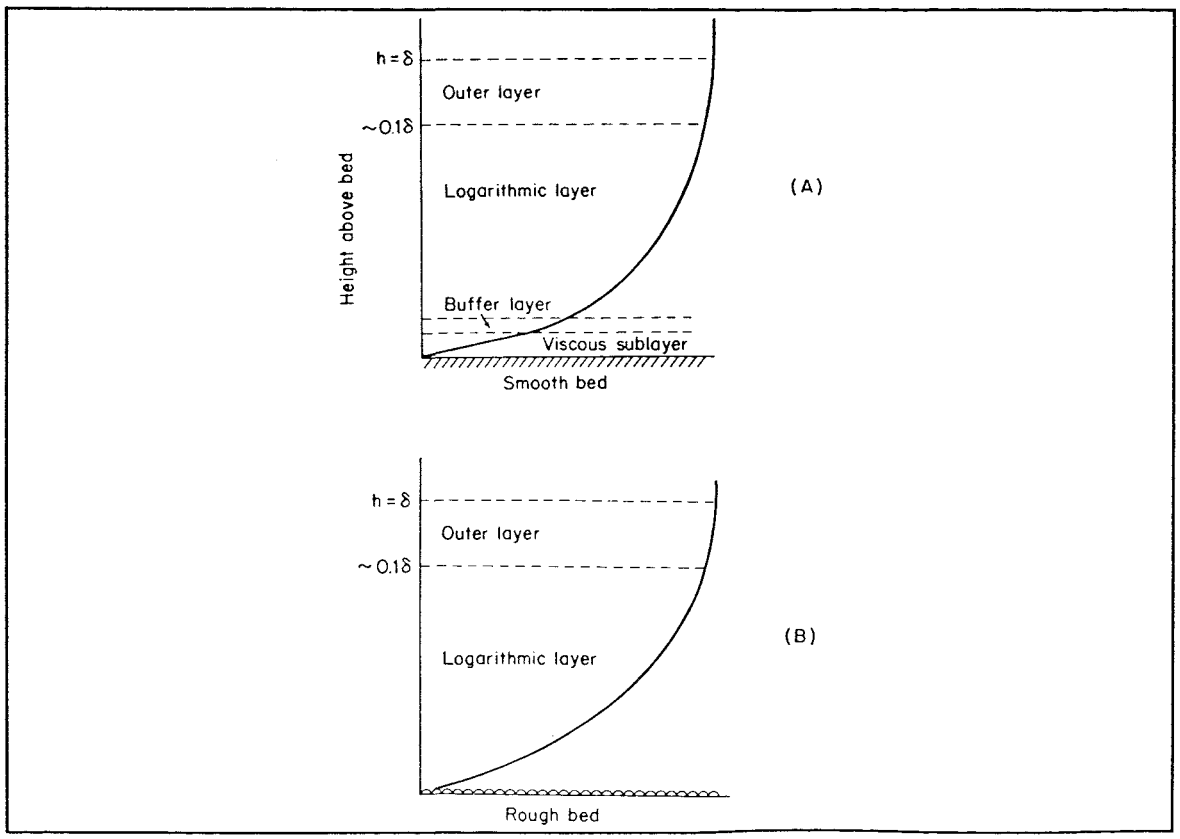

Fig. 2.2. Diagrammatic representation of the velocity profiles for (A) Smooth turbulent, and (B) Rough turbulent flow. The thickness of the layers are not to scale (from Dyer, 1986).

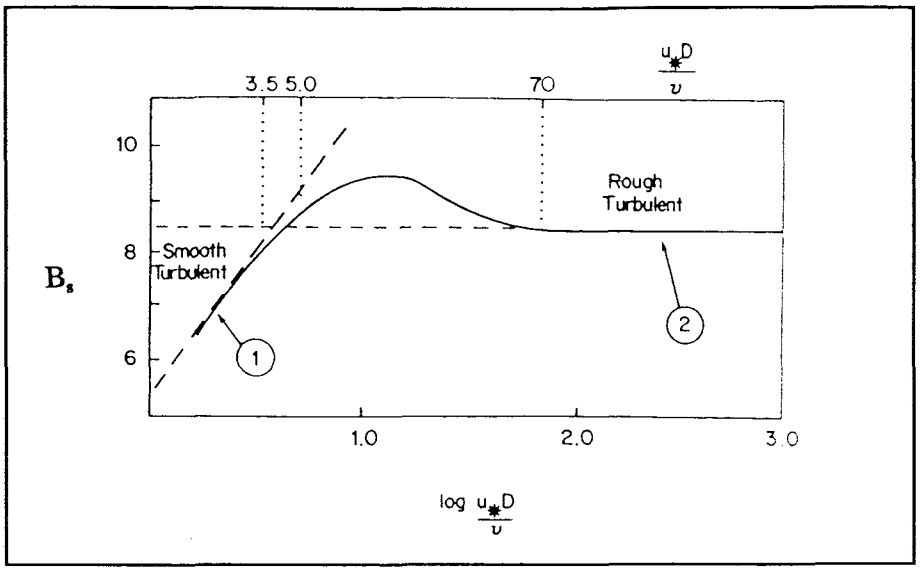

Fig. 2.3. Roughness function B_s plotted against grain Reynolds number: Curve 1, Equation 2.11; Curve 2, Equation 2.12; and Solid line, observed values (from Dyer, 1986).

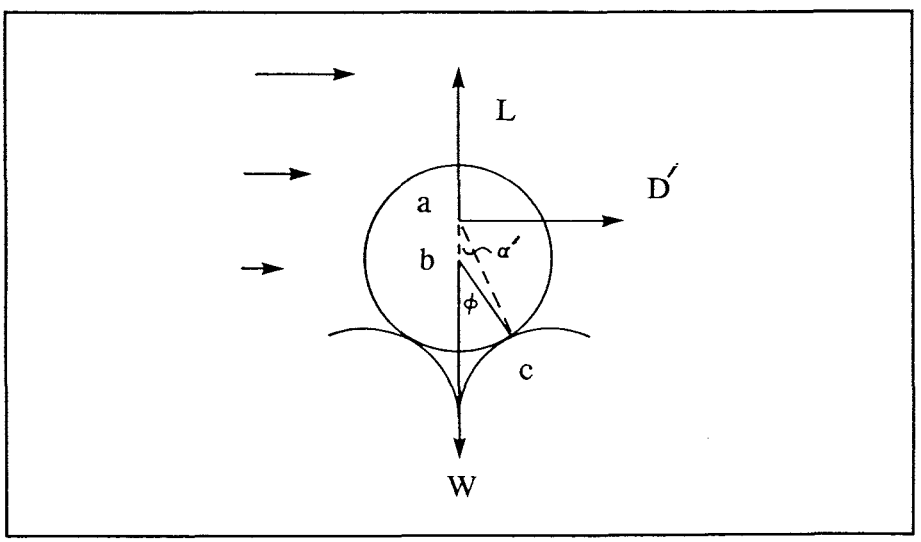

Fig. 2.4. Forces acting on a static grain resting on a grain boundary (after Dyer, 1986). For explanation of terms, see text.

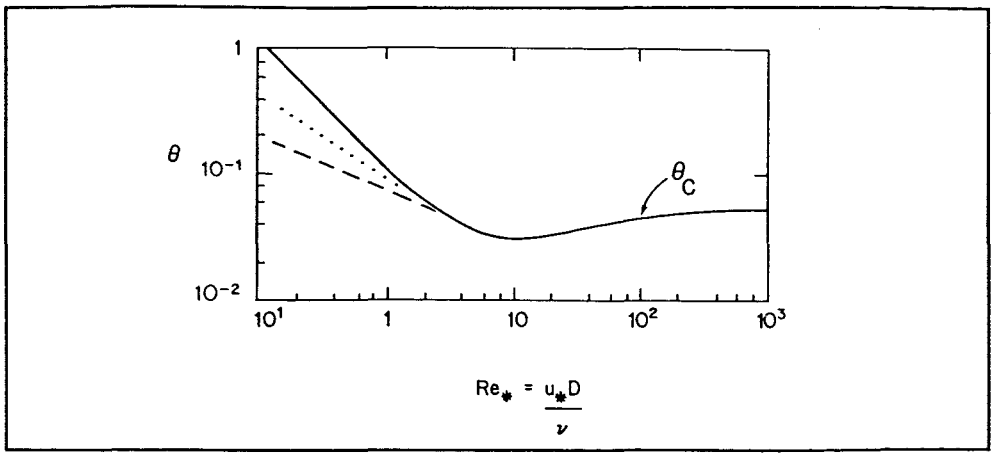

Fig. 2.5. Shields threshold curve (solid line), compared with the results of White (1970, dashed line) and those of Grass (1970, dotted line) (from Dyer, 1986).

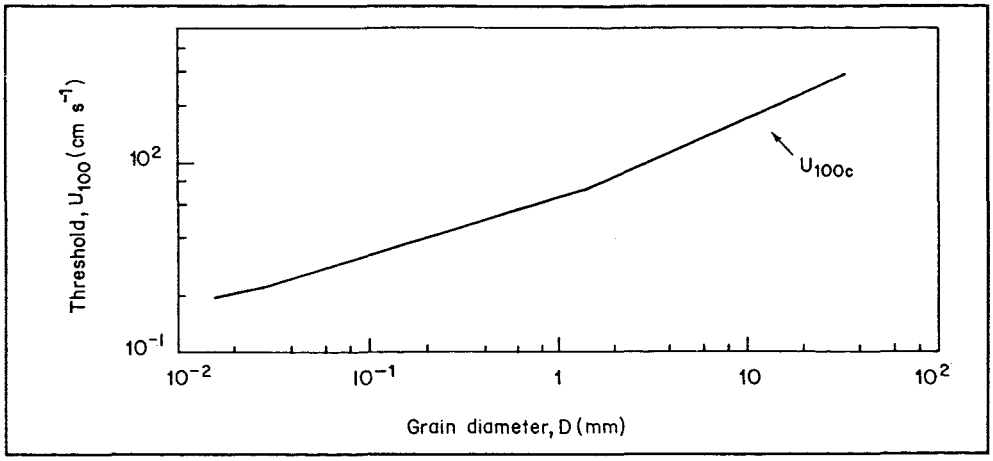

Fig. 2.6. Curve of the observed values of the threshold of motion, on a flat bed (from Dyer, 1986).

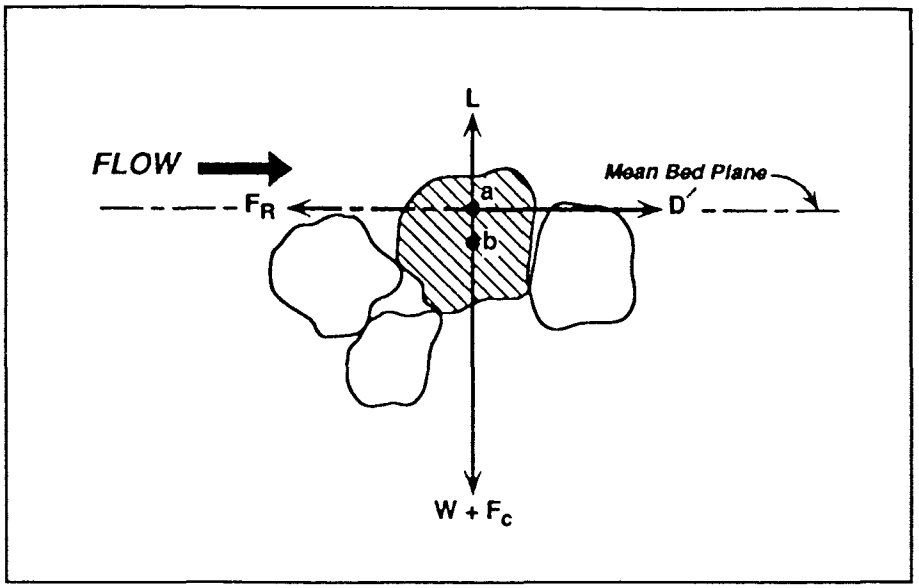

Fig. 2.7. Forces acting on a sediment grain at the surface of a cohesive bed subjected to unidirectional flow (after Mehta & Lee, 1994). For details, see text.

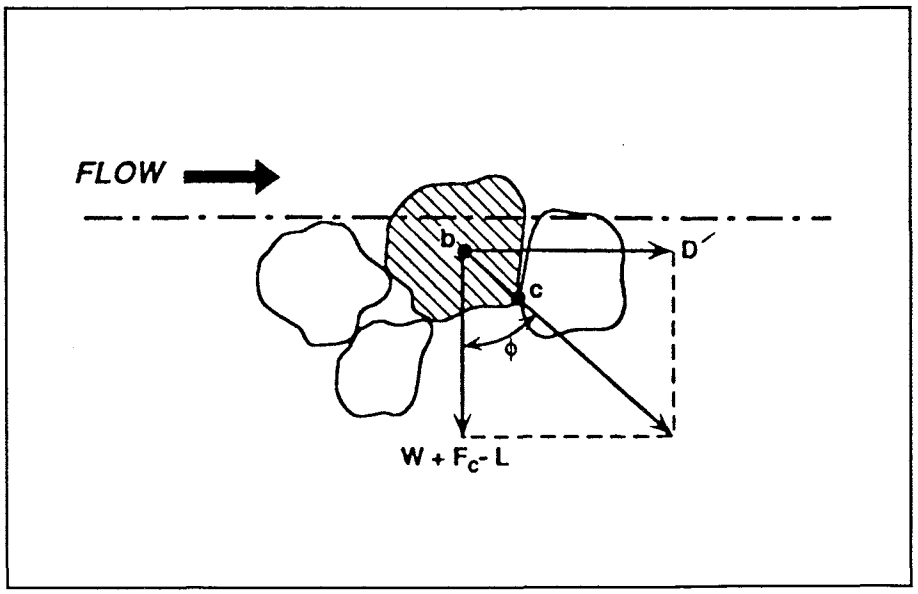

Fig. 2.8. Force diagram at incipient grain transport (after Mehta & Lee, 1994). For details, see text.

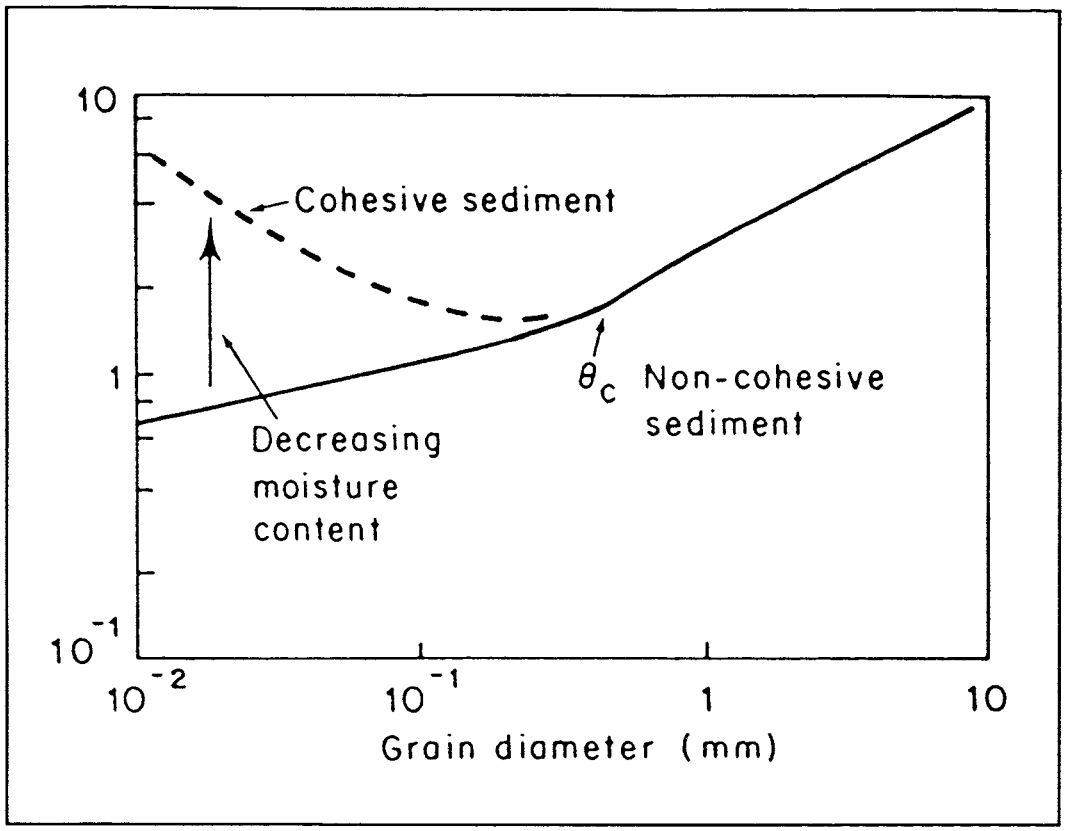

Fig. 2.9. Threshold curve for muddy sediments. The dashed line is only approximate, since the actual threshold for mud depends upon mineralogy, concentration etc (from Dyer, 1986).

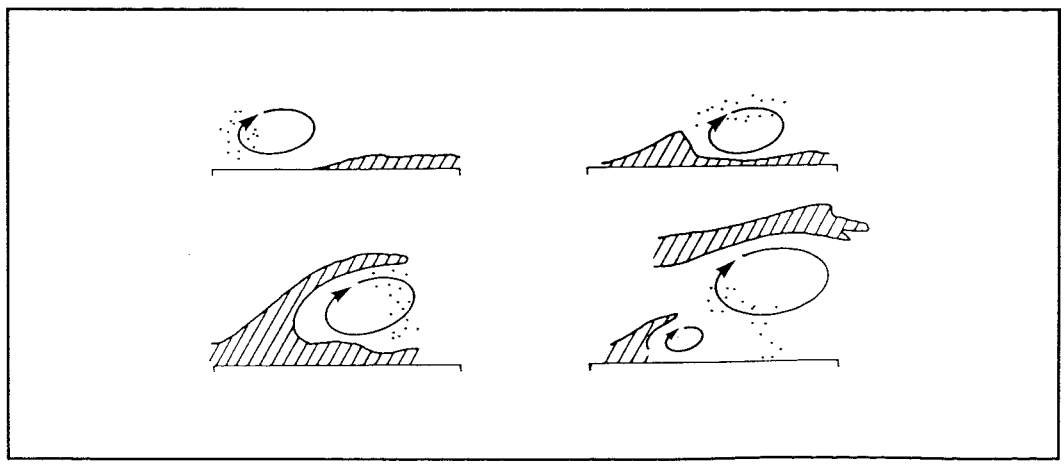

Fig. 2.10. Diagrammatic sequence of suspension caused by a burst. Shaded area is a zone of low velocity fluid (from Dyer, 1986).

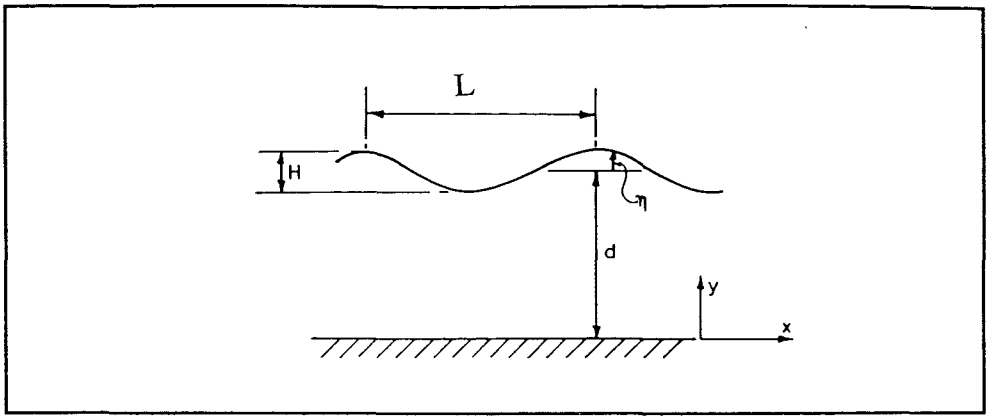

Fig. 2.11. Definition sketch for progressive waves (from Sleath, 1984).

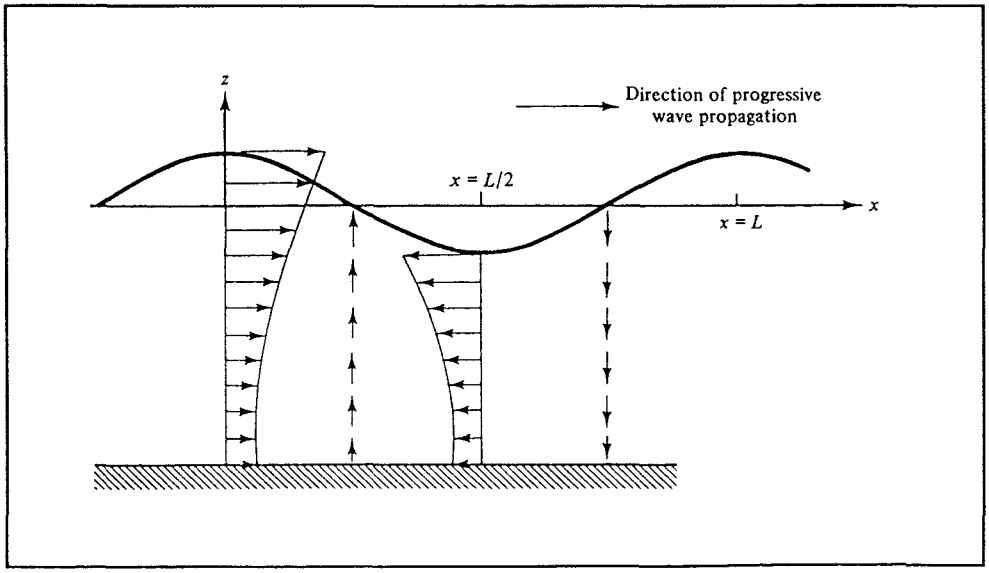

Fig. 2.12. Water particle velocities in a progressive wave (from Dean & Dalrymple, 1992).

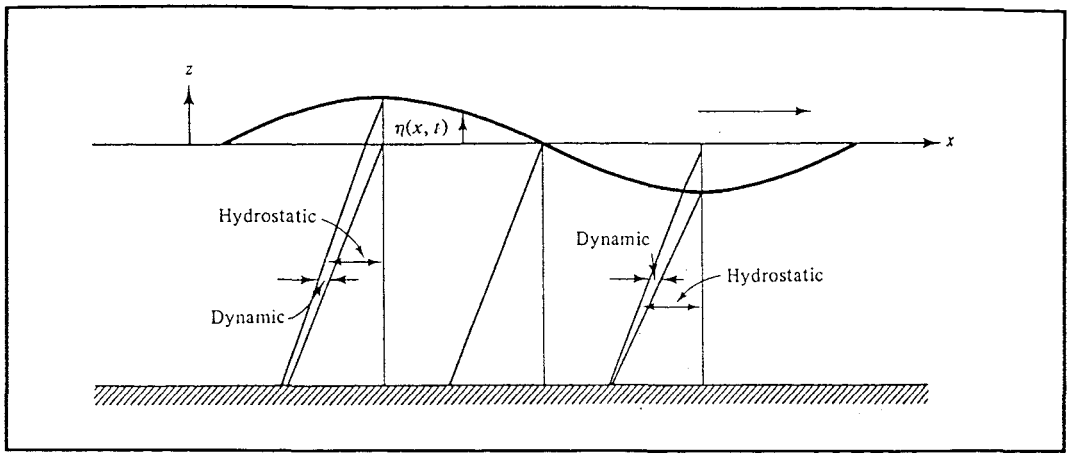

Fig. 2.13. Hydrostatic and dynamic pressure components, at various phase positions in a progressive water wave (from Dean & Dalrymple, 1992).

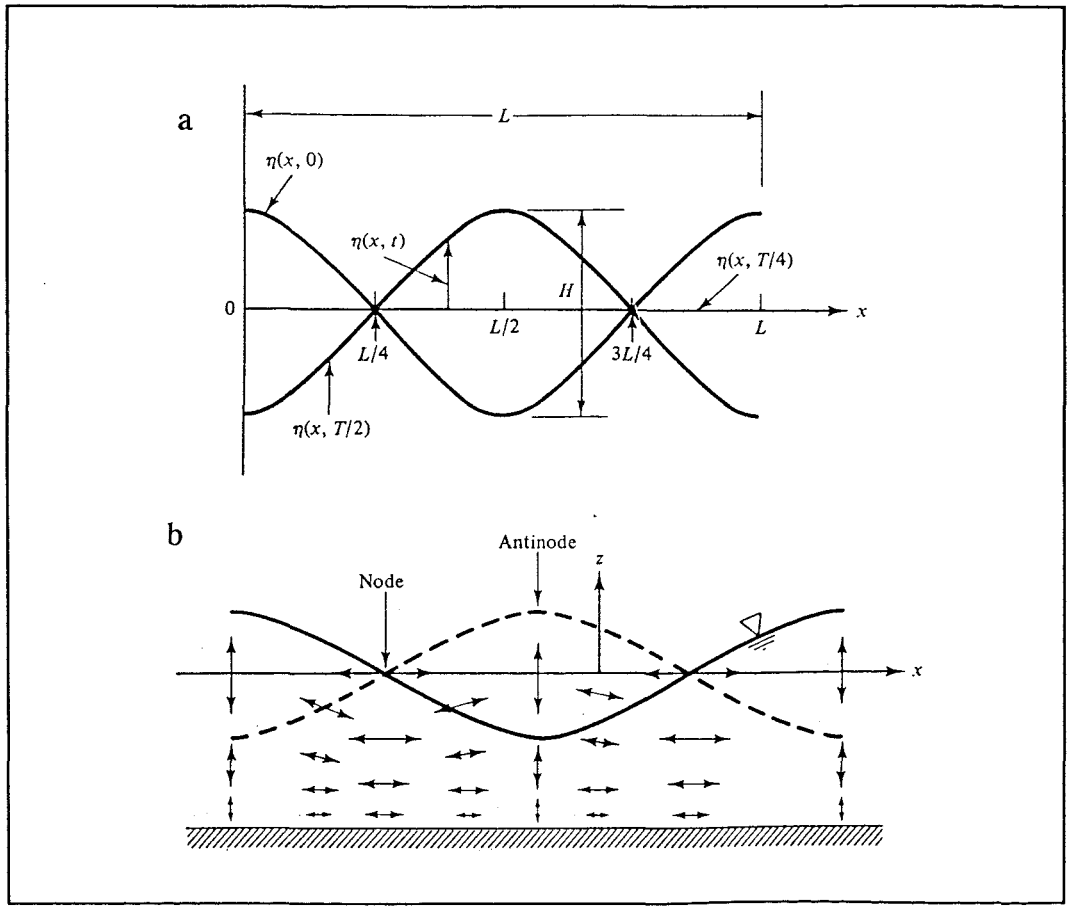

Fig. 2.14. (a) Water surface displacement associated with a standing water wave, and (b) distribution of water particle velocities in a standing water wave (from Dean & Dalrymple, 1992).

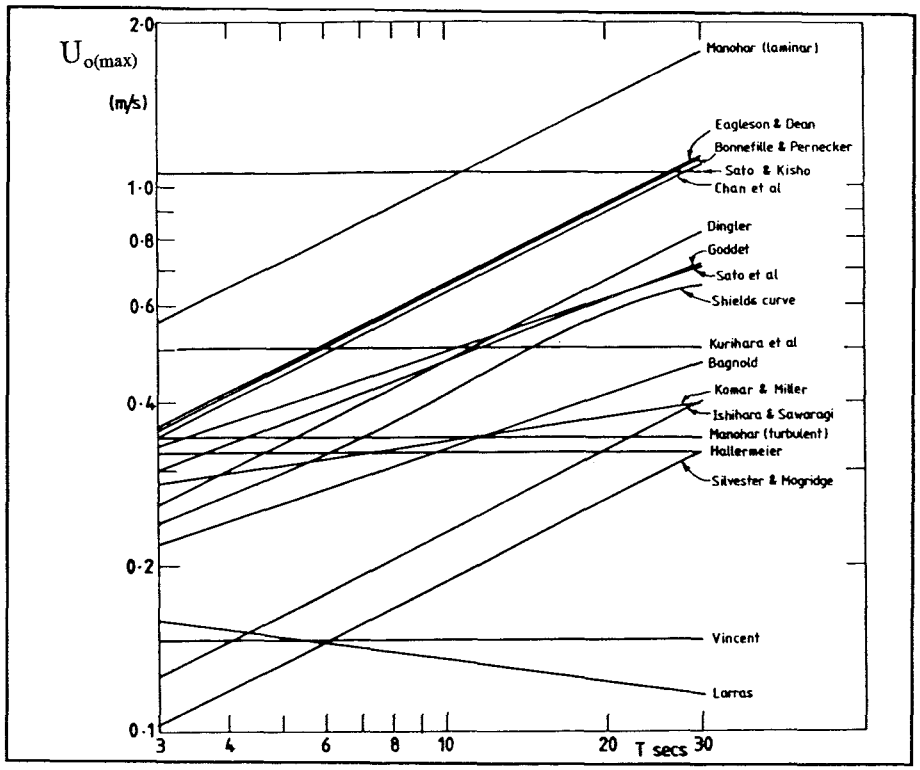

Fig. 2.15. Comparison of critical values of $U_{o(max)}$ predicted by various initial motion formulae, for 0.8 mm sand in fresh water at 20°C (after Sleath, 1984).

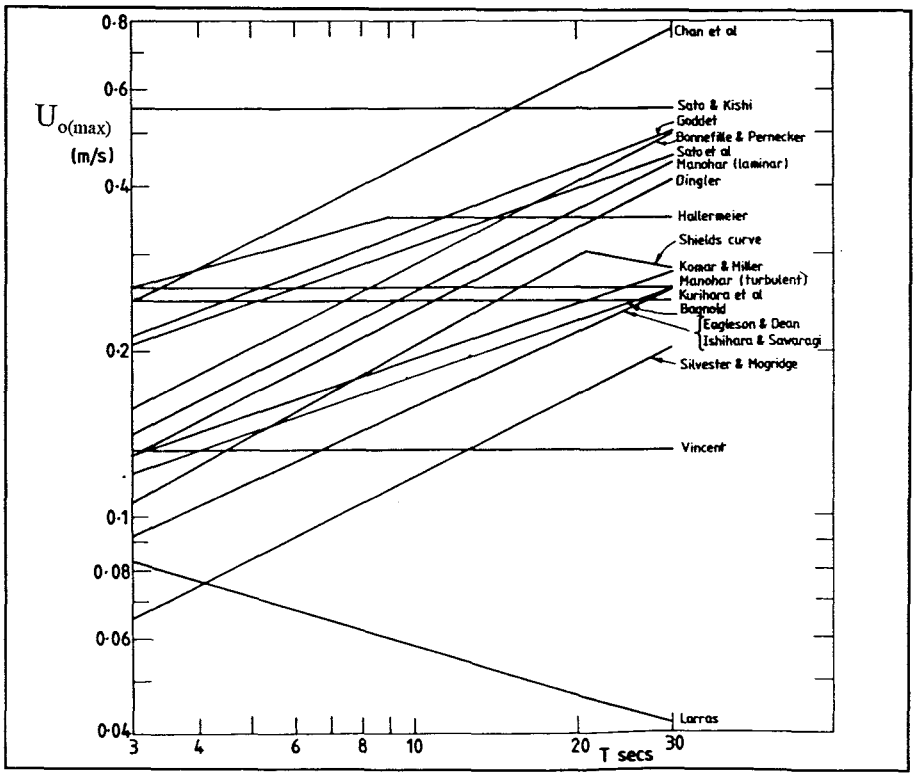

Fig. 2.16. Comparison of critical values of $U_{o(max)}$ predicted by various initial motion formulae, for 0.2 mm sand in fresh water at 20°C (after Sleath, 1984).

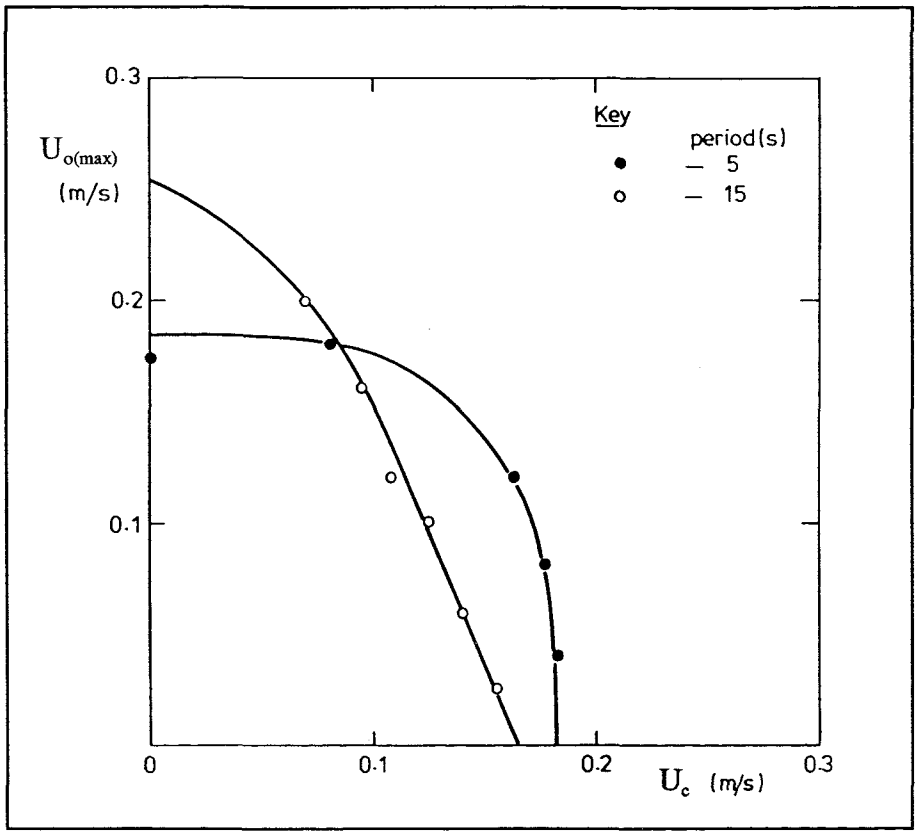

Fig. 2.17. Variation in $U_{o(max)}$ with the critical value of U_c under combined steady and oscillatory flow (after Hammond & Collins, 1979).

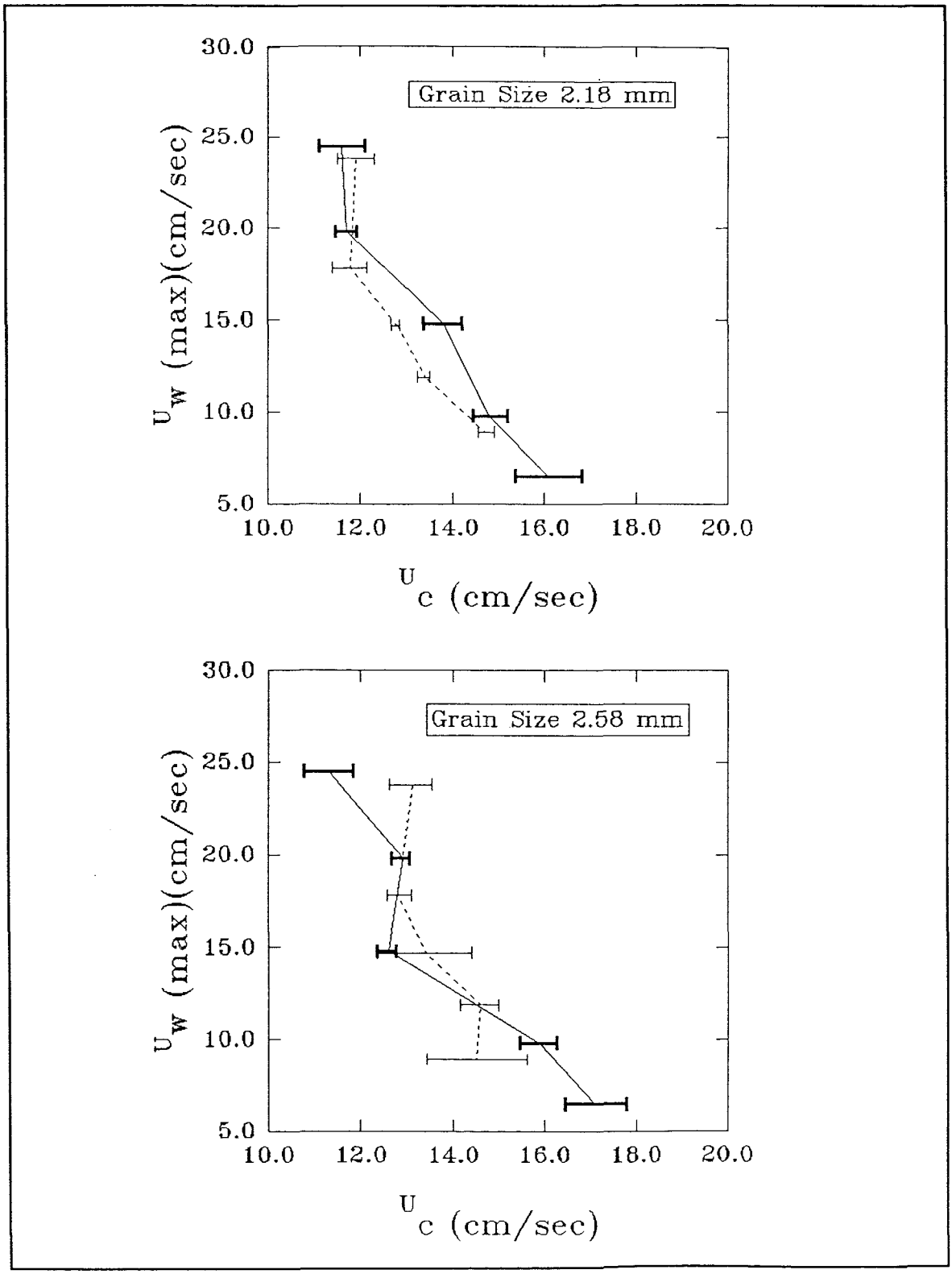

Fig. 2.18. Critical velocity combinations (solid line: 6 s, dashed line: 10 s) for the threshold of gravel movement: thick error bars—wave period of 6 s; thin error bars—wave period of 10 s. (from Panagiotopoulos et al., 1994).

CHAPTER 3

EXPERIMENTAL EQUIPMENT AND TESTED MATERIAL

3. EXPERIMENTAL EQUIPMENT AND TESTED MATERIAL

3.1. INTRODUCTION

This Chapter describes the instrumentation used in the investigation of the erosion threshold and pore pressure generation within sand-mud deposits; it emphasises the principles of operation and limitations of this equipment. Likewise, a brief description of the nature of the studied material is presented.

The principal instrumentation used, in each of the hydrodynamic experiments, were: a unidirectional laboratory, flume incorporating an oscillating tray; a plate positioning system; Laser Doppler Anemometer; video monitoring equipment; pore pressure transducers; and data acquisition and analysis equipment.

3.2. HYDRODYNAMIC APPARATUS

3.2.1. The Recirculating Flume

The flume (Fig. 3.1, supplied by Armfield Hydraulic Engineering Ltd) used in the present study (5.00 m long, 0.30 m wide and 0.45 m deep) has a rectangular cross section, with an open top with glass-sided walls. Water is pumped from a reservoir tank, through an adjustable gate valve, into a constant-head discharge tank. From the discharge tank, water flows along the channel through the working test section, over an adjustable tail gate and back into the discharge tank. The speed of flow is controlled by the adjustable valve, which is located next to an electric pump. The water depth can be set by controlling the height of the adjustable tail gate. Calibration studies carried out by Tomlinson (1993) have shown that the use of a horse-hair baffle (installed at

the entrance to the channel section) is necessary for the damping of excessive turbulence created by the pump and establishing a uniform flow structure within the flume.

3.2.2. Oscillating Plate

Inside the flume, an aluminium plate 3.00 m long, 0.25 m wide and 0.020 m thick is oscillated sinusoidally; this simulates wave action, with periods ranging from 2 to 20 s.

It is well known that the motion of waves in shallow water produces an increasingly flat elliptical orbit of fluid motion on approaching the sea-bed. At the sea-bed itself, in such water depths, a 'to and fro' motion predominates (Fig. 3.2). As an alternative to moving the water with respect to the bed, therefore, several researchers (see Manohar, 1955; Sleath, 1976; George & Sleath, 1978; Hammond & Collins, 1979; Katori *et al.*, 1984; Panagiotopoulos *et al.*, 1994) have adopted the principle of moving the bed with respect to the water. This option has been applied within the present investigation. In addition, according to Stokes theory, the velocity distribution above a plate oscillating in its own plane, in a tank of still water, is the same as that produced beneath water waves travelling above a stationary bed.

The oscillating plate system is best described by reference to the cross section shown in Fig. 3.3. Eight blocks, machined from water-lubricated material (supplied by Orkot Enginneering Plastics Ltd), are attached to an aluminium framework. The machining on the blocks is such that the framework slides onto the two lengths of the aluminium channel, which are fixed to the base of the flume. Within each block, 10 holes are drilled into the

side resting on top of the channel. A stainless steel ball bearing is positioned in each of the holes in the block, with the diameter of each bearing (10 mm) such that it protrudes above the upper surface of the block (by 1 mm). The aluminium oscillating plate rests then on the ball bearings. Horizontal movement relies upon the the ball bearings rolling within the Orkot blocks. As the ball bearings roll a distance equal to their circumference, then the aluminium plate travels in the horizontal direction a distance equal to one diameter of the bearings. A stainless steel wire is connected to each end of the moving plate and, by means of a system of pulleys, is attached to an intermediate sliding mechanism; this moves to and fro, in a direction parallel to the water flow (Fig. 3.1). The intermediate sliding mechanism is driven by a long connecting rod (1.8 m in length) which is attached, by means of a pin, to one of eight points along the radius of a rotating flywheel (Hammond & Collins, 1979; Williams, 1984) (Fig. 3.1). The period of rotation of the flywheel can be set by a control knob on a variable speed motor and measured automatically by a digital stop-watch; this is connected to a micro-switch mounted on the flywheel frame.

The motion of the moving plate deviates from pure simple harmonic, in proportion to the ratio between the length (L) of the connecting rod (see above) and the plate displacement amplitude (A_o) (Fig. 3.4). Assuming no errors in the inter-connecting system between the flywheel and the plate (e.g. friction in the pulleys and slackness in the wires), the deviation of the plate's geometric displacement and velocity from the sinusoidal motion of the flywheel can be determined by differentiation, as outlined below.

(i) For the sinusoidal motion of the flywheel, displacement is defined as

$$s(t) = A_o \cos\Theta \tag{3.1}$$

whilst velocity is defined as

$$\frac{ds}{dt} = \frac{-2\pi A_o}{T} \sin\Theta \tag{3.2}$$

where Θ is equal to $2\pi t/T$.

(ii) For the geometric motion of the plate (Fig. 3.4), displacement is given by

$$s(t) = A_o \sin\Theta + [L^2 - (A_o \cos\Theta)^2]^{\frac{1}{2}} - [L^2 - A_o^2]^{\frac{1}{2}} \tag{3.3}$$

whilst velocity is given by:

$$\frac{ds}{dt} = \frac{\pi A_o}{T} 2\cos\Theta + \frac{A_o \sin 2\Theta}{[L^2 - A_o^2 \cos^2\Theta]^{\frac{1}{2}}} \tag{3.4}$$

Using the above relationships, Tomlinson (1993) compared the theoretical deviation of the plate motion to that of the flywheel. Further, this investigator observed the actual deviation of the plate motion through the use of information provided by the plate positioning system (Section 3.2.3). It was concluded that there was a small offset between the curves representing the sinusoidal and geometric plate displacements, when the oscillation periods were larger than 5 s. This offset was greatest at the points of maximum plate displacement. In addition, at the same points, it was observed that the actual plate displacement (as measured by the plate positioning system) was not identical to the geometric curve of motion. This difference can be explained by the fact that the interconnecting system (i.e. pulley system wires) presents a low level of slackness when the plate approaches the locations of maximum displacement. However, this was not considered a significant error in the erosion threshold determination of the present study, since grain movement was not observed during these parts

of the (wave) oscillation cycle. During the remainder of the cycle, the curve of actual displacement is similar with those of the sinusoidal and geometric displacements. For oscillation periods smaller than 5 s, Tomlinson (1993) observed that the actual plate displacement curves were identical to the sinusoidal and geometric displacement curves, throughout the entire wave cycle. This pattern can be explained by the fact that, when the wave (oscillation period) is relatively small (i.e. the plate acceleration is high) then the interconnecting wire will remain tauter than in the case of longer periods (> 5 s). However, it is possible that the plate itself is likely to overrun, due to the increased inertia of the system.

The use of the oscillating plate mechanism to simulate wave action on the sea-bed is not without criticism. Various authors (Lhermitte, 1960; Kalkanis, 1964; Carstens *et al.*, 1969; and Davies & Wilkinson, 1977) have identified limitations in the use of oscillating beds; for example, they may be subjected to significant forces, related to bed acceleration. However, these effects can be minimised by avoiding the conditions of short period waves combined with large wave amplitudes. For the present investigation, inertial forces could not affect the critical motion of the sediment beds, because of the restricted grain size used in the experiments (Sleath, 1984). Further, Lhermitte (op. cit.) has expressed reservations about the absense of a free-stream pressure gradient. Nevertheless, such a limitation is only significant when the water depth is small compared to the diameter of the sediment grains. In support of use of the oscillating system, good agreement has been found between ripple formation using oscillating tray rigs and oscillating (pumping) water tunnels (Sleath, 1984). An alternative method of 'laboratory-simulated' wave action

on the sea-bed is by making use of an oscillating water tunnel (Rance & Warren, 1968). However, this particular method does not allow the superimposition of a steady current.

3.2.3. Plate Positioning System

The motion of the plate is monitored by making use of a 10-turn potentiometer. A perspex carriage is clamped to the stainless steel wire, which is attached (through the pulley wheel system) to either end of the oscillating plate. The carriage slides on two parallel stainless steel tube bars. A thread is attached to the carriage, extending to a small pulley wheel; this is mounted on the 10 turn potentiometer. The potentiometer is powered by 5 volts, from the reference voltage channel on the card of the analogue equipment (Section 3.6). As the plate moves to and fro, so does the perspex carriage. In turn, this causes the potentiometer wheel to rotate, producing a change in the output voltage. The output voltage is then fed back into one of the input channels of the analogue card.

3.3. LASER DOPPLER ANEMOMETER (LDA)

The instrument (supplied by DANTEC, Bristol) is based upon the principle that particles of fine-grained detritus, contained within the flow, travel at the same speed as the ambient flow itself.

A 5 mW helium-neon laser (Fig. 3.5 and Plate 3.1) emits a beam. Within an optical unit, the beam is split into two beams; these are polarised into mutually perpendicular directions, intersecting at a point where the velocity measurements are made. The point of intersection of the two beams is known as the Measurement Control Volume

(MCV) (Fig. 3.5). Some of the light travelling through the intersection point is reflected by the fine-grained particles contained within the flow, causing a frequency shift in the emitted light. A diode detector (Fig. 3.5) aligned carefully with the reference beam receives, therefore, two light signals; one with a frequency shift caused by the reflection from the particles, whilst the other has the frequency of the emitted light. The difference (F_d) between the two frequencies is determined by the detector. A frequency tracker receives then the signal F_d, which is used to calculate the particle speed and consequently the water speed. The frequency tracker unit produces an analogue or digital output signal, proportional to the calculated water velocity.

With the laser beam passing through a 30 cm focal convex lens and the beam separation option set at 4.5 cm, the elliptical shape of the Measuring Control Volume (MCV) has major and minor axes length of 0.08 cm and 0.03 cm, respectively. Due to the finite volume of the Measurement Control Volume (MCV), the system averages the velocities of a number of particles at any given time. The frequency of the light scattered by a particle travelling through the Measuring Control Volume (MCV) depends upon the rate at which the particle crosses the wavefronts, emitted by the incident light source. Since the diode detector is aligned coaxially with the reference beam, only light passing through the MCV is detected (any other light arriving at the diode is at a great angle).

The relationship between F_d and the fluid speed (U) is given by

$$F_d = KU \tag{3.5}$$

where K is the calibration factor for the laser, which is dependent upon the optical unit and the wavelength of the

laser light; and it is calculated from:

$$K = \frac{\lambda}{2\sin\frac{\theta}{2}} \qquad (3.6)$$

In this investigation, K was found to be 0.4152 cm/s/kHz. Hence, the final Equation relating water velocity to doppler frequency is:

$$U = 0.4152 F_d \qquad (3.7)$$

The frequency shift (F_d) registered by the detector is sent to the frequency tracker, where it is amplified and filtered. A voltage controlled oscillator, which produces a voltage proportional to its frequency, is set to scan by a phase detector until it matches the enhanced signal. At the point where the two frequencies are equal, the system is said to be 'in lock'. The voltage from the controlled oscillator is then sent to a 'sample and hold' device and, subsequently, to an analogue output socket. When the system is 'out of lock', the analogue signal is maintained at the existing level. At the same time, the voltage controlled oscillator continues to scan over the selected frequency range, until it matches the incoming doppler frequency signal.

The temporal response of the laser system is dependent upon the inertia of the reflecting particles. Since the size of these particles is of the order of the wavelength of the laser light, the errors are considered to be negligible. The system cannot measure flow velocities less than 0.5 cm s^{-1}. Further, it is incapable of providing any indication of flow direction. The accuracy of the system is ±0.2% of the selected frequency range. For the purposes of the present study, the selected frequency range was retained at 10-100 kHz; hence, the instrumental error was of the order of ±0.2 cm s^{-1}. Resolution of the low amplitude velocity fluctuations is

limited by electrical and optical noise.

Two of the main advantages of using the Laser Doppler Anemometer (LDA), as a flow measuring device, are: firstly, this system has a high temporal response to instantaneous velocity changes (<0.002 s)—this is far greater than the resolution required for the present study; and secondly, the small size of the Measuring Control Volume (MCV), together with the fact that the Anemometer does not interfere with the flow, allows the instrument to be positioned within the boundary layer, close to the sediment bed to an accuracy of ±0.15 mm.

The LDA was calibrated twice at different time-spans during the entire investigation; this was to secure measurements of high accuracy. Calibration results of the LDA are shown in Fig. 3.6 and listed in Tables 3.1 and 3.2.

3.4. PRESSURE TRANSDUCERS

For the experimental aims of the present study, two pressure sensors were used: one was located beneath the sediment/water interface, whilst the other was installed at the surface of the oscillating plate.

These instruments (Fig. 3.7, supplied by Druck Ltd: type PDCR 810, operating pressure range 0-70 mb) are based upon a high performance pressure sensor (core), to which has been added an electron beam-welded pressure connector and an electrical connector assembly. The core itself is an accurate pressure transducer, incorporating a high integrity silicon diaphragm and titanium module; this is combined with a pcb assembly and advanced compensation techniques, which provide excellent performance over extended temperature ranges. The final assembly is

electron beam-welded and encapsulated.

The transducers are designed to provide accurate linear measurements (a combined non-linearity and hysteresis of ±0.1%), with an error of +0.02% of the full pressure range.

An interface box supplied the transducers with power, amplifying their output from a 0-17 mvolt range to the 0-5 volt range of the data logger.

3.5. EQUIPMENT FOR THRESHOLD OBSERVATION

Video monitoring equipment, which includes a Sony CCD-V800 Hi-8 portable video camera, used in conjuction with a Sony PVM-1444QM monitor, was used to observe and record critical sediment erosion conditions. To improve visual inspection of the sediment beds examined, magnifying glasses (x3, x5) and plastic transparent sheets (x3) were used. The magnifying glasses were placed in front of the glass-sided walls of the flume test section, whilst the magnifying sheets were located in front of the monitor screen.

3.6. COMPUTER AND DATA ACQUISITION CARD

Data were collected, stored and analysed in a 486 PC computer (supplied by Elonex); this is equipped with a data acquisition card (A/D card). The card has 16 single-ended analogue input channels, of which only 4 were used (for the LDA, plate positioning system and pressure transducers). Fig. 3.8 and Tables 3.3 to 3.5 display the calibration of the channels to which the LDA and the pressure sensors were connected. The maximum A/D sampling rate is 30 kHz in direct memory access mode. The analogue input rate was switched to the ±5 volt setting.

A computer program was written such that, at any moment, the curves representing the horizontal water velocity, the position of the oscillating plate and the water pressure (in the pores of the sediment and at the surface of the moving plate) were being displayed on the screen of the computer monitor. In order to obtain signals of high fidelity (cleared from electrical noise), 4 low-pass filters were used in conjuction with the instruments which were connected to the analogue (A/D) card (see above).

3.7. SAMPLES EXAMINED

The sand component of the soils (sediments) examined was angular, fine-grained quartz (supplied by Hepworth Minerals), in one of two mono-sized distributions, with D_{50} equal to 152.5 μm and 215 μm.

The cohesive component was a natural estuarine silt-clay sediment, referred to as Combwich mud, obtained (in 1987) from the River Parrett, Severn Estuary (UK); its particle size distribution was determined using a Micromeritics 5100 Sedi-Graph. The analysis was repeated five times (Table 3.6) showing that approximately 20% of the mass of the mud was less than 2 μm in diameter (clay-sized material) (Fig. 3.9). On the basis of an x-ray diffraction analysis (performed by the Engineering Department of Oxford University), the clay mineralogy of this fraction was 56% illite, 26% expansive clays (undefined), 11% kaolinite and 7% chlorite. Further, a similar analysis of the silt-sized fraction revealed the presence of 45% quartz, 20% calcite, 15% feldspars and 20% clay minerals (illite and kaolinite). Hence, the overall clay mineral content of the Combwich mud was 36%. Classification in relation to the Atterberg limit tests has defined this particular mud as an inorganic clay

(with a measured organic content of less than 4%) of very high plasticity with a liquid limit of 85% and plasticity index of 49%.

In designing the experiments, particular attention was placed upon the fact that very few laboratory investigations have been carried out on sand-mud admixtures. Therefore, it was decided, for the purposes of the control of laboratory conditions, that the samples would be made artificially. The two unimodal sands were mixed separately with various proportions of the Combwich mud i.e. 5%, 10%, 20%, 30%, 40% and 50%, by dry weight (these percentages correspond to 1.8%, 3.6%, 7.2%, 10.8%, 14.4% and 18% of clay). The mixing process (accomplished by mechanical stirring) was designed to produce homogeneous samples, with a structure formed by natural settling; in this, the relative magnitudes of the sand and mud components were accurately known. The mixtures were derived by combining dry sand, wet mud and added tap water. Thus, a dense slurry which could be mixed easily was obtained. The samples with higher mud contents were more dilute than those with lower mud contents. Each sample was mixed for 20 min, then allowed to settle for 24 hours to ensure that the overlying water was clear. This excess water was carefully removed subsequently using a pipette. At this stage, sediment mixtures could be transferred to the flume test section to be examined under various hydrodynamic conditions. The median diameters (D_{50}) of the admixtures are shown on Table 3.7; these have been calculated using the following formula

$$D_{50} = aD_{50\,(sand)} + bD_{50\,(mud)} \qquad \textbf{(3.8)}$$

where a and b are the percentages of the sand and mud components of the mixed soils, respectively.

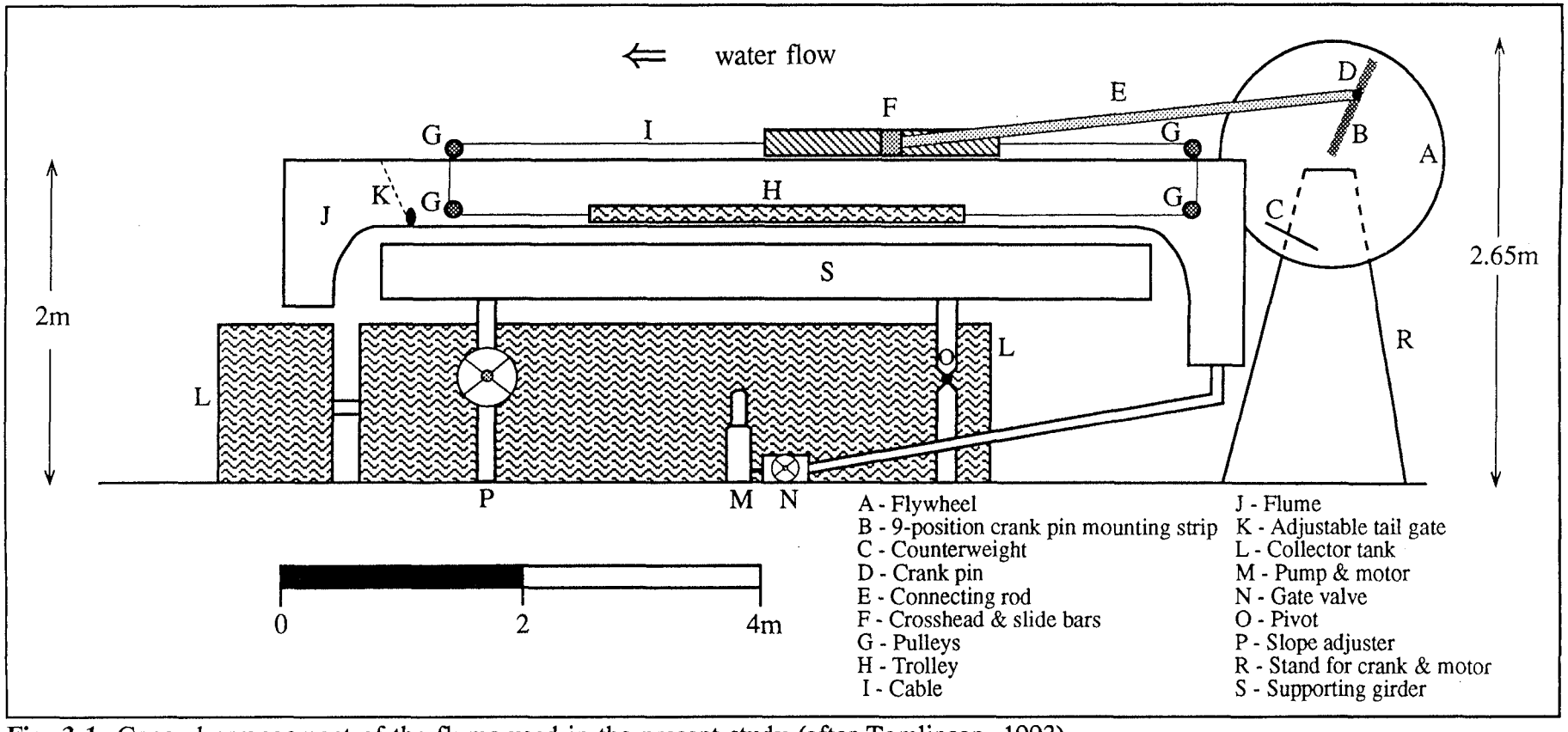

Fig. 3.1. General arrangement of the flume used in the present study (after Tomlinson, 1993).

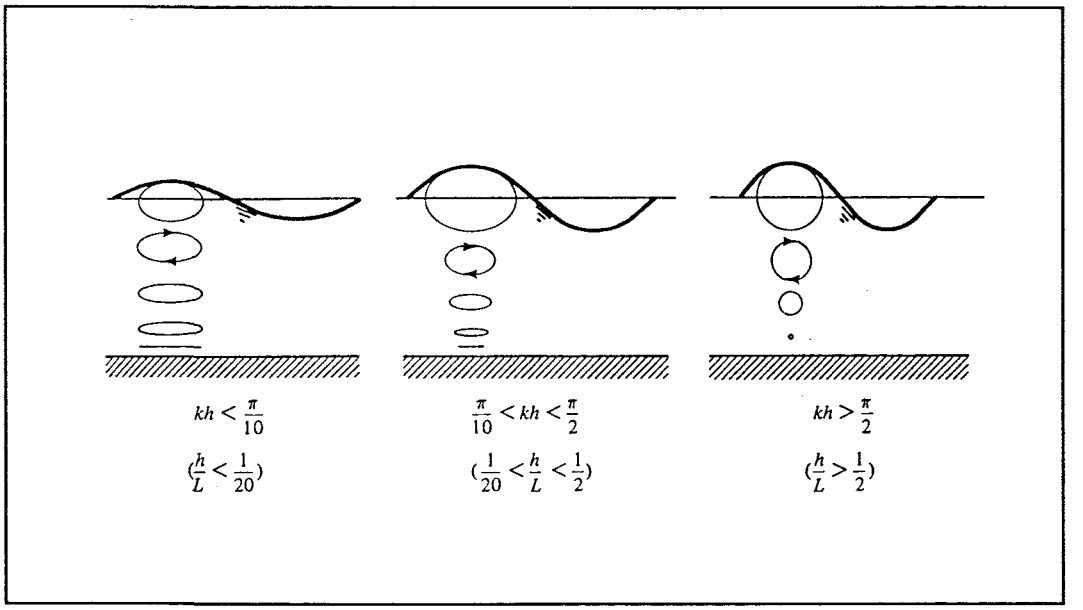

Fig. 3.2. Water particle trajectories in progressive water waves of different relative depths (from Dean & Dalrymple, 1992).

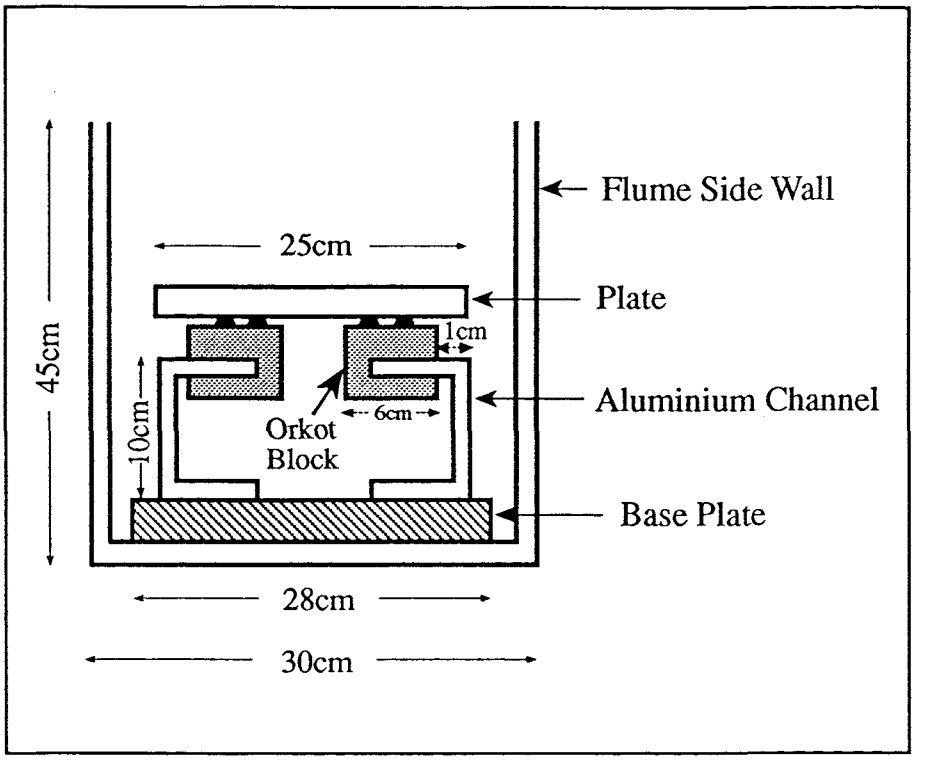

Fig. 3.3. Cross section demonstrating, the mechanism of the oscillating plate (from Tomlinson, 1993).

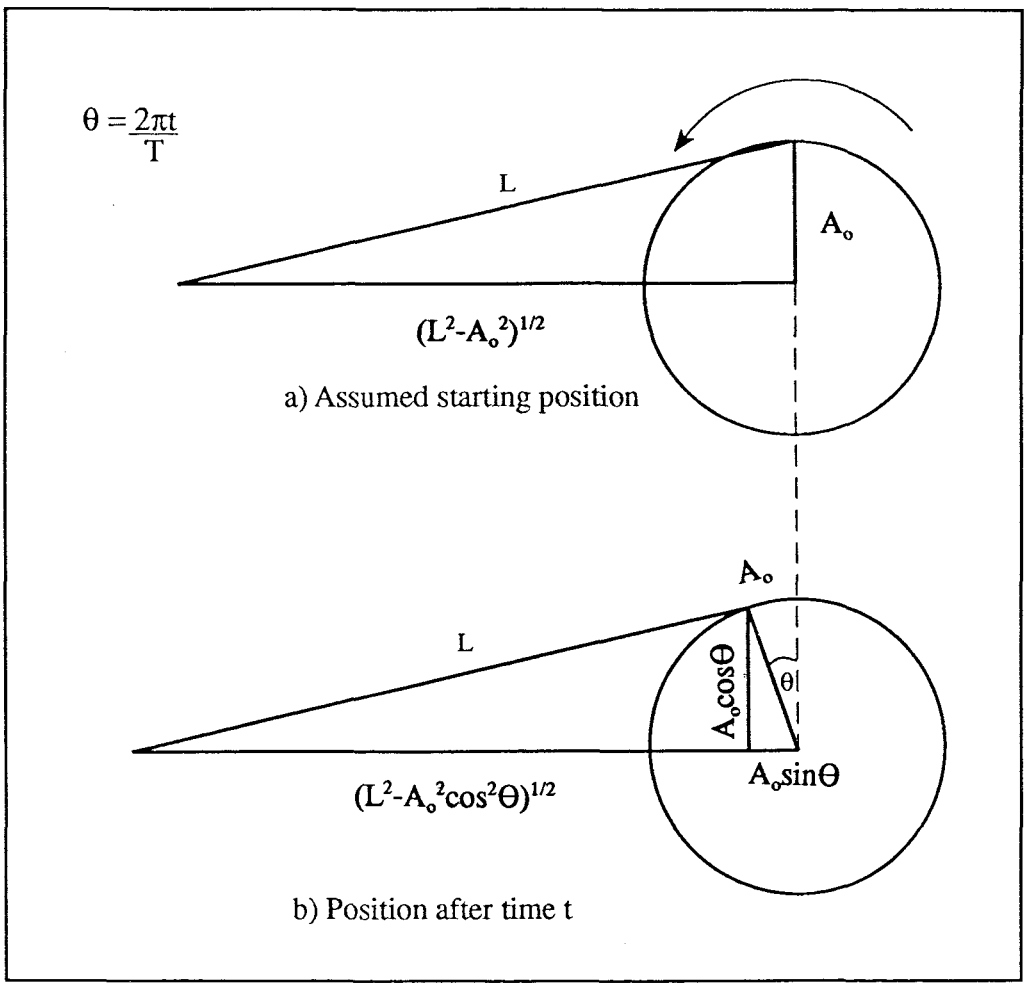

Fig.3.4. Schematic representation of the geometric motion of the oscillating plate (after Tomlinson, 1993).

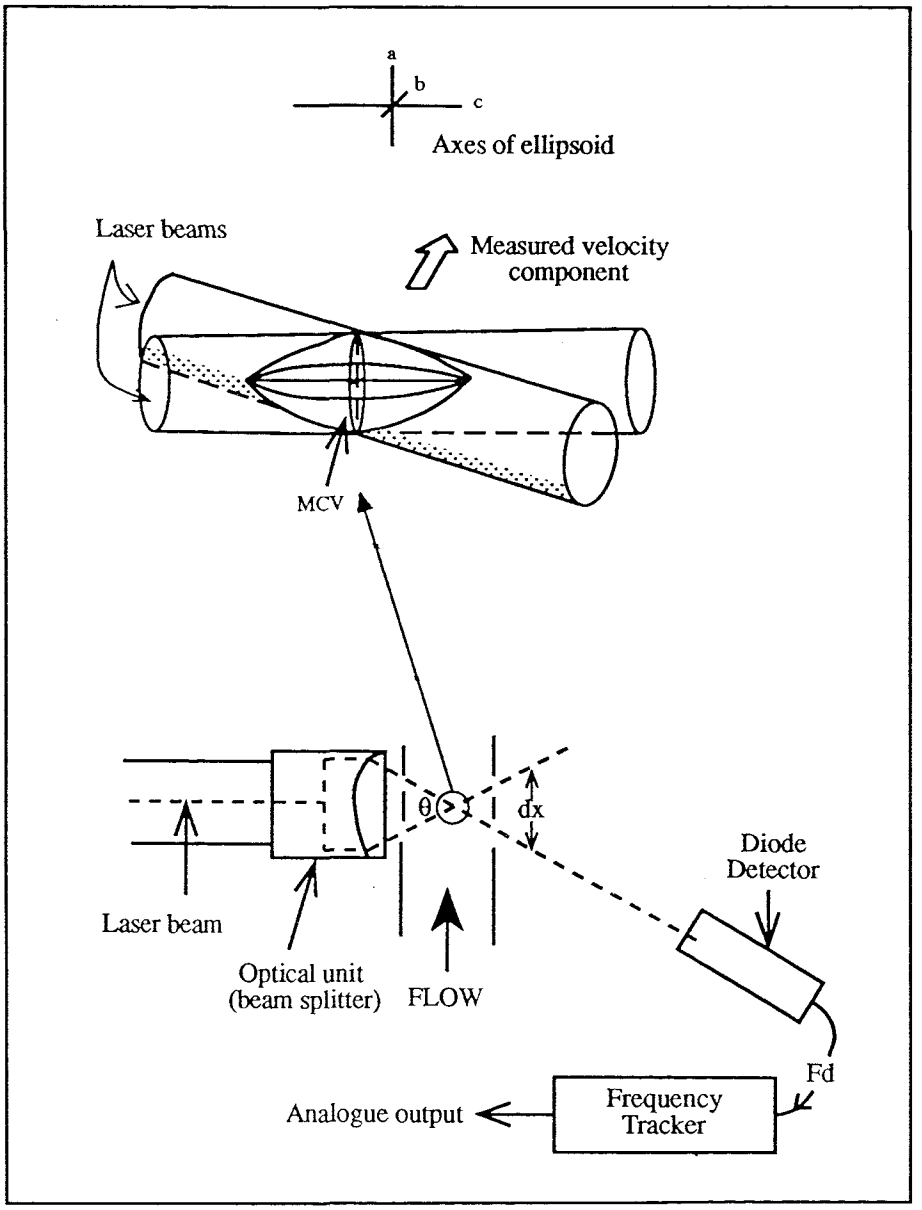

Fig. 3.5. Laser Doppler Anemometer arrangement (from Tomlinson, 1993).

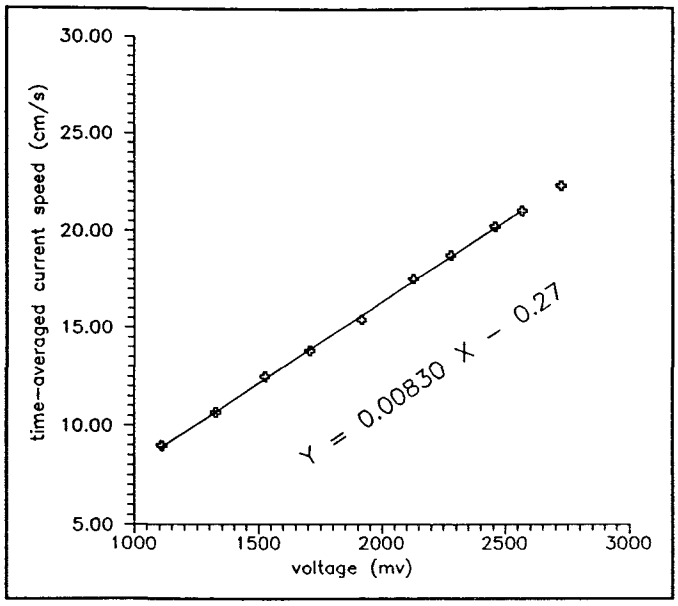

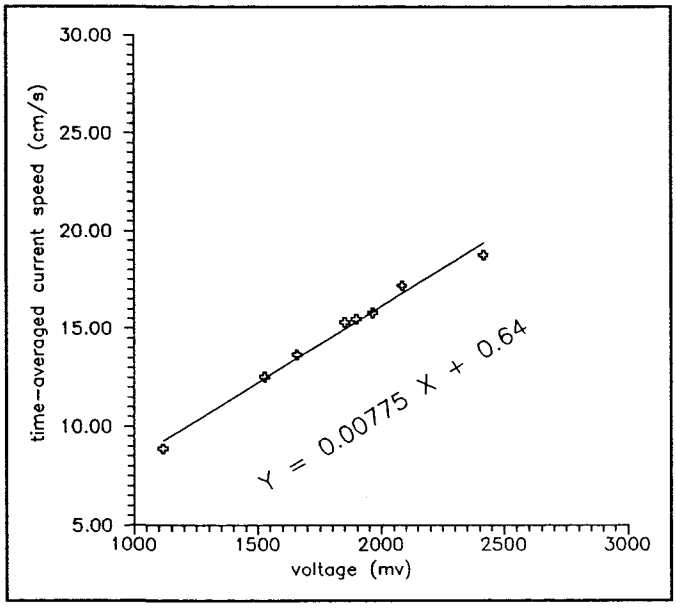

Fig. 3.6. Calibration formulae for the channel of the data acquisition sustem, to which the Laser Doppler Anemometer (LDA) was connected.

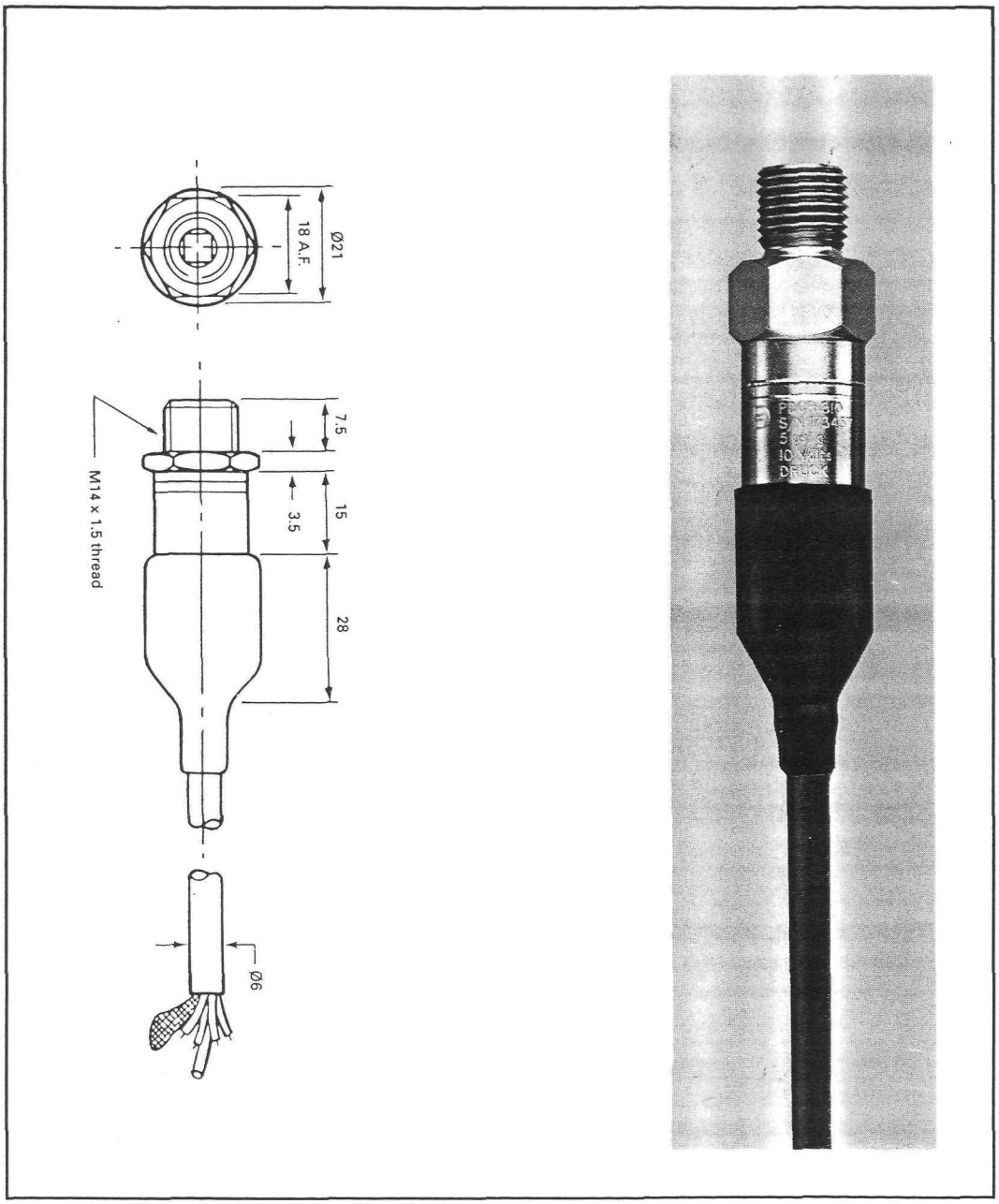

Fig. 3.7. Pore pressure transducer.

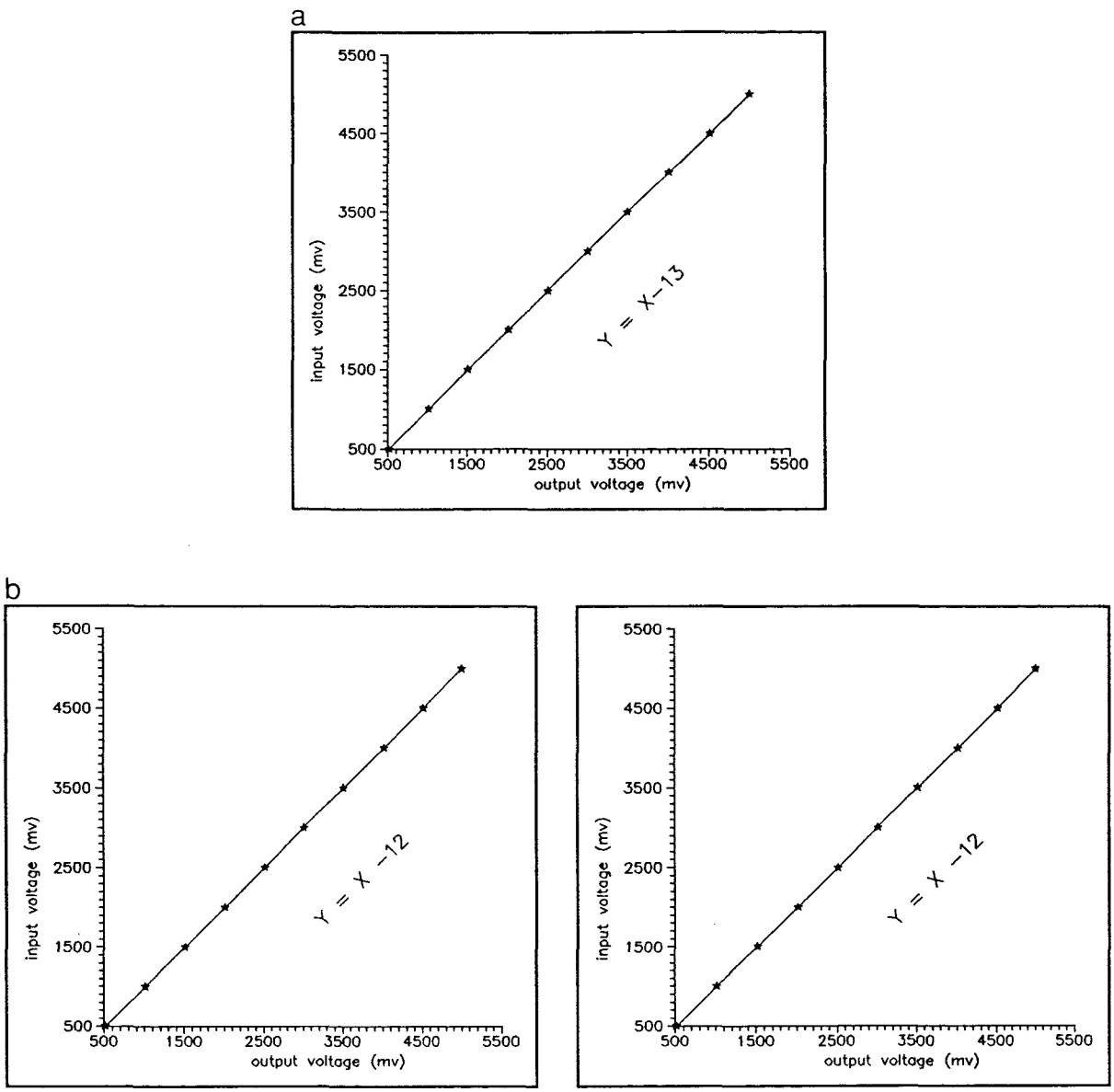

Fig. 3.8. Calibration of the channels of the data acquisition card to which (a) the LDA and (b) the pressure sensors were connected.

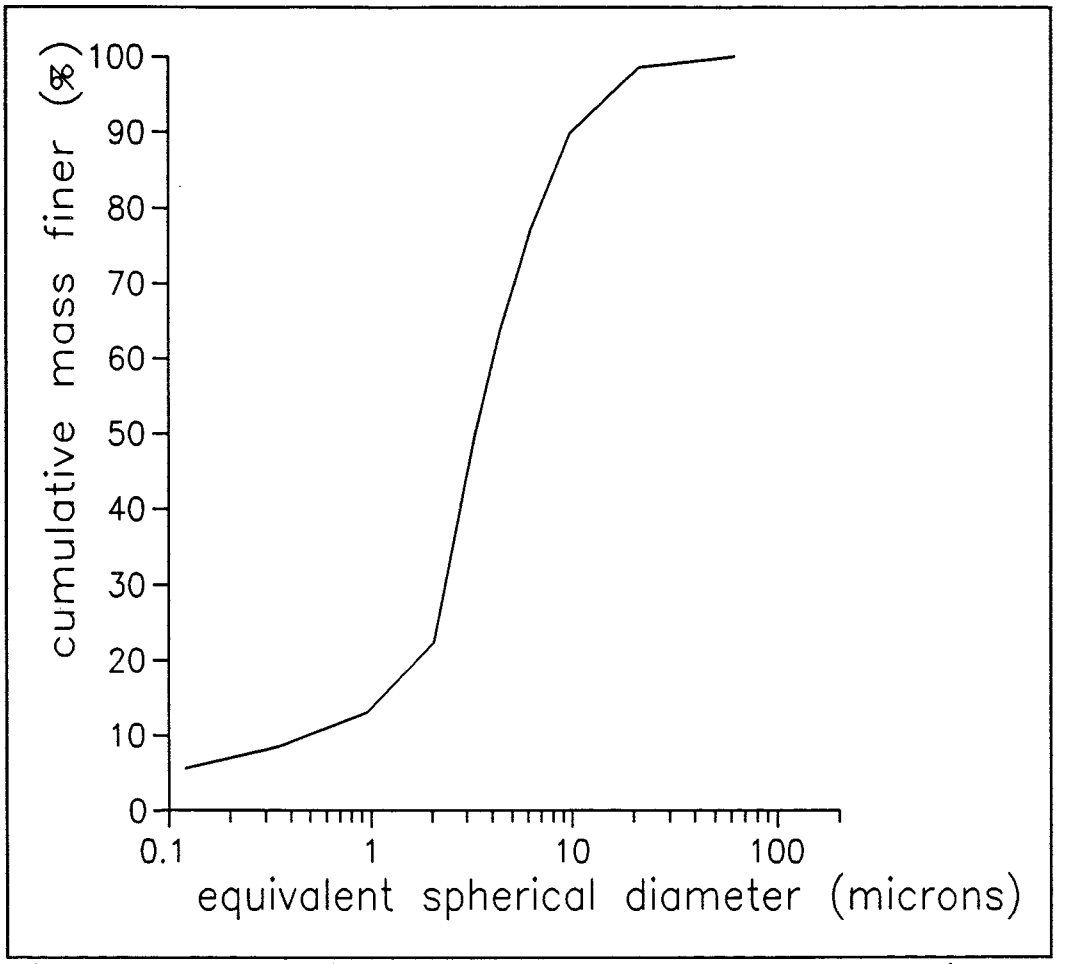

Fig. 3.9. Grain size distribution of the mud fraction of the sand-mud beds.

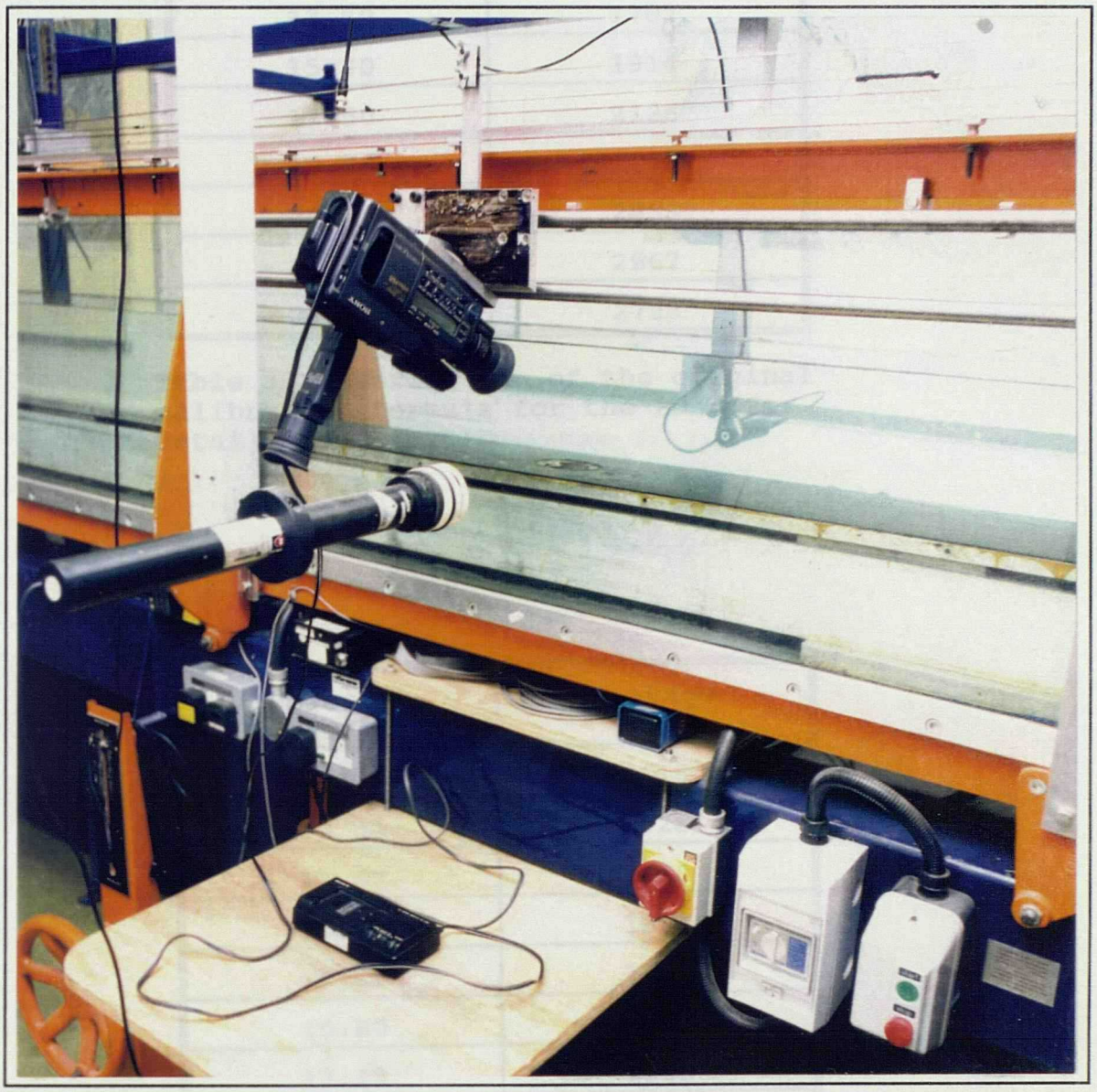

Plate 3.1. Laser Doppler Anemometer and video camera arrangement.

velocity (cm/s)	voltage (mv)
9.00	1110
10.70	1326
12.50	1527
13.80	1707
15.40	1914
17.50	2126
18.70	2278
20.20	2458
21.00	2567
22.30	2723

Table 3.1. Derivation of the original calibration formula for the LDA (for details, see text).

velocity (cm/s)	voltage (mv)
8.87	1116
12.54	1528
13.67	1658
15.32	1851
15.47	1898
15.80	1964
17.18	2085
18.76	2416

Table 3.2. Derivation of a new calibration formula for the LDA (for details, see text).

input voltage (mv)	output voltage (mv)
500	508
1002	1013
1499	1510
2002	2013
2498	2510
3002	3014
3497	3509
4003	4015
4498	4510
5003	5000

Table 3.3. Calibration of the channel of the data acquisition card, to which the Laser Doppler Anemometer (LDA) was connected.

input voltage (mv)	output voltage (mv)
501	511
1002	1012
1499	1509
2001	2011
2500	2512
3000	3012
3499	3510
4004	4016
4500	4512
5000	5000

Table 3.4. Calibration of the channel of the data acquisition card to which the pressure transducer, located beneath the sediment/water interface, was connected.

input voltage (mv)	output voltage (mv)
501	510
999	1009
1505	1515
2002	2013
2497	2510
3001	3013
3502	3514
3998	4009
4502	4514
5002	5000

Table 3.5. Calibration of the channel of the data acquisition card to which the pressure transducer, located at the surface of the oscillating plate, was connected.

grain diameter (μm)	analysis 1	analysis 2	analysis 3	analysis 4	analysis 5	averaged mass finer (%)
	mass finer (%)	mass finer (%)	mass finer (%)	mass finer (%)	mass finer (%)	
62.50	99.9	99.9	100.0	100.0	100.0	100.0
31.25	99.4	99.5	99.6	99.5	99.8	99.6
15.63	97.9	97.8	97.9	97.1	97.4	97.6
7.81	84.9	86.4	86.6	85.6	86.3	86.0
3.91	61.0	60.7	57.1	59.6	57.8	59.2
1.95	20.8	20.2	19.1	19.4	20.7	20.0
0.98	12.8	13.6	13.1	12.7	13.9	13.2
0.49	9.4	9.9	9.2	9.9	10.0	9.7
0.24	7.1	7.3	6.8	6.9	7.7	7.2
0.12	5.6	5.5	5.9	6.1	4.9	5.6

Table 3.6. Grain size analysis of the mud fraction of the sediment mixtures.

median diameter of sand component D_{50} (μm)	median diameter of mud component D_{50} (μm)	percentg. of sand component %	percentg. of mud component %	mean diameter of mixture particles D (μm)
152.5	3.46	100	0	152.5
		95	5	145.0
		90	10	137.6
		80	20	122.7
		70	30	107.8
		60	40	92.9
		50	50	78.0
215.0	3.46	100	0	215.0
		95	5	204.4
		90	10	193.8
		80	20	172.7
		70	30	151.5
		60	40	130.4
		50	50	109.2

Table 3.7. Estimation of the mean size of the artificially-produced mixtures.

CHAPTER 4

METHODOLOGY

4. METHODOLOGY

4.1. INTRODUCTION

This Chapter incorporates an outline of the experimental methods adopted to investigate the scientific objectives of the present investigation. In the performance of the experiments (mainly hydrodynamic), the advantages and limitations of each item of experimental equipment were considered carefully. At the commencement of the project, a series of aims were identified; these are outlined below.

(i) To define a specific programme of laboratory measurements related to erosion threshold experiments.

(ii) To gain any necessary experience in equipment presently available and develop further instrumentation.

(iii) To undertake research into boundary layer structure, under unidirectional flow conditions, in order to define subsequently the flow regime related to the initiation of sediment movement i.e. whether the flow regime was laminar or smooth/transitional/rough turbulent (Note: The boundary layer structure under other flow conditions i.e. waves or waves/currents combined, was determined based upon the theoretical definitions proposed by other investigators).

(iv) To perform the erosion threshold tests themselves, under steady or oscillatory currents, separately or in combination.

(v) To determine the pore (water) pressure response of the mixed (sand and mud) sediment deposits, under oscillatory and combined flow conditions.

(vi) Finally, to determine the shear strength of the sediments used in the erodibility tests, through liquid limit and yield stress measurements.

4.2. SCIENTIFIC OBJECTIVES

The main objective of the study was to carry out erosion threshold experiments on 14 sediment deposits, consisting of angular fine-grained quartz sands (D_{50} of 152.5 μm and 215 μm), mixed with various proportions of an estuarine mud, under unidirectional currents, waves and combined flows (waves and currents acting simultaneously). In this way, the critical erosion conditions, in terms of current speed/maximum wave velocity or current/wave-induced bed shear stress could be defined. Hence, the influence of clay mineral content on the erodibility of mixed beds could be examined.

Another fundamental aspect of the investigation was to consider also the influence of the clay content on the pore water pressure response of the sediment beds, under the action of waves or co-linear waves and currents. Further, to examine any possible correlation between the threshold of movement and the pore pressure response.

Finally, a secondary aim of the investigation was to examine any relationships between the critical erosion bed shear stresses and particular physical properties of the sand-mud admixtures, such as liquid limit and yield stress.

4.3. EXPERIMENTAL DESIGN

The equipment used throughout the hydrodynamic study has been described in Chapter 3. Calibration curves were incorporated into the software, which was written to analyse the raw data. Instrument accuracy was considered in the analysis of the results.

The required equipment was available prior to the

commencement of the present research, except for the pore pressure sensors. Thus, the experiments could be performed according to the procedure outlined in Section 4.1. The order in which the results were obtained is outlined below.

(a) A boundary layer (flow) investigation was carried out using the Laser Doppler Anemometer (LDA) at 3 cross-sections along the plane of motion of the oscillating plate, to investigate the influence of the moving plate itself and of the side-walls of the flume on the flow structure. Such measurements were undertaken in the vicinity of the test section, which incorporated the samples.

(b) In an extension of the boundary layer study, vertical velocity profiles were measured (using the LDA) above sediment beds which consisted only of the sand components of the mixed deposits. These profiles were established at 3 different unidirectional flow rates, to obtain information concerning the flow regimes associated with these flow rates.

(c) In order to investigate the water content consistency of specific sand-mud admixtures, the mixing process was repeated 4 times. On each occasion, the water content of the samples was determined, in triplicate (B.S. 1377, 1975).

(d) Decisions were made, then, concerning the erosion threshold criteria to be adopted. Likewise, on how the data acquisition equipment should be set up (including data collection and software production) and on establishing the optimum location for the flow measuring device (LDA) and the pressure transducers, for the hydrodynamic tests.

(e) Some preliminary measurements were undertaken using the pressure sensors, in order to examine their functional behaviour.

(f) At this stage, the threshold experiments were

undertaken, under various flow conditions i.e. unidirectional, oscillatory and in combination. During the erosion tests, under waves and the co-linear combined action of waves and steady currents, a pore pressure time-series (at 20 mm beneath the sediment/water inteface) was obtained.
(g) Finally, liquid limit and yield stress measurements were obtained using a (standard) fall cone penetrometer (B.S. 1377, 1975) and the Bohlin rheometer, respectively. The latter tests were carried out at the Simon Environmental Technological Centre of UMIST.

4.4. EROSION THRESHOLD CRITERIA

Some of the most frequently used threshold criteria have been described in Chapter 2; these have been used in other studies, under unidirectional, oscillatory and combined flow regimes. The majority of the observations were based upon some pre-defined or, indeed, undefined visual observations of the investigators (Kramer, 1935; Bagnold, 1946; Manohar, 1955; Chepil, 1959; Neil, 1967; Rathbun & Guy, 1967; Collins & Rigler, 1982). Such experimental studies, related to the threshold of sediment motion, have established widely-recognised results.

In order to compare successfully the threshold results of a particular sediment test bed, with sediments deposited within different geological environments, it is advantageous to quantify the threshold criterion i.e. by counting a particular number of grains or clusters of grains in motion, rather than qualifying the critical condition on the basis of visual observation. Hence, it was decided to apply this particular approach to the present investigation. However, this approach was possible only for the tests associated with the steady

current flows. For the remainder of the experimental conditions, the critical condition for sediment motion could not be quantified (see below).

4.4.1. Unidirectional Flow

The available quantitative threshold criteria are those of Vanoni (1964) and Neil & Yalin (1969).

The latter criterion, which is considered as the most objective, could not be applied to the present threshold determinations undertaken here. This approach is based upon the counting of unimodal grains. In contrast, the erodibility of the muddier samples of the study (mud content > 20%) was characterised by the dislodgement of small clusters (20-40 aggregates s^{-1}) of various sizes. In addition, it was extremely difficult to use this latter criterion successfully, since the mean size of the sediments examined was very small (i.e. < 250 μm). Therefore, the Vanoni criterion was selected for the threshold determinations of the unidirectional flow tests. Vanoni (op. cit.) undertook experiments in a flume, 0.39 m wide by 3.60 m long, to determine the shear stress for critical motion of fine-grained sediments in a growing boundary layer. Determinations were made for two sediment types: a quartz sand with a mean sieve size of 102 μm and glass beads with a mean sedimentation diameter of 37 μm. The intensity of sediment motion was determined on the basis of the frequency of bursts of motion over a small surface area of a sample, varying from 7 to 18 mm in diameter. When the frequency of bursts reduced to between 1/3 and 1 burst s^{-1}, critical conditions for the initiation of motion were considered to prevail. For the present investigation, when the burst frequency of sediment movement over an area of 20 mm diameter reached the value of 1 burst s^{-1}, the threshold of sediment

movement was considered to have been established.

4.4.2. Oscillatory Flow

The Vanoni criterion could not be applied for the oscillatory tests, since the bursting process identified is not related to wave-formed boundary layers. Therefore, the dislodgement of a small amount of sediment in the upper layer of an horizontally-smoothed bed was used as the appropriate threshold criterion.

4.4.3. Combined Flow

Although bursting events were observed under these experimental conditions, the short time-periods of sediment movement did not permit a reliable estimation of the burst frequency. Hence, the threshold criterion similar to that used in the oscillatory flow tests was applied.

4.5. EXPERIMENTAL PROCEDURE

Some of the experiments and associated calibrations were outlined in Section 4.3; these have provided the necessary information on the most appropriate experimental arrangement for each of the hydrodynamic experiments. On the basis of these results and information derived from the instrument manufacturer's manuals, various decisions were made concerning the experimental set up; these are outlined below.
(i) The sampling frequency for the LDA, the plate positioning system and the 2 pressure sensors was established at 20 Hz. This particular frequency was selected since the video camera system also records at this rate. Such a matching frequency enables the results of visual observations made during the experiments to be

correlated with the corresponding digital information, provided by the different instruments. However, this option was not used in the final analysis, since only mean flow rates were considered.

(ii) A data analysis program has been written using the calibration formulae for the LDA and the 2 pressure transducers. This approach has provided the facility of obtaining statistical information on any portion of the digital record i.e. mean, standard deviation and standard error.

(iii) Based upon the results of the research into the boundary layer, under unidirectional flow, it was decided to locate the LDA at 4 mm above the sediment bed, since the results obtained showed that this particular location was within the constant stress layer.

(iv) Subsequently, the unidirectional current speed measurements made using the LDA were used to provide time-mean values. Analysis of several 2 min and 4 min velocity records at 4 mm above the sediment/water interface, showed that a cumulative mean value obtained after 2 min is to within 0.3 cm s^{-1} of the cumulative mean, after 4 min. Considering that the LDA accuracy is ± 0.2 cm s^{-1}, it was decided that a reliable time-mean value of steady current speed could be obtained after 2 min.

(v) Water pressure measurements obtained using the two transducers were used to provide only the standard deviation, as the offset of the sensors (for unknown reasons) was quite variable. In addition, it was decided that mean pressure values would not be meaningful within the data analysis, since the thickness of the sediment deposits examined was only 20 mm. Analysis of several 2 min and 4 min pressure records showed that a standard deviation obtained after 2 min was to within 0.02 cm of pressure head, of the standard deviation after 4 min. As the accuracy of the sensors is 0.014 cm of pressure head,

it was concluded that a reliable standard deviation could be obtained over a 2 min measurement period.

(vi) The test section used throughout the entire study was in the form of a circular recess (located at the centre of the oscillating tray), 9.8 cm in diameter and 2 cm deep (Fig. 4.1). A 100 cm long rubber mat was attached to the oscillating plate, whilst an aperture equal to the diameter of the test section was cut into the mat overlying the plate recess (Plate 4.1). Red sand, to contrast with the quartz sand under study, and with a grain size similar to the sand component of the mixture being investigated, was fixed to the rubber mat. Such an approach was adopted to simulate a naturally-deposited sediment bed. Finally, before each of the threshold experiments, the test-bed was smoothed gently, in order to create a flattened water/sediment interface level with the surrounding red sand. The pore water pressure sensor, during oscillatory and combined flows, was located at 2 cm beneath the sediment/water interface (Fig. 4.1); it was separated from the soil (sample) by a porous material (filter paper).

(vii) In order to determine the number of unidirectional flow experiments which would derive a reliable mean critical erosion value, 20 threshold tests were carried out on a monosized sediment bed of 152.5 μm size (median diameter). Threshold conditions were reached within a constant period of time (2 min), of increasing the flow from zero. Such an approach was adopted in order to eliminate increased resistance, in response to extended flow duration (cf. Tomlinson, 1993). Vanoni's 'bursts of sediment motion' were used as the threshold criterion and the critical current speeds were measured 4 mm above the sediment/water interface. Figure 4.2 and Table 4.1 show the results of the latter preliminary study. Comparing each of the (20) derived critical values, with the overall mean value, the deviation from the mean ranges

from +0.76 to -0.72 cm s^{-1}. Comparing now the mean of 2 or 4 values each time with the mean of the 20 values, the deviations range from +0.75 to -0.47 cm s^{-1} and +0.28 to -0.25 cm s^{-1}, respectively. Consequently, all the deviations from the mean of the 20 values lie close to the measurement error of the LDA (i.e. ±0.20 cm s^{-1}). Hence, the repetition of each of the threshold experiments 4 times at least, provides a reliable determination of the critical parameter investigated.

4.6. EXPERIMENTAL INVESTIGATIONS

4.6.1. Erosion Threshold Determinations

This experimental phase of the investigation incorporates one of the principle aims of the study, which was to investigate the influence of various clay contents on the erodibility of a non-cohesive sediment (fine sand). The experiments were carried out under unidirectional, oscillatory and combined flow regimes.

A limited number of studies have been undertaken on sand-mud admixtures in the laboratory, under unidirectional currents alone (Grissinger *et al.*, 1981; Nalluri & Alvarez, 1992; Torfs, 1994) or purely oscillatory motion (Van Rijn, 1987; Williamson & Ockenden 1992). In addition, there does not appear to be any literature on studies which have been performed under combined flows (currents superimposed upon waves). Hence, since the present experiments provide data on an aspect of sediment dynamics which has not yet been studied sufficiently, it was considered that the samples used throughout the study should be prepared artificially (rather than collected naturally). Principally, this meant that the samples consisted of an artificial, unimodal fine sand fraction (99% quartz content) and a naturally-deposited mud. In

the natural environment, for comparison, sand-mud deposits contain a fine-grained sand fraction, rather than a medium- or coarse-sized sand component. The sediment admixtures examined have been described in detail in Section 3.7. However, it should be mentioned here that the consistency in the water content of particular samples, derived from the mixing process (accomplished using mechanical stirring), showed that the adopted method of mixing (Section 3.7) was reliable (reproducible to within ±2%; see Section 6.2).

In order to investigate the erodibility associated with sand-mud deposits, 14 different soils were tested under various hydrodynamic conditions. Four series of experiments were undertaken; these are referred to as Set 1, Set 2, Set 3 and Set 4 (see below).

Set 1: During this experimental phase, the erodibility of sediment deposits was examined under the action of a steady (freshwater) unidirectional current. Threshold was reached within a particular time period of (2 min), of increasing the unidirectional flow from zero. Such an approach was adopted to eliminate any increase in bed resistance, caused by an extended flow duration (Section 4.6.2). Each experiment was repeated between 6 and 8 times. Following each threshold experiment, the water content of the sample mixtures was determined. For this determination, three sub-samples, of approximately 15 g, were taken from the upper 5 mm of the various deposits.

Set 2: During this particular study, the sediment samples were subjected to various pre-threshold unidirectional current speeds (70%, 80% and 90% of the critical value defined by the Set 1 experiments), over different time periods (5 min, 10 min and 20 min). These experiments allowed the effect of current-induced shear stresses, at

values lower than critical conditions, on the erosional behaviour of the sediment beds to be examined i.e. stress history (see below). The erosion tests represented by Set 2 were repeated 3-4 times.

Set 3: These tests were performed to investigate the erodibility of the same deposits as those tested under unidirectional flow, under the action of (simulated) waves. Wave action was generated by the sinusoidally-oscillating plate within the flume. Plate displacements (strokes) of 0.283 m, 0.378 m, 0.468 m and 0.568 m were used throughout the experiments. Once again, emphasis was placed upon the rapid (i.e. within 2 min, as in Set 1) fulfilment of the threshold criterion. Each experiment was undertaken 6-8 times.

Set 4: Throughout this experimental phase, the erosion threshold of the sand-mud admixtures was determined under the simultaneous action of (simulated) waves and co-linear steady currents i.e. combined flow. Specific oscillatory wave periods (6 and 10 s) and particular strokes were selected for this operation. Each test was carried out 4 times.

Two sand-roughened (D_{50} of sand used—152.5 μm and 215 μm, respectively) rubber mats had been prepared prior to the commencement of the threshold tests. Each mat was attached to the oscillating plate, when sediment beds with a correspondingly sized sand component were investigated.

4.6.2. Effect of Pre-threshold Conditions on the Threshold of Sediment Movement (Unidirectional Flow)

In order to understand the concept of the threshold of sediment motion, several researchers (e.g. Miller

et al., 1977) have reviewed all the available data concerning the threshold of sediment movement on flat beds, in the laboratory. When plotted on a Shields diagram, these data showed a large degree of scatter in the various determinations. Miller *et al.* (op. cit.) attributed this scatter to the fact that the various researchers had used different threshold criteria. Although the researches specified this particular criterion, the characteristics of the flow immediately before threshold was reached were not determined; this appears to be important as explained below.

A body suspended in a moving fluid will orientate itself in such a way that can offer minimum resistance to the fluid (Rusnak, 1957). Further, as the flow speed increases over a sediment bed, there will come a moment where at least one particle (or cluster of particles) will move. This particle may re-orientate itself (perhaps to offer less resistance to the flow and, therefore, more resistance to erosion) or it may roll along the bed in the direction of the flow. As it rolls, the particle will collide with other grains, which might then be dislodged themselves. Alternatively, the particles may re-arrange themselves more compactly with grains or clusters surrounding them. This process may take place for any number of moving grains or clusters. Provided that the observed grain transport rate is less than that required for the selected threshold criterion, then the bed is able to continue arranging itself in this manner, offering more resistance to erosion. It is also possible that, at certain critical flow rates, some grains or aggregates will re-orientate themselves without the observer noticing. It follows that the length of time over which the sediment particles have a chance to re-locate themselves will increase further the probability that the bed will become more resistant to erosion.

Further, it could be expected that, as long as the amount of grains or aggregates moving (per unit time) is less than the critical transport rate associated with the selected threshold criterion, the resistance will be increased further in relation to the number of grains in motion (since the bed has an increased opportunity for re-organisation).

This speculative sequence of events was considered too important to ignore within the context of the experimental procedure. Consequently, a series of experiments (Set 2,) was designed to investigate the effects of pre-threshold stress history, on the critical conditions themselves.

4.6.3. Pore Pressure Measurements

During the oscillatory (Set 3) and combined flow (Set 4) a pore water pressure time-series was recorded at critical conditions. Measurements were obtained from a transducer located at 20 mm beneath the sediment/water interface. Another pressure sensor was available during the combined flow tests; this was located 8 cm upstream of the first sensor, on the surface of the oscillating plate (Fig. 4.3). This sensor recorded pressure fluctuations in the water column itself. Thus, on the basis of calculating the difference in the standard deviations of the pressure records from both transducers, a precise measure of water pressure fluctuation attenuation, caused by the presence of the sediment, could be obtained.

Further, an investigation into the relationship between critical erosion conditions and pore (water) pressure was carried out, under specific oscillatory flow conditions. In these experiments, the erosion threshold condition was

approached in a number of stages (5). Water pressure was monitored during each step, using both of the pressure sensors. For these measurements, the sensors were located in the same positions as those used during the combined flow tests (see above). Comparison of the attenuations in the water pressure fluctuations, caused by the presence of the sediment and derived from all the pressure records, would indicate any correlation between critical motion and pore pressure.

4.6.4. Liquid Limit and Yield Stress Measurements

Sediment shear strength, for comparison with threshold determinations, can be defined on the basis of liquid limit (LL) and yield stress (τ_y) tests. Within the context of the present investigation these tests were used: (i) to examine the influence of clay content on sediment properties; and (ii) to establish any relationship between physical properties and the threshold of movement.

4.7. EXPERIMENTAL PROCESS

4.7.1. Erosion Threshold Experiments

The arrangement of the Laser Doppler Anemometer (LDA), video camera, sediment sample and pore pressure transducers is shown schematically in Figs 4.3 and 4.4. The experimental procedure adopted to investigate the threshold of movement is outlined below.

Unidirectional flow

(i) The flume pump was switched on and it was allowed to warm up for at least half an hour.
(ii) 24 hours after mixing, the sediment samples were

inserted carefully into the test area, avoiding any compaction of the bed.
(iii) The beds were levelled with a plastic straight edge, in such a way that the direction of the resmoothing action was maintained at right angles to the water flow.
(iv) The flume was filled gradually with water, in such a way as to minimise any disturbance of the sediment bed. Following infilling, any loose grains upstream of, and in the vicinity of the test section, were removed.
(v) The samples were retained in a water depth of 11 cm (Fig. 4.1) and, at a zero flow rate for 30 min, in order to adjust to their new depositional conditions.
(vi) The Measurement Control Volume of the LDA (Section 3.3) was positioned at 4 mm above the sediment/water interface (Note: The reference point for any vertical distance was the upper grain surface of the sand roughened mat).
(vii) The data acquisition equipment was set up, so that it could be activated at the appropriate time. This arrangement included an input into the data file of the name of the experiment, the flow type, the initial water depth and ambient water temperature.
(viii) The title of the experiment was prepared, then recorded by the video camera.
(ix) The height alignment and orientation of the LDA was checked. The instrument was positioned vertically and horizontally, to an accuracy of 0.25 mm, using a graduated scale.

Definition of the threshold of sediment movement

For the experiments undertaken as Set 2, involving pre-threshold velocities acting over various time-periods, the water flow rate control valve was opened gradually. In this way, the desired flow rate was established over a

constant time-period (2 min)[1]. Once this flow rate had been established, a stopwatch was activated in order to monitor the flow duration. The pre-threshold velocity was recorded by the LDA, in the middle of the pre-stress period.

The procedure outlined below was adopted for the experiments of Set 1 and within the stress history tests (Set 2), immediately following the pre-stress period. The aim, at this particular stage in the experiment, was to establish threshold conditions within 2 min of increasing the existing flow rate; if this was not managed, then the experiment was aborted and repeated. The precise procedure adopted is described below.

(i) The flow was increased gradually until very weak 'initial motion' was observed; these were unstable grains or clusters of grains, caused by the levelling process. At this point the video camera was activated.

(ii) The flow was increased further by opening the flume pump control valve, in 1/4 turn increments at 10-15 s intervals, until 'critical erosion' conditions were reached.

(iii) Upon reaching a critical condition, the data acquisition equipment was activated in order to record the current speed over a 2 min period. Once this recording time had elapsed, the experiment was completed.

A critical transport rate of 1 burst s^{-1} was established visually, then compared with the video recording corresponding with this critical condition. The recordings demonstrated that the observed (threshold) condition only rarely corresponded exactly to

[1]Note: In view of the fact that it was extremely difficult to achieve the exact percentage of the pre-threshold velocity after 2 min, a considerable amount of effort was introduced in achieving the desired value.

1 burst s^{-1}. Hence, current speeds and bed shear stresses associated with experiments characterised by burst s^{-1} ratios closer to unity were selected for the subsequent analysis.

During incipient motion, the flow depth in the flume ranged from 16 cm to 20 cm. The corresponding water temperatures were approximately 19°C.

Oscillatory flow

The maximum horizontal plate velocity [$U_{o(max)}$], simulating the maximum wave-induced orbital velocity just outside the wave boundary layer, was used as the critical (threshold) parameter defining erosion of the bed. This variable was calculated using the expression

$$U_{o(max)} = \frac{2\pi A_o}{T} \qquad \textbf{(4.1)}$$

where A_o (stroke=$2A_o$) is the amplitude of the horizontal displacement of the moving plate. The period (T) of the plate oscillation was measured by timing the rotation of the flywheel.

These tests were carried out using 4 trolley (plate) displacements of 0.283 m, 0.378 m, 0.468 m and 0.568 m. The strokes correspond to the circumferences of differing crankpin settings on the flywheel (Fig. 3.1). The experimental procedure adopted to establish the threshold of movement, for this particular series of tests, is outlined below.

(a) Initially, steps (i), (ii), (iii), (iv) and (v) described for unidirectional flow tests were followed.

(b) A particular wave condition (stroke) was fixed, then the flywheel was set to rotate at a speed equivalent to a long period wave (10 s). Subsequently, the period of

rotation was reduced gradually until a few individual grains or clusters began to move; these related to the sample preparation (cf. unidirectional flow conditions). At this point in the procedure the video camera was activated.
(c) The (wave) period was decreased then in steps of 0.25 s, until the threshold of bed motion was observed. If critical erosion conditions persisted for over three wave cycles, then the experimental details were noted. If the threshold criterion had not been satisfied within 2 min of activating the flywheel (see also Tomlinson, 1993) then the experiment was aborted and repeated.
(d) Having established threshold conditions, the maximum plate velocity was calculated using Equation 4.1.
(e) Movement of the oscillating plate was stopped, then the next experimental run was prepared.

For the data analysis, maximum wave-induced velocities and bed shear stresses associated with experiments characterised by critical transport rates similar with those observed under unidirectional flow tests, were selected.

During the experiments, the water temperature ranged from 17°C to 19°C.

Combined (unidirectional current and wave-induced) flow

These tests were undertaken using wave periods of 6 s and 10 s. The former periods were combined with 3 wave strokes (0.283 m, 0.378 m and 0.468 m), whilst the latter periods utilised 4 (0.283 m, 0.378 m, 0.468 m and 0.568 m). The procedure adopted for the establishment of threshold is described below.
(a) The initial experimental set up was established, according to stages (i), (ii), (iii), (iv) and (v)

described for the unidirectional flow tests.
(b) The suitable crankpin position was set on the flywheel.
(c) The motor for the flywheel was started and, with the aid of a digital stopwatch, the appropriate period of oscillation (6 s or 10 s) was established. This procedure was undertaken as rapidly and carefully as possible, in order to reduce the potential effect of pre-threshold velocity on the bed; however, not so rapidly as to disturb the configuration of the bed itself.
(d) Having fixed the oscillation (wave) period, the unidirectional flow was increased from zero to the point where a few grains or clusters were moving; these related, once again, to the sample preparation (see above). At this point in the procedure, the video camera was activated.
(e) The final flow increments were controlled using the flow rate valve, until critical conditions had been established. The observer was satisfied that threshold condition had been reached, if this condition was established over at least 3 successive wave cycles. This procedure was established within a 2 min time period as set out for the previous flow conditions i.e. unidirectional and oscillatory flow.
(f) The maximum plate velocity was calculated using Equation 4.1.
(g) The motion of the plate was halted and positioned then in such a way that the middle of the test section was located at 4 mm beneath the Measuring Control Volume of the LDA, which was already switched on. The data acquisition equipment was reset, in order to monitor the unidirectional current component of the combined flow regime. After the logging period (2 min) had elapsed, the experiment was completed and preparations for the next run were initiated.

The flow depth during the tests ranged from 13 cm to 17 cm, whilst the water temperature varied between 18°C and 20°C.

4.7.2. Pore Pressure Response Determination

Three sets (referred to as A, B and C) of pore (water) pressure time-series were obtained, under oscillatory and combined flows, using the pressure transducers specified in Section 3.4.

The pressure sensors became available at different times during the experimental period. Hence, the measurements of Set A were undertaken during the erosion oscillatory flow tests (Set 3) when the first of the sensors was available. The sensor itself was calibrated by fitting it into the base of a burette, from which the tap had been removed. With the burette vertical and the transducer located at its base, the sensor output was logged for various measured heights of water in the tube. The heights were then converted into pressures (mbars). Figure 4.5 and Table 4.2 present the results of the calibration.

In order to interpret the pore pressure values it was considered that a preliminary investigation, referred to as Study A, should be undertaken. For a range of oscillatory (wave) periods and strokes, the water pressure was monitored (over 2 min) in the absence of sediment from the test section. The pressure transducer was located in the same position as that utilised during the oscillatory flow erosion tests. Tables 4.3 to 4.6 present the results of this particular study. From these data, it can be seen that the magnitude of the dynamic water pressure fluctuation (represented by the standard deviation values, multiplied by $\sqrt{2}$), provided that

oscillatory period remains constant, is variable. This discrepancy can be as much as 0.09 cm of (static) pressure head; it can be attributed to electrical noise, associated with the pressure signal. The noise level associated with this experimental phase ranged from 0.06-0.09 cm of pressure head. Additionally, it can be demonstrated that water pressure fluctuations increase as the wave period decreases; this is provided that the wave stroke remains constant.

The trends identified above have been taken into consideration in the analysis of pore pressure data, obtained during the Set A series of measurements. The procedure adopted to obtain the relevant pore pressures (for Set A) is outlined below.
At the establishment of critical erosion conditions, the data acquisition equipment was activated. The data file name was input and a 2 min pressure signal, produced by the sensor located 20 mm below the sediment/water interface, was obtained.

The other two sets of pore pressure measurements were undertaken when the second sensor had been acquired. To improve the results obtained, electrical noise associated with the pressure signals was reduced; for this, a modern electric power supply was purchased. In this way, the noise inherent in the pressure signals was reduced to between 0.04 cm and 0.06 cm of pressure head.

The new pressure sensor was calibrated following the same procedure as adopted for the original system (Fig. 4.6 and Table 4.7). Further, the first sensor needed to be re-calibrated, because of the use of the new power supply (Fig. 4.7 and Table 4.8).

In order to examine the functional behaviour of both of

the sensors, a preliminary study (Study B), was undertaken, under various oscillatory flow conditions and in the absence of sediment. The transducers were located in the same positions as those used during the erosional combined flow erosion tests (Set 4). The results of this study are listed in Tables 4.9 to 4.12. Once again, the dynamic water pressure fluctuations increase with a decrease in wave period; this is provided that the plate displacement is maintained constant. Further, standard deviations of the signals derived by each of the transducers, provided that wave period remains constant, appear a maximum discrepancy of 0.04 cm of pressure head; this value is lower than that observed during Study A (0.09 cm). This difference can be explained by the lower noise level (0.04-0.06 cm) associated with the pressure signals, during this particular experimental phase. Also, it may be noted that the records derived by the sensor situated within the test section were characterised by larger fluctuations, compared to those produced by the sensor located on the surface of the plate. A typical example of this pattern is listed in Table 4.11, for wave periods ranging from 3.97 s to 5.70 s; this can be attributed to small eddies created by the oscillatory plate motion, inside the empty test section. Finally, comparing the shape of the pressure signals obtained from both of the transducers (Figs 4.8 to 4.11), it may be concluded that no particular differences are observed.

Comparison of the standard deviations of the pressure records obtained by the sensor located within the test section, of Study B (Tables 4.9 to 4.12) with the corresponding values of Study A (Tables 4.3 to 4.6), shows that for the same oscillatory period the signal standard deviations are dissimilar. For example, at a wave stroke and period of 0.378 m and 3.54 s, respectively, the mean standard deviations of the

pressure signal during study B and study A were 0.56 cm and 0.68 cm of pressure head, respectively (Tables 4.4 and 4.10). This discrepancy can be attributed: (i) to the different levels of electrical noise associated with Studies A and B; and (ii) to a seiche phenomenon created within the flume and caused by the motion of the oscillating plate.

The trends identified above were considered in the analysis of the pore pressure data obtained during the Set B and Set C measurements.

Pore pressures related to Set B were obtained during the erosion threshold experiments, under combined flow, as outlined below.
When the observer was satisfied that threshold of movement had been reached, the data acquisition system was activated and logged over a 2 min time period. Thus, recordings from the sensor located below the sediment surface and that on the surface of the oscillating plate were obtained.

Set C pore pressure measurements relate to specific wave conditions. Determination of the erosion threshold was approached in a number (5) of steps, each corresponding to a different maximum plate velocity. During each of the wave conditions, pressure records from both sensors were obtained. At the last stage (5th), critical erosion parameters were redefined; this was in order to undertake a comparison with those defined during the Set 3 erosion tests.

4.7.3. Liquid Limit and Rheological Measurements

(a) Liquid limit

The liquid limits (LL) of the (remoulded) sediment deposits, with mud contents > 5%, were determined using the fall cone penetrometer method (B.S. 1377, 1975). This standard method is based upon the measurement of penetration into the soil of a standardised cone, of specified mass. At the liquid limit, the penetration of the cone is 20 mm. The procedure adopted to determine liquid limits is outlined below.

(1) A sample of 200-250 g of a specific sediment mixture was placed on a glass plate and mixed thoroughly with a a small amount of distilled water, using two palette knives or spatulas. More water was added to the soil, a little at a time, in order to create a thick homogeneous paste.

(2) The paste was placed into an air-tight container, then sealed. The mixture was left over a curing period of 24 hours in a cool place, to allow water to permeate through the mass of the soil.

(3) The soil was removed from the container after it had matured; it was remixed with the spatulas for at least 10 min, in order to obtain a uniform distribution of water.

(4) An amount of the soil paste was placed into a metal cup, avoiding on trapping air. The upper surface was smoothed off, level with the rim of the cup.

(5) The cone of the penetrometer was lowered carefully, so that the tip of the cone just touched the soil surface. The reading (R1) of the dial gauge was noted and recorded, to the nearest 0.1 mm.

(6) The cone was allowed to fall by pressing a release button for 5 s; after this, the new reading (R2) of the dial gauge was recorded to the nearest 0.1 mm. The

difference between R1 and R2 was recorded as the cone penetration.

(7) The cone was lifted and cleaned carefully. A little more wet soil was added to the cup (without trapping air) and its surface was smoothed off. Stages 5 and 6 were then repeated. If the second cone penetration reading was different from the first by less than 0.5 mm, then the average value was recorded and the water (moisture) content was measured. If the second penetration differed by between 0.5 and 1 mm from the first, a third test was carried out. Provided that the overall range did not exceed 1 mm, the average of the three penetrations was recorded and the water (moisture) content was measured. If the overall range exceeded 1 mm, the soil was removed from the metal cup and remixed, with the test being repeated.

(8) The soil which remained in the cup was remixed with the remainder of the sample on the glass plate, together with some additional distilled water, until a uniform and softer consistency was obtained. The cup was cleaned and dried, with stages 4-7 being repeated at least three more times i.e. making 4 in all. A range of penetration values, from about 15 mm to 25 mm, should be covered.

(9) Each cone penetration (mm) was plotted against the corresponding water content, as shown in Figs 4.12 and 4.13. From these graphs, the water content corresponding to a cone penetration of 20 mm was read off. This result was recorded as the liquid limit for the sediment mixture tested.

Tables 4.13 to 4.22 show results derived from liquid limit (cone penetrometer) tests.

(b) Rheological testing

The rheological testing on the sand-mud mixtures of the

present study was performed using a Bohlin rheometer. These measurements defined the yield stress (τ_y) of the sediments. The experimental procedure is described below. Small sub-samples of the soil under investigation were placed into a small closed-bottom metal cylinder, 8 cm in depth and 4 cm in internal diameter. The cylinder was inserted then into the Bohlin rheometer and a four-blade rheometer vane was inserted. A series of preliminary tests were run, to ascertain: (a) the upper limits of the shear stress required to obtain the yield stress of each sediment sample; and (b) the intervals needed to permit an accurate determination of the yield stress.

Each sample was set up to run for 30 intermediate steps, over 300 s i.e. a step interval of 10 s. Preliminary experiments suggested an upper shear stress limit of 50 Pa (N m^{-2}).

The yield stress of a particular mixed sediment from the present investigation was determined five times, with the mean value considered as the representative yield stress for the soil.

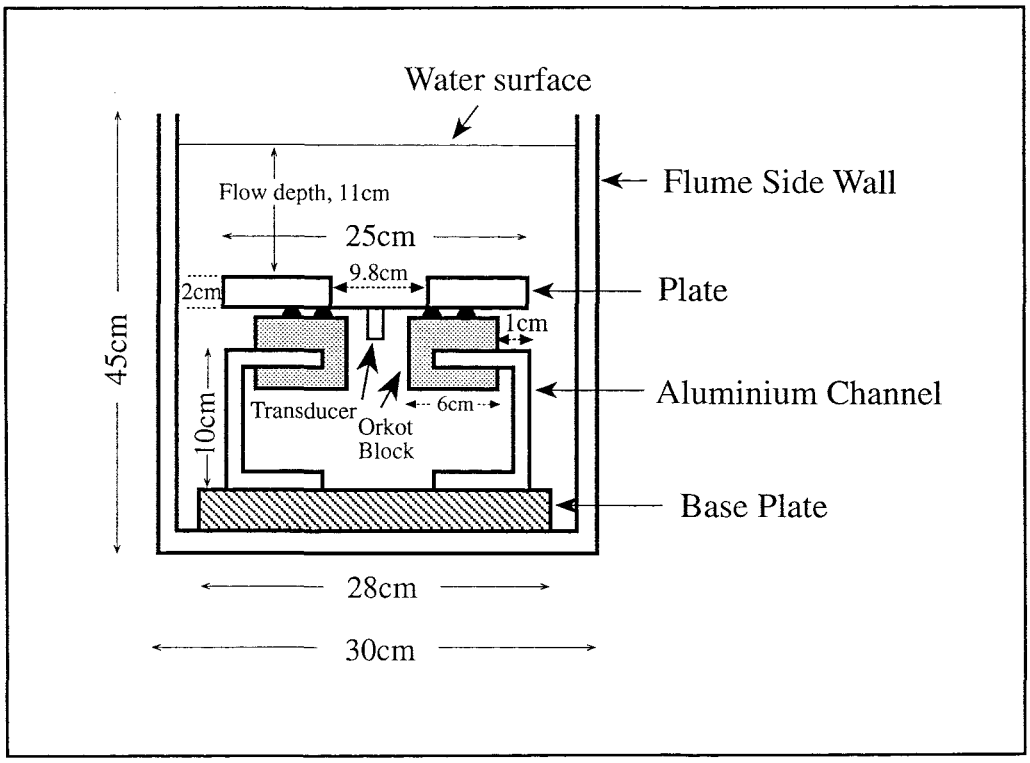

Fig. 4.1. Cross section of the flume, showing the circular test section containing the sample and the location of the pore pressure sensor (schematic).

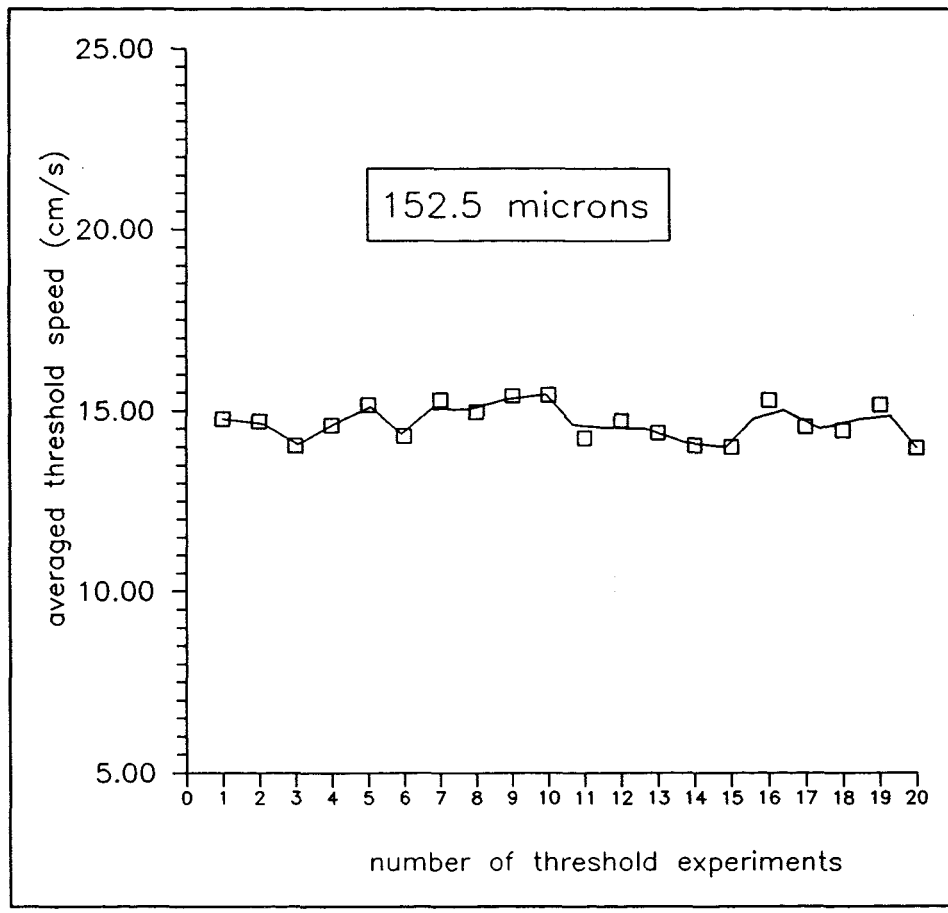

Fig. 4.2. Observational consistency in defining the threshold of sediment movement, for a 152.5 μm monosized sample.

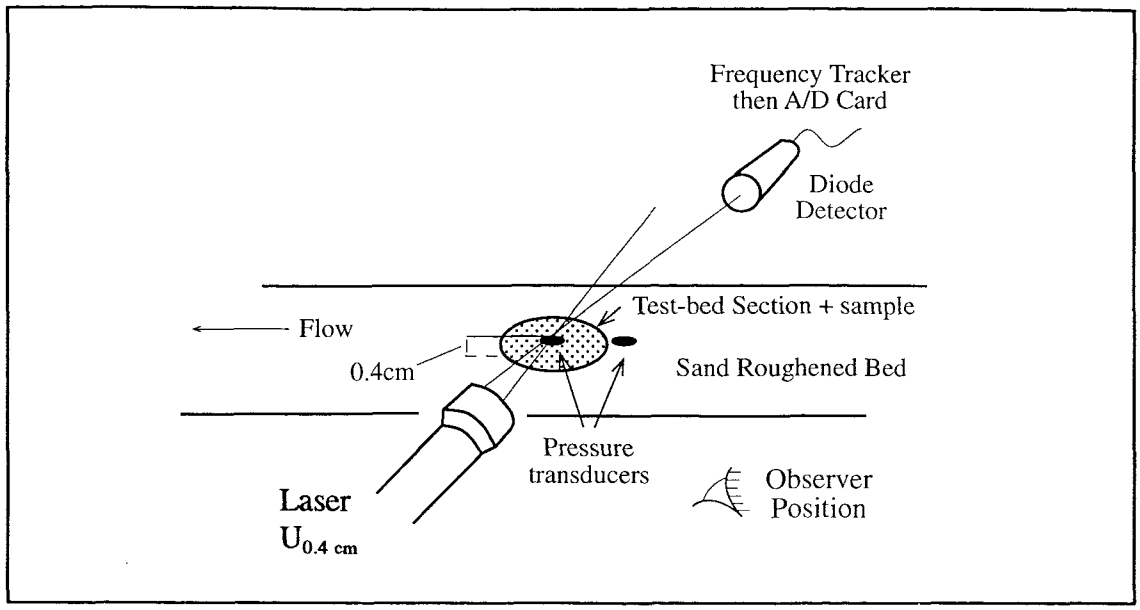

Fig. 4.3. Schematic representation of the experimental set up during the hydrodynamic tests, under a combined flow regime.

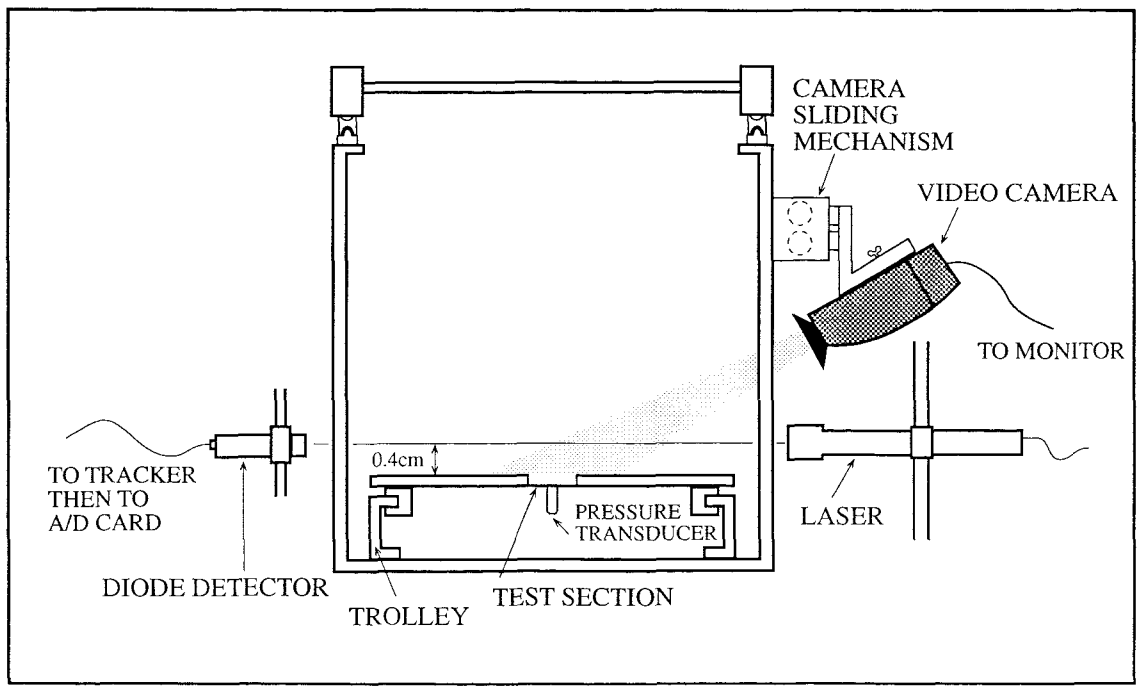

Fig. 4.4. Cross section of the flume, displaying the experimental arrangement of the video camera, Laser Doppler Anemometer (LDA) and pore pressure transducer.

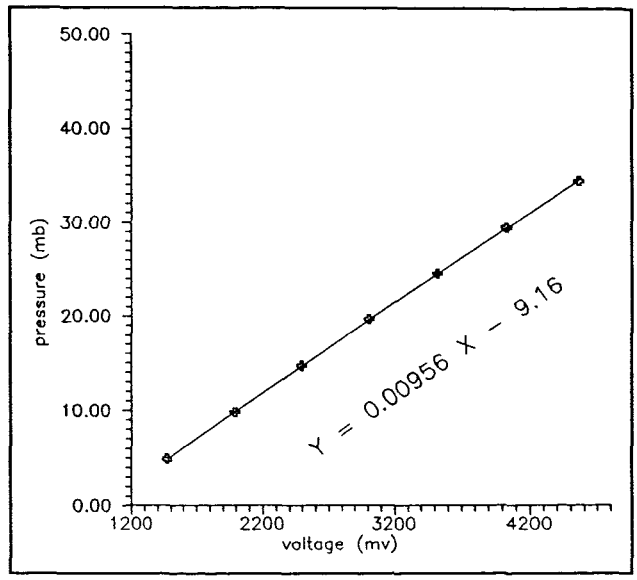

Fig. 4.5. Initial calibration of the pressure sensor, located within the test section and beneath the sediment/water interface.

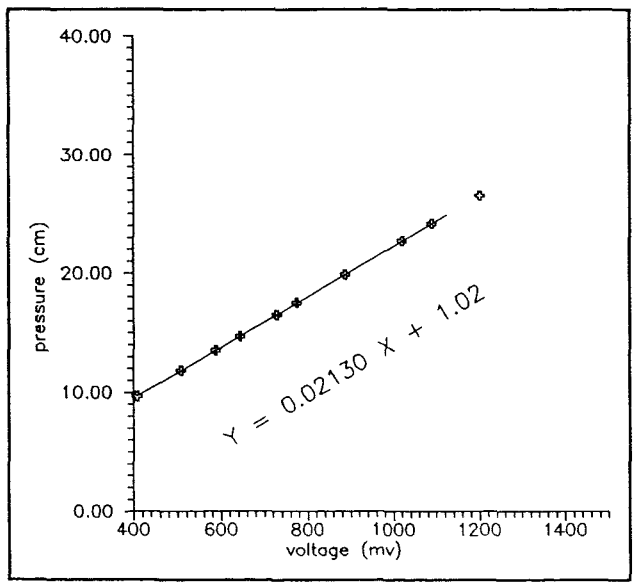

Fig. 4.6. Calibration of the pressure sensor located at the surface of the oscillating plate.

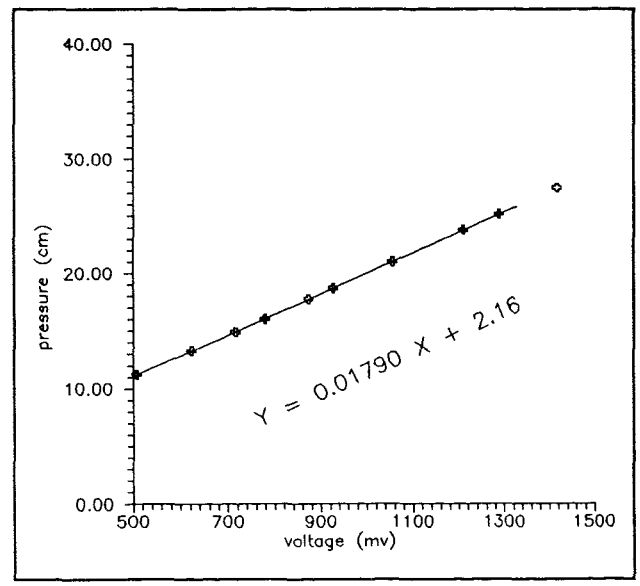

Fig. 4.7. Re-calibration of the pressure sensor situated beneath the sediment/water interface, following the introduction of a new power supply (see text).

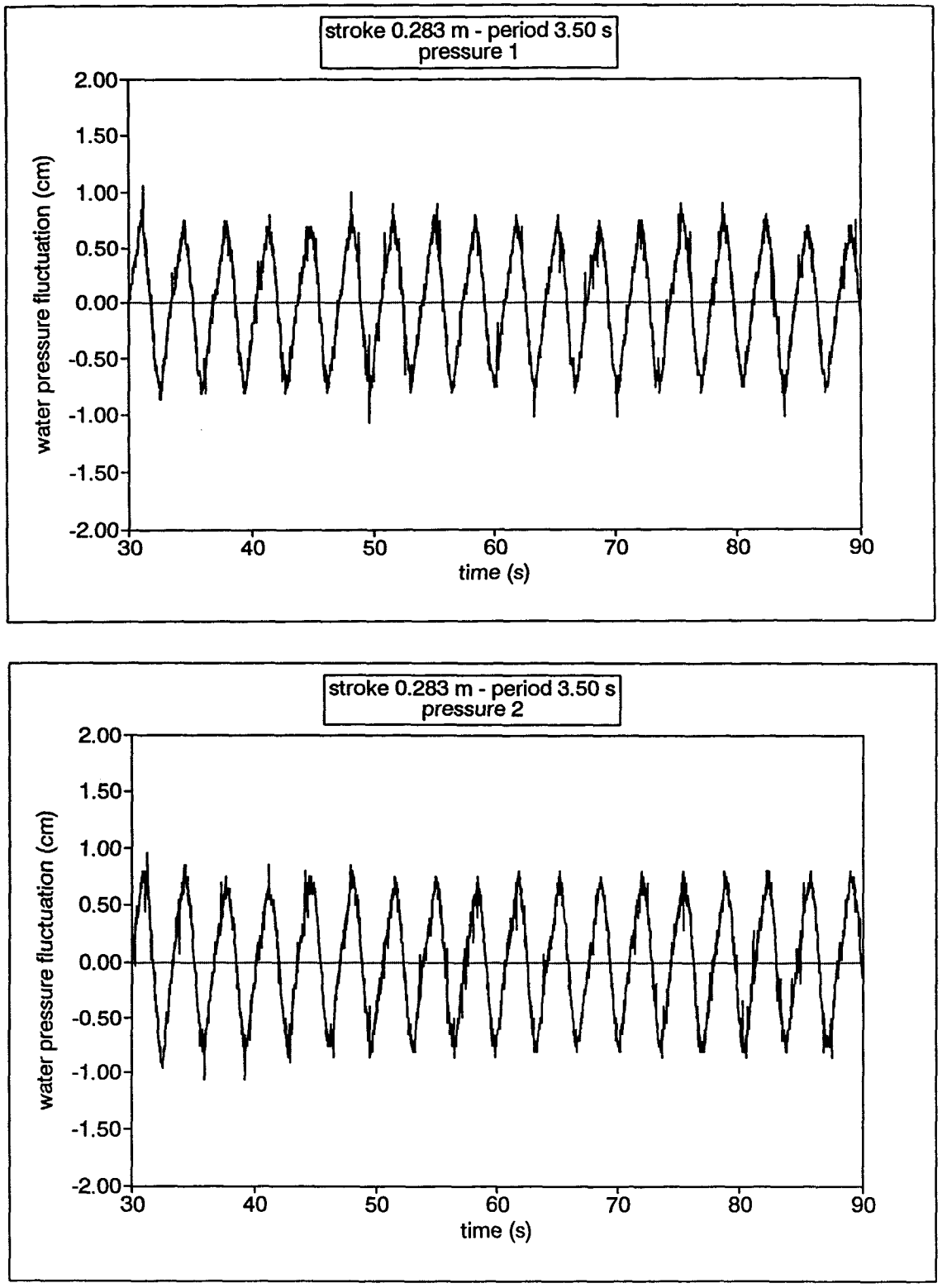

Fig. 4.8. Pressure signals obtained during Study B. Key: Pressure 1 obtained from the sensor located at the top of the oscillating plate; pressure 2 obtained from the sensor located in the test section.

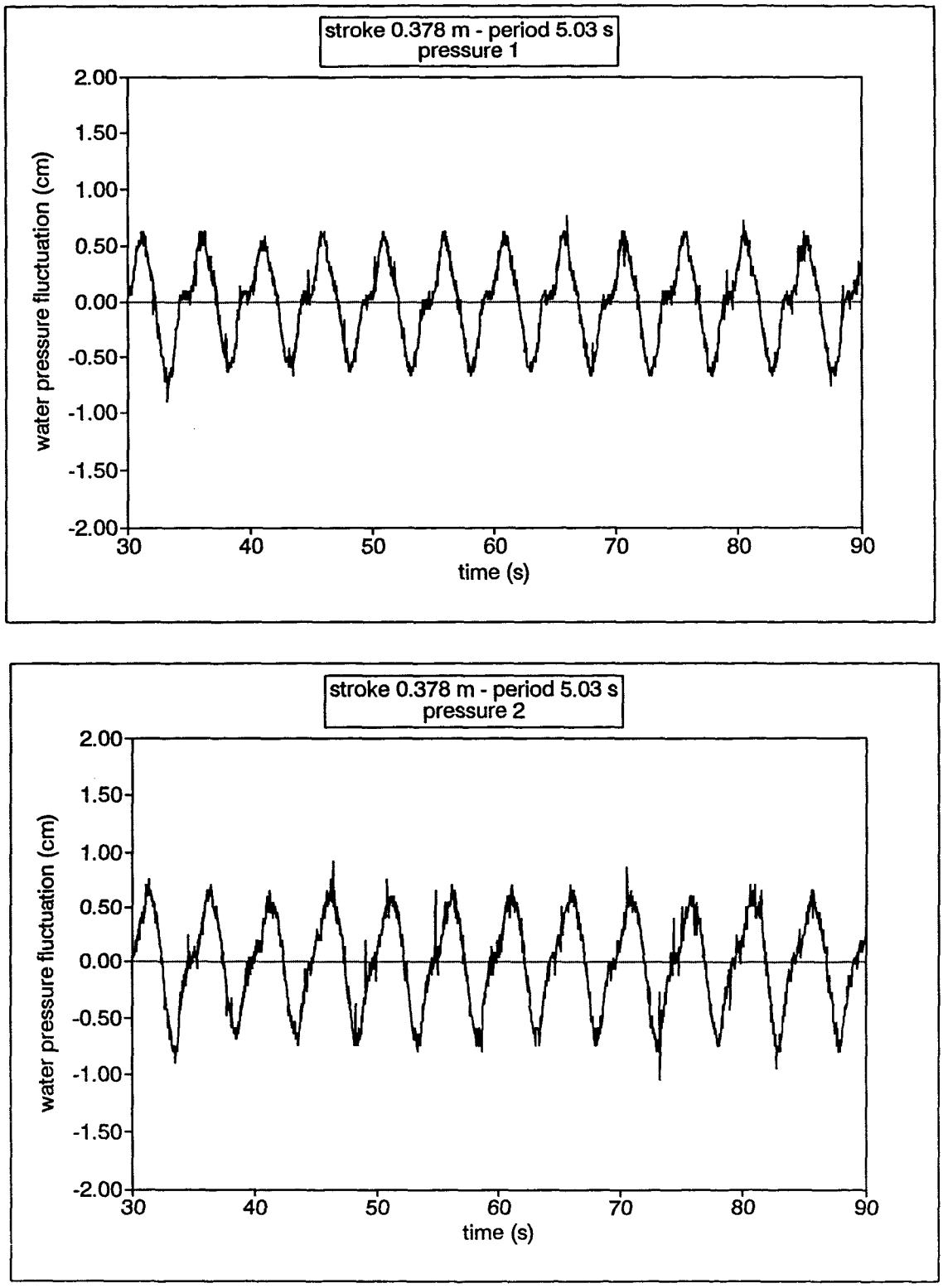

Fig. 4.9. Pressure signals obtained during Study B. Key: Pressure 1 obtained from the sensor located at the top of the oscillating plate; pressure 2 obtained from the sensor located in the test section.

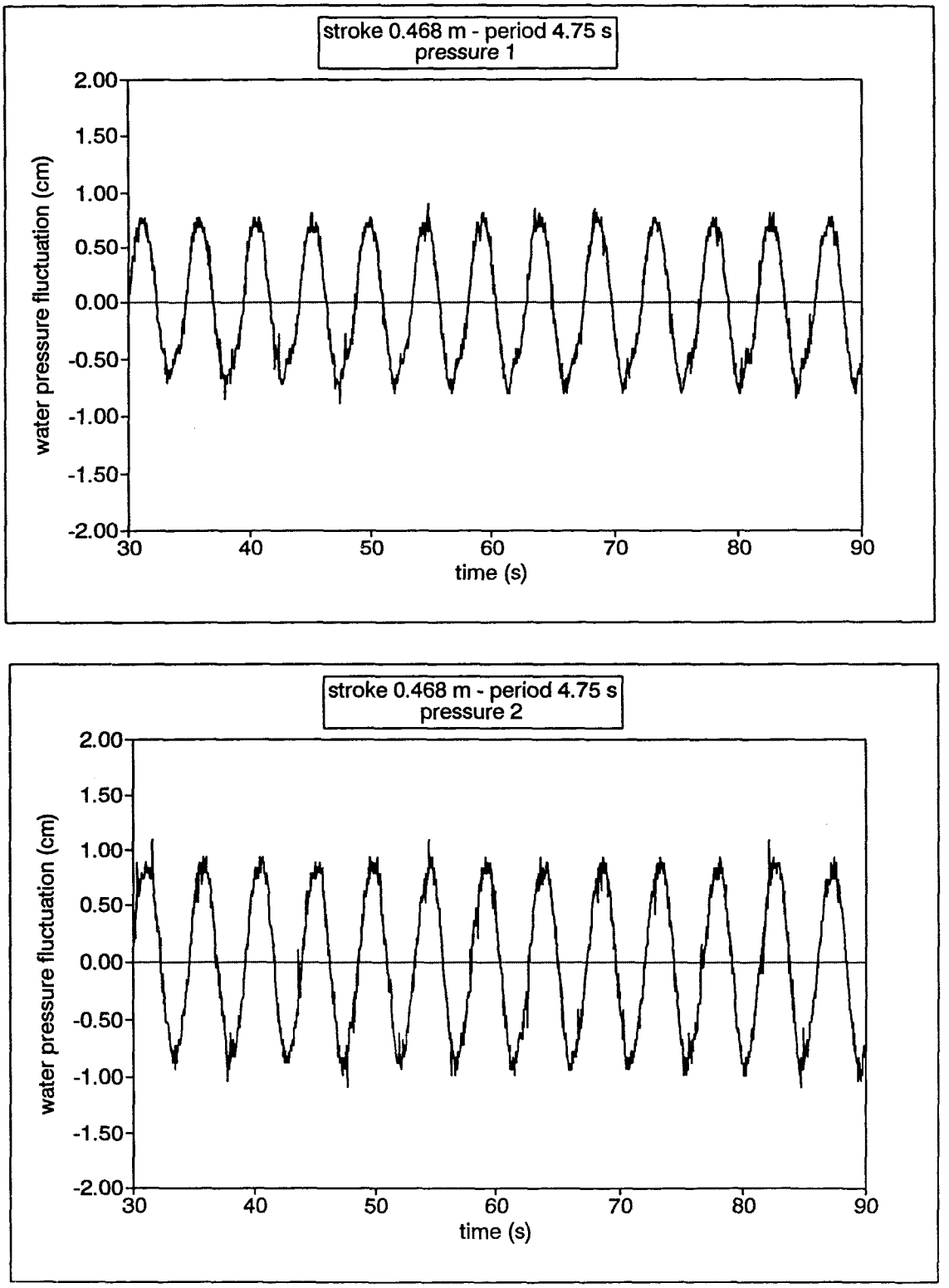

Fig. 4.10. Pressure signals obtained during Study B. Key: Pressure 1 obtained from the sensor located at the top of the oscillating plate; pressure 2 obtained from the sensor located in the test section.

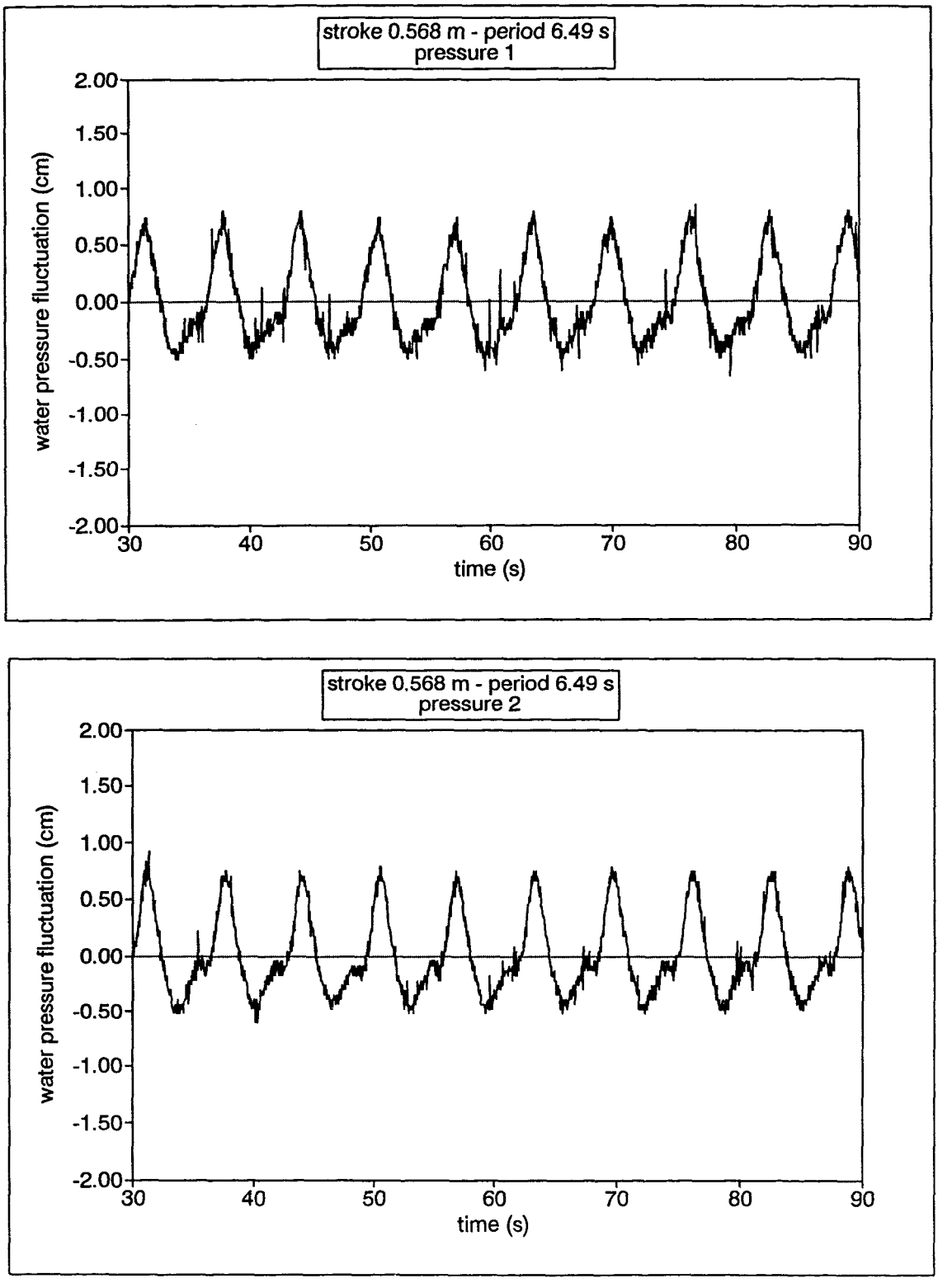

Fig. 4.11. Pressure signals obtained during Study B. Key: Pressure 1 obtained from the sensor located at the top of the oscillating plate; pressure 2 obtained from the sensor located in the test section.

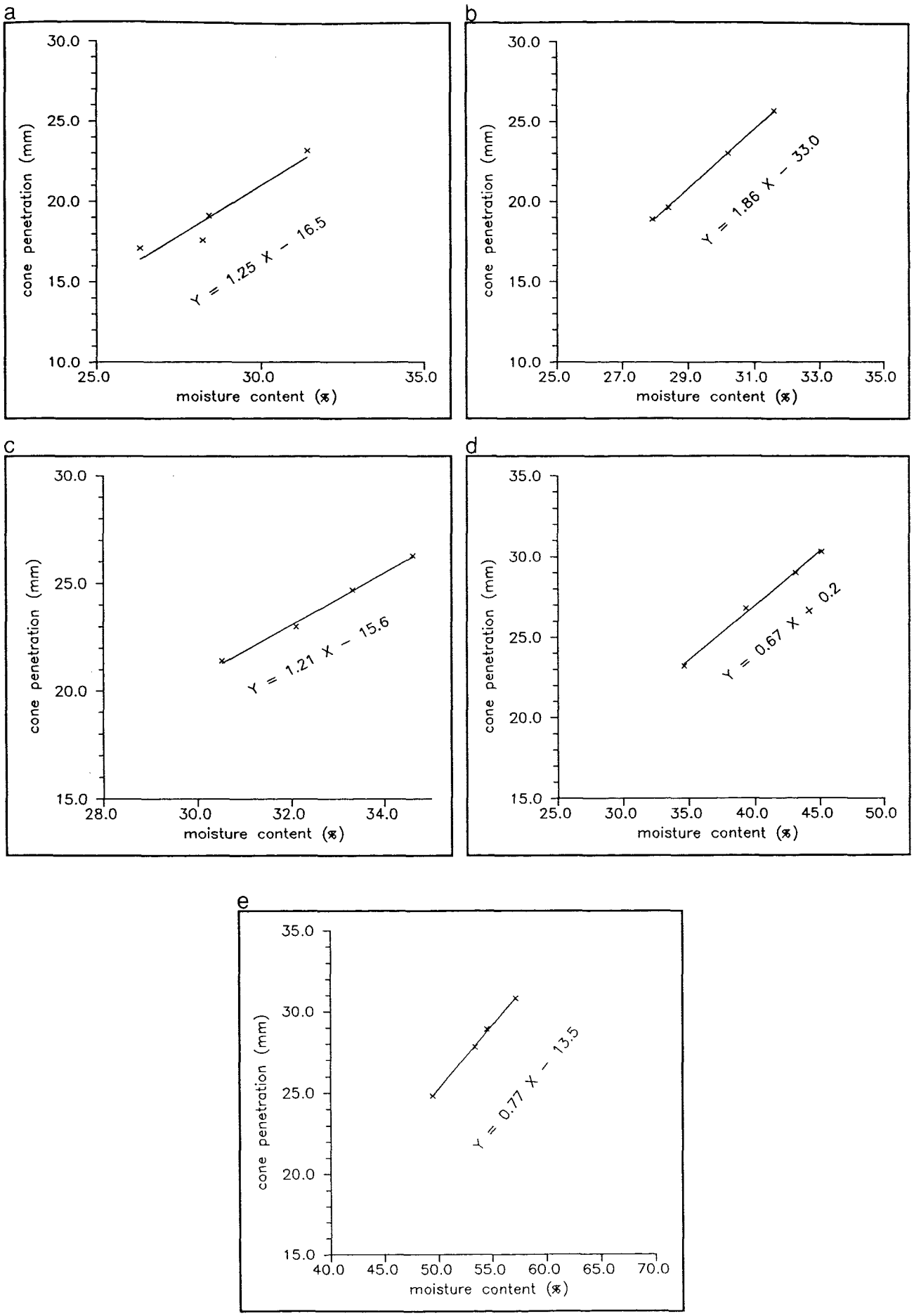

Fig. 4.12. Liquid limit test results for mixtures containing the 152.5 μm sands together with: (a) 10% mud; (b) 20% mud; (c) 30% mud; (d) 40% mud; and (e) 50% mud.

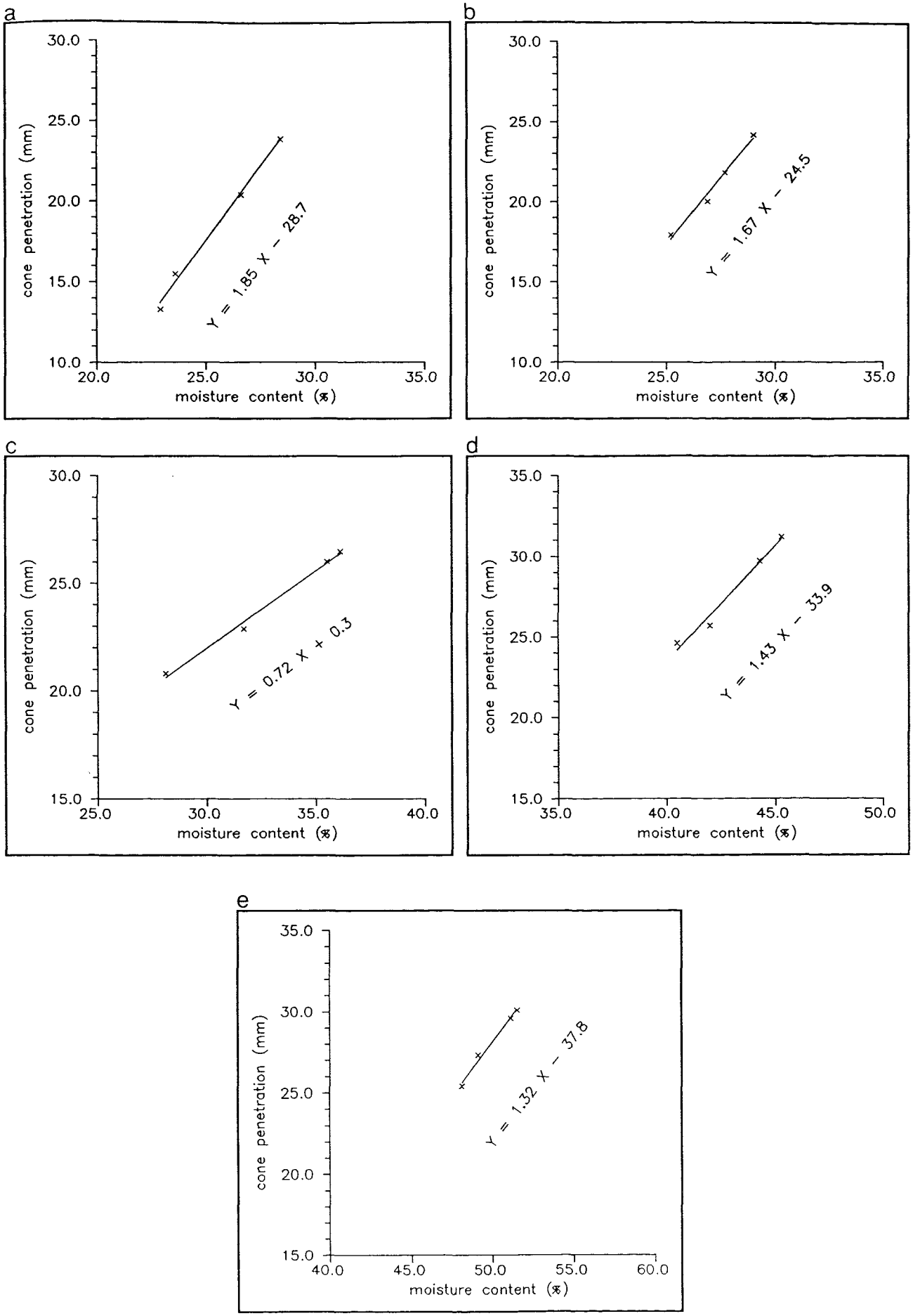

Fig. 4.13. Liquid limit test results for mixtures containing the 215 μm sands together with: (a) 10% mud; (b) 20% mud; (c) 30% mud; (d) 40% mud; and (e) 50% mud.

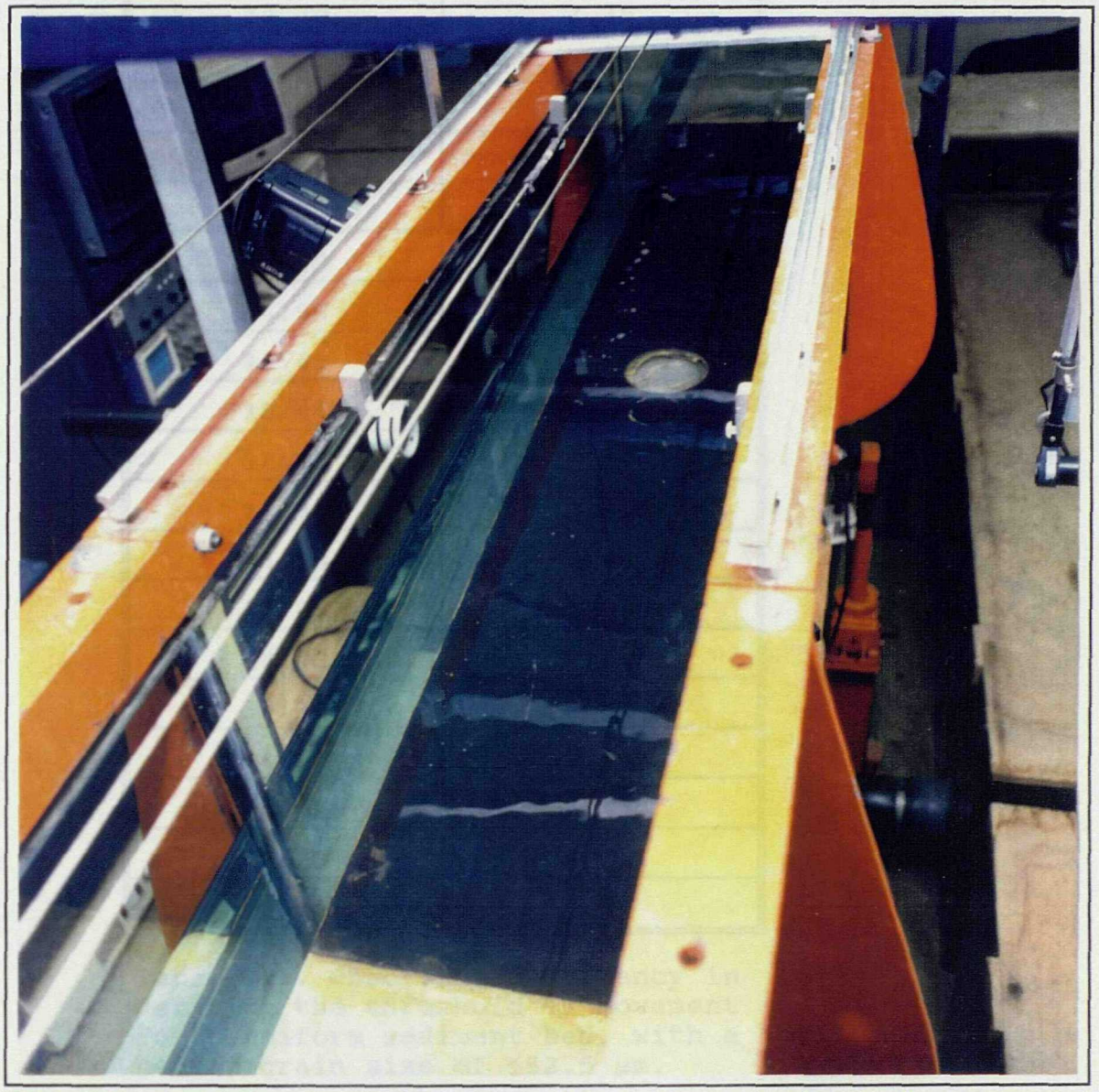

Plate 4.1. General plan view of the oscillating bed, incorporating the circular test area and surrounding sand-covered rubber mat.

averaged cr. current speed $U_{c(0.4\ cm)}$ (cm/s)	standard deviation σ (cm/s)
14.77	2.34
14.70	2.35
14.04	2.32
14.60	2.37
15.15	2.47
14.30	2.33
15.29	2.72
14.96	2.36
15.41	2.56
15.44	2.63
14.25	2.48
14.73	2.69
14.38	2.49
14.03	2.33
14.00	2.46
15.30	2.90
14.56	2.38
14.46	2.41
15.18	2.56
13.96	2.41

Table 4.1. Observer consistency in defining the threshold of movement for a uniform sediment bed, with a median grain size of 152.5 μm.

pressure head (cm)	pressure (mb)	voltage (mv)
5	4.91	1472
10	9.81	1991
15	14.72	2494
20	19.62	3006
25	24.53	3519
30	29.43	4031
35	34.34	4560

Table 4.2. Data used for the derivation of the calibration formula for the pressure transducer located beneath the sediment/water interface.

period of oscillation (s)	st.deviation of water pressure (cm)	mean st.dev. of water pressure (cm)
2.00	0.63 0.60 0.57 0.57	0.59
2.65	0.55 0.58 0.55 0.56	0.56
2.97	0.56 0.56 0.55 0.56	0.56
3.22	0.53 0.51 0.46 0.49	0.50
3.44	0.54 0.52 0.51 0.50	0.52
3.79	0.55 0.50 0.56 0.52	0.53
4.05	0.53 0.53 0.51 0.51	0.52
4.34	0.42 0.45 0.39 0.47	0.43
4.76	0.39 0.38 0.36 0.41	0.39
5.59	0.31 0.31 0.28 0.29	0.30
5.82	0.24 0.22 0.23 0.23	0.23

Table 4.3. Water pressure measurements for different periods of oscillation, in the absence of sediment. Wave stroke of 0.283 m.

period of oscillation (s)	st.deviation of water pressure (cm)	mean st.dev. of water pressure (cm)
2.82	0.66 0.70 0.67 0.69	0.68
3.02	0.69 0.69 0.69 0.68	0.68
3.33	0.66 0.66 0.67 0.67	0.67
3.54	0.70 0.65 0.69 0.69	0.68
3.77	0.58 0.62 0.57 0.57	0.59
4.01	0.59 0.51 0.53 0.50	0.53
4.32	0.49 0.49 0.50 0.50	0.50
4.63	0.50 0.51 0.51 0.49	0.50
4.90	0.47 0.50 0.45 0.47	0.47
5.15	0.41 0.37 0.36 0.45	0.40
5.64	0.35 0.32 0.31 0.35	0.33
6.28	0.20 0.20 0.20 0.19	0.20
6.67	0.19 0.19 0.19 0.19	0.19

Table 4.4. Water pressure measurements for different periods of oscillation, in the absence of sediment. Wave stroke of 0.378 m.

period of oscillation (s)	st.deviation of water pressure (cm)	mean st.dev. of water pressure (cm)
3.26	0.84 0.82 0.83 0.82	0.83
3.47	0.81 0.78 0.82 0.78	0.80
3.89	0.77 0.75 0.78 0.75	0.76
4.28	0.76 0.76 0.76 0.75	0.76
4.61	0.75 0.75 0.75 0.75	0.75
4.87	0.79 0.76 0.74 0.80	0.77
5.11	0.79 0.76 0.75 0.80	0.78
5.44	0.65 0.65 0.63 0.63	0.64
5.64	0.57 0.57 0.56 0.56	0.57
5.83	0.42 0.45 0.46 0.41	0.44
6.32	0.26 0.27 0.23 0.24	0.25

Table 4.5. Water pressure measurements for different periods of oscillation, in the absence of sediment. Wave stroke of 0.468 m.

period of oscillation (s)	st.deviation of water pressure (cm)	mean st.dev. of water pressure (cm)
5.22	0.74 0.76 0.72 0.70	0.73
5.64	0.65 0.65 0.63 0.63	0.64
5.80	0.52 0.47 0.49 0.54	0.51
6.00	0.39 0.39 0.39 0.38	0.39
6.37	0.36 0.36 0.35 0.37	0.36
6.87	0.33 0.33 0.34 0.34	0.34

Table 4.6. Water pressure measurements for different periods of oscillation, in the absence of sediment. Wave stroke of 0.568 m.

pressure head (cm)	voltage (mv)
9.70	408
11.85	508
13.54	587
14.73	643
16.52	728
17.51	774
19.90	887
22.74	1020
24.21	1088
26.58	1200

Table 4.7. Data used in the derivation of the calibration formula for the pressure transducer located at the surface of the oscillating plate.

pressure head (cm)	voltage (mv)
11.25	507
13.30	623
14.93	715
16.08	778
17.79	873
18.74	926
21.04	1055
23.80	1208
25.20	1287
27.49	1416

Table 4.8. Data used in the derivation of the new calibration formula for the pressure transducer located beneath the surface of the sediment deposit.

period of oscillation (s)	pressure 1 σ (cm)	pressure 2 σ (cm)
2.03	0.54 0.54 0.55 0.54	0.55 0.55 0.56 0.55
2.27	0.52 0.52 0.52 0.53	0.55 0.56 0.55 0.55
2.52	0.52 0.52 0.52 0.52	0.54 0.56 0.53 0.54
2.78	0.51 0.51 0.50 0.50	0.53 0.52 0.53 0.52
3.02	0.51 0.51 0.51 0.50	0.53 0.52 0.52 0.53
3.26	0.49 0.48 0.49 0.48	0.49 0.49 0.48 0.49
3.50	0.48 0.49 0.47 0.48	0.49 0.50 0.49 0.49
3.74	0.47 0.45 0.47 0.47	0.50 0.50 0.51 0.50
4.01	0.44 0.44 0.44 0.43	0.47 0.46 0.47 0.47
4.27	0.37 0.37 0.37 0.37	0.40 0.39 0.39 0.40
5.94	0.20 0.21 0.20 0.20	0.22 0.23 0.22 0.22

Table 4.9. Water pressure measurements for different periods of oscillation, in the absence of sediment. Wave stroke of 0.283 m (Note: Pressure 1 is obtained from the sensor situated at the top of the trolley, whilst pressure 2 relates to the sensor located within the test section).

period of oscillation (s)	pressure 1 σ (cm)	pressure 2 σ (cm)
2.78	0.52 0.52 0.52 0.52	0.56 0.56 0.56 0.55
3.01	0.52 0.52 0.52 0.53	0.57 0.57 0.55 0.57
3.28	0.52 0.51 0.51 0.51	0.55 0.55 0.56 0.53
3.54	0.51 0.51 0.50 0.52	0.56 0.53 0.56 0.57
3.80	0.47 0.47 0.48 0.47	0.49 0.49 0.49 0.49
4.00	0.45 0.45 0.45 0.45	0.48 0.48 0.48 0.47
4.24	0.43 0.44 0.43 0.42	0.48 0.48 0.48 0.48
4.54	0.41 0.41 0.40 0.40	0.46 0.46 0.46 0.44
4.74	0.40 0.42 0.39 0.38	0.44 0.43 0.44 0.43
5.03	0.38 0.38 0.37 0.40	0.42 0.40 0.42 0.43
6.05	0.25 0.25 0.25 0.23	0.28 0.28 0.28 0.28

Table 4.10. Water pressure measurements for different periods of oscillation, in the absence of sediment. Wave stroke of 0.378 m (Note: Pressure 1 is obtained from the sensor situated at the top of the trolley, whilst pressure 2 relates to the sensor located within the test section).

period of oscillation (s)	pressure 1 σ (cm)	pressure 2 σ (cm)
3.97	0.56 0.56 0.56 0.56	0.62 0.60 0.61 0.63
4.25	0.54 0.54 0.55 0.51	0.62 0.62 0.63 0.60
4.47	0.53 0.53 0.53 0.51	0.61 0.61 0.61 0.60
4.75	0.52 0.52 0.52 0.52	0.62 0.62 0.61 0.61
4.97	0.44 0.44 0.45 0.42	0.57 0.56 0.57 0.56
5.24	0.42 0.42 0.42 0.42	0.53 0.53 0.53 0.53
5.53	0.39 0.39 0.38 0.38	0.52 0.52 0.52 0.52
5.70	0.36 0.36 0.37 0.35	0.44 0.45 0.44 0.42
6.02	0.33 0.33 0.33 0.33	0.35 0.34 0.34 0.35

Table 4.11. Water pressure measurements for different periods of oscillation, in the absence of sediment. Wave stroke of 0.468 m (Note: Pressure 1 is obtained from the sensor situated at the top of the trolley, whilst pressure 2 relates to the sensor located within the test section).

period of oscillation (s)	pressure 1 σ (cm)	pressure 2 σ (cm)
5.24	0.66 0.67 0.66 0.66	0.69 0.68 0.68 0.70
5.50	0.63 0.63 0.63 0.63	0.64 0.64 0.62 0.65
5.75	0.58 0.57 0.57 0.58	0.59 0.59 0.59 0.59
5.98	0.45 0.45 0.45 0.44	0.44 0.44 0.43 0.43
6.26	0.38 0.37 0.37 0.38	0.38 0.38 0.38 0.38
6.49	0.36 0.36 0.36 0.36	0.36 0.37 0.36 0.36
6.77	0.36 0.36 0.36 0.34	0.37 0.37 0.36 0.37
7.05	0.35 0.35 0.34 0.34	0.35 0.34 0.34 0.35

Table 4.12. Water pressure measurements for different periods of oscillation, in the absence of sediment. Wave stroke of 0.568 m (Note: Pressure 1 is obtained from the sensor situated at the top of the trolley, whilst pressure 2 relates to the sensor located within the test section).

test number	cone penetration (mm)	averaged penetration (mm)	water content (%)
1	17.27 16.88	17.1	26.3
2	17.44 17.96 17.33	17.6	28.2
3	19.08 19.16	19.1	28.4
4	23.43 23.05	23.2	31.4

Table 4.13. Liquid limit (cone penetrometer) measurements for the sediment mixture containing the 152.5 micron sand and 10% mud (LL=29.2%).

test number	cone penetration (mm)	averaged penetration (mm)	water content (%)
1	18.82 18.89	18.9	27.9
2	19.59 19.63	19.6	28.4
3	23.08 22.94	23.0	30.2
4	25.42 25.99 25.58	25.7	31.6

Table 4.14. Liquid limit (cone penetrometer) measurements for the sediment mixture containing the 152.5 micron sand and 20% mud (LL=28.5%).

test number	cone penetration (mm)	averaged penetration (mm)	water content (%)
1	21.53 21.19	21.4	30.5
2	23.22 22.83	23.0	32.1
3	24.94 24.05 25.06	24.7	33.3
4	26.02 26.84 25.96	26.3	34.6

Table 4.15. Liquid limit (cone penetrometer) measurements for the sediment mixture containing the 152.5 micron sand and 30% mud (LL=29.4%).

test number	cone penetration (mm)	averaged penetration (mm)	water content (%)
1	23.26 23.08	23.2	34.6
2	26.97 26.53	26.8	39.3
3	29.23 28.46 29.25	29.0	43.1
4	30.23 30.74 29.84	30.3	45.1

Table 4.16. Liquid limit (cone penetrometer) measurements for the sediment mixture containing the 152.5 micron sand and 40% mud (LL=29.6%).

test number	cone penetration (mm)	averaged penetration (mm)	water content (%)
1	24.22 25.05 25.19	24.8	49.4
2	27.64 27.88	27.8	53.4
3	28.99 28.85	28.9	54.5
4	30.46 31.39 30.64	30.8	57.2

Table 4.17. Liquid limit (cone penetrometer) measurements for the sediment mixture containing the 152.5 micron sand and 50% mud (LL=43.5%).

test number	cone penetration (mm)	averaged penetration (mm)	water content (%)
1	13.17 13.36	13.3	22.9
2	15.21 15.92 15.31	15.5	23.6
3	20.89 20.01 20.37	20.4	26.6
4	24.56 23.63 23.57	23.9	28.4

Table 4.18. Liquid limit (cone penetrometer) measurements for the sediment mixture containing the 215 micron sand and 10% mud (LL=26.3%).

test number	cone penetration (mm)	averaged penetration (mm)	water content (%)
1	17.84 17.99	17.9	25.2
2	20.22 19.65 20.26	20.0	26.9
3	21.94 21.28 22.03	21.8	27.7
4	24.53 23.66 24.52	24.2	29.0

Table 4.19. Liquid limit (cone penetrometer) measurements for the sediment mixture containing the 215 micron sand and 20% mud (LL=26.6%).

test number	cone penetration (mm)	averaged penetration (mm)	water content (%)
1	20.33 21.13 20.79	20.8	28.1
2	22.68 23.14	22.9	31.7
3	26.04 25.89	26.0	35.5
4	26.51 26.50	26.5	36.1

Table 4.20. Liquid limit (cone penetrometer) measurements for the sediment mixture containing the 215 micron sand and 30% mud (LL=27.4%).

test number	cone penetration (mm)	averaged penetration (mm)	water content (%)
1	24.11 24.64 24.97	24.6	40.5
2	25.08 25.97 26.12	25.7	42.0
3	29.75 29.59	29.7	44.3
4	31.23 31.15	31.2	45.3

Table 4.21. Liquid limit (cone penetrometer) measurements for the sediment mixture containing the 215 micron sand and 40% mud (LL=37.7%).

test number	cone penetration (mm)	averaged penetration (mm)	water content (%)
1	25.12 25.59	25.4	48.1
2	27.01 27.72 27.09	27.3	49.1
3	29.41 29.73	29.6	51.1
4	30.10 30.06	30.1	51.5

Table 4.22. Liquid limit (cone penetrometer) measurements for the sediment mixture containing the 215 micron sand and 50% mud (LL=44.0%).

CHAPTER 5

BOUNDARY LAYER RESEARCH

5. BOUNDARY LAYER RESEARCH

5.1. INTRODUCTION

This Chapter describes the methods (and the subsequent) results obtained to: (i) identify the overall structure of the water flow within the flume channel; and (ii) define the character of the prevailing boundary layer during the experiments, under various hydrodynamic conditions.

Unidirectional flow structure definition was succeeded by the measurement of vertical velocity profiles using the LDA. The oscillatory (wave) boundary layer was not investigated experimentally, since the flow velocity measuring device (LDA) of the present study could not operate under reversing flow conditions. Hence, identification of the wave boundary layer, during the threshold tests, was accomplished based upon the theoretical concepts postulated by other investigators. Theoretical assumptions were used also for the determination of the combined flow regimes.

Another objective of this initial study was to examine the feasibility of utilising the flume arrangement to simulate natural conditions in the laboratory. Further, to establish a method for determining the critical bed shear stress for use in the threshold experiments.

5.2. UNIDIRECTIONAL FLOW RATES

The objectives for undertaking boundary layer research, under unidirectional flow, is summarised below.
(i) A series of vertical velocity profiles (Series 1) were measured, in order to establish the overall nature of the flow within the flume. These velocity profiles

involved the examination of the effects of the glass-sided walls and oscillating plate mechanism on the overlying flow structure. Particular attention, during the experiments, was paid to the flow overlying the test section (a circular recess within the bed). Generally, this preliminary study tested the feasibility of using the flume to simulate naturally-occuring (unidirectional) tidal or river flows.

(ii) Another series of velocity profiles (Series 2) contributed to the investigation of unidirectional boundary layers above sediment beds; these consisted only of the sand fractions used to form the mixed deposits investigated during the present project. These boundary layers were formed under the action of various (3) flow rates i.e. slow, medium and fast. The fundamental objective of these measurements was to provide an insight into the different flow regimes, associated with unidirectional currents.

5.2.1. Experimental Approach

The validity of the measured flow velocities in this research is dependent on a number of factors. Mainly, these factors concern the accuracy of the measurement capability of the Laser Dopper Anemometer (LDA), the positional errors of the instrument, and the accuracy of the A/D conversion system (Section 3.6). Another possible limitation which requires examination is the effect of the presence of the oscillating plate mechanism, together with the side walls, on the flow structure; this is particularly important in the area of the flow which incorporates the test-bed section. Finally, the unidirectional current is produced by an electrical pump; this may fluctuate, causing deviation in the speed over a particular time period.

In order to establish that the above conditions had not affected either the boundary layer determinations or the threshold determinations, a particular experimental procedure was adopted as outlined below.

(i) For velocity profiles undertaken under Series 1, the LDA was used to provide information over three different cross sections along the oscillating plate, under a medium flow rate. At each cross section, vertical profiles (for successive heights of 1 cm, 3 cm, 5 cm, 7 cm, 9 cm and 11 cm) were measured at various distances (0 cm, 2 cm, 4 cm, 6 cm, 8 cm, 10 cm, 12 cm and 13 cm) from the main longitudinal axis of the plate. The two extreme cross sections were located at the points of maximum displacement of the test bed, from its mean position, encountered in the oscillatory and combined flow threshold tests i.e. 0.284 m. The results of the Series 1 measurements are listed in Table 5.1 and discussed subsequently in Section 5.2.2.

(ii) In order to establish the presence of any fluctuations in the power supply and flow generated by the electrical pump, the flow speed in the flume was logged at 20 Hz for 30 min. The LDA data were analysed then, using a Fourier transform method; this permitted the investigation of fluctuations at a frequency of 8 Hz, or less. The results obtained showed that fluctuations were not present within this frequency range.

(iii) Generally, the positional error of the instruments causes some experimental uncertainty. For example, the vertical dimension of the LDA Measuring Control Volume (MCV) results in the intergration of flow velocity measurements over a distance of 0.03 cm. Further, the accuracy of the location of the MCV using the graduated ruler, was considered to be ±0.125 cm. For repeatability, the ruler was placed in the same position for each new location of the MCV. The positional error of the MCV is only significant, therefore, in the region immediately

adjacent to the bed.

(iv) Another problem inherent in flume-type studies is the various bed roughnesses, which the flow experiences, along the length of the flume. Such differing roughnesses cause the flow to be 'non-uniform', in a downstream direction. Each time the streamlines meet a new roughness element, this results in modification to the boundary layer. As described in Section 4.5, the test-bed was surrounded by a rubber mat; this was covered with sand of the same median grain size as that contained within the sand-mud deposits investigated. The adoption of this experimental procedure ensured: (i) that overall flow conditions were turbulent; and (ii) that the boundary layer was as fully developed as possible, by the time it was overlying the test section of the bed. Possible modifications of the boundary layer, on coming into contact with different roughness elements, is shown in Fig. 5.1. The diagram shows that the velocity profiles measured above the sediment/water interface may incorporate the effects of a number (4) of partially-developed boundary layers.

It is possible to estimate the boundary layer thickness, under laminar flow conditions, using the expression

$$\delta = 5\left(\frac{\nu X}{U_s}\right)^{0.5} \qquad \textbf{(5.1)}$$

where X is the distance from the point of initiation of the boundary layer, in the downstream direction, and U_s is the velocity in the free stream. As explained in Section 2.2.1, there will be a critical point where the flow becomes unstable and exhibits small fluctuations i.e. 'the transitional point'. Likewise, there is a location where fully developed turbulent flow dominates. The values of X representing the locations where initially laminar, then fully developed turbulent flow

predominates, are given by $5x10^5$ and $3x10^6$ times the value of ν/U_s, respectively. A free stream flow speed of 25 cm s^{-1} suggests that fully developed turbulent flow is established at a distance of 8 m from the leading edge of the plate. This assessment is a strong indication of the necessity of surrounding the test section with a roughened bed. The farther upstream that the roughened section of the bed commences, then the farther upstream will be the transition to turbulent flow: similarly, the thicker will be the boundary layer associated with that roughness (since turbulent flow is much more efficient at transferring momentum than laminar flow).

5.2.2. Series 1 Velocity Profiles: Results and Discussion

The overall water flow structure within the flume channel close to the side walls and near to the oscillating plate was analysed, with particular attention being paid to flow over the test section. These results are presented in Table 5.1. It was not necesary to plot each of the velocity profiles, measured by the LDA, since the trends in the flow speed distribution can be extracted from Table 5.1.

For all the profiles at each of the 3 cross sections (middle and extreme upstream/downstream), the current speed increases with elevation above the bed. This trend must be expected in an infinitely-long channel, with a constant bed roughness and where the downstream pressure gradient is zero (dP/dX=0), provided that the boundary layer is extended throughout the whole of the depth of flow. In addition, along the same channel, the flow speed may be expected to increase with lateral distance from the side walls; this is to a point where the velocity at any elevation is greatest at the central longitudinal axis of the channel. The latter trend is not verified by

the present velocity profiles, as the data show that the maximum speeds occur on the left-hand side of the flume (in a downstream direction). This problem maybe is due to the pump inlet and appears to be inherent with this type of laboratory flume (Nash, 1987). Further, Table 5.1 indicates that the shapes of the lateral velocity profiles become flatter with elevation above the bed. This characteristic may be explained by the fact that, just above the plate surface and next to the glass walls of the flume (i.e. a vertical distance of 1 cm and lateral distances of ±13 cm), the combined influence of the plate and flume side walls retard the flow to a greater extent; this is in comparison to positions higher up in the profile.

In the threshold experiments, the measured unidirectional component of velocity assumes that the flow is both steady and uniform at all sections along the major axis of the plate (through which the test bed would pass). The results listed in Table 5.1 show that the flow speeds do not change significantly, at the same positions in each of the sections. However the flow streamlines will constantly try to realign, from the point where they enter the horizontal channel to where they meet the rails of the oscillating plate; finally, when they meet the plate itself (notwithstanding the different roughness elements encountered along the plate). Since the relative magnitudes of the velocity measurements obtained at the same positions in the different cross sections were not significantly different, the flow was considered to be steady and uniform.

Particular attention was paid in the measurement programme to flow over the test bed, in order to assess the possible effects of the side walls. With reference to Table 5.1 the flow appears to be reasonably uniform

within the 12 cm wide central part of the flume (±6 cm from the major axis of the plate). Although the velocity measurements imply that there is a difference of approximately 2 cm s^{-1} across this zone, this was considered to be not significant. During the threshold tests the movement of sediment did not appear to occur in any particular region of the test bed; this confirms the interpretation of flow characteristics, described previously.

5.2.3. Series 2 Velocity Profiles

The main aim of these particular measures was to investigate the nature of the velocity profiles for three different unidirectional flow rates, over (2) beds of unimodal sand (152.5 μm and 215 μm in diameter). These sand fractions were the sand component of the sediments examined for the purposes of the present investigation. This approach was adopted here, in an attempt to become acquainted with the turbulent flow expressions and terms associated with them. Although every effort was made during the threshold experiments (which incorporated a current component) to ensure that the flow above the test section was a fully-developed turbulent boundary layer, no initial assumptions were made regarding the flow regime. Hence, construction of the various velocity profiles demonstrated if turbulence, within the boundary layer, was developed or not.

For the construction of the boundary layer profiles, time-averaged current speeds (U) in the downstream direction were measured for a height (y) range of 0.4-10.0 cm, above the central area of the sediment/ water interface. If the flow was laminar, then a plot of y against U would yield a straight line. If the flow was turbulent, the corresponding plot would produce a curve,

which in a semi-logarithmic graph and with the height (y) on the logarithmic scale, would be a straight line (see below).

Having plotted the data, the graphs were examined closely in an attempt to identify any obvious linear trends. If any portion of the graph exhibited such a trend, this implied that the flow velocity profile was logarithmic; it was, therefore, turbulent in character. All the plots exhibited some degree of linearity, as expected. Having identified the flow as being turbulent, it remained to be determined whether or not the flow was rough, transitional or smooth (Section 2.2.2). This classification is somewhat difficult since the limits for each type of flow regime are set by $5<Re_*<70$, where Re_* (the grain Reynolds number) is equal to U_*k_s/ν. Since the shear velocity (U_*) is unknown, then the grain Reynolds number cannot be evaluated. As a result of this iterative problem, a graphical method was adopted to estimate U_* and, subsequently, Re_*; this is outlined below.

Firstly, all the measured values (Tables 5.2 to 5.7) from each boundary layer profile were plotted semi-logarithmically i.e. with the vertical distance from the sediment/water interface on a logarithmic scale (Figs 5.2 to 5.4). Then simulated velocity profiles, corresponding to known shear velocities, were compared with the observations. Such data were derived using the 'Universal Law of the Wall' for a smooth boundary (Eq. 2.11) and a rough boundary (Eq. 2.12), using U_* increments of 0.05 cm s^{-1} and heights ranging from 0.01 cm up to the upper limit of the constant stress layer[1]. In this way, an estimation of the shear velocity could be obtained.

[1]Note: See Middleton & Southard (1984) for the structure of unidirectional steady current boundary layers.

Subsequently, incorporating these shear velocity values into the formula used to derive the grain Reynolds number (see above) and substituting k_s (roughness length) with D_{50} of the beds, a determination of the type of the formed boundary layer was possible.

152.5 μm sediment bed: Results and discussion

The results are displayed in Figs 5.2a, 5.2b, 5.3a, 5.3b, 5.4a and 5.4b. The experimental points (x) follow generally a linear scale (logarithmic structure) within the lower part (constant stress layer) of the boundary layer. Regression analysis undertaken on these data derives correlation coefficients (r^2) of 0.98, 0.99 and 0.96, for slow, medium (close to the threshold of motion) and fast unidirectional flow rates, respectively. All these coefficients are significant at the 99% confidence level. Therefore, the overlying boundary layer is characterised by a turbulent flow regime.

Superimposing now the simulated (solid lines) velocity profiles (with slopes representative of different shear velocities (U_*)), derived by the 'Law of the Wall' for a smooth boundary, on the measured data which lie within the constant stress layer (Figs 5.2a, 5.3a and 5.4a), the following shear velocities values are produced: for a slow flow rate, U_*=0.70 cm s^{-1}; for a medium flow rate, U_*=1.00 cm s^{-1}; and for a fast flow rate, U_*=1.25 cm s^{-1}. Likewise, a comparison of the measured constant stress layer data with simulated profiles derived by the 'Law of the Wall' for a rough boundary, produces shear velocities of 0.60 cm s^{-1}, 0.90 cm s^{-1} and 1.18 cm s^{-1}, for a slow, medium and fast flow rate, respectively.

The derived shear velocities outlined above produce grain Reynolds numbers of < 5; this is the limit between the

smooth turbulent and transitional flow regimes (Sleath, 1984). Hence, the flow regime inside the inner part of the unidirectional flow boundary layer of the present investigation may be characterised as *smooth turbulent*. On the basis of this analysis, it is logical to assume that, for the finer-grained bed material examined in terms of erosion threshold and under flow conditions incorporating unidirectional currents, the associated boundary layer could be characterised in relation to smooth turbulent flow.

215 μm sediment bed: Results and discussion

An analysis, identical to that adopted for the velocity profiles associated with the 152.5 μm sand bed, was applied to the results related to the 215 μm sand bed (Figs 5.2c, 5.2d, 5.3c, 5.3d, 5.4c and 5.4d). Turbulent flow was verified by the high correlation coefficients (r^2=0.94 to 0.97) of the regression analysis, through the data points related to the lower part of the boundary layers.

Further, shear velocities were evaluated for all the flow rates, using the graphical method (see previously). Once again, subsequent calculation of the grain Reynolds numbers produced values less than 5. Therefore, in this particular case, the steady current-induced boundary layer could be defined as *smooth turbulent*.

5.2.4. The Derivation of Bed Shear Stress Related to the Threshold Experiments

Critical shear velocities associated with the threshold experiments were obtained using the expression for turbulent flow over a smooth boundary (Eq. 2.11). For the calculation of the shear velocities, U was substituded by

the recorded mean critical current speed, for y=0.4 cm. This height was located inside the constant stress layer, as the measured vertical velocity profiles (Series 2) showed (see, for example, Figs 5.3a and 5.3c). The water temperature during the threshold tests was approximately 19°C; thus, the kinematic viscosity of water was taken as 10^{-6} m^2 s^{-1}.

The current-induced bed shear stresses (τ_o) were calculated using the relationship

$$\tau_o = \rho U_*^2 \qquad (5.2)$$

where ρ is the water density (1000 kg m^{-3})

5.3. OSCILLATORY FLOW

Flow regime inside the wave boundary layers developed during the oscillatory flow erosion experiments have been examined as a function of the wave Reynolds number [$RE=U_{o(max)c}.A_o/\nu$] (the water temperature during the tests ranged from 17°C to 19°C; hence, the kinematic viscosity was taken as 10^{-6} m^2 s^{-1}) and the parameter A_o/D_{50}, according to the various published definitions, have been presented by Li (1954), Kajiura (1968) and Sleath (1974).

Li (op. cit.), undertaking measurements on trays of sediment (sand) oscillated in still water, observed that at values of RE higher than $1.6x10^5$ the flow was not turbulent throughout the complete wave cycle. Turbulence set in soon after the velocity passed its maximum, disappearing when the flow reversed. The value defined above is in reasonable agreement with a value of $RE=10^5$ recommended by Jonsson (1980) for design purposes. Vincent (1957) and Lhermitte (1958) performed experiments in wave flumes and identified RE values which were much lower than that proposed by Li (op. cit.). Lhermitte

(1958) has suggested that the much earlier transition to a smooth turbulent flow regime, observed by himself and Vincent (1957), was caused by a fundamental difference between their experimental arrangement and that of Li (1954). It has been shown elsewhere that, relative to axes fixed in the bed, the velocity distribution close to a bed oscillating in its own plane in still water is identical (for a given value of X) to the first-order solution for waves over a stationery bed. This result relates to both smooth and rough beds, provided that the roughness length (k_s) is small compared with the wavelength. However, second-order effects such as the mass transport velocity in the boundary layer over a flat bed, are not reproduced in an oscillating tray. Nevertheless, in most natural situations these effects are small and, consequently, it seems unlikely that they would have much influence on the transition from laminar to turbulent flow.

Further, Kajiura (1968), performing tests with oscillating beds of sand or gravel, has suggested that the transition from a laminar to turbulent flow regime occurs at wave Reynolds numbers (RE) defined by:

$$RE = 104\left(\frac{A_o}{D_{50}}\right) \qquad \textbf{(5.3)}$$

Finally, Sleath (1974, 1988) has argued that, for the onset of fully-developed turbulence, the most appropriate expression is:

$$RE = 5770\left(\frac{A_o}{D_{50}}\right)^{0.45} \qquad \textbf{(5.4)}$$

Based upon the concepts outlined above, the wave boundary layer formed during the oscillatory threshold tests can be characterised by a *laminar* flow regime (Fig. 5.5).

5.3.1. Shear Stress Calculation

The critical maximum wave-induced shear stress [$\tau_{o(max)}$] necessary to erode the sand-mud mixtures examined, under various wave conditions, was calculated using the 'Quadratic Stress Law',

$$\tau_{o(max)} = \frac{1}{2} f_w \rho U_{o(max)}^2 \qquad (5.5)$$

where the friction factor (f_w) used was abstracted from published curves (Kamphuis, 1975; see Fig. 5.6).

5.4. COMBINED FLOW REGIME

The boundary layers developed during the combined flow threshold tests, related to the co-linear and simultaneous action of steady currents and simulated waves, were studied by considering each component of the combined flow regime separately. For this analysis, it has been assumed that the current and oscillatory components do not affect each other; in other words, they have been considered to be uncoupled. According to Lighthill (1954), the above assumption is a good approximation to the problem, provided that the frequency of the oscillation periods is high enough to produce a thin oscillatory (wave) boundary layer, compared with the overall thickness of the steady current flow. The established wave conditions during the combined flow threshold tests were characterised by periods of 6 s and 10 s, associated with near-bed wave amplitudes of 0.283 m, 0.378 m, 0.468 m and 0.568 m. According to Jonsson's (1980) oscillatory boundary layer flow model, such wave conditions produce wave boundary layers with a thickness of a few millimetres. Therefore, comparison of the thickness of these oscillatory boundary layers with the flow depth developed during the combined flow tests

(13-17 cm) indicates that Lighthill's (1954) approach can be applied satisfactorily to the determination of the combined flow regime of the present study.

In addition, Sleath (1984) has presented a model which suggests that the combination of waves and currents at short wave periods is 'incomplete' i.e. that, due to the brief existence of oscillatory flow in any one direction, the wave boundary layer is not allowed sufficient time to be developed fully. Hence, in this case, the wave and current flows are said to be decoupled. The periods (6 s and 10 s) of the wave component of the present study of threshold under a combined flow regime may be considered as relatively short; therefore, Sleath's (op. cit.) condition is satisfied.

Considering the concepts outlined above, the combined boundary layer created during the threshold tests can be determined as outlined below.
(i) Based upon the investigation of the unidirectional current boundary layer (Section 5.2.3), it can be assumed that the flow regime within the boundary layer induced by the steady current component of the combined flow may be characterised as *smooth turbulent*.
(ii) Considering the definitions used for the determination of the oscillatory boundary layer (Section 5.3), the boundary layer induced by the wave component of the combined flow may be characterised as *laminar* (Fig. 5.7) [Note: It should be mentioned here that the boundaries appearing in Fig. 5.7 have been defined under purely oscillatory flow. The superimposition of a steady current probably causes modification of their present location. However, considering the assumption that steady current and oscillatory components were uncoupled, during the experiments, it may be concluded that the position of the boundaries of Fig. 5.7 does not change

significantly].

Considering the above discussion, the structure of the combined flow regime during the threshold tests can now be specified: a turbulent steady current is superimposed upon a thin laminar oscillatory boundary layer, which acts effectively as an additional roughness element for the unidirectional component (Grant & Madsen, 1979). This increased roughness, experienced by the unidirectional flow, increases the turbulent activity in the region enveloping the lower part of the steady (unidirectional) current-induced boundary layer. Hence, at the moment of the threshold of movement of sediment grains (since the oscillatory component in the combined flow experiments acting alone is insufficient to cause sediment motion), the turbulent eddies produced by the current component will penetrate into the laminar wave boundary layer and induce sediment movement; this occurs at a critical phase within the wave cycle.

The above mechanism was indicated on the basis of observation of bursts of grain/cluster motion when the oscillating plate was moving in a direction opposite to that of the steady current; this was at a phase in the wave period just after the mid-stroke position of the trolley.

5.4.1. Shear Stress Calculation

A first approximation of the applied shear stress may be derived from the vector sum of the current and wave stress components, derived independently:

$$\tau_{wc} = \tau_w + \tau_c \qquad (5.6)$$

Such linear superimposition is likely to be valid under laminar, rather than turbulent, flows.

In addition to linear superimposition, five methods/models can be used to calculate the resultant stresses under combined wave and current flows: (i) Jonsson (1966b); (ii) Bijker (1966); (iii) Grant & Madsen (1979); (iv) Christoffersen & Jonsson (1985); and (v) Sleath (1991). A very brief outline of each of these models is presented below.

Jonsson's (op. cit.) method is based upon the introduction of a combined wave-current friction factor (f_{cw}), defined by the individual wave (f_w) and current (f_c) factors:

$$f_{wc} = \frac{U_y f_c + U_{o(max)} f_w}{U_y + U_{o(max)}} \qquad \textbf{(5.7)}$$

The combined maximum shear stress is given then by:

$$\tau_{wc} = \frac{1}{2} \rho f_{wc} (U_y + U_{o(max)})^2 \qquad \textbf{(5.8)}$$

Bijker's (op. cit.) approach is one of the earliest and most commonly used, particularly for coastal engineering purposes. The method estimates the resultant combined wave-current shear stress (averaged over half the wave period) as

$$\frac{\tau_{wc}}{\tau_c} = 1 + \frac{1}{2} \left(\xi \frac{U_{o(max)}}{U_{da}} \right)^2 \qquad \textbf{(5.9)}$$

where U_{da} is the depth averaged mean water flow speed and ξ is a parameter dependent upon the mean water depth, physical roughness and the ratio of the thickness of the wave boundary layer to that of the laminar sub-layer.

The Grant & Madsen (op. cit.) and Cristoffersen & Jonsson (op. cit.) models are 'two layer models'. The wave boundary layer is confined to a level very close to the

sea bed, whereas that of the steady current extends from the wave boundary layer up to the water surface. Non-linear interaction of the oscillatory and steady flows, near a rough boundary, produces an increased turbulence which increases the shear within the wave boundary layer; this causes increased flow dissipation to be experienced by the current, as a result of an apparent roughness (y_{oa}) in excess of that related to the physical bed surface. The model solution for the velocity profile above the wave boundary layer (δ_w) is given by:

$$U_y = \frac{U_{*c}}{k} \ln\left(\frac{y}{y_{oa}}\right), \quad for\ y > \delta_w \qquad (5.10)$$

Inside the boundary layer it is expressed as

$$U_y = \frac{U_{*c}^2}{kU_{*cw}} \ln\left(\frac{y}{y_{oa}}\right), \quad for\ y < \delta_w \qquad (5.11)$$

where the apparent roughness height (y_{oa}) is due to both the wave boundary layer and the physical roughness (y_o) and U_{*cw} is the shear velocity inside the wave boundary layer (Note: The subscript 'cw' denotes wave shear velocity estimated taking into consideration the effect of the mean current). An iterative procedure is used whereby wave and current shear stresses are estimated from the mean velocity at a reference level, wave period, and the oscillatory component of the velocity. The maximum resultant shear stress is:

$$\tau_{wc} = \tau_c + \tau_{cw} \qquad (5.12)$$

Sleath's (1991) model has been developed to be more applicable to relatively rough beds. In this approach, no division into wave and current boundary layers is undertaken. According to this model, the wave friction factor is defined by:

$$f_w = 0.048 \left(\frac{A_o}{K_s}\right)^{-\frac{1}{4}} \qquad (5.13)$$

The solution for the mean velocity is

$$U_y = \frac{U_{*c}}{k} \ln\left(\frac{y + y_s}{y_o + y_s}\right) \qquad (5.14)$$

where y_s is a function of the wave eddy viscosity.

For the present investigation, the combined critical shear stress was calculated assuming linear interaction between the processes. Thus, the shear stresses have been calculated for the waves and currents separately, then added to produce the total critical shear stress. According to Kemp & Simons (1982) and Lee-Young & Sleath (1988), this method may be considered sufficiently accurate to be used for intermediate and turbulent flow conditions.

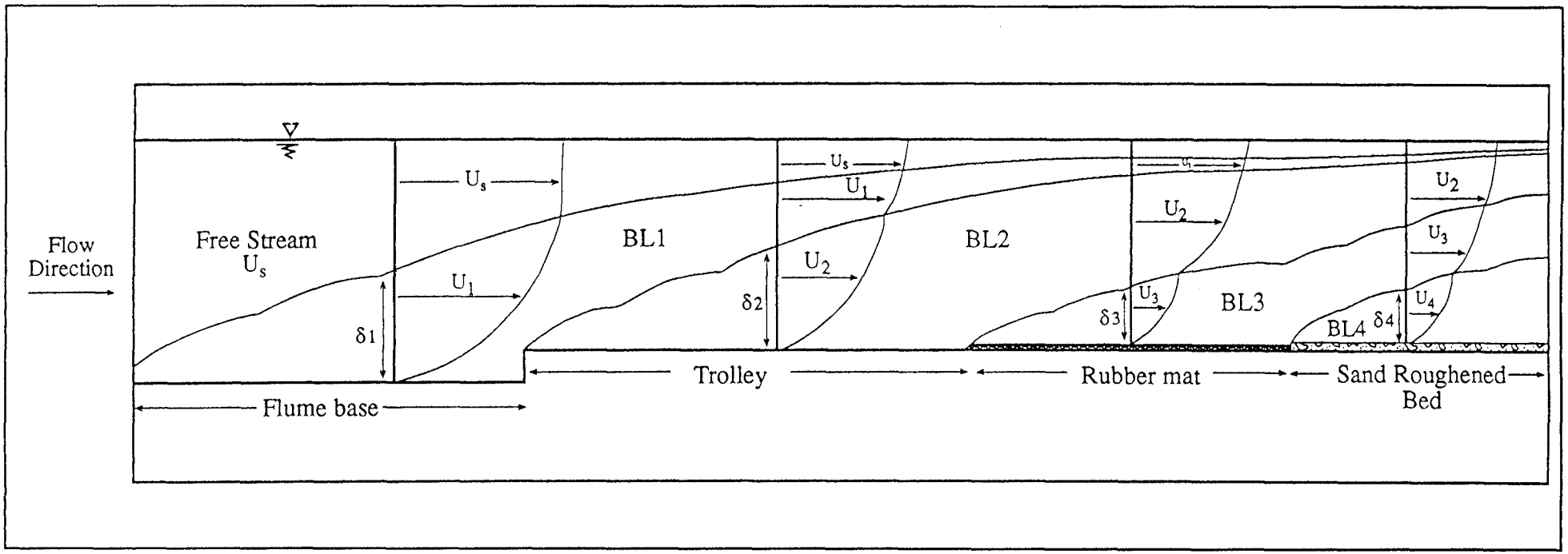

Fig. 5.1. Boundary layer modifications along the flume channel (schematic). Key: BL1, BL2, BL3, BL4—boundary layers; $\delta 1$, $\delta 2$, $\delta 3$, $\delta 4$—thickness of boundary layers; U_1, U_2, U_3, U_4—flow velocity within boundary layers; and U_s—free stream velocity.

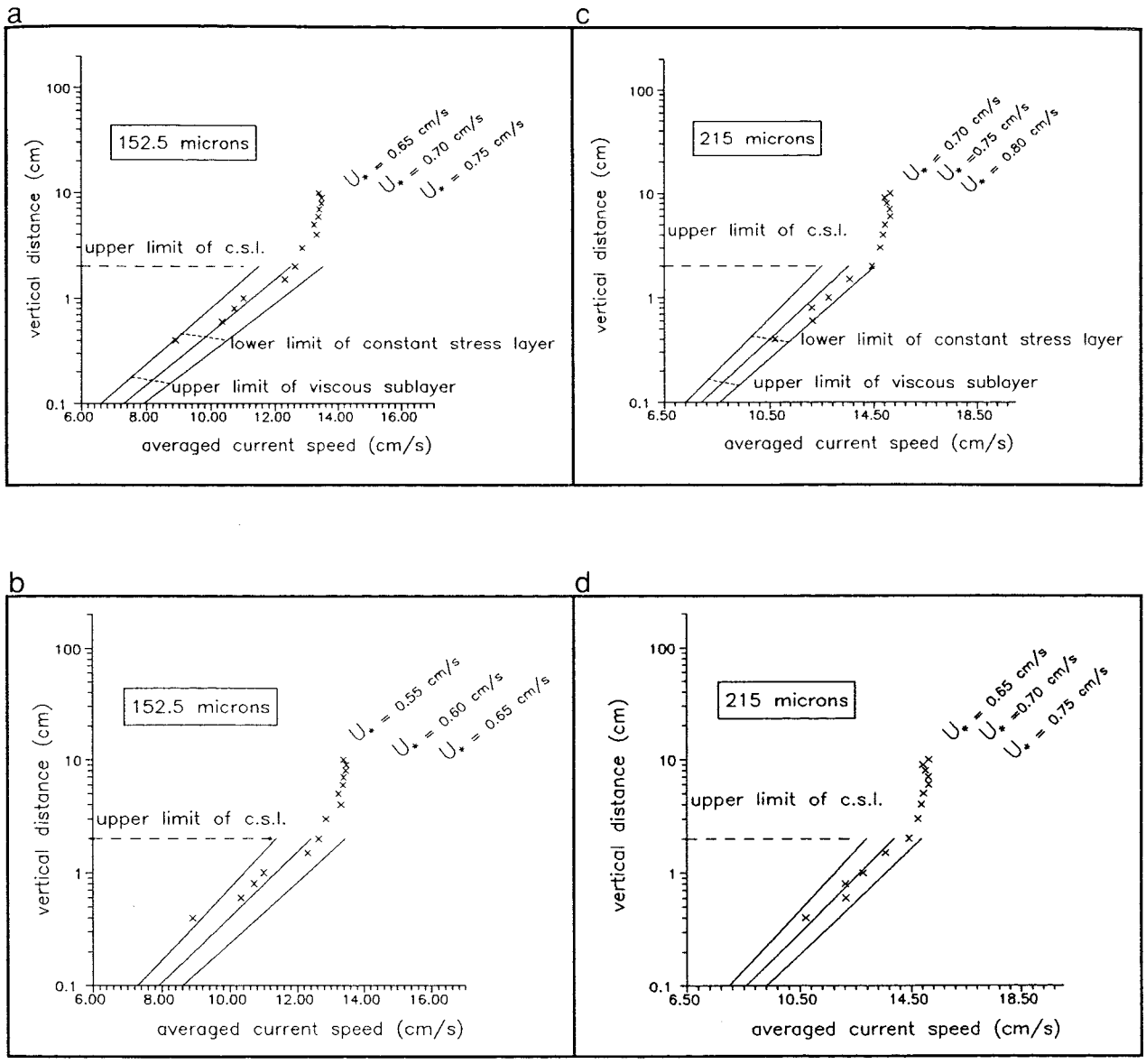

Fig. 5.2. Determination of shear velocity (U_*) above the sediment/water interface, for sand of 152.5 μm or 215 μm in size, associated with a *slow* flow rate, using the 'Law of the Wall' for (a,c) smooth and (b,d) rough boundaries (solid lines—simulated velocity profiles, x—measured velocity profile in the flume). The apparent boundaries of the constant stress layer (c.s.l.) and viscous sub-layer have been drawn in accordance with the definitions presented by Middleton & Southard (1984).

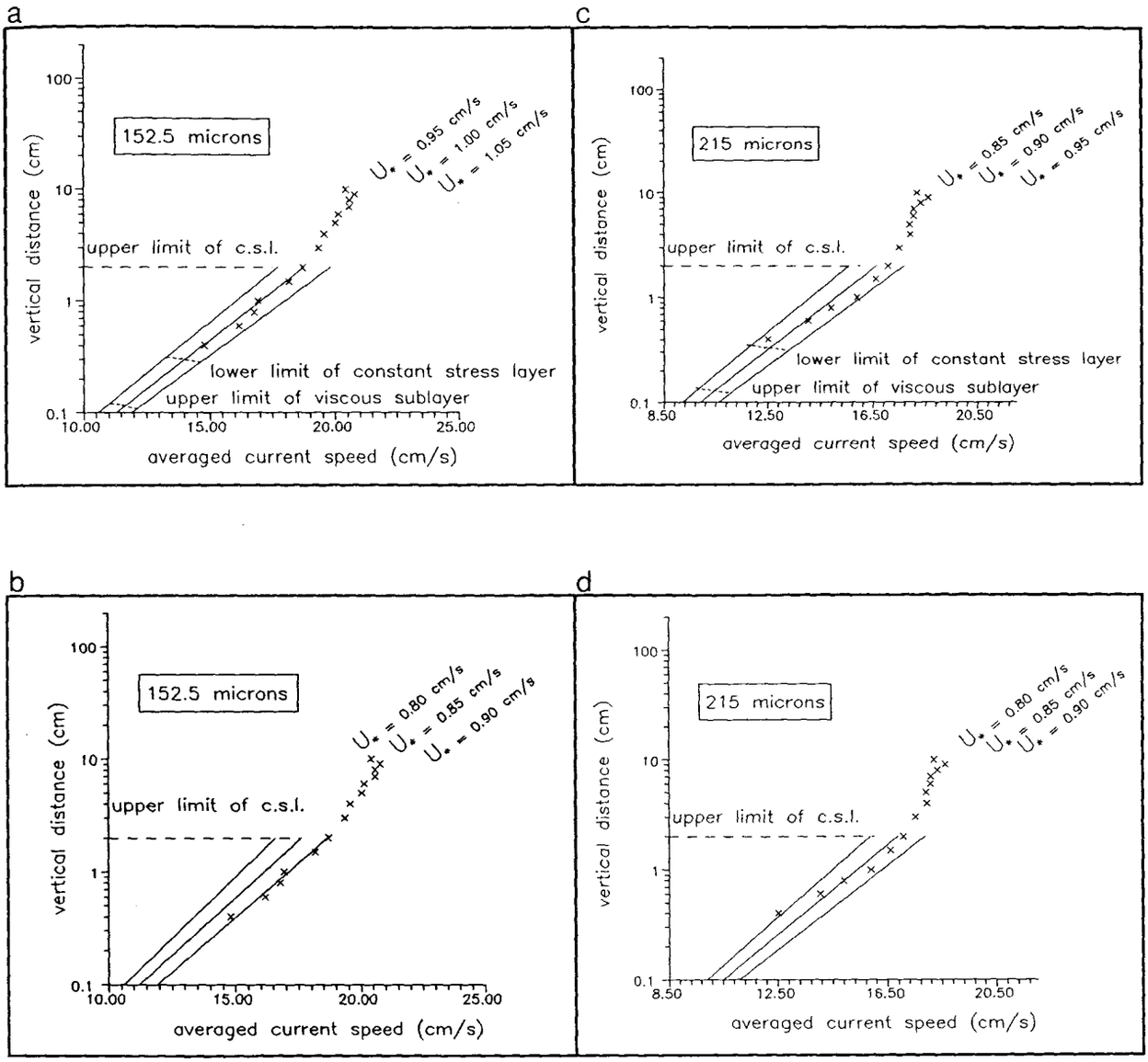

Fig. 5.3. Determination of shear velocity (U_*) above the sediment/water interface, for sand of 152.5 μm or 215 μm in size, associated with a *medium* flow rate using the 'Law of the Wall' for (a,c) smooth and (b,d) rough boundaries (solid lines—simulated velocity profiles, x—measured velocity profile in the flume). The apparent boundaries of the constant stress layer (c.s.l.) and viscous sub-layer have been drawn in accordane with the definitions presented by Middleton & Southard (1984).

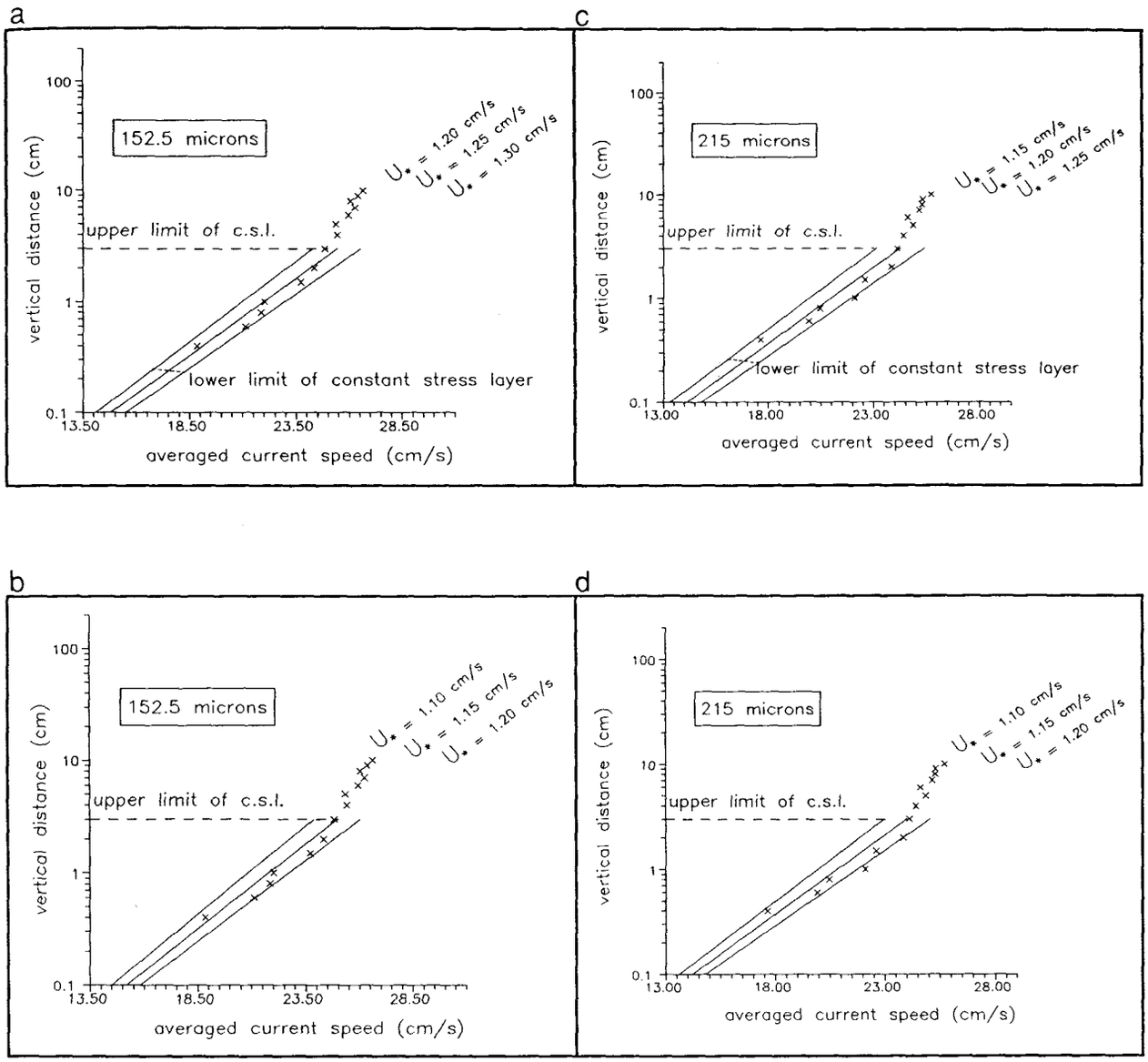

Fig. 5.4. Determination of shear velocity (U_*) above the sediment/water interface, for sand of 152.5 μm or 215 μm in size, associated with a *fast* flow rate, using the 'Law of the Wall' for (a,c) smooth and (b,d) rough boundaries (solid lines—simulated velocity profiles, x—measured velocity profile in the flume). The apparent boundaries of the constant stress layer (c.s.l.) and viscous sub-layer have been drawn in accordance with definitions presented by Middleton & Southard (1984).

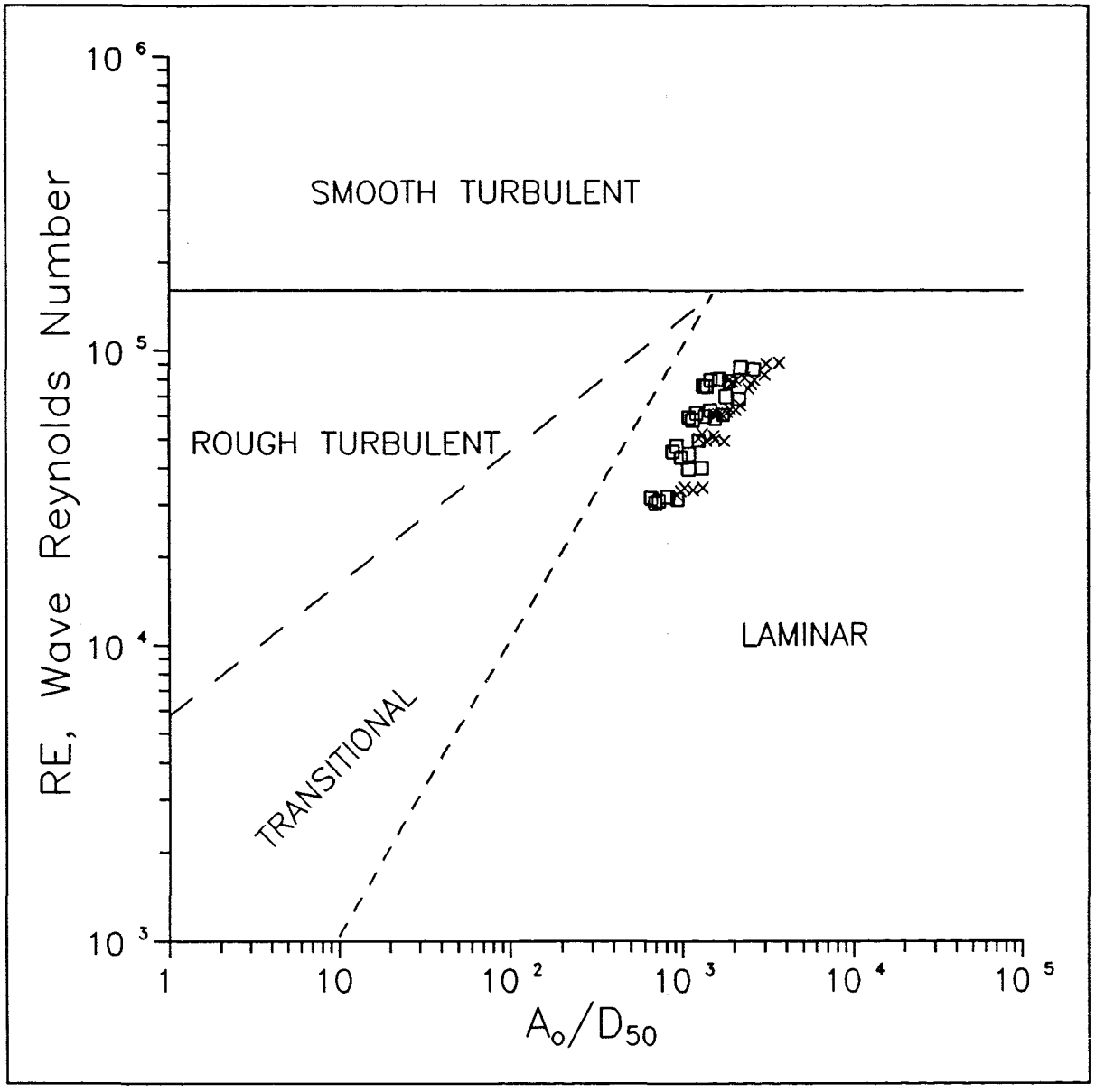

Fig. 5.5. Boundary layer conditions under the action of (simulated) waves, during the erodibility experiments, according to the definitions of: Li, 1954 (solid line); Kajiura, 1968 (small-stroke dashed line); and Sleath, 1974 (large-stroke dashed line). Key: x, mixtures containing 152.5 μm sands; and □, mixtures containing 215 μm sands.

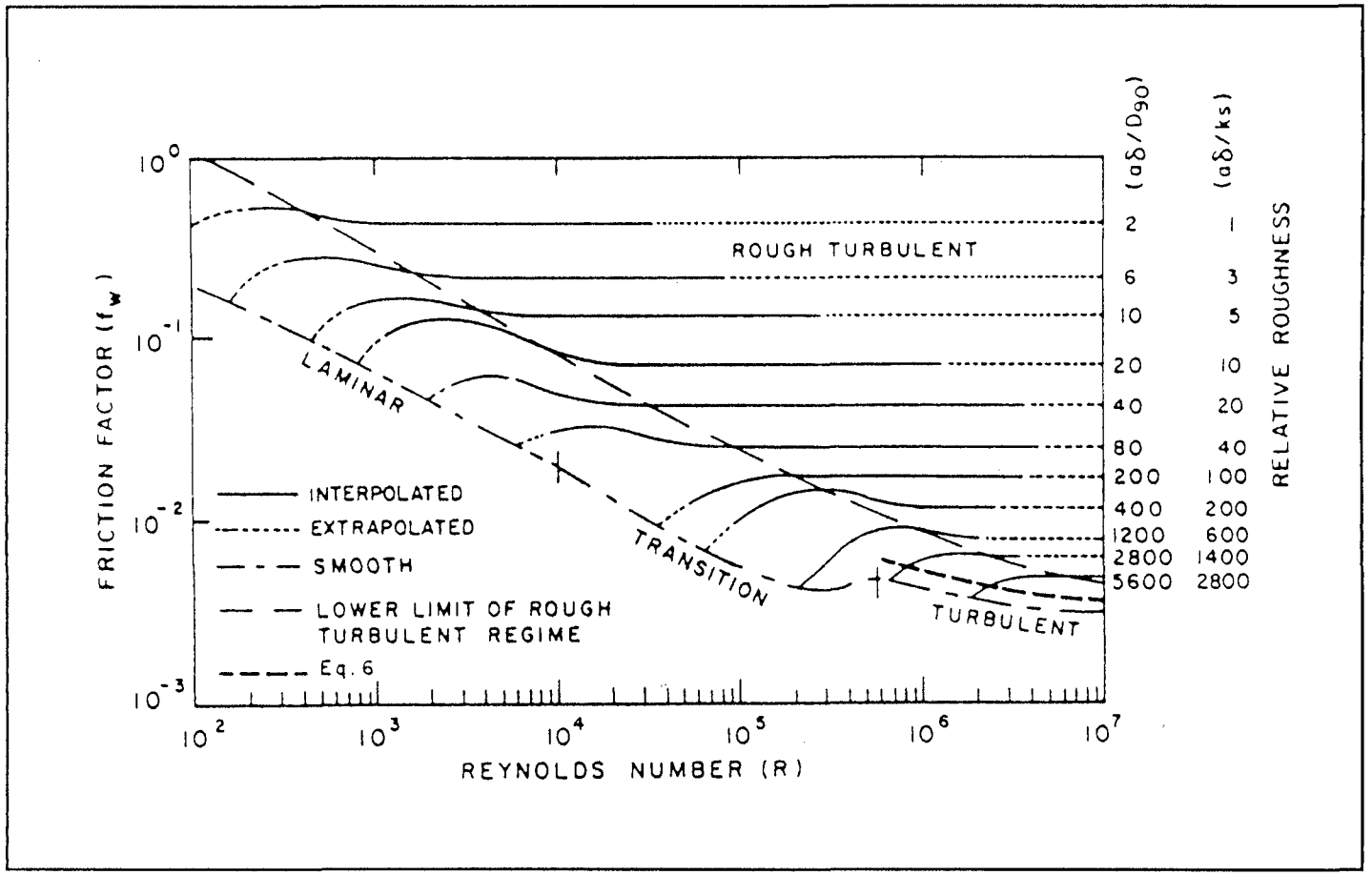

Fig. 5.6. Wave friction factor design diagram (from Kamphuis, 1975).

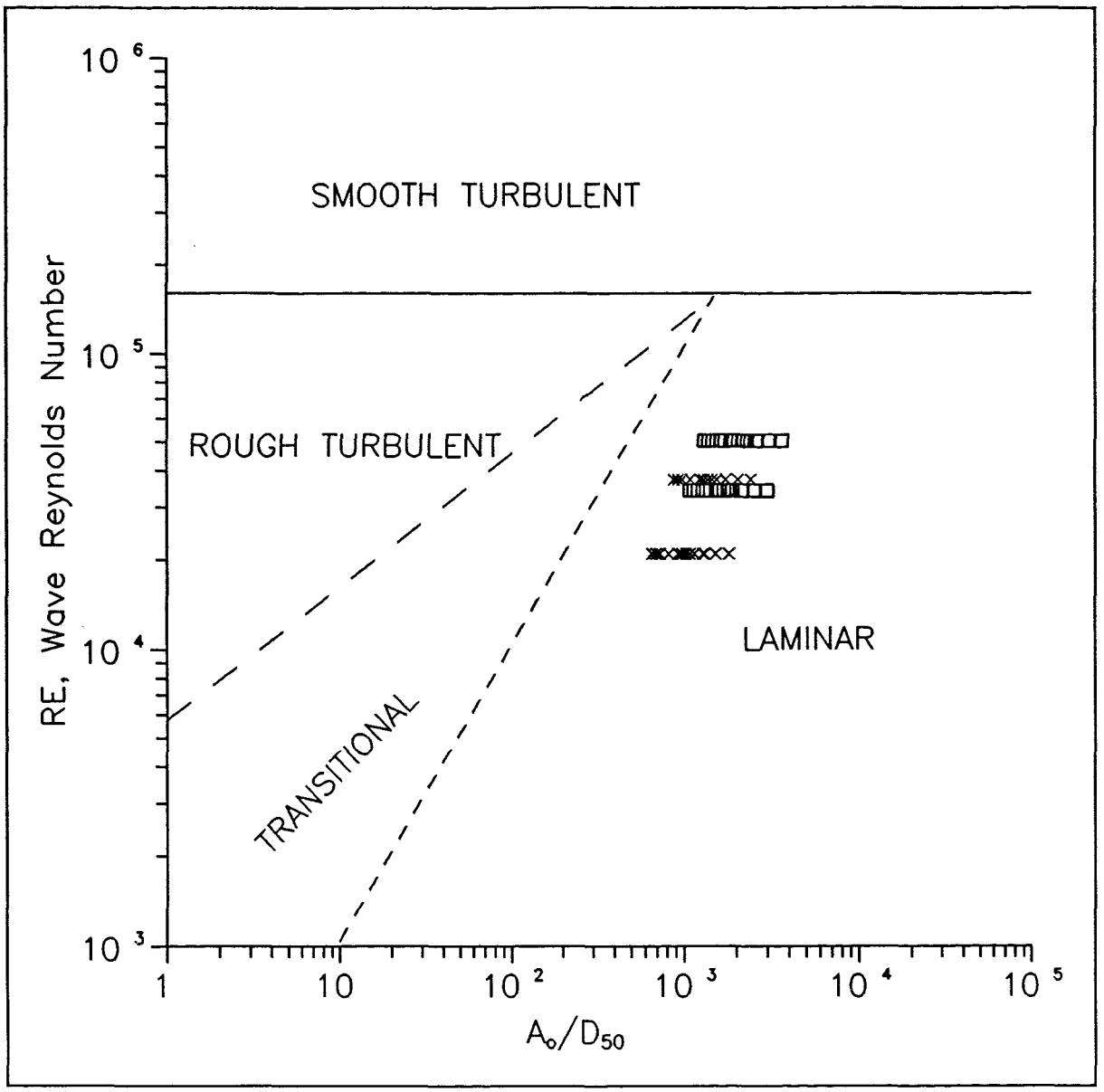

Fig. 5.7. Flow regime definition of the oscillatory component, during the erodibility experiments under combined flow [Li, 1954 (solid line); Kajiura, 1968 (small-stroke dashed line; and Sleath, 1974 (large-stroke dashed line)]. Key: x, wave periods of 10 s; and □, wave periods of 6 s.

MIDDLE CROSS SECTION															
height above the plate (cm)	LEFT SIDE OF THE FLUME (looking downstream) distance (cm) from the major axis of the moving plate							plate major axis	RIGHT SIDE OF THE FLUME (looking downstream) distance (cm) from the major axis of the moving plate						
	13	12	10	8	6	4	2	0	2	4	6	8	10	12	13
	CURRENT SPEED (cm/s)														
11	26.68	26.46	25.66	24.91	24.89	25.66	25.79	26.31	26.59	26.40	25.25	25.08	24.73	25.05	25.14
9	26.14	26.13	25.53	24.96	25.13	25.78	25.80	26.26	26.70	26.69	25.38	24.94	24.38	24.62	24.15
7	24.89	25.40	25.34	25.23	25.34	24.74	25.94	26.19	26.38	26.24	25.28	24.48	23.67	23.19	22.83
5	22.65	24.41	25.30	25.13	25.83	25.14	25.82	25.34	26.08	25.80	24.48	23.98	22.43	20.78	20.32
3	20.82	23.05	24.43	25.42	24.78	25.10	25.91	25.07	24.69	25.15	24.16	23.46	21.98	19.54	18.59
1	20.05	22.88	22.48	24.58	24.21	24.15	23.66	22.76	22.54	22.44	22.70	22.88	21.76	20.65	18.98
EXTREME UPSTREAM CROSS SECTION															
11	26.06	26.50	25.99	25.86	26.09	26.61	26.69	26.65	26.78	26.72	26.10	26.07	25.78	25.52	24.83
9	25.37	25.76	25.94	25.90	26.19	26.45	26.37	26.58	26.76	26.50	25.70	25.50	25.10	24.84	23.31
7	23.71	24.92	25.60	25.85	25.81	25.58	26.16	25.48	26.25	25.98	25.39	24.83	24.19	22.89	22.80
5	21.88	23.54	25.26	25.48	26.15	25.71	26.10	25.23	25.55	25.13	24.35	24.22	22.75	21.20	20.90
3	20.55	22.61	24.64	25.38	24.98	25.67	25.94	24.50	23.54	23.41	23.17	23.65	22.35	19.85	19.06
1	17.78	20.96	21.86	23.34	22.88	23.39	23.78	21.91	21.61	20.94	21.86	22.09	20.97	18.44	16.87
EXTREME DOWNSTREAM CROSS SECTION															
11	27.08	26.76	25.22	23.97	23.33	24.15	24.76	25.66	25.97	25.69	24.21	24.09	23.79	24.90	25.37
9	26.71	26.38	25.14	24.08	23.86	24.34	25.22	26.03	26.58	26.40	24.50	24.03	23.58	24.70	24.06
7	25.36	25.65	25.00	24.27	24.13	24.70	25.71	26.36	26.76	26.47	25.15	24.28	24.27	23.68	23.82
5	22.82	24.79	25.18	24.65	24.98	24.82	25.47	25.59	26.33	26.37	24.55	24.10	22.96	21.19	20.64
3	20.79	23.11	24.38	25.22	24.44	24.88	25.78	25.83	25.58	25.88	24.80	24.17	21.42	19.14	19.02
1	18.56	20.73	21.70	25.03	24.58	25.07	24.51	23.32	22.46	23.16	23.15	22.78	21.61	19.56	16.99

Table 5.1. Velocity measurements defining the overall structure of the unidirectional flow within the experimental flume channel (for explanation, see text).

vertical distance y (cm)	averaged current speed U (cm/s)	standard deviation σ (cm/s)
0.4	8.90	1.95
0.6	10.33	1.66
0.8	10.72	1.75
1.0	11.01	1.61
1.5	12.31	1.33
2.0	12.64	0.94
3.0	12.86	0.92
4.0	13.32	0.84
5.0	13.24	0.95
6.0	13.38	0.92
7.0	13.40	0.96
8.0	13.47	0.86
9.0	13.48	0.93
10.0	13.39	1.02

Table 5.2. Measured vertical velocity profile above the sediment/water interface containing only sand of 152.5 microns size, for a *slow* unidirectional flow rate.

vertical distance y (cm)	averaged current speed U (cm/s)	standard deviation σ (cm/s)
0.4	14.81	2.40
0.6	16.17	2.19
0.8	16.77	2.13
1.0	16.91	2.12
1.5	18.14	1.74
2.0	18.70	1.85
3.0	19.35	1.50
4.0	19.56	1.48
5.0	20.02	1.32
6.0	20.14	1.36
7.0	20.57	1.30
8.0	20.58	1.39
9.0	20.79	1.52
10.0	20.43	1.55

Table 5.3. Measured vertical velocity profile above the sediment/water interface containing only sand of 152.5 microns size, for a *medium* flow rate.

vertical distance y (cm)	averaged current speed U (cm/s)	standard deviation σ (cm/s)
0.4	18.87	3.06
0.6	21.14	2.81
0.8	21.87	2.78
1.0	22.05	2.63
1.5	23.72	2.40
2.0	24.35	1.99
3.0	24.84	2.16
4.0	25.44	1.86
5.0	25.35	2.14
6.0	25.96	1.97
7.0	26.27	1.70
8.0	26.06	1.86
9.0	26.39	1.79
10.0	26.64	1.77

Table 5.4. Measured vertical velocity profile above the sediment/water interface containing only sand of 152.5 microns size, for a *fast* unidirectional flow rate.

vertical distance y (cm)	averaged current speed U (cm/s)	standard deviation σ (cm/s)
0.4	10.70	2.06
0.6	12.13	1.83
0.8	12.11	1.80
1.0	12.75	1.70
1.5	13.56	1.48
2.0	14.42	1.11
3.0	14.74	1.09
4.0	14.86	0.97
5.0	14.93	1.03
6.0	15.13	1.00
7.0	15.11	1.06
8.0	15.00	1.16
9.0	14.91	1.06
10.0	15.12	1.15

Table 5.5. Measured vertical velocity profile above the sediment/water interface containing only sand of 215 microns size, for a *slow* unidirectional flow rate.

vertical distance y (cm)	averaged current speed U (cm/s)	standard deviation σ (cm/s)
0.4	12.51	2.21
0.6	14.03	2.15
0.8	14.91	1.90
1.0	15.89	1.91
1.5	16.61	1.48
2.0	17.08	1.24
3.0	17.51	1.32
4.0	17.94	1.15
5.0	17.91	1.31
6.0	18.06	1.25
7.0	18.07	1.22
8.0	18.33	1.39
9.0	18.62	1.41
10.0	18.20	1.30

Table 5.6. Measured vertical velocity profile above the sediment/water interface containing only sand of 215 microns size, for a *medium* unidirectional flow rate.

vertical distance y (cm)	averaged current speed U (cm/s)	standard deviation σ (cm/s)
0.4	17.65	3.68
0.6	19.91	2.38
0.8	20.46	2.54
1.0	22.12	2.40
1.5	22.60	2.17
2.0	23.84	1.90
3.0	24.11	1.77
4.0	24.41	1.52
5.0	24.85	1.59
6.0	24.60	1.88
7.0	25.15	1.91
8.0	25.29	1.77
9.0	25.31	1.87
10.0	25.70	1.74

Table 5.7. Measured vertical velocity profile above the sediment/water interface containing only sand of 215 microns size, for a *fast* unidirectional flow rate

CHAPTER 6

RESULTS AND DISCUSSION: UNIDIRECTIONAL FLOW

6. RESULTS AND DISCUSSION: UNIDIRECTIONAL FLOW

6.1. EROSION THRESHOLD DETERMINATIONS

In order to examine the reproducibility of the threshold determinations, using the experimental and observational techniques described in Chapter 4, statistical analyses were applied to the results obtained. The Set 1 and Set 2 experiments yielded standard deviations in the threshold, about the mean, of ±3% and ±2%, respectively. Hence, the order of magnitude of the error in the results and their reproducibility is about ±2.5%. Such a small error in the results provides justification for the selection of the Vanoni threshold criterion in the steady flow tests. However, it should be mentioned here that the difficulty in determining the exact moment at which the Vanoni criterion was satisfied for any particular sediment was, without doubt, the most difficult task in the experimental procedure. Likewise, it was identified that the finer-grained (muddier) mixtures were the most difficult to observe.

The experimental methodology (Chapter 4) describes how the unidirectional current speed was increased from zero (Set 1 tests) or a pre-threshold value (Set 2 tests) to a threshold speed, within a constant time period (2 min). Initially, the flow speed was increased rapidly; closer to the onset of sediment movement, it was increased more slowly (i.e. at 1/4 turn increments on the pump control valve). If individual grains or clusters of particles had begun to move in bursts, within 2 min of implementing the flow characteristics, then the experiment was considered to be satisfactory up until that point. The problem then was to establish critical erosion conditions as soon as possible, in order to prevent any potential stress

history effects on the derived value for the threshold current speed, $U_{c(0.4\ cm)}$ (cf. Tomlinson, 1993). This procedure proved to be a particularly difficult operation, since the threshold of movement process appeared to show no definite pattern. For example, in a particular test, the required critical transport rate was observed immediately after observing the initial bursts of grain movement; in another, it took several increments on the pump control valve (hence, more time) following observation of the initial sediment motion. The reason for this was that although some bursts of grain or cluster movement existed constantly, these were insufficient to satisfy the Vanoni criterion.

The method by which erosion threshold is defined, through extrapolating known measurements of sediment transport to a point where no transport takes place, was not adopted for the present study; doubts about its accuracy have been raised. According to several authors (Paintal, 1971; Taylor & Vanoni, 1972; Graf & Pazis, 1977; Lavelle & Mojfeld, 1987), there is not any flow velocity (other than zero) for which no sediment transport takes place. For example, Paintal (op. cit.) has reported flux measurements in a flume for particles with diameters of between 2.5 mm and 22.2 mm, as low as 6.9×10^{-9} g cm^{-1} s^{-1}. These grain sizes are larger than those used in the present study; however, such transport rates could be measured only when the sediment flux was allowed to accumulate for periods of up to 70 hours. Such results should be considered against the reliability of the threshold method outlined above.

It has been mentioned already that the establishment of erosion threshold conditions, during Set 1 and Set 2 tests, was achieved by turning the pump control valve in

1/4 turn increments. Thus, the actual increment required for critical motion could have been less than 1/4 turn. This possibility was investigated by undertaking velocity measurements for different flow rates, using the LDA located at a vertical distance of 0.4 cm above the roughened rubber mat. The results obtained showed that the addition of 3 sets of 1/4 turn increments, on a particular flow rate, could increase the flow by 0.5-1.0 cm s^{-1}. Considering that the actual flow rates required for threshold should be distributed statistically between, the valve settings, the probability that the error in the critical flows was 1 cm s^{-1} is relatively small.

6.2. DATA COLLECTED

The results of the threshold experiments, in the absence of any stress history of the bed (Set 1), are listed in Tables 6.1 to 6.3. Tables 6.1 and 6.2 represent time-averaged critical current speeds, at 0.4 cm above the sediment/water interface, with their standard deviations (σ); these are a measure of the existing turbulence level within the boundary layer. Also the σ value, for each particular run, is useful in estimating peak velocities; at such times, sediment movement is considered to occur (Grass, 1970). Table 6.3 lists the mean threshold current speeds for each of the mixtures tested together with the subsequent critical bed shear stress exerted by the fluid.

Graphical representation of the results in Tables 6.1 and 6.2 is shown in Fig. 6.1, where threshold current speed is plotted against mud content (M). These data indicate improved erosion predictability for mixtures associated with the larger sand size fraction (D_{50}=215 μm). The

standard error of fluctuation in threshold current speeds is, in general, lower than that observed for admixtures of the smaller grained sands. Further, the standard error bars are larger for the muddier admixtures (M > 30%); this implies greater difficulty in defining threshold, compared to that of the sandier deposits.

The influence of the clay (mineral) content on the erosion threshold of the mixed deposits is evident on Fig. 6.1. An incremental increase in the mud (and, subsequently, clay) content of the samples causes an increase in the critical (threshold) current speed. This increment would appear to be small at mud contents < 30%, corresponding to about 11% of clay; it is higher when the mud content (M) exceeds 30-40%. This trend is more apparent for the 215 μm sand admixtures. Furthermore, the threshold current speeds related to both mixtures demonstrate that the sediments associated with the smaller sand size (D_{50}=152.5 μm) are more difficult to erode.

The results of the water content measurements are presented in Tables 6.4 and 6.5. The water contents defined before the hydrodynamic tests are, for a particular sediment mixture, relatively consistent (reproducibility to within ±2%); this is indicative of an effective and reproducable mixing technique. Water content definitions, following the threshold tests of Set 1 (Tables 6.4 and 6.5) are, generally, lower than those derived before the threshold experiments. This difference can be attributed to the remoulding process, during the sediment loading in the flume test-section.

Variation in the soil bulk density, with mud content, is shown in Fig. 6.2. The densities were derived assuming

that the sediment mixtures were saturated; these were based upon the water content measurements, following the Set 1 threshold tests. Although a reduction in sediment bulk density with mud content is significant, it does not appear to affect the sediment erodibility (cf. Fig. 6.1). This relationship contrasts with that for non-cohesive granular materials, where stiffness and shear strength correlate positively with bulk density (Kraus & Smith, 1994).

Threshold results related to sediment beds subjected to a stress history (Set 2 tests) are listed in Tables 6.6 to 6.33. The data presented in Tables 6.6 to 6.19 demonstrate various combinations of pre-threshold current speeds (Note: Speeds of 70%, 80% and 90% of the original threshold could not be set accurate, hence, only an approximate condition was established) and flow durations, together with the newly-derived critical (threshold) values for each of the mixed sediments. Representative new mean threshold current speeds and subsequently derived bed shear stresses, for different stress levels, are shown in Tables 6.20 to 6.33.

Stress history effects on the threshold of movement are shown in Figs 6.3 to 6.6. These plots have been derived using the data presented in Tables 6.6 to 6.19. Generally, a more prolonged and intense stress history can increase considerably the original erosion threshold value of the sediment deposits (compare the relative positions of solid lines on the Figs, with dashed lines which represent the threshold conditions for a bed without any stress history). However, in some cases, the entrainment thresholds of the sediment beds without any stress history are higher than those related to beds subjected to particular stress histories (Figs 6.4b and

6.6b). In addition, Figs 6.3 to 6.6 show that, if the pre-stress period is fixed, then the critical (threshold) current speed increases with the pre-stress unidirectional flow velocity. Likewise, if the pre-stress velocity is fixed, then the threshold current speed increases with an increasing pre-stress period. However, the latter case is only a general trend. There are situations where, for a fixed pre-stress velocity, the threshold level decreases with increasing pre-stress duration (Figs 6.3b, 6.3c, 6.3d, 6.4a, 6.4b, 6.5b, 6.5c, 6.5d, 6.6a, 6.6c).

6.3. DISCUSSION

6.3.1. Set 1 Experimental Data

(a) Previous studies

Generally, other investigators have observed that the addition of small amounts (i.e. 5-10%, by mass) of cohesive material (clay) to sand enhances the erosion resistance of sediment deposits. On the other hand, small amounts of sand added to pure mud deposits can decrease or increase the erosion resistance; in some cases, an addition of 50% of sand can increase the critical erosion shear stress by a factor of 2 (Torfs *et al.*, 1995). Finally, there are other examples where the influence of the clay content on the erodibility of sediments is not significant. Experimental evidence confirming these trends is summarised below.

Flume experiments performed on 11 mixed sediments (Smerdon & Beasley, 1961), obtained from the bed of the Missiuri River (USA) and characterised by various levels of cohesion (with clay contents ranging from 15-58%),

have demonstrated that the critical tractive force was correlated positively and (significantly) with clay content (expressed as a percentage) (Fig. 6.7a).

Likewise, Peirce *et al.* (1970) have examined sediments with clay contents ranging from 0-31%, obtained from different locations within the Mersey Estuary (UK), showing that erodibility of the various soils differed considerably (by a factor of 10) and decreased with clay content (Fig. 6.7a).

Grissinger *et al.* (1981) have studied, in a portable flume, the erosion of streambank material (with sand contents ranging from 45% to 84%) of low cohesion sampled from Georgia, Alabama, Mississipi and Tennessee (USA); it was shown that the clay content of the mixtures correlated positively, and significantly, with the critical erosion shear stress.

Similarly, flume experiments (Kamphuis & Hall, 1983) carried out under steady (unidirectional) currents on mud-sand admixtures (with sand quantities of 1-50%), obtained from the bed of the Mackenzie River (Canada), have revealed that erosion resistance increased with clay content (Fig. 6.7b). The size of the eroded particles tended to be larger for mixtures with higher sand contents.

Unidirectional flow experiments (Nalluri & Alvarez, 1992), carried out on artificial sand-clay deposits with clay contents < 30%, have shown: (i) that critical erosion shear stresses are increased dramatically by several orders of magnitude, depending upon the type/ concentration of the cohesive additive, compared with non-cohesive sediments alone; and (ii) that the mode of

erosion for the cohesive sediment beds is in terms of clusters of various sizes.

In a somewhat different approach, Jones *et al.* (1993), introducing the photogrammetric analysis of cliff deposits located at Thompson Island (USA), showed that the highest rates of cliff erosion were associated generally with material containing the highest sand:mud ratios.

A unidirectional flume investigation (Torfs, 1994) into the erodibility of mixed non-cohesive/cohesive sediments has indicated a *transition zone* between the mode of the erosion of cohesionless (low percentages of fines) and cohesive sediments (high clay content). With smectite, for example, the transition occured at clay percentages of between 7% and 13%; for kaolinite, the transition was present for clay contents > 8-10% (Fig. 6.8).

In contrast with the trends outlined above, especially those postulated by Kamphuis and Hall (1983), laboratory and *in-situ* erodibility tests performed on artificially-prepared mud-sand mixtures (with sand contents not exceeding 50%) (Williamson & Ockenden, 1992) and naturally-mixed sediments (predominately muddy) (Williamson, 1992), have indicated that the presence of sand *increased* the shear stress required for erosion. In this case, it would appear that the sand assisted drainage of the sediments, resulting in more rapid compaction (cf. Terwindt & Breusers, 1972). However, in most cases, the mud appears to have been consolidated to a (surface) shear strength greater than the critical erosion stress required for sand (McCave, 1984).

Finally, flume experiments performed on natural sediment

mixtures, sampled from different offshore locations in Texas (USA), containing different proportions of sand, silt and clay (Smerdon, 1964; Moherek, 1978), showed similar erodibility between the various mixtures Figs 6.7a and 6.7b).

(b) The present study

On the basis of earlier arguments (Dyer, 1986; Raudkivi, 1990), that a clay mineral content of 5-10% (by weight) is high enough to dominate the sediment erodibility characteristics, the relationship shown on Fig. 6.1 can be explained. In a bed of pure sand, no cohesion exists between the particles: the pores between the particles are filled with water (and, sometimes, air). As the mud content (M) increases, the clay mineral content (consisting predominately of illite, kaolinite and expansive clays) acts as a binding agent for the sand and silt quartz grains of the sediment deposit i.e. cohesive forces exist between the sand/silt and clay particles, increasing their resistance to erosion. From the double layer theory (Section 2.3.2), it may be concluded that sand/silt-clay bonds are relatively strong, as the sand and silt quartz particles do not carry clouds of ions around them. Hence, these bonds are not dependent upon the composition of the pore water. Therefore, the strength of a sandy bed with small amounts of clay minerals is determined by the strength of the clay-sand/silt bonds and will increase with increasing the clay content. At a critical clay (mineral) content of 11-14%, the sand/silt quartz particles become separated from each other and a matrix of clay particles is formed, which incorporates the sand and silt grains. Now, the shear strength of the deposit will be determined by the strengths of the sand/silt-clay and clay-clay bonds. The

strength of the clay-clay bonds is a function of the composition of the pore water for a given mineralogical composition. It has been shown (Kandiah, 1974) that, in a fresh water enviromment, clay-clay bonds are stronger than sand-clay bonds. Therefore, erosion of the muddier samples of the present study (clay quantities > 11-14%) will be controlled mainly by the resistance of their clay fraction. Taking into consideration that this clay is particularly cohesive (Stone & James, 1992), it is quite reasonable for the muddier mixtures to withstand the more intense steady current flows.

It should be noted that the presence of organic matter within the mud fraction of the present admixtures, although limited in amount (< 4%), could lead to the development of microbial communities which might contribute to the stability of the beds. However, in order that these microbial communities should act in this way, they need to be grown in sufficiently dense populations; this could happen, but provided that organic or inorganic nutrients existed in the water environment and that enough time (some days) was allowed for the development of microbes. During the present investigation, the water was free of nutrients and individual sets of hydrodynamic experiments were not undertaken over very long time periods (a few hours, maximum). Hence, microbial influence on the observed increased sediment stability can be considered as insignificant.

The greater resistance to erosion shown by the mixed sediment deposits associated with the finer sands (Fig. 6.1) may be explained: (i) in relation to adhesive and cohesive forces between the smaller grains; and (ii) by the fact that the smaller sand grains tend to have

higher friction angles (ϕ) and, therefore, can withstand higher traction forces (Kirchner et *al.*, 1990). The latter authors have measured friction angles in water-worked sediment beds and have demonstrated a negative power-law correlation between friction angle and median grain size of the bed.

The trend identified above is consistent approximately with the Hjulstrom's curve (1935); this was prepared originally to explain the relationship between the depth-averaged velocity across the transverse profile of a river and the size of unimodal sediment particles, for the three states of erosion, transportation and deposition.

Comparing now the results of the present study (Table 6.3) with these of previous investigations (Smerdon & Beasley, 1961; Peirce *et al.*, 1970; Kamphuis *et al.*, 1983; and Torfs, 1994; Figs 6.7 and 6.8), it is clear that there is a considerable dissimilarity related to the incremental rate of change of critical shear stress in relation to an increase in the clay content within a sediment. Such variability may be the result of experimental error, variation in experimental techniques, clay properties (i.e. clay fabric, interparticle bonding, clay colloid chemistry), and the use of different criteria to define the onset of erosion.

Figure 6.9 presents a comparison of the results of the present study with the Miller *et al.* (1977) envelope. This erosion band was produced by selecting various threshold data, derived in laboratory flumes, concerning non-cohesive particles (rounded or spherical, of nearly uniform in size). The presence of cohesion in sand-mud admixtures has a marked influence on the rate of the

critical shear stress increment, as compared with that related to non-cohesive sediments; this is represented by the solid lines shown in Fig. 6.9. The increase in critical shear stress associated with sand-mud admixtures, as the Re. value becomes gradually lower, is more dramatic. This pattern is similar to that identified by the Nalluri & Alvarez (1992) investigation (Fig. 6.9) (Note: The different orientation in the latter data is due to the fact that these researchers have calculated Re. on the basis of the D_{50} of the mixture being the median diameter of the predominant sand fraction). Finally, it is surprising that the critical shear stresses associated with the sandier deposits of the present study lie below the Miller *et al.* (1977) band (Fig. 6.9). The sand fraction of the sediments used in the present investigation is angulary shaped; therefore, they should be characterised by higher friction angles (Kirchner *et al.*, 1990) and, subsequently, by higher tractive forces than those associated with Miller *et al.* (op. cit.) envelope.

6.3.2. Stress History (Set 2 Experiments)

The only mention of the effects of stress history on sediment erodibility appears to be that of Madsen & Grant (1976), in attempting to explain their oscillatory flow data plotting above the Shields curve. Consequently, this section of the text describes the importance of stress history to threshold experiments, offering a possible mechanism which can explain the stabilisation effects of the stress process.

Grass (1970) introduced the concept that each individual sediment particle on a bed can be ascribed a certain critical shear stress value τ_{grain} which, if exceeded, the

particle moves. The values of τ_{grain} can be combined into a probability density function. In a similar manner, a probability density function can be produced for the instantaneous shear stress that each surface particle receives from the overlying flow (τ_{flow}). Both of these distributions have exactly the same number of values of shear stress, as in the population samples. For any surface grain on the bed, at any instant if $\tau_{flow} > \tau_{grain}$, then the grain will move. Upon increasing the flow speed from zero, the maximum instantaneous shear stress applied to the bed is insufficient to erode even the particle requiring the least shear stress to cause it to move. Hence, the two distributions do not overlap and surface grains do not move.

An observer, having noted that there is not any movement over a nominal period of time, then increases the flow rate by a nominal increment (Note: 'nominal' is used here because information regarding the period of observation over which it was decided whether or not critical flow conditions had been reached, is not presented in the literature; further, if critical flow conditions had not been reached, there is not any information available regarding the increment in current speed for the next period of observation to commence). The observer increases then the flow rate, until conditions are reached where the highest value of the shear stress τ_{flow} is equal to the shear stress τ_{grain} required to move the most unstable grain on the bed. At this point, there is a very remote possibility that this shear stress will be applied to the most unstable grain: It is more likely, however, that this stress will be applied to a grain which has a higher value of τ_{grain}. Hence, at this stage there is unlikely to be any movement on the bed.

The observer increases, therefore, the flow such that the two distributions overlap; this increases the probability that, for any particular grain, the value of τ_{flow} which is applied is greater than or equal to its own critical value (τ_{grain}). At this stage, a few grains are likely to be moving and the observer has to decide whether or not the selected threshold criterion has been satisfied. If critical conditions have been met, then the experiment may be assumed to have been completed. Otherwise, the observer increases the flow rate once again, so that a condition is reached eventually whereby the amount of grains where $\tau_{flow} \geq \tau_{grain}$ satisfy the threshold criterion.

The stress history influence will be initiated as the flow velocity is increased, from a zero value: at this time, the unworked sediment bed has its loosest packing arrangement, incorporating numerous pore spaces (Kirchner *et al.*, 1990). Laminar flow forces within the viscous sub-layer of the boundary layer may cause the most unstable grains (or clusters of grains) to pivot, to establish a more stable position. As the flow becomes more turbulent, the weakest eddies penetrate the bed and flow through the pore spaces within the sediment. Approaching the threshold of motion which depends upon the selection of the threshold criterion and the rate at which flow is increased, the permeating flow creates skin friction on the loosely-packed grains; this causes them to shift gradually, or vibrate. In this way, the bed becomes more compact and resistant to erosion. Grains or aggregates which do not satisfy the threshold criterion find more stable positions; these are either their initial locations (if they have settled slightly, or if they have re-orientated themselves to find a more streamlined position (Rusnak, 1957)) or positions farther downstream. Grains (or aggregates) being transported

collide with other grains or clusters of grains, causing them either to settle into a more stable location or be eroded themselves.

Experiments in which the overlying water flow has been increased slowly will produce a compact bed sample with strong particle interlocking; therefore, it would be more resistant to erosion. If the flow is increased rapidly, turbulent eddies approach the sediment bed with high energy whilst the sediment is still highly porous and, hence, when the interlocking is weak.

It is apparent, therefore, that the effect of stress history will depend upon the selection of a threshold criterion. Thus, before a criterion requiring a significant level of sediment transport is satisfied, it may be subject to more stress history discrepancies. For example, if the threshold criterion is satisfied when transport rate is Q in a particular experiment, then the criterion is not satisfied when transport rate is < Q, but the bed has an increased opportunity for compaction. Hence, the probability density function of τ_{grain} will change. It is arguable then that the probability density function for τ_{grain} will change constantly, to become more resistant to erosion from the moment the flow rate is increased from zero.

Figures 6.10 and 6.11 show the variations of the critical bed shear stress with mud content, under different stress levels. These data reveal a more significant change in the erosional behaviour of sediment mixtures with M > 40%, as compared with that related to beds without any stress history; this is represented by the dashed lines in Figs 6.10 and 6.11. This pattern provides evidence that an additional process to that outlined

above (i.e. stress history) must contribute to the stability of the intergranular structure of such mixtures. Previous experiments undertaken under steady flow conditions (Institution of Civil Engineers, 1985) have shown that, when a cohesive sediment is subjected to prolonged flows below the erosion threshold, there is a 'time-hardening' effect; with this, the resistance to erosion increases in response to rapid consolidation of the sediment bed. Hence, the muddiest deposits (M > 40%) of the present study may be subjected to this particular process, during the stress history tests.

In conclusion, it should be noted that stress history results related to sediment erodibility emphasise the difficulty in defining *in-situ* critical motion conditions. In coastal and shallow marine environments, physico-chemical and biological factors, together with prolonged flow durations and variable wave- or current-induced shear stresses applied to the natural sediment beds, could alter their primary erosive characteristics.

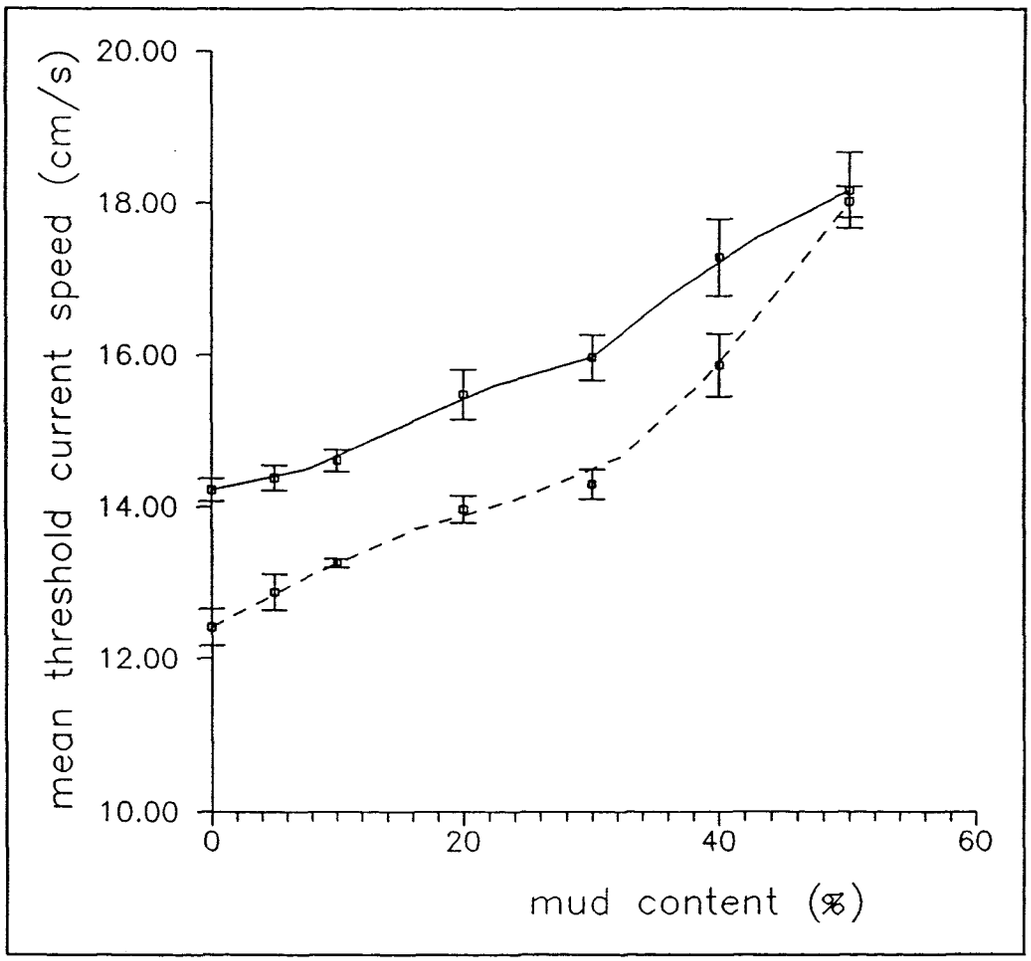

Fig. 6.1. Variation in the mean threshold current speed, with mud content, for mixed sediments under unidirectional flow. The mean and standard error of the mean are shown (Key: Solid line—mixtures containing the 152.5 μm sands; and dashed line—mixtures containing the 215 μm sands).

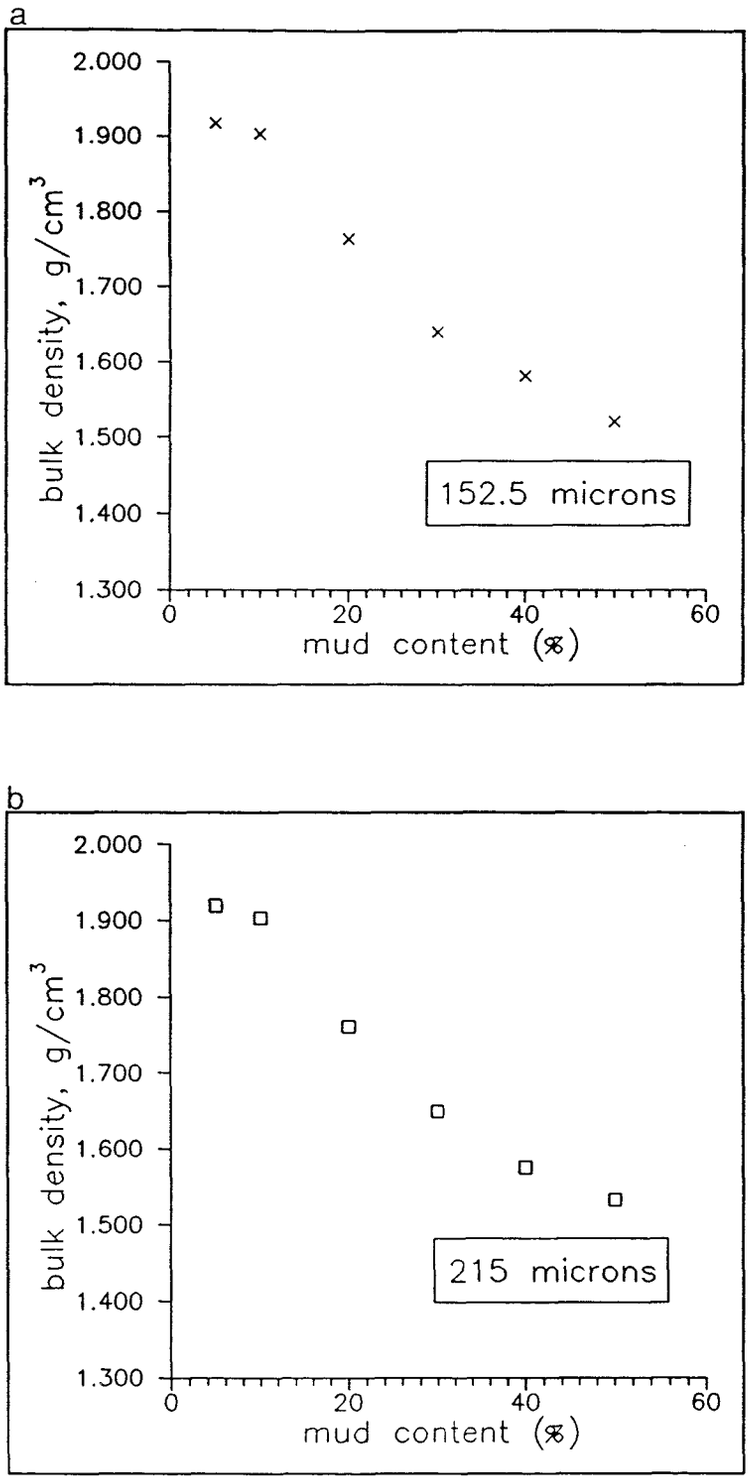

Fig. 6.2. Variation in the bulk density with mud content, for the various sediments under investigation: (a) 152.5 μm sand mixtures; and (b) 215 μm sand mixtures.

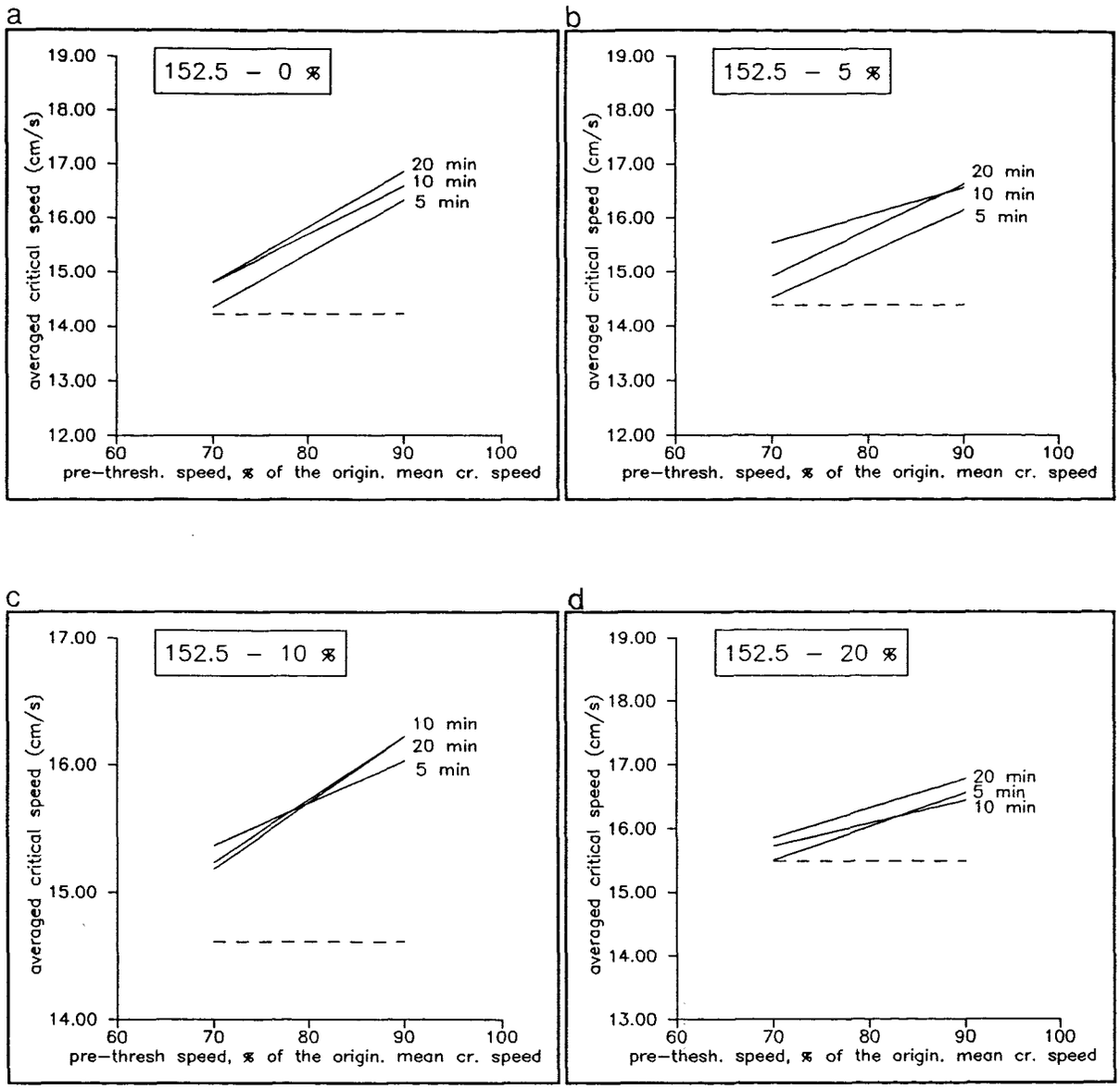

Fig. 6.3. The influence of stress history on the original threshold current speed (dashed line) of the mixtures containing the 152.5 μm sands and mud contents of 0%. 5%, 10% and 20%, respectively (Note: Values close to the edges of the solid lines represent unidirectional flow durations).

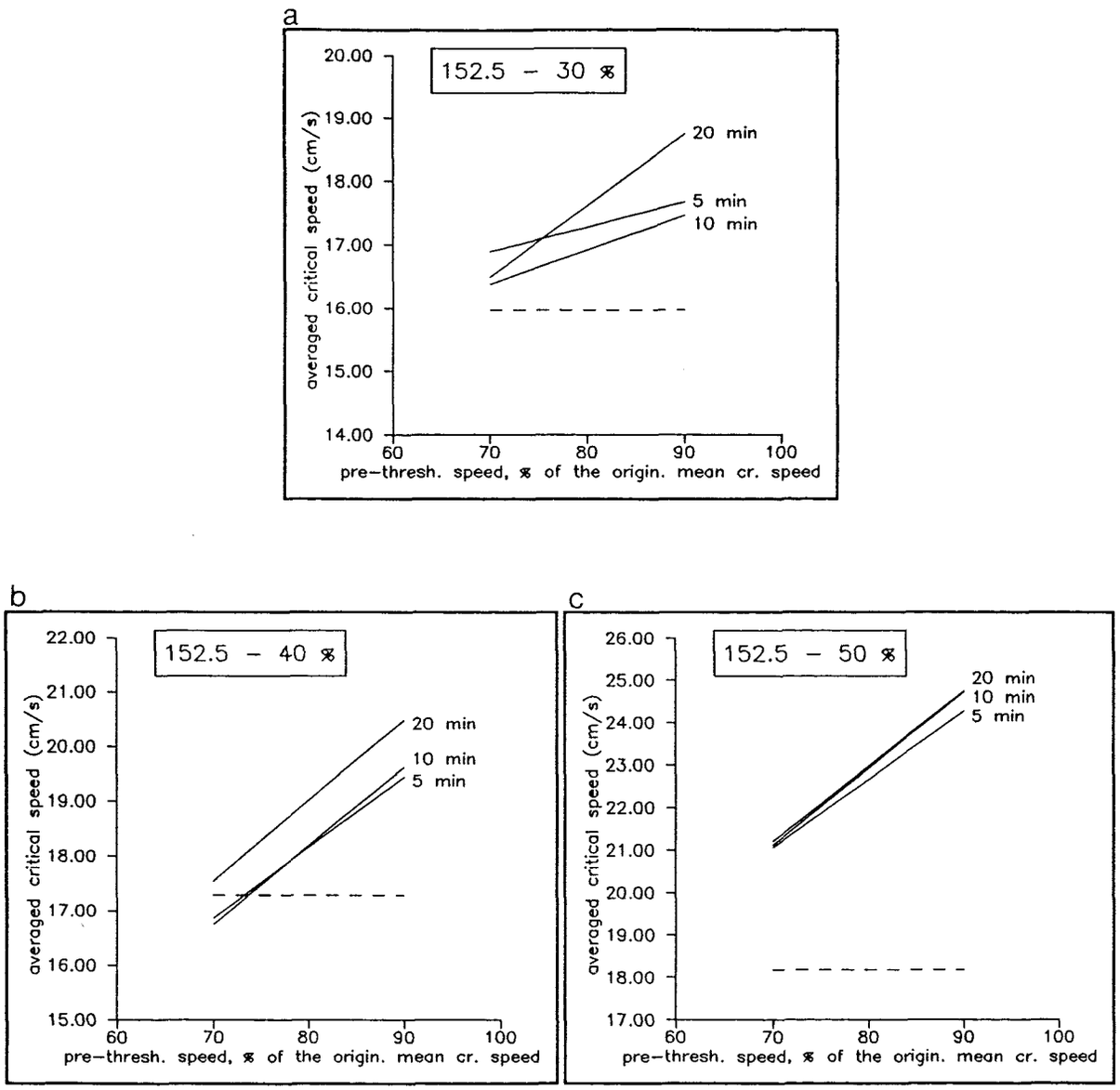

Fig. 6.4. The influence of stress history on the original threshold current speed (dashed line) of the mixtures containing the 152.5 μm sands and mud contents of 30%, 40% and 50%, respectively (Note: Values close to the edges of the solid lines represent unidirectional flow durations).

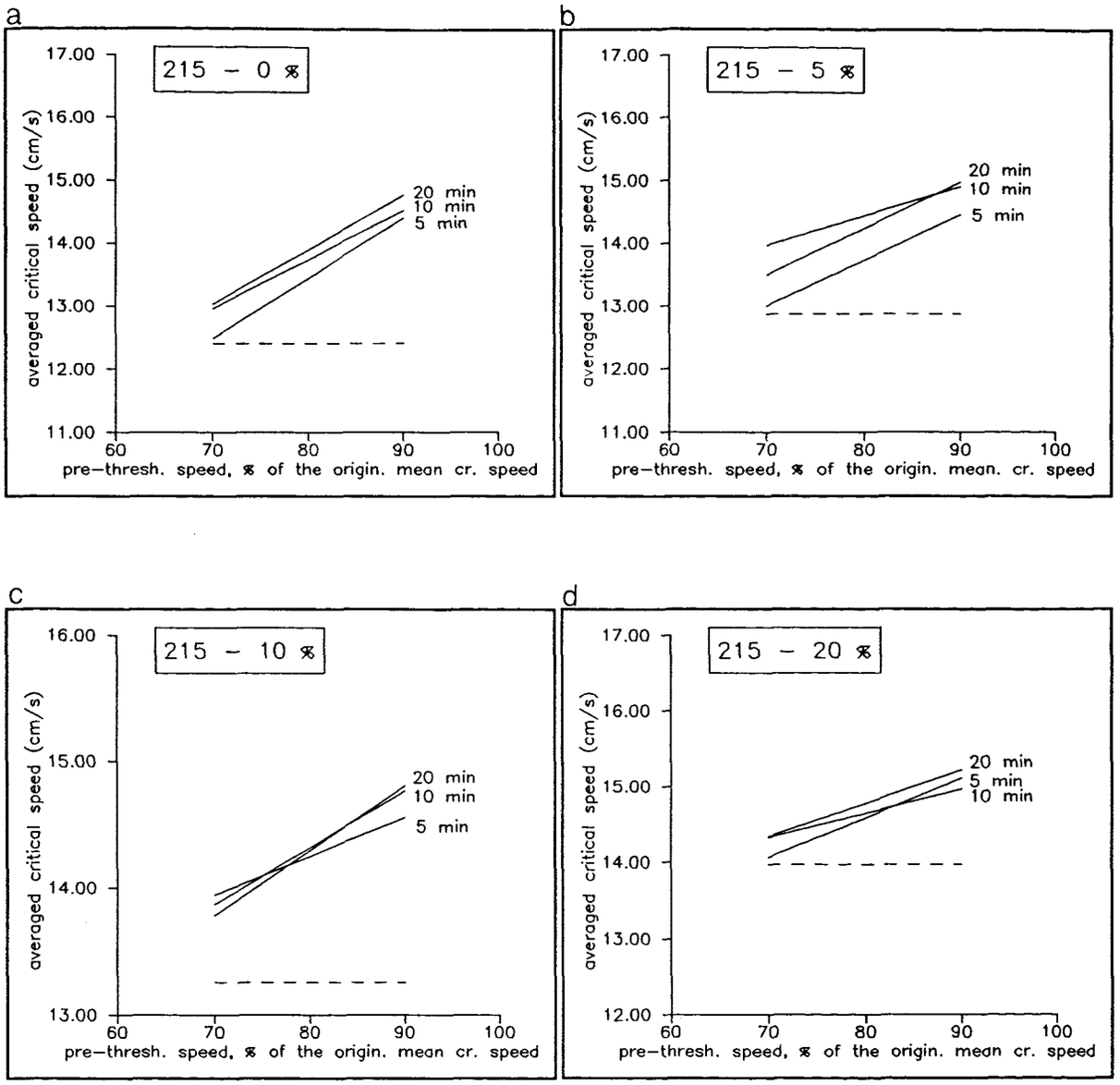

Fig. 6.5. The influence of stress history on the original threshold current speed (dashed line) of the mixtures containing the 215 μm sands and mud contents of 0%, 5%, 10% and 20%, respectively (Note: Values close to the edges of the solid lines represent unidirectional flow durations).

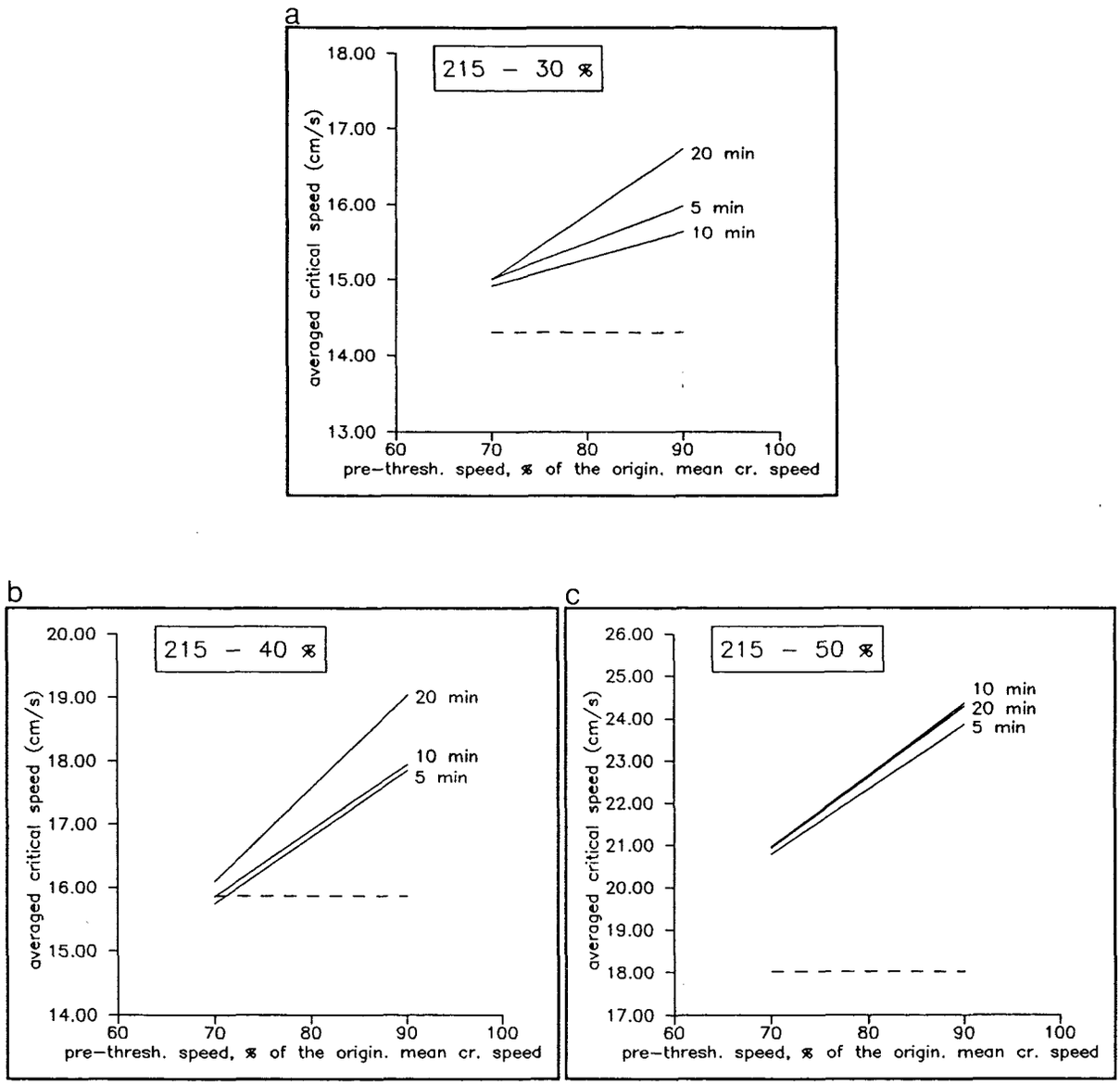

Fig. 6.6. The influence of stress history on the original threshold current speed (dashed line) of the mixtures containing the 215 μm sands and mud contents of 30%, 40% and 50%, respectively (Note: Values close to the edges of the solid lines represent unidirectional flow durations).

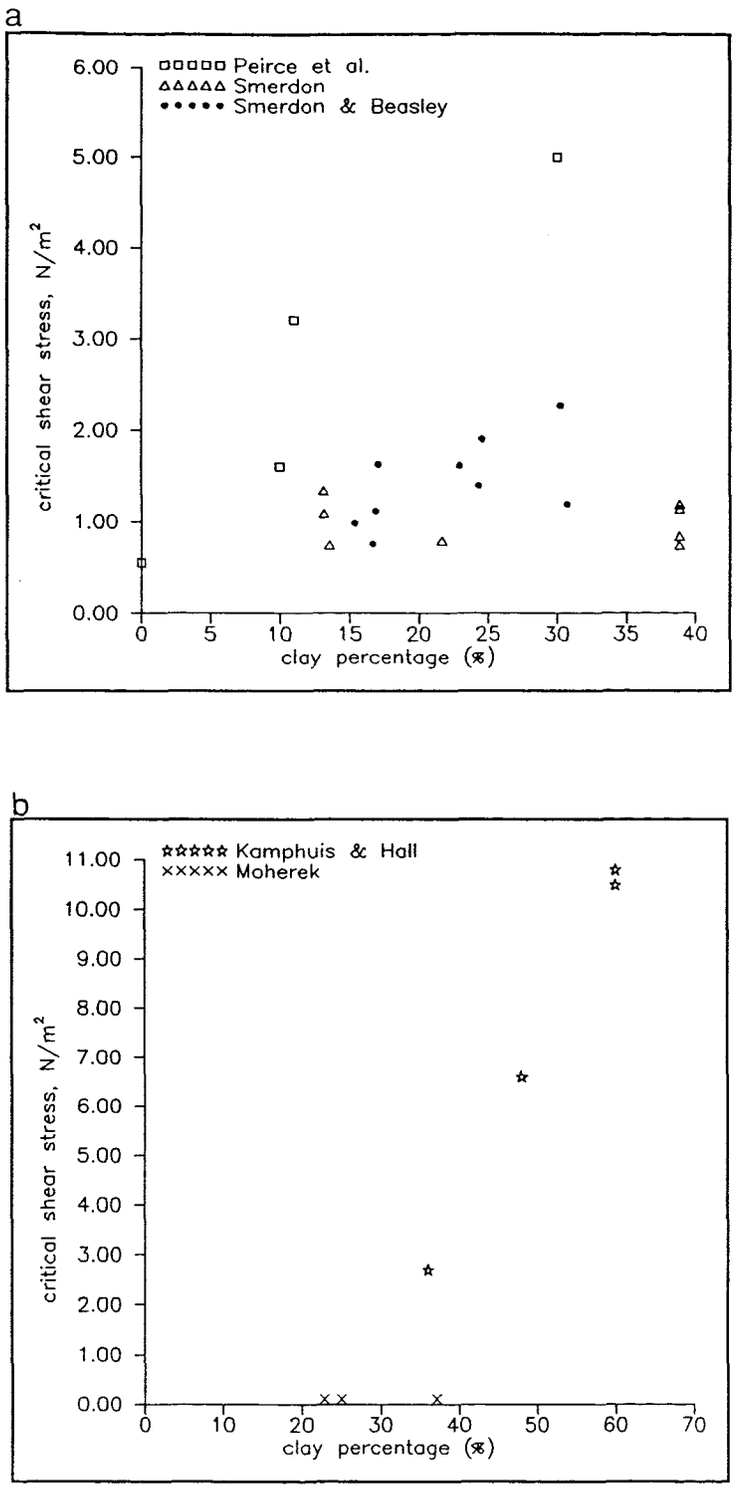

Fig. 6.7. Incipient motion, for various natural sand-mud admixtures, determined by the laboratory studies of Smerdon & Beasley (1961); Smerdon (1964); Peirce *et al.* (1970); Moherek (1978); and Kamphuis & Hall (1983).

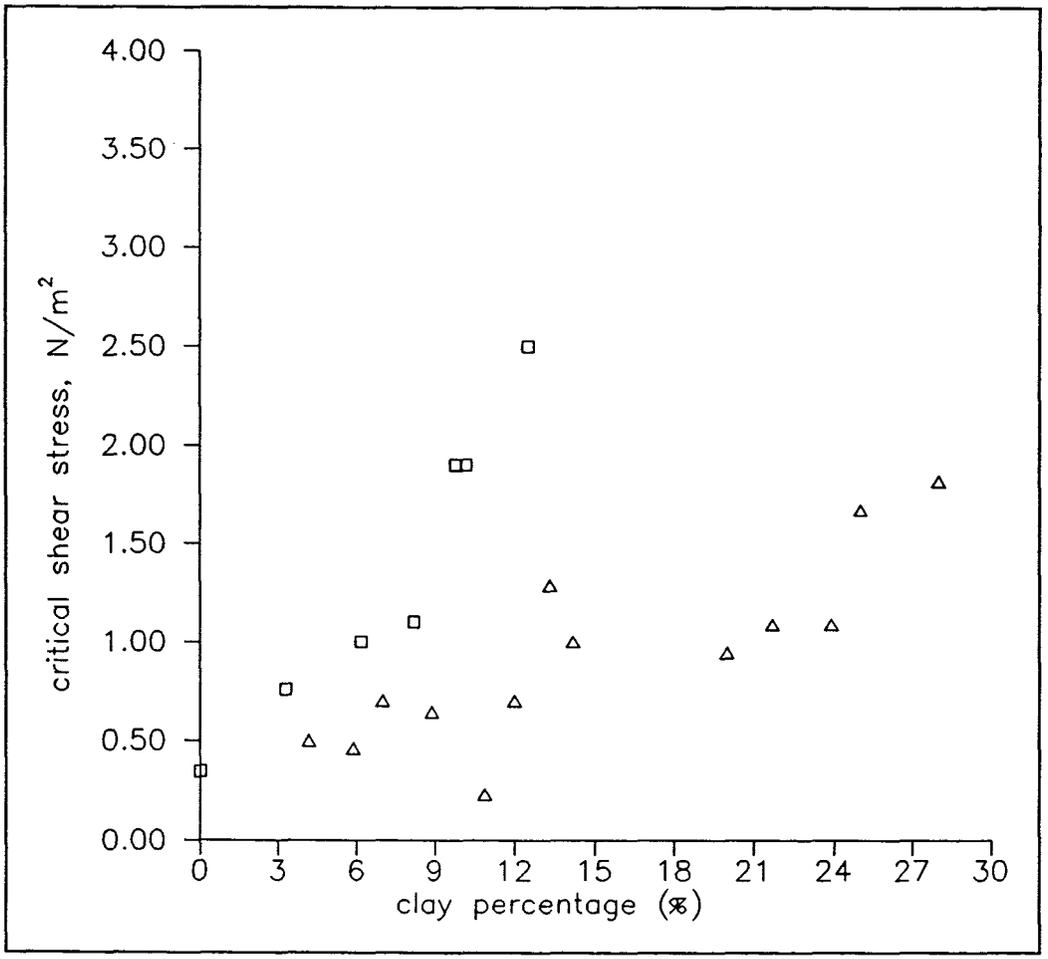

Fig. 6.8. Incipient motion determined for different types of cohesive additive (clay minerals) (Key: □, kaolinite; ▵, smectite) (after Torfs, 1994).

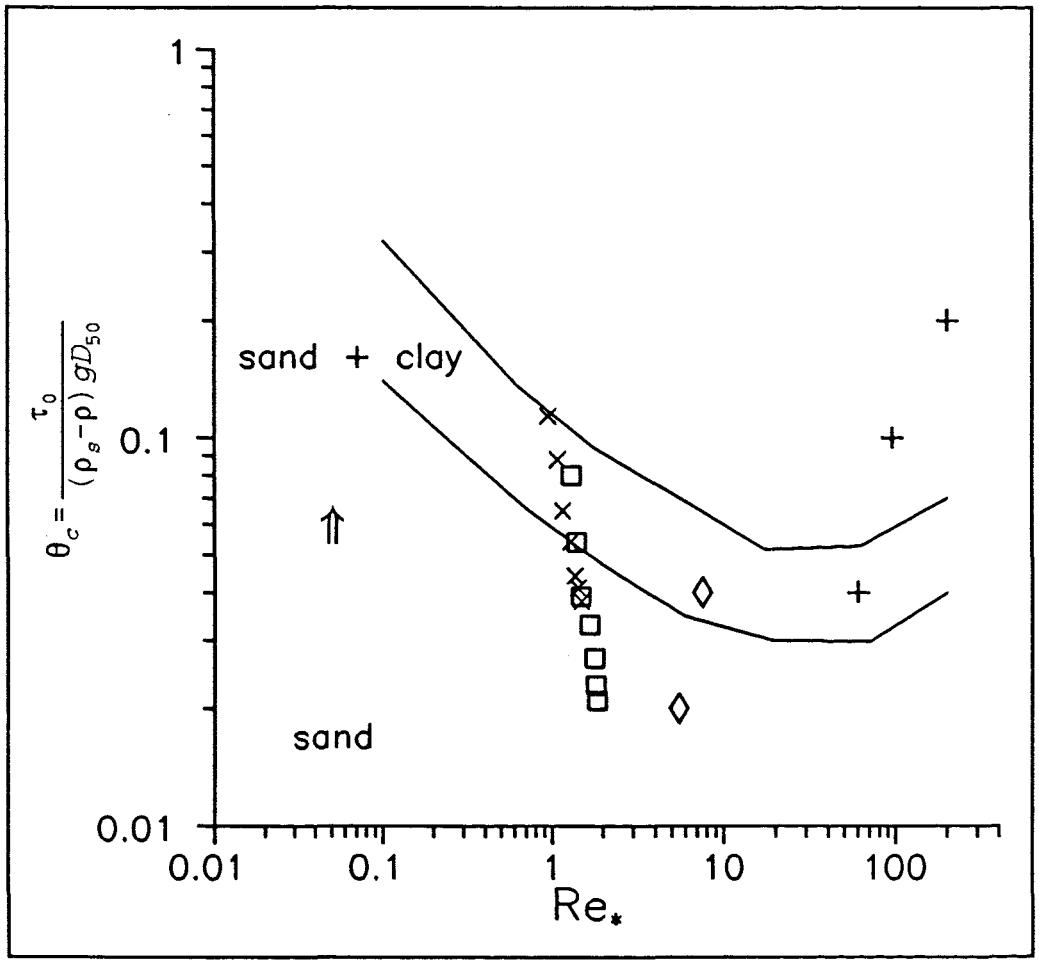

Fig. 6.9. Comparison of the results of the present study (x, □) with those of the Nalluri & Alvarez (1992) investigation (◇, +) and the Miller *et al.* (1977) envelope (solid lines). Key: x, mixtures of 152.5 μm sand; □, mixtures of 215 μm sand; ◇, mixtures of 500 μm sand; and +, mixtures of 2000 μm sand.

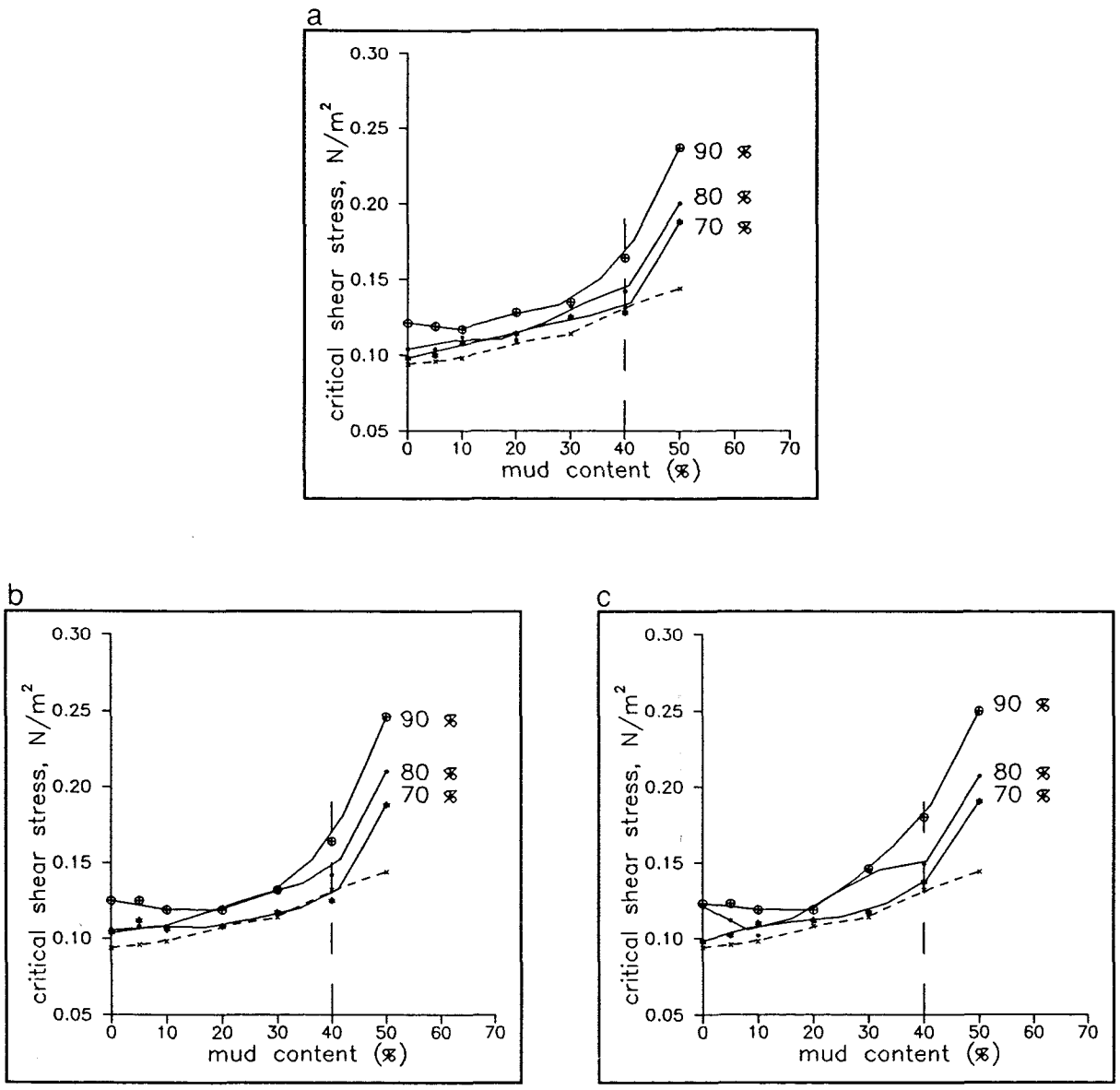

Fig. 6.10. Variation in the critical erosion shear stress with mud content, for mixtures containing 152.5 μm sands, under different pre-threshold current speeds (70%, 80% and 90% of the original critical value) and flow durations of: (a) 5 min; (b) 10 min; and (c) 20 min (Note: The small-stroke dashed lines represent sediment beds without any stress history).

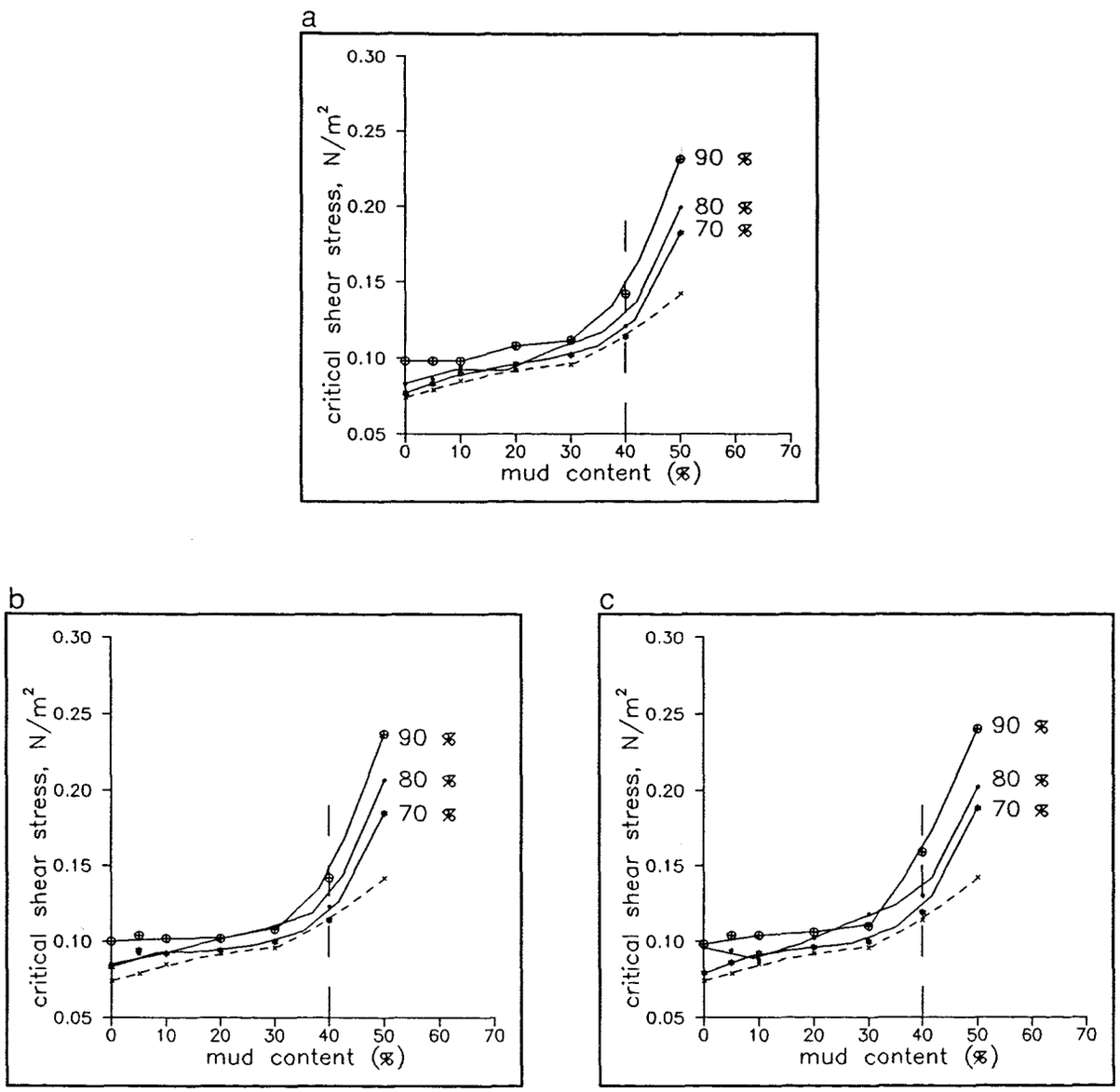

Fig. 6.11. Variation in the critical erosion shear stress with mud content, for mixtures containing 215 μm sands, under different pre-threshold current speeds (70%, 80% and 90% of the original critical value) and flow durations of: (a) 5 min; (b) 10 min; and (c) 20 min (Note: The small-stroke dashed lines represent sediment beds without any stress history).

mud content (%)	avrg. cr. cur. speed $U_{c(0.4\ cm)}$ (cm/s)	standard deviation σ (cm/s)
0	14.32	2.49
0	14.54	2.42
0	13.82	2.22
0	14.21	2.32
5	14.29	2.26
5	14.31	2.10
5	14.07	2.38
5	14.85	2.19
10	14.22	2.40
10	14.56	2.32
10	14.86	2.56
10	14.80	2.44
20	15.94	2.61
20	15.85	2.32
20	15.61	2.46
20	14.52	2.31
30	16.09	2.89
30	16.02	2.64
30	16.60	2.44
30	15.15	2.37
40	18.62	2.68
40	17.49	2.79
40	16.36	2.45
40	16.68	2.51
50	17.46	2.62
50	19.07	2.76
50	17.17	2.69
50	18.98	3.00

Table 6.1. Experimental results obtained under unidirectional flow, for sediments containing a sand component of 152.5 microns size (in the absence of any stress history of the bed).

mud content (%)	avrg. cr. cur. speed $U_{c(0.4\ cm)}$ (cm/s)	standard deviation σ (cm/s)
0	12.89	2.42
0	12.63	2.47
0	12.36	2.27
0	11.76	2.37
5	12.38	2.35
5	12.89	2.29
5	12.72	2.52
5	13.50	2.41
10	13.15	2.31
10	13.19	2.30
10	13.29	2.27
10	13.41	2.18
20	14.16	2.39
20	13.54	2.25
20	13.84	2.17
20	14.34	2.26
30	14.01	2.50
30	14.77	2.33
30	14.48	2.68
30	13.95	2.51
40	14.83	2.54
40	15.55	2.51
40	16.51	2.81
40	16.58	2.56
50	17.81	2.89
50	17.90	3.03
50	17.74	3.00
50	18.62	2.92

Table 6.2. Experimental results obtained under unidirectional flow, for sediments containing a sand component of 215 microns size (in the absence of any stress history of the bed).

size of sand component (microns)	mud content (%)	mean critical current speed (cm/s)	mean critical shear stress τ_c (N/m^2)
152.5	0	14.22	0.094
	5	14.38	0.096
	10	14.61	0.098
	20	15.48	0.108
	30	15.97	0.114
	40	17.29	0.132
	50	18.17	0.144
215	0	12.41	0.074
	5	12.87	0.079
	10	13.26	0.085
	20	13.97	0.092
	30	14.30	0.096
	40	15.87	0.114
	50	18.02	0.142

Table 6.3. Derived mean critical current speeds and shear stresses under unidirectional flow rates, for sediment beds without any stress history.

mud content (%)	water content (%)	water content (%)
5	32.5	30.2
5	32.3	
5	34.4	
5	34.1	
10	41.2	31.2
10	40.1	
10	41.0	
10	41.2	
20	54.1	43.9
20	57.2	
20	56.5	
20	55.3	
30	66.9	59.7
30	67.5	
30	69.2	
30	67.5	
40	81.2	69.5
40	81.8	
40	82.5	
40	84.5	
50	89.4	82.1
50	90.1	
50	91.9	
50	90.8	

Table 6.4. The moisture content for each of the mixtures tested (containing the 152.5 micron sand component) *before* the threshold experiment (2nd column) and *after* the threshold experiment (3rd column).

mud content (%)	water content (%)	water content (%)
5	38.1	30.0
5	37.2	
5	37.9	
5	37.2	
10	42.5	31.2
10	43.5	
10	43.1	
10	41.8	
20	52.7	44.1
20	51.7	
20	54.1	
20	53.6	
30	60.3	58.2
30	61.0	
30	61.8	
30	62.1	
40	75.1	70.6
40	77.0	
40	74.5	
40	75.4	
50	88.0	79.2
50	87.6	
50	85.9	
50	89.0	

Table 6.5. The moisture content for each of the mixtures tested (containing the 215 micron sand component) *before* the threshold experiment (2nd column) and *after* the threshold experiment (3rd column).

pre-thresh. speed % of the original mean critical current speed	flow duration (min)	averaged pre-thresh. speed $U_{0.4\ cm}$ (cm/s)	standard deviat. σ (cm/s)	new averaged critical current speed $U_{c(0.4\ cm)}$ (cm/s)	standard deviat. σ (cm/s)
65-69	5	9.55	2.21	13.82	2.55
	5	9.45	2.08	15.12	2.68
	10	9.73	2.00	15.27	2.75
	10	9.77	1.99	14.88	2.37
	20	9.31	2.38	14.48	2.51
	20	9.25	2.30	14.54	2.60
73-84	5	10.39	2.46	15.20	2.53
	5	11.29	2.37	15.00	2.72
	10	11.83	2.18	14.91	2.45
	10	12.01	2.27	15.40	2.61
	20	11.96	2.30	15.87	2.69
	20	11.65	2.31	16.99	2.75
85-92	5	12.92	2.27	15.92	2.56
	5	13.10	2.35	16.97	2.93
	10	12.89	2.27	17.38	2.74
	10	12.11	2.23	16.35	2.70
	20	12.07	2.30	16.53	3.05
	20	12.06	2.26	16.60	2.72

Table 6.6. Experimental results, under unidirectional flow, with a stress history of the bed containing only sand of 152.5 microns in size.

pre-thresh. speed % of the original mean critical current speed	flow duration (min)	averaged pre-thresh. speed $U_{0.4\ cm}$ (cm/s)	standard deviat. σ (cm/s)	new averaged critical current speed $U_{c(0.4\ cm)}$ (cm/s)	standard deviat. σ (cm/s)
66-75	5	9.58	2.01	14.58	2.37
	5	9.55	1.97	14.71	2.34
	10	10.00	2.03	15.98	2.58
	10	10.71	2.18	15.65	2.37
	20	10.05	2.15	15.08	2.53
	20	10.76	2.26	14.73	2.62
76-80	5	11.20	2.29	14.85	2.60
	5	11.44	2.28	15.30	2.60
	10	10.95	2.30	15.55	2.65
	10	11.10	1.99	15.41	2.34
	20	11.08	2.12	14.99	2.43
	20	10.91	2.07	16.64	2.40
84-91	5	12.03	2.25	16.38	2.44
	5	12.60	2.12	16.16	2.48
	10	13.13	2.29	17.37	2.56
	10	12.53	2.11	16.33	2.60
	20	12.04	2.30	16.02	2.56
	20	12.61	2.18	17.20	2.48

Table 6.7. Experimental results, under unidirectional flow, with a stress history of the bed containing sand of 152.5 microns in size and with 5% mud.

pre-thresh. speed % of the original mean critical current speed	flow duration (min)	averaged pre-thresh. speed $U_{0.4\ cm}$ (cm/s)	standard deviat. σ (cm/s)	new averaged critical current speed $U_{c(0.4\ cm)}$ (cm/s)	standard deviat. σ (cm/s)
66-73	5	9.60	2.07	15.96	2.52
	5	9.97	2.31	14.79	2.35
	10	10.31	2.21	15.09	2.63
	10	10.64	2.25	15.57	2.60
	20	10.14	2.17	15.88	2.44
	20	10.19	2.07	15.24	2.55
76-84	5	11.88	2.16	15.55	2.55
	5	11.66	2.07	15.82	2.44
	10	11.56	2.16	15.87	2.39
	10	12.26	2.11	15.20	2.42
	20	12.00	2.10	14.75	2.58
	20	11.05	2.09	15.13	2.32
85-92	5	12.59	2.13	16.24	2.29
	5	12.59	2.25	15.83	2.49
	10	12.93	2.16	16.37	2.62
	10	13.50	2.32	16.26	2.48
	20	12.96	2.34	16.71	2.63
	20	12.44	2.33	16.49	2.69

Table 6.8. Experimental results, under unidirectional flow, with a stress history of the bed containing sand of 152.5 microns in size and with 10% mud.

pre-thresh. speed % of the original mean critical current speed	flow duration (min)	averaged pre-thresh. speed $U_{0.4\ cm}$ (cm/s)	standard deviat. σ (cm/s)	new averaged critical current speed $U_{c(0.4\ cm)}$ (cm/s)	standard deviat. σ (cm/s)
66-72	5	10.32	2.03	16.05	2.59
	5	10.50	2.10	15.67	2.29
	10	10.46	2.12	15.47	2.52
	10	10.27	2.00	15.53	2.08
	20	11.15	1.83	15.87	2.58
	20	10.99	1.82	15.72	2.89
74-81	5	11.39	2.37	14.49	2.25
	5	12.10	1.99	16.14	2.35
	10	12.56	2.16	16.28	2.61
	10	11.75	1.97	16.79	2.62
	20	12.38	2.18	16.28	2.46
	20	12.28	2.13	16.60	2.83
81-91	5	13.15	2.26	16.00	2.76
	5	13.37	2.37	17.83	2.70
	10	13.21	2.17	16.07	2.58
	10	12.61	2.31	16.35	2.67
	20	14.14	2.11	16.72	2.56
	20	13.30	2.22	16.72	2.48

Table 6.9. Experimental results, under unidirectional flow, with a stress history of the bed containing sand of 152.5 microns in size and with 20% mud.

pre-thresh. speed % of the original mean critical current speed	flow duration (min)	averaged pre-thresh. speed $U_{0.4\ cm}$ (cm/s)	standard deviat. σ (cm/s)	new averaged critical current speed $U_{c(0.4\ cm)}$ (cm/s)	standard deviat. σ (cm/s)
65-70	5	10.70	2.12	17.42	2.52
	5	10.91	2.04	16.03	2.48
	10	11.06	2.06	15.73	2.37
	10	10.46	2.11	16.66	2.87
	20	10.90	2.04	15.65	2.43
	20	11.23	2.14	16.75	2.69
75-84	5	12.59	2.12	17.95	2.47
	5	11.98	2.03	17.25	2.49
	10	13.34	2.19	16.76	2.71
	10	13.30	2.33	17.78	2.59
	20	12.96	2.23	18.61	2.55
	20	12.86	2.42	17.74	2.59
85-92	5	14.68	2.45	17.63	2.84
	5	14.40	2.33	17.40	2.44
	10	13.56	2.29	16.86	2.33
	10	14.54	2.34	17.70	2.68
	20	13.93	2.26	18.66	2.53
	20	14.17	2.31	18.27	2.76

Table 6.10. Experimental results, under unidirectional flow, with a stress history of the bed containg sand of 152.5 microns in size and with 30% mud.

pre-thresh. speed % of the original mean critical current speed	flow duration (min)	averaged pre-thresh. speed $U_{0.4\ cm}$ (cm/s)	standard deviat. σ (cm/s)	new averaged critical current speed $U_{c(0.4\ cm)}$ (cm/s)	standard deviat. σ (cm/s)
68-73	5	11.84	2.13	17.46	2.43
	5	12.06	1.99	16.54	2.71
	10	12.36	2.16	16.50	2.70
	10	11.71	2.01	17.16	2.41
	20	12.19	2.02	17.46	2.64
	20	12.54	2.05	18.04	2.84
76-80	5	13.51	2.19	17.60	2.77
	5	13.75	2.05	18.17	2.49
	10	13.09	2.20	18.73	2.93
	10	13.87	2.34	17.32	2.79
	20	13.40	2.26	19.54	2.80
	20	13.62	2.16	17.68	2.61
87-91	5	15.32	2.37	19.42	2.92
	5	15.68	2.29	19.73	2.95
	10	15.50	2.42	19.84	2.65
	10	15.48	2.33	19.57	2.48
	20	15.41	2.24	20.63	2.88
	20	15.00	2.33	20.75	2.83

Table 6.11. Experimental results, under unidirectional flow, with a stress history of the bed containing sand of 152.5 microns in size and with 40% mud.

pre-thresh. speed % of the original mean critical current speed	flow duration (min)	averaged pre-thresh. speed $U_{0.4\ cm}$ (cm/s)	standard deviat. σ (cm/s)	new averaged critical current speed $U_{c(0.4\ cm)}$ (cm/s)	standard deviat. σ (cm/s)
67-71	5	12.68	2.20	22.25	3.27
	5	12.85	2.03	20.20	3.13
	10	12.90	2.17	21.83	3.08
	10	12.95	2.51	20.60	3.31
	20	12.21	2.02	22.08	3.06
	20	12.46	2.24	20.82	3.12
75-82	5	13.63	2.10	23.41	3.18
	5	13.85	2.15	21.25	3.25
	10	14.20	2.32	23.38	3.09
	10	14.73	2.08	22.06	3.35
	20	14.90	2.07	23.14	3.22
	20	14.50	2.13	21.82	3.18
86-91	5	16.02	2.32	25.61	3.25
	5	16.18	2.41	23.25	3.32
	10	15.62	2.25	25.55	3.12
	10	15.95	2.37	24.11	3.05
	20	16.53	2.32	25.73	3.18
	20	16.22	2.18	24.26	3.29

Table 6.12. Experimental results, under unidirectional flow, with a stress history of the bed containing sand of 152.5 microns in size and with 50% mud.

pre-thresh. speed % of the original mean critical current speed	flow duration (min)	averaged pre-thresh. speed $U_{0.4\ cm}$ (cm/s)	standard deviat. σ (cm/s)	new averaged critical current speed $U_{c(0.4\ cm)}$ (cm/s)	standard deviat. σ (cm/s)
66-72	5	8.62	1.85	12.66	2.42
	5	8.19	2.01	12.59	2.37
	10	8.35	1.92	13.33	2.33
	10	8.85	2.20	12.98	2.38
	20	8.80	1.89	12.83	2.57
	20	8.94	2.14	12.80	2.69
75-83	5	10.05	2.17	13.27	2.82
	5	10.17	2.36	13.09	2.78
	10	10.30	2.32	13.12	2.71
	10	9.92	2.41	13.59	2.62
	20	9.31	2.08	13.85	2.65
	20	9.85	2.11	14.83	2.31
87-92	5	10.95	2.35	14.09	2.87
	5	10.80	2.37	14.99	2.82
	10	11.35	2.22	15.17	2.92
	10	11.00	2.18	14.27	2.55
	20	11.42	2.47	14.42	2.62
	20	11.12	2.02	14.68	2.68

Table 6.13. Experimental results, under unidirectional flow, with a stress history of the bed containing only sand of 215 microns in size.

pre-thresh. speed % of the original mean critical current speed	flow duration (min)	averaged pre-thresh. speed $U_{0.4\ cm}$ (cm/s)	standard deviat. σ (cm/s)	new averaged critical current speed $U_{c(0.4\ cm)}$ (cm/s)	standard deviat. σ (cm/s)
68-74	5	9.23	1.95	13.41	2.25
	5	9.32	1.98	12.81	2.22
	10	8.95	2.15	14.30	2.29
	10	8.74	2.18	14.00	2.62
	20	9.06	2.27	13.69	2.60
	20	9.51	2.29	13.38	2.52
78-81	5	10.08	2.31	13.30	2.72
	5	10.23	1.99	13.69	2.71
	10	10.04	2.25	14.11	2.25
	10	10.35	2.37	13.99	2.39
	20	10.43	2.14	13.41	2.42
	20	10.41	2.05	14.89	2.48
83-92	5	10.68	2.28	14.66	2.42
	5	11.05	2.37	14.47	2.38
	10	11.54	2.19	15.55	2.81
	10	11.71	2.29	14.62	2.88
	20	11.32	2.34	14.54	2.57
	20	11.63	2.16	15.49	2.61

Table 6.14. Experimental results, under unidirectional flow, with a stress history of the bed containing sand of 215 microns in size and with 5% mud.

pre-thresh. speed % of the original mean critical current speed	flow duration (min)	averaged pre-thresh. speed $U_{0.4\ cm}$ (cm/s)	standard deviat. σ (cm/s)	new averaged critical current speed $U_{c(0.4\ cm)}$ (cm/s)	standard deviat. σ (cm/s)
67-72	5	8.95	2.06	13.42	2.33
	5	9.23	1.97	14.48	2.29
	10	9.35	2.13	13.70	2.41
	10	8.88	2.18	14.26	2.47
	20	9.30	2.16	14.41	2.28
	20	9.55	2.20	13.83	2.42
76-83	5	10.63	1.98	14.11	2.41
	5	10.08	1.96	14.36	2.32
	10	10.38	2.25	14.40	2.51
	10	11.01	2.19	13.79	2.49
	20	10.52	2.27	13.59	2.37
	20	10.44	2.21	13.94	2.61
84-93	5	12.08	2.31	14.75	2.65
	5	11.13	2.28	14.37	2.64
	10	12.21	2.35	14.99	2.81
	10	12.33	2.25	14.76	2.47
	20	11.85	2.30	15.17	2.40
	20	11.76	2.18	14.97	2.55

Table 6.15. Experimental results, under unidirectional flow, with a stress history of the bed containing sand of 215 microns in size and with 10% mud.

pre-thresh. speed % of the original mean critical current speed	flow duration (min)	averaged pre-thresh. speed $U_{0.4\ cm}$ (cm/s)	standard deviat. σ (cm/s)	new averaged critical current speed $U_{c(0.4\ cm)}$ (cm/s)	standard deviat. σ (cm/s)
68-71	5	9.83	1.72	14.69	2.81
	5	9.50	1.91	13.94	2.68
	10	9.61	2.01	14.64	2.33
	10	9.71	2.13	13.72	2.30
	20	9.92	2.11	14.42	2.54
	20	9.70	2.19	14.19	2.59
76-82	5	10.99	2.22	13.90	2.60
	5	10.91	2.23	14.25	2.52
	10	10.62	2.13	14.70	2.36
	10	11.19	2.31	15.16	2.39
	20	11.46	2.29	14.70	2.71
	20	11.22	2.09	14.98	2.66
85-90	5	11.87	2.27	14.64	2.89
	5	11.93	2.32	16.09	2.65
	10	12.51	2.33	14.70	2.82
	10	11.99	2.21	14.94	2.59
	20	12.41	2.40	15.09	2.44
	20	12.57	2.16	15.29	2.39

Table 6.16. Experimental results, under unidirectional flow, with a stress history of the bed containing sand of 215 microns in size and with 20% mud.

pre-thresh. speed % of the original mean critical current speed	flow duration (min)	averaged pre-thresh. speed $U_{0.4\ cm}$ (cm/s)	standard deviat. σ (cm/s)	new averaged critical current speed $U_{c(0.4\ cm)}$ (cm/s)	standard deviat. σ (cm/s)
66-72	5	9.95	2.11	15.40	2.46
	5	9.82	2.18	14.36	2.41
	10	9.44	2.21	14.49	2.76
	10	10.25	2.02	15.01	2.55
	20	10.30	1.93	14.41	2.71
	20	10.00	1.95	15.19	2.68
76-83	5	10.95	2.21	16.07	2.52
	5	10.87	2.08	15.44	2.89
	10	11.42	2.22	15.19	2.83
	10	11.40	2.29	16.02	2.73
	20	11.87	2.17	16.66	2.66
	20	11.05	2.12	15.89	2.58
87-93	5	12.88	2.53	15.99	2.39
	5	12.75	2.41	15.69	2.62
	10	12.44	2.40	15.10	2.48
	10	12.61	2.48	15.84	2.68
	20	13.30	2.62	16.70	2.84
	20	13.25	2.52	16.36	2.79

Table 6.17. Experimental results, under unidirectional flow, with a stress history of the bed containing sand of 215 microns in size and with 30% mud.

pre-thresh. speed % of the original mean critical current speed	flow duration (min)	averaged pre-thresh. speed $U_{0.4\,cm}$ (cm/s)	standard deviat. σ (cm/s)	new averaged critical current speed $U_{c(0.4\,cm)}$ (cm/s)	standard deviat. σ (cm/s)
69-72	5	11.25	2.12	16.03	2.33
	5	10.95	2.01	15.79	2.44
	10	11.01	2.18	15.94	2.51
	10	10.99	2.02	16.04	2.52
	20	11.43	1.88	15.74	2.49
	20	11.31	2.06	16.84	2.47
78-81	5	12.48	2.21	16.16	2.81
	5	12.86	2.18	16.78	2.77
	10	12.38	2.25	17.19	2.48
	10	12.53	2.12	16.10	2.73
	20	12.82	2.19	17.93	2.68
	20	12.75	2.24	16.44	2.66
88-91	5	14.35	2.41	17.82	2.77
	5	13.96	2.39	18.21	2.91
	10	13.99	2.53	18.20	2.93
	10	14.29	2.33	17.96	2.65
	20	14.31	2.34	19.03	2.70
	20	14.44	2.29	19.44	2.92

Table 6.18. Experimental results, under unidirectional flow, with a stress history of the bed containing sand of 215 microns in size and with 40% mud.

pre-thresh. speed % of the original mean critical current speed	flow duration (min)	averaged pre-thresh. speed $U_{0.4\ cm}$ (cm/s)	standard deviat. σ (cm/s)	new averaged critical current speed $U_{c(0.4\ cm)}$ (cm/s)	standard deviat. σ (cm/s)
66-72	5	12.81	2.24	22.07	3.05
	5	12.22	2.02	19.83	3.21
	10	12.97	2.07	21.62	3.33
	10	12.33	2.51	20.43	3.01
	20	11.89	2.19	21.89	3.11
	20	12.05	2.16	20.45	3.21
78-83	5	14.09	2.09	23.01	3.15
	5	14.72	2.11	20.98	3.36
	10	14.34	2.13	23.19	3.08
	10	14.06	2.32	21.88	3.11
	20	14.96	2.26	22.66	3.21
	20	14.49	2.08	21.62	3.30
88-92	5	16.58	2.42	24.99	3.22
	5	16.51	2.37	23.07	3.27
	10	15.86	2.43	25.04	3.08
	10	15.97	2.17	23.81	3.16
	20	16.01	2.31	25.02	3.20
	20	16.19	2.30	24.06	3.28

Table 6.19. Experimental results, under unidirectional flow, with a stress history of the bed containing sand of 215 microns in size and with 50% mud.

pre-thresh. speed % of the original mean critical current speed	flow duration (min)	new mean critical current speed (cm/s)	new mean critical shear stress τ_c (N/m^2)
65-69	5	14.47	0.098
	10	15.08	0.104
	20	14.51	0.098
73-84	5	15.10	0.104
	10	15.16	0.106
	20	16.43	0.121
85-92	5	16.45	0.121
	10	16.87	0.125
	20	16.57	0.123

Table 6.20. The derived mean values of the critical parameters studied in the stress history experiments (sand size, 152.5 microns; 0% mud).

pre-thresh. speed % of the original mean critical current speed	flow duration (min)	new mean critical current speed (cm/s)	new mean critical shear stress τ_c (N/m^2)
66-75	5	14.65	0.100
	10	15.82	0.112
	20	14.91	0.102
76-80	5	15.08	0.104
	10	15.48	0.108
	20	15.82	0.112
84-91	5	16.27	0.119
	10	16.85	0.125
	20	16.61	0.123

Table 6.21. The derived mean values of the critical parameters studied in the stress history experiments (sand size, 152.5 microns; 5% mud).

pre-thresh. speed % of the original mean critical current speed	flow duration (min)	new mean critical current speed (cm/s)	new mean critical shear stress τ_c (N/m^2)
66-73	5	15.38	0.108
	10	15.33	0.106
	20	15.56	0.110
76-84	5	15.69	0.112
	10	15.54	0.108
	20	14.94	0.102
85-92	5	16.04	0.117
	10	16.32	0.119
	20	16.60	0.123

Table 6.22. The derived mean values of the critical parameters studied in the stress history experiments (sand size, 152.5 microns; 10% mud).

pre-thresh. speed % of the original mean critical current speed	flow duration (min)	new mean critical current speed (cm/s)	new mean critical shear stress τ_c (N/m^2)
66-72	5	15.86	0.114
	10	15.50	0.108
	20	15.80	0.112
74-81	5	15.32	0.106
	10	16.54	0.121
	20	16.44	0.121
81-91	5	16.92	0.128
	10	16.21	0.119
	20	16.72	0.123

Table 6.23. The derived mean values of the critical parameters studied in the stress history experiments (sand size, 152.5 microns; 20% mud).

pre-thresh. speed % of the original mean critical current speed	flow duration (min)	new mean critical current speed (cm/s)	new mean critical shear stress τ_c (N/m^2)
65-70	5	16.73	0.125
	10	16.20	0.117
	20	16.20	0.117
75-84	5	17.60	0.135
	10	17.27	0.132
	20	18.18	0.144
85-92	5	17.52	0.135
	10	17.28	0.132
	20	18.47	0.146

Table 6.24. The derived mean values of the critical parameters studied in the stress history experiments (sand size, 152.5 microns; 30% mud).

pre-thresh. speed % of the original mean critical current speed	flow duration (min)	new mean critical current speed (cm/s)	new mean critical shear stress τ_c (N/m^2)
68-73	5	17.00	0.128
	10	16.83	0.125
	20	17.75	0.137
76-80	5	17.89	0.139
	10	18.03	0.142
	20	18.61	0.149
87-91	5	19.58	0.164
	10	19.71	0.164
	20	20.69	0.180

Table 6.25. The derived mean values of the critical parameters studied in the stress history experiments (sand size, 152.5 microns; 40% mud).

pre-thresh. speed % of the original mean critical current speed	flow duration (min)	new mean critical current speed (cm/s)	new mean critical shear stress τ_c (N/m^2)
67-71	5	21.23	0.188
	10	21.22	0.188
	20	21.45	0.190
75-82	5	22.33	0.204
	10	22.72	0.210
	20	22.48	0.207
86-91	5	24.43	0.237
	10	24.83	0.246
	20	25.00	0.250

Table 6.26. The derived mean values of the critical parameters studied in the stress history experiments (sand size, 152.5 microns; 50% mud).

pre-thresh. speed % of the original mean critical current speed	flow duration (min)	new mean critical current speed (cm/s)	new mean critical shear stress τ_c (N/m^2)
66-72	5	12.63	0.077
	10	13.16	0.083
	20	12.82	0.079
75-83	5	13.18	0.083
	10	13.36	0.085
	20	14.34	0.096
87-92	5	14.54	0.098
	10	14.72	0.100
	20	14.55	0.098

Table 6.27. The derived mean values of the critical parameters studied in the stress history experiments (sand size, 215 microns; 0% mud).

pre-thresh. speed % of the original mean critical current speed	flow duration (min)	new mean critical current speed (cm/s)	new mean critical shear stress τ_c (N/m^2)
68-74	5	13.11	0.083
	10	14.15	0.094
	20	13.54	0.086
78-81	5	13.50	0.086
	10	14.05	0.092
	20	14.15	0.094
83-92	5	14.57	0.098
	10	15.09	0.104
	20	15.02	0.104

Table 6.28. The derived mean values of the critical parameters studied in the stress history experiments (sand size 215 microns; 5% mud).

pre-thresh. speed % of the original mean critical current speed	flow duration (min)	new mean critical current speed (cm/s)	new mean critical shear stress τ_c (N/m^2)
67-72	5	13.95	0.090
	10	13.98	0.092
	20	14.12	0.092
76-83	5	14.24	0.094
	10	14.10	0.092
	20	13.77	0.088
84-93	5	14.56	0.098
	10	14.88	0.102
	20	15.07	0.104

Table 6.29. The derived mean values of the critical parameters studied in the stress history experiments (sand size, 215 microns; 10% mud).

pre-thresh. speed % of the original mean critical current speed	flow duration (min)	new mean critical current speed (cm/s)	new mean critical shear stress τ_c (N/m^2)
68-71	5	14.32	0.096
	10	14.18	0.094
	20	14.31	0.096
76-82	5	14.08	0.092
	10	14.93	0.102
	20	14.84	0.102
85-90	5	15.37	0.108
	10	14.82	0.102
	20	15.19	0.106

Table 6.30. The derived mean values of the critical parameters studied in the stress history experiments (sand size, 215 microns; 20% mud).

pre-thresh. speed % of the original mean critical current speed	flow duration (min)	new mean critical current speed (cm/s)	new mean critical shear stress τ_c (N/m^2)
66-72	5	14.88	0.102
	10	14.75	0.100
	20	14.80	0.100
76-83	5	15.76	0.112
	10	15.61	0.110
	20	16.28	0.118
87-93	5	15.84	0.112
	10	15.47	0.108
	20	16.53	0.110

Table 6.31. The derived mean values of the critical parameters studied in the stress history experiments (sand size, 215 microns; 30% mud).

pre-thresh. speed % of the original mean critical current speed	flow duration (min)	new mean critical current speed (cm/s)	new mean critical shear stress τ_c (N/m^2)
69-72	5	15.91	0.114
	10	15.99	0.114
	20	16.29	0.119
78-81	5	16.47	0.121
	10	16.65	0.123
	20	17.19	0.130
88-91	5	18.02	0.142
	10	18.08	0.142
	20	19.24	0.159

Table 6.32. The derived mean values of the critical parameters studied in the stress history experiments (sand size, 215 microns; 40% mud).

pre-thresh. speed % of the original mean critical current speed	flow duration (min)	new mean critical current speed (cm/s)	new mean critical shear stress τ_c (N/m^2)
66-72	5	20.95	0.182
	10	21.03	0.185
	20	21.17	0.188
78-83	5	22.00	0.199
	10	22.54	0.207
	20	22.14	0.202
88-92	5	24.03	0.231
	10	24.43	0.237
	20	24.54	0.240

Table 6.33. The derived mean values of the critical parameters studied in the stress history experiments (sand size, 215 microns; 50% mud).

CHAPTER 7

RESULTS AND DISCUSSION: OSCILLATORY FLOW

7. RESULTS AND DISCUSSION: OSCILLATORY FLOW

7.1. ERODIBILITY EXPERIMENTS

7.1.1. Threshold Determinations

A statistical analysis of the data derived under wave conditions (Set 3 experiments) has demonstrated that the error associated with them is around ±4%. This error is higher than that associated with the unidirectional flow results (Section 6.1). The fact that the threshold criterion applied to the steady flow tests is more objective than that used for the oscillatory flow results (Section 4.4.2) may explain sufficiently this discrepancy.

The experimental procedure for the establishment of threshold conditions, under simulated waves, has been described in detail in Chapter 4. In all the experiments, the wave period was reduced gradually in 0.25 s decrements, until sediment movement ocurred. The possibility that the error associated with the definition of the critical (threshold) wave period was as large as the interval of the period decrement (0.25 s) is somewhat limited. This error should be distributed statistically between the boundaries of each period reduction.

Resonance phenomena

At the time at which the erosion threshold experiments were being performed, resonance (between the water mass and the oscillating plate) was observed for the majority of the critical periods of the plate oscillation. Hence, a series of water velocity and pressure measurements were carried out, for periods of oscillation ranging from 3.20 s up to 9.20 s, using the Laser Doppler Anemometer

(LDA) and a pressure transducer. The pressure sensor was located inside the water column of the flume test section, at 7 cm above the mid-stroke position of the moving plate. The LDA was aligned vertically over the transducer, measuring the water orbital velocity at a height of 5 cm above the oscillating plate. Although the LDA was unable to identify reverse flows, it was considered that the instrument could be used for the investigation of the observed resonance conditions. Simultaneously with the water pressure and orbital velocity recordings, the position of the oscillating carriage was recorded using the plate positioning system.

On the one hand, therefore, the resonance could be verified by observing the existence of a standing wave inside the water column of the flume channel. On the other hand, it was feasible, on the basis of the recordings associated with the water orbital velocity and plate position, to calculate the phase difference between these two parameters. Consequently, taking into account this phase difference and the plate position at which threshold of movement was observed to commence (approximately 45° before the plate reached the mid-stroke position), then using Equation 2.46 which describes the variation of the horizontal water orbital velocity at the bed under a standing wave, the influence of the horizontal water velocity component could be established. This flow was established in response to a standing wave, over the critical horizontal maximum plate velocity.

Simultaneous recordings of water pressure and horizontal (wave) orbital velocity, at the same location inside the flume, are shown in Figs 7.1 to 7.4. For both periods of plate oscillation (3.20 s and 9.20 s) and for all the strokes (i.e. the horizontal displacement of the plate),

the peaks in the water orbital velocity[1] correspond with the nodal positions within the wave form in the flume; these are represented by the pressure recordings. This data set confirms that a standing wave is developed inside the flume, because of resonance between the water mass and the oscillating carriage.

The influence of the additional horizontal velocity component ($U_{o,sw}$), caused by the standing wave, over the critical movement definition is shown on Table 7.1. The Table lists the parameters which have been used to calculate this extra horizontal water velocity (it must be taken into consideration that critical motion was observed to commence 45° before the plate reached the mid-stroke position). The results obtained demonstrate that the standing wave-induced velocity component represents only a low percentage of the maximum plate velocity (the parameter used as 'critical' in the oscillatory flow experiments). These percentages are lower than the error associated with the critical motion defined under oscillatory flow (±4%). Consequently, it is concluded that the observed resonance could not alter significantly the threshold data obtained.

7.1.2. Data Collected

The results of the oscillatory flow experiments are listed in Tables 7.2 to 7.15. These Tables present critical (threshold) oscillatory (wave) periods and maximum oscillatory velocities, calculated using Equation 4.1, for each of the experiments. The shorter oscillation periods recorded during the entire set of experiments was for the mixtures containing mud contents

[1]Note: The flats which appear when the velocity values are at a minimum are due to the malfunction of the anemometer (LDA), under reversing flow conditions.

(M) > 30%, and for strokes of 0.283 m and 0.378 m. These periods are lower than the limits (3.5 s for a stroke of 0.283 m and 3.9 s for a stroke of 0.378 m) suggested by Hammond & Collins (1979), in order the inertial forces exerted on the sediment particles do not affect the critical motion of the beds. These investigators proposed earlier that the horizontal acceleration of a sinusoidally-oscillating plate should not exceed a value of g/20; this was based upon the argument that if the vertical gravity force is 20 times greater than the horizontal inertial force, then the effects of the horizontal force can be considered to have a negligible effect on the threshold process. This condition is not satisfied in the case of the muddier admixtures, for wave strokes of 0.283 m and 0.378 m (see above). However, according to other arguments (Sleath, 1984; Voulgaris *et al.*, 1995), the smaller the size of the sediment particles, then the lower is the significance of the gravity force; subsequently, the smaller is the influence of inertia on the threshold of sediment motion. Further, Davies & Wilkinson (1977) have suggested conditions which should be satisfied in order that the results of tests of incipient motion which make use of oscillating beds, can be valid:

$$0.82 D \sqrt{\frac{2\pi}{T\nu}} < 1 \qquad (7.1)$$

This expression places a limit upon the magnitude of the inertial force, in relation to the fluid force. The left hand part of this expression (Eq. 7.1) increases with grain diameter (D) and decreases with oscillatory (wave) period (T). In the present study, every combination of D and T used produces values of less than 1. Hence, the prescribed limitation is satisfied throughout the present series of experiments.

Figures 7.5 and 7.6 display the results of the oscillatory flow tests in terms of maximum plate (wave) velocity against mud content (M), under an increasing wave stroke. In the domain M $\leq$ 30% there is not any particular pattern to the results: in general, the critical maximum wave-induced velocity appears to be unaffected by an increasing mud concentration. With M in excess of 30%, a reasonable linear positive relationship exists between the critical maximum wave velocity and the mud content. In addition, deposits associated with the smaller sized sands (152.5 μm) require more intense wave conditions in order to be eroded. Further, a gradual increase in the wave stroke causes a reduction in the slope of the above established linear functions. For example, in the case of 152.5 μm sand admixtures, these slopes reach values of 0.98, 0.66, 0.38 and 0.20 for wave strokes of 0.283 m, 0.378 m, 0.468 m and 0.568 m, respectively (Fig. 7.5). The corresponding gradients related to the 215 μm sand admixtures (with increasing wave stroke) are 0.30, 0.29, 0.21 and 0.14, respectively. Likewise, a decrease in the maximum wave-induced velocity and, subsequently, in the wave (oscillation) period, produces a same result provided that the stroke remains constant (cf. Figs 7.5a and 7.6a; 7.5b and 7.6b; 7.5c and 7.6c; 7.5d and 7.6d). These results imply that, under calmer wave conditions (lower near-bed wave amplitudes and longer wave periods), the erodibility of muddier mixtures (M > 30%) differ distinctly in relation to the behaviour of the other sand-mud deposits investigated. However, further experimental work is needed on mixtures containing different sizes of sand fraction, in order to confirm the behaviour observed and described above.

The results presented in Tables 7.16 to 7.19 relate to the mean critical maximum wave-induced shear stress, for each of the admixtures tested, under a particular wave

stroke. The shear stresses have been calculated using Equation 5.5. A comparison of the wave-induced critical shear stresses, with the corresponding unidirectional current-induced stresses (Table 6.3), shows that the former are much higher than the latter. Hence, assuming the wave boundary layer developed during the experimental process was a laminar flow regime (Section 5.3) and considering the unidirectional flow boundary as *smooth turbulent* (Section 5.2.3), then it may be concluded that the efficiency of the laminar flow forces to erode a sediment is much lower than the corresponding competence of the turbulent flow forces.

7.1.3. Discussion

All investigations undertaken into new areas of research must provide a link between the level of the existing knowledge and the results of an investigation, in order to validate the findings. However, to the writer's knowledge, only two studies have examined until now the effect of waves on the erodibility of mixed (sand-mud) sediment deposits.

Firstly, a laboratory flume study performed by Van Rijn (1987) investigated the effect of various wave conditions (periods and heights ranging from 1.5 s to 2.5 s and 0.02 m to 0.10 m, respectively) on the erosional behaviour of mixtures of kaolinite and fine sand. This research was undertaken in a wave flume, with the waves generated in saline water (31 ‰) by a simple wave paddle. The results indicated that a sediment bed consisting of 75% kaolinite and 25% fine sand showed the same erosional behaviour as a pure (100%) kaolinite bed. On the other hand, a bed consisting of 25% kaolinite and 75% fine sand did not display the same behaviour as a pure (100%) sand bed. Because of the presence of the kaolinite which acted

as a binding agent, there was strong surpression of the sand ripples; these were not larger than 2 mm, whilst heights of 10 mm were observed for a pure sand bed under the influence of the same wave conditions. As a result, sand concentrations above the bed were much lower (by a factor of 35) than those measured in case of a pure sand bed.

Latterly, Williamson & Ockenden (1992) have investigated the erosion characteristics of estuarine mud beds, containing various amounts of fine sand (with sand contents ranging from 0-40%), under the action of waves of increasing significant height (i.e. 0.03 m 0.06 m and 0.12 m). These tests, undertaken in saline waters, showed that the most prominent feature during the experimental period was layering of the beds, with sand added during the wave tests. The sediment beds had developed a fluidised and less dense upper layer early on the experiments. The presence of the (2) layers indicated that the upper part of the bed might have been fluidised prior to erosion; this was supported also by a decrease in the bulk density. In addition, the height of the bed did not appear to have fallen when erosion occurred; instead, the bed level appeared to have risen during erosion, which may have indicated fluidisation during erosion. Further, the results showed that the erosion rates were an order of magnitude higher for the mud (only) beds, than for the beds containing additional sand. This observation indicated that the sand inhibited erosion and reduced the erosion rates. According to Williamson & Ockenden (op. cit.) the presence of sand within the mud matrix might have increased the strength of the bed, making it more resistant to fluidisation and subsequent erosion.

It is not possible to compare the results of the present

study directly with those of the investigations described above, since different experimental equipment and techniques have been used. However, it is useful to undertake a comparison of the general trends observed. Although the samples used throughout the present study show some similarities with those examined by Williamson & Ockenden (1992), the trends identified in both studies are in conflict. In contrast, the results of Van Rijn (1987) support the findings of the present investigation.

It is conventional to relate wave oscillation periods, at threshold, to maximum wave velocities [$U_{o(max)}$] (see, for example, Sleath (1984)); these are presented in Figs 7.7 to 7.10. Particular emphasis in the following discussion is paid to: (i) the degree of scatter in the results, for particular experimental conditions so that the predictability of threshold occurence might be investigated; and (ii) the linearity of the plots and the gradients of the lines of best fit, through the observations represented on each of the graphs. The latter data sets might be used then to indicate the type of flow regime (laminar or turbulent) or the effects of various sediment properties on the erosion threshold of the beds.

The results for the 152.5 μm sand mixtures are shown in Figs 7.7 and 7.8. The data presented indicate a positive relationship between maximum wave (plate) velocity [$U_{o(max)}$] and wave period (T), for $M \leq 30\%$, a negative correlation can be identified for $M > 30\%$.

Further, there does not appear to be any general trend in the range in the scatter of the $U_{o(max)}$ values, for any of the sediment beds or with increasing wave period. The usual scatter, for each of the particular tests, lies approximately within the range of 0.5-3.5 cm s^{-1}. Several

sets of observations show, however, a greater degree of scatter in the $U_{o(max)}$ values. For example, for a wave period within the range of 3.5-4.2 s (Fig. 7.7d), the scatter is of the order of 4.3 cm s^{-1}. For a wave period range of 2.0-2.8 s (Fig. 7.8b), the scatter is of the order of 12.9 cm s^{-1}. For wave period ranges of 2.8-3.3 s and 5.2-5.9 s (Fig. 7.8c), the scatter is of the order of 6.8 cm s^{-1} and 3.9 cm s^{-1}, respectively. Generally, the excess scatter appears to be higher for the shorter wave periods. However, since the observations are limited, it is somewhat difficult to identify whether it is due to experimental uncertainty or is significant scientifically.

Figures 7.7 and 7.8 show also that the relationship between $U_{o(max)}$ and T appears to be linear. Hence, a line of best fit might be drawn through these variables (shown as a dashed line on the Figs). However, in some cases, the correlation coefficients (r^2) of the regression lines are not significant (Figs 7.7a, 7.7b and 7.7d). In addition, it is worth noting that there is a reversal in the gradients of the regression lines associated with admixtures with M > 30% (Figs 7.8b and 7.8c). In general, such a reversal is indicative of a change in the flow regime, or the physical parameters of the sediment beds (Sleath, 1984). As the regime during all the oscillatory flow experiments remained laminar (Section 5.3), it may be concluded that the trends indicate some modification to the physical characteristics and properties of the muddier sediment deposits. Such a pattern will be demonstrated in the results presented below, in relation to pore water pressures, liquid limits and the rheological properties of the deposits.

Finally, the results for the 215 μm sand admixtures are shown on Figs 7.9 and 7.10. Once again, there is a linear

(with r^2 significant at the 95% confidence level) positive correlation between $U_{o(max)}$ and T, for M $\leq$ 30%; this changes to a linear negative relationship, not significant, when the mud content is in excess of 30%. This modification implies, once again that the physical characterisics of the muddier sediments may have changed drastically. Further, the scatter of the $U_{o(max)}$ values in relation to the various sediment beds and wave periods shows a random distribution. Such scatter, for each particular experiment, ranges usually from 0.5-2.5 cm s^{-1}. The fact that some of the observations demonstrate a higher level of scatter in $U_{o(max)}$ values may be attributed to experimental error. For example, in Fig. 7.9c, for a wave period range of 5.2-5.8 s, the scatter is of the order of 3.0 cm s^{-1}. In Fig. 7.10b, for wave period ranges of 3.0-3.7 s and 4.5-5.3 s, the scatter is of the order of 5.5 cm s^{-1} and 5.4 cm s^{-1}, respectively. Finally, in Fig. 7.10c, for wave period ranges of 3.0-3.4 s, 3.5-4.1 s and 5.6-6.3 s, the scatter is of the order of 3.9 cm s^{-1}, 4.6 cm s^{-1} and 3.6 cm s^{-1}, respectively.

A review of the raw data plots (Figs 7.7 to 7.10), representing all the oscillatory flow threshold experiments, demonstrates that the degree of scatter in the experimental results appears to be random. Since there is not any obvious trend, the only conclusion which can be drawn from the results is that there is a degree of uncertainty inherent in the oscillatory flow experiments; this may be attributed to threshold observation variability, together with the statistical nature of the bed arrangement. Such uncertainty causes scatter in the threshold results, which overrides any predictability in the threshold conditions associated with the laminar flow regime prevailing during the hydraulic tests. This summary demonstrates also that all of the relationships shown on Figs 7.7 to 7.10 indicate

some degree of linearity, which suggests that a line of best fit can be drawn through all the points using standard regression techniques. This procedure was undertaken in an attempt to investigate any potential change in the physical parameters of the mixed sediment beds. In describing these graphs, it is appreciated that the lines of best fit were derived on the basis of only limited (4) values of wave stroke. Hence, if the results from one of the experimental conditions were defective in some way (e.g. through observational errors of judgement), this would have had a significant influence on the gradient of the regression line. Therefore, only apparent trends can be inferred from the relationships obtained.

Finally, some attempt has been made to undertake a comparison of the data of the present study with the Komar & Miller (1974) expression (Eq. 2.80), as represented by the solid line in Figs 7.7 to 7.10. This expression was derived originally to describe the erosion threshold conditions related to rounded non-cohesive unimodal sediments, under laminar flow regimes. The data of several investigators, including Bagnold (1946), Manohar (1955) and Rance & Warren (1968), were incorporated into this wide-ranging synthesis. Although threshold results related to the present study are underestimated in the expression, due mainly to the angular shape of the sand fraction of the mixtures (Section 6.3.1), for $M \leq 30\%$ and the majority of the sediment beds (Figs 7.7a, 7.7b, 7.7c, 7.7d, 7.8a, 7.9b and 7.10a), the Komar & Miller (op. cit.) function may describe adequately the rate of incremental increase of the maximum wave-induced velocity with wave period. This association is indicated by the parallel trend between the dashed and solid lines on the Figs. In the domain $M > 30\%$, there is a reversal in the slopes of the dashed

and solid lines (Figs 7.8b, 7.8c, 7.10b and 7.10c); this implies that the admixtures with the larger mud quantities are purely cohesive in character. Consequently, the Komar & Miller formula (1974) is insufficient to describe the behaviour of such sedimentary material.

7.2. PORE PRESSURE RESPONSE

7.2.1. Introduction

In recent years, the effect of wave loading on the seabed has become of increasing importance in the design of offshore structures (Bjerrum, 1973). In particular, such loading may produce shear stresses sufficient to overcome the shear strength of the soils, resulting in their failure. Further, repetitive wave loading can cause an increase in the ambient pore water pressure; this may lead, under extreme conditions, to liquefaction of the sediment bed (Seed & Rahman, 1978; Foda & Tzang, 1994).

There is a general absence of studies concerned with the influence of a clay fraction on pore water pressures within sandy deposits, under wave loading. However, specifically (Thomas & Sills, 1994), pore water pressure has been measured at various levels beneath the sediment/water interface in various shallow water deposits (South Wales, UK). Pore pressure fluctuations within the muddy beds were found to be much lower than those associated with the sandy beds. Pressure dampening may well have been due to the presence of gasses inside the pore spaces within the sediment deposits (Thomas & Sills, op. cit.)

7.2.2. Data Collected and Discussion

(a) Set A

Pore water pressure measurements, at the threshold of movement under oscillatory flow, are shown on Figs 7.11 to 7.30. Additionally, standard deviations of the pore pressure recordings are shown on Tables 7.2 to 7.15. Unfortunately, functional problems with the pressure sensor during the tests associated with the 215 μm sand admixtures and for wave strokes greater than 0.283 m, have limited the pore pressure records available. Nevertheless, some trends can be identified.

Each pore pressure signal is the combined result of the sinusoidal motion (acceleration and deceleration) of the oscillating plate and the standing wave formed within the flume during the experiments (Section 7.1.1). In several cases, the standing wave has affected the shapes of the pressure output in such a way that they deviate from the purely sinusoidal form (see, for example, Figs 7.23 to 7.26). The results show overall, a significant reduction in the pore pressure fluctuation amplitude for the most of the more-difficulty eroded muddier samples (M > 30%) (in contrast, in the absence of any fine-grained sediments, the amplitude of the water pressure fluctuation increases as the wave period decreases (Tables 4.4 to 4.7)). This pattern appears to be more intense for the shorter wave periods (Figs 7.11 to 7.14, 7.15 to 7.18 and 7.27 to 7.30). It is very interesting that the observed dampening of the pore pressure fluctuations occurs within the upper 20 mm of the sediment deposits. Therefore, the effect of the increased clay (mineral) content can be considered as substantial on this physical response of the sediment deposits.

The decrease in pore pressure fluctuations associated with the muddier admixtures may be explained in terms of observations made elsewhere. For example, it is well known from field studies (Wit & Kranenburg, 1992) that the measured level of attenuation, for different wave heights, is the result of the dissipation of energy within the sediment bed. Such dissipation is likely to depend mainly upon the rheological properties, controlled principally by the nature and magnitude of the clay mineral content (Ando & Yamamoto, 1991). Therefore, it may be suggested that muddier admixtures of sediments are characterised by distinct changes in their rheological properties as demonstrated by the yield stress determinations (Chapter 9). Such changes may explain any reduction in the pore pressure amplitude. Another explanation for the dampening of the pore water pressure fluctuations could be that, at clay contents exceeding 11% to 14% there is probably a radical decrease in the sediment permeability. Hsu & Jeng (1993) have investigated pore pressures and effective stresses, induced by short-crested waves, for a (95%) partially-saturated anisotropic soil matrix of infinite depth. These investigators showed that a reduction in the soil permeability can lead to a reduction in the pore pressure amplitude, within the upper layer of the sediment deposit.

The trends outlined above are relevant to the interpretation of Figs 7.7 to 7.10 (see above), concerning the modification of the physical characteristics of the muddier deposits.

(b) Set C

The objectives related to these particular pore pressure measurements were: (i) to validate pore pressure

attenuation within the muddier admixtures, identified during Set A; and (ii) to examine the possible correlation of pore pressure amplitude with the threshold of sediment motion. The results of these measurements are listed in Tables 7.20 to 7.33: The terms 'pressure 1' and 'pressure 2', in the description, refer to output obtained from the sensors located at the surface of the oscillating plate and beneath the sediment/water interface, respectively.

In general, there is attenuation of the signal transmitted into the bed: this shows a dependence upon wave stroke and period (see below) and is more evident for sediments with M > 30%. However, the majority of the measured pressure attenuations associated with the admixtures with M ≤ 30% must be considered with some caution. Such attenuations have been derived from σ values representing a pressure difference (pressure 1 - pressure 2) which lies within the range of the electrical noise (0.05 cm), inherent in the water pressure signals.

The changes in pore pressure fluctuation with an increasing mud content, for a particular wave stroke and various oscillation (wave) period ranges, are shown on Figs 7.31 to 7.38. Once again, dampening of the pore pressure amplitude is evident within the muddier admixtures. Further, the dampening is more intense for the shorter wave periods (see, for example, Figs 7.31, 7.33 and 7.35). Finally, at a particular wave period, any reduction in pore pressure fluctuations within the muddier sediments is higher for the longer wave strokes (compare, for example, Figs 7.31a and 7.32b; 7.33a and 7.34c; and 7.35b and 7.36c).

Characteristic pressure records related to Figs 7.31c and 7.37b are shown in Figs 7.39 to 7.42 and 7.43 to 7.46,

respectively.

Based upon the results of previous observations (Foda & Tzang, 1994), an attempt has been made here to investigate the influence of pore pressure amplitudes on the threshold of sediment movement. Any such correlation might lead to a reconsideration of theoretical concepts concerning the threshold of movement of loosely-consolidated, but solid, boundaries. The previous studies have identified a resonant stage, in the laboratory, during the complex process of soil fluidisation by water waves. Massive fluidisation failure was observed consistently, following internal resonance events (i.e. the amplification of the pore pressure fluctuation) within a silty bed (with a mean grain size of 50 μm). The weakening effect of this resonance was observed to endure long periods of consolidation. Wave reloading, following such consolidation on a pre-resonated silty soil, resulted in a recurrence of similar massive fluidisation failure. Analysis of the pore pressure records has indicated that the resonant events were the result of strong channelling of the seepage flow within the silt bed. For the present study, therefore, it was decided to examine whether or not a similar resonant stage existed at threshold.

For the above purpose, threshold (critical) conditions were approached gradually in (5) steps (with each step corresponding to a different $U_{o(max)}$ value). Attenuation of the pressure heads, transmitted into the sediment bed, were calculated. An anticipated trend, which might indicate correlation between the pore pressure amplitude and the erodibility of the sediments, might be as follows: (i) as threshold is approached, the attenuation of pressure transmitted into the bed would be constant or increase; and (ii) at the moment of threshold, an

apparent reduction of this attenuation could appear i.e. with the pore pressure fluctuation amplified with reference to the amplitude of the pressure head, produced by particular wave conditions.

Pressure attenuations associated with sediment mixtures with M > 30% (Tables 7.25, 7.26, 7.32 and 7.33) were used in the analysis; these were considered as the most reliable (see above) data sets. The results are shown in Figs 7.47 and 7.48, where the oscillation (wave) period is plotted against pressure attenuation, for the various wave strokes. Generally, pressure attenuation increases as the wave period decreases and threshold of particle movement is approached. Further, at the moment of critical motion, the pressure attenuation continues to show a further increase; only in two cases is the trend reversed. Such reversal is shown in Fig. 7.47b, related to the 152.5 μm sand mixtures containing 50% of mud. Here, for strokes of 0.283 m and 0.468 m (shown as dashed lines on the Fig.) the pressure attenuation increases initially; during critical conditions, it displays some reduction (see Table 7.26, for a listing of the pressure attenuation values). Hence, the pore pressure fluctuation is amplified in relation to the amplitude of the pressure head (measured by the sensor located at the surface of the plate) caused by the prevailing wave conditions. However, reduction in the attenuation of the pressure is not particularly high. Thus, it may be assumed that the reduction is due to experimental error, caused by the noise inherent to the pressure signals. In conclusion, the results of the present study do not indicate any relationship between the observed pore pressure amplitude and threshold of movement.

For comparison, Figs 7.49 to 7.51 and 7.52 to 7.54 show the pressure records relevant to the 0.283 m and 0.468 m

wave strokes of Fig. 7.47b, respectively. Figs 7.55 to 7.57 and 7.58 to 7.60 display pressure records relevant to the 0.378 wave stroke of Fig. 7.48a and 0.283 m wave stroke of Fig. 7.48b, respectively.

Finally, during the Set C measurements, the erosion threshold of various sand-mud mixtures was again defined (see Tables 7.20 to 7.33), in order to examine the reliability of the earlier threshold determinations under oscillatory flow (the Set 2 tests). Such a comparison showed that the newly derived thresholds were contained within the reproducibility limit (±4%) of the earlier determinations.

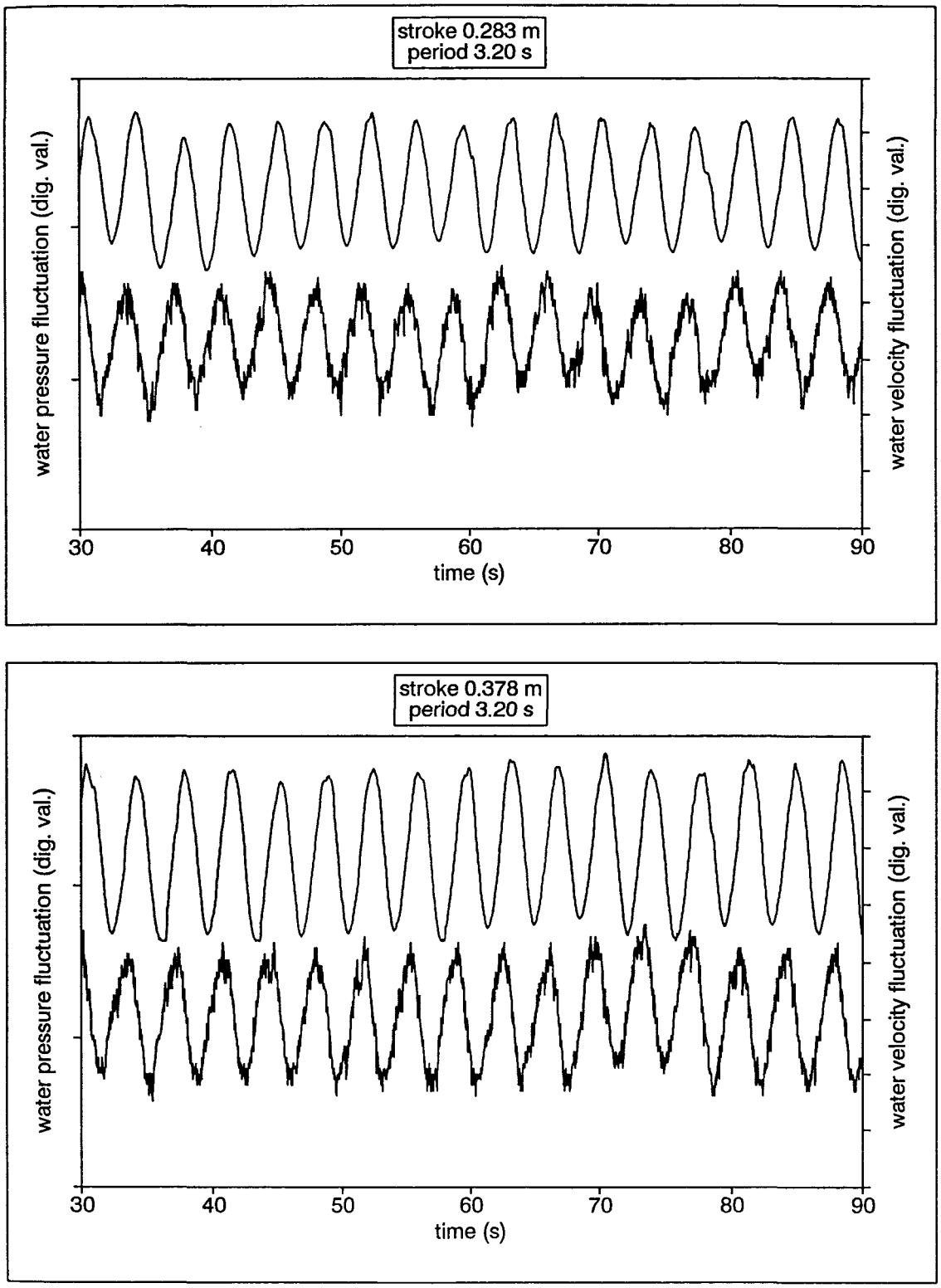

Fig. 7.1. Simultaneous water velocity (upper plot) and pressure (lower plot) measurements, demonstrating the existence of a standing wave in the flume during the oscillatory hydraulic experiments (strokes of 0.283 m and 0.378 m; and period of 3.20 s).

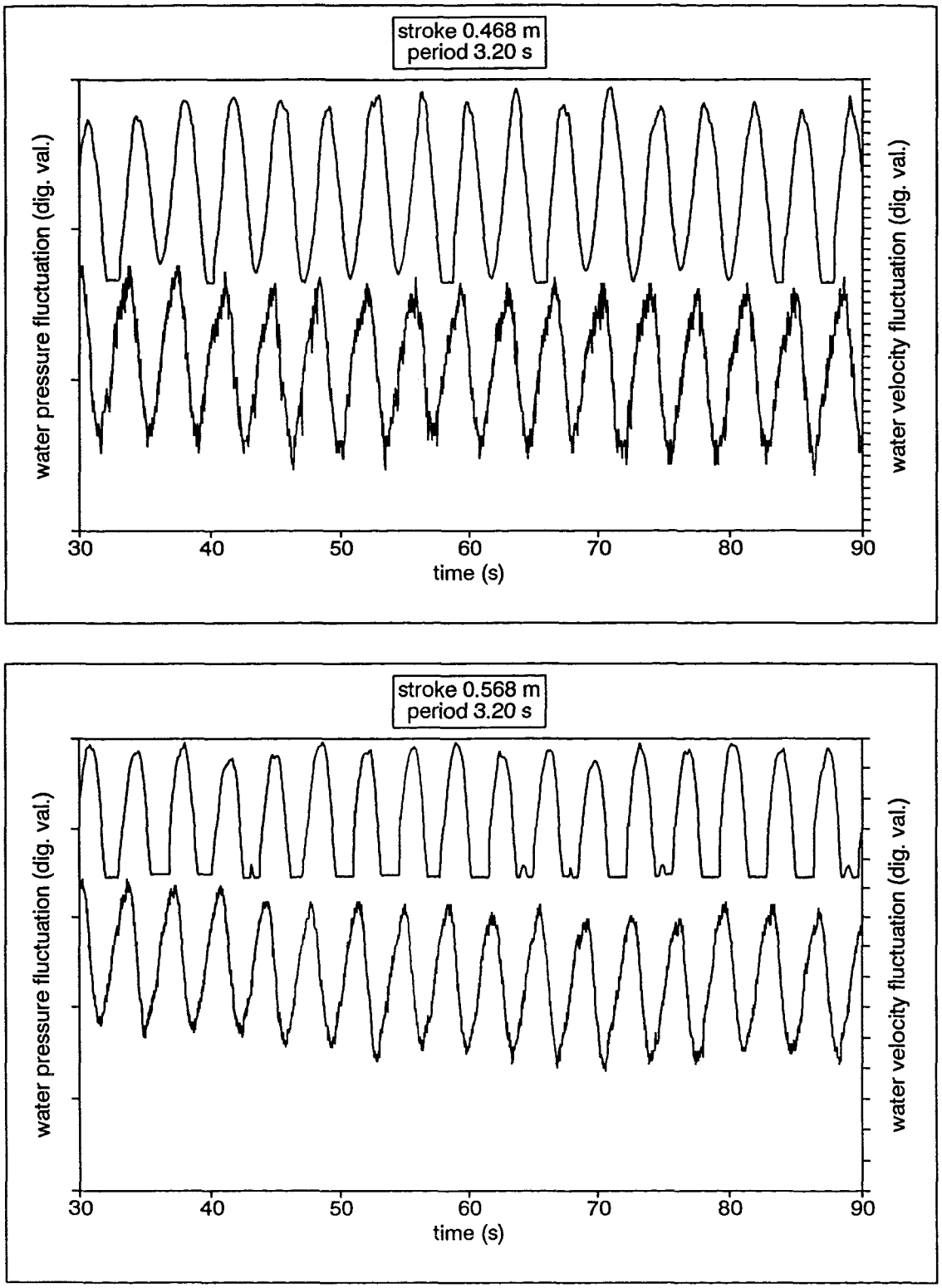

Fig. 7.2. Simultaneous water velocity (upper plot) and pressure (lower plot) measurements, demonstrating the existence of a standing wave in the flume during the oscillatory hydraulic experiments (strokes of 0.468 m and 0.568 m; and period of 3.20 s).

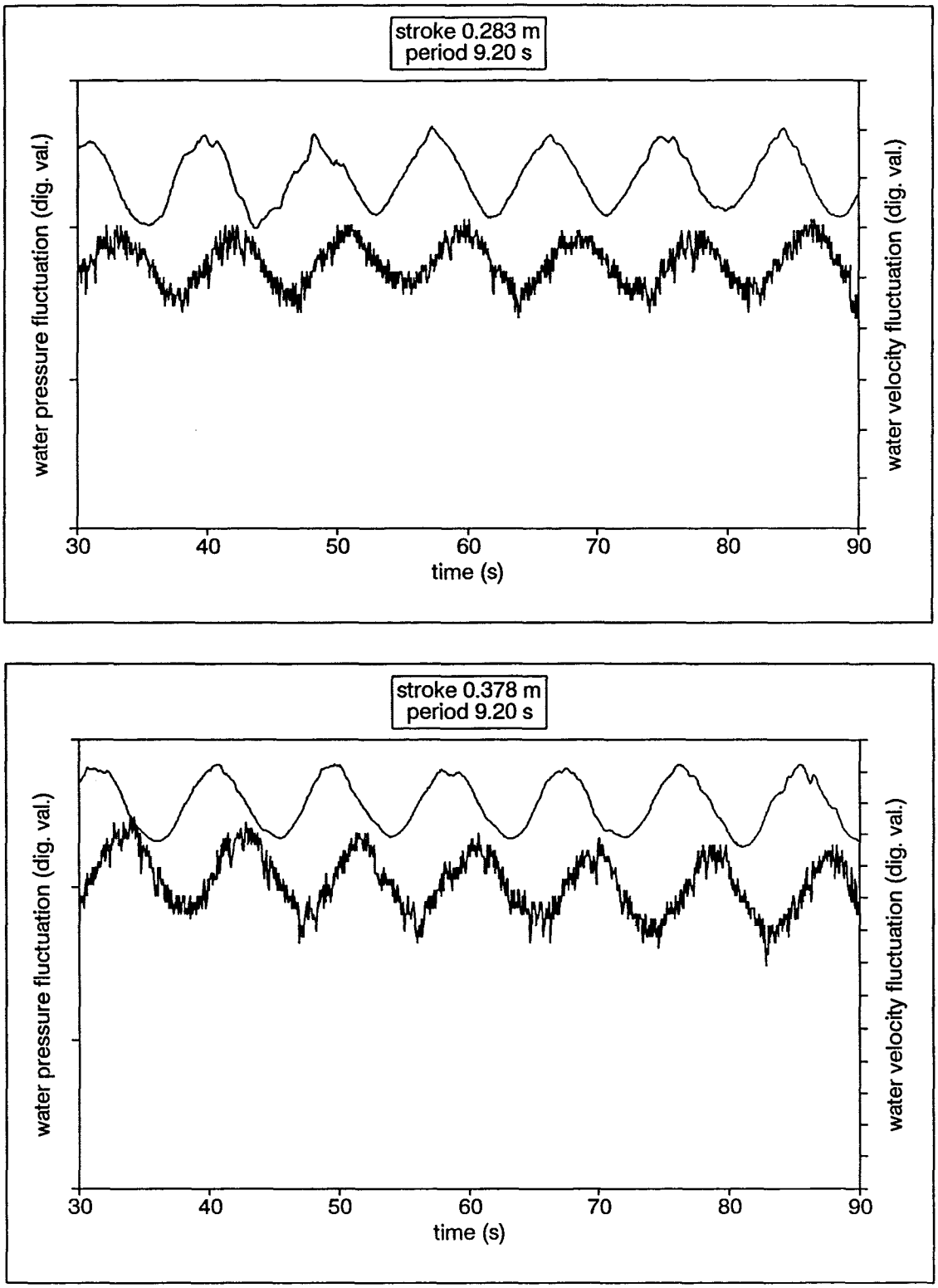

Fig. 7.3. Simultaneous water velocity (upper plot) and pressure (lower plot) measurements, demonstrating the existence of a standing wave in the flume during the oscillatory hydraulic experiments (strokes of 0.283 m and 0.378 m; and period of 9.20 s).

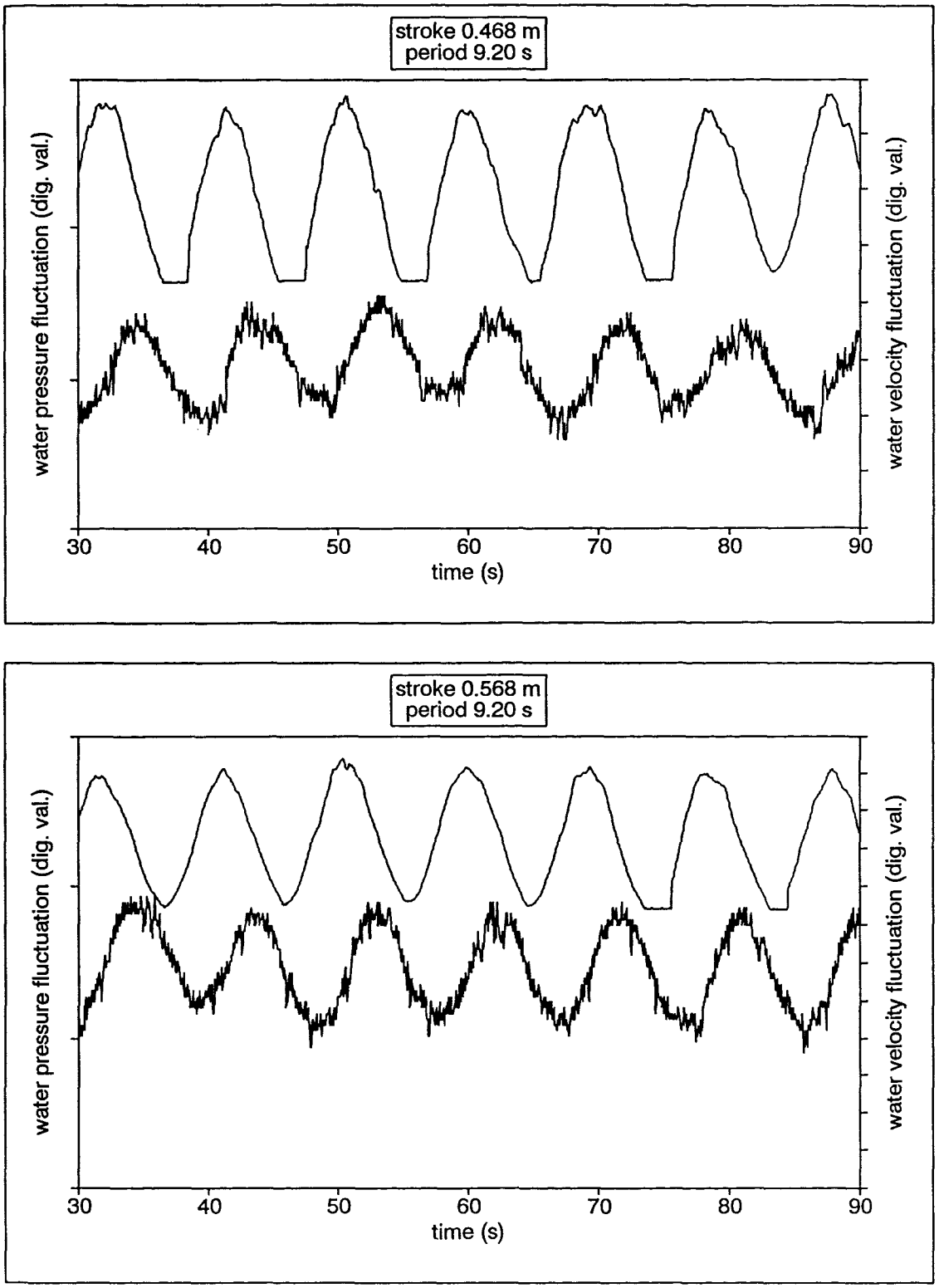

Fig. 7.4. Simultaneous water velocity (upper plot) and pressure (lower plot) measurements, demonstrating the existence of a standing wave in the flume during the oscillatory hydraulic experiments (strokes of 0.468 m and 0.568 m; and period of 9.20 s).

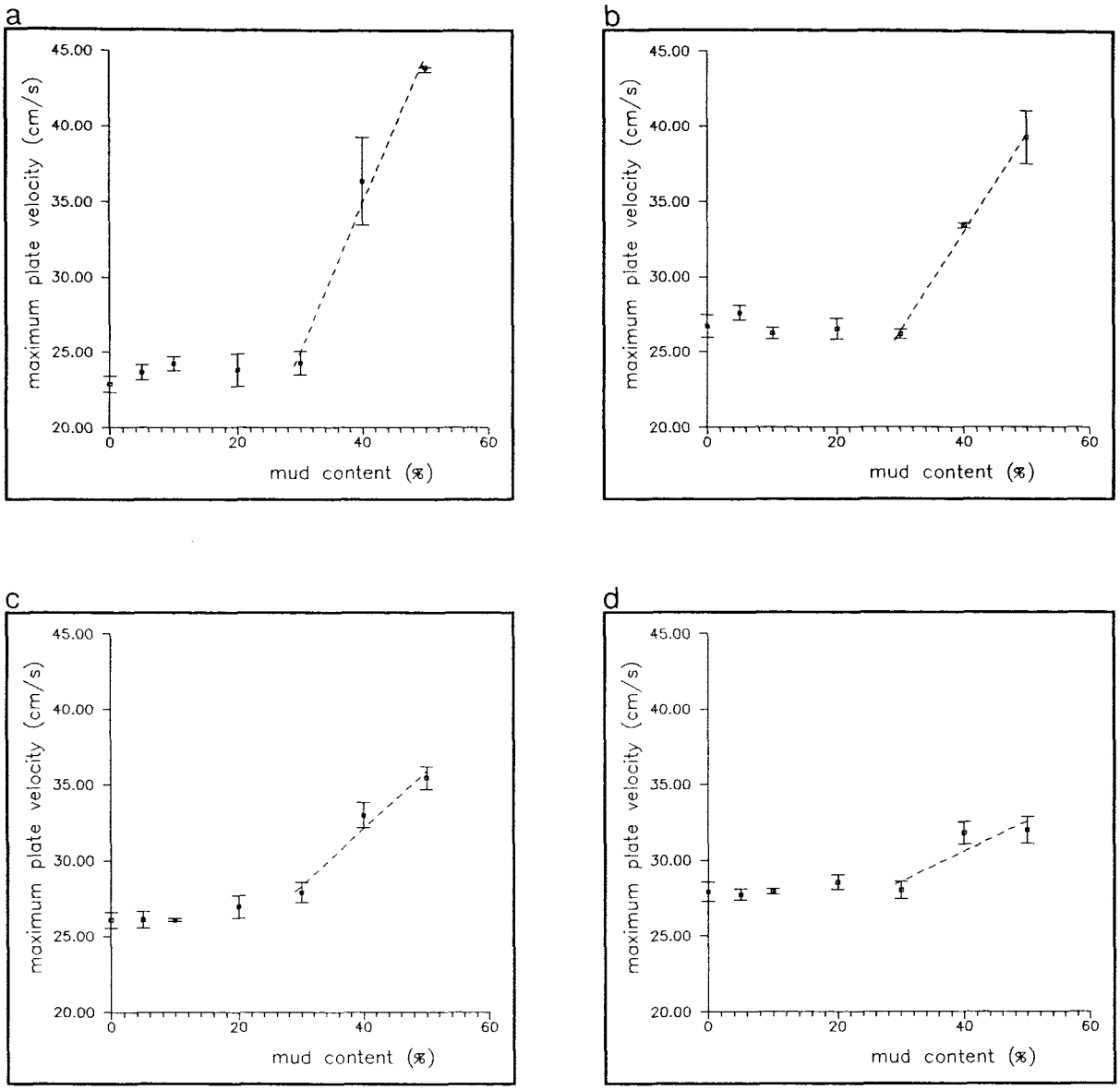

Fig. 7.5. Variation in critical maximum plate (wave) velocity, with the mud content of sediments containing 152.5 μm sands and under the action of simulated waves, for strokes of:
(a) 0.283 m; (b) 0.378 m; (c) 0.468 m; and (d) 0.568 m (Note: The mean and the standard error of the mean are displayed).

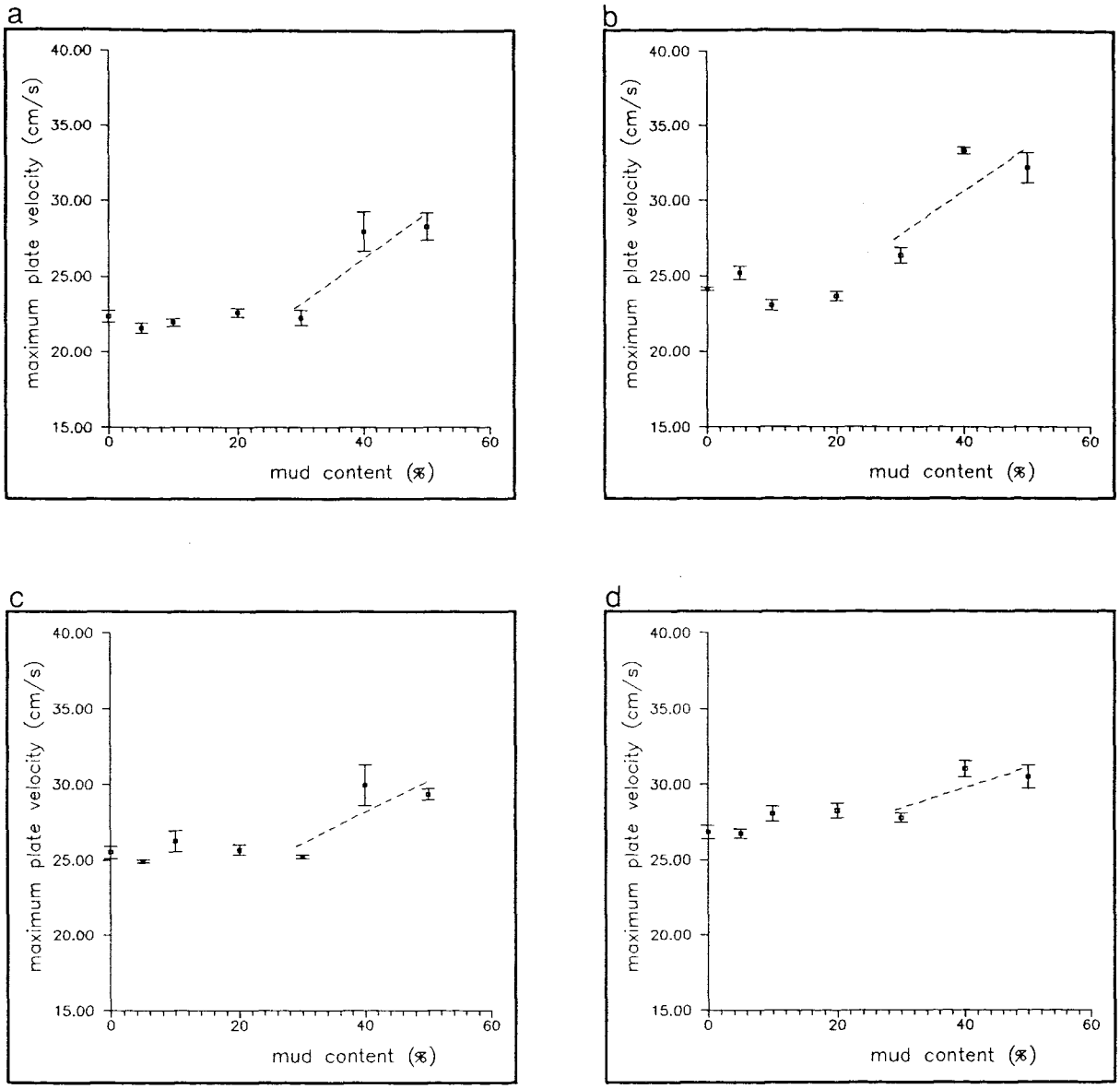

Fig. 7.6. Variation in critical maximum plate (wave) velocity, with the mud content of sediments containing 215 μm sands and under the action of simulated waves, for strokes of:
(a) 0.283 m; (b) 0.378 m; (c) 0.468 m; and (d) 0.568 m (Note: The mean and the standard error of the mean are displayed).

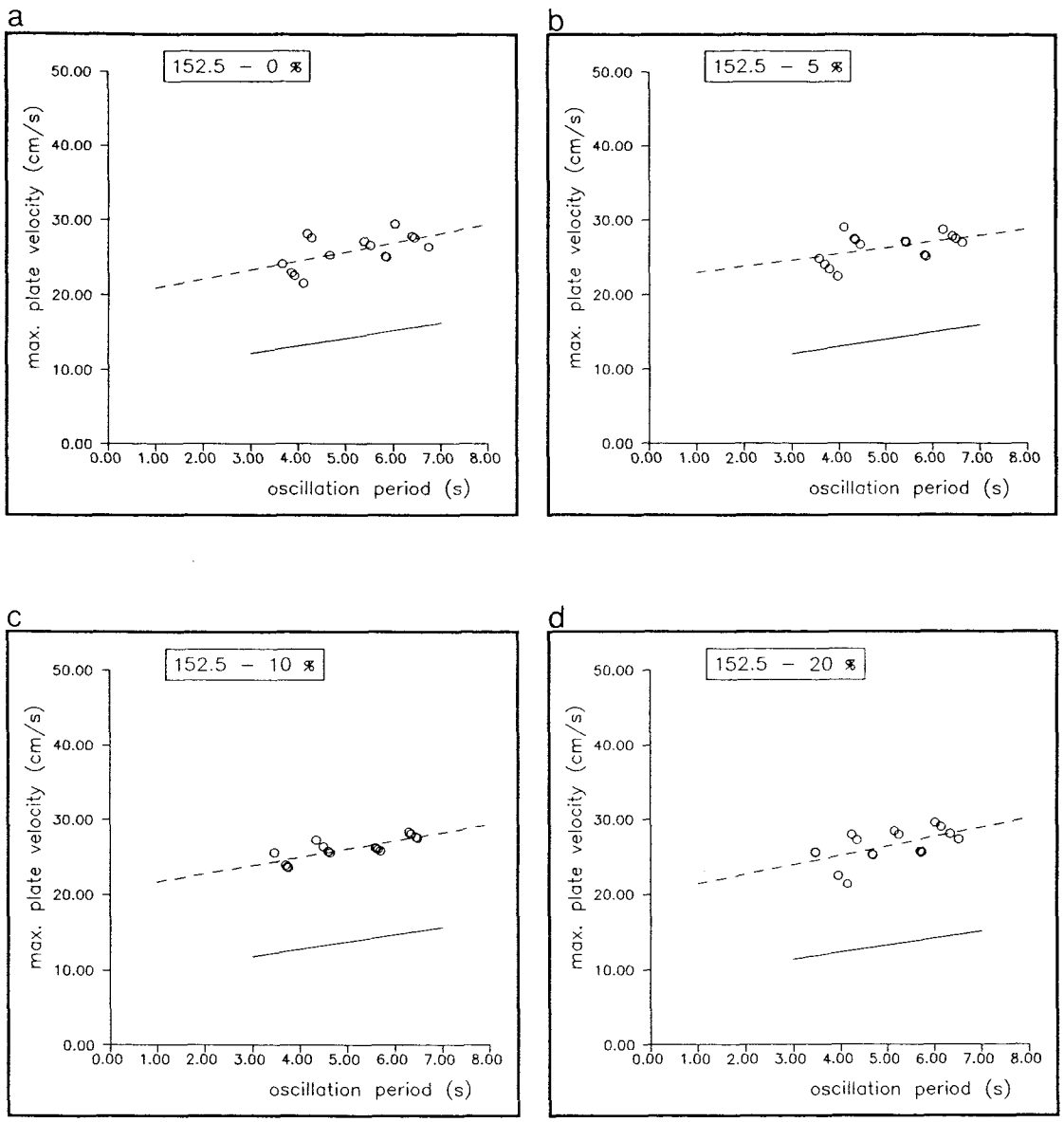

Fig. 7.7. The threshold conditions under oscillatory flow, for various sand-mud admixtures, compared with the Komar & Miller expression (solid line).

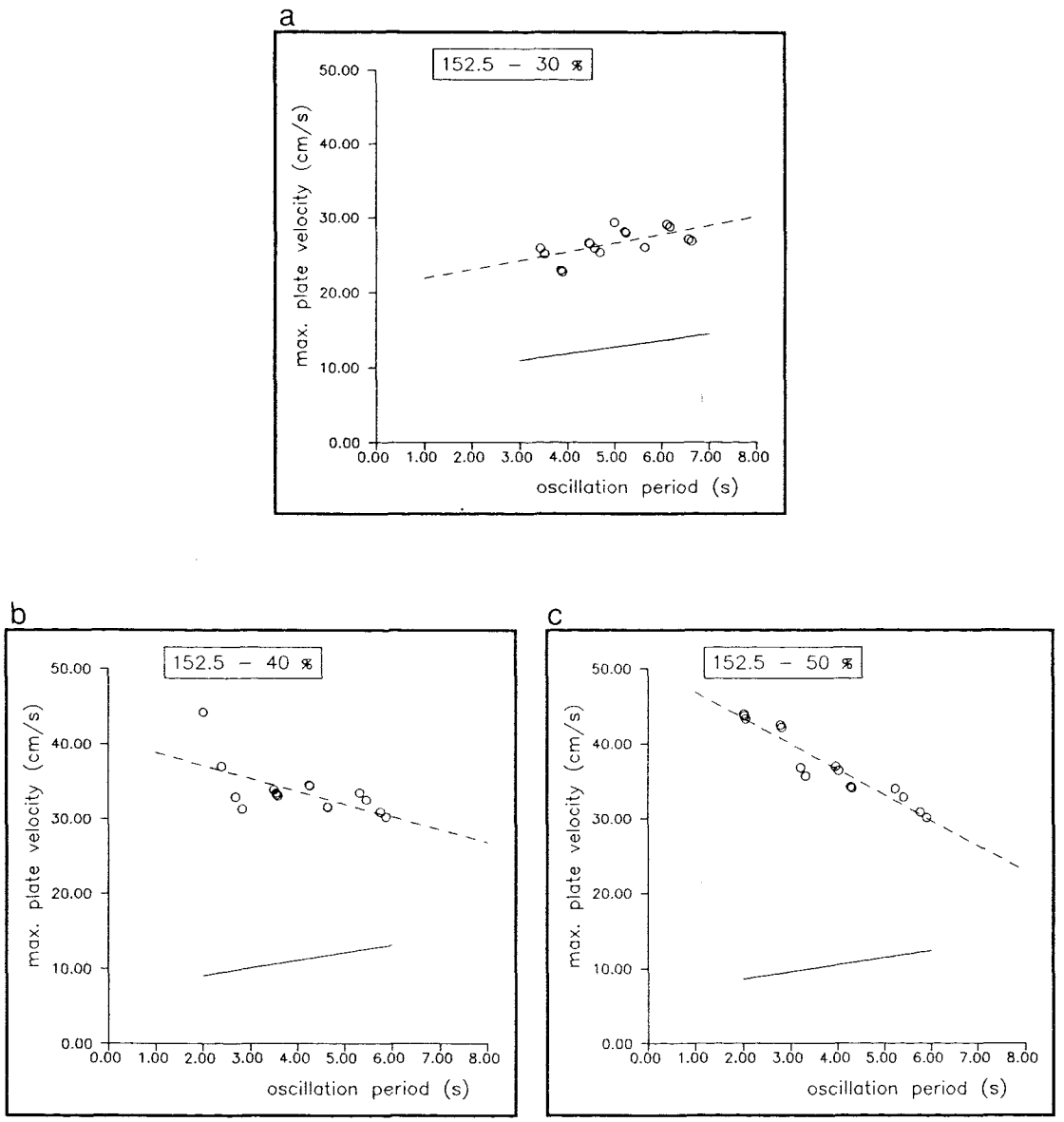

Fig. 7.8. The threshold conditions under oscillatory flow, for various sand-mud admixtures, compared with the Komar & Miller expression (solid line).

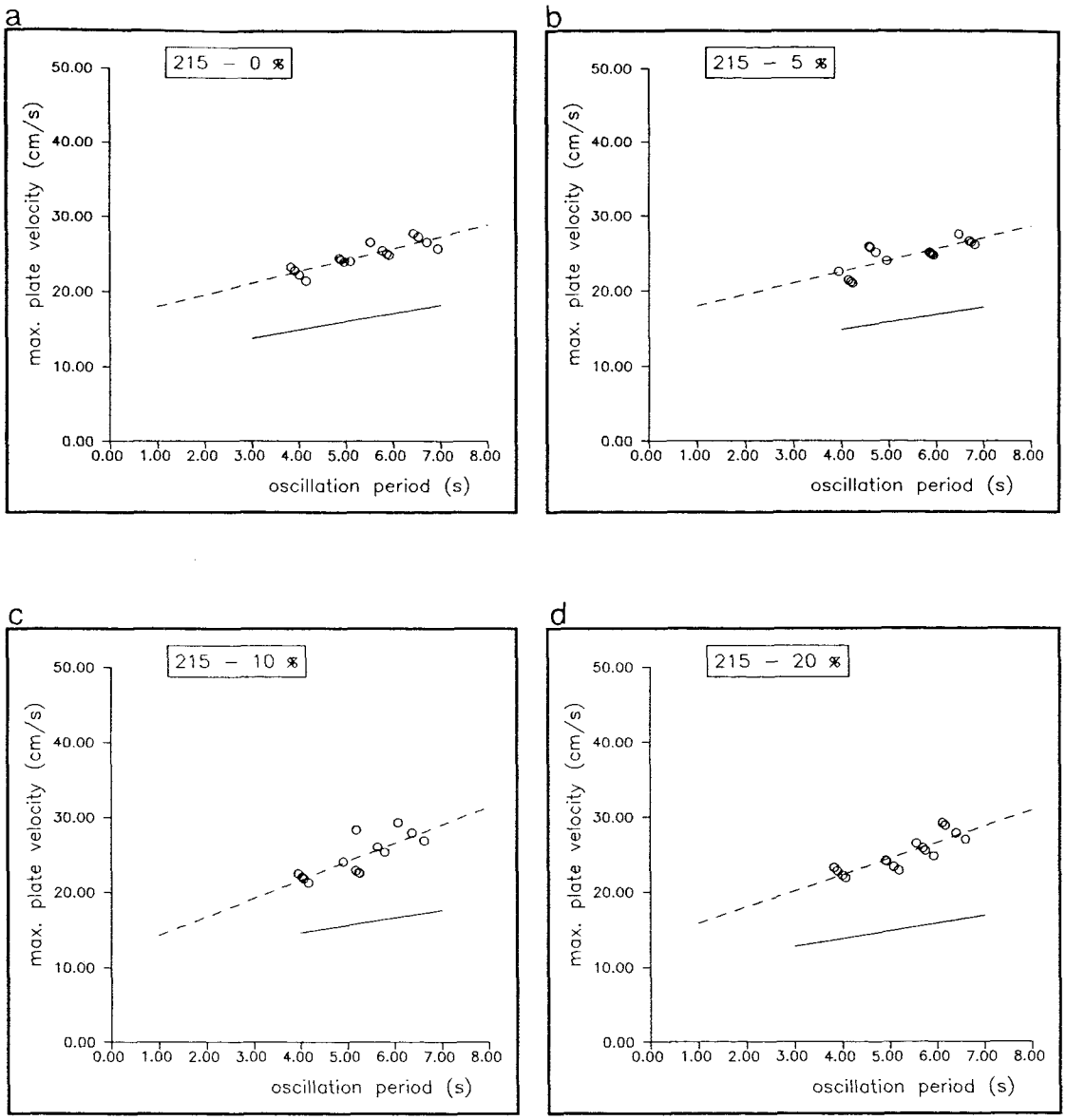

Fig. 7.9. The threshold conditions under oscillatory flow, for various sand-mud admixtures, compared with the Komar & Miller expression (solid line).

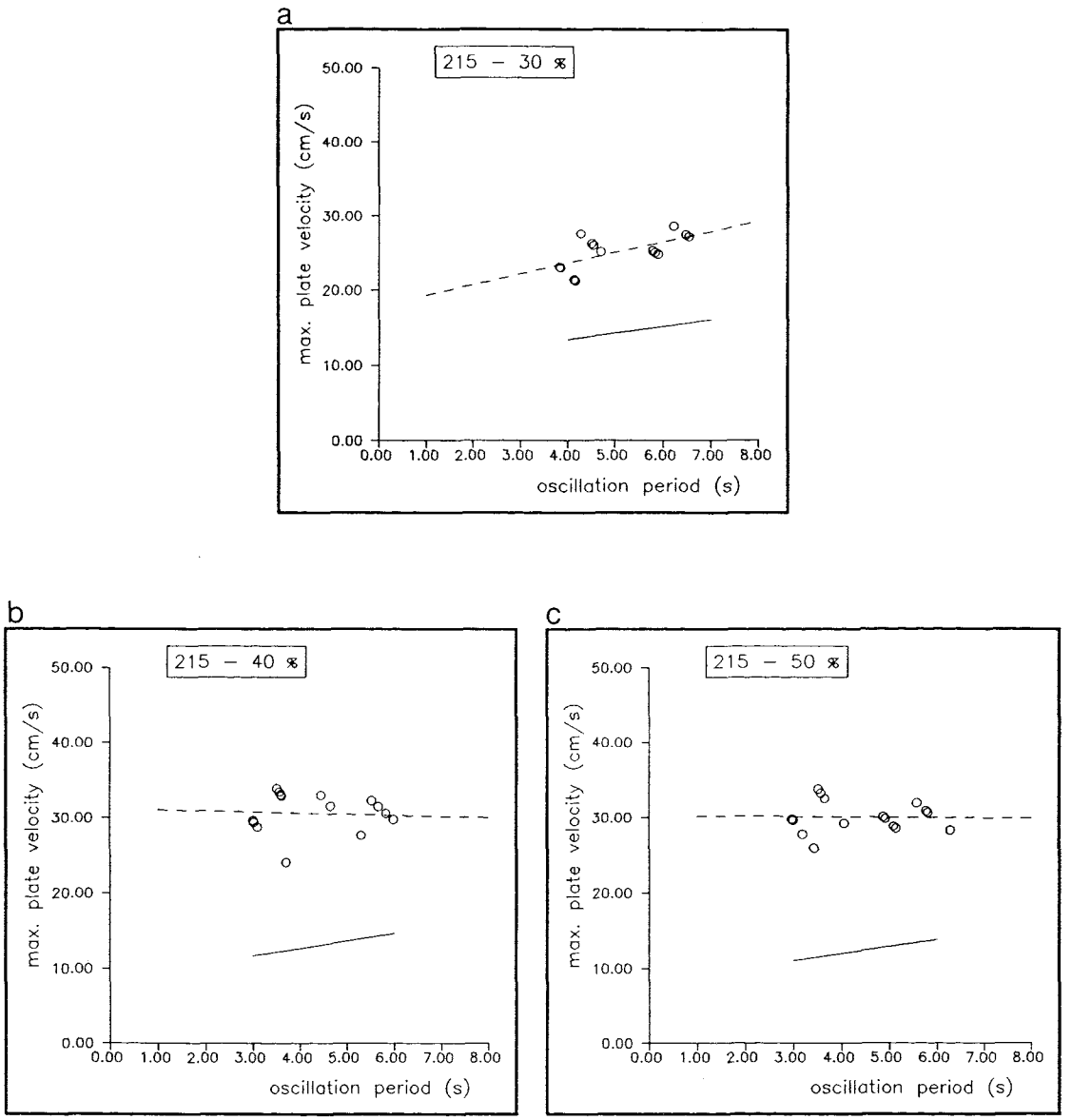

Fig. 7.10. The threshold conditions under oscillatory flow, for various sand-mud admixtures, compared with the Komar & Miller expression (solid line).

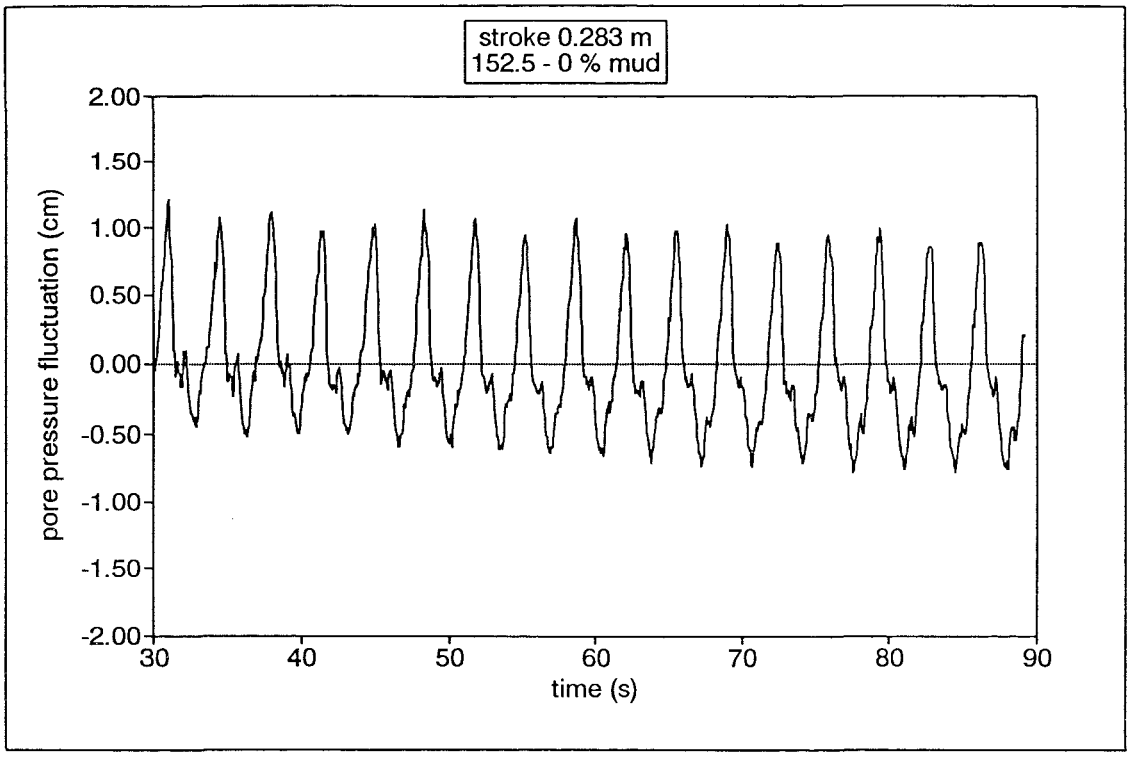

Fig. 7.11. Pore water pressure measurements obtained at 2 cm below the sediment/water interface, for the sediment bed containing only sand of 152.5 μm size, under a wave stroke of 0.283 m.

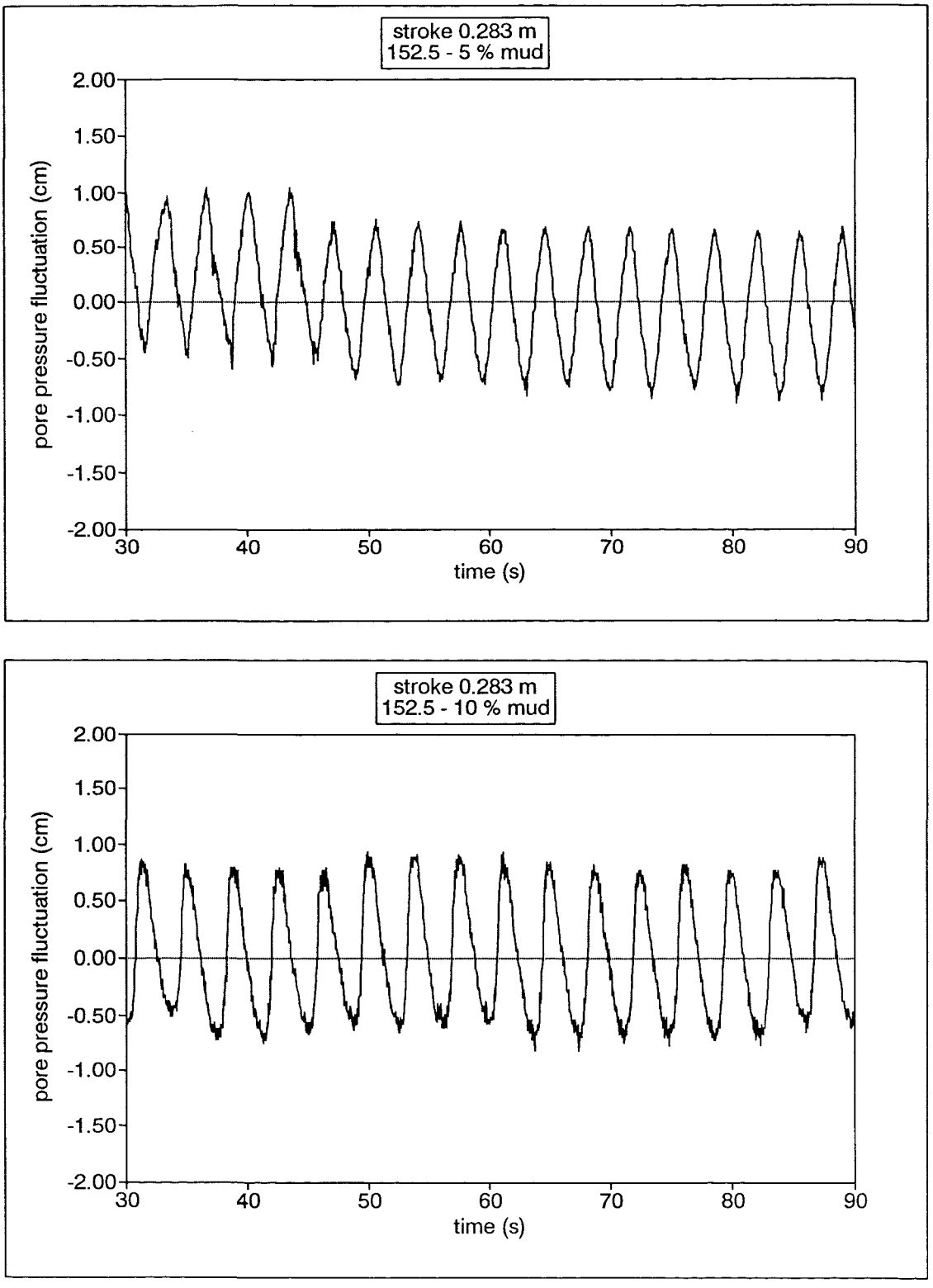

Fig. 7.12. Pore water pressure measurements obtained at 2 cm below the sediment/water interface, for the sediment beds containing the 152.5 μm sand fraction and mud contents of 5% and 10% respectively, under a wave stroke of 0.283 m.

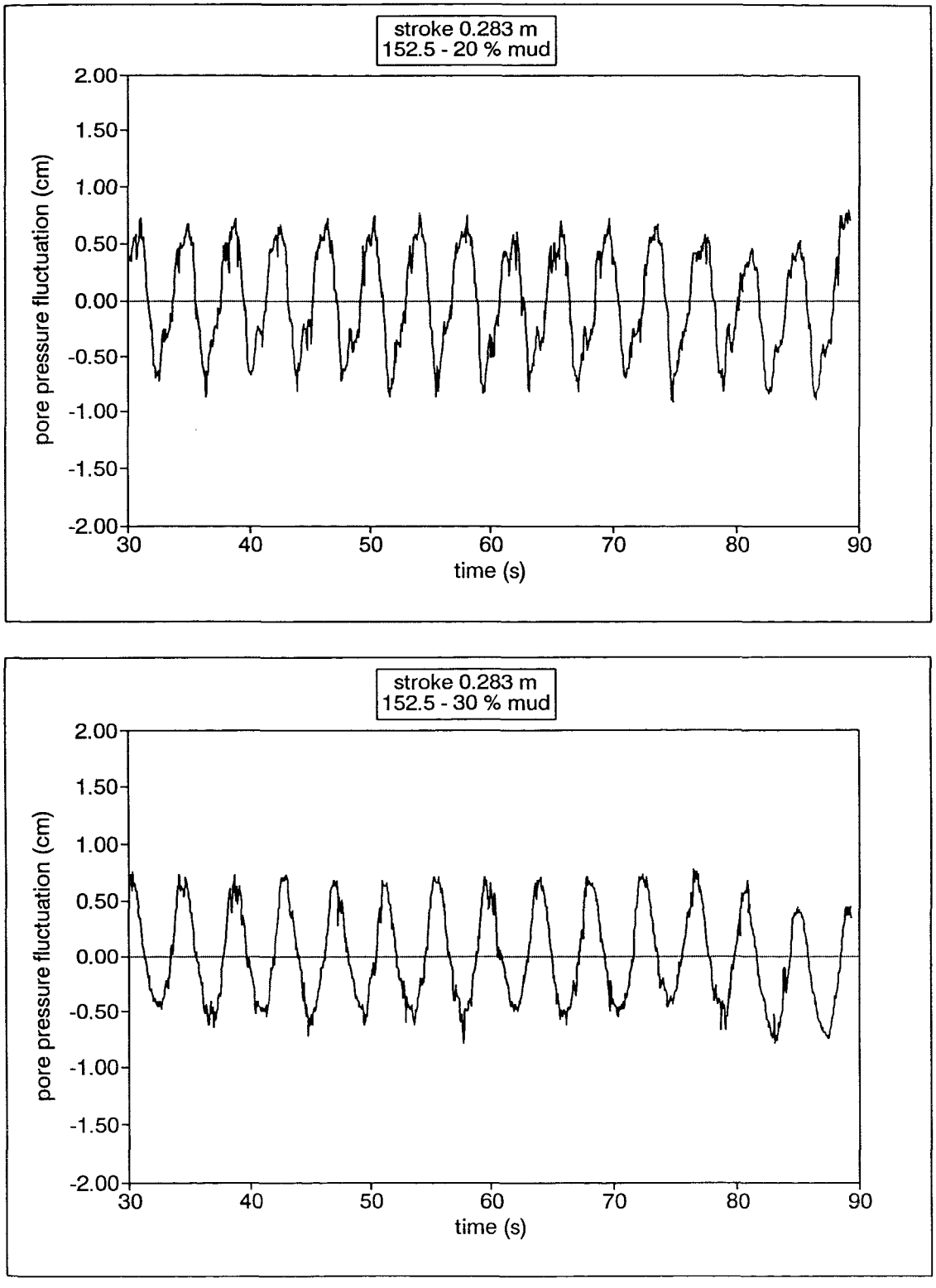

Fig. 7.13. Pore water pressure measurements obtained at 2 cm below the sediment/water interface, for the sediment beds containing the 152.5 μm sand fraction and mud contents of 20% and 30% respectively, under a wave stroke of 0.283 m.

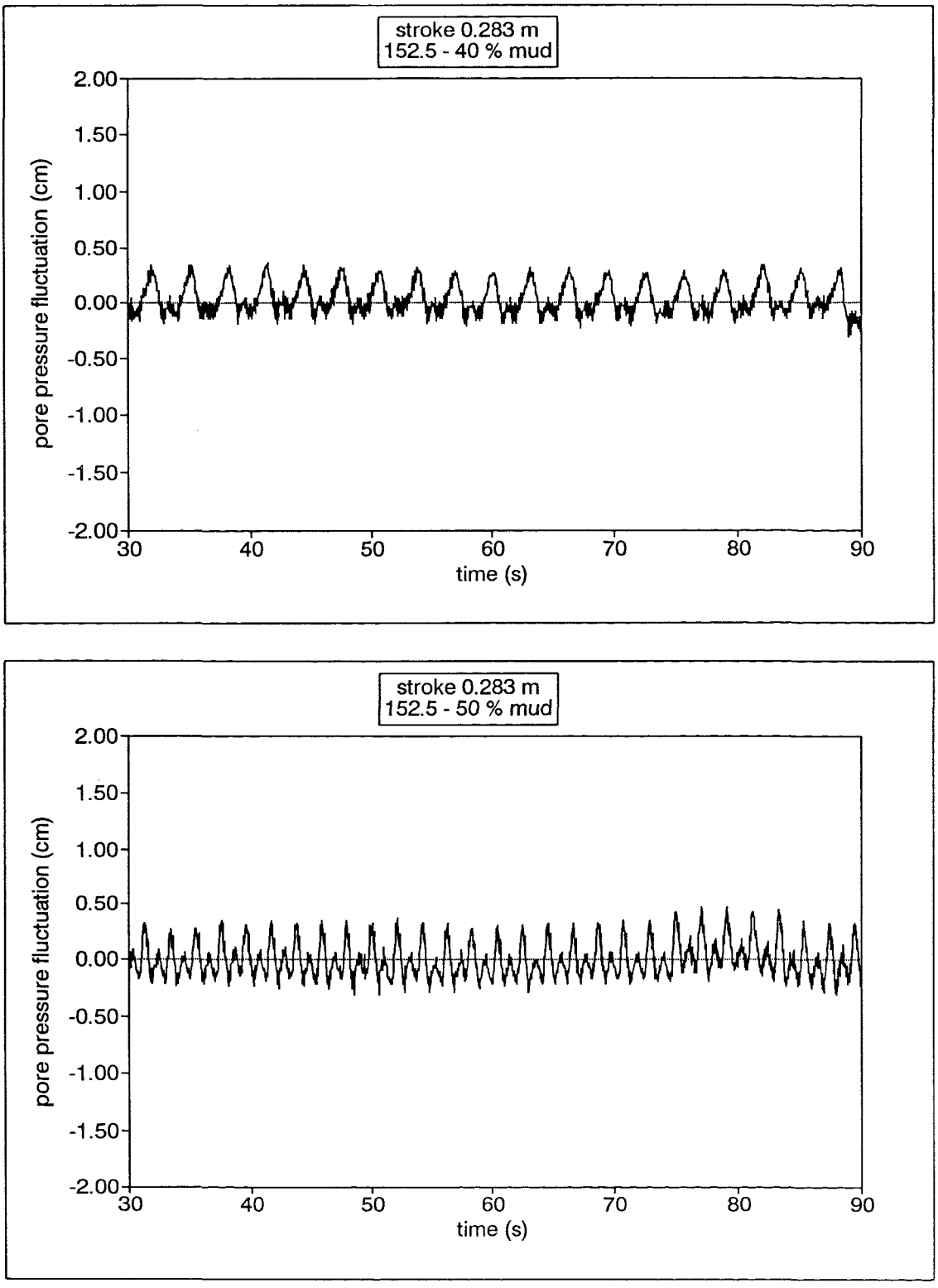

Fig. 7.14. Pore water pressure measurements obtained at 2 cm below the sediment/water interface, for the sediment beds containing the 152.5 μm sand fraction and mud contents of 40% and 50% respectively, under a wave stroke of 0.283 m.

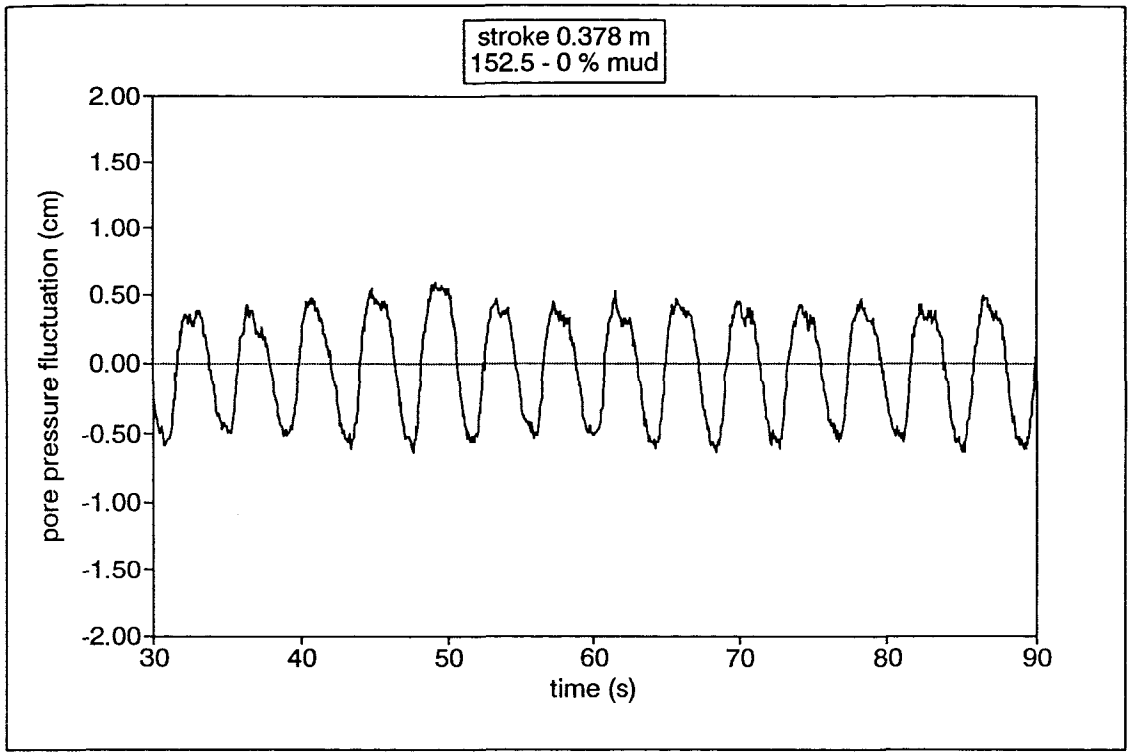

Fig. 7.15. Pore water pressure measurements obtained at 2 cm below the sediment/water interface, for the sediment bed containing only sand of 152.5 μm size, under a wave stroke of 0.378 m.

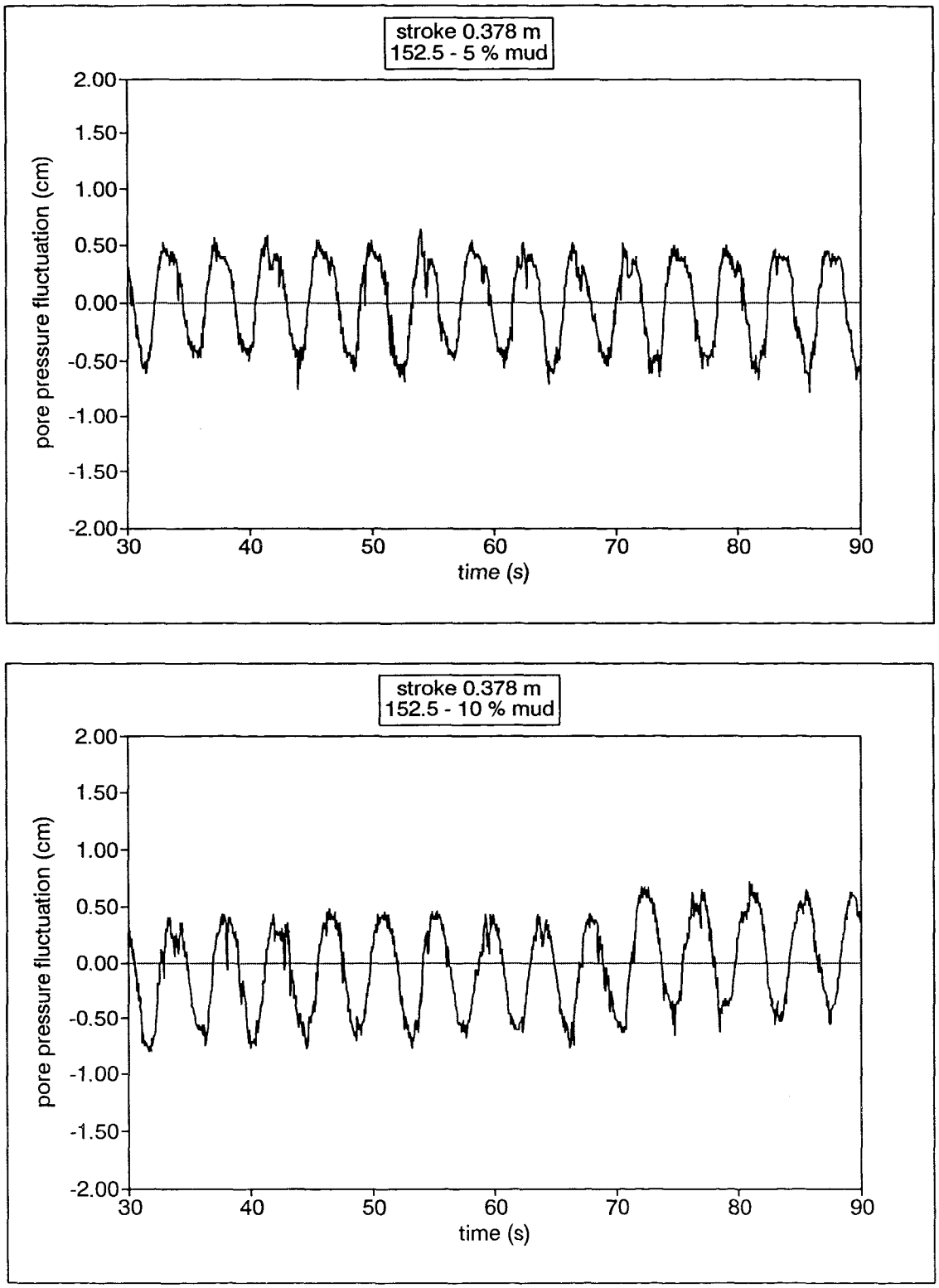

Fig. 7.16. Pore water pressure measurements obtained at 2 cm below the sediment/water interface, for the sediment beds containing the 152.5 μm sand fraction and mud contents of 5% and 10% respectively, under a wave stroke of 0.378 m.

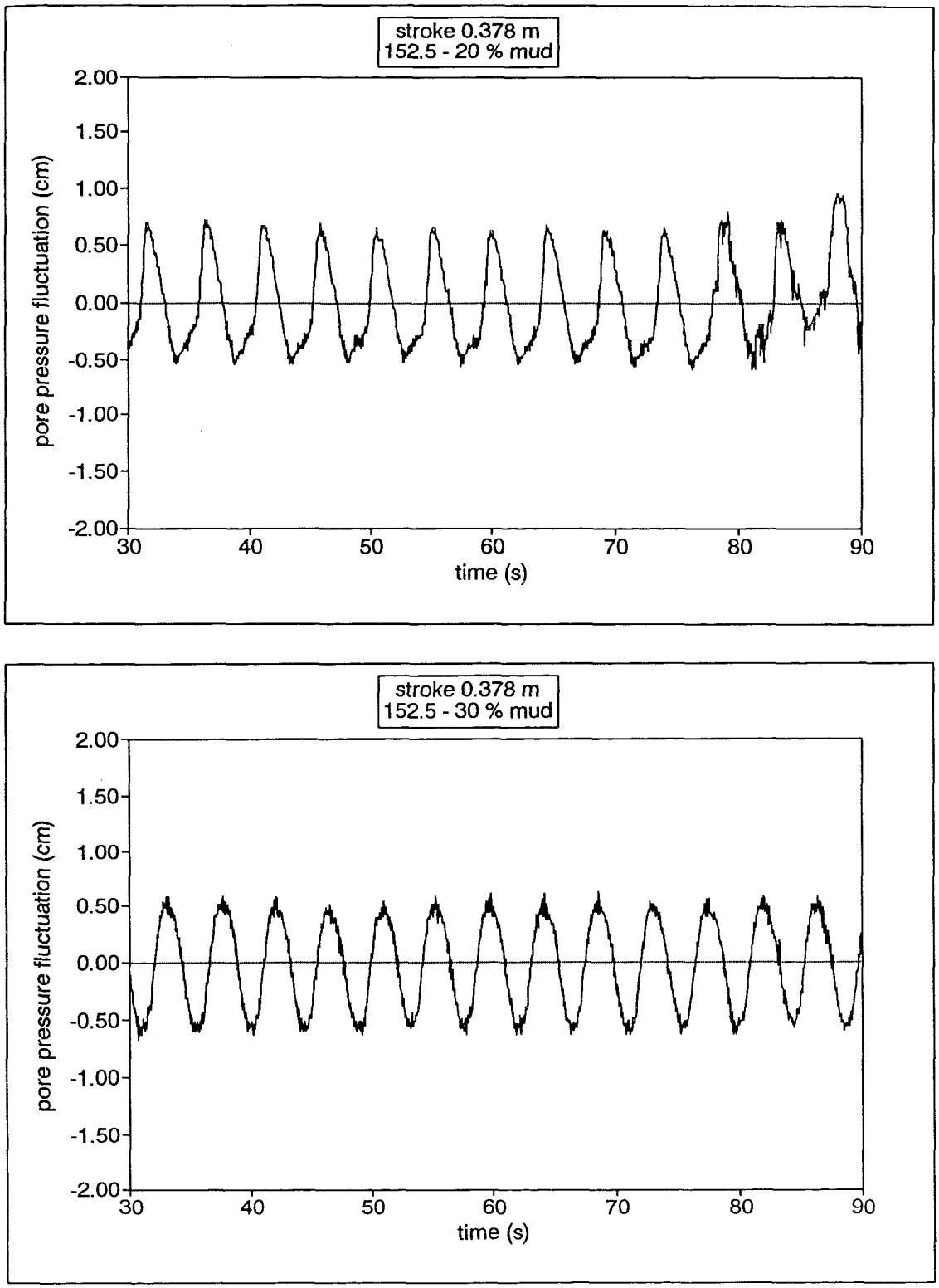

Fig. 7.17. Pore water pressure measurements obtained at 2 cm below the sediment/water interface, for the sediment beds containing the 152.5 μm sand fraction and mud contents of 20% and 30% respectively, under a wave stroke of 0.378 m.

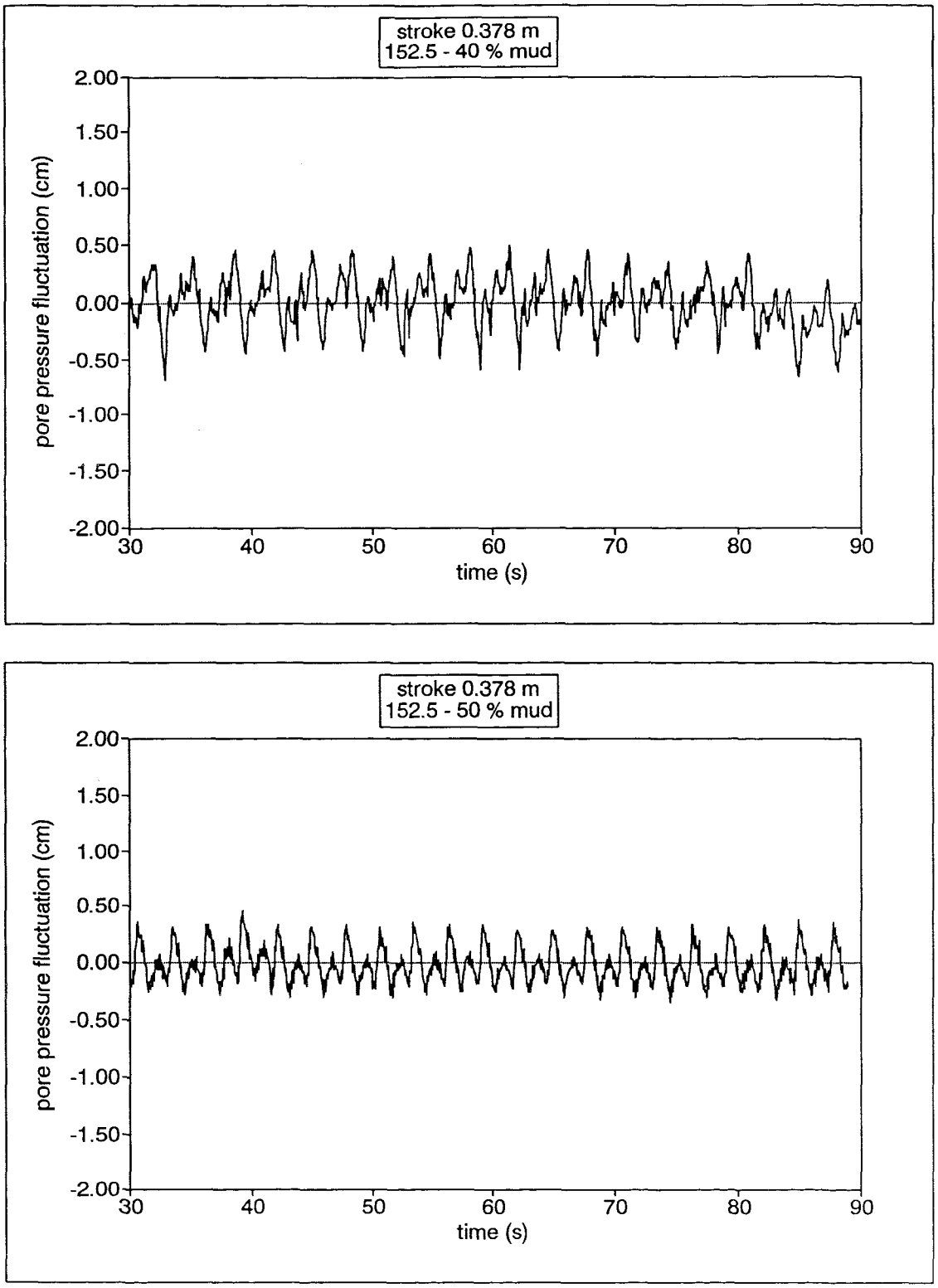

Fig. 7.18. Pore water pressure measurements obtained at 2 cm below the sediment/water interface, for the sediment beds containing the 152.5 μm sand fraction and mud contents of 40% and 50% respectively, under a wave stroke of 0.378 m.

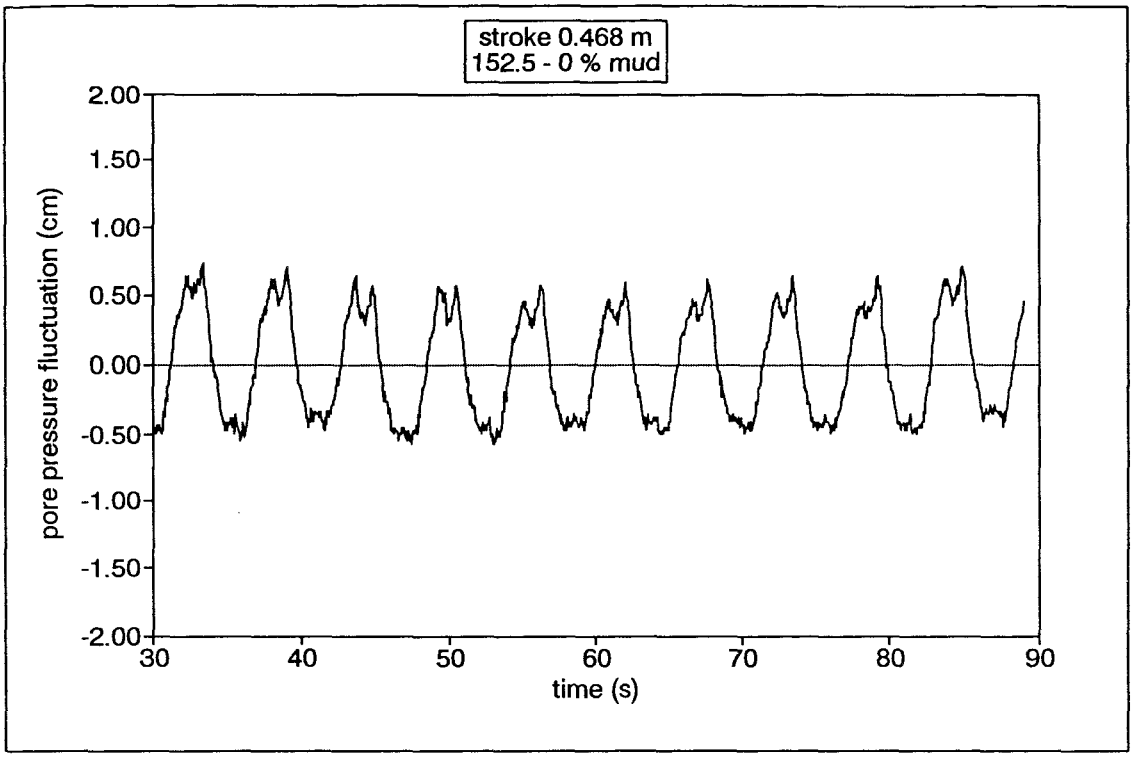

Fig. 7.19. Pore water pressure measurements obtained at 2 cm below the sediment/water interface, for the sediment bed containing only sand of 152.5 μm size, under a wave stroke of 0.468 m.

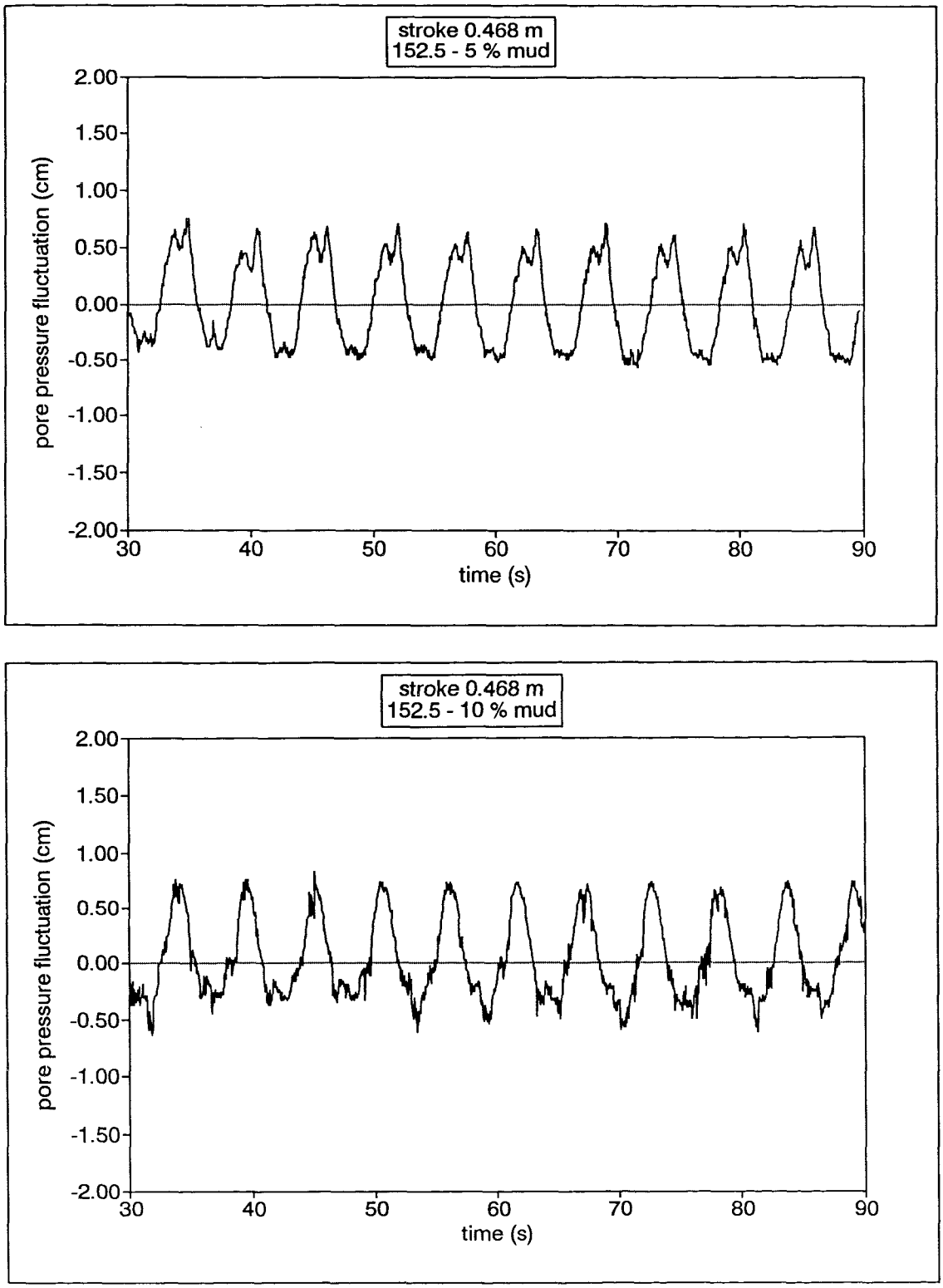

Fig. 7.20. Pore water pressure measurements obtained at 2 cm below the sediment/water interface, for the sediment beds containing the 152.5 μm sand fraction and mud contents of 5% and 10% respectively, under a wave stroke of 0.468 m.

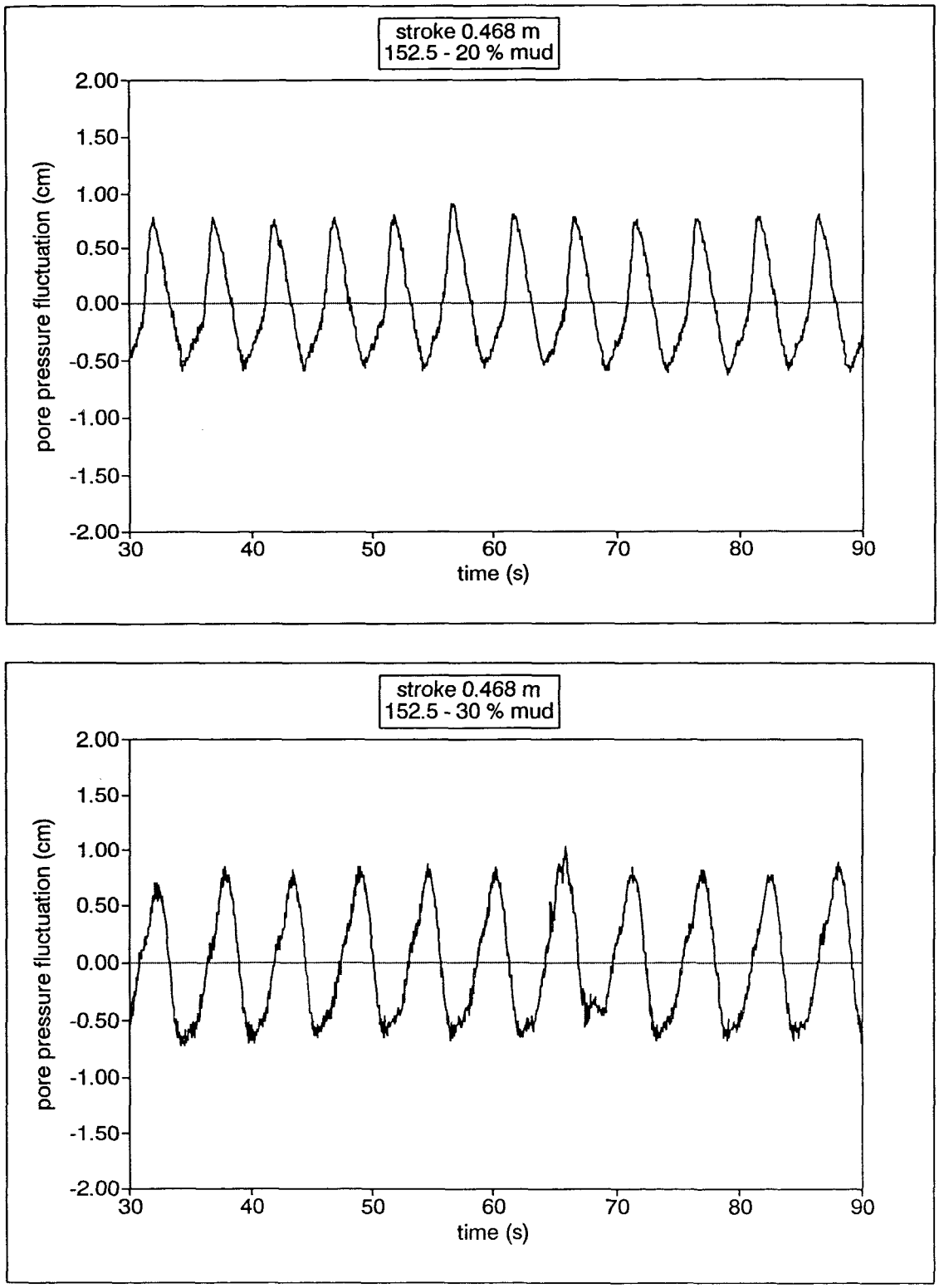

Fig. 7.21. Pore water pressure measurements obtained at 2 cm below the sediment/water interface, for the sediment beds containing the 152.5 μm sand fraction and mud contents of 20% and 30% respectively, under a wave stroke of 0.468 m.

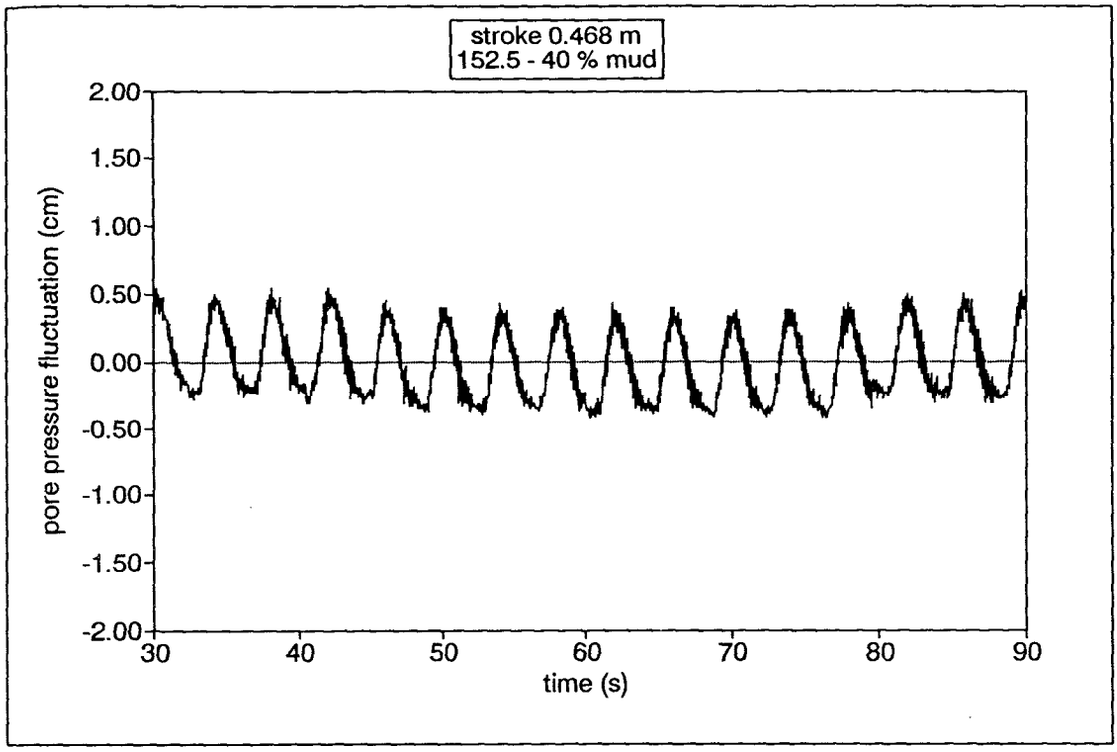

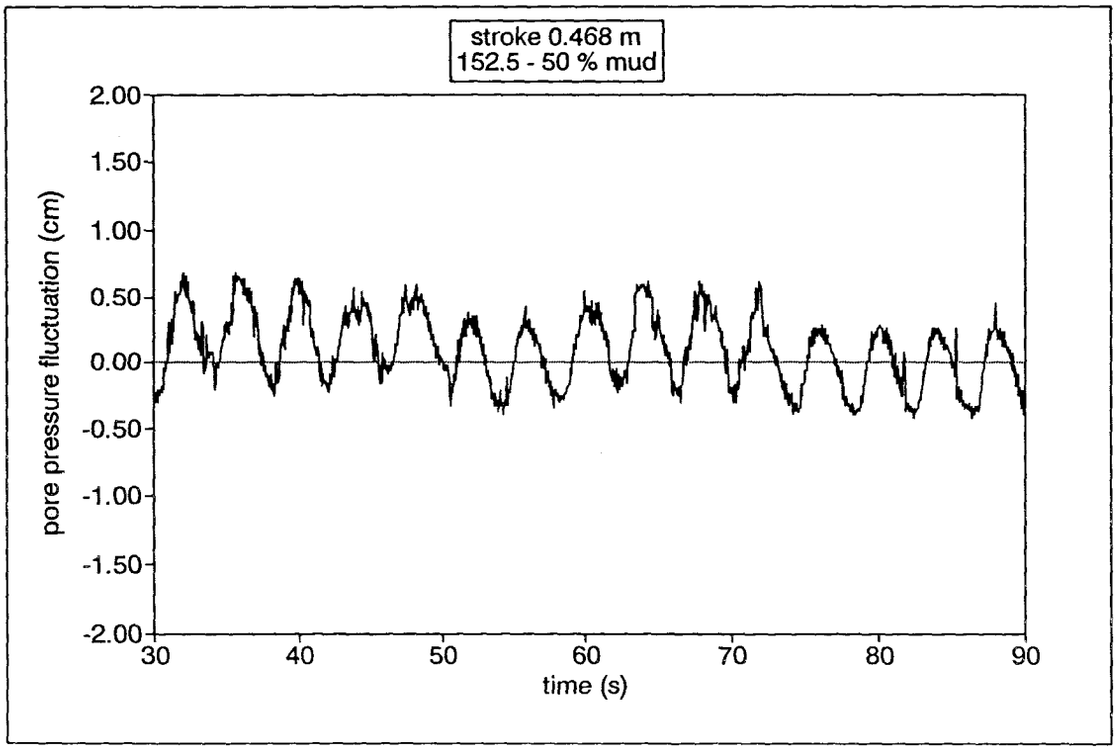

Fig. 7.22. Pore water pressure measurements obtained at 2 cm below the sediment/water interface, for the sediment beds containing the 152.5 μm sand fraction and mud contents of 40% and 50% respectively, under a wave stroke of 0.468 m.

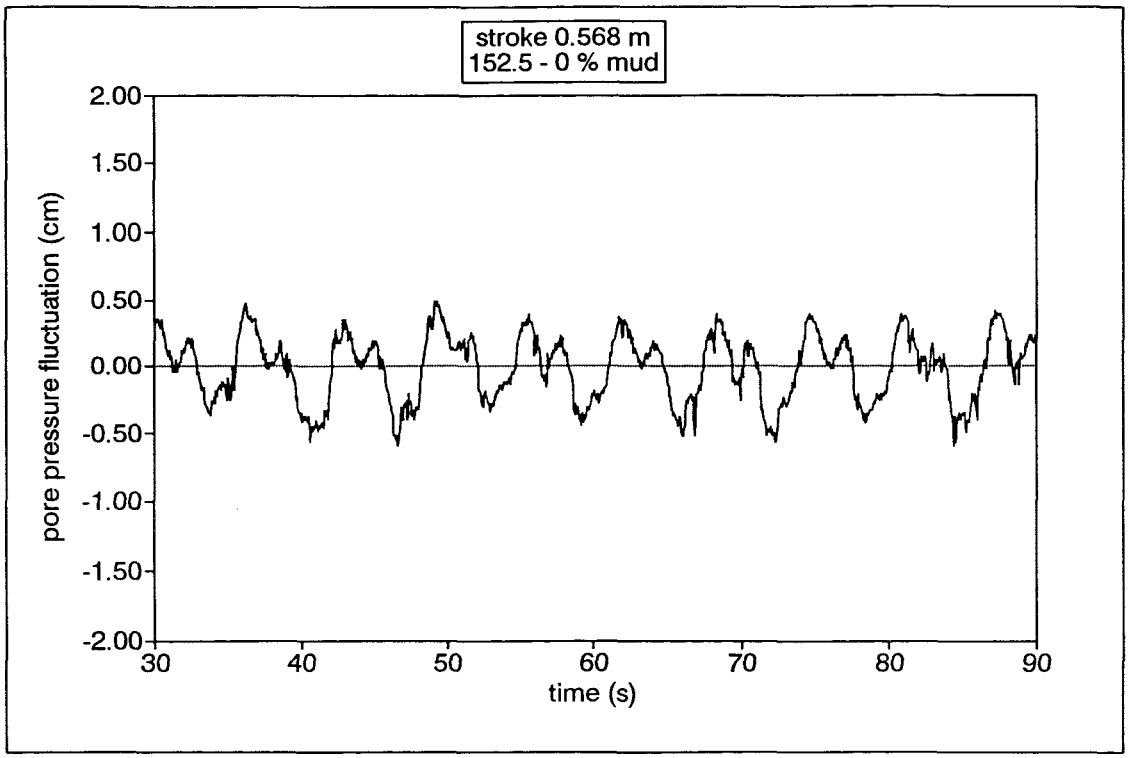

Fig. 7.23. Pore water pressure measurements obtained at 2 cm below the sediment/water interface, for the sediment bed containing only sand of 152.5 μm size, under a wave stroke of 0.568 m.

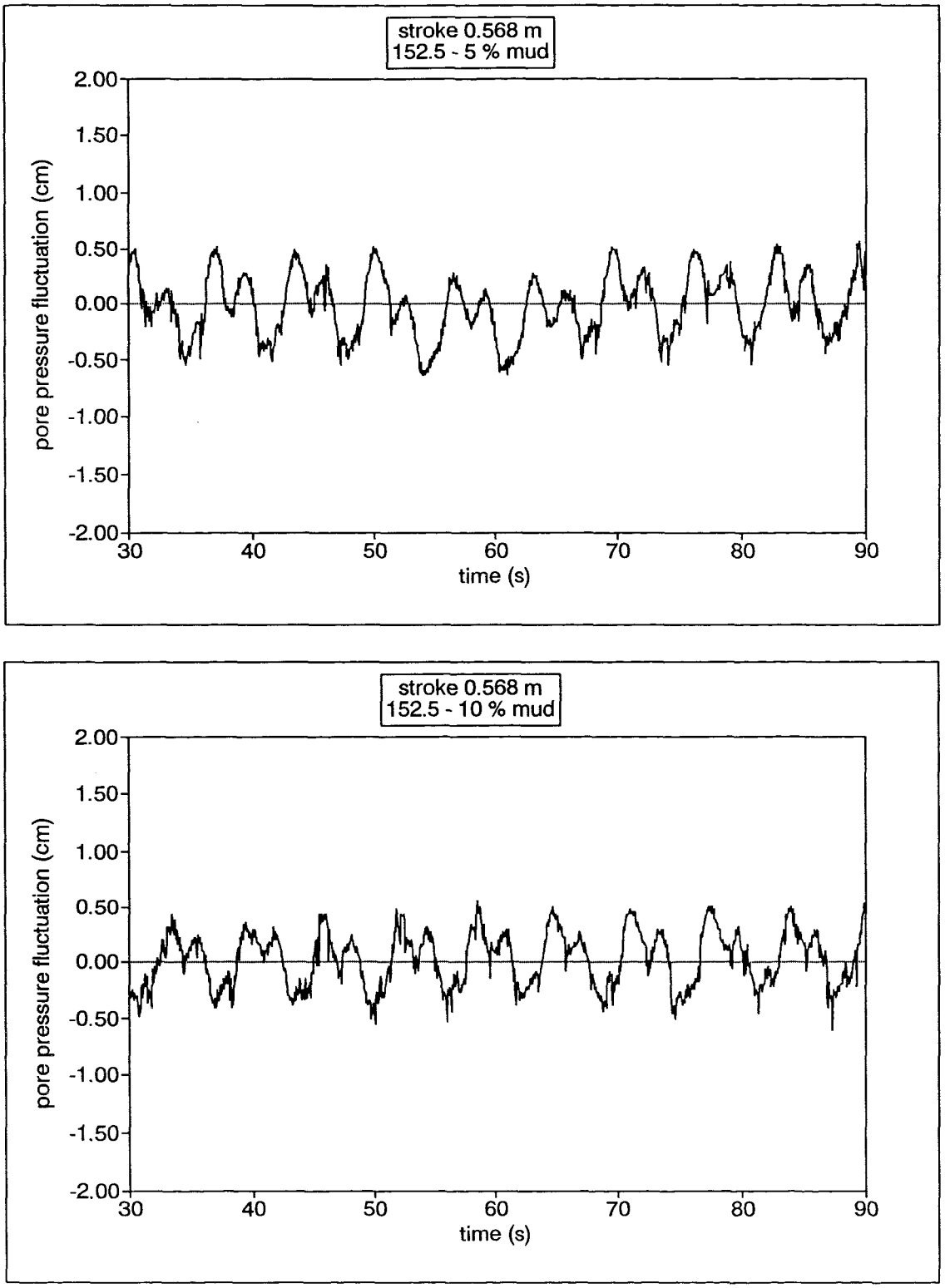

Fig. 7.24. Pore water pressure measurements obtained at 2 cm below the sediment/water interface, for the sediment beds containing the 152.5 μm sand fraction and mud contents of 5% and 10% respectively, under a wave stroke of 0.568 m.

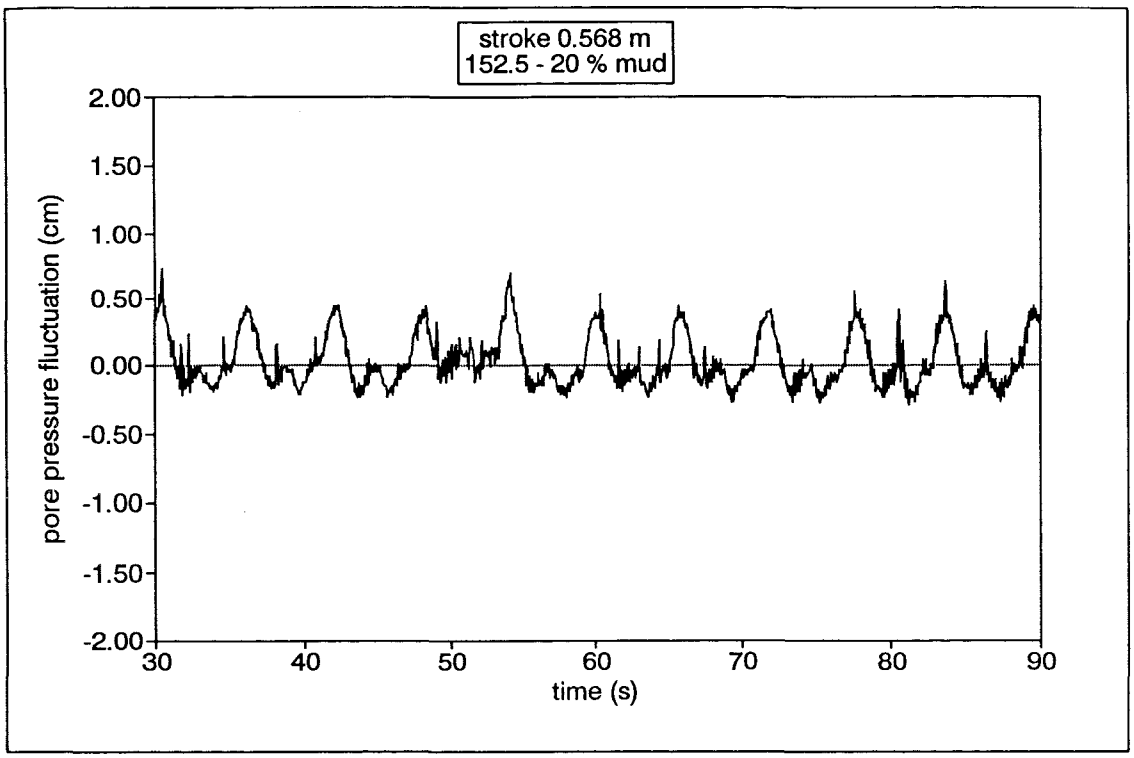

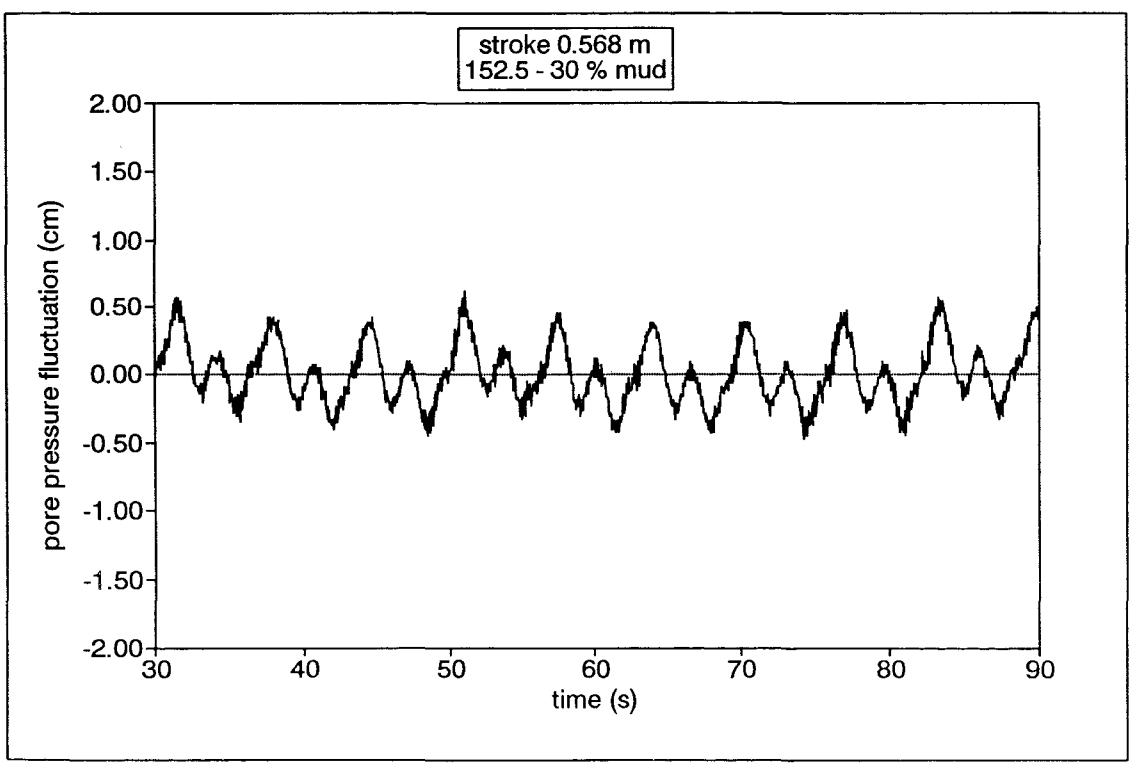

Fig. 7.25. Pore water pressure measurements obtained at 2 cm below the sediment/water interface, for the sediment beds containing the 152.5 μm sand fraction and mud contents of 20% and 30% respectively, under a wave stroke of 0.568 m.

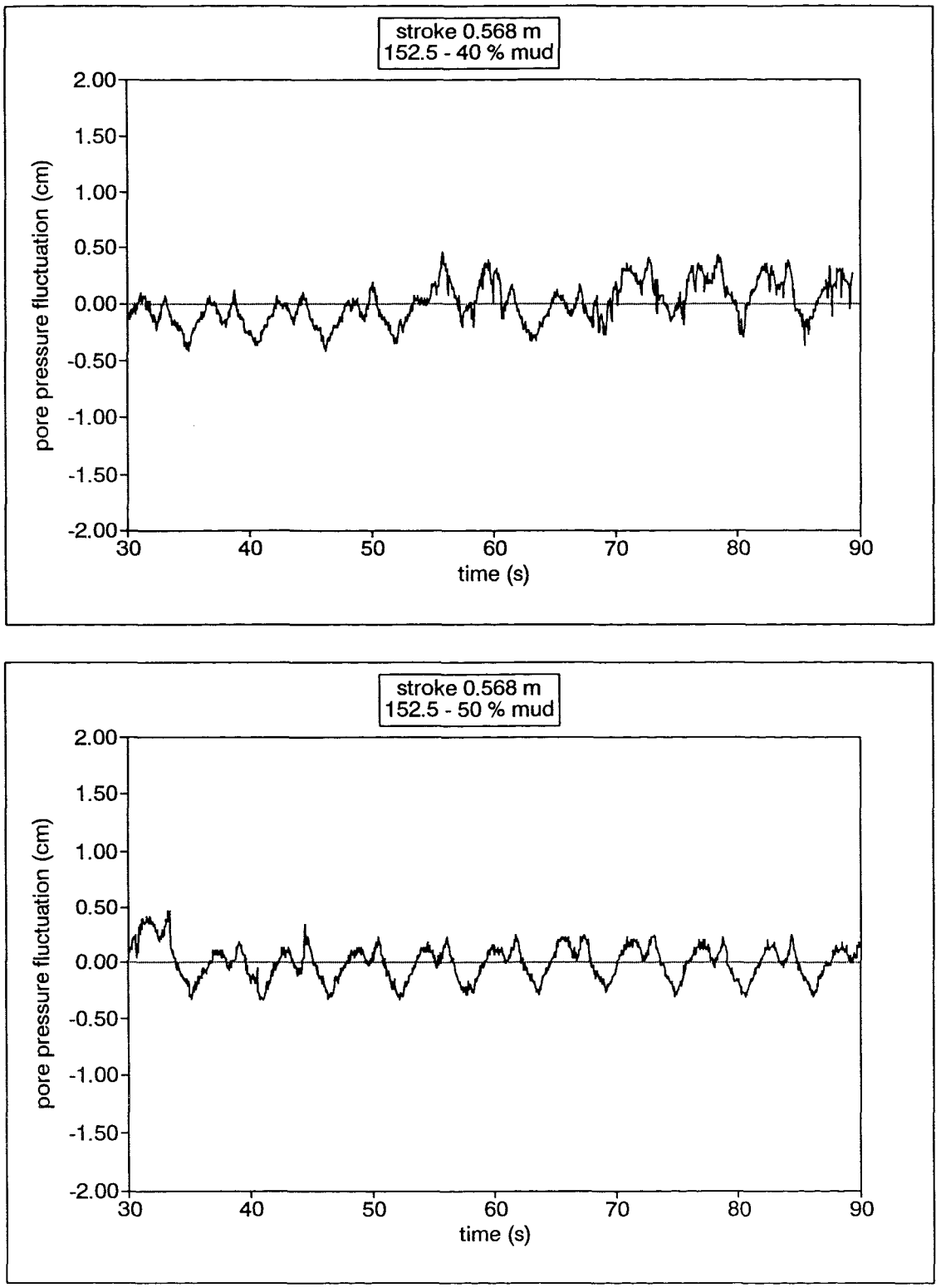

Fig. 7.26. Pore water pressure measurements obtained at 2 cm below the sediment/water interface, for the sediment beds containing the 152.5 μm sand fraction and mud contents of 40% and 50% respectively, under a wave stroke of 0.568 m.

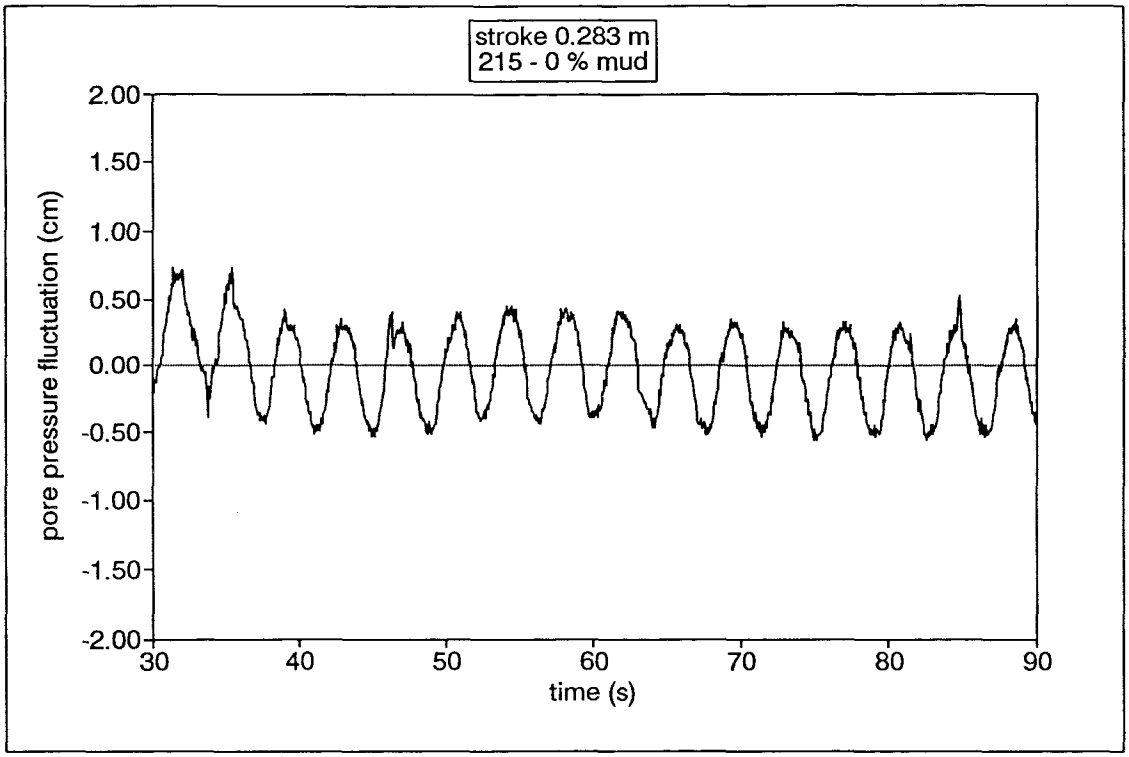

Fig. 7.27. Pore water pressure measurements obtained at 2 cm below the sediment/water interface, for the sediment bed containing only sand of 215 μm size, under a wave stroke of 0.283 m.

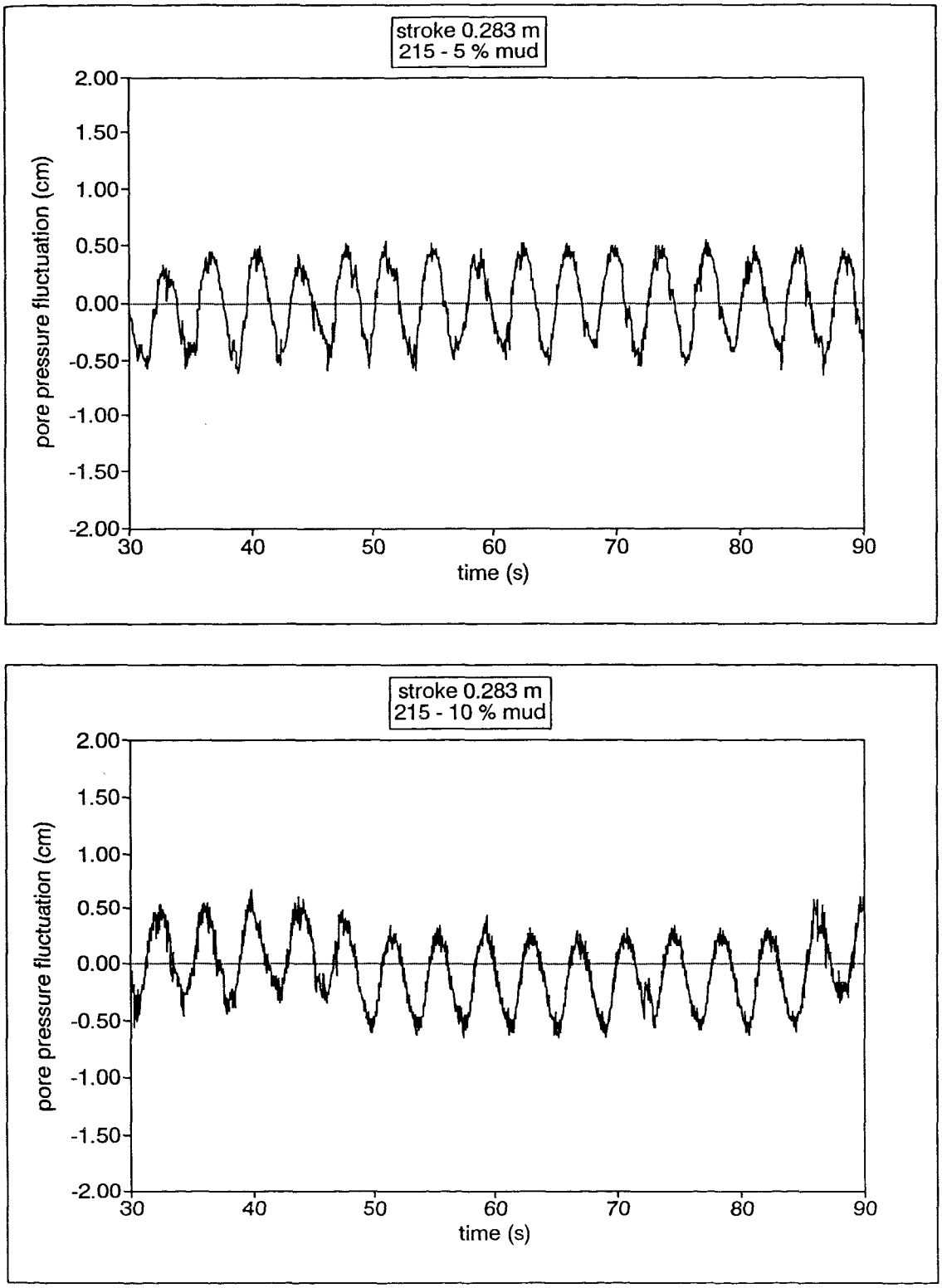

Fig. 7.28. Pore water pressure measurements obtained at 2 cm below the sediment/water interface, for the sediment beds containing the 215 μm sand fraction and mud contents of 5% and 10% respectively, under a wave stroke of 0.283 m.

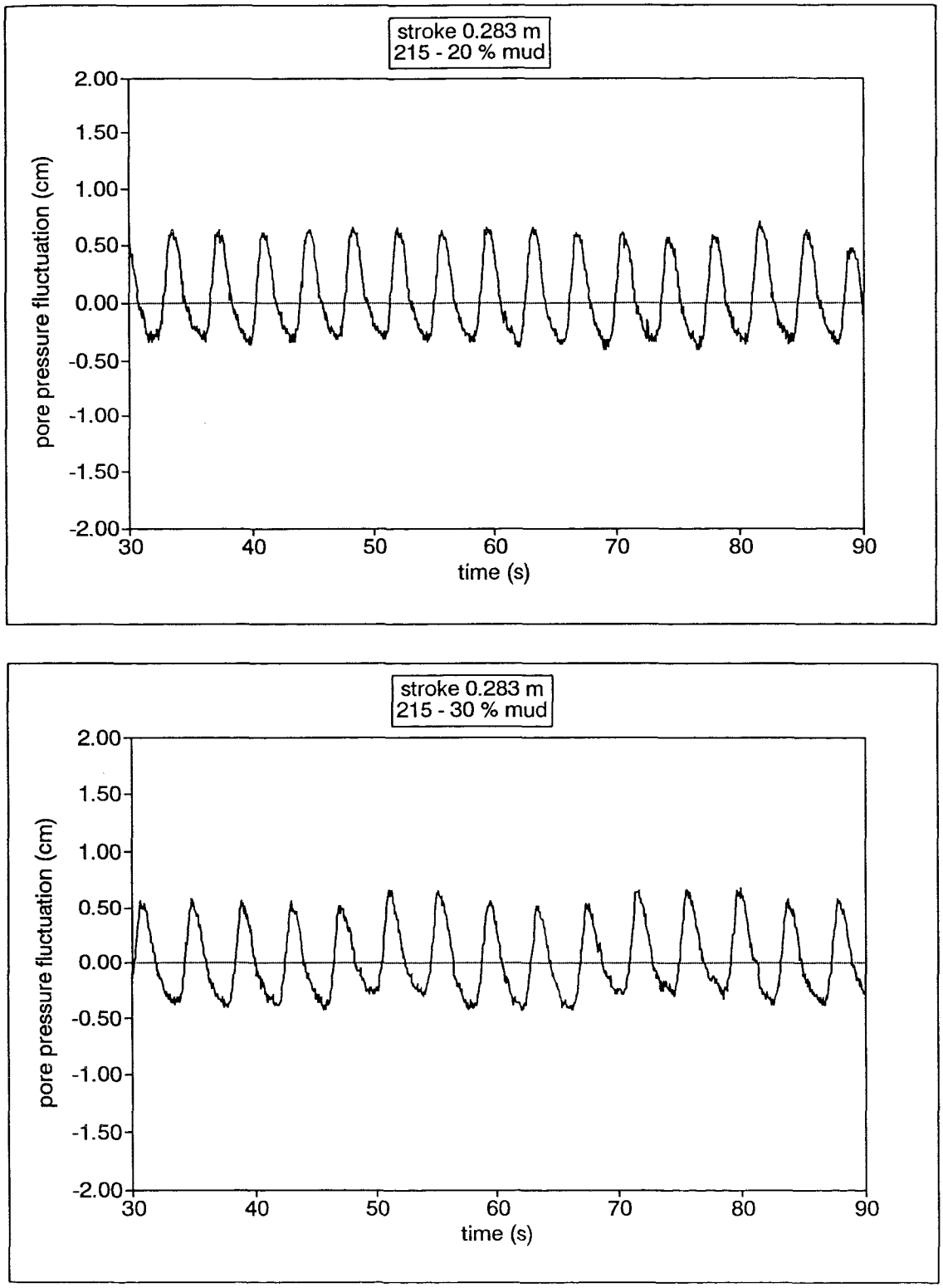

Fig. 7.29. Pore water pressure measurements obtained at 2 cm below the sediment/water interface, for the sediment beds containing the 215 μm sand fraction and mud contents of 20% and 30% respectively, under a wave stroke of 0.283 m.

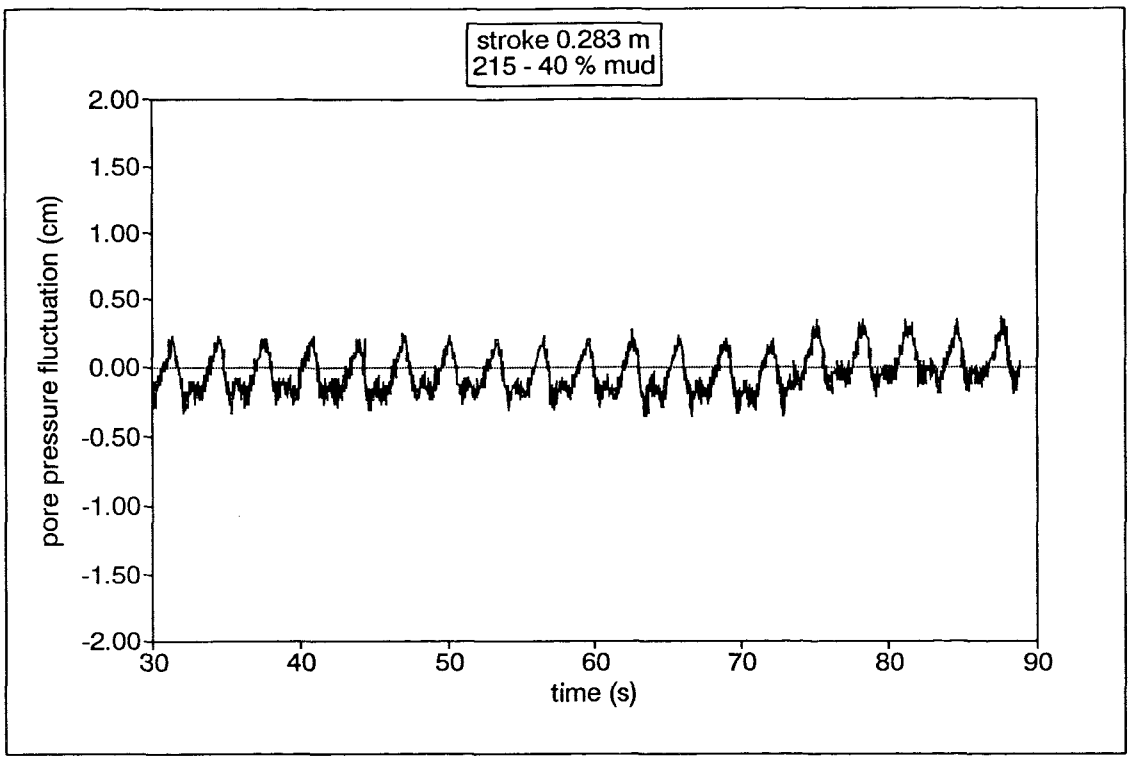

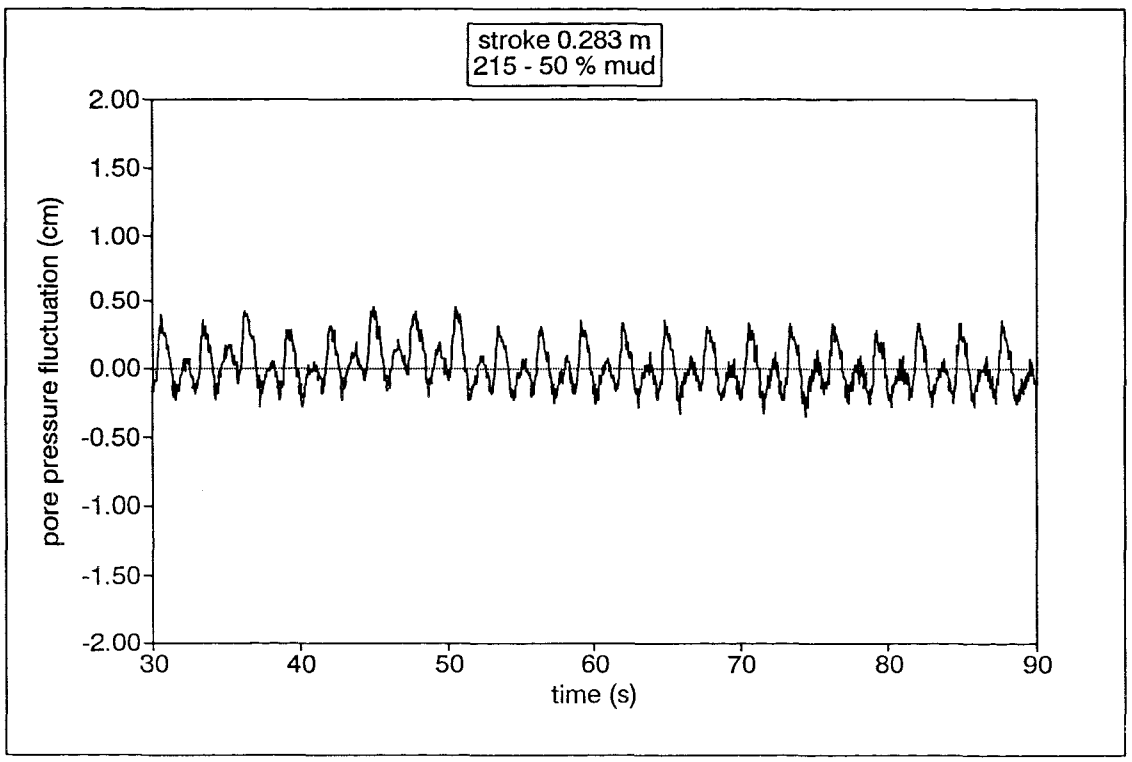

Fig. 7.30. Pore water pressure measurements obtained at 2 cm below the sediment/water interface, for the sediment beds containing the 215 μm sand fraction and mud contents of 40% and 50% respectively, under a wave stroke of 0.283 m.

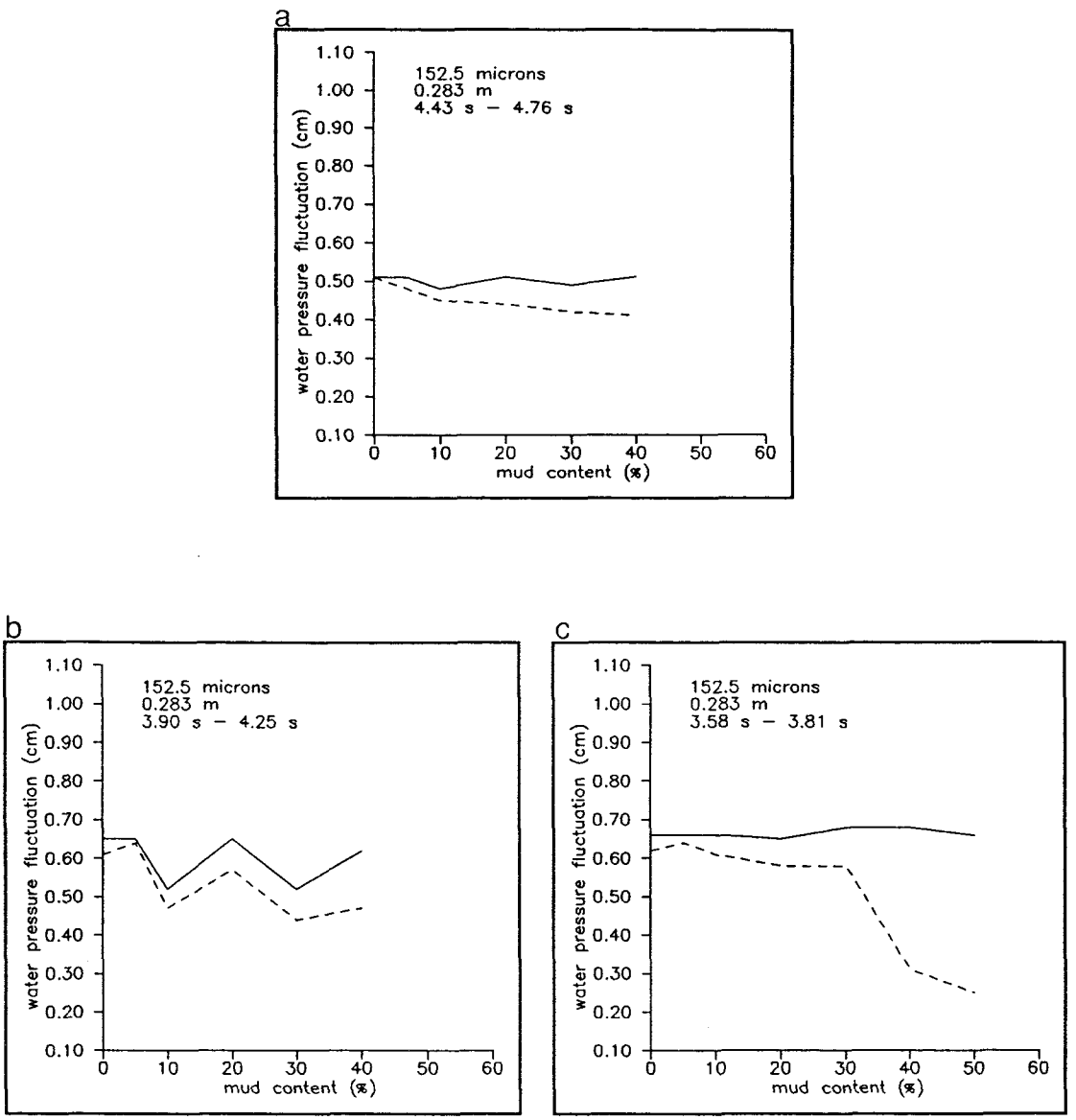

Fig. 7.31. Variation in pore pressure fluctuation (dashed line) with mud content, for the 152.5 μm sand admixtures, under a wave stroke of 0.283 m and wave (oscillation) period ranges of: (a) 4.43-4.76 s; (b) 3.90-4.25 s; and (c) 3.58-3.81 s (Key: Solid line—amplitude of pressure head transmitted into the bed).

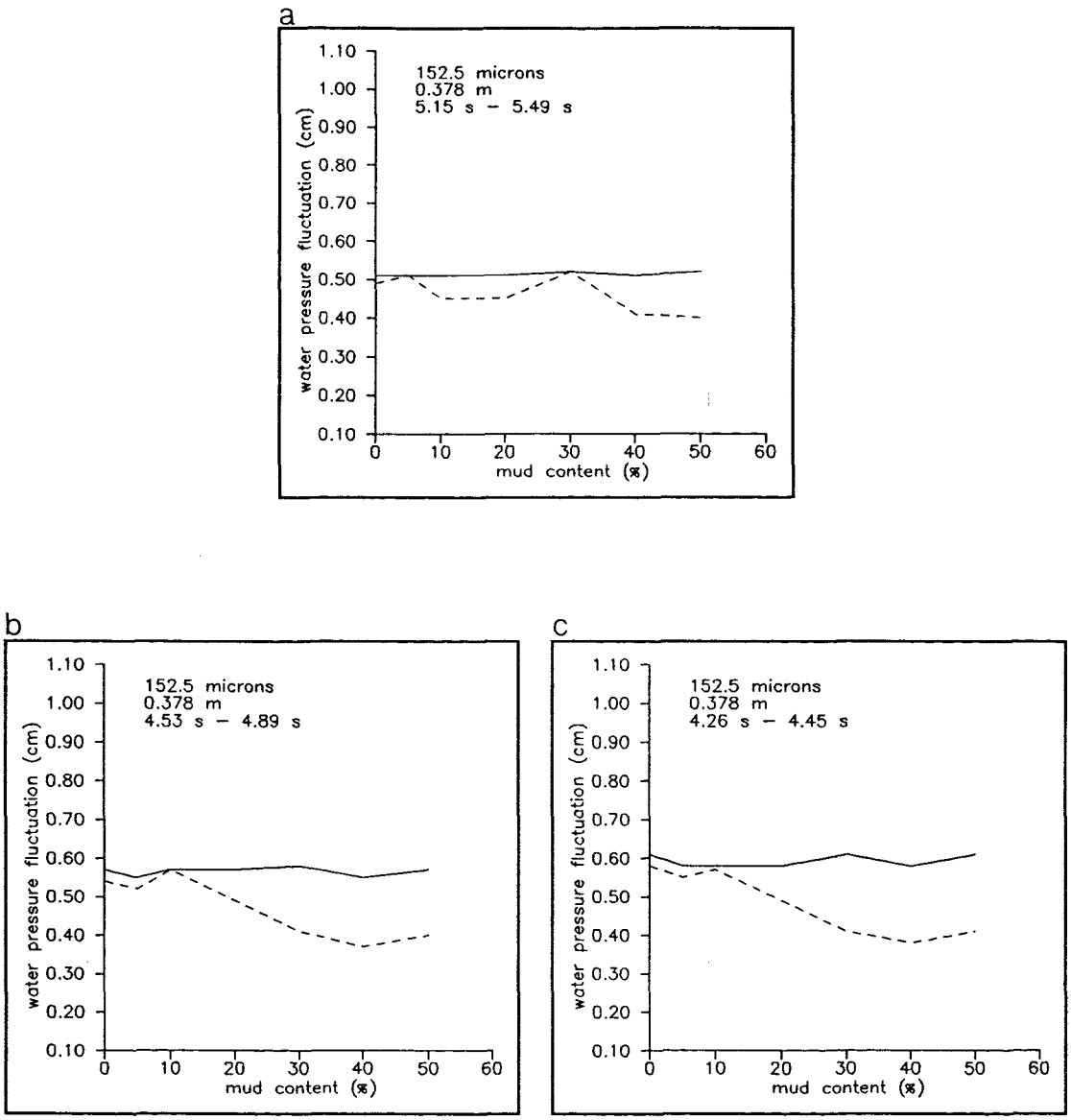

Fig. 7.32. Variation in pore pressure fluctuation (dashed line) with mud content, for the 152.5 μm sand admixtures, under a wave stroke of 0.378 m and wave (oscillation) period ranges of: (a) 5.15-5.49 s; (b) 4.53-4.89 s; and (c) 4.26-4.45 s (Key: Solid line—amplitude of pressure head transmitted into the bed).

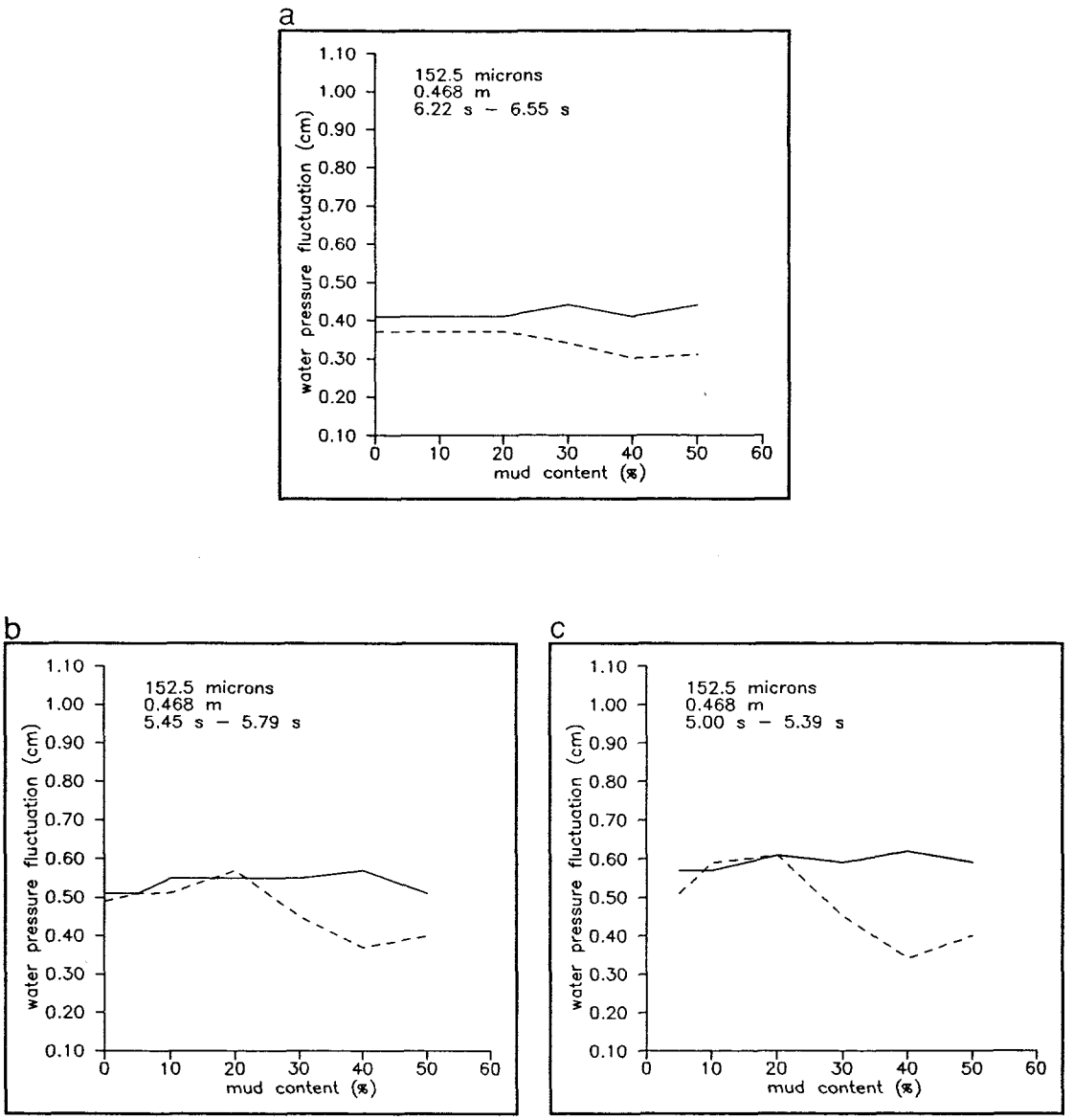

Fig. 7.33. Variation in pore pressure fluctuation (dashed line) with mud content, for the 152.5 μm sand admixtures, under a wave stroke of 0.468 m and wave (oscillation) period ranges of: (a) 6.22-6.55 s; (b) 5.45-5.79 s; and (c) 5.00-5.39 s (Key: Solid line—amplitude of pressure head transmitted into the bed).

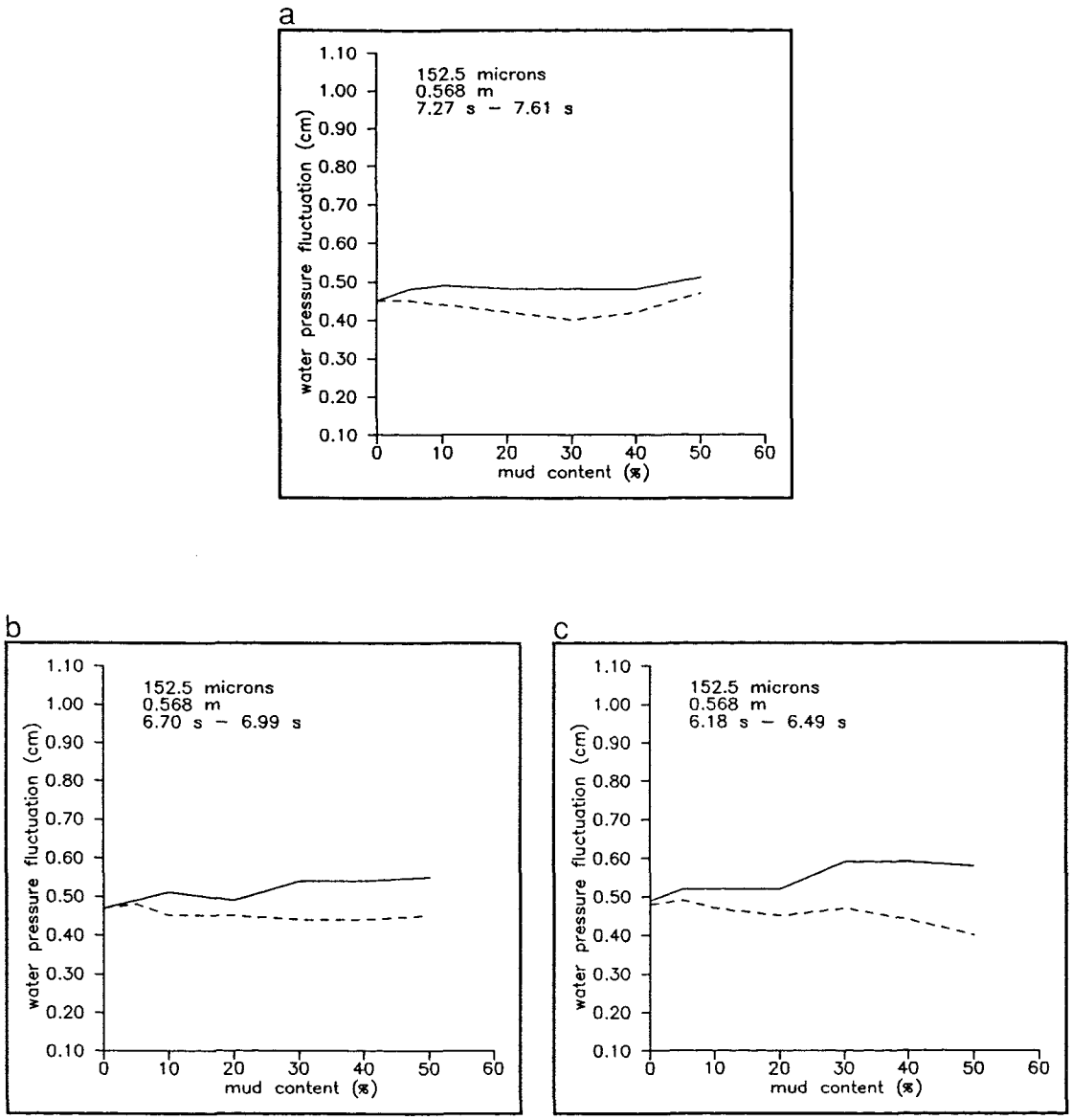

Fig. 7.34. Variation in pore pressure fluctuation (dashed line) with mud content, for the 152.5 μm sand admixtures, under a wave stroke of 0.568 m and wave (oscillation) period ranges of: (a) 7.27-7.61 s; (b) 6.70-6.99 s; and (c) 6.18-6.49 s (Key: Solid line—amplitude of pressure head transmitted into the bed).

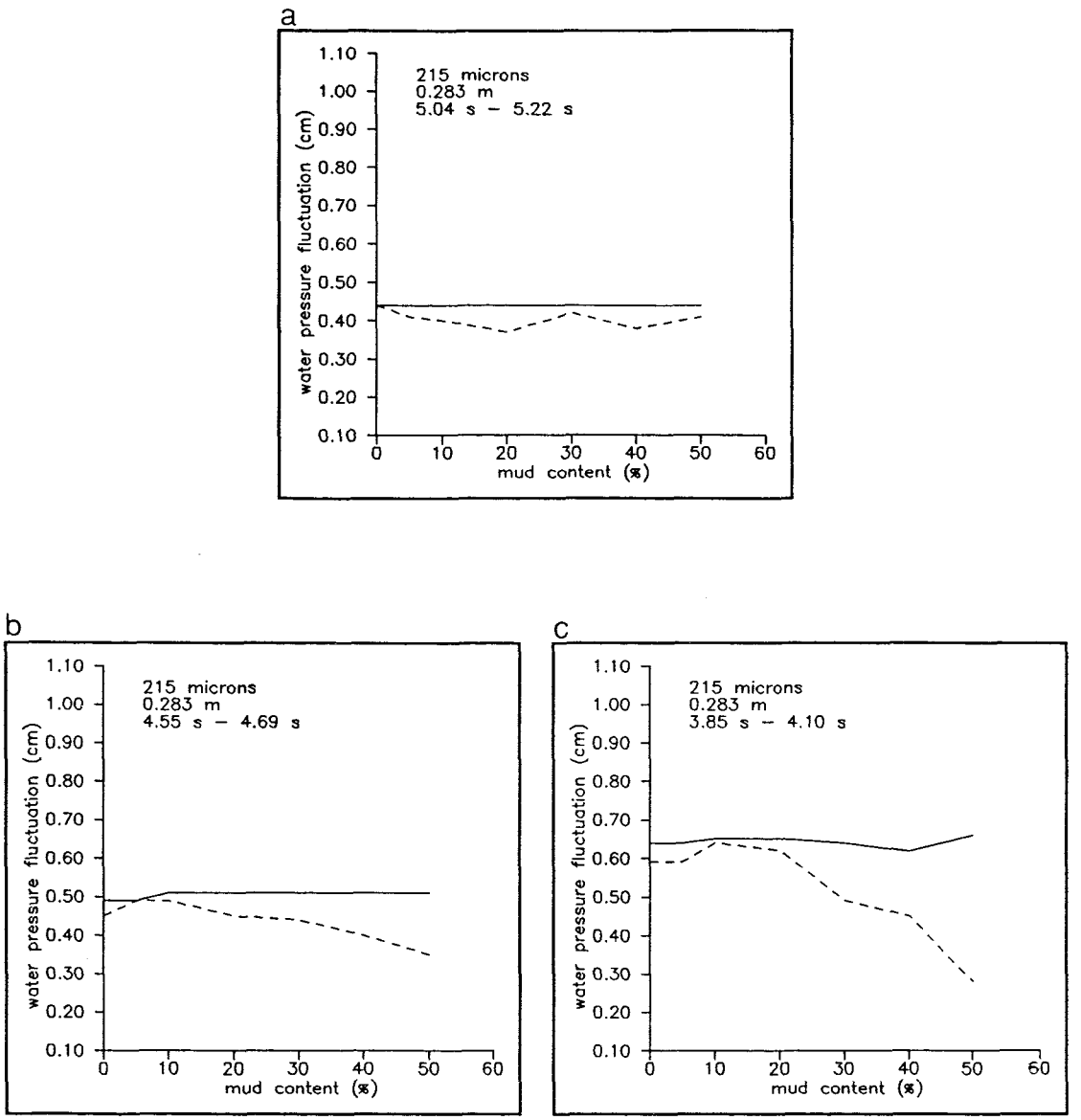

Fig. 7.35. Variation in pore pressure fluctuation (dashed line) with mud content, for the 215 μm sand admixtures, under a wave stroke of 0.283 m and wave (oscillation) period ranges of: (a) 5.04-5.22 s; (b) 4.55-4.69 s; and (c) 3.85-4.10 s (Key: Solid line—amplitude of pressure head transmitted into the bed).

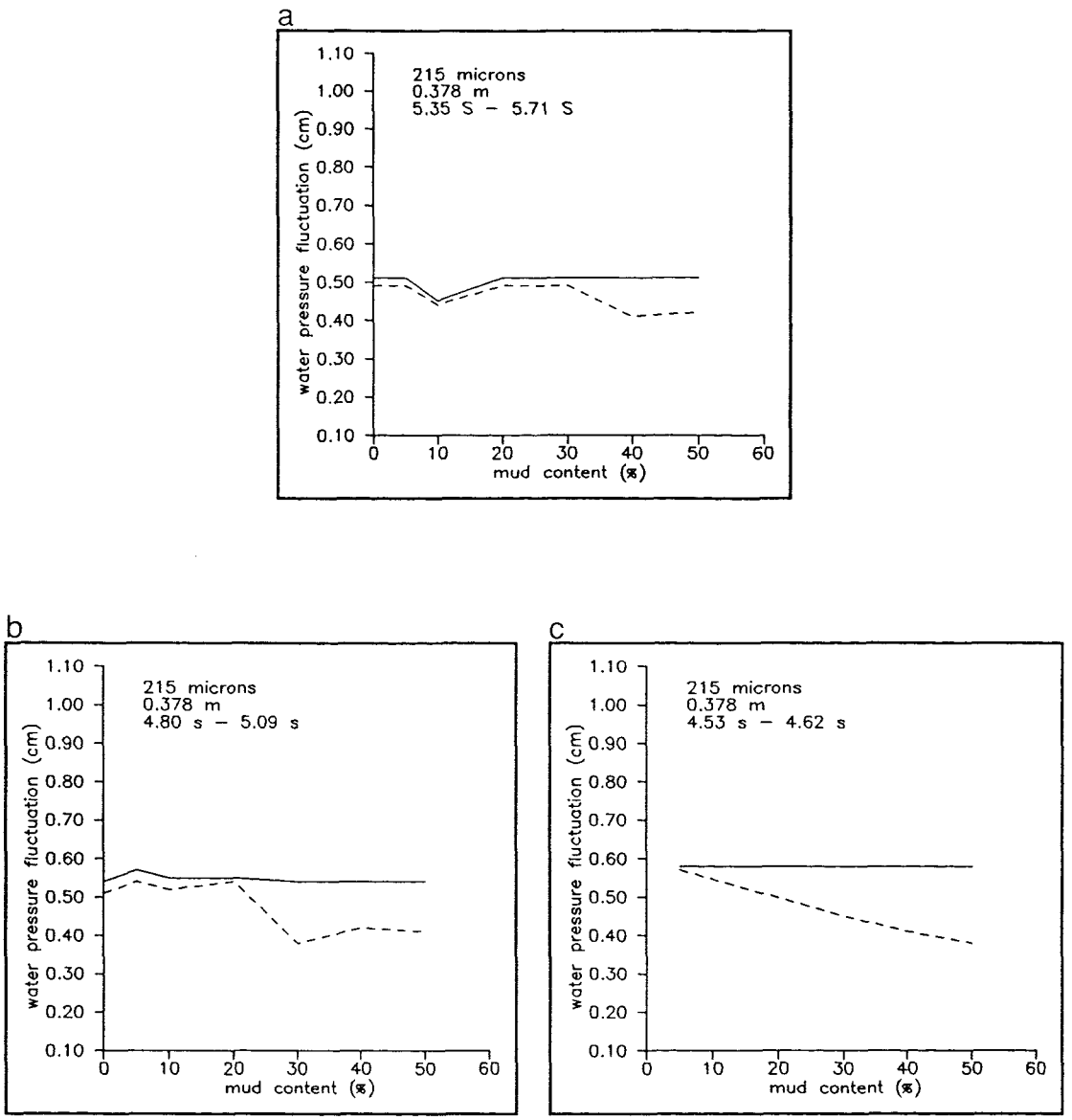

Fig. 7.36. Variation in pore pressure fluctuation (dashed line) with mud content, for the 215 μm sand admixtures, under a wave stroke of 0.378 m and wave (oscillation) period ranges of: (a) 5.35-5.71 s; (b) 4.80-5.09 s; and (c) 4.53-4.62 s (Key: Solid line—amplitude of pressure head transmitted into the bed).

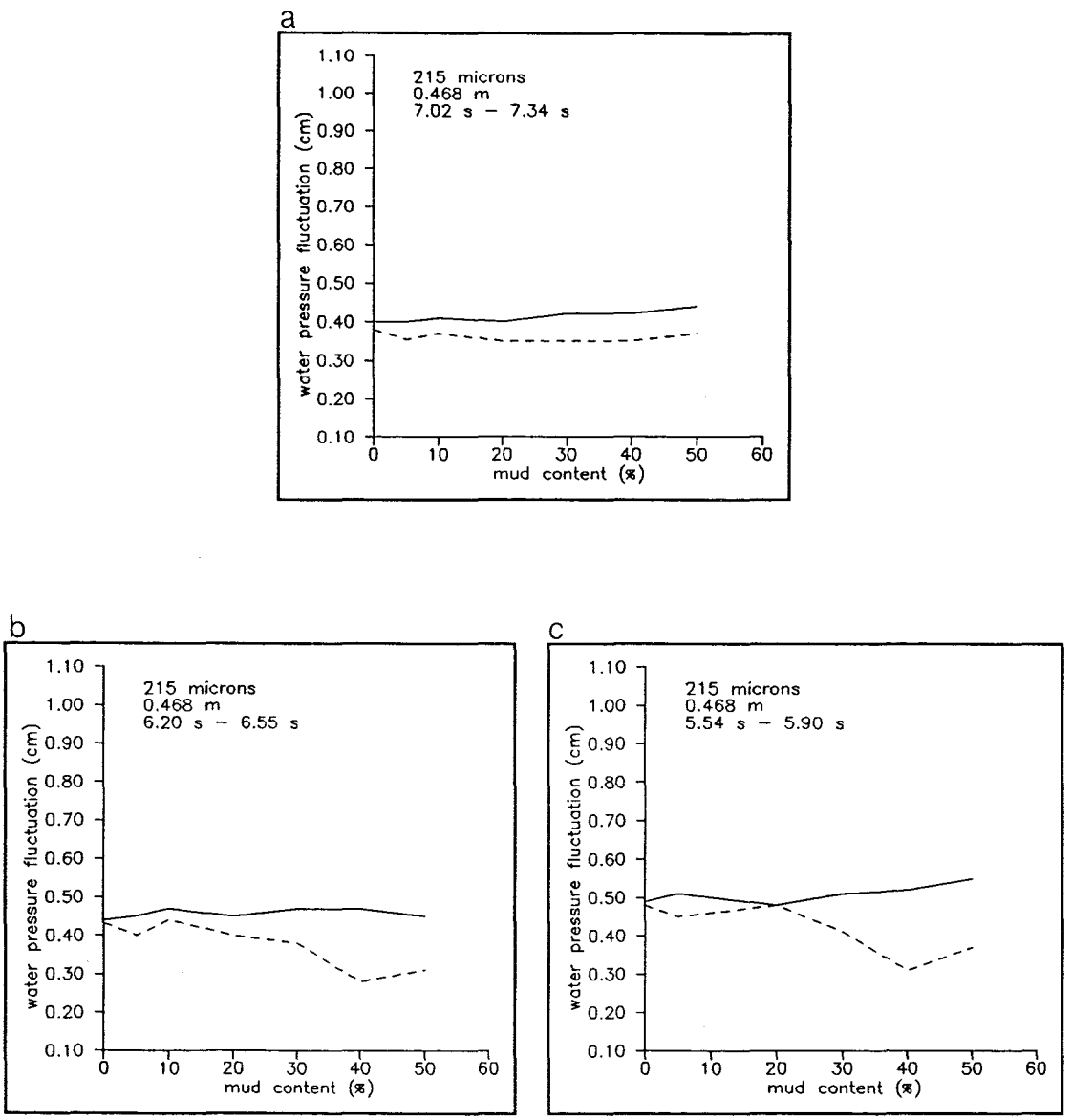

Fig. 7.37. Variation in pore pressure fluctuation (dashed line) with mud content, for the 215 μm sand admixtures, under a wave stroke of 0.468 m and wave (oscillation) period ranges of: (a) 7.02-7.34 s; (b) 6.20-6.55 s; and (c) 5.54-5.90 s (Key: Solid line—amplitude of pressure head transmitted into the bed).

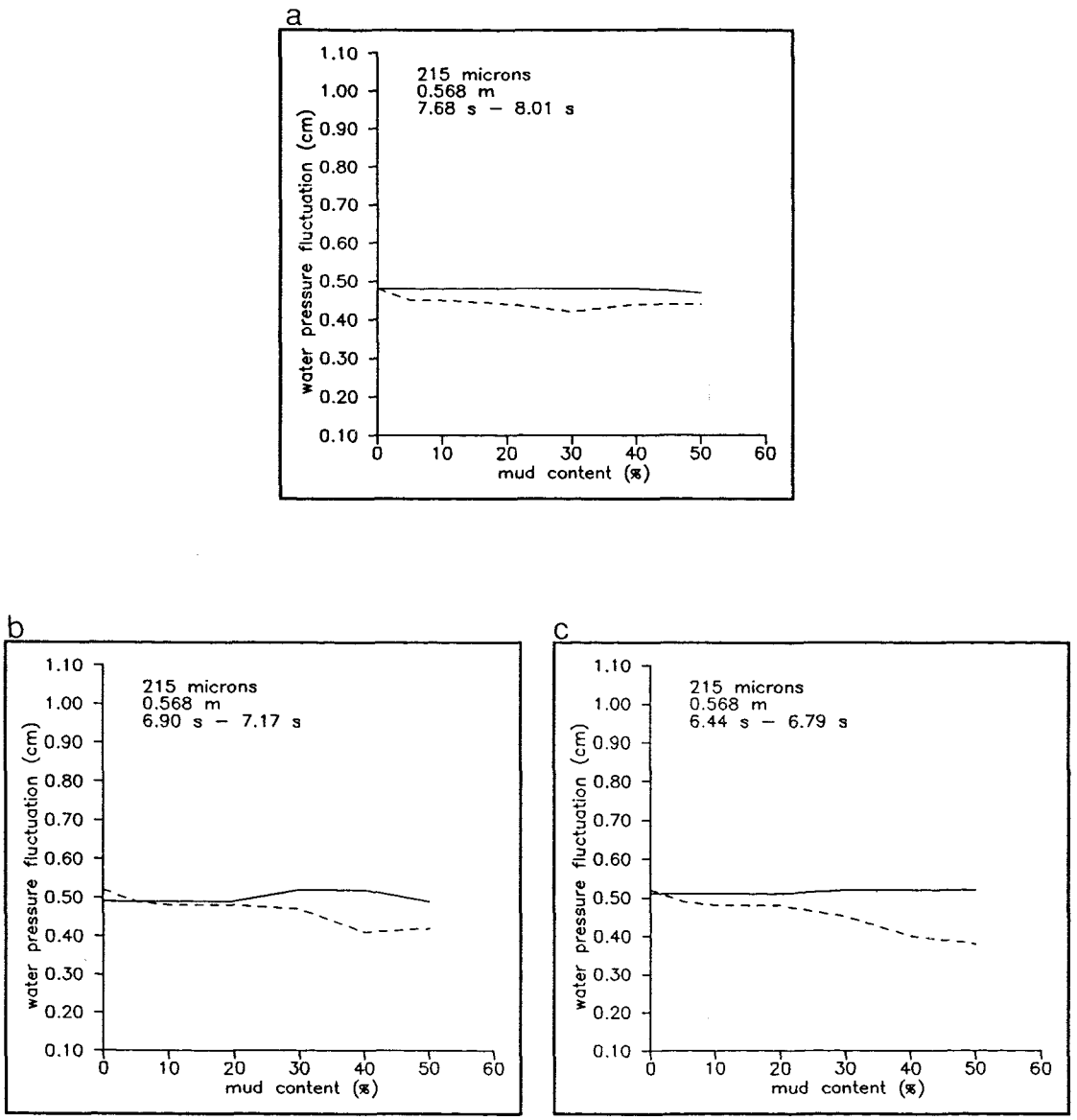

Fig. 7.38. Variation in pore pressure fluctuation (dashed line) with mud content, for the 215 μm sand admixtures, under a wave stroke of 0.568 m and wave (oscillation) period ranges of: (a) 7.68-8.01 s; (b) 6.90-7.17 s; and (c) 6.44-6.79 s (Key: Solid line—amplitude of pressure head transmitted into the bed).

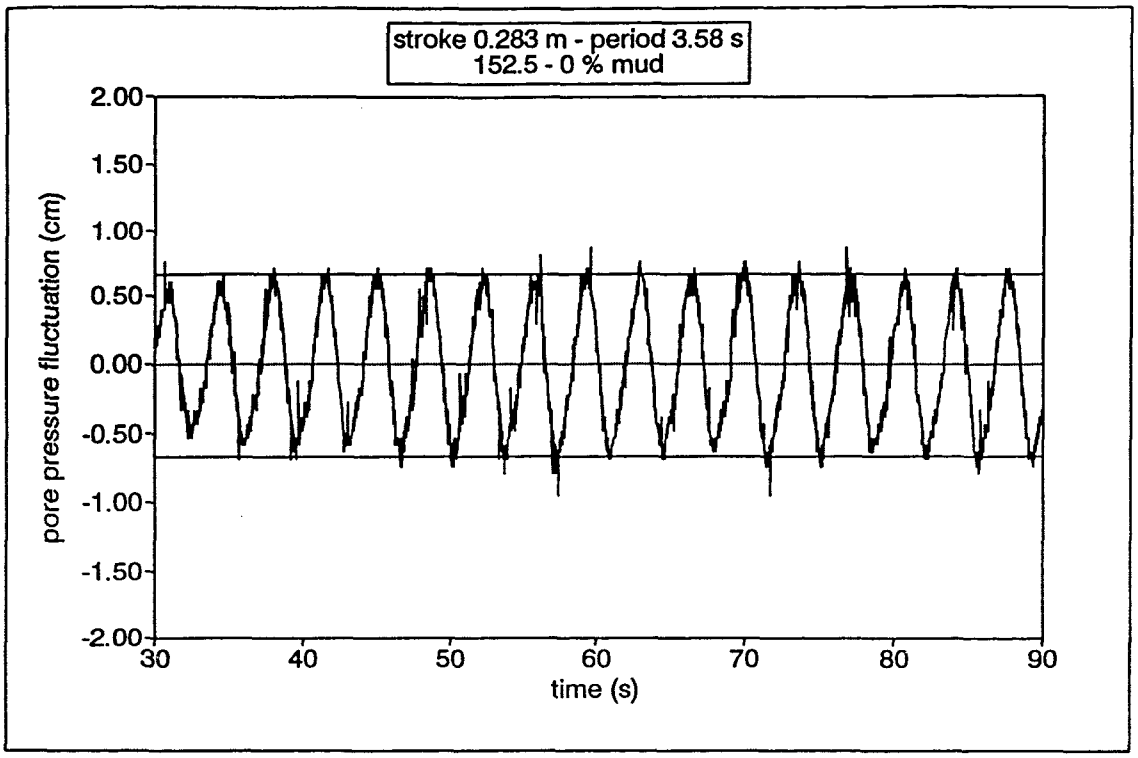

Fig. 7.39. Pore pressure record in relation to the amplitude of the pressure head (solid lines) transmitted into the sediment bed containing only the 152.5 μm sand, under a wave stroke of 0.283 m and period of 3.58 s.

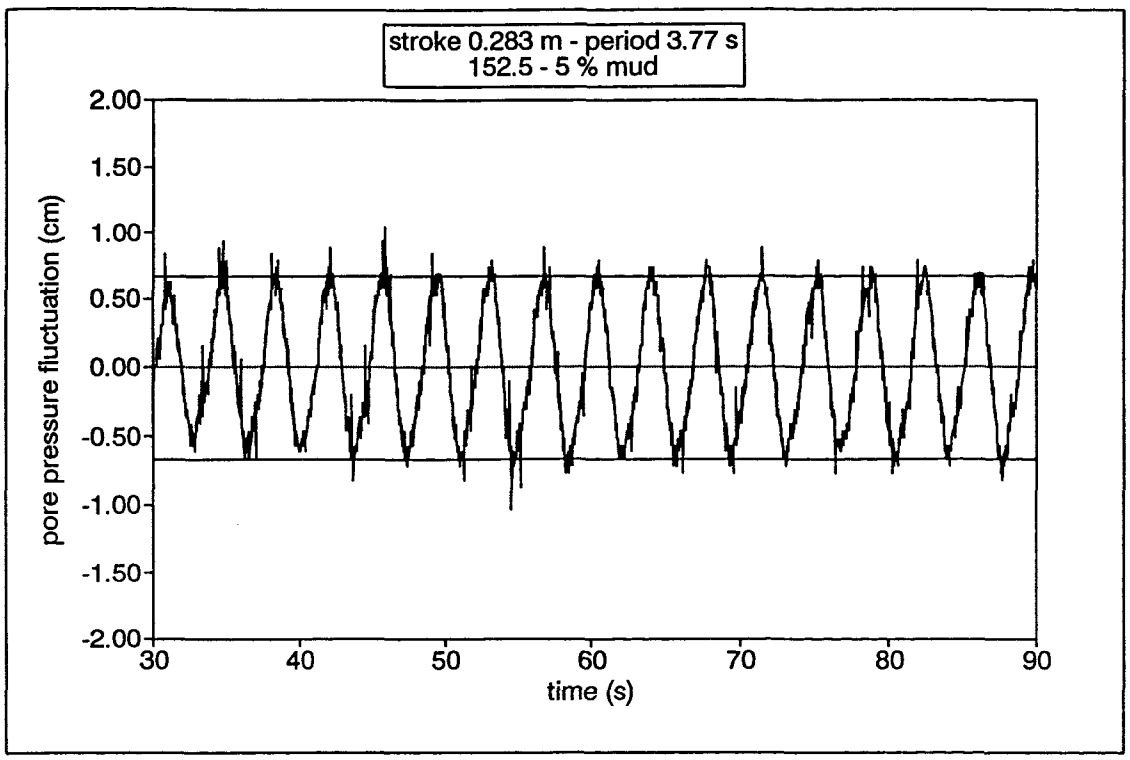

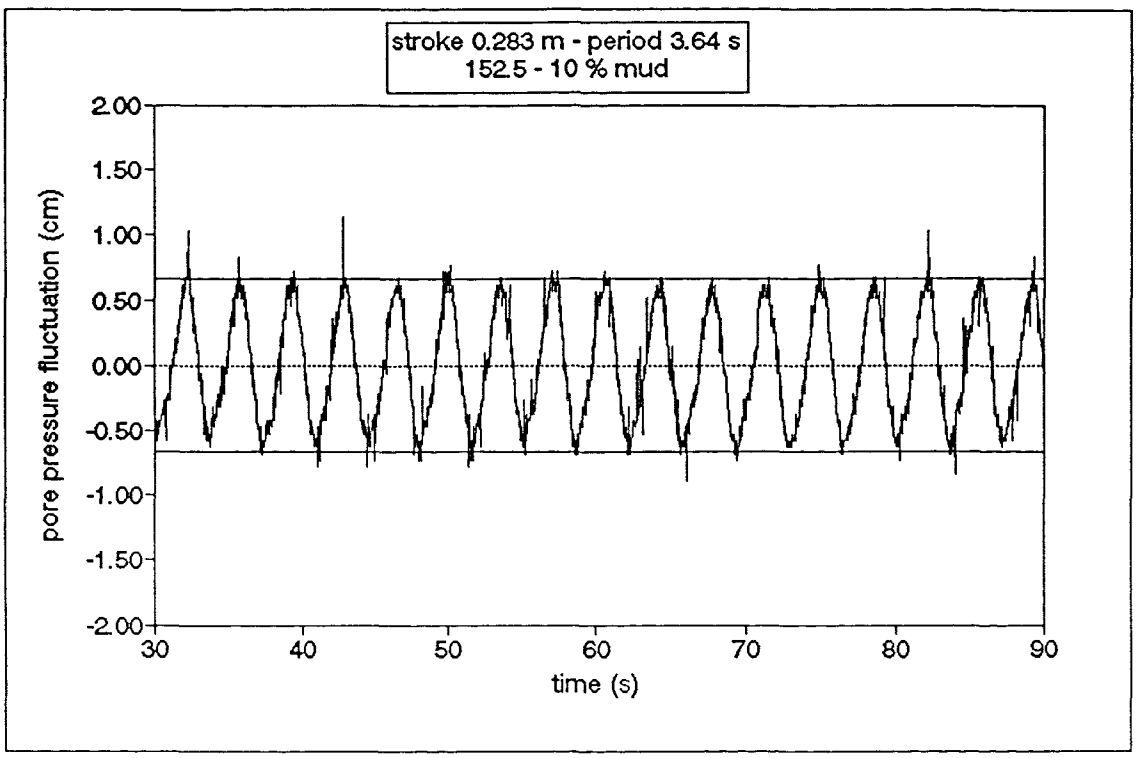

Fig. 7.40. Pore pressure records in relation to the amplitude of the pressure head (solid lines) transmitted into the 152.5 μm sand admixtures containing 5% and 10% of mud respectively, under a wave stroke of 0.283 m and periods of 3.77 s and 3.64 s, respectively.

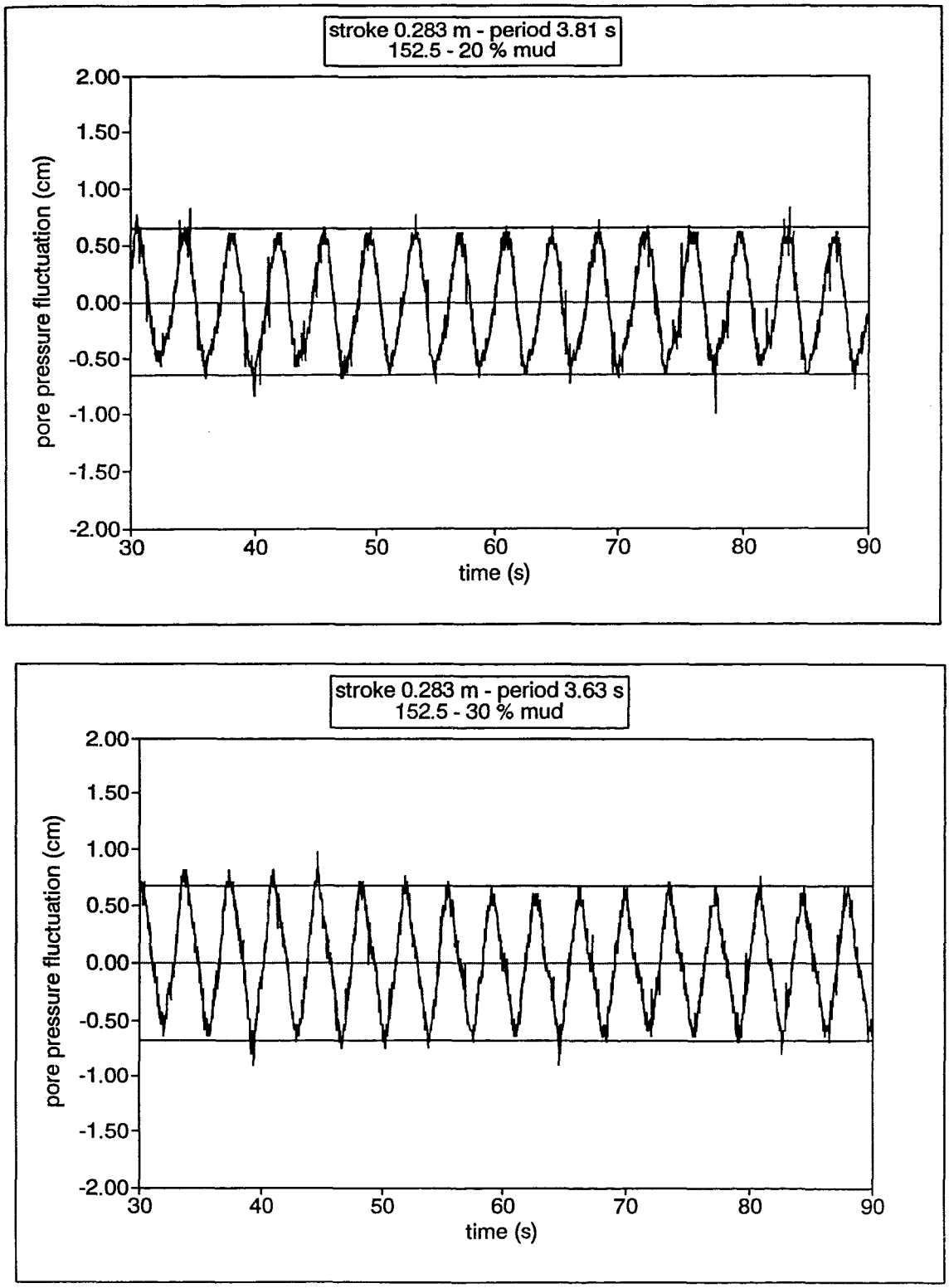

Fig. 7.41. Pore pressure records in relation to the amplitude of the pressure head (solid lines) transmitted into the 152.5 μm sand admixtures containing 20% and 30% of mud respectively, under a wave stroke of 0.283 m and periods of 3.81 s and 3.63 s, respectively.

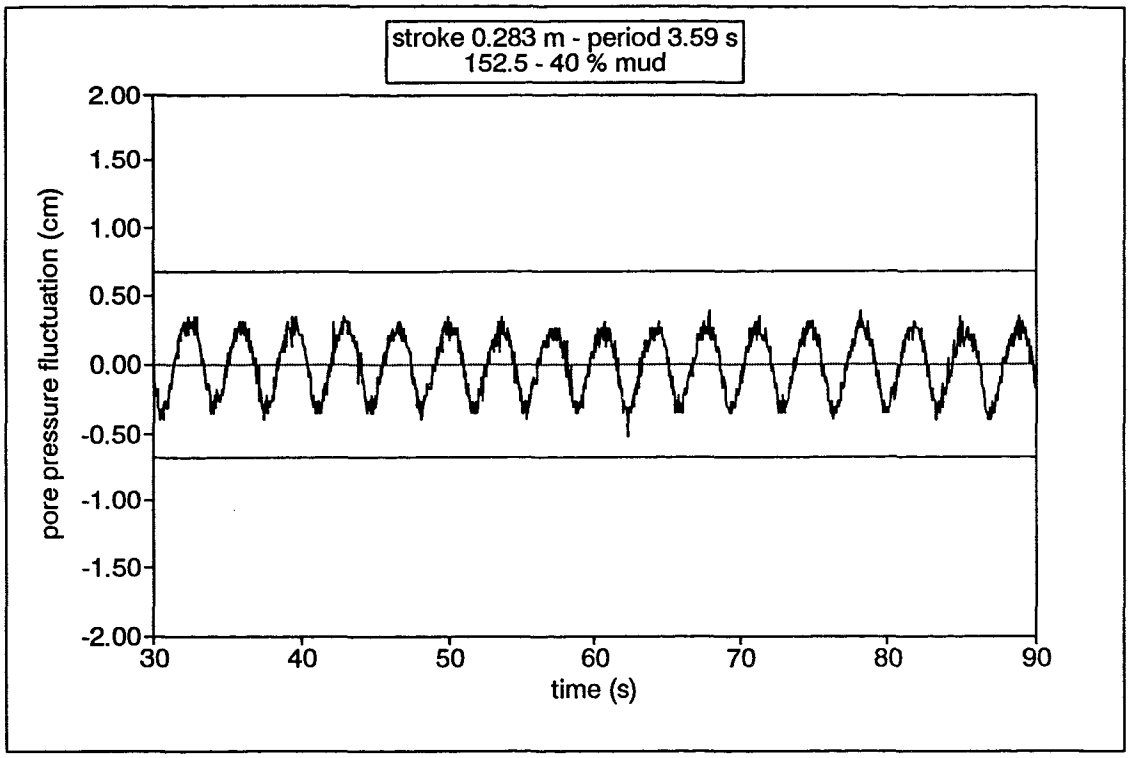

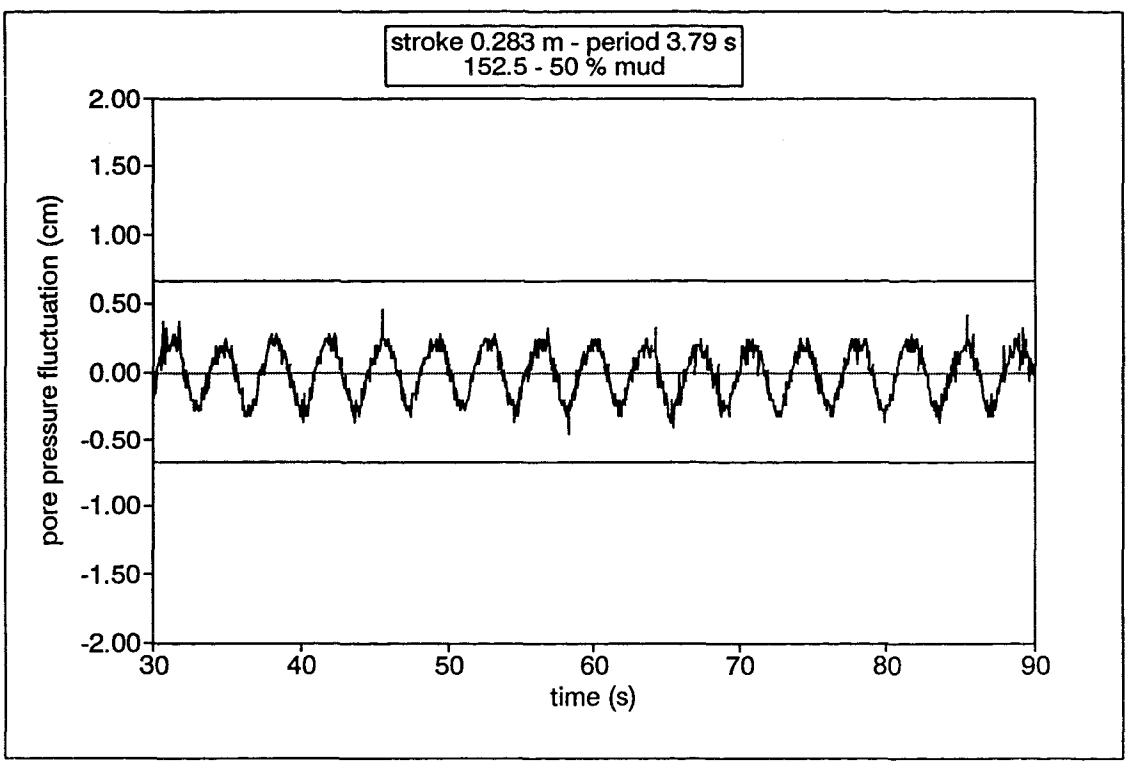

Fig. 7.42. Pore pressure records in relation to the amplitude of the pressure head (solid lines) transmitted into the 152.5 μm sand admixtures containing 40% and 50% of mud respectively, under a wave stroke of 0.283 m and periods of 3.59 s and 3.79 s, respectively.

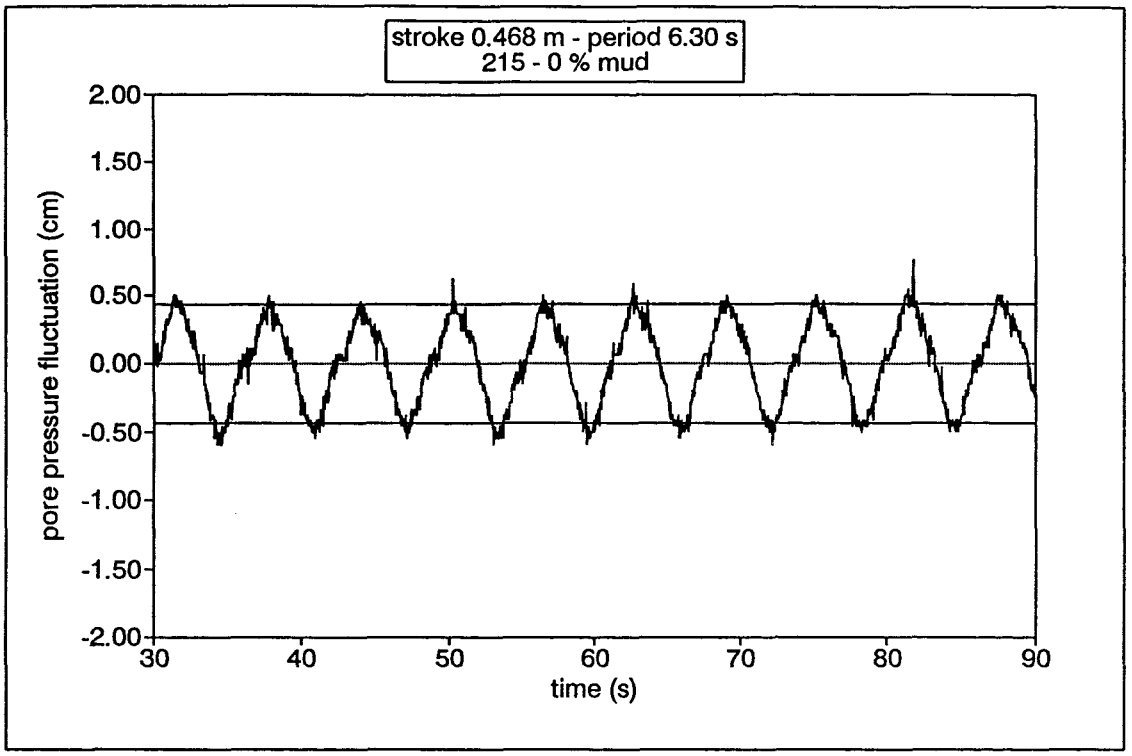

Fig. 7.43. Pore pressure record in relation to the amplitude of the pressure head (solid lines) transmitted into the sediment bed containing only the 215 μm sand, under a wave stroke of 0.468 m and period of 6.30 s.

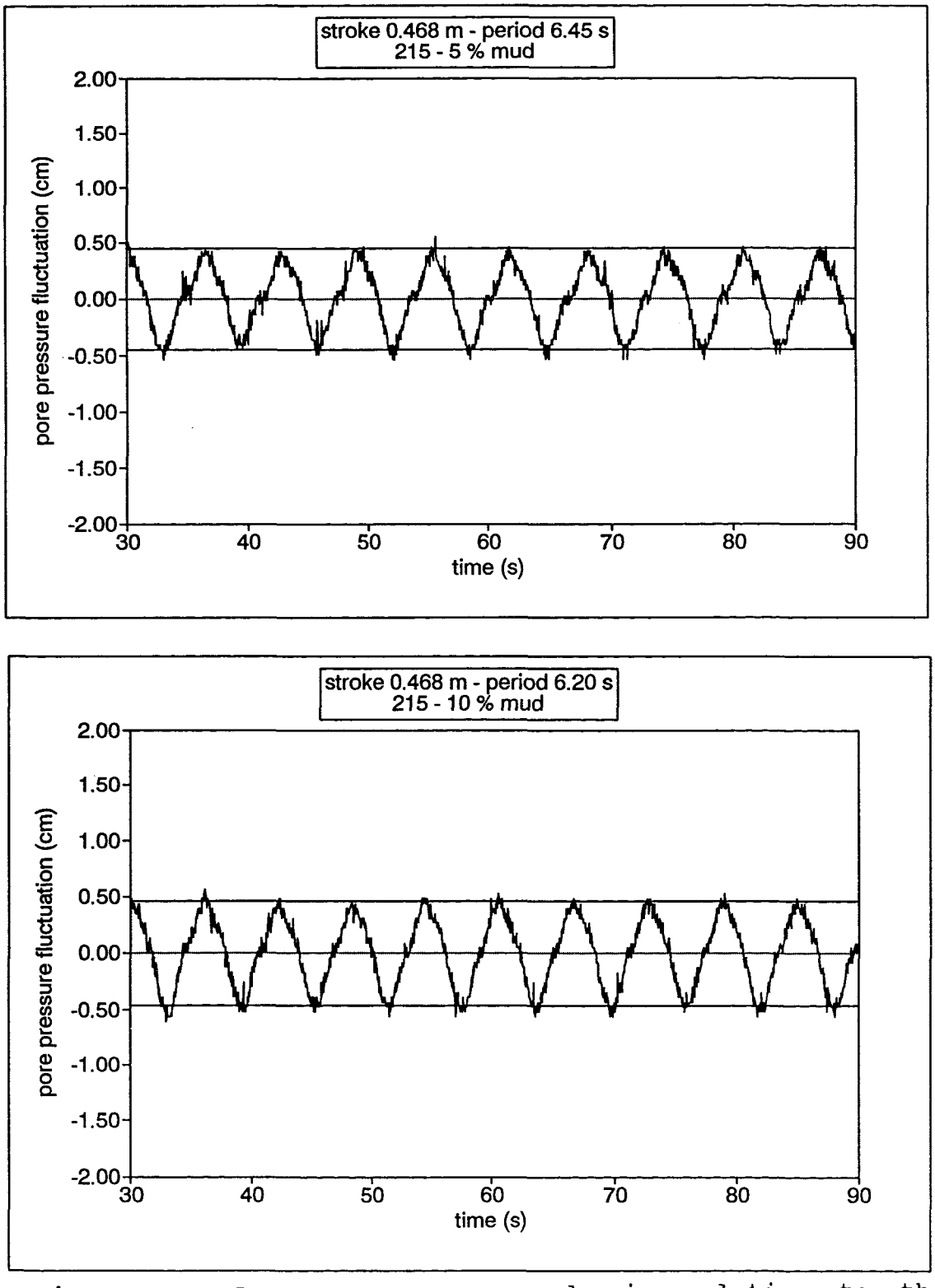

Fig. 7.44. Pore pressure records in relation to the amplitude of the pressure head (solid lines) transmitted into the 215 μm sand admixtures containing 5% and 10% of mud respectively, under a wave stroke of 0.468 m and periods of 6.45 s and 6.20 s, respectively.

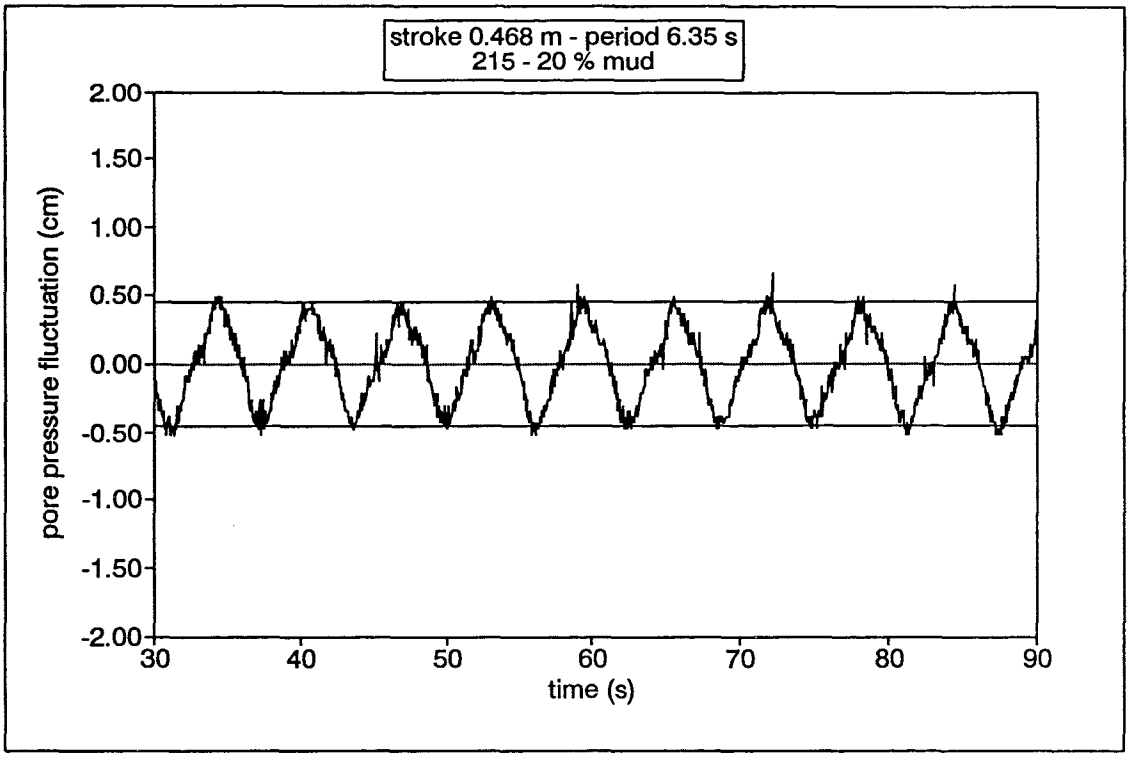

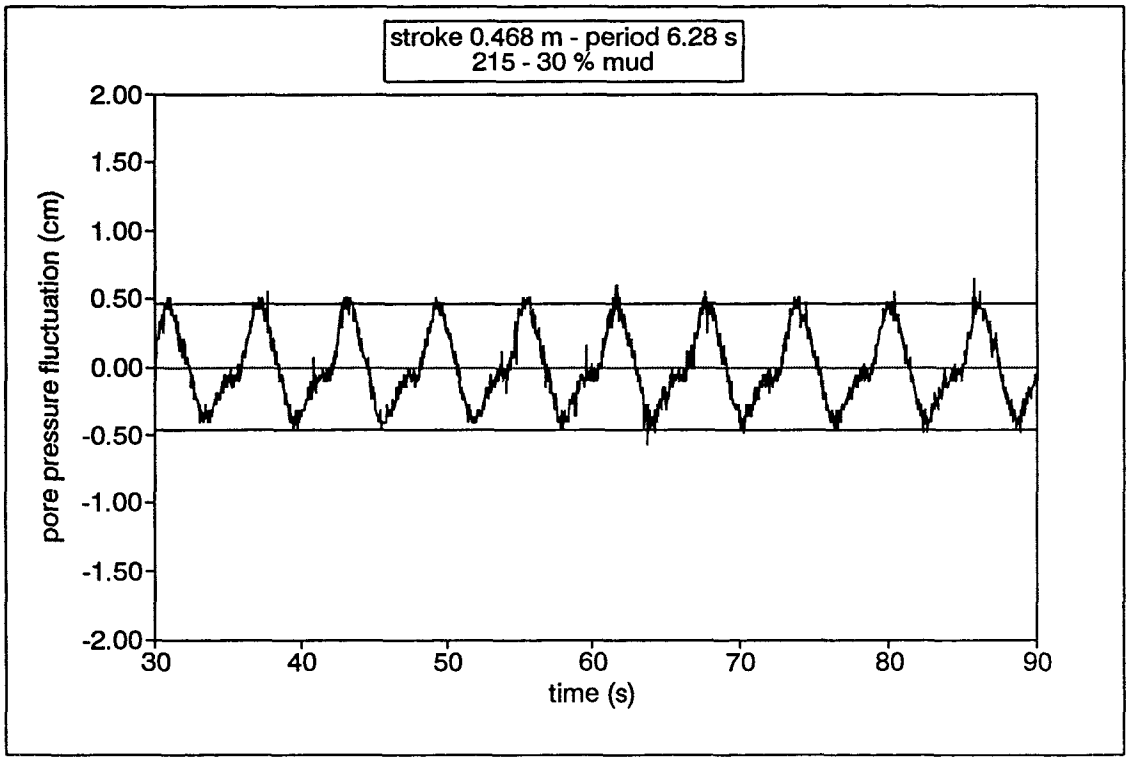

Fig. 7.45. Pore pressure records in relation to the amplitude of the pressure head (solid lines) transmitted into the 215 μm sand admixtures containing 20% and 30% of mud respectively, under a wave stroke of 0.468 m and periods of 6.35 s and 6.28 s, respectively.

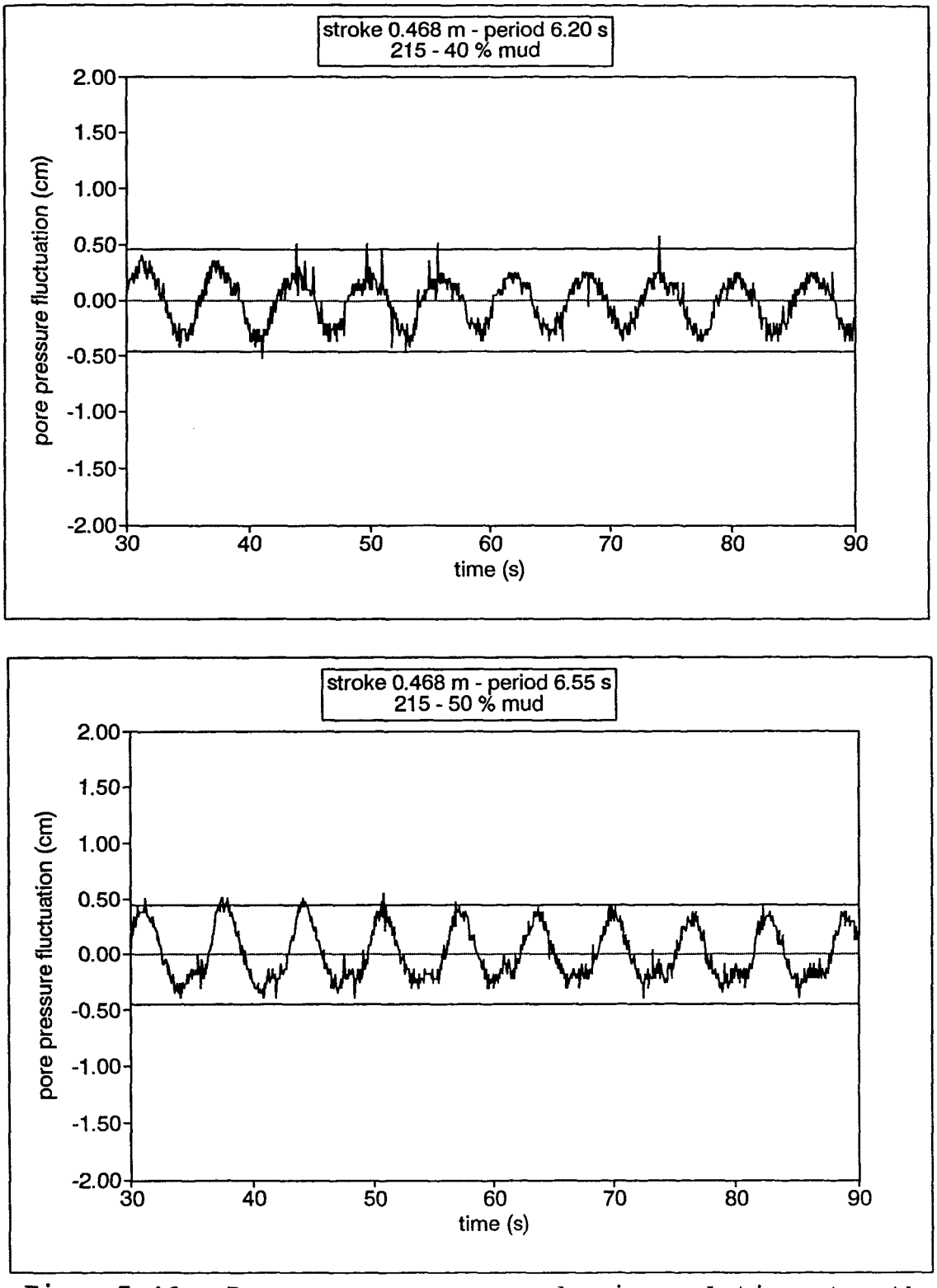

Fig. 7.46. Pore pressure records in relation to the amplitude of the pressure head (solid lines) transmitted into the 215 μm sand admixtures containing 40% and 50% of mud respectively, under a wave stroke of 0.468 m and periods of 6.20 s and 6.55 s, respectively.

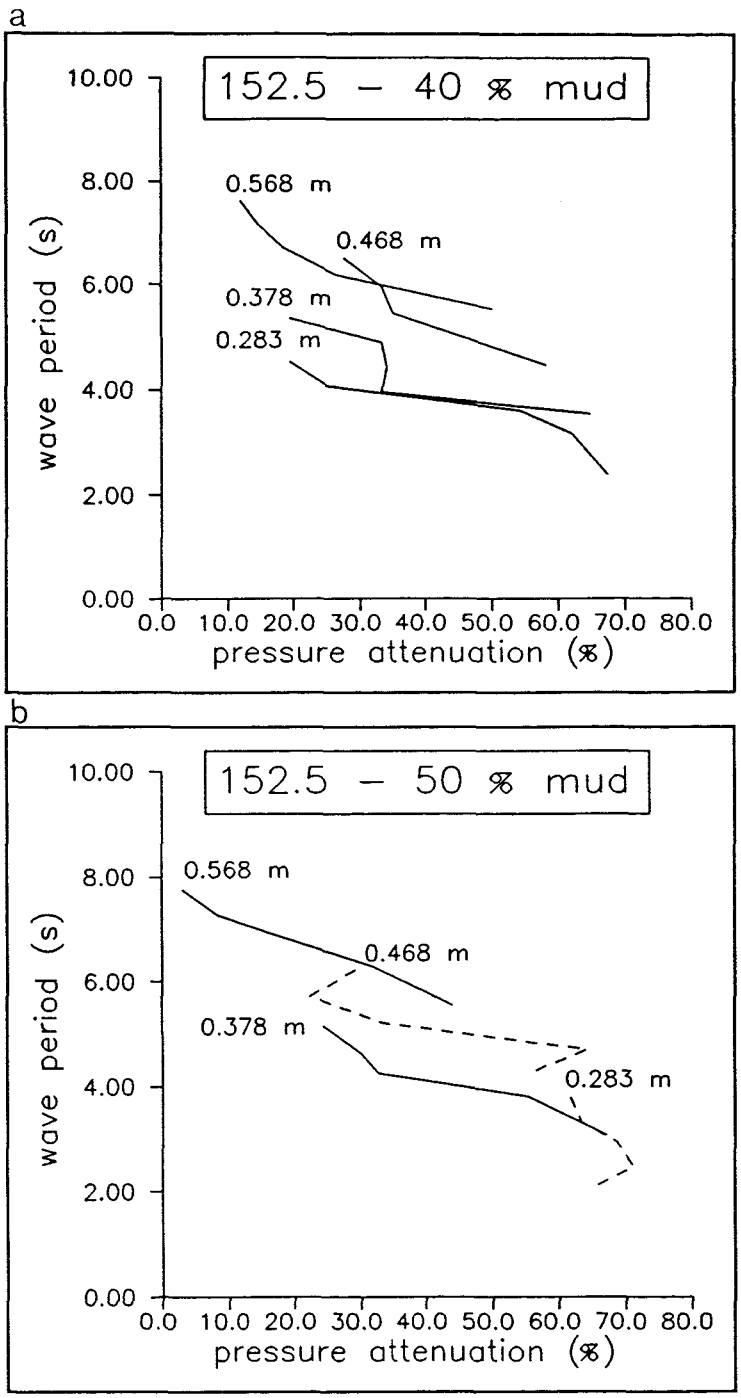

Fig. 7.47. Variation in the attenuation of the pressure head transmitted into the 152.5 μm sediment admixtures containing 40% and 50% of mud respectively, as threshold conditions are approached (Note: Values close to the edges of the curves represent particular wave strokes).

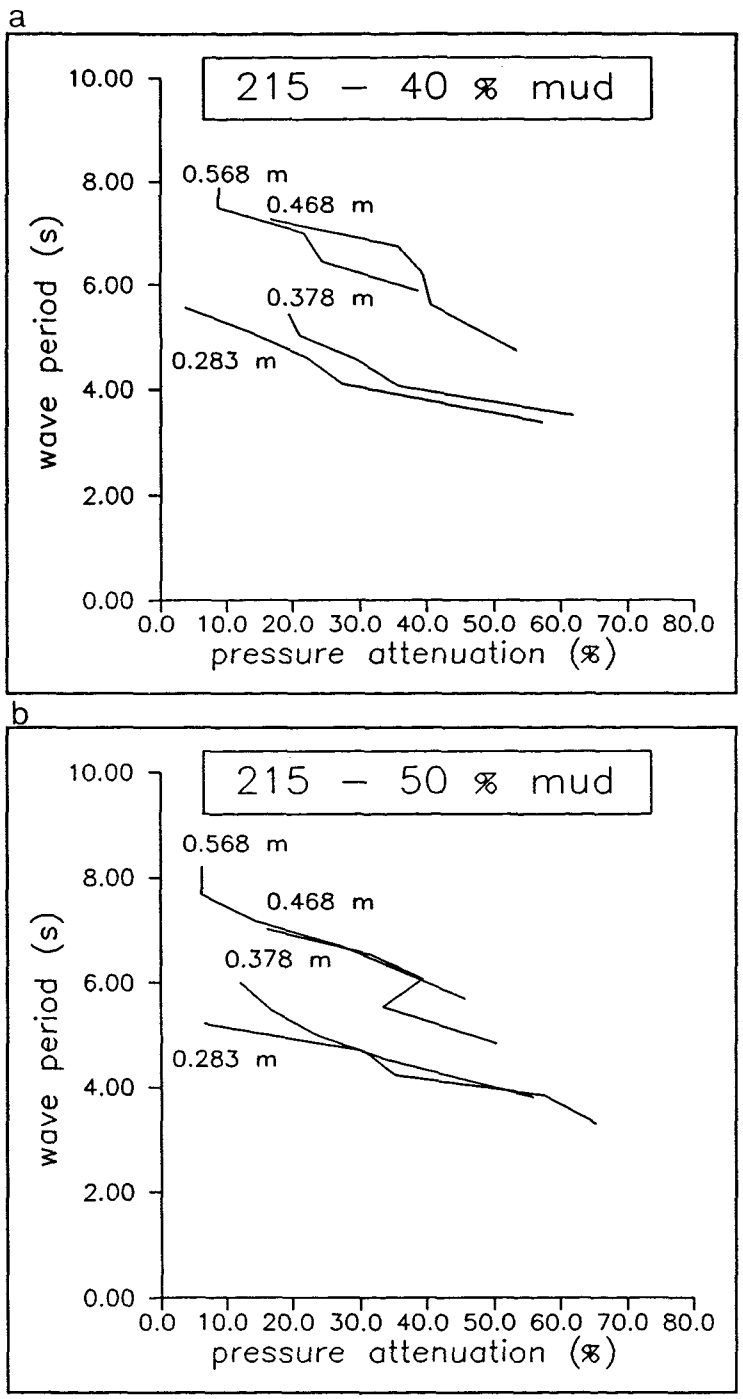

Fig. 7.48. Variation in the attenuation of the pressure head transmitted into the 215 μm sediment admixtures containing 40% and 50% of mud respectively, as threshold conditions are approached (Note: Values close to the edges of the curves represent particular wave strokes).

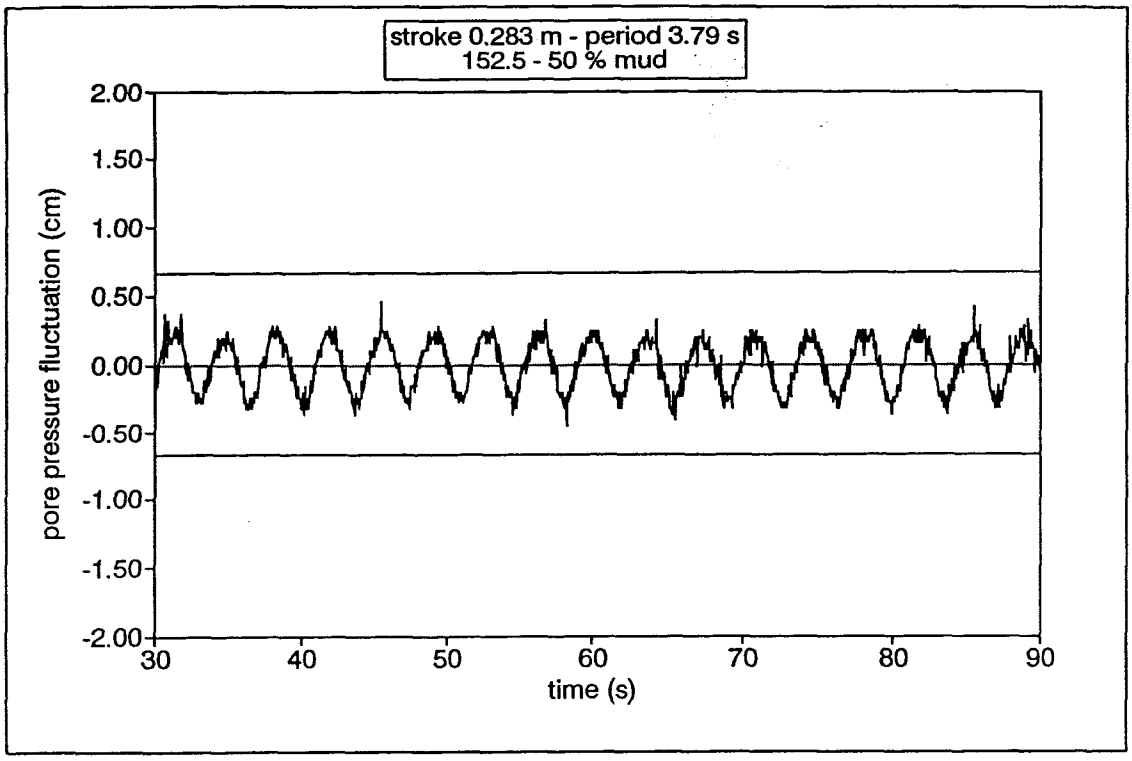

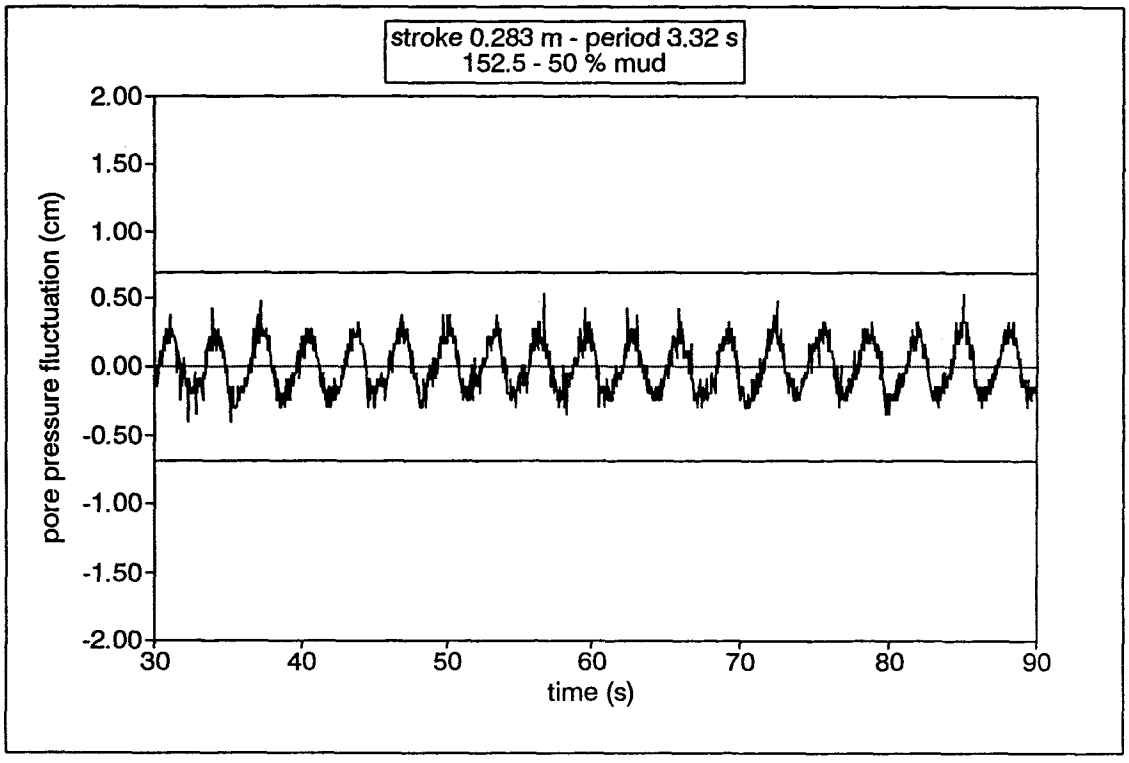

Fig. 7.49. Pore pressure records as threshold is approached in relation to the amplitude of the pressure head (solid lines) transmitted into the 152.5 μm sand admixture containing 50% of mud, under a wave stroke of 0.283 m (wave periods of 3.79 s and 3.32 s).

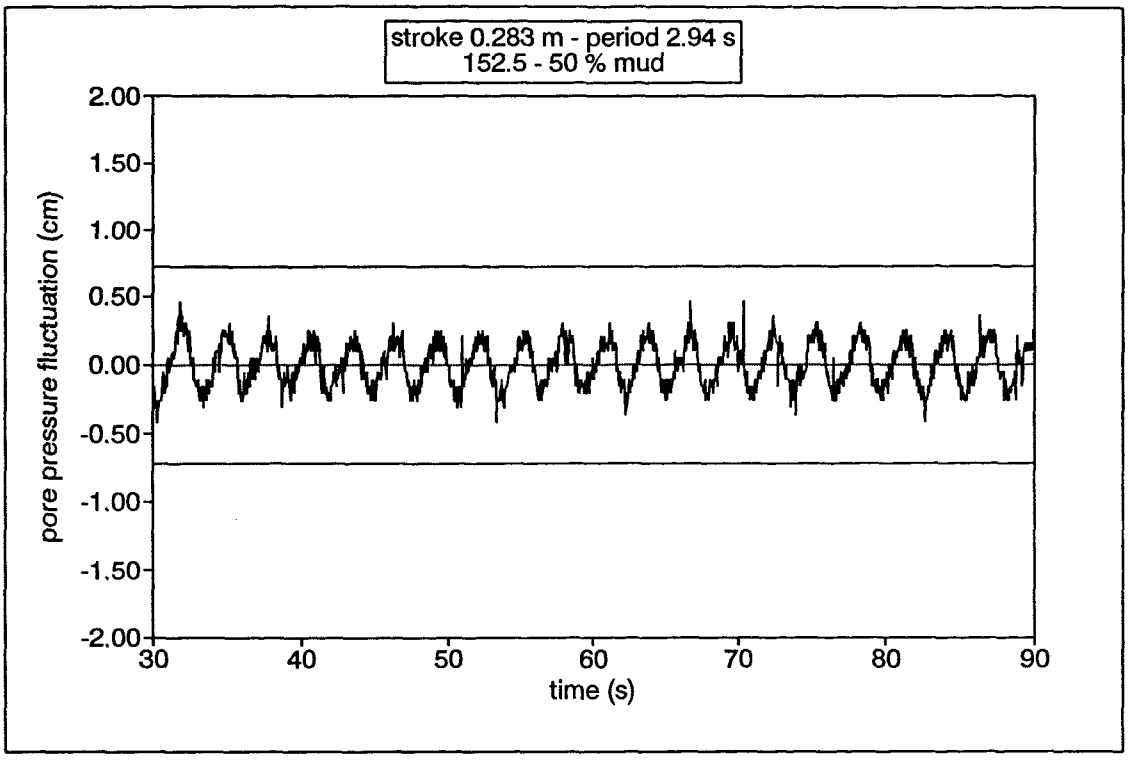

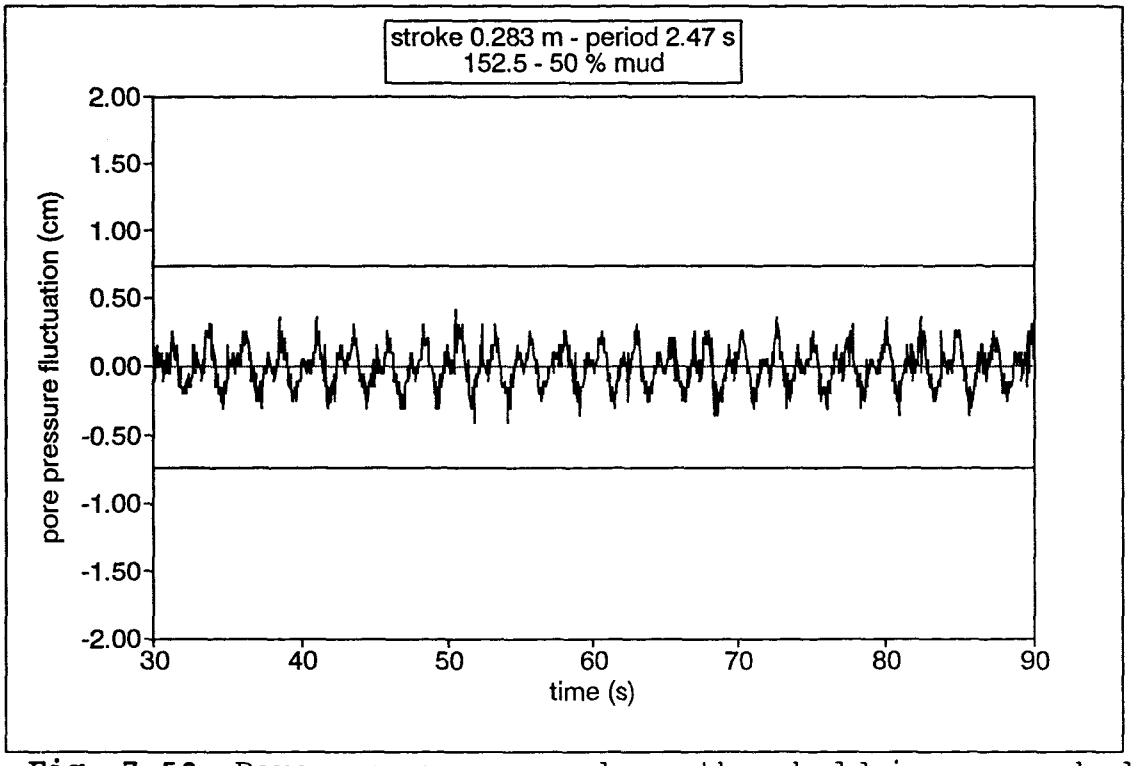

Fig. 7.50. Pore pressure records as threshold is approached in relation to the amplitude of the pressure head (solid lines) transmitted into the 152.5 μm sand admixture containing 50% of mud, under a wave stroke of 0.283 m (wave periods of 2.94 s and 2.47 s).

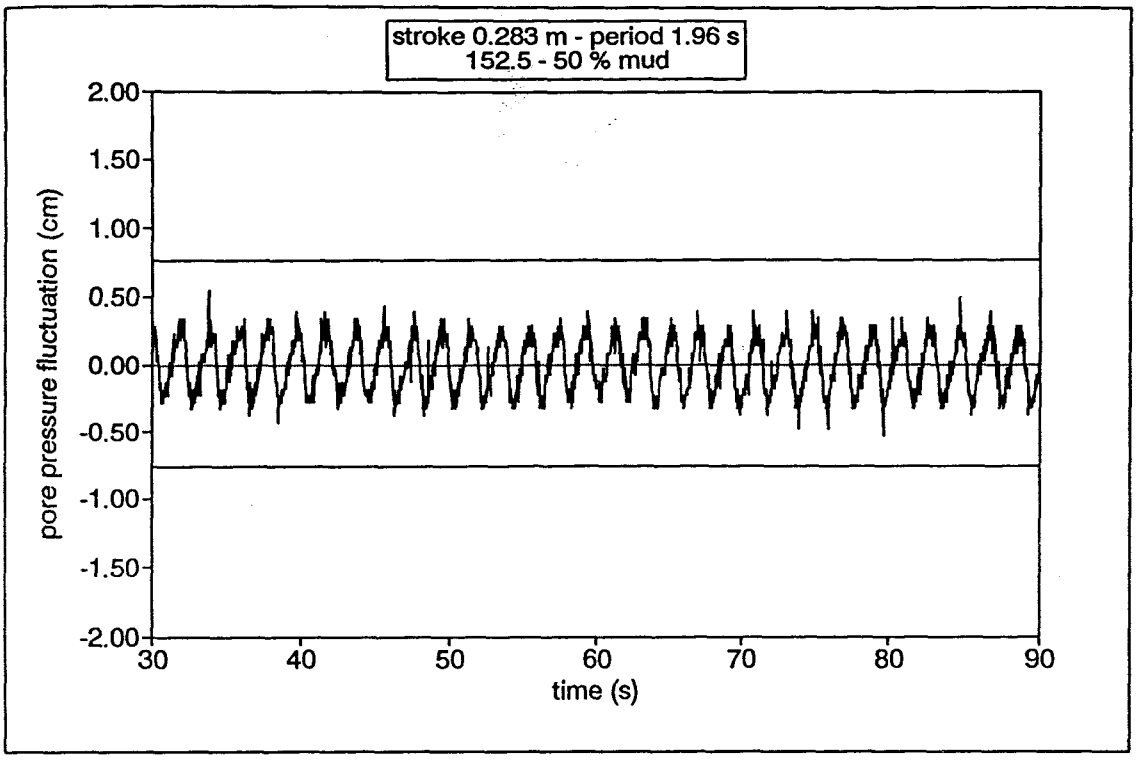

Fig. 7.51. Pore pressure record at threshold in relation to the amplitude of the pressure head (solid lines) transmitted into the 152.5 μm sand admixture containing 50% of mud, under a wave stroke of 0.283 m (wave period of 1.96 s).

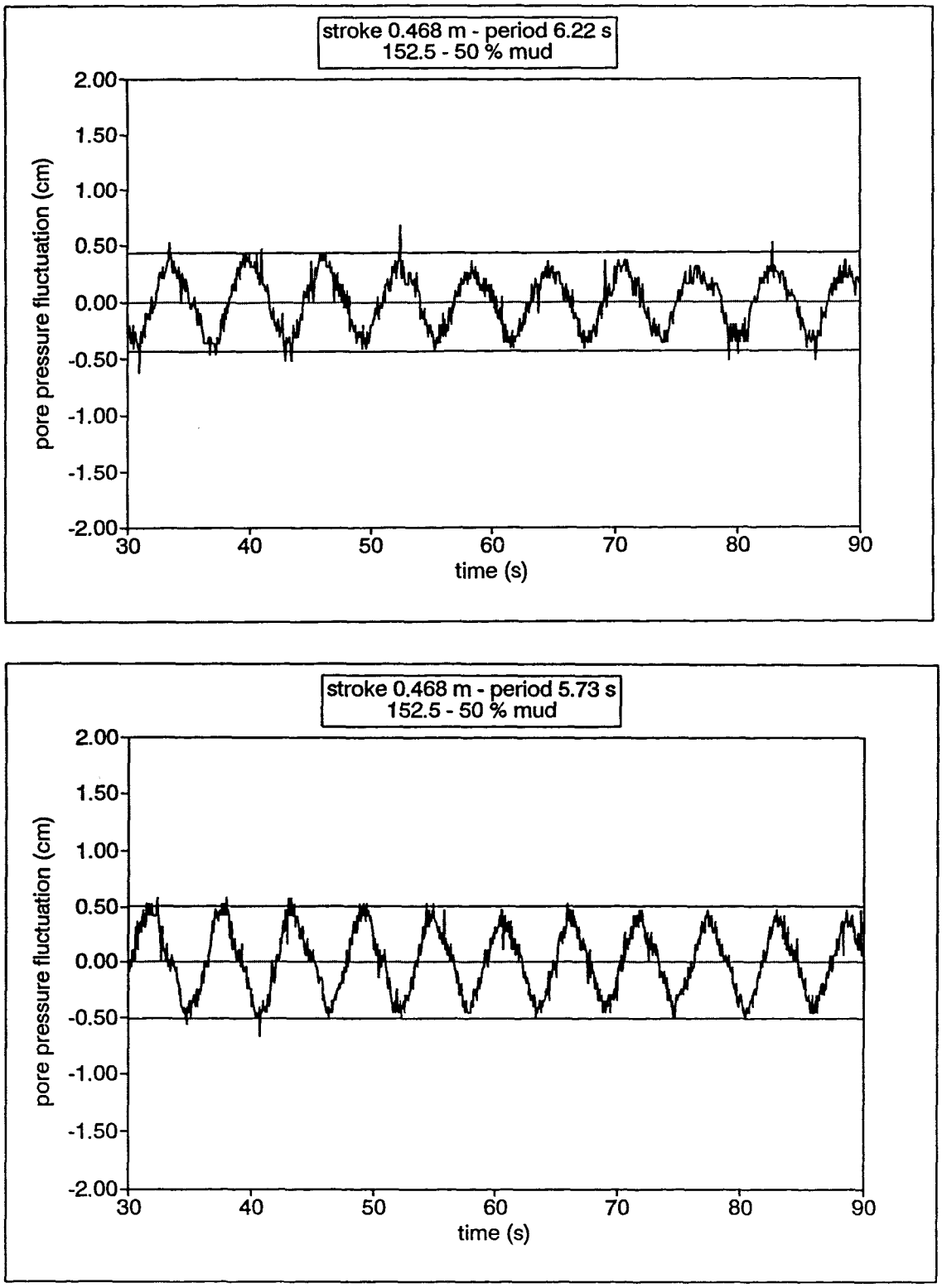

Fig. 7.52. Pore pressure records as threshold is approached in relation to the amplitude of the pressure head (solid lines) transmitted into the 152.5 μm sand admixture containing 50% of mud, under a wave stroke of 0.468 m (wave periods of 6.22 s and 5.73 s).

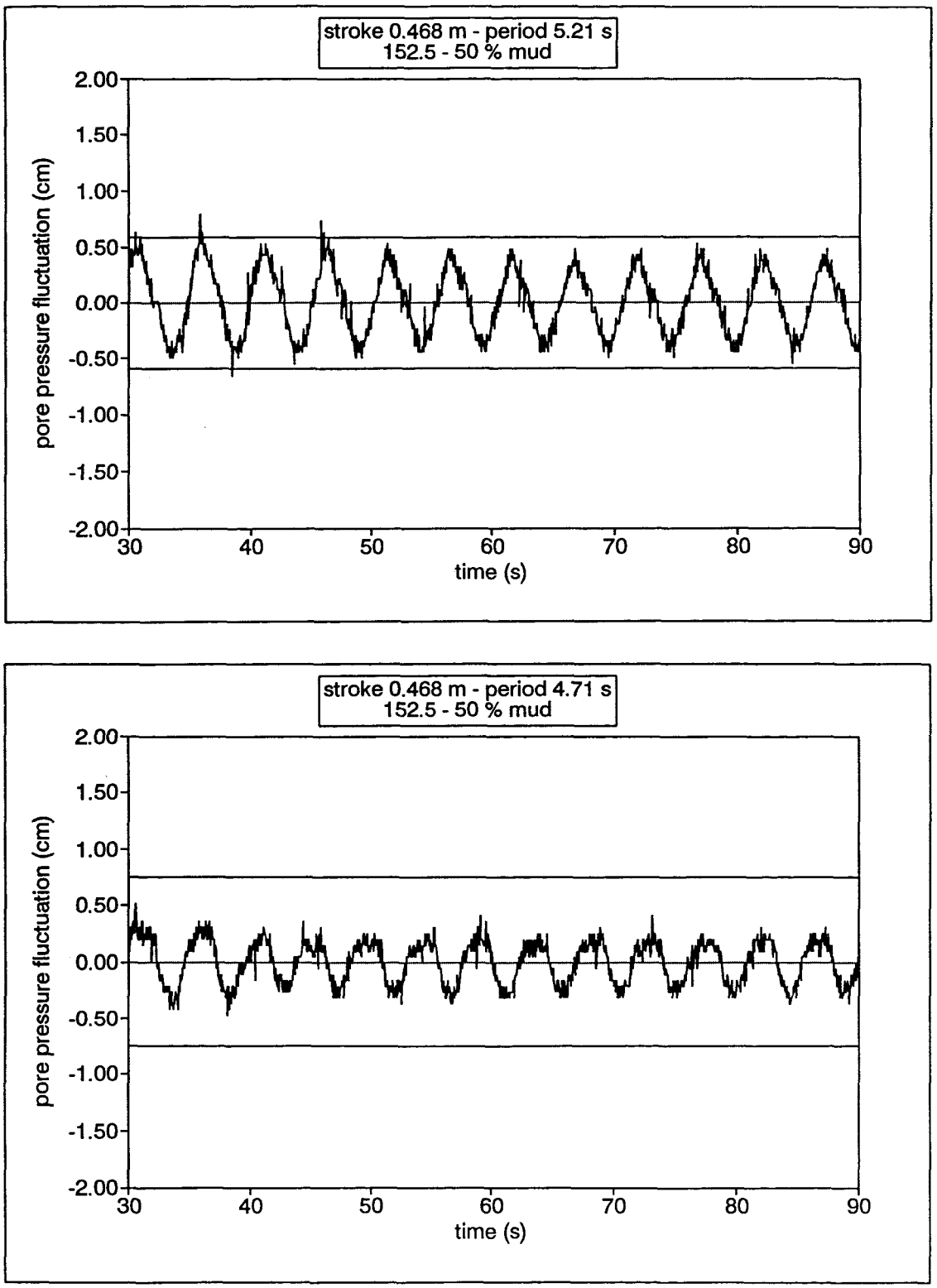

Fig. 7.53. Pore pressure records as threshold is approached in relation to the amplitude of the pressure head (solid lines) transmitted into the 152.5 μm sand admixture containing 50% of mud, under a wave stroke of 0.468 m (wave periods of 5.21 s and 4.71 s).

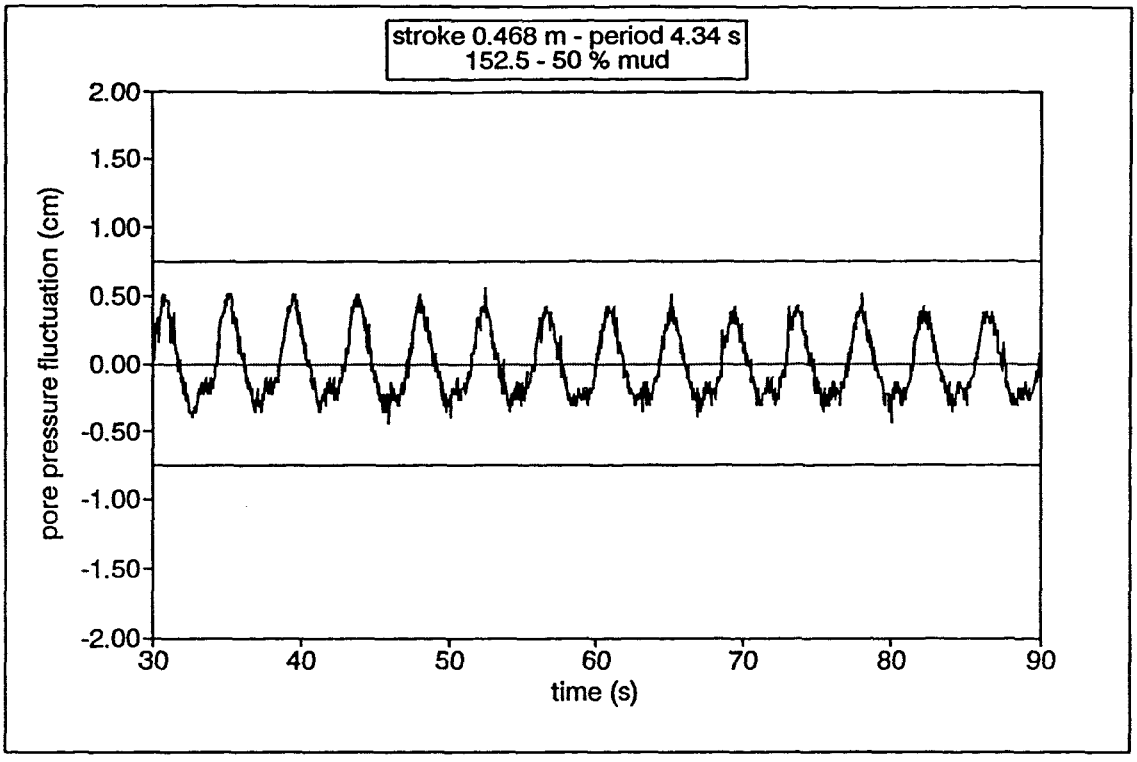

Fig. 7.54. Pore pressure record at threshold in relation to the amplitude of the pressure head (solid lines) transmitted into the 152.5 μm sand admixture containing 50% of mud, under a wave stroke of 0.468 m (wave period of 4.34 s).

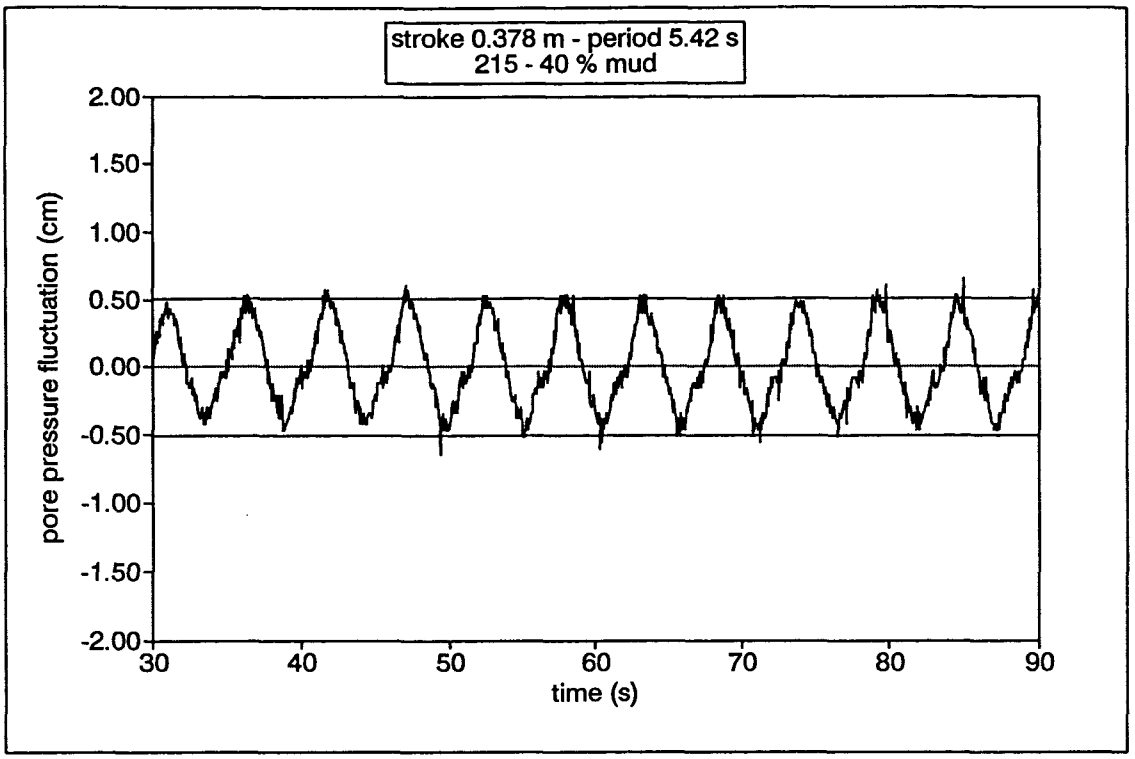

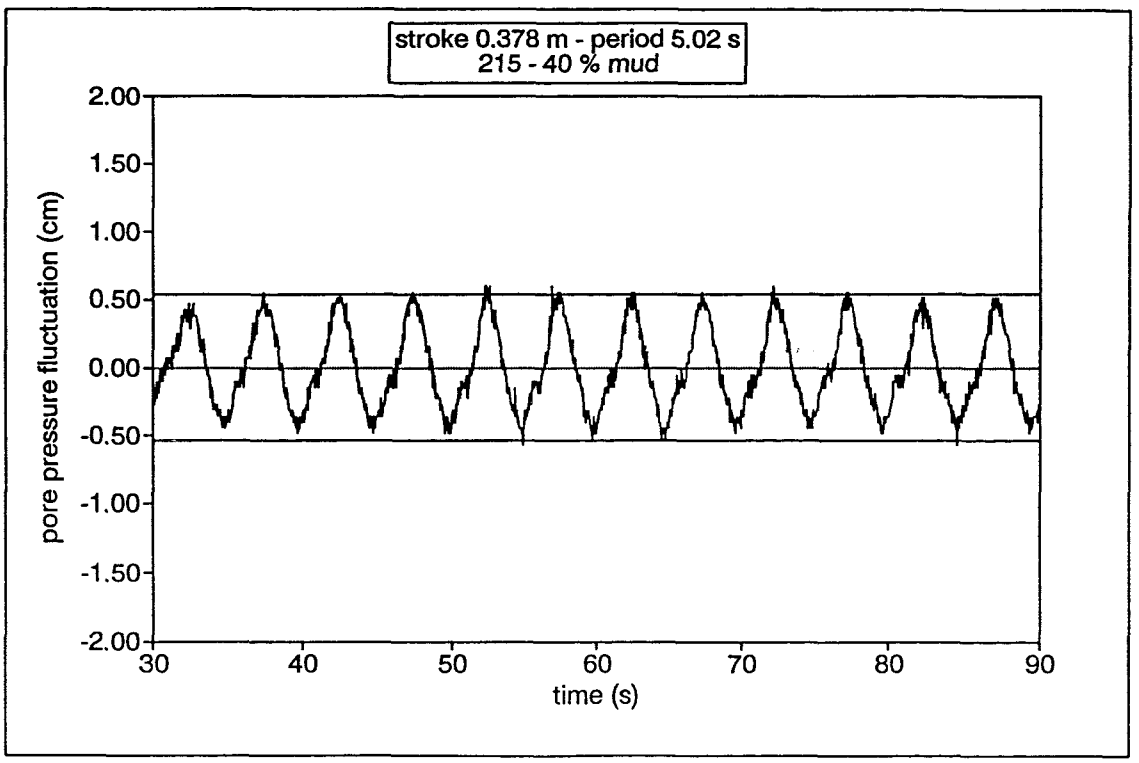

Fig. 7.55. Pore pressure records as threshold is approached in relation to the amplitude of the pressure head (solid lines) transmitted into the 215 μm sand admixture containing 40% of mud, under a wave stroke of 0.378 m (wave periods of 5.42 s and 5.02 s).

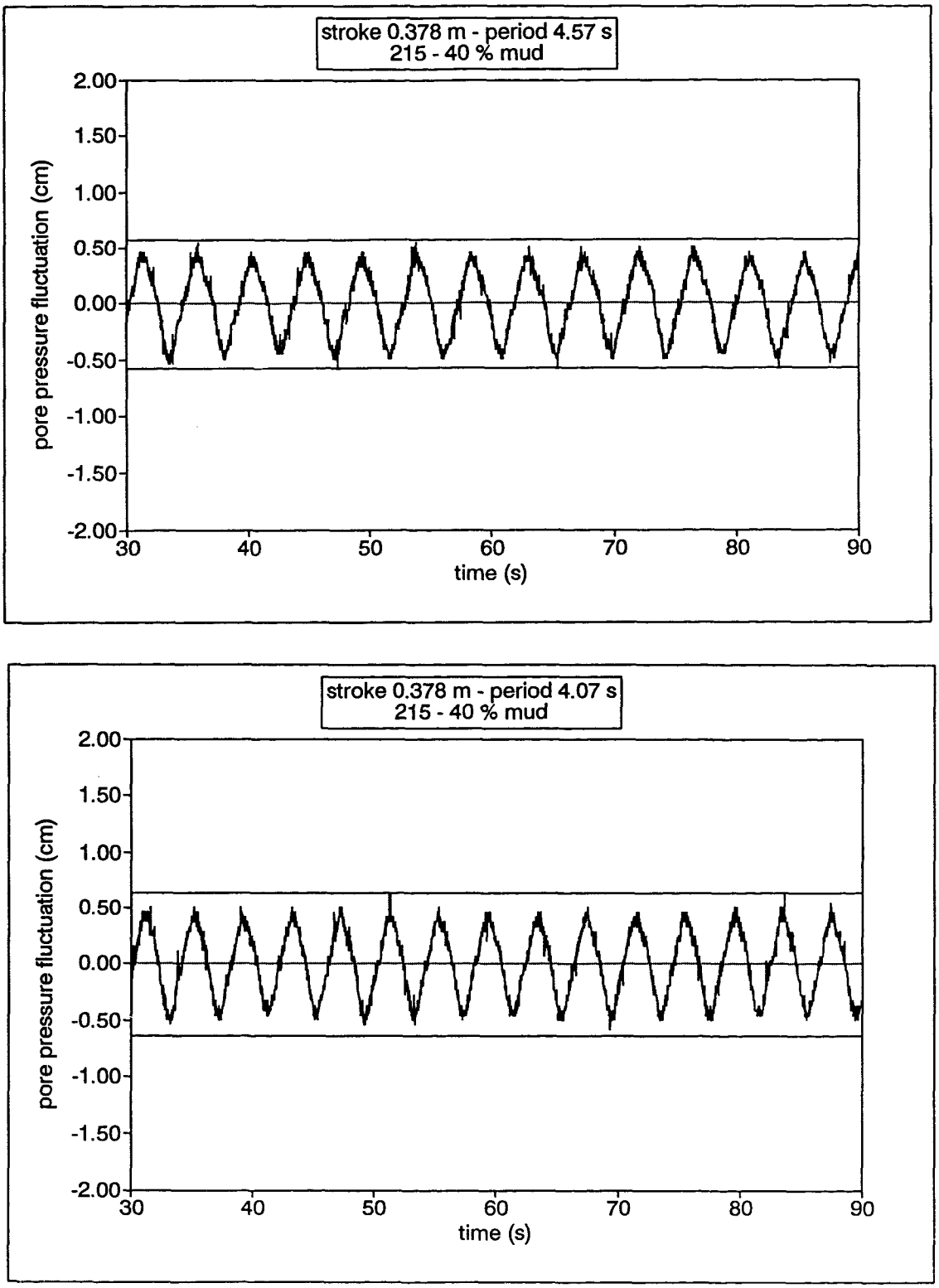

Fig. 7.56. Pore pressure records as threshold is approached in relation to the amplitude of the pressure head (solid lines) transmitted into the 215 μm sand admixture containing 40% of mud, under a wave stroke of 0.378 m (wave periods of 4.57 s and 4.07 s).

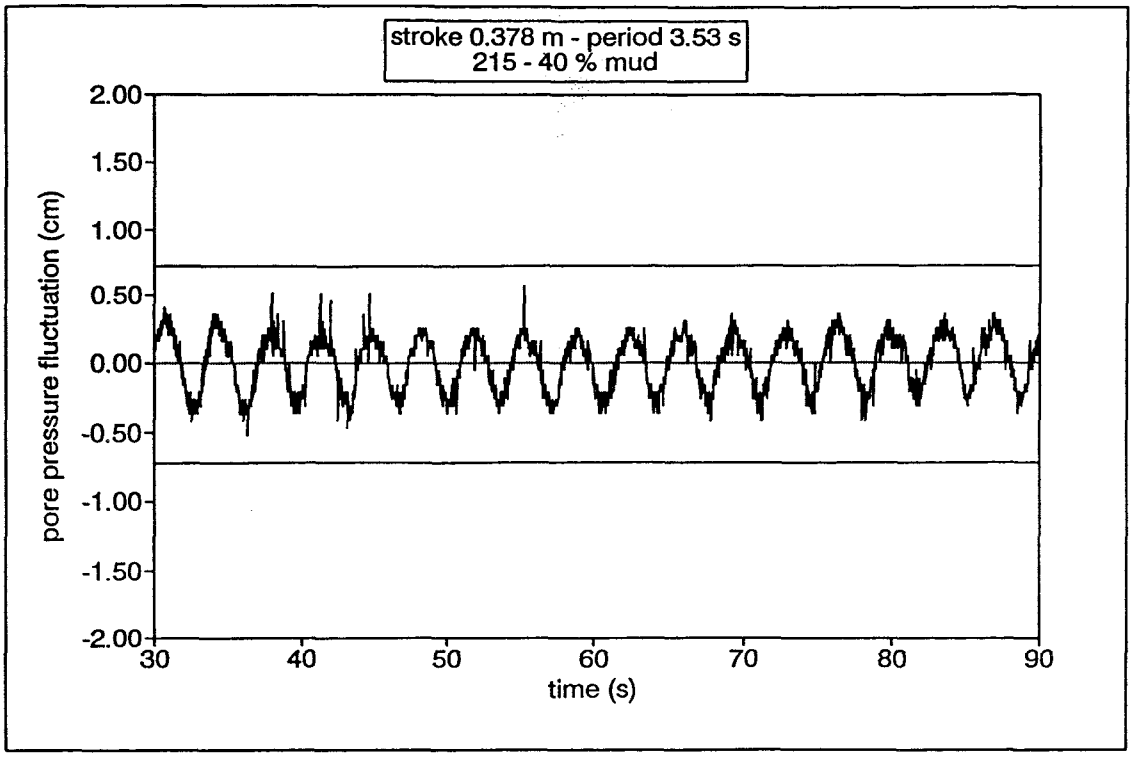

Fig. 7.57. Pore pressure record at threshold in relation to the amplitude of the pressure head (solid lines) transmitted into the 215 μm sand admixture containing 40% of mud, under a wave stroke of 0.378 m (wave period of 3.53 s).

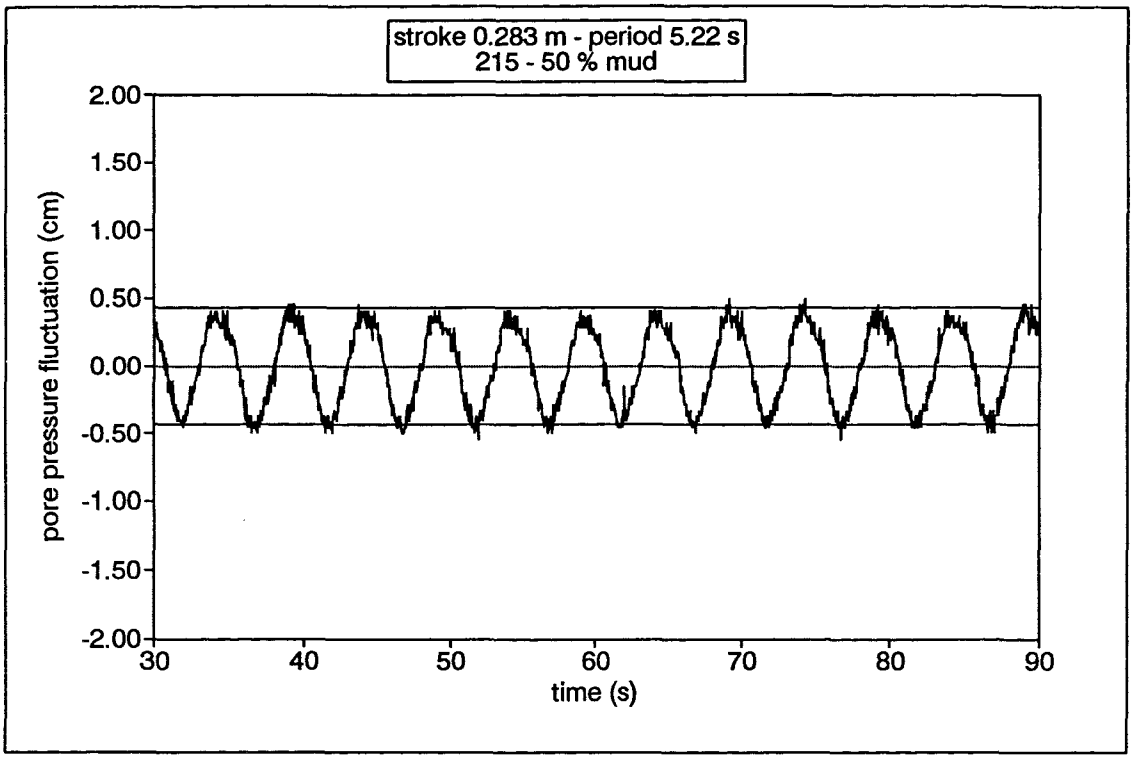

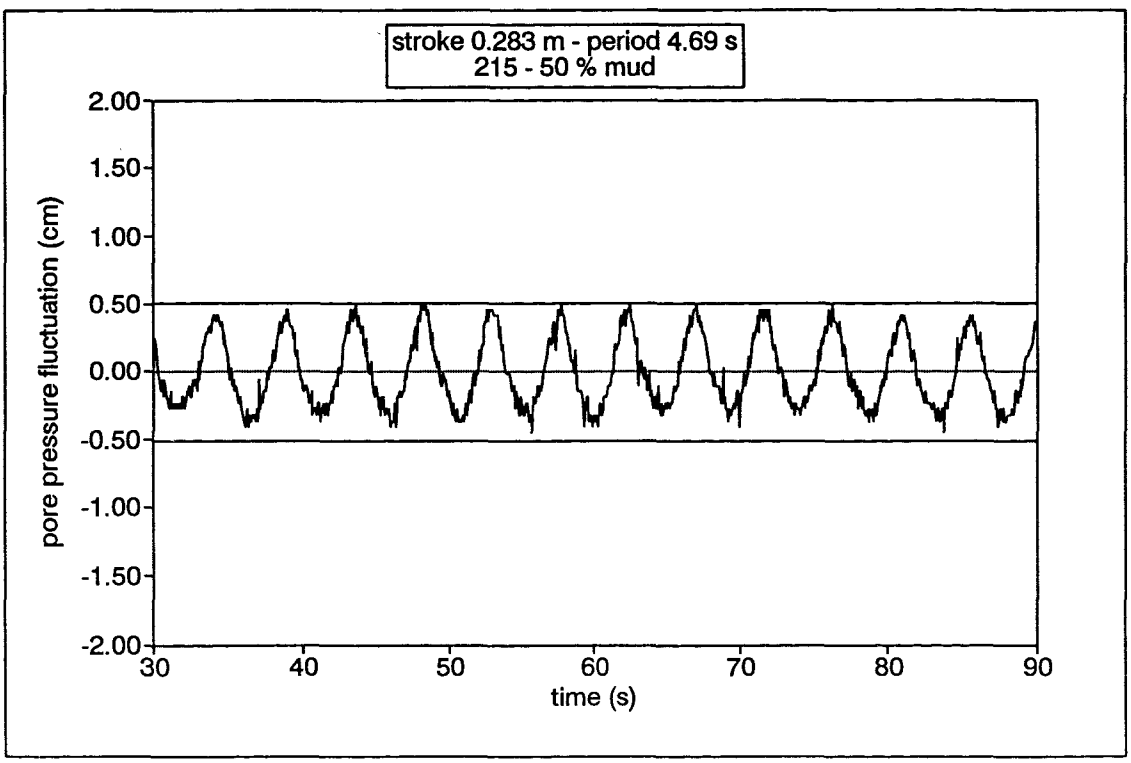

Fig. 7.58. Pore pressure records as threshold is approached in relation to the amplitude of the pressure head (solid lines) transmitted into the 215 μm sand admixture containing 50% of mud, under a wave stroke of 0.283 m (wave periods of 5.22 s and 4.69 s).

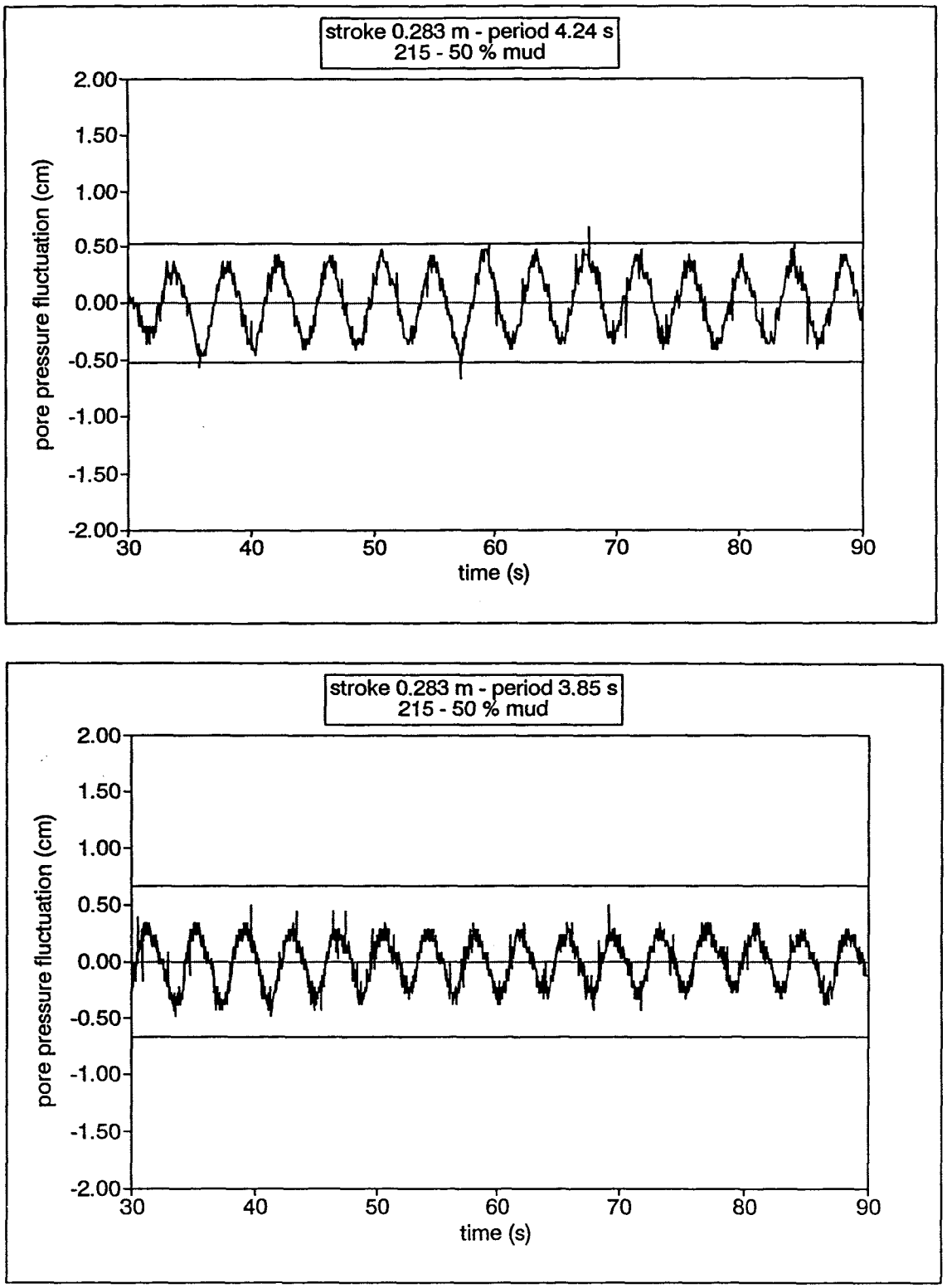

Fig. 7.59. Pore pressure records as threshold is approached in relation to the amplitude of the pressure head (solid lines) transmitted into the 215 μm sand admixture containing 50% of mud, under a wave stroke of 0.283 m (wave periods of 4.24 s and 3.85 s).

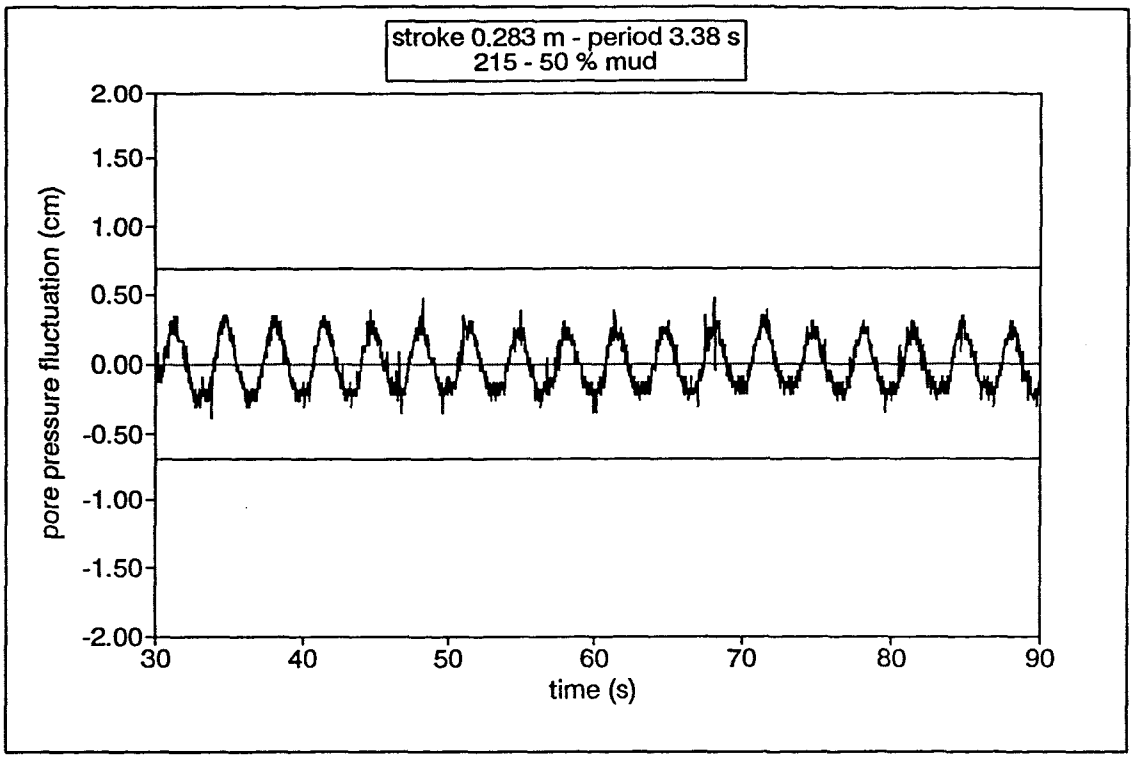

Fig. 7.60. Pore pressure record at threshold in relation to the amplitude of the pressure head (solid lines) transmitted into the 215 μm sand admixture containing 50% of mud, under a wave stroke of 0.283 m (wave period of 3.38 s).

period of oscillation T (s)	stroke $2A_o$ (m)	amplitude of plate velocity $U_{o(max)}$ (cm/s)	amplitude of hor.water vel. at the bed under the stand. wave (cm/s)	phase difference between hor. water velocity and plate velocity (degrees)	hor.component of velocity acting on the bed at the moment of threshold $U_{o,sw}$ (cm/s)	proportion of $U_{o,sw}$ to the amplitude of plate velocity (%)	wave number K (m^{-1})
3.20	0.283	27.77	6.02	-32	0.31	1.1	1.9959
3.20	0.378	37.09	7.45	-31	0.44	1.2	1.9959
3.20	0.468	45.92	8.51	-30	0.57	1.2	1.9959
3.20	0.568	55.74	12.19	-32	0.62	1.1	1.9959
4.20	0.283	21.16	5.29	-31	0.31	1.5	1.5162
4.20	0.378	28.56	6.50	-31	0.38	1.3	1.5162
4.20	0.468	34.99	8.22	-30	0.55	1.6	1.5162
4.20	0.568	44.46	11.04	-30	0.74	1.7	1.5162
5.20	0.283	17.89	4.79	-32	0.24	1.3	1.2230
5.20	0.378	22.83	6.05	-32	0.31	1.4	1.2230
5.20	0.468	28.96	7.91	-31	0.46	1.6	1.2230
5.20	0.568	33.01	10.29	-31	0.60	1.8	1.2230
6.20	0.283	14.33	4.44	-32	0.22	1.5	1.0250
6.20	0.378	19.34	5.74	-33	0.25	1.3	1.0250
6.20	0.468	24.12	7.58	-31	0.44	1.8	1.0250
6.20	0.568	28.77	9.78	-31	0.57	2.0	1.0250
7.20	0.283	12.04	4.20	-34	0.15	1.2	0.8222
7.20	0.378	16.49	5.52	-32	0.28	1.7	0.8222
7.20	0.468	19.41	7.35	-33	0.32	1.6	0.8222
7.20	0.568	24.77	9.54	-32	0.48	1.9	0.8222
8.20	0.283	10.29	4.01	-33	0.17	1.7	0.7744
8.20	0.378	13.97	5.79	-34	0.21	1.5	0.7744
8.20	0.468	18.92	7.35	-33	0.32	1.7	0.7744
8.20	0.568	20.95	9.35	-33	0.40	1.9	0.7744
9.20	0.283	9.66	4.04	-34	0.15	1.6	0.6901
9.20	0.378	12.90	5.71	-33	0.25	1.9	0.6901
9.20	0.468	15.97	7.54	-33	0.33	2.1	0.6901
9.20	0.568	19.39	8.99	-34	0.33	1.7	0.6901

Table. 7.1. Resonance phenomena and their significance to the modification of the critical erosion conditions. Note: The values of $U_{o,sw}$ have been calculated taking into account that the threshold of movement was observed to start approximately 45° before the oscillating plate reached the mid-stroke position.

stroke (m)	critical period of oscillation (s)	max.vel. of oscillation (cm/s)	st.deviation of pore pressure (cm)	mean max. vel. of oscillation (cm/s)	mean critical period of oscillation (s)	mean st. deviation of pore pressure (cm)
0.283	3.86	23.02	0.49	22.88	3.89	0.48
0.283	3.92	22.67	0.50			
0.283	4.11	21.62	0.46			
0.283	3.67	24.21	0.47			
0.378	4.67	25.42	0.39	26.71	4.46	0.37
0.378	4.28	27.73	0.35			
0.378	4.67	25.42	0.38			
0.378	4.20	28.26	0.36			
0.468	5.83	25.21	0.38	26.07	5.65	0.38
0.468	5.85	25.12	0.38			
0.468	5.39	27.26	0.37			
0.468	5.51	26.67	0.37			
0.568	6.74	26.46	0.26	27.91	6.40	0.25
0.568	6.03	29.58	0.24			
0.568	6.44	27.69	0.25			
0.568	6.39	27.91	0.25			

Table 7.2. Experimental results obtained under oscillatory flow (sand size, 152.5 microns; 0% mud).

stroke (m)	critical period of oscillation (s)	max.vel. of oscillation (cm/s)	st.deviation of pore pressure (cm)	mean max. vel. of oscillation (cm/s)	mean critical period of oscillation (s)	mean st. deviation of pore pressure (cm)
0.283	3.80	23.38	0.49	23.65	3.76	0.50
0.283	3.70	24.02	0.51			
0.283	3.97	22.38	0.51			
0.283	3.58	24.82	0.50			
0.378	4.32	27.48	0.39	27.60	4.31	0.36
0.378	4.10	28.95	0.37			
0.378	4.35	27.29	0.33			
0.378	4.45	26.67	0.34			
0.468	5.42	27.11	0.42	26.10	5.64	0.39
0.468	5.83	25.21	0.38			
0.468	5.86	25.08	0.38			
0.468	5.44	27.01	0.38			
0.568	6.42	27.78	0.31	27.71	6.44	0.28
0.568	6.49	27.48	0.25			
0.568	6.22	28.67	0.26			
0.568	6.63	26.90	0.28			

Table 7.3. Experimental results obtained under oscillatory flow (sand size, 152.5 microns; 5% mud).

stroke (m)	critical period of oscillation (s)	max.vel. of oscillation (cm/s)	st.deviation of pore pressure (cm)	mean max. vel. of oscillation (cm/s)	mean critical period of oscillation (s)	mean st. deviation of pore pressure (cm)
0.283	3.71	23.95	0.51	24.22	3.67	0.50
0.283	3.76	23.63	0.48			
0.283	3.75	23.70	0.47			
0.283	3.47	25.61	0.52			
0.378	4.64	25.58	0.40	26.25	4.53	0.40
0.378	4.61	25.75	0.39			
0.378	4.50	26.38	0.39			
0.378	4.35	27.29	0.40			
0.468	5.61	26.19	0.37	26.09	5.63	0.37
0.468	5.69	25.83	0.37			
0.468	5.64	26.06	0.36			
0.468	5.59	26.29	0.37			
0.568	6.34	28.13	0.25	27.94	6.39	0.25
0.568	6.47	27.57	0.24			
0.568	6.29	28.35	0.25			
0.568	6.44	27.69	0.25			

Table 7.4. Experimental results obtained under oscillatory flow (sand size, 152.5 microns; 10% mud).

stroke (m)	critical period of oscillation (s)	max.vel. of oscillation (cm/s)	st.deviation of pore pressure (cm)	mean max. vel. of oscillation (cm/s)	mean critical period of oscillation (s)	mean st. deviation of pore pressure (cm)
0.283	3.46	25.68	0.47	23.80	3.76	0.47
0.283	3.95	22.50	0.47			
0.283	4.15	21.41	0.46			
0.283	3.47	25.61	0.47			
0.378	4.69	25.31	0.38	26.51	4.49	0.39
0.378	4.23	28.06	0.35			
0.378	4.35	27.29	0.41			
0.378	4.68	25.36	0.43			
0.468	5.15	28.53	0.45	26.97	5.46	0.44
0.468	5.74	25.60	0.42			
0.468	5.71	25.74	0.41			
0.468	5.25	27.99	0.46			
0.568	6.52	27.35	0.20	28.53	6.26	0.20
0.568	6.34	28.13	0.20			
0.568	6.14	29.05	0.21			
0.568	6.03	29.58	0.20			

Table 7.5. Experimental results obtained under oscillatory flow (sand size, 152.5 microns; 20% mud).

stroke (m)	critical period of oscillation (s)	max.vel. of oscillation (cm/s)	st.deviation of pore pressure (cm)	mean max. vel. of oscillation (cm/s)	mean critical period of oscillation (s)	mean st. deviation of pore pressure (cm)
0.283	3.52	25.24	0.46	24.25	3.68	0.44
0.283	3.86	23.02	0.41			
0.283	3.43	25.91	0.43			
0.283	3.89	22.84	0.44			
0.378	4.68	25.36	0.36	26.15	4.54	0.38
0.378	4.45	26.67	0.38			
0.378	4.57	25.97	0.39			
0.378	4.46	26.61	0.37			
0.468	5.22	28.15	0.51	27.91	5.28	0.48
0.468	5.24	28.04	0.46			
0.468	5.64	26.06	0.50			
0.468	5.00	29.39	0.44			
0.568	6.57	27.15	0.22	28.01	6.38	0.22
0.568	6.12	29.14	0.24			
0.568	6.63	26.90	0.20			
0.568	6.18	28.86	0.21			

Table 7.6. Experimental results obtained under oscillatory flow (sand size, 152.2 microns; 30% mud).

stroke (m)	critical period of oscillation (s)	max.vel. of oscillation (cm/s)	st.deviation of pore pressure (cm)	mean max. vel. of oscillation (cm/s)	mean critical period of oscillation (s)	mean st. deviation of pore pressure (cm)
0.283	2.01	44.21	0.14	36.36	2.49	0.15
0.283	2.40	37.03	0.14			
0.283	2.70	32.91	0.15			
0.283	2.84	31.29	0.15			
0.378	3.57	33.25	0.19	33.41	3.55	0.23
0.378	3.59	33.06	0.24			
0.378	3.55	33.43	0.27			
0.378	3.50	33.91	0.23			
0.468	4.66	31.53	0.23	33.01	4.46	0.25
0.468	4.26	34.50	0.26			
0.468	4.27	34.41	0.27			
0.468	4.65	31.60	0.22			
0.568	5.89	30.28	0.18	31.8	5.62	0.19
0.568	5.77	30.91	0.19			
0.568	5.48	32.55	0.18			
0.568	5.33	33.46	0.20			

Table 7.7. Experimental results obtained under oscillatory flow (sand size, 152.5 microns; 40% mud).

stroke (m)	critical period of oscillation (s)	max.vel. of oscillation (cm/s)	st.deviation of pore pressure (cm)	mean max. vel. of oscillation (cm/s)	mean critical period of oscillation (s)	mean st. deviation of pore pressure (cm)
0.283	2.05	43.35	0.16	43.78	2.03	0.16
0.283	2.02	43.99	0.14			
0.283	2.03	43.77	0.15			
0.283	2.02	43.99	0.17			
0.378	3.32	35.75	0.13	39.35	3.04	0.15
0.378	2.79	42.54	0.15			
0.378	2.81	42.24	0.17			
0.378	3.22	36.86	0.16			
0.468	4.31	34.10	0.26	35.46	4.15	0.27
0.468	4.29	34.25	0.27			
0.468	4.03	36.46	0.26			
0.468	3.97	37.02	0.27			
0.568	5.77	30.91	0.17	32.01	5.59	0.17
0.568	5.91	30.18	0.16			
0.568	5.42	32.91	0.19			
0.568	5.24	34.04	0.17			

Table 7.8. Experimental results obtained under oscillatory flow (sand size, 152.5 microns; 50% mud).

stroke (m)	critical period of oscillation (s)	max.vel. of oscillation (cm/s)	st.deviation of pore pressure (cm)	mean max. vel. of oscillation (cm/s)	mean critical period of oscillation (s)	mean st. deviation of pore pressure (cm)
0.283	4.01	22.16	0.36	22.36	3.98	0.32
0.283	3.91	22.73	0.28			
0.283	4.16	21.36	0.34			
0.283	3.83	23.20	0.30			
0.378	5.09	23.98	X	24.14	4.95	X
0.378	4.86	24.42	X			
0.378	4.96	23.93	X			
0.378	4.90	24.22	X			
0.468	5.77	25.47	X	25.51	5.77	X
0.468	5.52	26.62	X			
0.468	5.91	24.86	X			
0.468	5.86	25.08	X			
0.568	6.94	25.70	X	26.83	6.65	X
0.568	6.43	27.74	X			
0.568	6.71	26.58	X			
0.568	6.53	27.31	X			

Table 7.9. Experimental results obtained under oscillatory flow (sand size, 215 microns; 0% mud). Key: X, transducer not functioning.

stroke (m)	critical period of oscillation (s)	max.vel. of oscillation (cm/s)	st.deviation of pore pressure (cm)	mean max. vel. of oscillation (cm/s)	mean critical period of oscillation (s)	mean st. deviation of pore pressure (cm)
0.283	4.23	21.01	0.32	21.56	4.13	0.31
0.283	3.94	22.55	0.31			
0.283	4.19	21.21	0.31			
0.283	4.14	21.46	0.31			
0.378	4.58	25.92	X	25.21	4.71	X
0.378	4.95	23.98	X			
0.378	4.72	25.15	X			
0.378	4.60	25.80	X			
0.468	5.91	24.86	X	24.93	5.90	X
0.468	5.94	24.74	X			
0.468	5.85	25.12	X			
0.468	5.88	24.99	X			
0.568	6.81	26.19	X	26.72	6.68	X
0.568	6.74	26.46	X			
0.568	6.69	26.66	X			
0.568	6.47	27.57	X			

Table 7.10. Experimental results obtained under oscillatory flow (sand size, 215 microns; 5% mud). Key: X, transducer not functioning.

stroke (m)	critical period of oscillation (s)	max.vel. of oscillation (cm/s)	st.deviation of pore pressure (cm)	mean max. vel. of oscillation (cm/s)	mean critical period of oscillation (s)	mean st. deviation of pore pressure (cm)
0.283	4.17	21.31	0.27	21.92	4.06	0.31
0.283	4.03	22.05	0.34			
0.283	4.07	21.83	0.29			
0.283	3.95	22.50	0.32			
0.378	5.26	22.57	X	23.05	5.15	X
0.378	5.18	22.91	X			
0.378	4.92	24.12	X			
0.378	5.25	22.61	X			
0.468	5.64	26.06	X	26.26	5.61	X
0.468	5.80	25.34	X			
0.468	5.19	28.31	X			
0.468	5.80	25.34	X			
0.568	6.38	27.95	X	28.03	6.37	X
0.568	6.63	26.90	X			
0.568	6.38	27.95	X			
0.568	6.08	29.33	X			

Table 7.11. Experimental results obtained under oscillatory flow (sand size, 215 microns; 10% mud). Key: X, transducer not functioning.

stroke (m)	critical period of oscillation (s)	max.vel. of oscillation (cm/s)	st.deviation of pore pressure (cm)	mean max. vel. of oscillation (cm/s)	mean critical period of oscillation (s)	mean st. deviation of pore pressure (cm)
0.283	3.82	23.26	0.34	22.57	3.94	0.34
0.283	4.06	21.89	0.35			
0.283	3.99	22.27	0.32			
0.283	3.89	22.84	0.33			
0.378	4.93	24.08	X	23.63	5.03	X
0.378	4.91	24.17	X			
0.378	5.08	23.36	X			
0.378	5.18	22.91	X			
0.468	5.93	24.78	X	25.66	5.73	X
0.468	5.55	26.48	X			
0.468	5.69	25.83	X			
0.468	5.75	25.56	X			
0.568	6.11	29.19	X	28.25	6.32	X
0.568	6.17	28.91	X			
0.568	6.40	27.87	X			
0.568	6.60	27.02	X			

Table 7.12. Experimental results obtained under oscillatory flow (sand size, 215 microns; 20% mud). Key: X, transducer not functioning.

stroke (m)	critical period of oscillation (s)	max.vel. of oscillation (cm/s)	st.deviation of pore pressure (cm)	mean max. vel. of oscillation (cm/s)	mean critical period of oscillation (s)	mean st. deviation of pore pressure (cm)
0.283	3.85	23.08	0.28	22.25	4.00	0.32
0.283	4.17	21.31	0.35			
0.283	4.14	21.46	0.33			
0.283	3.84	23.14	0.31			
0.378	4.51	26.32	X	26.32	4.52	X
0.378	4.55	26.09	X			
0.378	4.29	27.67	X			
0.378	4.71	25.20	X			
0.468	5.84	25.16	X	25.21	5.83	X
0.468	5.90	24.91	X			
0.468	5.79	25.38	X			
0.468	5.79	25.38	X			
0.568	6.54	27.27	X	27.77	6.43	X
0.568	6.47	27.57	X			
0.568	6.47	27.57	X			
0.568	6.22	28.67	X			

Table 7.13. Experimental results obtained under oscillatory flow (sand size, 215 microns; 30% mud). Key: X, transducer not functioning.

stroke (m)	critical period of oscillation (s)	max.vel. of oscillation (cm/s)	st.deviation of pore pressure (cm)	mean max. vel. of oscillation (cm/s)	mean critical period of oscillation (s)	mean st. deviation of pore pressure (cm)
0.283	3.09	28.76	0.16	27.97	3.20	0.16
0.283	3.02	29.42	0.16			
0.283	3.69	24.08	0.17			
0.283	3.00	29.62	0.16			
0.378	3.61	32.88	X	33.32	3.56	X
0.378	3.59	33.06	X			
0.378	3.50	33.91	X			
0.378	3.55	33.43	X			
0.468	5.31	27.67	X	29.97	4.93	X
0.468	5.31	27.67	X			
0.468	4.66	31.53	X			
0.468	4.45	33.02	X			
0.568	5.67	31.46	X	31.02	5.76	X
0.568	5.99	29.77	X			
0.568	5.83	30.59	X			
0.568	5.53	32.25	X			

Table 7.14. Experimental results obtained under oscillatory flow (sand size, 215 microns; 40% mud). Key: X, transducer not functioning.

stroke (m)	critical period of oscillation (s)	max.vel. of oscillation (cm/s)	st.deviation of pore pressure (cm)	mean max. vel. of oscillation (cm/s)	mean critical period of oscillation (s)	mean st. deviation of pore pressure (cm)
0.283	2.98	29.82	0.15	28.28	3.15	X
0.283	3.43	25.91	0.13			
0.283	3.00	29.62	0.16			
0.283	3.20	27.77	0.14			
0.378	3.57	33.25	X	32.21	3.70	X
0.378	4.06	29.23	X			
0.378	3.65	32.52	X			
0.378	3.51	33.82	X			
0.468	5.14	28.59	X	29.36	5.00	X
0.468	5.09	28.87	X			
0.468	4.88	30.11	X			
0.468	4.92	29.87	X			
0.568	5.77	30.91	X	30.48	5.86	X
0.568	5.81	30.70	X			
0.568	5.58	31.96	X			
0.568	6.29	28.35	X			

Table 7.15. Experimental results obtained under oscillatory flow (sand size, 215 microns; 50% mud). Key: X, transducer not functioning.

sand size (microns)	mud percentage (%)	friction factor (f_w)	critical maximum wave shear stress $\tau_{w(max)c}$ (N/m^2)
152.5	0	0.0100	0.262
	5	0.0100	0.280
	10	0.0100	0.293
	20	0.0100	0.283
	30	0.0100	0.294
	40	0.0085	0.562
	50	0.0075	0.719
215	0	0.0100	0.250
	5	0.0100	0.232
	10	0.0100	0.240
	20	0.0100	0.254
	30	0.0100	0.248
	40	0.0090	0.352
	50	0.0090	0.360

Table 7.16. Critical shear stresses related to simulated wave action, for a plate displacement of 0.283 m.

sand size (microns)	mud percentage (%)	friction factor (f_w)	critical maximum wave shear stress $\tau_{w(max)c}$ (N/m^2)
152.5	0	0.0085	0.303
	5	0.0085	0.324
	10	0.0085	0.293
	20	0.0085	0.299
	30	0.0085	0.291
	40	0.0075	0.419
	50	0.0070	0.542
215	0	0.0085	0.248
	5	0.0085	0.270
	10	0.0085	0.226
	20	0.0085	0.237
	30	0.0085	0.294
	40	0.0075	0.416
	50	0.0075	0.389

Table 7.17. Critical shear stresses related to simulated wave action, for a plate displacement of 0.378 m.

sand size (microns)	mud percentage (%)	friction factor (f_w)	critical maximum wave shear stress $\tau_{w(max)c}$ (N/m^2)
152.5	0	0.0075	0.255
	5	0.0075	0.255
	10	0.0075	0.255
	20	0.0075	0.273
	30	0.0075	0.292
	40	0.0070	0.381
	50	0.0070	0.440
215	0	0.0075	0.244
	5	0.0075	0.233
	10	0.0075	0.259
	20	0.0075	0.247
	30	0.0075	0.238
	40	0.0070	0.314
	50	0.0070	0.302

Table 7.18. Critical shear stresses related to simulated wave action, for a plate displacement of 0.468 m.

sand size (microns)	mud percentage (%)	friction factor (f_w)	critical maximum wave shear stress $\tau_{w(max)c}$ (N/m^2)
152.5	0	0.0070	0.273
	5	0.0070	0.269
	10	0.0070	0.273
	20	0.0070	0.285
	30	0.0070	0.275
	40	0.0060	0.303
	50	0.0060	0.307
215	0	0.0070	0.252
	5	0.0070	0.250
	10	0.0070	0.275
	20	0.0070	0.279
	30	0.0070	0.270
	40	0.0060	0.289
	50	0.0060	0.279

Table 7.19. Critical shear stresses related to simulated wave action, for a plate displacement of 0.568 m.

stroke (m)	wave period (s)	pressure 1 σ (cm)	pressure 2 σ (cm)	pressure attenuation (%)	$U_{o(max)}$ (cm/s)
0.283	5.89	0.20 0.20	0.19 0.19	5.0	15.09
	5.48	0.26 0.26	0.26 0.26	0	16.22
	4.99	0.31 0.31	0.30 0.30	3.2	17.81
	4.43	0.36 0.36	0.36 0.37	0	20.06
	3.90* 3.58*	0.46* 0.47*	0.43* 0.44*	6.5* 6.4*	22.79* 24.82*
0.378	6.45	0.24 0.23	0.21 0.20	12.5	18.40
	6.06	0.25 0.25	0.24 0.24	4.0	19.59
	5.47	0.36 0.36	0.35 0.35	2.8	21.70
	5.15	0.36 0.36	0.35 0.35	2.8	23.05
	4.79* 4.29*	0.40* 0.43*	0.38* 0.41*	5.0* 4.7*	24.78* 27.67*
0.468	7.40	0.28 0.27	0.24 0.24	14.3	19.86
	7.01	0.28 0.28	0.24 0.24	14.3	20.96
	6.47	0.29 0.29	0.26 0.25	10.3	22.71
	6.20	0.31 0.31	0.28 0.28	9.7	23.70
	5.99* 5.77*	0.33* 0.36*	0.31* 0.35*	6.1* 2.8*	24.53* 25.47*
0.568	8.35	0.33 0.33	0.32 0.32	3.0	21.36
	8.03	0.32 0.32	0.31 0.31	3.1	22.21
	7.40	0.32 0.32	0.32 0.31	0	24.10
	6.99	0.33 0.33	0.33 0.34	0	25.52
	6.63* 6.49*	0.34* 0.35*	0.34* 0.34*	0* 2.9*	26.90* 27.48*

Table 7.20. Pore pressure measurements obtained under oscillatory flow (sand size, 152.5 μm; 0% mud). The values marked with an asterisk were obtained during the threshold of sediment motion.

stroke (m)	wave period (s)	pressure 1 σ (cm)	pressure 2 σ (cm)	pressure attenuation (%)	$U_{o(max)}$ (cm/s)
0.283	5.90	0.20 0.20	0.19 0.19	5.0	15.06
	5.52	0.25 0.25	0.25 0.26	0	16.10
	4.99	0.31 0.31	0.30 0.30	3.2	17.81
	4.49	0.36 0.36	0.34 0.34	5.6	19.79
	3.93* 3.77*	0.46* 0.47*	0.45* 0.45*	2.2* 4.3*	22.61* 23.57*
0.378	6.43	0.24 0.24	0.21 0.21	12.5	18.46
	6.00	0.25 0.25	0.25 0.25	0	19.78
	5.49	0.36 0.36	0.36 0.35	0	21.62
	4.89	0.39 0.39	0.37 0.37	5.1	24.27
	4.40* 4.06*	0.41* 0.45*	0.39* 0.42*	4.9* 6.7*	26.98* 29.23*
0.468	7.40	0.28 0.28	0.24 0.24	14.3	19.86
	7.00	0.28 0.28	0.24 0.25	10.7	20.99
	6.52	0.29 0.29	0.26 0.26	10.3	22.54
	6.19	0.31 0.31	0.29 0.28	6.5	23.74
	5.79* 5.24*	0.36* 0.40*	0.36* 0.36*	0* 10.0*	25.38* 28.04*
0.568	8.43	0.33 0.33	0.31 0.30	6.1	21.16
	8.00	0.33 0.32	0.32 0.31	3.0	22.29
	7.50	0.34 0.34	0.32 0.32	5.9	23.78
	6.91	0.35 0.35	0.34 0.34	2.9	25.81
	6.61* 6.38*	0.36* 0.37*	0.33* 0.35*	8.3* 5.4*	26.98* 27.95*

Table 7.21. Pore pressure measurements under oscillatory flow (sand size, 152.5 μm; 5% mud). The values marked with an asterisk were obtained during the threshold of sediment motion.

stroke (m)	wave period (s)	pressure 1 σ (cm)	pressure 2 σ (cm)	pressure attenuation (%)	$U_{c(max)}$ (cm/s)
0.283	5.63	0.25 0.25	0.22 0.22	12.0	15.78
	5.15	0.30 0.30	0.29 0.28	3.3	17.25
	4.68	0.34 0.33	0.32 0.31	5.9	18.99
	4.20	0.37 0.37	0.33 0.33	10.8	21.16
	3.64* 3.49*	0.47* 0.48*	0.43* 0.43*	8.5* 10.4*	24.41* 25.46*
0.378	6.40	0.24 0.24	0.20 0.20	16.7	18.55
	5.98	0.25 0.25	0.23 0.22	8.0	19.85
	5.49	0.36 0.36	0.32 0.32	11.1	21.62
	5.01	0.38 0.38	0.36 0.35	5.3	23.69
	4.64* 4.45*	0.40* 0.41*	0.40* 0.40*	0* 2.4*	25.58* 26.67*
0.468	7.48	0.27 0.27	0.24 0.24	11.1	19.65
	7.06	0.28 0.28	0.24 0.23	14.3	20.81
	6.48	0.29 0.29	0.26 0.26	10.3	22.68
	5.98	0.33 0.33	0.31 0.31	6.1	24.57
	5.59* 5.39*	0.39* 0.40*	0.39* 0.42*	0* 0*	26.29* 27.26*
0.568	8.30	0.33 0.33	0.30 0.30	9.1	21.49
	7.78	0.34 0.34	0.30 0.30	11.8	22.92
	7.36	0.34 0.35	0.31 0.31	11.4	24.23
	6.80	0.36 0.36	0.32 0.32	11.1	26.23
	6.41* 6.35*	0.37* 0.37*	0.33* 0.34*	10.8* 8.1*	27.82* 28.09*

Table 7.22. Pore pressure measurements obtained under oscillatory flow (sand size, 152.5 μm; 10% mud). The values marked with an asterisk were obtained during the threshold of sediment motion.

	wave period (s)	pressure 1 σ (cm)	pressure 2 σ (cm)	pressure attenuation (%)	$U_{o(max)}$ (cm/s)
0.283	5.95	0.20 0.20	0.18 0.18	10.0	14.93
	5.47	0.25 0.25	0.25 0.25	0	16.25
	4.95	0.31 0.30	0.28 0.27	9.7	17.95
	4.54	0.36 0.36	0.31 0.31	13.9	19.57
	3.95* 3.81*	0.46* 0.46*	0.40* 0.41*	13.0* 10.9*	22.50* 23.32*
0.378	6.48	0.23 0.23	0.19 0.19	17.4	18.32
	6.00	0.25 0.25	0.23 0.23	8.0	19.78
	5.49	0.36 0.36	0.32 0.31	11.1	21.62
	5.00	0.38 0.38	0.33 0.32	13.2	23.74
	4.74* 4.39*	0.40* 0.41*	0.35* 0.36*	12.5* 12.2*	25.04* 27.04*
0.468	7.40	0.28 0.27	0.23 0.22	17.9	19.86
	6.95	0.28 0.28	0.24 0.24	14.3	21.14
	6.55	0.29 0.29	0.26 0.26	10.3	22.44
	5.95	0.33 0.33	0.30 0.30	9.1	24.70
	5.53* 5.28*	0.39* 0.43*	0.40* 0.43*	0* 0*	26.57* 27.83*
0.568	8.55	0.32 0.32	0.30 0.30	6.3	20.86
	7.98	0.33 0.33	0.29 0.29	12.1	22.35
	7.54	0.34 0.33	0.30 0.30	11.8	23.65
	6.95	0.35 0.35	0.32 0.32	8.6	25.66
	6.44* 6.15*	0.37* 0.42*	0.32* 0.37*	13.5* 11.9*	27.69* 29.00*

Table 7.23. Pore pressure measurements obtained under oscillatory flow (sand size, 152.5 μm; 20% mud). The values marked with an asterisk were obtained during the threshold of sediment motion.

stroke (m)	wave period (s)	pressure 1 σ (cm)	pressure 2 σ (cm)	pressure attenuation (%)	$U_{o(max)}$ (cm/s)
0.283	5.71	0.25 0.25	0.22 0.22	12.0	15.56
	5.31	0.30 0.30	0.30 0.29	0	16.73
	4.76	0.35 0.35	0.30 0.29	14.3	18.67
	4.25	0.37 0.36	0.31 0.31	16.2	20.91
	3.63* 3.59*	0.48* 0.48*	0.41* 0.41*	14.6* 14.6*	24.48* 24.75*
0.378	6.47	0.23 0.23	0.22 0.22	4.3	18.34
	6.03	0.25 0.25	0.22 0.22	12.0	19.68
	5.49	0.37 0.37	0.37 0.36	0	21.62
	4.96	0.38 0.38	0.28 0.28	26.3	23.93
	4.53* 4.27*	0.41* 0.43*	0.29* 0.29*	29.3* 32.6*	26.20* 27.80*
0.468	7.49	0.27 0.27	0.21 0.21	22.2	19.62
	6.91	0.29 0.28	0.23 0.22	20.7	21.27
	6.38	0.31 0.31	0.24 0.24	22.6	23.03
	5.84	0.36 0.36	0.31 0.31	13.9	25.16
	5.46* 5.21*	0.39* 0.42*	0.32* 0.32*	17.9* 23.8*	26.91* 28.21*
0.568	8.38	0.32 0.32	0.28 0.28	12.5	21.28
	7.95	0.32 0.32	0.28 0.28	12.5	22.43
	7.49	0.34 0.33	0.28 0.28	17.6	23.81
	6.93	0.38 0.38	0.31 0.31	18.4	25.74
	6.20* 6.13*	0.42* 0.43*	0.33* 0.33*	21.4* 23.3*	28.77* 29.09*

Table 7.24. Pore pressure measurements obtained under oscillatory flow (sand size, 152.5 μm; 30% mud). The values marked with an asterisk were obtained during the threshold of sediment motion.

stroke (m)	wave period (s)	pressure 1 σ (cm)	pressure 2 σ (cm)	pressure attenuation (%)	$U_{o(max)}$ (cm/s)
0.283	4.53	0.36 0.36	0.29 0.29	19.4	19.62
	4.07	0.44 0.44	0.33 0.32	25.0	21.83
	3.59	0.48 0.48	0.22 0.22	54.2	24.75
	3.16	0.50 0.50	0.19 0.19	62.0	28.12
	2.54* 2.24*	0.52* 0.52*	0.17* 0.17*	67.3* 67.3*	34.99* 39.67*
0.378	5.35	0.36 0.36	0.28 0.29	19.4	22.19
	4.89	0.39 0.39	0.26 0.26	33.3	24.27
	4.42	0.41 0.41	0.27 0.27	34.1	26.85
	3.96	0.45 0.45	0.30 0.30	33.3	29.97
	3.57* 3.48*	0.51* 0.51*	0.18* 0.18*	64.7* 64.7*	33.25* 34.11*
0.468	6.50	0.29 0.29	0.21 0.21	27.6	22.61
	5.95	0.33 0.33	0.22 0.22	33.3	24.70
	5.45	0.40 0.39	0.26 0.26	35.0	26.96
	5.00	0.44 0.44	0.25 0.23	45.5	29.39
	4.66* 4.24*	0.53* 0.54*	0.21* 0.24*	60.4* 55.6*	31.53* 34.66*
0.568	7.61	0.34 0.34	0.30 0.30	11.8	23.44
	7.18	0.35 0.35	0.30 0.30	14.3	24.84
	6.70	0.38 0.38	0.31 0.31	18.4	26.62
	6.18	0.42 0.42	0.31 0.31	26.2	28.86
	5.68* 5.36*	0.58* 0.64*	0.29* 0.32*	50.0* 50.0*	31.40* 33.27*

Table 7.25. Pore pressure measurements obtained under oscillatory flow (sand size, 152.5 μm; 40% mud). The values marked with an asterisk were obtained during the threshold of sediment motion.

stroke (m)	wave period (s)	pressure 1 σ (cm)	pressure 2 σ (cm)	pressure attenuation (%)	$U_{o(max)}$ (cm/s)
0.283	3.79	0.47 0.46	0.18 0.18	61.7	23.45
	3.32	0.49 0.49	0.18 0.18	63.3	26.77
	2.94	0.50 0.51	0.14 0.17	68.6	30.23
	2.47	0.52 0.52	0.15 0.15	71.2	35.98
	2.13* 1.96*	0.53* 0.54*	0.18* 0.20*	66.0* 63.0*	41.72* 45.34*
0.378	5.15	0.37 0.37	0.28 0.27	24.3	23.05
	4.64	0.40 0.40	0.28 0.28	30.0	25.58
	4.26	0.43 0.43	0.29 0.29	32.6	27.86
	3.82	0.47 0.47	0.21 0.21	55.3	31.07
	3.25* 2.91*	0.51* 0.52*	0.17* 0.17*	66.7* 67.3*	36.52* 40.79*
0.468	6.22	0.31 0.31	0.22 0.22	29.0	23.63
	5.73	0.36 0.36	0.28 0.28	22.2	25.65
	5.21	0.41 0.43	0.27 0.29	33.3	28.21
	4.71	0.53 0.53	0.19 0.18	64.2	31.20
	4.34* 4.16*	0.53* 0.54*	0.24* 0.24*	54.7* 55.6*	33.86* 35.33*
0.568	7.75	0.33 0.33	0.32 0.32	3.0	23.01
	7.27	0.36 0.36	0.33 0.33	8.3	24.53
	6.86	0.39 0.39	0.32 0.32	17.9	26.00
	6.29	0.41 0.41	0.28 0.28	31.7	28.35
	5.75* 5.34*	0.55* 0.65*	0.33* 0.34*	40.0* 47.7*	31.02* 33.40*

Table 7.26. Pore pressure measurements obtained under oscillatory flow (sand size, 152.5 μm; 50% mud). The values marked with an asterisk were obtained during the threshold of sediment motion.

stroke (m)	wave period (s)	pressure 1 σ (cm)	pressure 2 σ (cm)	pressure attenuation (%)	$U_{o(max)}$ (cm/s)
0.283	6.03	0.20 0.20	0.18 0.18	10.0	14.74
	5.54	0.26 0.26	0.26 0.27	0	16.04
	5.16	0.31 0.31	0.31 0.31	0	17.22
	4.63	0.35 0.35	0.32 0.32	8.6	19.19
	4.09* 3.95*	0.44* 0.45*	0.42* 0.42*	4.5* 6.7*	21.73* 22.50*
0.378	6.90	0.24 0.24	0.21 0.21	12.5	17.20
	6.41	0.25 0.25	0.22 0.22	12.0	18.52
	6.01	0.25 0.25	0.26 0.25	0	19.75
	5.41	0.36 0.36	0.35 0.35	2.8	21.94
	5.06* 4.96*	0.38* 0.38*	0.36* 0.36*	5.3* 5.3*	23.46* 23.93*
0.468	7.71	0.26 0.26	0.25 0.25	3.8	19.06
	7.28	0.28 0.27	0.27 0.26	3.6	20.19
	6.87	0.29 0.29	0.27 0.29	3.4	21.39
	6.30	0.30 0.32	0.30 0.30	3.2	23.33
	5.81* 5.71*	0.35* 0.35*	0.34* 0.33*	2.9* 5.7*	25.29* 25.74*
0.568	8.80	0.33 0.33	0.34 0.34	0	20.27
	8.33	0.33 0.32	0.33 0.33	0	21.41
	7.79	0.34 0.34	0.34 0.34	0	22.89
	7.43	0.35 0.35	0.35 0.35	0	24.00
	7.14* 6.79*	0.35* 0.36*	0.37* 0.37*	0* 0*	24.98* 26.27*

Table 7.27. Pore pressure measurements obtained under oscillatory flow (sand size, 215 μm; 0% mud). The values marked with an asterisk were obtained during the threshold of sediment motion.

stroke (m)	wave period (s)	pressure 1 σ (cm)	pressure 2 σ (cm)	pressure attenuation (%)	$U_{o(max)}$ (cm/s)
0.283	5.98	0.20 0.20	0.19 0.18	5.0	14.86
	5.52	0.26 0.27	0.27 0.29	0	16.10
	5.10	0.31 0.31	0.29 0.29	6.5	17.42
	4.63	0.35 0.35	0.35 0.34	0	19.19
	4.20* 3.99*	0.38* 0.45*	0.36* 0.42*	5.3* 6.7*	21.16* 22.27*
0.378	6.79	0.24 0.24	0.20 0.20	16.7	17.48
	6.35	0.25 0.25	0.21 0.20	16.0	18.69
	5.85	0.30 0.30	0.29 0.29	3.3	20.29
	5.35	0.36 0.36	0.35 0.35	2.8	22.19
	4.80* 4.62*	0.40* 0.41*	0.38* 0.40*	5.0* 2.4*	24.73* 25.69*
0.468	7.77	0.27 0.27	0.24 0.24	11.1	18.91
	7.34	0.28 0.28	0.25 0.24	10.7	20.02
	6.84	0.31 0.31	0.27 0.27	12.9	21.48
	6.45	0.32 0.32	0.28 0.28	12.5	22.78
	5.81* 5.77*	0.36* 0.36*	0.32* 0.33*	11.1* 8.3*	25.29* 25.47*
0.568	8.55	0.33 0.33	0.32 0.32	3.0	20.86
	8.21	0.33 0.33	0.31 0.31	6.1	21.72
	7.72	0.34 0.34	0.32 0.32	5.9	23.10
	7.25	0.35 0.35	0.34 0.34	2.9	24.60
	6.90* 6.75*	0.35* 0.36*	0.35* 0.35*	0* 2.8*	25.85* 26.42*

Table 7.28. Pore pressure measurements obtained under oscillatory flow (sand size, 215 μm; 5% mud). The values marked with an asterisk were obtained during the threshold of sediment motion.

stroke (m)	wave period (s)	pressure 1 σ (cm)	pressure 2 σ (cm)	pressure attenuation (%)	$U_{\infty(max)}$ (cm/s)
0.283	6.06	0.20 0.20	0.17 0.17	15.0	14.66
	5.68	0.26 0.26	0.24 0.24	7.7	15.64
	5.08	0.31 0.31	0.27 0.29	9.7	17.49
	4.65	0.36 0.35	0.35 0.34	2.8	19.11
	4.02* 3.85*	0.44* 0.46*	0.41* 0.45*	6.8* 2.2*	22.10* 23.08*
0.378	7.11	0.22 0.22	0.18 0.18	18.2	16.69
	6.68	0.24 0.24	0.20 0.20	20.0	17.77
	6.23	0.25 0.25	0.22 0.22	12.0	19.05
	5.71	0.32 0.32	0.31 0.31	3.1	20.79
	4.95* 4.86*	0.39* 0.39*	0.36* 0.37*	7.7* 5.1*	23.98* 24.42*
0.468	7.62	0.27 0.27	0.24 0.25	7.4	19.29
	7.16	0.28 0.29	0.25 0.26	10.3	20.52
	6.61	0.31 0.31	0.27 0.27	12.9	22.23
	6.20	0.33 0.33	0.31 0.31	6.1	23.70
	5.44* 5.21*	0.40* 0.42*	0.38* 0.38*	5.0* 9.5*	27.01* 28.21*
0.568	8.44	0.34 0.33	0.31 0.31	8.8	21.13
	8.01	0.34 0.34	0.32 0.32	5.9	22.27
	7.47	0.35 0.35	0.33 0.33	5.7	23.88
	7.09	0.35 0.35	0.34 0.34	2.9	25.16
	6.53* 6.17*	0.36* 0.42*	0.34* 0.38*	5.6* 9.5*	27.31* 28.91*

Table 7.29. Pore pressure measurements obtained under oscillatory flow (sand size, 215 μm; 10% mud). The values marked with an asterisk were obtained during the threshold of sediment motion.

stroke (m)	wave period (s)	pressure 1 σ (cm)	pressure 2 σ (cm)	pressure attenuation (%)	$U_{o(max)}$ (cm/s)
0.283	5.99	0.20 0.20	0.17 0.17	15.0	14.84
	5.49	0.27 0.27	0.26 0.27	0	16.19
	5.04	0.31 0.31	0.27 0.25	16.1	17.63
	4.55	0.36 0.36	0.32 0.32	11.1	19.53
	4.04* 3.86*	0.44* 0.46*	0.41* 0.44*	6.8* 4.3*	22.00* 23.02*
0.378	6.88	0.23 0.23	0.19 0.19	17.4	17.25
	6.40	0.24 0.24	0.21 0.21	12.5	18.55
	6.03	0.25 0.25	0.24 0.24	4.0	19.68
	5.56	0.36 0.36	0.35 0.35	2.8	21.35
	5.00* 4.88*	0.38* 0.39*	0.37* 0.38*	2.6* 2.6*	23.74* 24.32*
0.468	7.80	0.27 0.27	0.24 0.24	11.1	18.84
	7.35	0.28 0.28	0.25 0.25	10.7	19.99
	6.80	0.31 0.31	0.27 0.27	12.9	21.61
	6.35	0.32 0.32	0.28 0.28	12.5	23.14
	6.03* 5.90*	0.33* 0.34*	0.31* 0.34*	6.1* 0*	24.37* 24.91*
0.568	8.41	0.34 0.34	0.31 0.31	8.8	21.21
	7.94	0.34 0.34	0.31 0.31	8.8	22.46
	7.21	0.35 0.35	0.33 0.32	5.7	24.74
	6.97	0.35 0.35	0.34 0.34	2.9	25.59
	6.52* 6.12*	0.36* 0.43*	0.34* 0.38*	5.6* 11.6*	27.35* 29.14*

Table 7.30. Pore pressure measurements obtained under oscillatory flow (sand size, 215 μm; 20% mud). The values marked with an asterisk were obtained during the threshold of sediment motion.

stroke (m)	wave period (s)	pressure 1 σ (cm)	pressure 2 σ (cm)	pressure attenuation (%)	$U_{o(max)}$ (cm/s)
0.283	6.04	0.20 0.20	0.17 0.18	10.0	14.71
	5.54	0.27 0.27	0.27 0.26	0	16.04
	5.13	0.31 0.31	0.30 0.29	3.2	17.32
	4.59	0.36 0.36	0.31 0.31	13.9	19.36
	3.94* 3.70*	0.45* 0.47*	0.35* 0.37*	22.2* 21.3*	22.55* 24.02*
0.378	6.52	0.24 0.23	0.21 0.20	12.5	18.20
	6.07	0.25 0.25	0.25 0.25	0	19.55
	5.60	0.36 0.36	0.35 0.35	2.8	21.20
	5.09	0.38 0.38	0.27 0.27	28.9	23.32
	4.56* 4.35*	0.41* 0.43*	0.32* 0.31*	22.0* 27.9*	26.03* 27.29*
0.468	7.83	0.28 0.28	0.24 0.24	14.3	18.77
	7.26	0.30 0.30	0.25 0.25	16.7	20.24
	6.78	0.31 0.31	0.25 0.27	16.1	21.67
	6.28	0.33 0.32	0.28 0.26	18.2	23.40
	5.68* 5.60*	0.36* 0.37*	0.29* 0.30*	19.4* 18.9*	25.87* 26.24*
0.568	8.41	0.34 0.34	0.31 0.31	8.8	21.21
	7.86	0.34 0.34	0.29 0.31	13.3	22.69
	7.35	0.35 0.35	0.32 0.32	8.6	24.27
	6.94	0.37 0.37	0.33 0.33	10.8	25.70
	6.52* 6.17*	0.37* 0.46*	0.32* 0.37*	13.5* 19.6*	27.35* 28.91*

Table 7.31. Pore pressure measurements obtained under oscillatory flow (sand size, 215 μm; 30% mud). The values marked with an asterisk were obtained during the threshold of sediment motion.

stroke (m)	wave period (s)	pressure 1 σ (cm)	pressure 2 σ (cm)	pressure attenuation (%)	$U_{o(max)}$ (cm/s)
0.283	5.55	0.27 0.27	0.26 0.26	3.7	16.01
	5.12	0.31 0.31	0.27 0.26	12.9	17.36
	4.60	0.36 0.36	0.28 0.28	22.2	19.32
	4.10	0.44 0.44	0.32 0.32	27.3	21.67
	3.59* 3.17*	0.48* 0.50*	0.21* 0.21*	56.3* 58.0*	24.75* 28.03*
0.378	5.42	0.36 0.35	0.28 0.30	19.4	21.90
	5.02	0.38 0.38	0.30 0.30	21.0	23.64
	4.57	0.41 0.41	0.29 0.28	29.3	25.97
	4.07	0.45 0.44	0.29 0.29	35.6	29.16
	3.53* 3.49*	0.51* 0.51*	0.20* 0.19*	60.8* 62.7*	33.62* 34.01*
0.468	7.26	0.30 0.30	0.25 0.24	16.7	20.24
	6.74	0.31 0.30	0.20 0.20	35.5	21.80
	6.20	0.33 0.33	0.20 0.20	39.4	23.70
	5.62	0.37 0.37	0.22 0.22	40.5	26.15
	4.78* 4.67*	0.53* 0.52*	0.25* 0.24*	52.8* 53.8*	30.74* 31.47*
0.568	7.88	0.34 0.34	0.31 0.31	8.8	22.63
	7.49	0.35 0.34	0.32 0.31	8.6	23.81
	6.99	0.37 0.37	0.29 0.29	21.6	25.52
	6.44	0.37 0.37	0.28 0.28	24.3	27.69
	6.03* 5.73*	0.45* 0.58*	0.32* 0.30*	28.9* 48.3*	29.58* 31.13*

Table 7.32. Pore pressure measurements obtained under oscillatory flow (sand size, 215 μm; 40% mud). The values marked with an asterisk were obtained during the threshold of sediment motion.

stroke (m)	wave period (s)	pressure 1 σ (cm)	pressure 2 σ (cm)	pressure attenuation (%)	$U_{\infty(max)}$ (cm/s)
0.283	5.22	0.31 0.31	0.29 0.28	6.5	17.02
	4.69	0.36 0.36	0.25 0.25	30.6	18.95
	4.24	0.38 0.36	0.24 0.24	35.1	20.96
	3.85	0.47 0.46	0.20 0.20	57.4	23.08
	3.38* 3.23*	0.49* 0.49*	0.17* 0.17*	65.3* 65.3*	26.29* 27.51*
0.378	6.00	0.25 0.25	0.22 0.22	12.0	19.78
	5.48	0.36 0.35	0.30 0.30	16.7	21.66
	4.99	0.38 0.38	0.29 0.28	23.7	23.79
	4.53	0.41 0.41	0.27 0.27	34.1	26.20
	3.89* 3.74*	0.47* 0.48*	0.22* 0.20*	53.2* 58.3*	30.51* 31.74*
0.468	7.02	0.31 0.31	0.26 0.26	16.1	20.93
	6.55	0.32 0.32	0.22 0.22	31.3	22.44
	6.08	0.33 0.33	0.20 0.20	39.4	24.17
	5.54	0.39 0.39	0.26 0.26	33.3	26.53
	4.95* 4.73*	0.44* 0.52*	0.26* 0.21*	40.9* 59.6*	29.69* 31.07*
0.568	8.20	0.33 0.33	0.31 0.31	6.1	21.75
	7.68	0.33 0.33	0.30 0.31	6.1	23.22
	7.17	0.35 0.35	0.30 0.29	14.3	24.87
	6.70	0.37 0.37	0.27 0.27	27.0	26.62
	5.84* 5.56*	0.52* 0.63*	0.31* 0.31*	40.4* 50.8*	30.54* 32.08*

Table 7.33. Pore pressure measurements obtained under oscillatory flow (sand size, 215 μm; 50% mud). The values marked with an asterisk were obtained during the threshold of sediment motion.

CHAPTER 8

RESULTS AND DISCUSSION: COMBINED FLOW

8. RESULTS AND DISCUSSION: COMBINED FLOW

8.1. EROSION TESTS

8.1.1. Threshold Determinations

A statistical analysis of the results produced under combined flow conditions (Set 4 of experiments) has demonstrated that the error associated with them is around ±6%. This value is higher than the error associated with the data derived under unidirectional and oscillatory flow conditions. The subjectivity of the threshold criterion used (Section 4.4.3), together with the complex interaction between the unidirectional current and oscillatory flow component, may explain the above discrepancy.

During the hydraulic tests, the resonance phenomena in the flume (cf. oscillatory flow experiments) did not appear to be significant, since the steady current component dampened considerably the standing wave development within the system. Hence, the threshold of movement (observed to occur when the oscillating plate was moving in a direction opposite to that of the steady current and at various phases after the mid-stroke position) could not be affected by this activity.

8.1.2. Data Collected

The experimental procedure for this particular series of tests has been described in Chapter 4. Briefly, the oscillating plate was set in motion with a particular period (T) and stroke ($2A_o$), in such a way that the required wave flow component was established as rapidly as possible. The unidirectional component was increased from zero, at a rate which allowed the threshold

conditions to be established within 2 min. If these conditions were not reached within this time period, the experiment was set up again and repeated.

The results from each of these tests are presented in Tables 8.1 to 8.14. In consideration of the information derived, it should be borne in mind that the oscillatory (wave) conditions [$U_{o(max)}$] were held constant, whilst the unidirectional current (U_c) was varied until a critical combination of $U_{o(max)}$ and U_c was achieved. In addition, the use of 6 s and 10 s wave periods and the restricted particle size of the samples did not allow the development of significant inertial forces on the individual sediment particles.

A statistical analysis of the results obtained under 10 s periods shows an increase in the average experimental scatter, with the near-bed wave amplitude (wave stroke); this implies a greater difficulty in the prediction of ereosion threshold. The scatter may be caused by a more complicated current-wave interaction, as wave conditions are intensified.

Figures 8.1 and 8.2 show the variation in critical (threshold) speed of the current component, with varying mud contents, for wave periods of 10 s and 6 s and strokes of 0.283 m, 0.378 m, 0.468 m and 0.568 m. The main trends observed from these graphs are described below.

(i) There is an incremental increase in the threshold speed of the current component with mud content (and, subsequently, with clay), for all the wave conditions established. This increase may be expressed in terms of a linear function, characterised by a high degree of significance. This relationship is shown in Figs 8.3 and 8.4, where the lines of best fit through the data relate

to correlation coefficients (r^2) ranging from 0.94-0.98 and 0.91-0.99, for admixtures associated with the 152.5 μm and 215 μm sands, respectively.
(ii) The mixtures associated with the larger sand fraction size require lower steady current speeds, in order to be entrained within the water movement.
(iii) A large increase in wave stroke (expressed as a near-bed wave amplitude) causes a relatively small reduction in the threshold speed of the steady current component of the combined flow regime (see also Figs 8.3 and 8.4).

It has been described (see above) that the results shown on Figs 8.3 and 8.4 demonstrate a positive and significant linear relationships between the threshold current speed and mud content, under various wave conditions. An additional observation concerns the parallel trend which characterises the regression lines. Considering that periods related to these lines (10 s and 6 s) are representative of locally wind-generated waves and oceanic swell, such relationships might be used to interpret the variation in erosion threshold conditions for combinations of near-bed unidirectional currents and 'typical' waves. Such an analysis could be undertaken for different wave heights and relative to different water depths; they should be particularly applicable to investigations in shallow water coastal environments, characterised by fine- to very fine-grained sediment deposits.

Tables 8.15 to 8.21 list combined flow critical erosion bed shear stresses, for each one of the samples tested, under specific wave conditions. Shear stresses, for use in the present study, have been calculated for the waves and currents separately; this is according to the procedures described for the unidirectional and

oscillatory flow threshold experiments (Sections 5.2.4 and 5.3.1). The relevant variables required in this procedure are listed in Tables 8.15 to 8.21. Wave friction factors have been extracted from the friction factor diagram of Kamphuis (1975) and, where necessary, the value of ν has been taken as 10^{-6} m^2 s^{-1} (since water temperature during the tests ranged from 18-20°C). The derived current- and wave-induced shear stresses have been added, to produce a combined critical bed shear stress; this assumes linear interaction between the superimposed waves and the unidirectional currents.

It is worth noting that higher threshold stresses are derived for the shorter period waves (see Tables 8.15 and 8.19; 8.16 and 8.20; 8.17 and 8.21). This observation can be explained by assuming that the combined flow threshold shear stress is 'different', under waves of different period i.e. that the forces on the bed particles act in different directions and are, consequently, of a different magnitude.

Graphical representation of the 'combined' shear stress, in relation to various mud contents, is shown in Figs 8.5 and 8.6. A positive and significant relationship between the two variables is apparent. The high correlation coefficients (r^2) of the regression lines, shown on the Figs 8.5 and 8.6, justify the assumption of a linear interaction between the processes for the calculation of bed shear stress. Further, it may be seen that, for a fixed wave period and particular sediment bed, an increase of the stroke of the wave component (i.e. an intensification of the wave conditions) causes generally an increase in the combined critical shear stress. This pattern implies that the wave boundary layer plays a protective role in the erosion of the bed caused by the superimposition of the unidirectional current. However,

in some cases, the above trend is reversed. For, example, in Figs 8.5a and 8.6a, the combined shear stresses under a wave stroke of 0.468 m are lower than those derived under a stroke of 0.378 m. This difference indicates that erosion of the bed does not depend only upon the magnitude of wave-induced shear stress, but is affected also by the particular way in which waves and currents interact.

Figures 8.7 to 8.10 present the critical velocity combinations used for all the samples tested, for both the wave periods used (6 s and 10 s). Each data point represents the mean of 4 experimental observations. Data lying on y and x axes represent threshold values obtained from purely unidirectional and oscillatory flow experiments, respectively. Likewise, the threshold value presented for oscillatory flow corresponds to the mean of the 4 (wave) strokes used in the investigation. An immediate impression created by the results is that there is a distinct difference in the required threshold value for the current component (U_c), between the 6 s and 10 s period experiments. For the 10 s periods and maximum wave-induced velocities [$U_{o(max)}$] > 9 cm s^{-1} and 6 s periods with $U_{o(max)}$ > 15 cm s^{-1}, the value of U_c decreases with increasing $U_{o(max)}$. Each of the data sets show that this decrease becomes increasingly greater for a 10 s wave period, than for a 6 s wave period. However, wave periods of 10 s and 6 s associated with maximum wave velocities < 9 cm s^{-1} and < 15 cm s^{-1} respectively produce usually threshold current speeds which are equal or greater than those derived under purely unidirectional flows (Figs 8.7, 8.8a, 8.9, 8.10a and 8.10b). This observation indicates that, for the less intense wave conditions, the protection afforded by the wave boundary layer to the sediment (see above) against the erosion competence of the superimposed steady current is at a maximum.

Therefore, in order for the bed to be eroded, the unidirectional current must have enough energy (at least initially) to disrupt the protective wave boundary layer and then to overcome the physical surface strength of the sediment bed. This limitation results in a threshold current speed which is similar to, or higher than, that required under purely steady flow conditions.

8.1.3. Discussion

The results presented in Figs 8.7 to 8.10 demonstrate that data for the 10 s period experiments plot, generally, lower than the 6 s period experiments. Wave periods of 6 s appear to require higher current speeds than the 10 s periods, in order that critical conditions be reached (especially when $U_{o(max)}$ is > 9 cm s^{-1}). Hence, the different shape of the curves between the 6 s and 10 s wave period combined flow experiments requires explanation.

The flow regimes which describe the wave boundary layers, for each of the combined flow experiments in the absence of a unidirectional current, are described in Section 5.4. The mechanisms which have caused the erosion of the samples in the experiments are likely to have been turbulent. This interpretation may be explained by the fact that all of the laminar wave boundary layers (which, in themselves, did not cause the sediment to erode) must have had turbulent unidirectional currents superimposed upon them. In addition, the observation of bursts of sediment motion, at the moment of threshold, supports this concept. The way in which the sediment particles could have been moved, in response to turbulent flow forces, is described below.

Lighthill (1954) and Sleath (1984) have argued that if

the frequency of wave oscillation is high enough, then the wave boundary layer is very thin compared with that of the steady flow; hence, waves and currents will be unaffected by each other. Within the context of the present investigation, it is possible, therefore, that the laminar wave boundary layer for the 6 s periods was thinner (therefore, more stable) than that associated with the 10 s periods. In this sense, the layer would have acted in a similar manner to the viscous sub-layer in smooth turbulent flow. Thus, the unidirectional current speed needed to be increased to a critical value which was higher than that related to 10 s period waves, in order to generate more turbulent energy and to break down the thinner and more stable 6 s wave boundary layer. Threshold of sediment movement would be generated through the evolution of turbulent eddies.

The unidirectional flow rate required to induce turbulence within the wave boundary layer depends upon the stability of the wave boundary layer i.e. how close it is to becoming transitional; this, in turn, depends upon the values of A_o/D and the wave Reynolds number (RE). Examples of studies which support this concept have been described by Ramaprian & Tu (1980). These investigators observed, that within the transitional range of the combined flows, flow in the wave-dominated region close to the bed was laminar during the accelerating part of the wave cycle; after this, the flow became fully turbulent. Hino *et al.* (1983) have explained this observation by the fact that the RE increases from zero at the start of the acceleration phase of the cycle, to a maximum when the velocity is at a maximum; this is at the start of the decelerating phase of the wave cycle. When RE is at maximum, therefore, the wave boundary layer is more unstable than at any other time (phase) during the cycle. Thus, the presence of the turbulent unidirectional

current serves to increase the flow instability.

Considering the explanation proposed by Ramaprian & Tu (1980) together with the fact that threshold of movement (under the action of turbulent flow forces) in combined flow experiments happened at various phases during the decelerating stage of the plate motion (when the direction of plate movement was opposite to that of the steady current), it may be assumed that the combined flow regime at threshold may be characterised as 'transitional'. The boundary layer will collapse into the transitional regime at a 'critical phase' in the wave cycle, when the instantaneous values of A_o/D and RE and the turbulent unidirectional current reach conditions such that the wave boundary layer cannot remain laminar. Turbulent eddies evolve, some of which travel towards the bed. If there are still viscous forces close to the bed then, in order to move the sediment, these turbulent eddies must have enough energy to penetrate this viscous-dominated region. If the eddies do not have enough energy and for the experiments in the present study, the unidirectional flow is increased; hence, the eddies have more kinetic energy when turbulence breaks out in the subsequent (wave) cycle. It is likely that the 'critical phase' (see above) will vary for different sediments and prevailing wave/current conditions. Indeed, the threshold of motion was observed to commence at various phases in the decelerating wave cycle of the combined flow regime.

The findings of the present investigation, that greater unidirectional flows are needed to satisfy threshold conditions under short (6 s) wave periods than for longer periods (10 s), are supported by the results of previous studies. Such results were concerned with the laboratory determination of the threshold of sands, under combined flow conditions, and are described below.

Hammond & Collins (1979) carried out such experiments on very well sorted mono-sized sands; these were supplied from an industrial source, ranging in size from fine- to coarse-grained sediments. Latterly, Tomlinson (1993) performed tests on artificial sediment beds of five mean grain sizes; these consisted of a mixture of seven 1/2 phi sieve sand fractions. Finally, Voulgaris *et al.* (1995) have described experiments undertaken on natural sands obtained from sandbanks in the Swansea Bay area of the Bristol Channel (UK). These sands consisted of subrounded particles, with a wide range of sorting. The threshold experiments associated with the above studies were all performed in an identical manner, using equipment similar to that used in the present study. Critical conditions of motion, in each case, were described quantitatively by reference to the Yalin (1972) criterion. In the studies of Hammond & Collins (op. cit.) and Tomlinson (op. cit.) only particles of a size which was equivalent to the median grain size of the sample were counted, when identifying threshold. However, during the Voulgaris *et al.* (op. cit.) experiments, no distinction could be made between sand grains of different sizes. Hence, the total number of grains (of any size) in motion were counted when identifying threshold conditions. Finally, the oscillatory flow regimes associated with the various investigations were characterised by laminar and transitional flow conditions; the unidirectional flow regimes by smooth turbulent and transitional flow conditions.

The results of the studies have been presented as a series of critical velocity combination plots, to illustrate the changing interactions of oscillatory and unidirectional currents in response to wave period modifications. A summary of the critical velocity combinations for the Voulgaris *et al.* (op. cit.) data,

with waves of 5 s and 15 s period, is shown as Fig. 8.11. In this representation short period waves appear to require stronger steady currents than the long period waves; this suggests that the same material is eroded more easily under the action of longer period waves. Further, a steep linear variation in the threshold combination below $U_{o(max)}$=24 cm s^{-1} is indicated, with a rapid reduction in the unidirectional component at higher wave velocities. For comparison, the results of the present study show that a rapid reduction in the unidirectional current component may occur when $U_{o(max)}$ is in excess of 15-20 cm s^{-1} (Figs 8.7 to 8.10). Finally, for $U_{o(max)}$ values up to the oscillatory threshold in the Voulgaris *et al.* (1995) data, current speeds which are a large proportion of unidirectional threshold are required. This trend has been identified also for the present data (especially for the 6 s wave periods) (see Figs 8.7 to 8.10).

Similar diagrams for the Hammond & Collins (1979) and Tomlinson (1993) data sets are displayed as Figs 8.12 and 8.13, respectively.

The data shown in Figs 8.11 and 8.12, for 5 s period waves, all display curves consisting of two distinct sections; these may be an indication of comparable fluid dynamic processes occurring in each of the cases. In contrast, the higher wave period (15 s) results, on Figs 8.11 and 8.12, appear to represent different processes. Here, there is less change in the gradient at high $U_{o(max)}$ values. The critical combination expressions representing these longer wave periods lie closer to straight lines between the individual flow 'end members' than the two-limbed curves of the shorter wave periods. This relationship would appear to suggest that the unidirectional flow has a greater influence on grain

threshold, under such conditions. In general, there is less difference between the results of the 5 s and 10 s period wave experiments in the Tomlinson (1993) data (Fig. 8.13), than between the 5 s and 15 s results in the other data sets (Figs 8.11 and 8.12). In several of the plots shown in Fig. 8.13, there is not a clearly defined difference between the patterns of the 5 s and 10 s data. However, this observation is not in agreement with the results of the present investigation.

In conclusion, the consistency of the wave period effect can be explained only by assuming a different mechanism related to the superimposition of wave-induced flows and mean currents, at the various wave periods. The combined velocity plots obtained from the present and previous investigations suggest that a high unidirectional flow needs to be maintained to achieve threshold of movement in the shorter wave period experiments.

8.2. PORE PRESSURE MEASURES

Pore pressure measurements, referred to as Set B, were carried out at threshold. Such experiments were undertaken in an effort to examine the combined influence of clay content and hydrodynamic parameters on pore pressure behaviour.

Standard deviations of the pressure head transmitted into the bed (pres.1) and pore pressure (pres.2) are listed in Tables 8.1 to 8.14. In addition, the attenuation levels (%) of the transmitted pressure head have been calculated. The first impression gained from the data sets is that water pressure attenuations, due to the presence of the sediment, do not exist for the 10 s wave period experiments; this is even characteristic of sediment mixtures associated with the highest mud

contents. Further, for the 6 s wave periods, considerable pressure attenuation exists only when the mud content is in excess of 30% and the near-bed wave amplitude is in excess of 0.378 m (Figs 8.14 to 8.21).

Comparison of the attenuations of the transmitted (into the sediment bed) pressure heads, observed during purely oscillatory flow tests, with attenuations derived under combined flow conditions and provided that wave conditions (wave period and stroke) are similar, shows that the latter values are somehow higher than the former. This is outlined below.

(i) For waves of 6 s period and a stroke of 0.468 m, the pressure attenuation levels under oscillatory flow, for mixtures associated with the 152.5 μm sands and containing mud percentages of 40% and 50%, are of the order of 33% and 25%, respectively. Under combined flow, the corresponding values are 38% and 39%, respectively.

(ii) For similar wave conditions as described above, the pressure attenuations under oscillatory flow, for the 215 μm sand mixtures with mud contents of 40% and 50%, are of the order of 40% and 39%, respectively. Under combined flow the corresponding values are 48% and 47%, respectively.

The observations described above imply that the steady current component of the combined flow regime may act as an additional dampening of the pore (water) pressure amplitude; this results in higher attenuations of the pressure head, transmitted into the bed.

The results listed in Tables 8.1 to 8.14 are presented in Figs 8.22 and 8.23. The Figs represent the variation in pore pressure amplitude with mud content of the samples, under particular combined flow conditions. The reduction in pore pressure fluctuations (for the 6 s wave periods)

within the muddier mixtures, identified during the oscillatory flow tests (Set A and Set C), is also apparent; however, this is to a higher degree than for the oscillatory flow experiments. Furthermore, the dampening appears to have a positive relationship with the near-bed wave amplitude (wave stroke). Once again (cf. pore pressure results under oscillatory flow), the clay mineral content may be considered as the major reason for this pore pressure amplitude reduction. However, the interaction of unidirectional current component of the combined flow regime with pore water oscillation may well be responsible for a further decrease in the pore pressure amplitude.

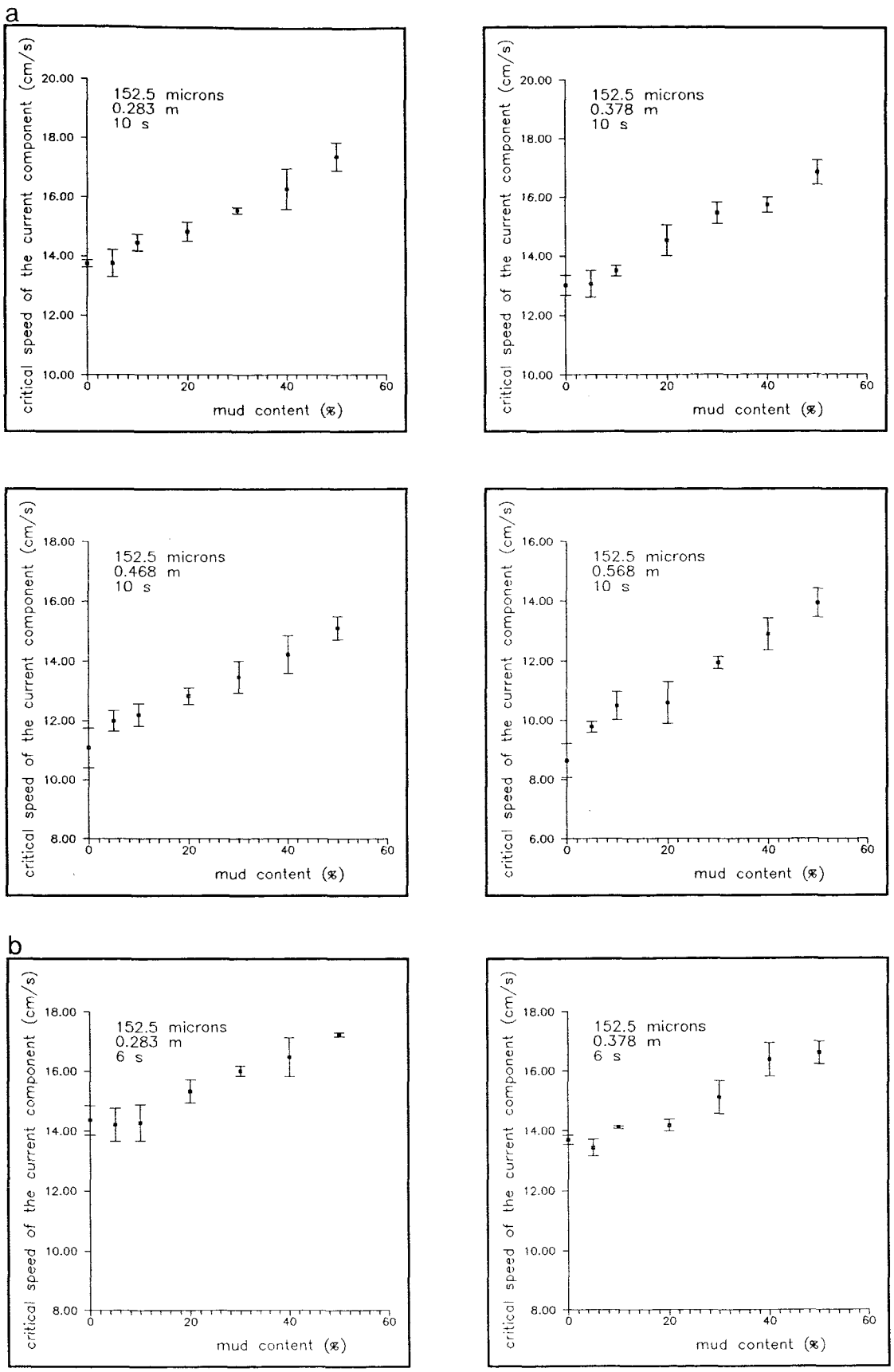

Fig. 8.1. Combined flow results associated with the 152.5 μm sand admixtures, for various wave strokes and periods of (a) 10 s and (b) 6 s (Key: The mean and the standard error of the mean are displayed).

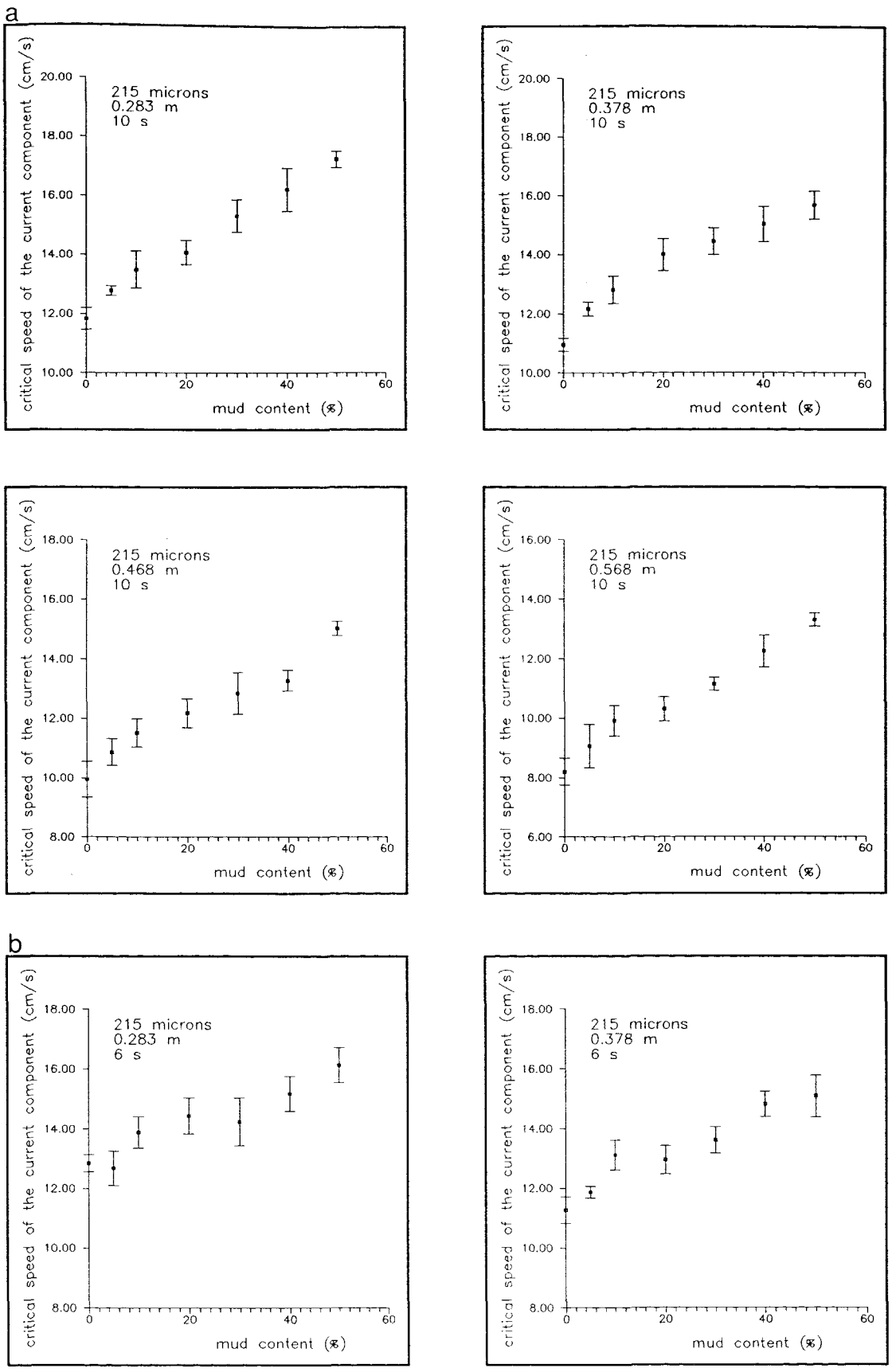

Fig. 8.2. Combined flow results associated with the 215 μm sand admixtures, for various wave strokes and periods of (a) 10 s and (b) 6 s (Key: The mean and the standard error of the mean are displayed).

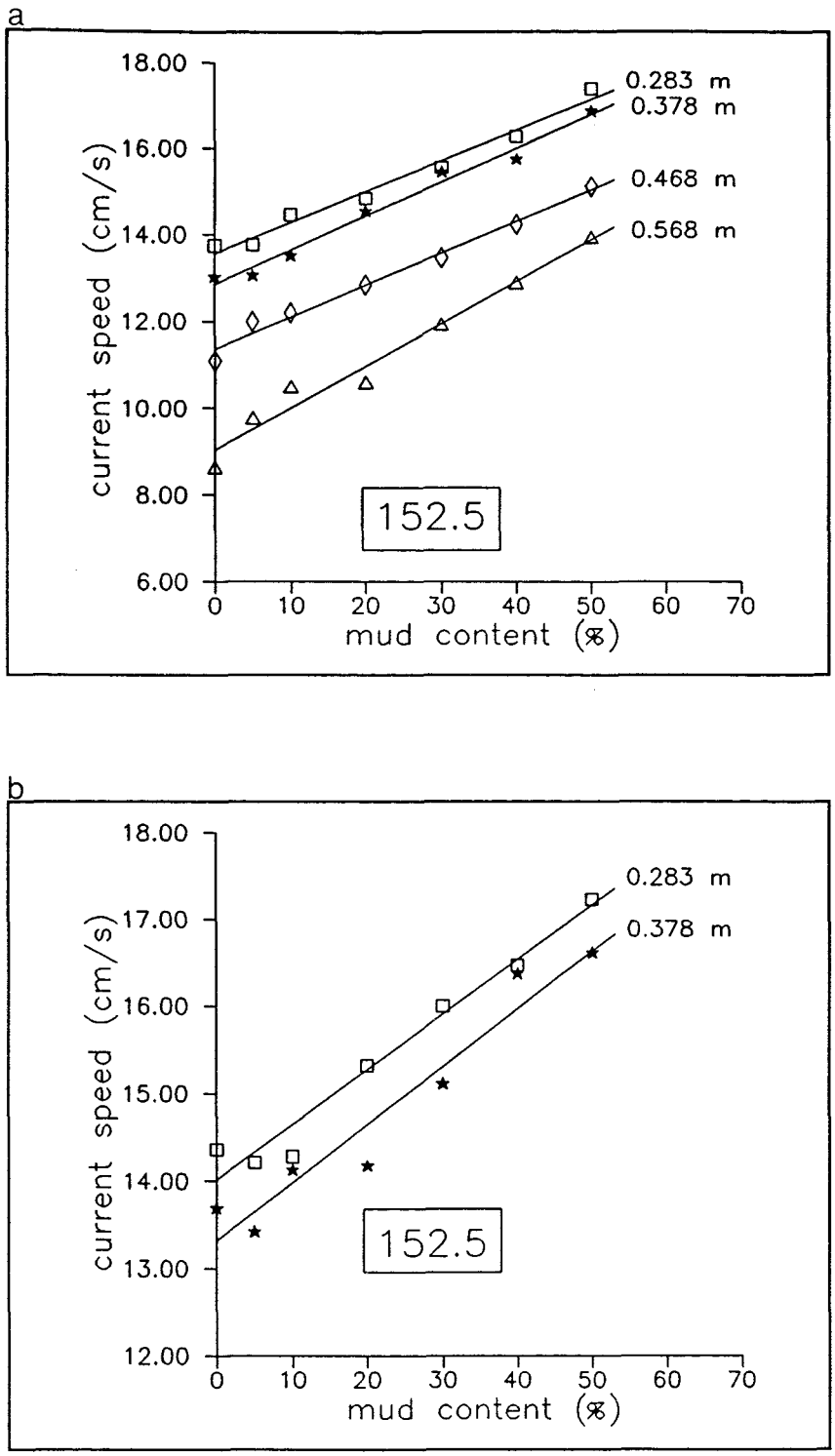

Fig. 8.3. Regression analysis for the mean threshold speeds of the current component related to the 152.5 μm sand admixtures, for near-bed wave amplitudes of 0.283 m, 0.378 m, 0.468 m and 0.568 m and periods of (a) 10 s and (b) 6 s.

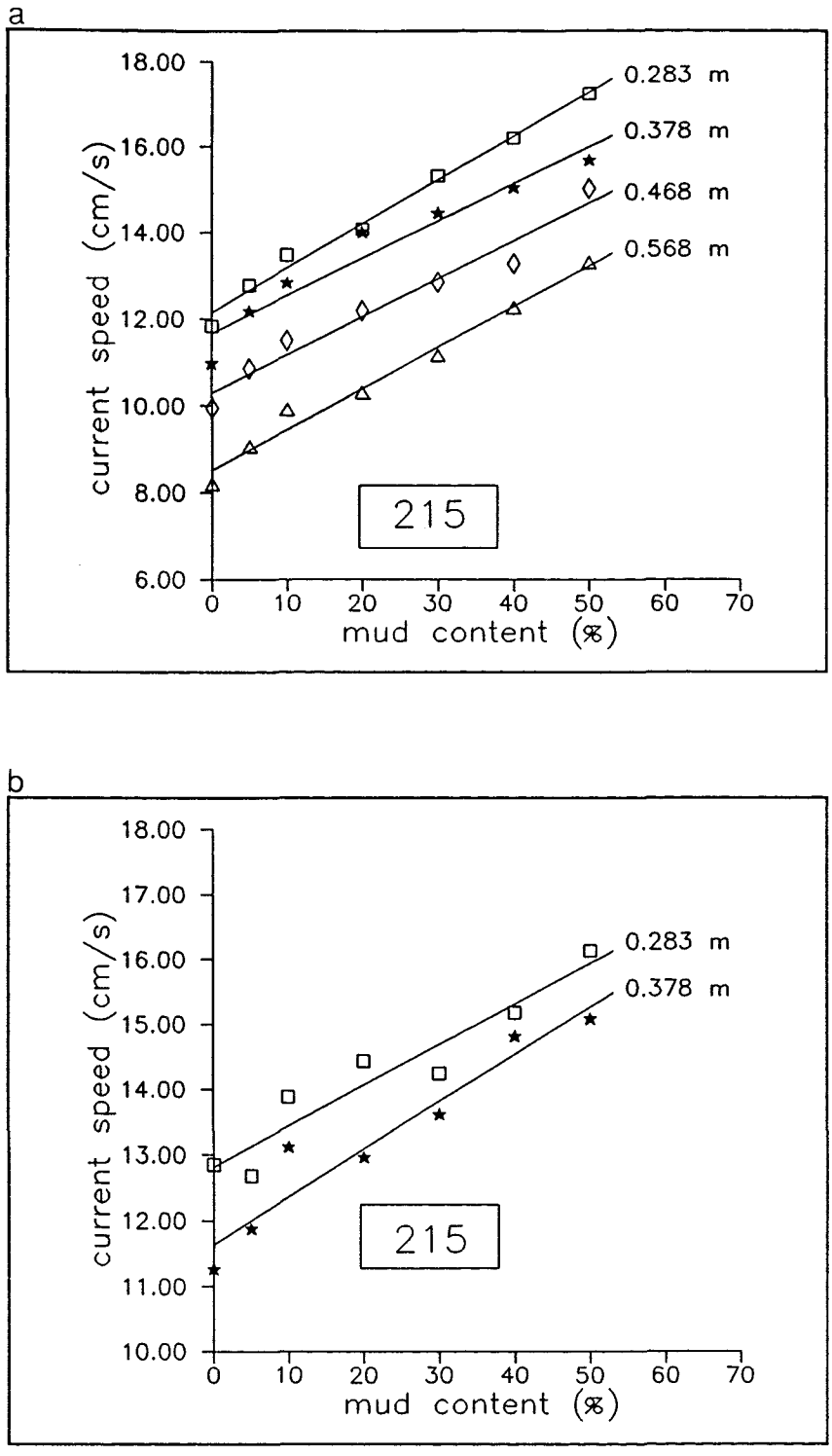

Fig. 8.4. Regression analysis for the mean threshold speeds of the current component related to the 215 μm sand admixtures, for near-bed wave amplitudes of 0.283 m, 0.378 m, 0.468 m and 0.568 m and periods of (a) 10 s and (b) 6 s.

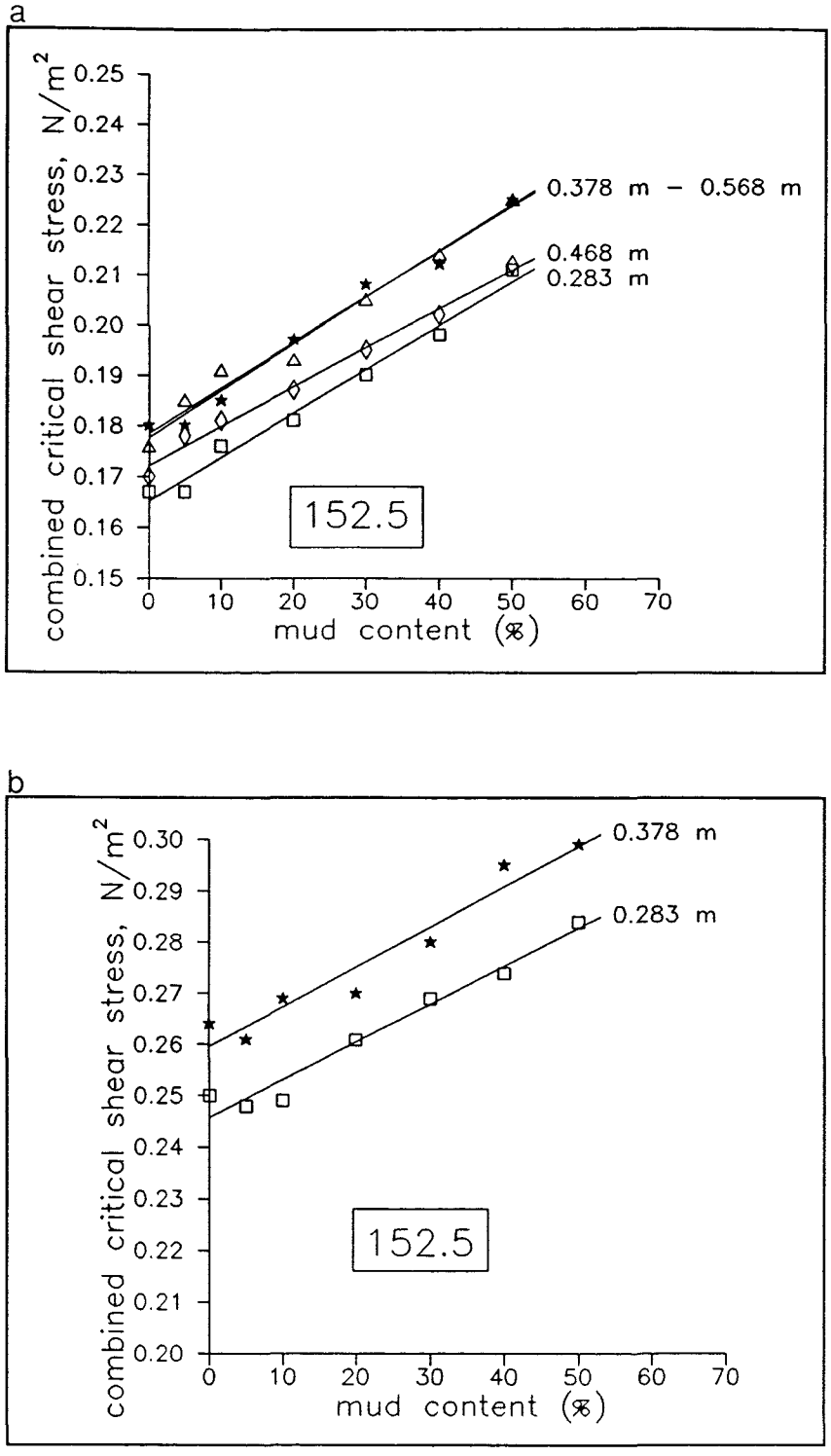

Fig. 8.5. Best-fit lines desribing the variation in combined critical bed shear stress with mud content, for mixtures associated with the 152.5 μm sands, under wave strokes of 0.283 m, 0.378 m, 0.468 m and 0.568 m and periods of (a) 10 s and (b) 6 s.

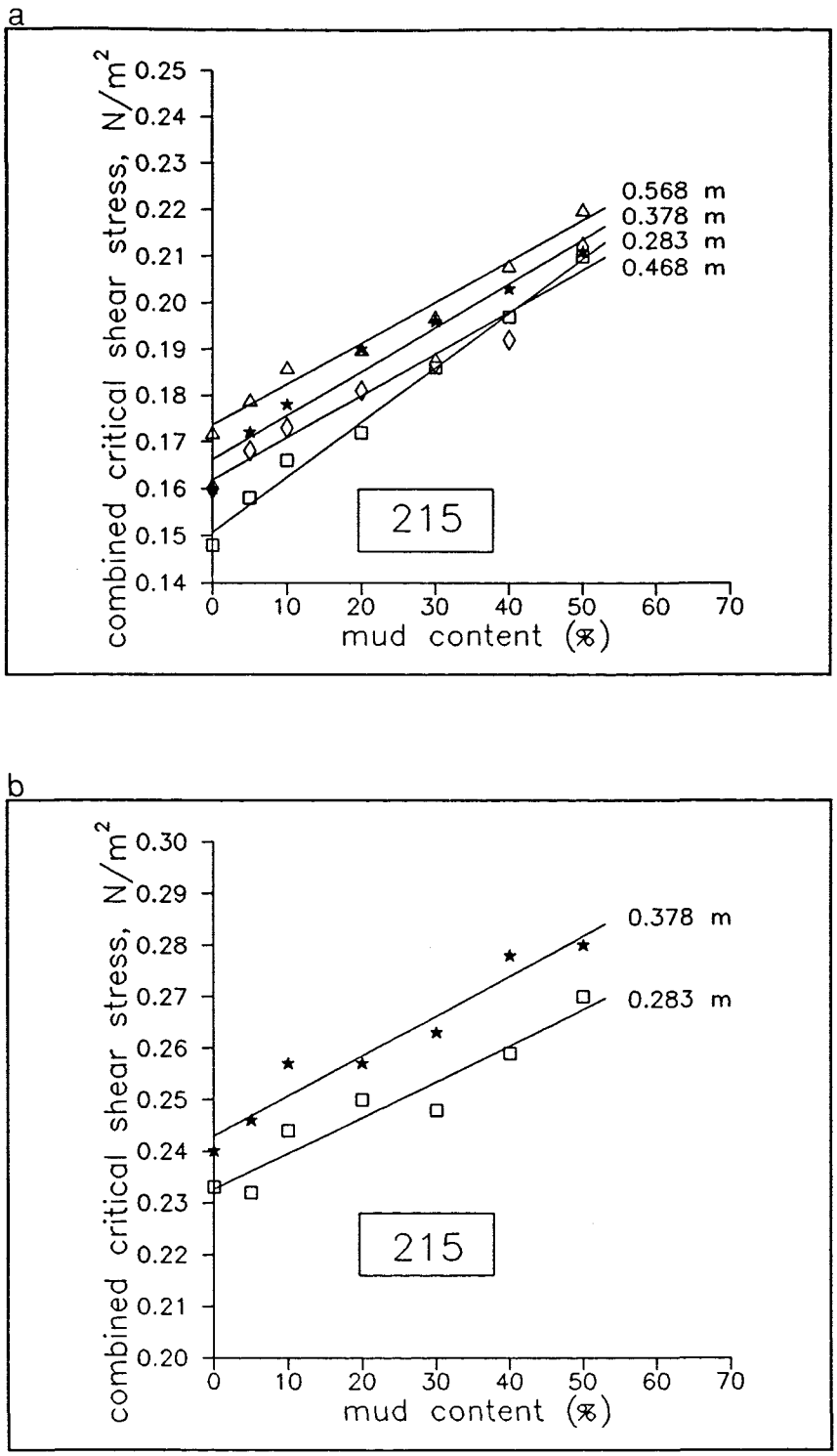

Fig. 8.6. Best-fit lines describing the variation in combined critical bed shear stress with mud content, for mixtures associated with the 215 μm sands, under wave strokes of 0.283 m, 0.378 m, 0.468 m and 0.568 m and periods of (a) 10 s and (b) 6 s.

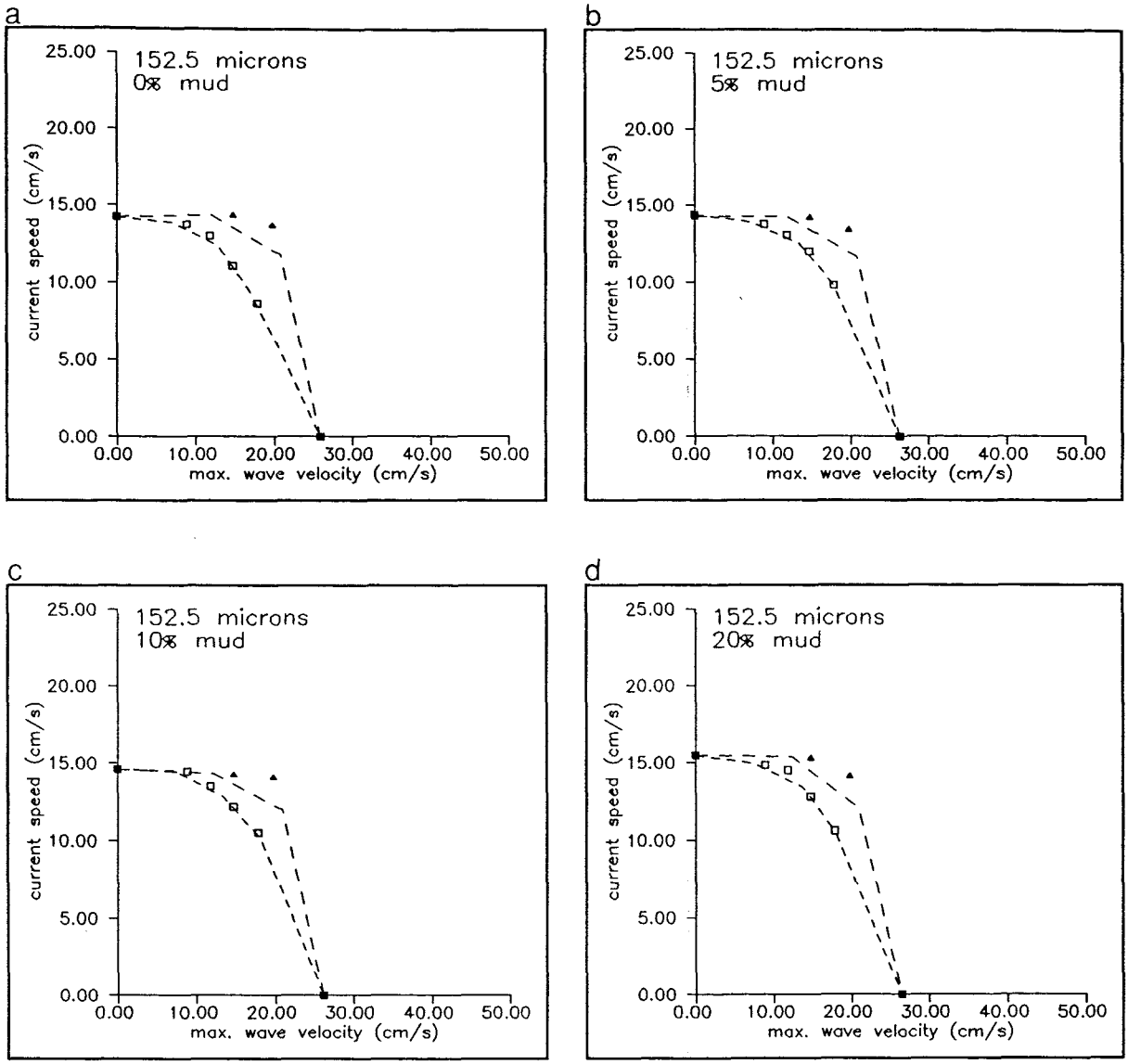

Fig. 8.7. Critical velocity combinations for the 152.5 μm sand admixtures containing 0%, 5%, 10% and 20% mud, respectively (Key: Large-stroke dashed line, 6 s period; small-stroke dashed line, 10 s period).

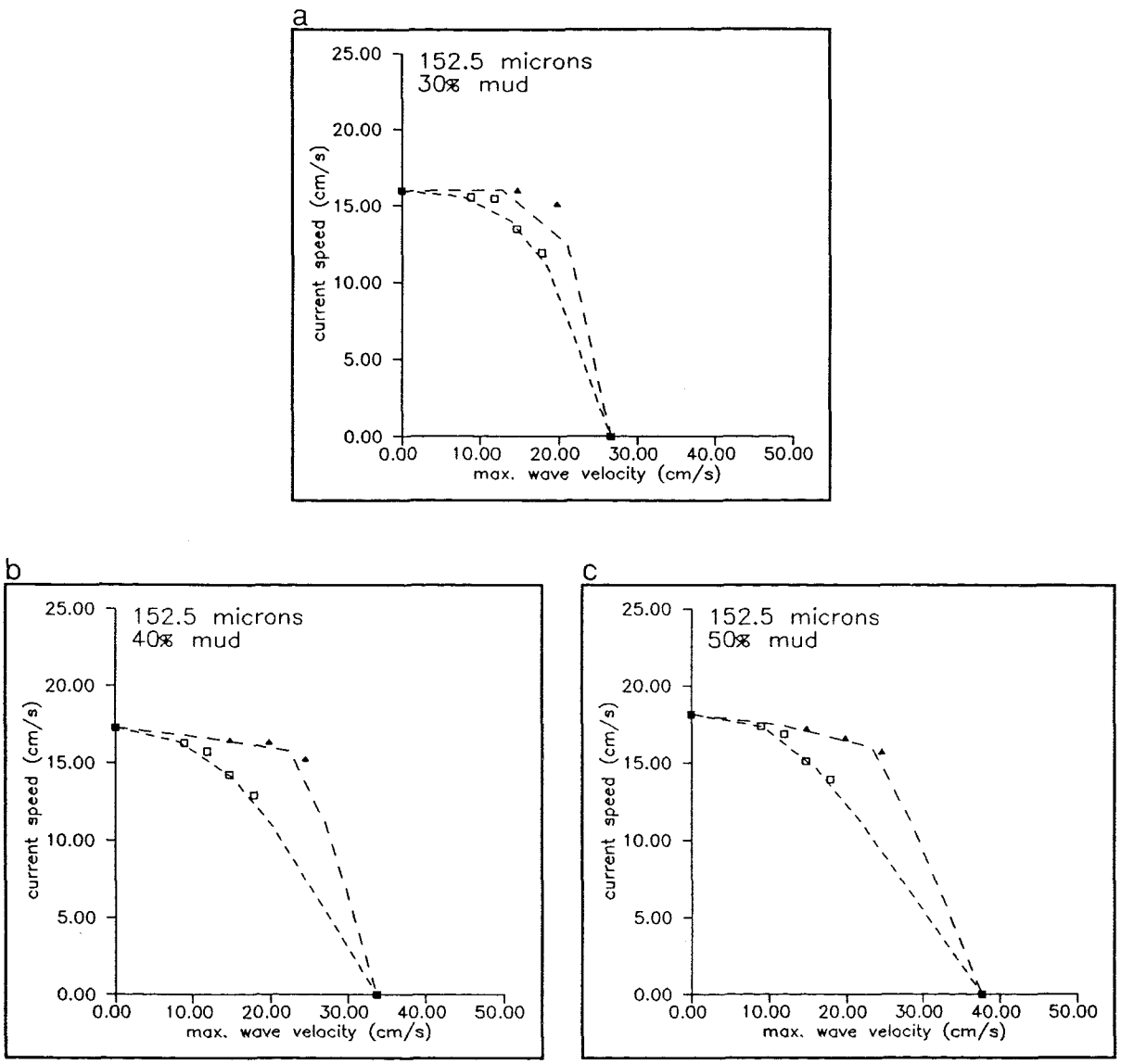

Fig. 8.8. Critical velocity combinations for the 152.5 μm sand admixtures containing 30%, 40% and 50% mud, respectively (Key: Large-stroke dashed line, 6 s period; small-stroke dashed line, 10 s period).

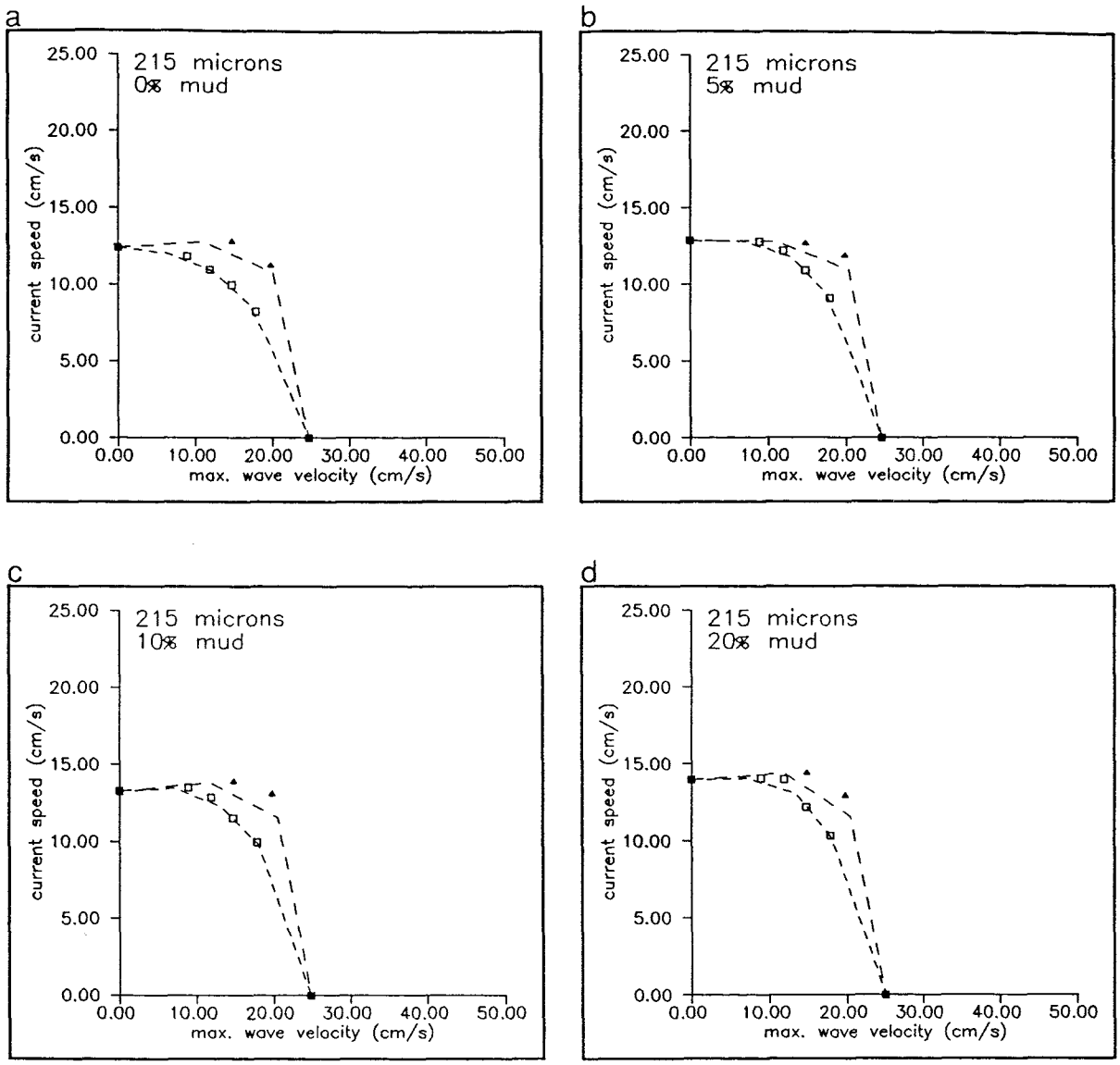

Fig. 8.9. Critical velocity combinations for the 215 μm sand admixtures containing 0%, 5%, 10% and 20% mud, respectively (Key: Large-stroke dashed line, 6 s period; small-stroke dashed line, 10 s period).

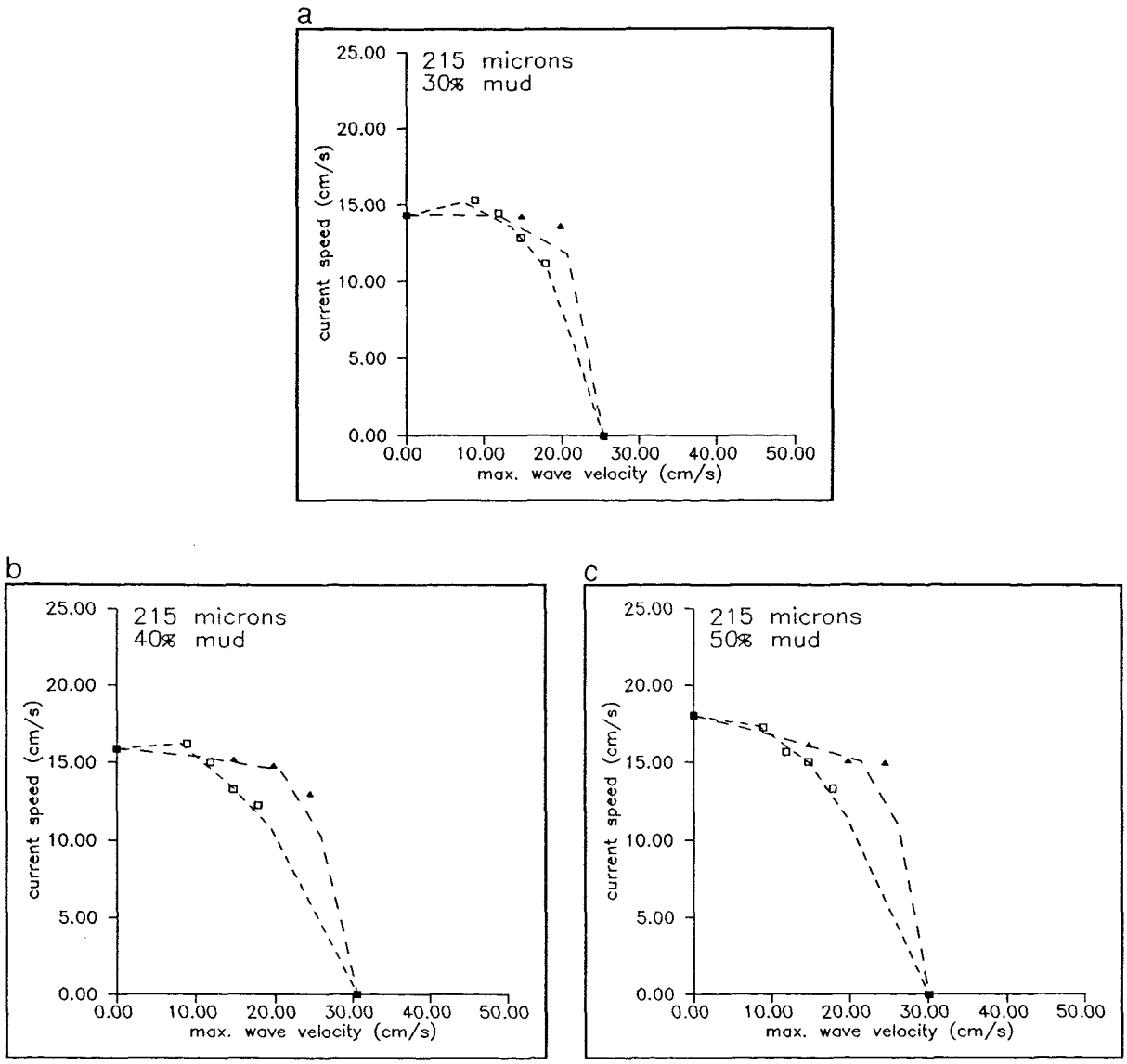

Fig. 8.10. Critical velocity combinations for the 215 μm sand admixtures containing 30%, 40% and 50% mud, respectively (Key: Large-stroke dashed line, 6 s period; small-stroke dashed line, 10 s period).

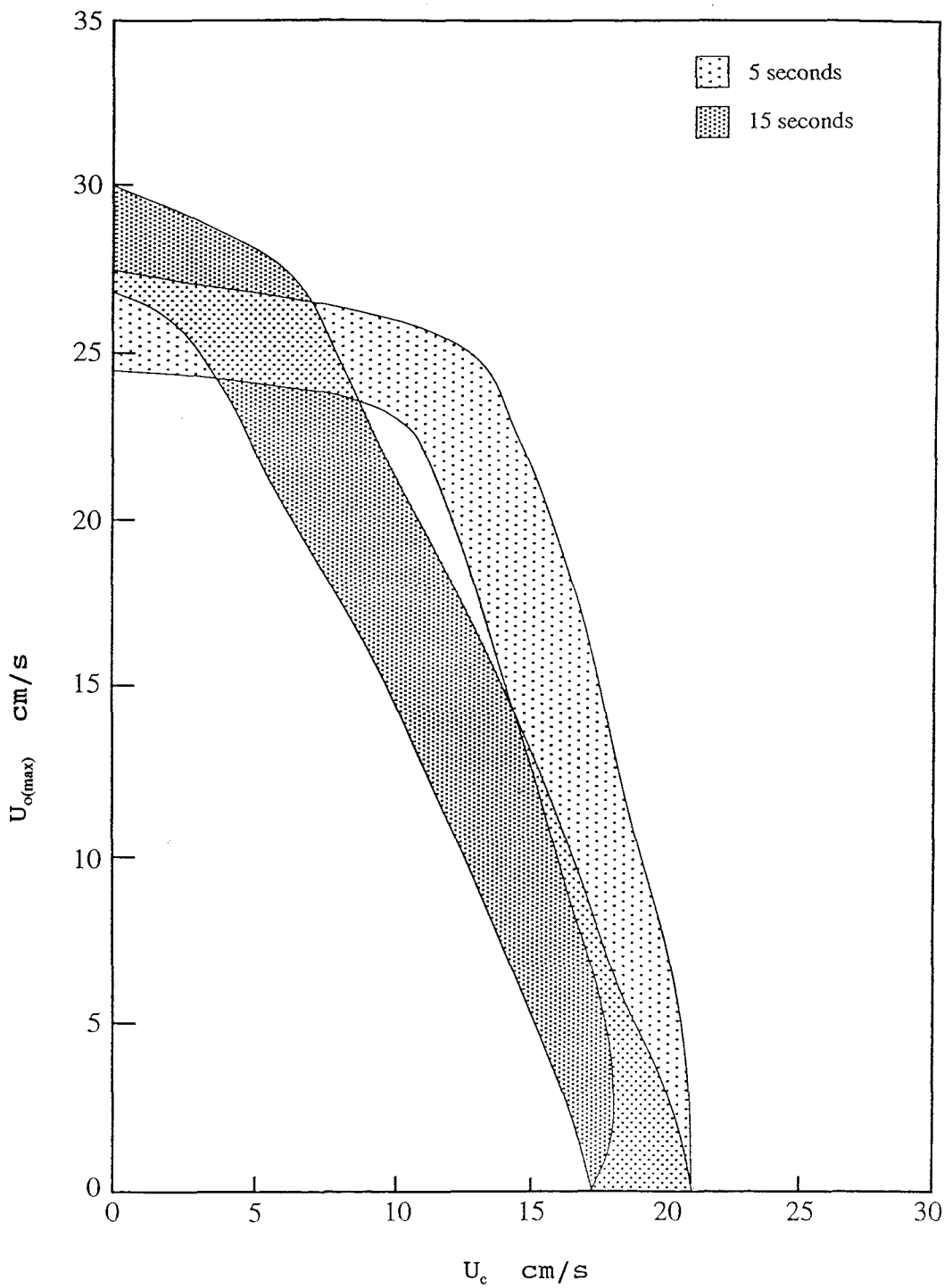

Fig. 8.11. Velocity combinations at threshold, under combined flow, for the Voulgaris *et al.* (1995) data sets. Each of the envelopes presented enclose 8 curves, derived from separate samples within the mean grain size range of 320-400 μm.

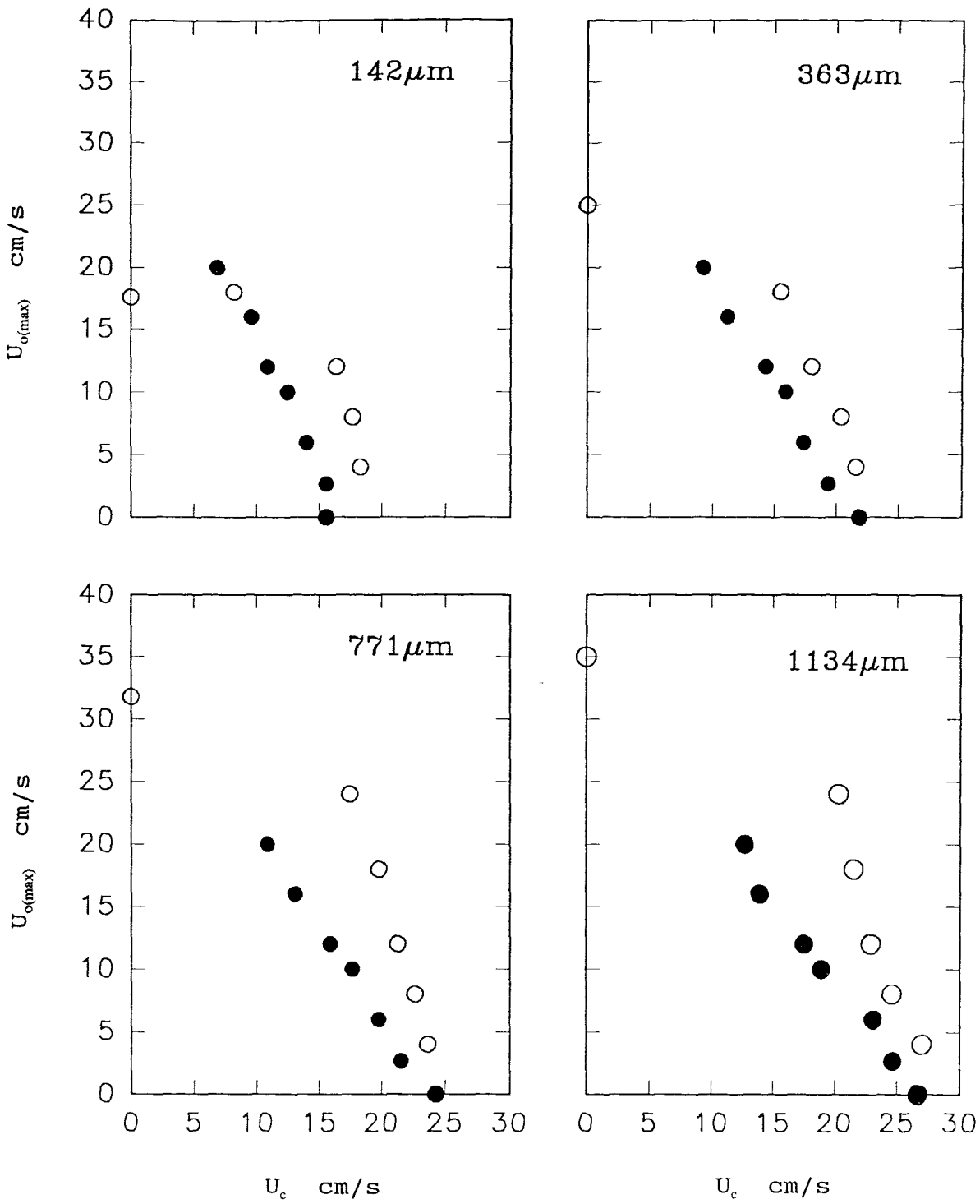

Fig. 8.12. Velocity combinations at threshold, under combined flow, for each grain size in the Hammond & Collins (1979) data set. Hollow circles represent 5 s period waves, filled circles represent 15 s period waves.

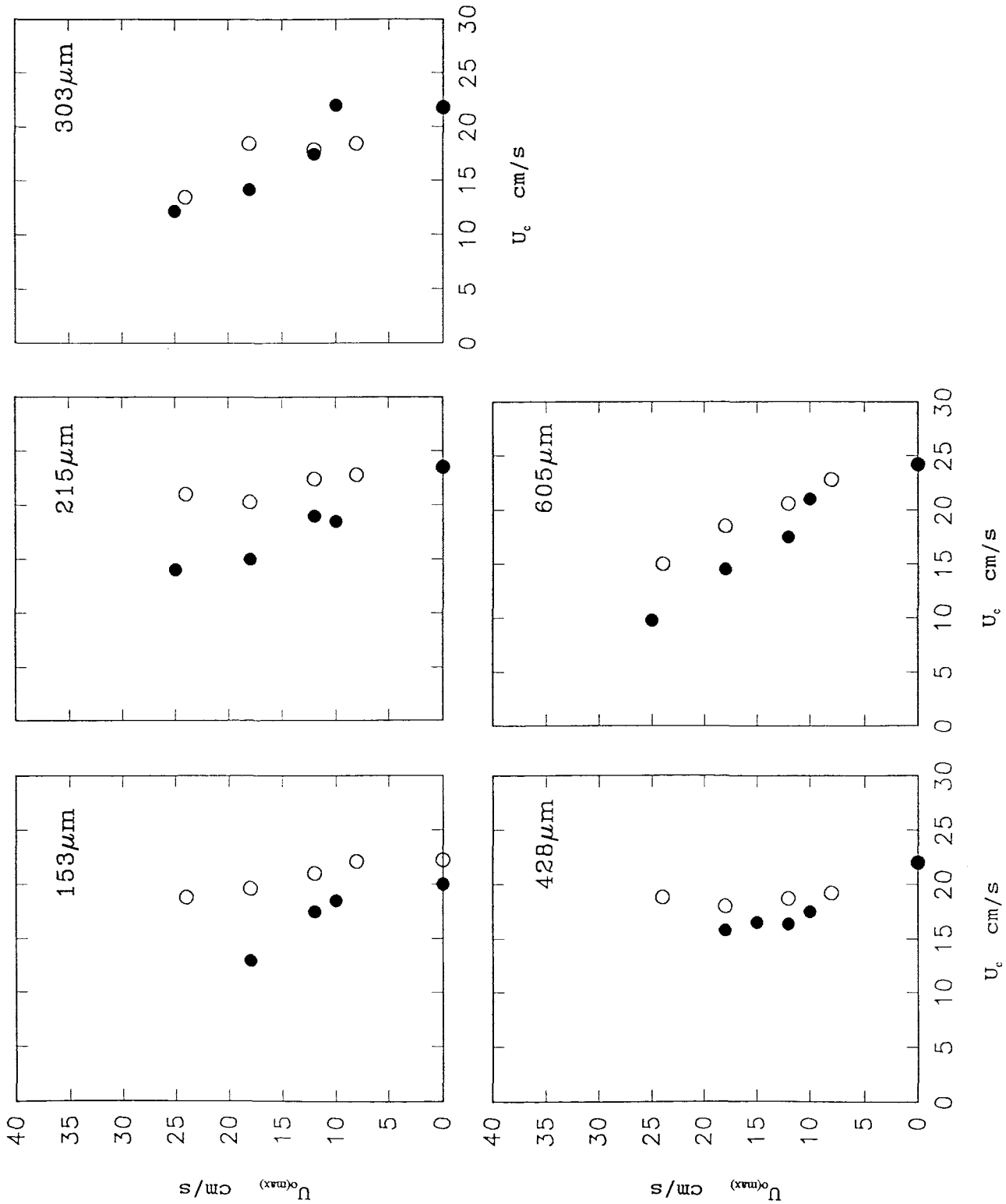

Fig. 8.13. Velocity combinations at threshold, under combined flow, for each grain size in the Tomlinson (1993) data set. Hollow circles represent 5 s period waves, filled circles represent 10 s period waves.

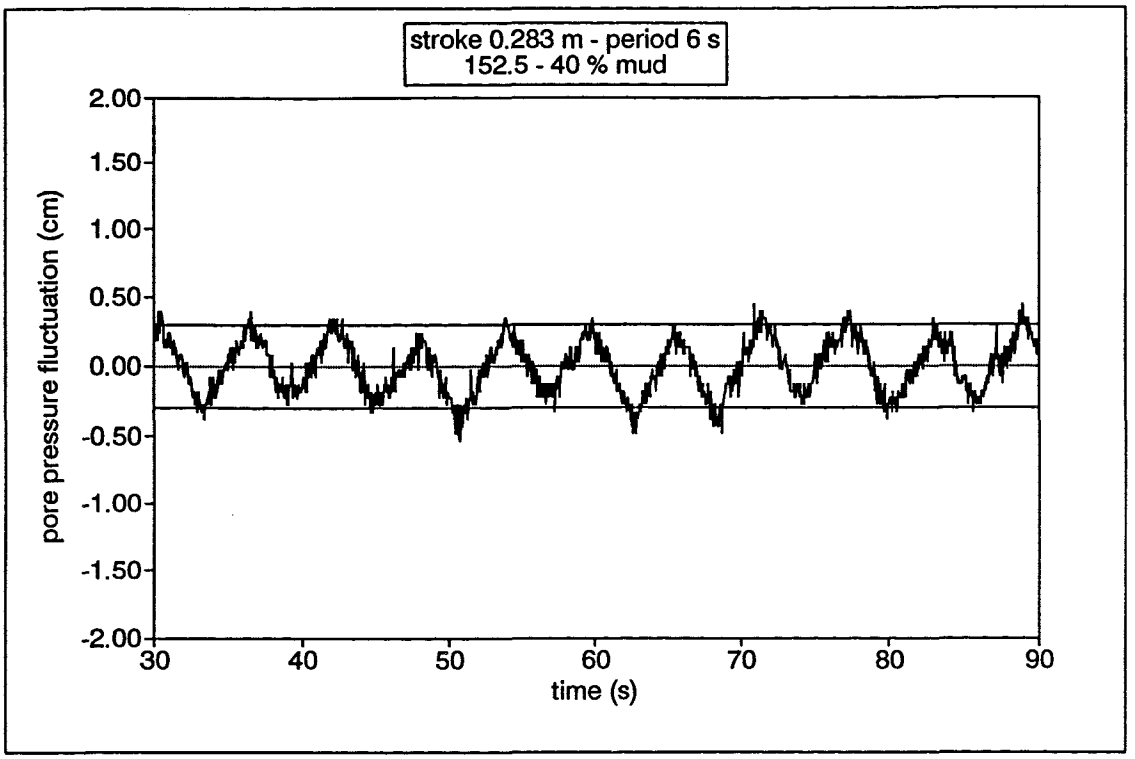

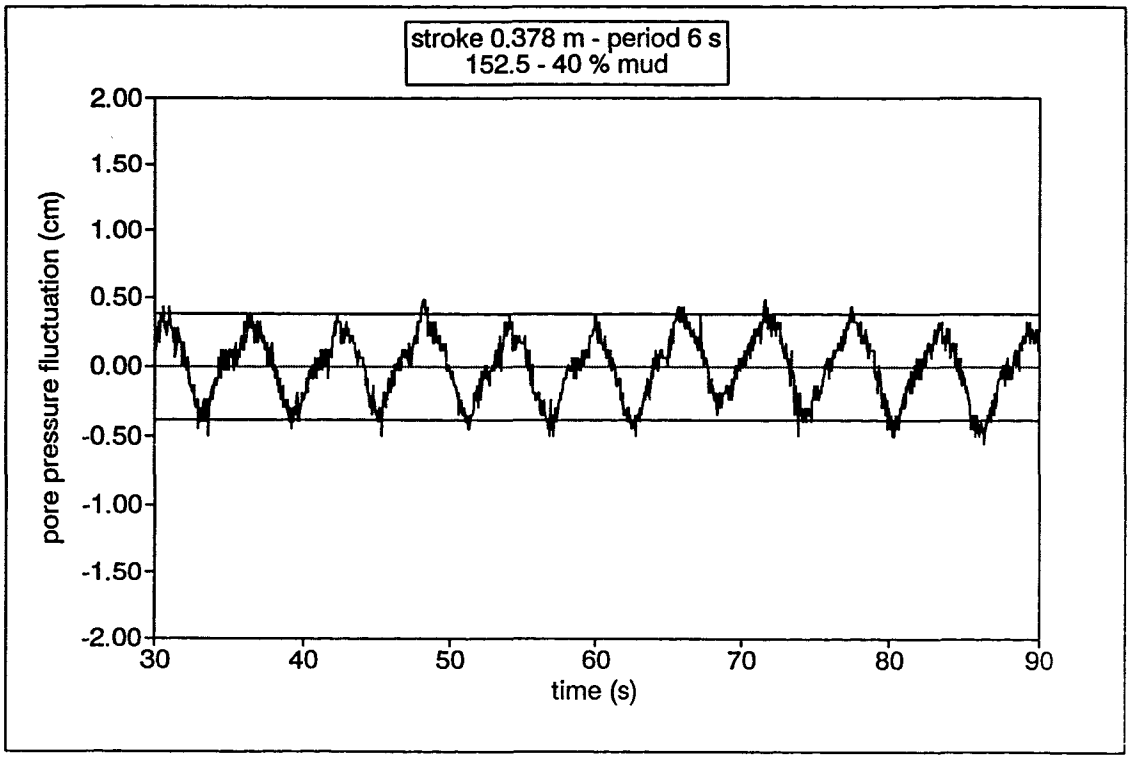

Fig. 8.14. Pore pressure records, under combined flow, with reference to the amplitude of the pressure head (solid lines) transmitted into the sediment bed containing the 152.5 μm sand fraction and 40% of mud. Data relate to wave strokes of 0.283 m and 0.378 m and a period of 6 s.

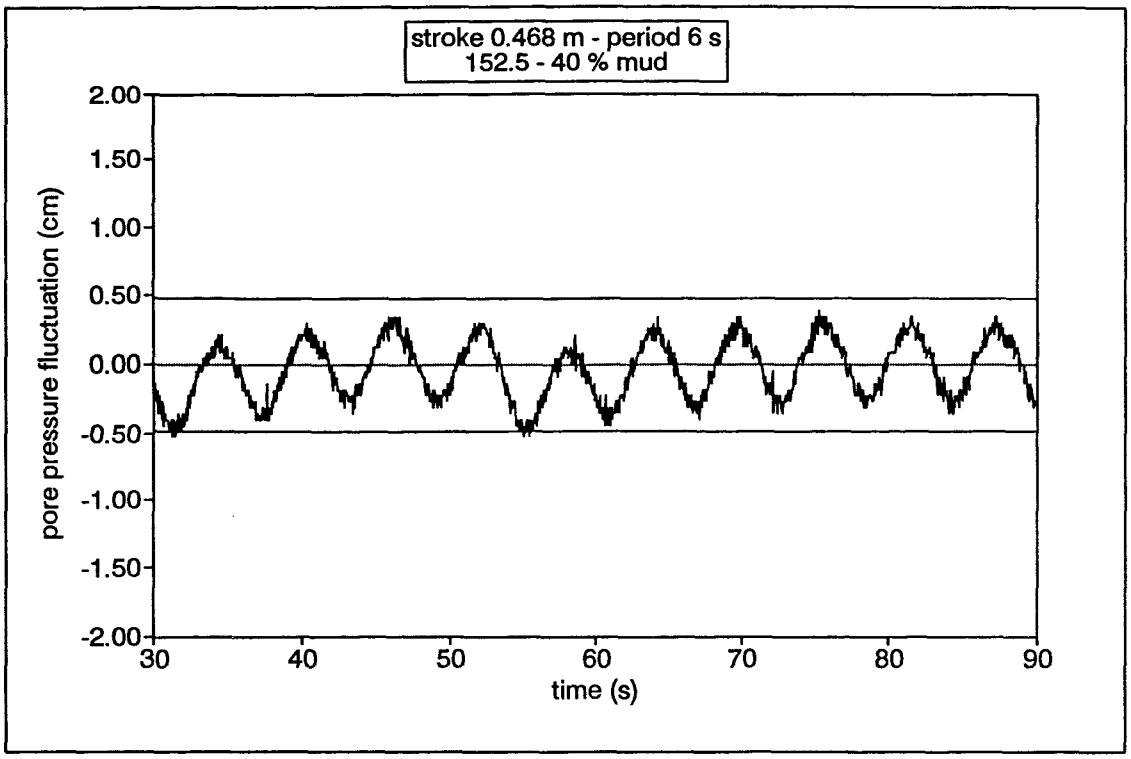

Fig. 8.15. Pore pressure record, under combined flow, with reference to the amplitude of the pressure head (solid lines) transmitted into the sediment bed containing the 152.5 μm sand fraction and 40% of mud. Data relate to a wave stroke of 0.468 m and period of 6 s.

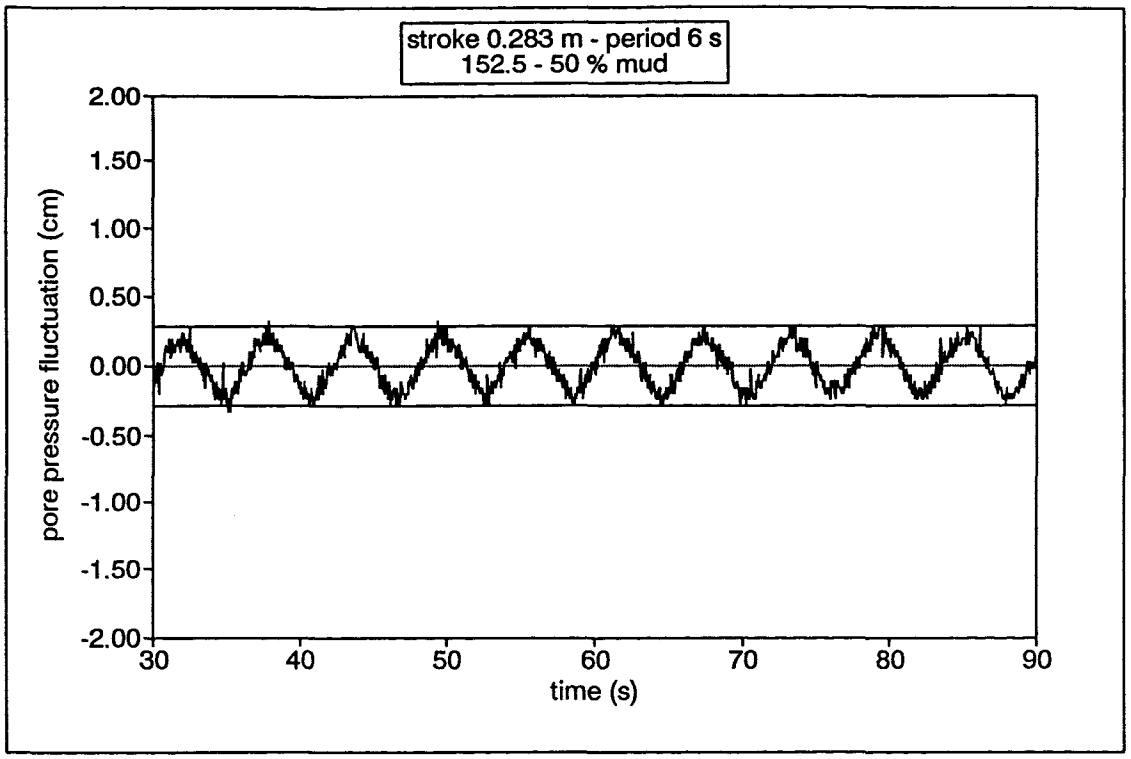

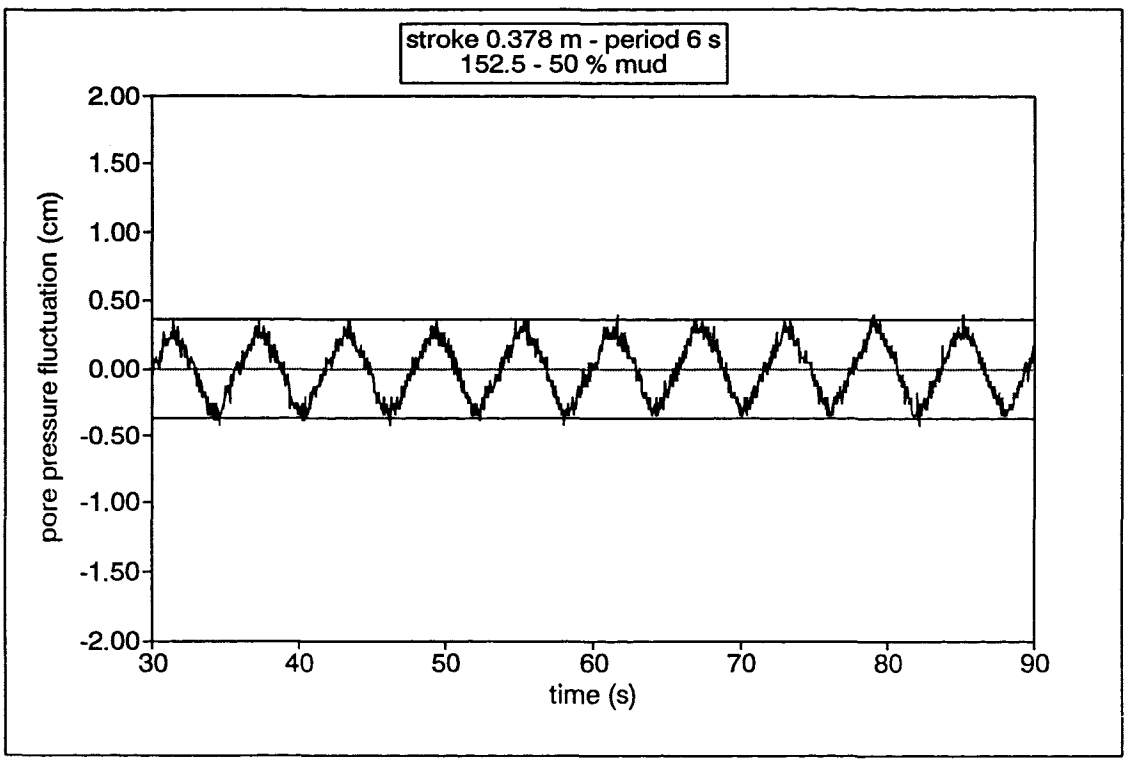

Fig. 8.16. Pore pressure records, under combined flow, with reference to the amplitude of the pressure head (solid lines) transmitted into the sediment bed containing the 152.5 μm sand fraction and 50% of mud. Data relate to wave strokes of 0.283 m and 0.378 m and a period of 6 s.

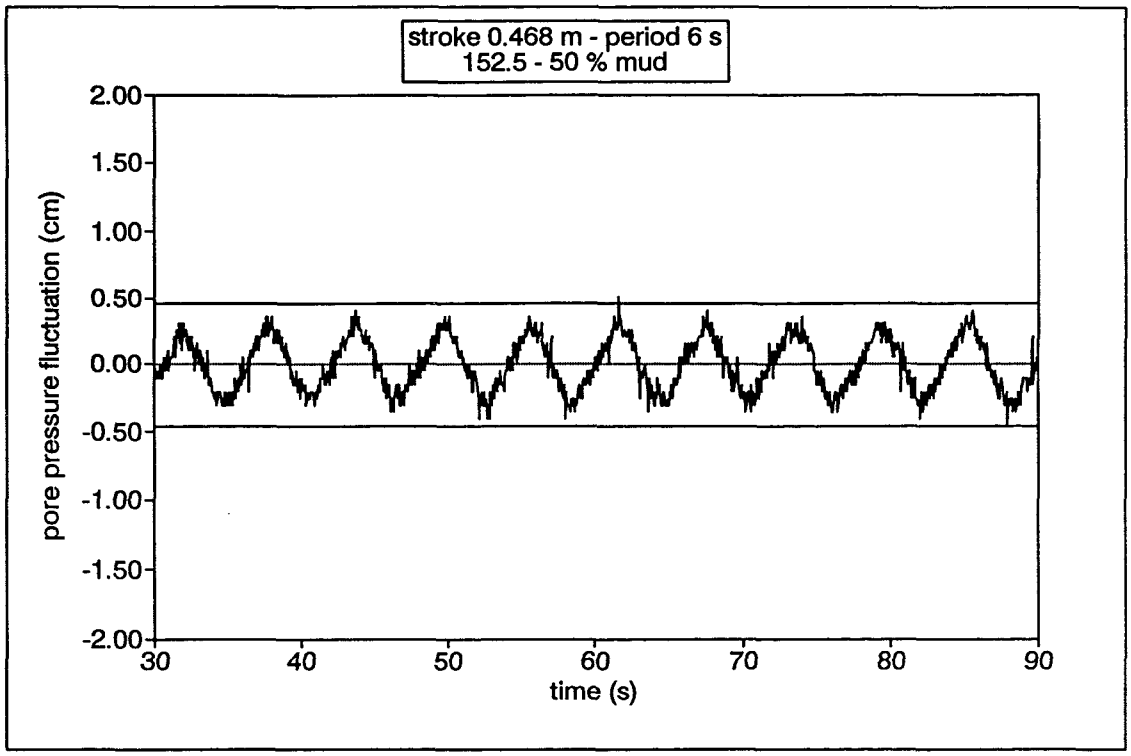

Fig. 8.17. Pore pressure record, under combined flow, with reference to the amplitude of the pressure head (solid lines) transmitted into the sediment bed containing the 152.5 μm sand fraction and 50% of mud. Data relate to a wave stroke of 0.468 m and period of 6 s.

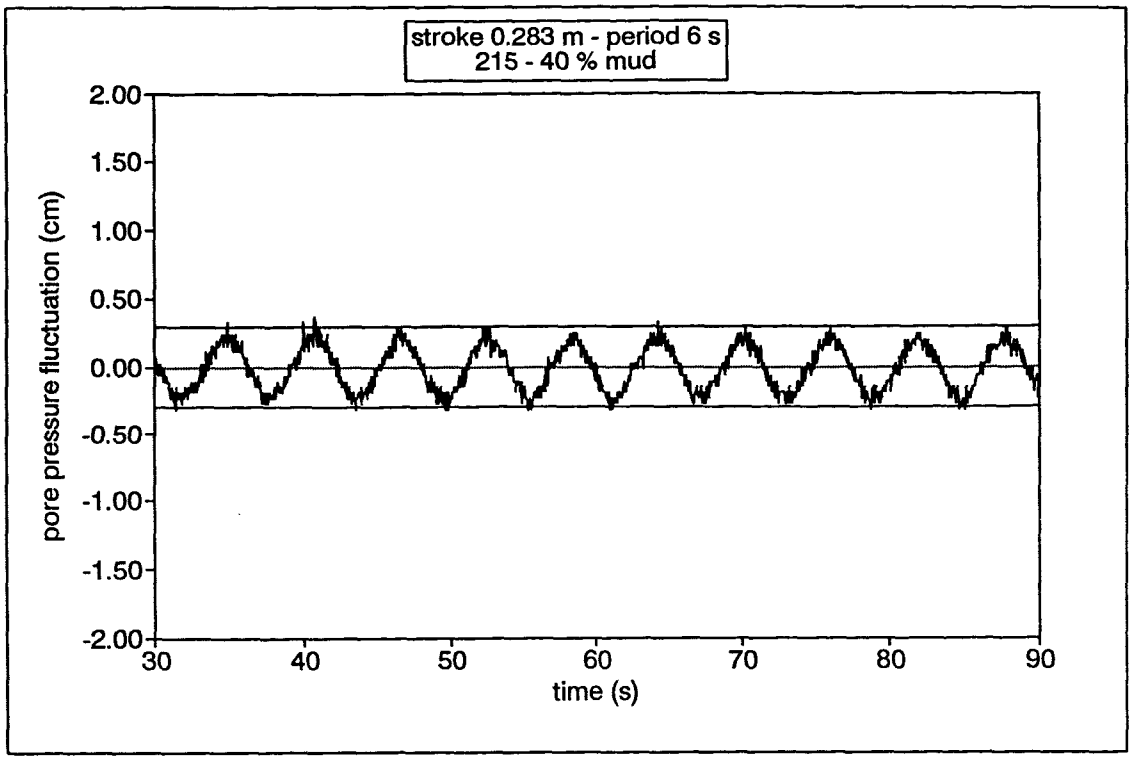

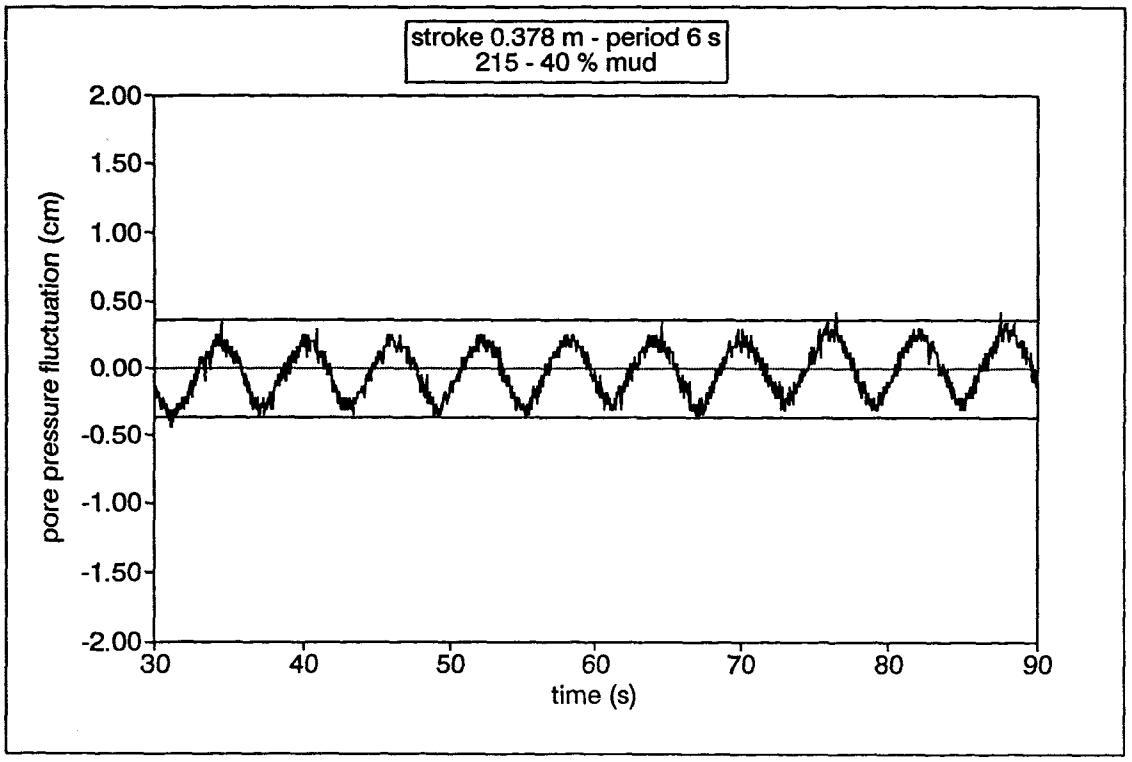

Fig. 8.18. Pore pressure records, under combined flow, with reference to the amplitude of the pressure head (solid lines) transmitted into the sediment bed containing the 215 μm sand fraction and 40% of mud. Data relate to wave strokes of 0.283 m and 0.378 m and a period of 6 s.

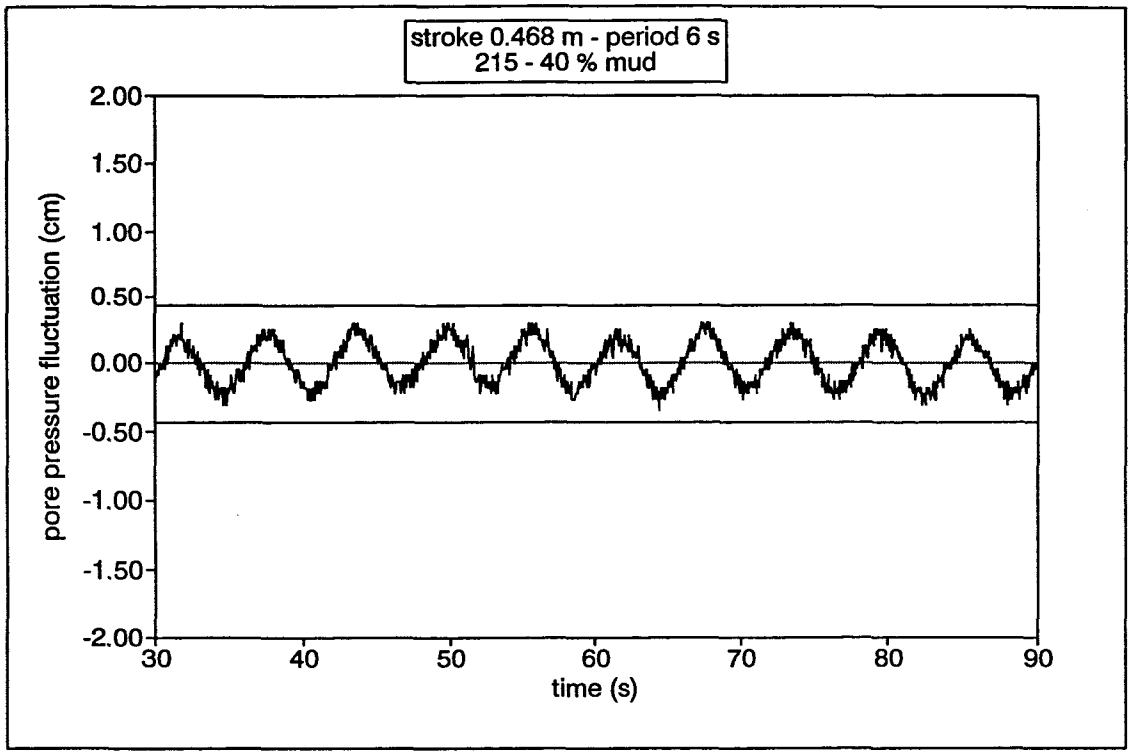

Fig. 8.19. Pore pressure record, under combined flow, with reference to the amplitude of the pressure head (solid lines) transmitted into the sediment bed containing the 215 μm sand fraction and 40% of mud. Data relate to a wave stroke of 0.468 m and period of 6 s.

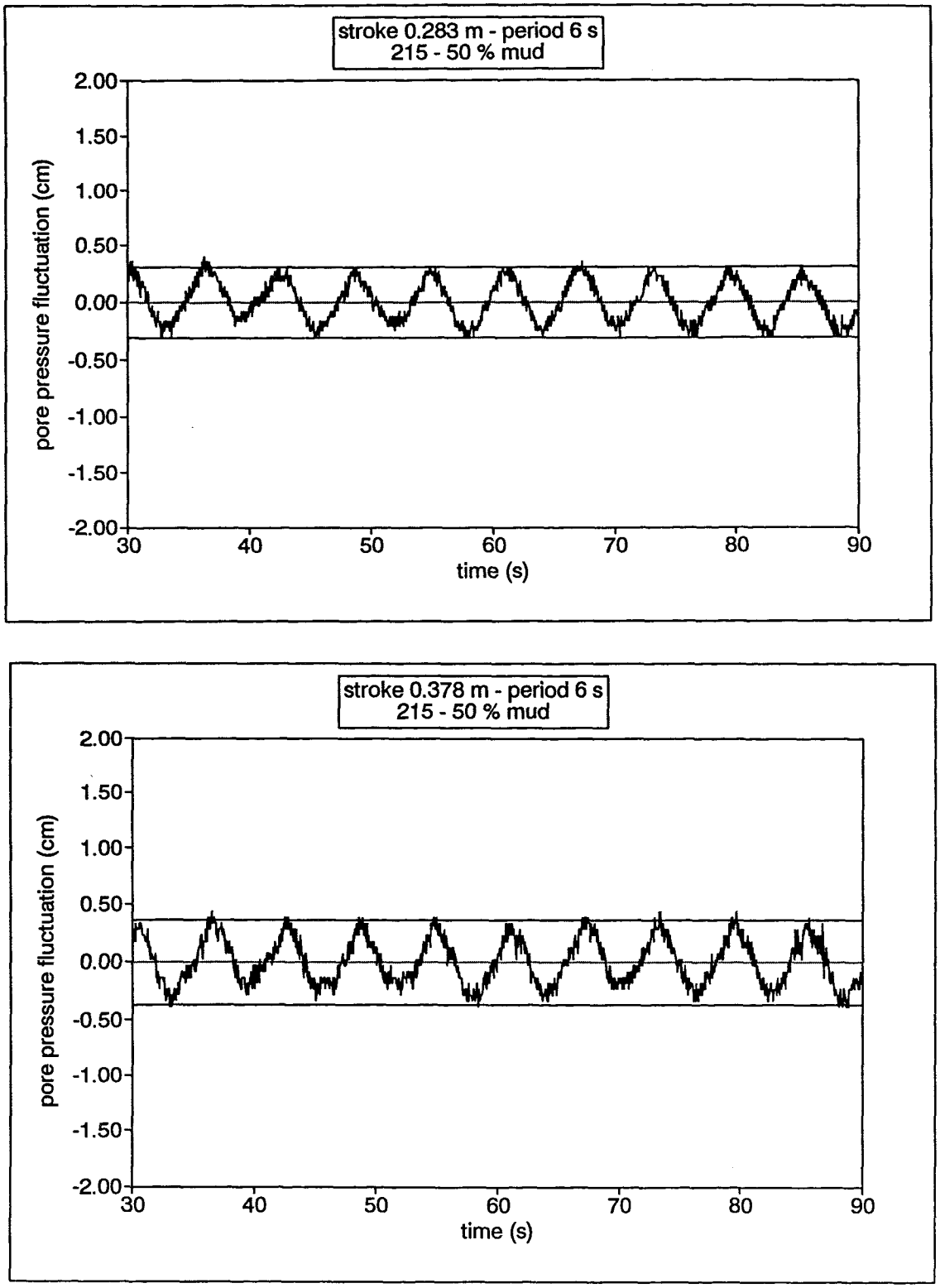

Fig. 8.20. Pore pressure records, under combined flow, with reference to the amplitude of the pressure head (solid lines) transmitted into the sediment bed containing the 215 μm sand fraction and 50% of mud. Data relate to wave strokes of 0.283 m and 0.378 m and a period of 6 s.

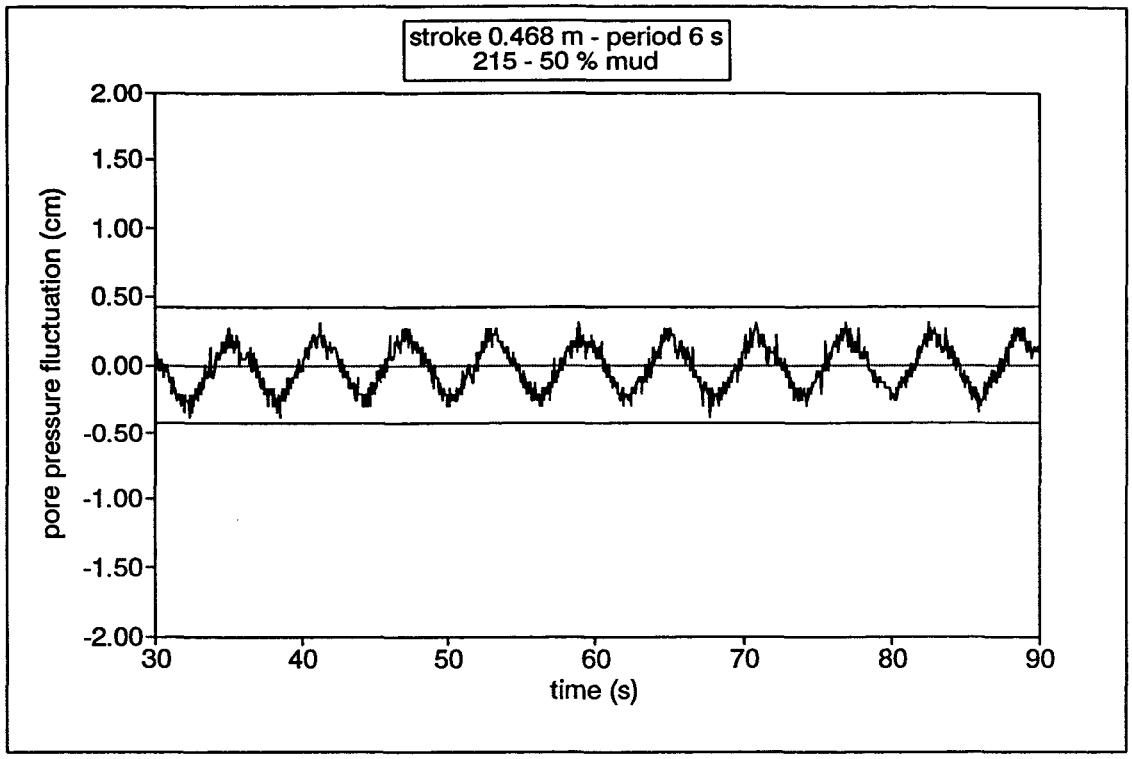

Fig. 8.21. Pore pressure record, under combined flow, with reference to the amplitude of the pressure head (solid lines) transmitted into the sediment bed containing the 215 μm sand fraction and 50% of mud. Data relate to a wave stroke of 0.468 m and period of 6 s.

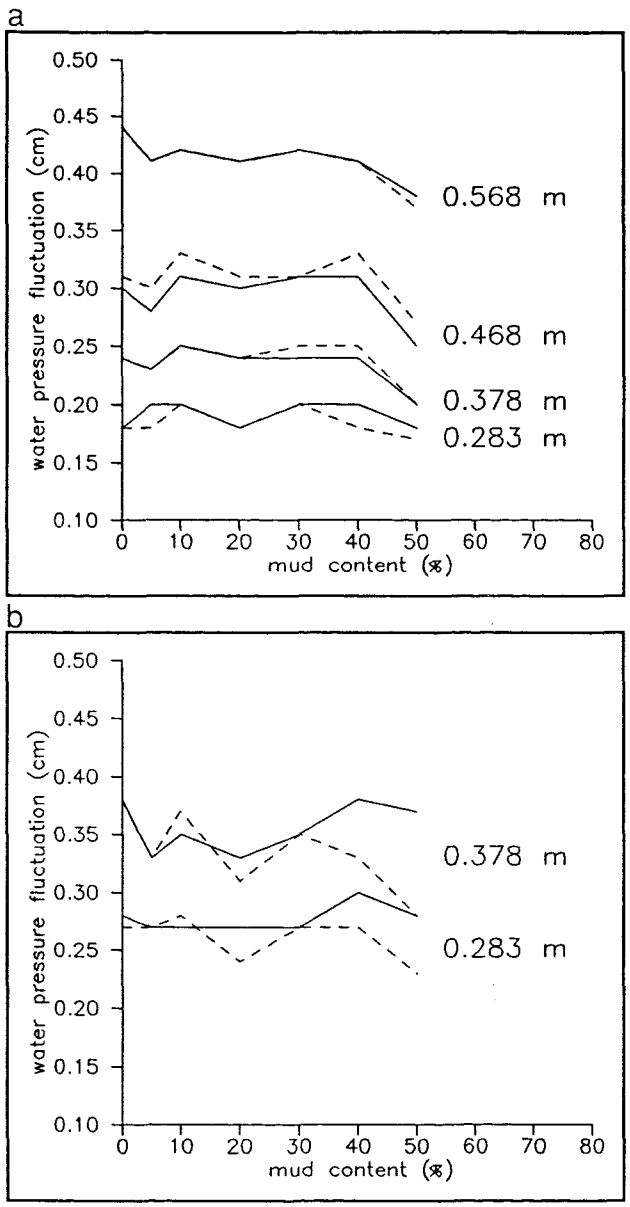

Fig. 8.22. Variation in pore pressure fluctuation (dashed line) with mud content and under combined flow conditions, for the 152.5 μm sand admixtures. Data shown for various wave strokes and periods of (a) 10 s and (b) 6 s. Key: Solid line—amplitude of pressure head transmitted into the bed.

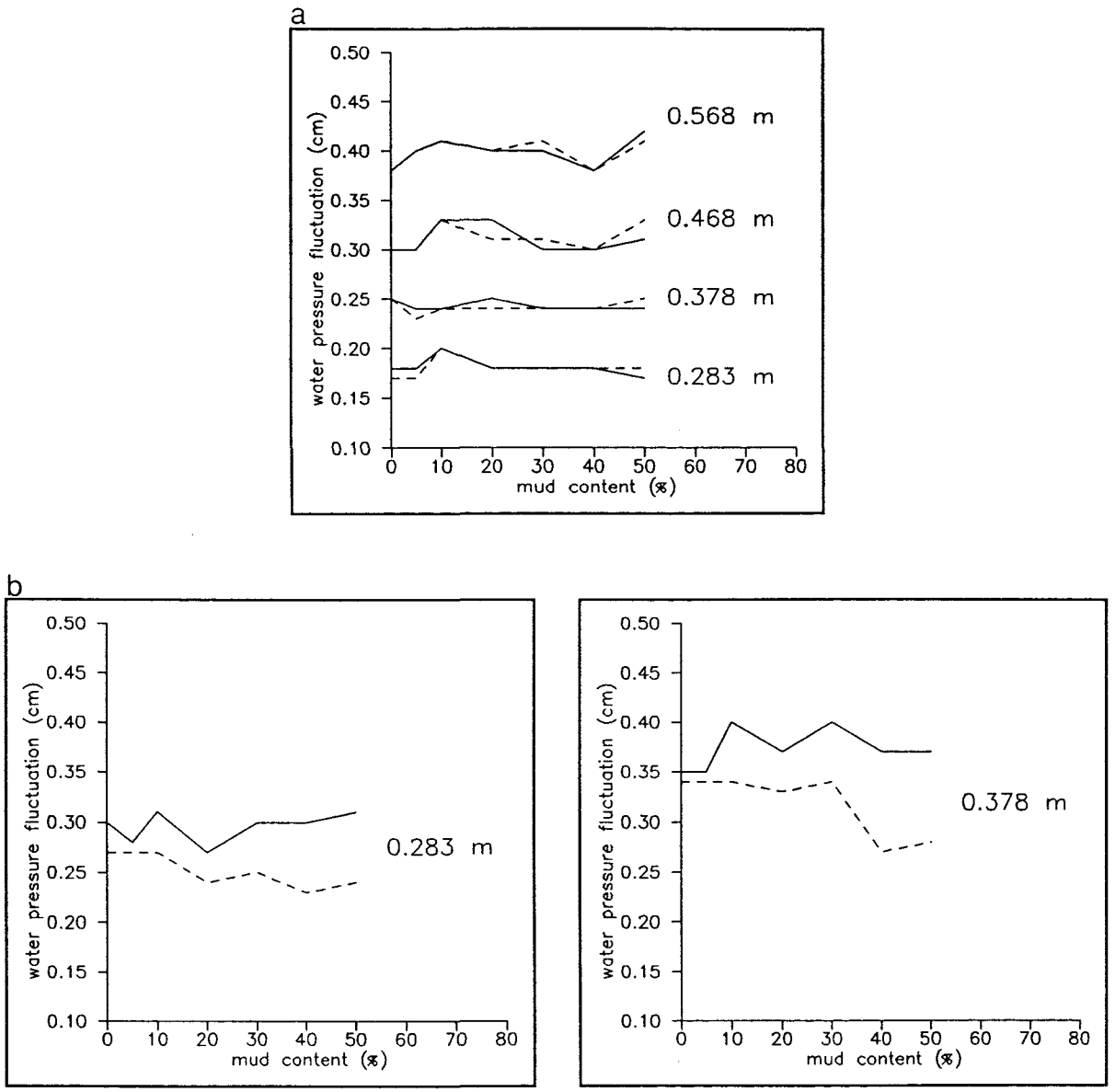

Fig. 8.23. Variation in pore pressure fluctuation (dashed line) with mud content and under combined flow conditions, for the 215 μm sand admixtures. Data shown for various wave strokes and periods of (a) 10 s and (b) 6 s. Key: Solid line—amplitude of pressure head transmitted into the bed.

stroke (m)	period (s)	$U_{o(max)}$ (cm/s)	U_c (cm/s)	σ (cm/s)	mean U_c (cm/s)	pres.1 σ (cm)	pres.2 σ (cm)	atten. (%)
0.283	6	14.81	15.82	2.21	14.36	0.20	0.19	5.0
			13.78	1.99		0.20	0.19	
			14.03	1.98		0.20	0.19	
			13.79	1.96		0.20	0.19	
0.378	6	19.78	13.74	1.93	13.69	0.26	0.26	0
			14.07	1.96		0.26	0.27	
			13.60	1.89		0.27	0.27	
			13.33	1.97		0.27	0.27	
0.283	10	8.89	13.95	1.98	13.74	0.13	0.13	0
			13.47	2.00		0.13	0.13	
			13.93	1.95		0.14	0.13	
			13.62	1.98		0.13	0.13	
0.378	10	11.87	13.54	1.88	13.01	0.17	0.16	0
			12.07	1.84		0.18	0.17	
			12.92	1.76		0.17	0.17	
			13.52	1.96		0.17	0.17	
0.468	10	14.70	9.80	1.59	11.08	0.21	0.22	0
			10.77	1.68		0.21	0.22	
			10.77	1.66		0.21	0.22	
			12.96	1.91		0.21	0.21	
0.568	10	17.84	9.61	1.71	8.64	0.31	0.30	0
			9.63	1.54		0.31	0.30	
			7.91	1.20		0.31	0.31	
			7.41	1.26		0.31	0.31	

Table 8.1. Experimental results obtained under combined flow conditions: Sand size, 152.5 μm; 0% mud.

stroke (m)	period (s)	$U_{o(max)}$ (cm/s)	U_c (cm/s)	σ (cm/s)	mean U_c (cm/s)	pres.1 σ (cm)	pres.2 σ (cm)	atten. (%)
0.283	6	14.81	12.85	1.89	14.21	0.19	0.19	0
			14.15	2.11		0.19	0.19	
			15.57	2.26		0.18	0.19	
			14.27	2.16		0.19	0.19	
0.378	6	19.78	13.08	1.99	13.42	0.23	0.23	0
			14.24	2.12		0.22	0.23	
			13.05	1.94		0.23	0.23	
			13.32	1.91		0.23	0.23	
0.283	10	8.89	15.09	2.18	13.76	0.13	0.13	7.1
			13.15	1.98		0.14	0.13	
			13.59	1.96		0.14	0.13	
			13.20	2.08		0.14	0.13	
0.378	10	11.87	13.87	2.09	13.05	0.17	0.16	0
			11.99	1.89		0.16	0.16	
			12.62	2.01		0.16	0.16	
			13.72	2.06		0.16	0.16	
0.468	10	14.70	11.32	1.87	11.99	0.20	0.21	0
			11.46	1.89		0.20	0.21	
			12.75	2.03		0.19	0.20	
			12.41	1.85		0.20	0.21	
0.568	10	17.84	9.38	1.82	9.78	0.29	0.30	0
			9.55	1.75		0.29	0.29	
			10.18	1.86		0.29	0.29	
			10.00	1.84		0.29	0.29	

Table 8.2. Experimental results obtained under combined flow conditions: Sand size, 152.5 μm; 5% mud.

stroke (m)	period (s)	$U_{o(max)}$ (cm/s)	U_c (cm/s)	σ (cm/s)	mean U_c (cm/s)	pres.1 σ (cm)	pres.2 σ (cm)	atten. (%)
0.283	6	14.81	16.07	2.41	14.28	0.18	0.19	0
			13.80	2.06		0.19	0.19	
			13.68	2.03		0.19	0.20	
			13.57	2.02		0.20	0.20	
0.378	6	19.78	14.18	2.17	14.12	0.25	0.26	0
			14.14	2.16		0.25	0.26	
			14.14	2.14		0.25	0.26	
			14.00	2.18		0.26	0.26	
0.283	10	8.89	13.88	2.05	14.45	0.14	0.14	0
			14.26	2.17		0.14	0.14	
			15.19	2.31		0.13	0.14	
			14.46	2.15		0.14	0.14	
0.378	10	11.87	13.37	1.97	13.50	0.18	0.18	0
			13.07	1.94		0.18	0.18	
			13.65	2.12		0.19	0.18	
			13.91	2.18		0.18	0.18	
0.468	10	14.70	11.29	1.82	12.19	0.22	0.23	0
			12.48	2.03		0.22	0.23	
			11.92	1.92		0.22	0.23	
			13.07	2.15		0.21	0.22	
0.568	10	17.84	11.75	1.90	10.49	0.30	0.30	0
			10.50	1.78		0.30	0.30	
			9.48	1.69		0.30	0.30	
			10.22	1.72		0.30	0.30	

Table 8.3. Experimental results obtained under combined flow conditions: Sand size, 152.5 μm; 10% mud.

stroke (m)	period (s)	$U_{o(max)}$ (cm/s)	U_c (cm/s)	σ (cm/s)	mean U_c (cm/s)	pres.1 σ (cm)	pres.2 σ (cm)	atten. (%)
0.283	6	14.81	14.92	2.06	15.32	0.18	0.16	10.5
			15.28	2.01		0.19	0.16	
			14.67	1.99		0.19	0.17	
			16.41	2.22		0.18	0.17	
0.378	6	19.78	13.77	1.93	14.17	0.23	0.23	4.3
			14.15	1.89		0.23	0.22	
			14.06	1.91		0.23	0.21	
			14.70	2.00		0.23	0.21	
0.283	10	8.89	15.01	2.09	14.83	0.13	0.13	0
			13.89	1.91		0.14	0.13	
			15.22	1.89		0.13	0.13	
			15.19	1.95		0.13	0.13	
0.378	10	11.87	15.44	1.97	14.52	0.17	0.17	0
			13.22	1.89		0.17	0.17	
			14.08	1.88		0.17	0.17	
			15.35	2.05		0.17	0.17	
0.468	10	14.70	12.93	1.98	12.83	0.21	0.22	0
			12.01	1.79		0.21	0.22	
			13.25	2.01		0.21	0.22	
			13.11	2.11		0.21	0.21	
0.568	10	17.84	9.07	1.76	10.60	0.29	0.29	0
			9.79	1.81		0.29	0.29	
			11.45	1.86		0.29	0.29	
			12.09	1.99		0.29	0.29	

Table 8.4. Experimental results obtained under combined flow conditions: Sand size, 152.5 μm; 20% mud.

stroke (m)	period (s)	$U_{o(max)}$ (cm/s)	U_c (cm/s)	σ (cm/s)	mean U_c (cm/s)	pres.1 σ (cm)	pres.2 σ (cm)	atten. (%)
0.283	6	14.81	16.42	2.47	16.00	0.19	0.19	0
			16.04	2.40		0.19	0.18	
			15.97	2.39		0.19	0.18	
			15.58	2.35		0.19	0.19	
0.378	6	19.78	16.54	2.51	15.11	0.24	0.24	0
			15.18	2.38		0.24	0.25	
			13.87	2.11		0.25	0.25	
			14.85	2.33		0.25	0.25	
0.283	10	8.89	15.62	2.37	15.55	0.13	0.14	0
			15.80	2.42		0.13	0.14	
			15.39	2.31		0.14	0.13	
			15.37	2.21		0.14	0.14	
0.378	10	11.87	14.51	2.36	15.45	0.17	0.18	0
			15.30	2.42		0.17	0.18	
			15.80	2.39		0.17	0.18	
			16.20	2.41		0.17	0.18	
0.468	10	14.70	13.94	2.08	13.46	0.22	0.22	0
			13.65	1.96		0.21	0.22	
			14.33	2.00		0.21	0.22	
			11.92	1.91		0.22	0.22	
0.568	10	17.84	12.17	2.02	11.93	0.30	0.30	0
			12.15	2.12		0.30	0.29	
			11.34	2.02		0.30	0.30	
			12.07	2.00		0.30	0.30	

Table 8.5. Experimental results obtained under combined flow conditions: Sand size, 152.5 μm; 30% mud.

stroke (m)	period (s)	$U_{o(max)}$ (cm/s)	U_c (cm/s)	σ (cm/s)	mean U_c (cm/s)	pres.1 σ (cm)	pres.2 σ (cm)	atten. (%)
0.283	6	14.81	16.47	2.16	16.47	0.21	0.19	9.5
			15.58	2.18		0.21	0.19	
			18.16	2.53		0.21	0.19	
			16.85	2.41		0.21	0.19	
0.378	6	19.78	15.27	2.10	16.37	0.27	0.23	14.8
			17.59	2.41		0.26	0.23	
			15.59	2.09		0.27	0.23	
			17.03	2.33		0.27	0.23	
0.468	6	24.49	14.96	1.92	15.27	0.34	0.21	38.2
			14.84	2.09		0.34	0.21	
			15.92	2.31		0.34	0.21	
			15.36	2.23		0.34	0.21	
0.283	10	8.89	18.27	2.46	16.28	0.13	0.13	7.1
			15.31	2.06		0.14	0.13	
			15.42	2.00		0.14	0.13	
			16.12	2.25		0.14	0.14	
0.378	10	11.87	15.85	2.20	15.74	0.17	0.17	0
			16.41	2.36		0.16	0.17	
			15.18	1.92		0.18	0.19	
			15.52	2.08		0.17	0.18	
0.468	10	14.70	15.25	2.02	14.22	0.21	0.22	0
			15.25	2.19		0.22	0.23	
			13.69	2.06		0.22	0.23	
			12.68	2.09		0.22	0.23	
0.568	10	17.84	11.94	2.24	12.89	0.29	0.29	0
			14.42	2.27		0.29	0.29	
			12.56	1.97		0.29	0.30	
			12.63	2.10		0.29	0.29	

Table 8.6. Experimental results obtained under combined flow conditions: Sand size, 152.5 μm; 40% mud.

stroke (m)	period (s)	$U_{o(max)}$ (cm/s)	U_c (cm/s)	σ (cm/s)	mean U_c (cm/s)	pres.1 σ (cm)	pres.2 σ (cm)	atten. (%)
0.283	6	14.81	17.10	2.23	17.23	0.21	0.16	20.0
			17.42	2.35		0.20	0.16	
			17.25	2.36		0.20	0.16	
			17.13	2.42		0.20	0.16	
0.378	6	19.78	15.77	2.36	16.61	0.26	0.20	23.1
			16.69	2.45		0.26	0.20	
			16.36	2.38		0.26	0.20	
			17.60	2.61		0.25	0.20	
0.468	6	24.49	14.69	2.29	15.73	0.33	0.20	39.4
			17.38	2.63		0.33	0.20	
			14.77	2.35		0.34	0.21	
			16.08	2.33		0.33	0.20	
0.283	10	8.89	17.64	2.63	17.38	0.14	0.13	7.7
			16.05	2.45		0.12	0.12	
			17.49	2.25		0.13	0.12	
			18.35	3.02		0.13	0.12	
0.378	10	11.87	17.18	2.60	16.86	0.14	0.14	0
			17.81	3.27		0.13	0.13	
			15.87	2.41		0.13	0.14	
			16.57	2.50		0.14	0.15	
0.468	10	14.70	14.58	2.49	15.11	0.18	0.19	0
			14.52	2.39		0.18	0.19	
			16.21	2.52		0.18	0.18	
			15.12	2.34		0.18	0.19	
0.568	10	17.84	14.25	2.39	13.93	0.27	0.26	3.7
			13.00	2.34		0.27	0.26	
			15.10	2.38		0.27	0.26	
			13.38	2.39		0.27	0.26	

Table 8.7. Experimental results obtained under combined flow conditions: Sand size, 152.5 μm; 50% mud.

stroke (m)	period (s)	$U_{o(max)}$ (cm/s)	U_c (cm/s)	σ (cm/s)	mean U_c (cm/s)	pres.1 σ (cm)	pres.2 σ (cm)	atten. (%)
0.283	6	14.81	12.91	1.91	12.85	0.21	0.19	9.5
			12.79	1.92		0.21	0.19	
			12.15	1.86		0.21	0.20	
			13.55	2.09		0.21	0.19	
0.378	6	19.78	11.25	1.78	11.26	0.25	0.24	4.0
			11.11	1.79		0.25	0.25	
			12.41	1.82		0.25	0.24	
			10.27	1.61		0.25	0.24	
0.283	10	8.89	11.54	1.61	11.83	0.13	0.12	7.7
			12.35	1.79		0.13	0.12	
			10.96	1.74		0.13	0.12	
			12.48	1.81		0.13	0.12	
0.378	10	11.87	11.03	1.81	10.96	0.18	0.18	0
			10.92	1.78		0.18	0.18	
			10.42	1.68		0.18	0.18	
			11.46	1.74		0.18	0.18	
0.468	10	14.70	11.28	1.72	9.95	0.21	0.20	0
			10.63	1.83		0.21	0.21	
			8.72	1.45		0.21	0.21	
			9.18	1.59		0.21	0.21	
0.568	10	17.84	9.46	1.66	8.20	0.26	0.26	0
			7.59	1.59		0.27	0.27	
			8.21	1.69		0.27	0.27	
			9.18	1.59		0.27	0.27	

Table 8.8. Experimental results obtained under combined flow conditions: Sand size, 215 μm; 0% mud.

stroke (m)	period (s)	$U_{o(max)}$ (cm/s)	U_c (cm/s)	σ (cm/s)	mean U_c (cm/s)	pres.1 σ (cm)	pres.2 σ (cm)	atten. (%)
0.283	6	14.81	12.56	2.17	12.68	0.20	0.19	5.0
			14.33	2.18		0.19	0.19	
			11.65	1.96		0.19	0.19	
			12.16	2.08		0.20	0.18	
0.378	6	19.78	11.40	2.01	11.87	0.24	0.24	4.0
			12.14	2.06		0.24	0.24	
			11.70	1.89		0.25	0.24	
			12.24	2.13		0.25	0.24	
0.283	10	8.89	12.63	2.20	12.77	0.12	0.12	7.7
			12.50	2.13		0.13	0.12	
			12.71	2.13		0.13	0.12	
			13.22	2.21		0.12	0.12	
0.378	10	11.87	11.59	2.03	12.16	0.17	0.16	5.9
			12.63	2.25		0.16	0.15	
			11.94	2.11		0.16	0.16	
			12.48	2.28		0.17	0.16	
0.468	10	14.70	10.86	2.14	10.86	0.21	0.20	0
			12.12	2.25		0.21	0.20	
			10.14	2.10		0.21	0.21	
			10.33	2.16		0.21	0.21	
0.568	10	17.84	10.31	2.07	9.06	0.27	0.27	0
			7.30	1.66		0.29	0.28	
			10.23	1.96		0.27	0.27	
			8.41	1.79		0.28	0.28	

Table 8.9. Experimental results obtained under combined flow conditions: Sand size, 215 μm; 5% mud.

stroke (m)	period (s)	$U_{o(max)}$ (cm/s)	U_c (cm/s)	σ (cm/s)	mean U_c (cm/s)	pres.1 σ (cm)	pres.2 σ (cm)	atten. (%)
0.283	6	14.81	13.21	2.12	13.88	0.22	0.19	13.6
			14.99	2.31		0.22	0.19	
			12.79	2.13		0.22	0.19	
			14.54	2.19		0.22	0.19	
0.378	6	19.78	12.50	2.14	13.11	0.28	0.24	14.3
			14.42	2.22		0.28	0.24	
			12.15	2.01		0.28	0.24	
			13.35	2.16		0.28	0.24	
0.283	10	8.89	12.71	2.12	13.47	0.14	0.14	0
			13.92	2.04		0.13	0.13	
			12.25	2.06		0.14	0.14	
			15.01	2.28		0.13	0.14	
0.378	10	11.87	12.04	2.14	12.81	0.18	0.17	0
			13.11	2.15		0.17	0.17	
			12.11	2.12		0.17	0.17	
			13.97	2.32		0.17	0.17	
0.468	10	14.70	10.94	1.91	11.50	0.23	0.23	0
			12.19	2.03		0.22	0.23	
			10.45	1.95		0.24	0.23	
			12.42	2.03		0.22	0.22	
0.568	10	17.84	10.16	1.71	9.91	0.28	0.28	0
			10.93	1.82		0.29	0.28	
			8.52	1.62		0.29	0.29	
			10.03	1.69		0.29	0.29	

Table 8.10. Experimental results obtained under combined flow conditions: Sand size, 215 μm; 10% mud.

stroke (m)	period (s)	$U_{o(max)}$ (cm/s)	U_c (cm/s)	σ (cm/s)	mean U_c (cm/s)	pres.1 σ (cm)	pres.2 σ (cm)	atten. (%)
0.283	6	14.81	13.25	2.18	14.43	0.19	0.17	10.5
			15.85	2.46		0.19	0.17	
			13.63	2.22		0.19	0.17	
			14.99	2.28		0.19	0.17	
0.378	6	19.78	14.37	2.21	12.95	0.26	0.23	11.5
			12.53	2.09		0.26	0.23	
			12.39	2.02		0.27	0.24	
			12.50	2.08		0.26	0.23	
0.283	10	8.89	13.57	2.26	14.06	0.14	0.13	0
			14.00	2.13		0.13	0.13	
			13.43	2.20		0.14	0.13	
			15.23	2.50		0.12	0.12	
0.378	10	11.87	13.03	2.09	13.99	0.18	0.17	5.5
			14.95	2.32		0.17	0.16	
			13.06	1.99		0.19	0.18	
			14.90	2.17		0.17	0.17	
0.468	10	14.70	11.18	1.93	12.18	0.24	0.23	4.3
			13.14	2.17		0.22	0.22	
			11.53	2.10		0.23	0.22	
			12.87	2.01		0.21	0.21	
0.568	10	17.84	9.46	1.59	10.30	0.28	0.28	0
			10.59	1.78		0.28	0.28	
			9.83	1.61		0.29	0.29	
			11.31	1.99		0.28	0.28	

Table 8.11. Experimental results obtained under combined flow conditions: Sand size, 215 μm; 20% mud.

stroke (m)	period (s)	$U_{o(max)}$ (cm/s)	U_c (cm/s)	σ (cm/s)	mean U_c (cm/s)	pres.1 σ (cm)	pres.2 σ (cm)	atten. (%)
0.283	6	14.81	12.41	2.09	14.24	0.21	0.17	14.3
			15.55	2.37		0.21	0.18	
			13.39	2.08		0.22	0.18	
			15.61	2.50		0.20	0.18	
0.378	6	19.78	12.38	2.08	13.61	0.28	0.24	14.3
			13.66	2.14		0.28	0.24	
			13.90	2.03		0.28	0.24	
			14.48	2.30		0.28	0.24	
0.283	10	8.89	15.61	2.42	15.31	0.14	0.14	0
			16.18	2.50		0.12	0.13	
			13.68	2.28		0.14	0.13	
			15.78	2.40		0.13	0.12	
0.378	10	11.87	15.00	2.46	14.44	0.16	0.16	0
			13.93	2.50		0.16	0.17	
			13.42	2.22		0.18	0.18	
			15.39	2.39		0.17	0.16	
0.468	10	14.70	11.08	2.10	12.84	0.21	0.21	0
			14.40	2.57		0.20	0.21	
			12.60	2.23		0.22	0.22	
			13.29	2.31		0.22	0.22	
0.568	10	17.84	10.66	1.69	11.15	0.29	0.29	0
			10.88	1.74		0.28	0.29	
			11.60	2.02		0.28	0.28	
			11.44	1.99		0.28	0.28	

Table 8.12. Experimental results obtained under combined flow conditions: Sand size, 215 μm; 30% mud.

stroke (m)	period (s)	$U_{o(max)}$ (cm/s)	U_c (cm/s)	σ (cm/s)	mean U_c (cm/s)	pres.1 σ (cm)	pres.2 σ (cm)	atten. (%)
0.283	6	14.81	16.09	2.58	15.18	0.21	0.16	23.8
			16.04	2.43		0.21	0.16	
			13.60	2.31		0.21	0.16	
			14.98	2.45		0.21	0.16	
0.378	6	19.78	13.54	2.37	14.81	0.26	0.19	26.9
			15.30	2.44		0.26	0.19	
			15.33	2.41		0.26	0.19	
			15.06	2.46		0.26	0.19	
0.468	6	24.49	12.74	2.33	13.00	0.31	0.16	48.4
			13.39	2.38		0.31	0.16	
			12.82	2.31		0.31	0.16	
			13.04	2.34		0.31	0.16	
0.283	10	8.89	14.73	2.43	16.21	0.13	0.13	0
			17.39	2.65		0.12	0.13	
			15.18	2.44		0.13	0.13	
			17.52	2.68		0.12	0.13	
0.378	10	11.87	14.51	2.48	15.03	0.17	0.17	0
			16.72	2.78		0.17	0.16	
			13.88	2.38		0.17	0.17	
			14.99	2.85		0.17	0.16	
0.468	10	14.70	13.71	2.47	13.27	0.21	0.20	0
			14.00	2.45		0.21	0.20	
			12.79	2.35		0.21	0.21	
			12.59	2.36		0.21	0.21	
0.568	10	17.84	11.03	2.21	12.25	0.27	0.27	0
			13.24	2.41		0.27	0.27	
			11.66	2.25		0.27	0.27	
			13.05	2.44		0.27	0.27	

Table 8.13. Experimental results obtained under combined flow conditions: Sand size, 215 μm; 40% mud.

stroke (m)	period (s)	$U_{o(max)}$ (cm/s)	U_c (cm/s)	σ (cm/s)	mean U_c (cm/s)	pres.1 σ (cm)	pres.2 σ (cm)	atten. (%)
0.283	6	14.81	14.52	2.17	16.13	0.22	0.17	22.7
			16.47	2.66		0.22	0.16	
			17.30	2.32		0.22	0.17	
			16.22	2.40		0.22	0.17	
0.378	6	19.78	14.17	2.16	15.08	0.26	0.20	23.1
			15.75	2.52		0.26	0.20	
			13.67	2.30		0.26	0.20	
			16.71	2.62		0.26	0.20	
0.468	6	24.49	13.81	2.21	14.96	0.30	0.16	46.7
			16.15	2.43		0.30	0.16	
			14.80	2.39		0.30	0.16	
			15.06	2.51		0.30	0.16	
0.283	10	8.89	17.95	2.71	17.24	0.13	0.13	0
			17.05	2.66		0.12	0.13	
			17.33	2.62		0.12	0.13	
			16.61	2.42		0.12	0.13	
0.378	10	11.87	14.96	2.50	15.67	0.16	0.17	0
			16.60	2.69		0.17	0.17	
			14.73	2.24		0.17	0.18	
			16.39	2.41		0.17	0.18	
0.468	10	14.70	14.77	2.25	15.02	0.22	0.22	0
			15.18	2.56		0.22	0.22	
			15.60	2.29		0.22	0.23	
			14.52	2.43		0.22	0.23	
0.568	10	17.84	13.65	2.32	13.30	0.30	0.30	0
			13.67	2.31		0.30	0.29	
			12.72	2.33		0.30	0.29	
			13.17	2.33		0.30	0.30	

Table 8.14. Experimental results obtained under combined flow conditions: Sand size, 215 μm; 50% mud.

sand size (microns)	mud percentage (%)	friction factor (f_w)	maximum wave shear stress $\tau_{w(max)}$ (N/m^2)	critical current shear stress τ_c ($N/m^{2)}$	combined shear stress τ_{cw} (N/m^2)
152.5	0	0.0200	0.079	0.088	0.167
	5			0.088	0.167
	10			0.097	0.176
	20			0.102	0.181
	30			0.111	0.190
	40			0.119	0.198
	50			0.132	0.211
215	0	0.0200	0.079	0.069	0.148
	5			0.079	0.158
	10			0.087	0.166
	20			0.093	0.172
	30			0.107	0.186
	40			0.118	0.197
	50			0.131	0.210

Table 8.15. Critical shear stresses due to the co-linear combined action of waves and currents, for a plate displacement of 0.283 m and wave period of 10 s.

sand size (microns)	mud percentage (%)	friction factor (f_w)	maximum wave shear stress $\tau_{w(max)}$ (N/m^2)	critical current shear stress τ_c ($N/m^{2)}$	combined shear stress τ_{cw} (N/m^2)
152.5	0	0.0140	0.099	0.081	0.180
	5			0.081	0.180
	10			0.086	0.185
	20			0.098	0.197
	30			0.109	0.208
	40			0.113	0.212
	50			0.126	0.225
215	0	0.0140	0.099	0.061	0.160
	5			0.073	0.172
	10			0.079	0.178
	20			0.091	0.190
	30			0.097	0.196
	40			0.104	0.203
	50			0.112	0.211

Table 8.16. Critical shear stresses due to the co-linear combined action of waves and currents, for a plate displacement of 0.378 m and wave period of 10 s.

sand size (microns)	mud percentage (%)	friction factor (f_w)	maximum wave shear stress $\tau_{w(max)}$ (N/m^2)	critical current shear stress τ_c ($N/m^{2)}$	combined shear stress τ_{cw} (N/m^2)
152.5	0	0.0100	0.108	0.062	0.170
	5			0.070	0.178
	10			0.073	0.181
	20			0.079	0.187
	30			0.087	0.195
	40			0.094	0.202
	50			0.104	0.212
215	0	0.0100	0.108	0.052	0.160
	5			0.060	0.168
	10			0.065	0.173
	20			0.073	0.181
	30			0.079	0.187
	40			0.084	0.192
	50			0.104	0.212

Table 8.17. Critical shear stresses due to the co-linear combined action of waves and currents, for a plate displacement of 0.468 m and wave period of 10 s.

sand size (microns)	mud percentage (%)	friction factor (f_w)	maximum wave shear stress $\tau_{w(max)}$ (N/m^2)	critical current shear stress τ_c ($N/m^{2)}$	combined shear stress τ_{cw} (N/m^2)
152.5	0	0.0085	0.135	0.041	0.176
	5			0.050	0.185
	10			0.056	0.191
	20			0.058	0.193
	30			0.070	0.205
	40			0.079	0.214
	50			0.090	0.225
215	0	0.0085	0.135	0.037	0.172
	5			0.044	0.179
	10			0.051	0.186
	20			0.055	0.190
	30			0.062	0.197
	40			0.073	0.208
	50			0.085	0.220

Table 8.18. Critical shear stresses due to the co-linear combined action of waves and currents, for a plate displacement of 0.568 m and wave period of 10 s.

sand size (microns)	mud percentage (%)	friction factor (f_w)	maximum wave shear stress $\tau_{w(max)}$ (N/m^2)	critical current shear stress τ_c ($N/m^{2)}$	combined shear stress τ_{cw} (N/m^2)
152.5	0	0.0140	0.154	0.096	0.250
	5			0.094	0.248
	10			0.095	0.249
	20			0.107	0.261
	30			0.115	0.269
	40			0.120	0.274
	50			0.131	0.284
215	0	0.0140	0.154	0.079	0.233
	5			0.078	0.232
	10			0.090	0.244
	20			0.096	0.250
	30			0.094	0.248
	40			0.105	0.259
	50			0.116	0.270

Table 8.19. Critical shear stresses due to the co-linear combined action of waves and currents, for a plate displacement of 0.283 m and wave period of 6 s.

sand size (microns)	mud percentage (%)	friction factor (f_w)	maximum wave shear stress $\tau_{w(max)}$ (N/m^2)	critical current shear stress τ_c ($N/m^{2)}$	combined shear stress τ_{cw} (N/m^2)
152.5	0	0.0090	0.176	0.088	0.264
	5			0.085	0.261
	10			0.093	0.269
	20			0.094	0.270
	30			0.104	0.280
	40			0.119	0.295
	50			0.123	0.299
215	0	0.0090	0.176	0.064	0.240
	5			0.070	0.246
	10			0.081	0.257
	20			0.081	0.257
	30			0.087	0.263
	40			0.102	0.278
	50			0.104	0.280

Table 8.20. Critical shear stresses due to the co-linear combined action of waves and currents, for a plate displacement of 0.378 m and wave period of 6 s.

sand size (microns)	mud percentage (%)	friction factor (f_w)	maximum wave shear stress $\tau_{w(max)}$ (N/m^2)	critical current shear stress τ_c ($N/m^{2)}$	combined shear stress τ_{cw} (N/m^2)
152.5	40	0.0075	0.225	0.107	0.332
	50			0.113	0.338
215	40	0.0075	0.225	0.081	0.306
	50			0.103	0.328

Table 8.21. Critical shear stresses due to the co-linear combined action of waves and currents, for a plate displacement of 0.468 m and wave period of 6 s.

CHAPTER 9

RESULTS AND DISCUSSION: LIQUID LIMIT AND RHEOLOGY

9. RESULTS AND DISCUSSION: LIQUID LIMIT AND RHEOLOGY

9.1. LIQUID LIMIT DETERMINATION

9.1.1. Introduction

Sedimentologists measure routinely the changes in the consistency of a sediment, using the Atterberg liquid limit. The liquid limit (LL) is the water content of a sediment-water mixture below which the material no longer behaves as a liquid i.e. the material has acquired a measurable shear strength. As a result of numerous tests, this value is suggested to lie between 2.0 and 2.5 KPa; however, 1.7 KPa is used normally as an average value (Faas, 1991).

The liquid limit (LL) can be defined only for sediments characterised by some degree of cohesion. Whilst the LL parameter is measured easily, it clearly does not measure the water content at the lower limit of the fluid (liquid) state (Been & Sills, 1985). Such a limitation is because the water content at which the development of a cohesive sediment structure occurs is many orders of magnitude greater than the water content observed at the (Atterberg) liquid limit.

9.1.2. Measurements

In addition to the erosion threshold determinations, an alternative method of defining the shear strength of sediments is a measurement of the liquid limit (LL). Such measurements can be accomplished using the (British Standard) fall cone penetrometer; this measures various penetrations, into the sediment, of a standard cone with an apex angle of 30° and weight of 0.78 N for different water (moisture) contents (for a detailed description of

the experimental process, see Section 4.7.3). The results derived from these particular tests are listed in Tables 4.13 to 4.22.

The variation in the liquid limit, in relation to the mud content (M) of the sediment mixtures used in the present study, is presented in Fig. 9.1. The trends identified are as follows:
(a) for M ≥ 10% but ≤ 30%, the cohesive forces between the sand and clay particles begin to develop and stabilise/increase slightly the liquid limit; and
(b) for M > 30-40%, the cohesive forces are established fully and the sediments behave cohesively—this causes an abrupt increase in the liquid limit.

The effect of the clay component of sand-clay mixtures on the liquid limit (LL), has been studied previously by various investigators. For example, a 'linear mixture law' has been identified as a reasonable expression of the relationship between liquid limit and clay content, provided that the clay component is > 10% for inorganic clays and > 20% for organic clays (Seed *et al.*, 1964b). A wide range of soil mixtures have been investigated by Sivapulliah & Sridharan (1985). These investigators concluded that the liquid limit could not be described in terms of a (linear mixture) law. However, a more detailed examination of the results reveals that the expression is valid when the clay is mixed with fine sand; this is in agreement with the earlier finding (see above). Finally, liquid limit measurements have been undertaken on artifically-prepared clay-sand mixtures; in these, the (medium size) sand content has ranged from 0% to 60% (Tan *et al.*, 1994). A linear mixture law, slightly modified to that proposed by Seed *et al.* (op. cit.), has been suggested,

$$LL_{mixture} = \frac{(100-S)}{100} LL_{clay} \qquad \textbf{(9.1)}$$

where S is the sand percentage contained within the total sediment deposit, given by

$$S = 100 \frac{m_s}{m_s + m_c} \qquad \textbf{(9.2)}$$

where m_s is the mass of sand added to the mixture, whilst m_c is the mass of clay (but, actually, the mass of the non-sand fraction (containing both the clay and the silt fractions)).

Comparison of the measured liquid limits related to the samples with M ≥ 30%, with Equation 9.1 (provided that the parameter LL_{clay} of this expression is substituted by the liquid limit of the mud fraction of the samples of the present study), demonstrates that the increase in the liquid limit identified can be described adequately. Such a relationship is especially characteristic of the 215 μm sand admixtures, as explained by this linear function; this is represented as a solid line in Fig. 9.1.

Although the linear mixture law of Tan *et al.* (1994) has been derived on the basis of liquid limit measures of various sand-clay admixtures, it has been argued by these investigators that the formula could also be valid for sand-mud admixtures. The present liquid limit results, although, somewhat limited in number, confirm this particular concept.

Several American investigators in the late 1950s and in the early 1960s (Dunn, 1959; Smerdon & Beasley, 1961; Carlson & Enger, 1963), together with more recent studies (Kamphuis & Hall, 1983), have established a general positive linear correlation between the liquid limit of

natural soils (with low sand contents) and the critical current-induced erosion shear stress. However, within a limited number of investigations (Gibbs, 1962), a reverse (negative) linear relationship has been demonstrated. Such a trend has been attributed to the fact that some soils may be expandable related to lower erosion thresholds. An attempt to examine if a similar relationship relates to the results obtained in the present investigation is shown in Fig. 9.2. Figs 9.2a and 9.2b were obtained under the action of currents and waves, respectively. The correlations associated with the 152.5 μm sand admixtures tend to be positive. However, correlations associated with admixtures of the larger sand fraction size (215 μm) are linear positive and are highly significant (at a confidence level of 98%).

9.2. RHEOLOGY

9.2.1. Introduction

Rheology relates to the study of flow and deformation behaviour of materials. The rheological behaviour of a material is described generally by an expression relating the applied stress to the shear (or deformation) rate, in the case of viscous materials, and deformation, in the case of elastic materials. The derived expression is based mainly upon experimental data sets.

On the basis of the results of various soils, their rheological behaviour is demonstrated only by that of the cohesive sediments. Correspondingly, the complexity of the behaviour of cohesive sediments is summarised effectively by the statement of Williams (1992): '*Cohesive sediments are, in general, non-linear, dispersive, dissipative, thixotropic and may display an apparent yield stress. As such, they are among the most*

difficult materials to characterise rheologically, while their physical characteristics (in particular the presence of large constituent particles or aggregates) impose severe rheometrical constraints. These considerations, not withstanding many of the widely-documentated guidelines for characterisation of non-Newtonian materials, may be usefully applied. The most pertinent issue in this case is that any succesful study must recognise that shear and time effects in these materials are coupled.'

The resultant shear stress τ of a viscous material is related to the shear rate γ according to Newton's Law,

$$d\tau = 2\mu d\gamma \qquad \textbf{(9.3)}$$

where μ is the dynamic viscosity and is a measure for the shear flow resistance, i.e. the internal friction of the material. Typical flow curves related to different types of fluids are shown in Fig. 9.3. Clearly, for some materials, the dynamic viscosity is not constant but is a function of the shear rate; such material is defined as non-Newtonian. Characteristic flows associated with non-Newtonian bodies are represented by Curves B and D as shown on Fig. 9.3. The response of these materials is treated often as an ideal Bingham behaviour, described in terms of an extrapolated yield stress τ_B and a Newtonian-like Bingham viscosity μ_B.

9.2.2. Rheological Curves and Yield Stress Definition

The relationship investigated during the rheological tests was variation in the instantaneous dynamic viscosity of the mixtures, under an increasing shear stress, with shear rate (the experimental procedure has been described in Section 4.7.3). From this particular relationship, yield stresses (τ_y) were derived; these were

defined as those shear stresses at which the viscosity could obtain its maximum value. In physical terms, the presence of a yield stress means that the material will not flow until the applied stress exceeds the yield value.

For the present investigation, the mixtures with mud contents < 20% could not exhibit any rheological behaviour (thus, it was not possible for a yield stress to be defined), since the quantity of the cohesive additive was not sufficient for these soils to attain such a property (see, for example, Fig. 9.4). In contrast, mixtures with M ≥ 20% behaved as pseudo(visco)-plastic material, displaying non-Newtonian behaviour at low shear rates. The relationship between shear stress and shear rate is exemplified in the results presented in Figs 9.5 to 9.12; these emphasise the 'shear-thinning' properties of these admixtures, at relatively low rates of shear. The variation in the viscosity, with shear rate, indicates that these mixtures exhibit marked shear-thinning when the mud content is in excess of 30% (notice the change in the shape of the viscosity curve maxima, as the mud content increases).

Theoretically, it may be expected that the addition of non-cohesive particles weakens the structural strength of a cohesive sediment. The influence of the sand content on the rheological behaviour of the mud has been investigated experimentally elsewhere by Migniot (1968, 1989) and O'Brien & Julien (1988). The relative presence of sand i.e. an increase in the sand concentration in relation to the total sediment concentration, decreases the rigidity (yield stress) of a sediment. From the data presented by Migniot (1989), it may be concluded also that the effect of adding sand particles to a muddy sediment is small; this is provided that the relative

sand concentration is less than 10%. O'Brien & Julien (1988) added sand to a 5-6% clay suspension and a 30% natural mud suspension. These investigators concluded that the viscosity did not decrease dramatically, until the sand concentrations added exceeded 20% (by volume).

The yield stresses determined for the mixtures investigated as part of the present investigation are listed in Table 9.1 and shown in Fig. 9.13. The low standard deviations of the mean values indicate very well homogenised samples. The results indicate that mixtures associated with the 215 μm sands are characterised by lower yield stresses than those associated with the 152.5 μm sand mixtures. Furthermore, an increase in the mud content and, subsequently, the clay mineral content causes an increase in the yield stress. The increase is dramatic when M > 30%. Such a change in the rheology of the muddier admixtures may explain the dampening in pore pressure, during the hydraulic experiments under oscillatory and combined flow conditions.

The resistance of a sediment deposit to erosion depends upon the inherent strength of the structure. From a theoretical point of view, it is a logical consequence to predict good (positive) correlations between yield stress and the critical shear stress at erosion. To date, the relationship between the two variables has not resulted in very good correlations, especially when the sediments tested were particularly muddy (for example, only Migniot (1968) and Otsubo & Muraoka (1988) have postulated highly significant correlations). This latter relationship may be attributed to thixotropic effects and the differences encountered between the field and laboratory conditions i.e. the sample structural history. Similar correlation attempted for the data of the present study has produced a satisfactory result (Fig. 9.14). Figs 9.14a and 9.14b

were obtained under the action of currents and waves, respectively. The relationships derived between the surface sediment erosion threshold and yield stress are both positive and significant (at a confidence level of 90%) for both the 152.5 μm and 215 μm sand admixtures.

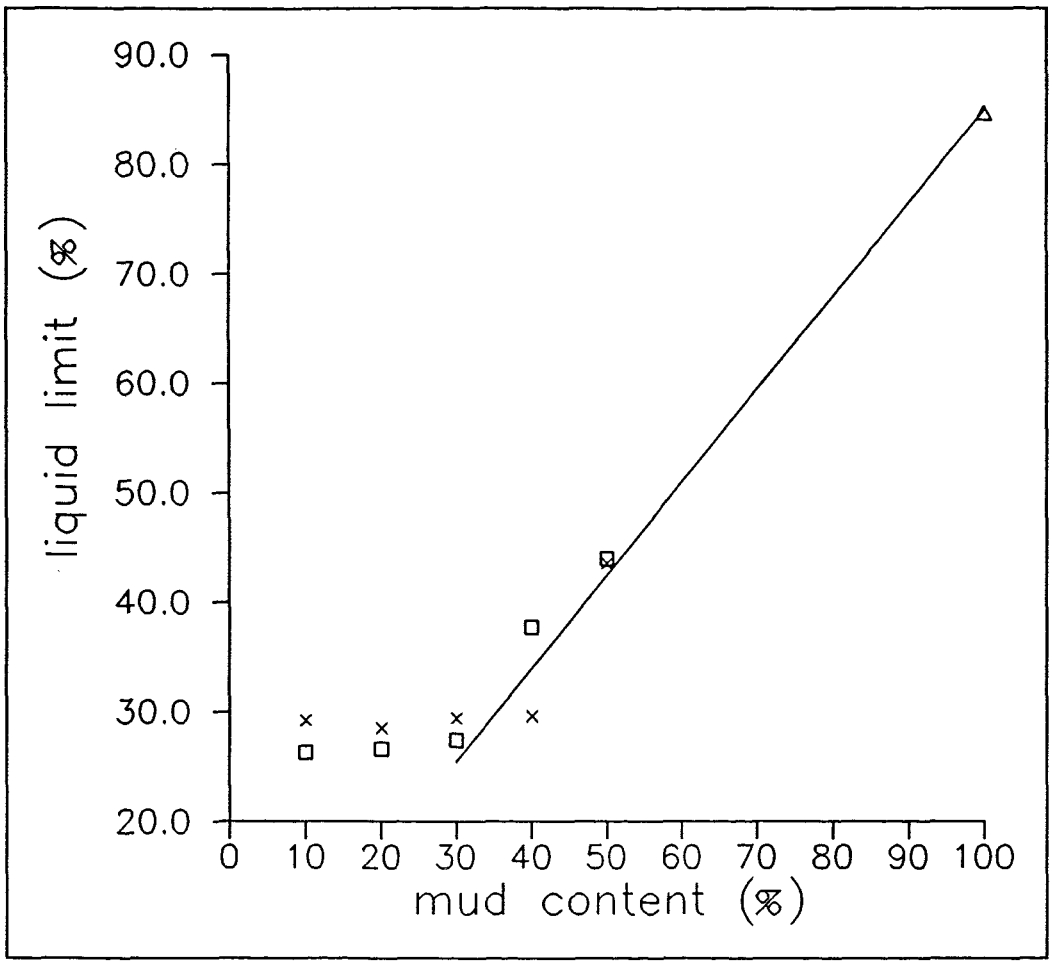

Fig. 9.1. Liquid limit variation with mud content, for sediments investigated for erodibility in the flume. Key: Solid line, 'linear mixture law' proposed by Tan *et al.* (1994); △, liquid limit of the mud; □, mixtures of 215 μm sand; and x, mixtures of 152.5 μm sand.

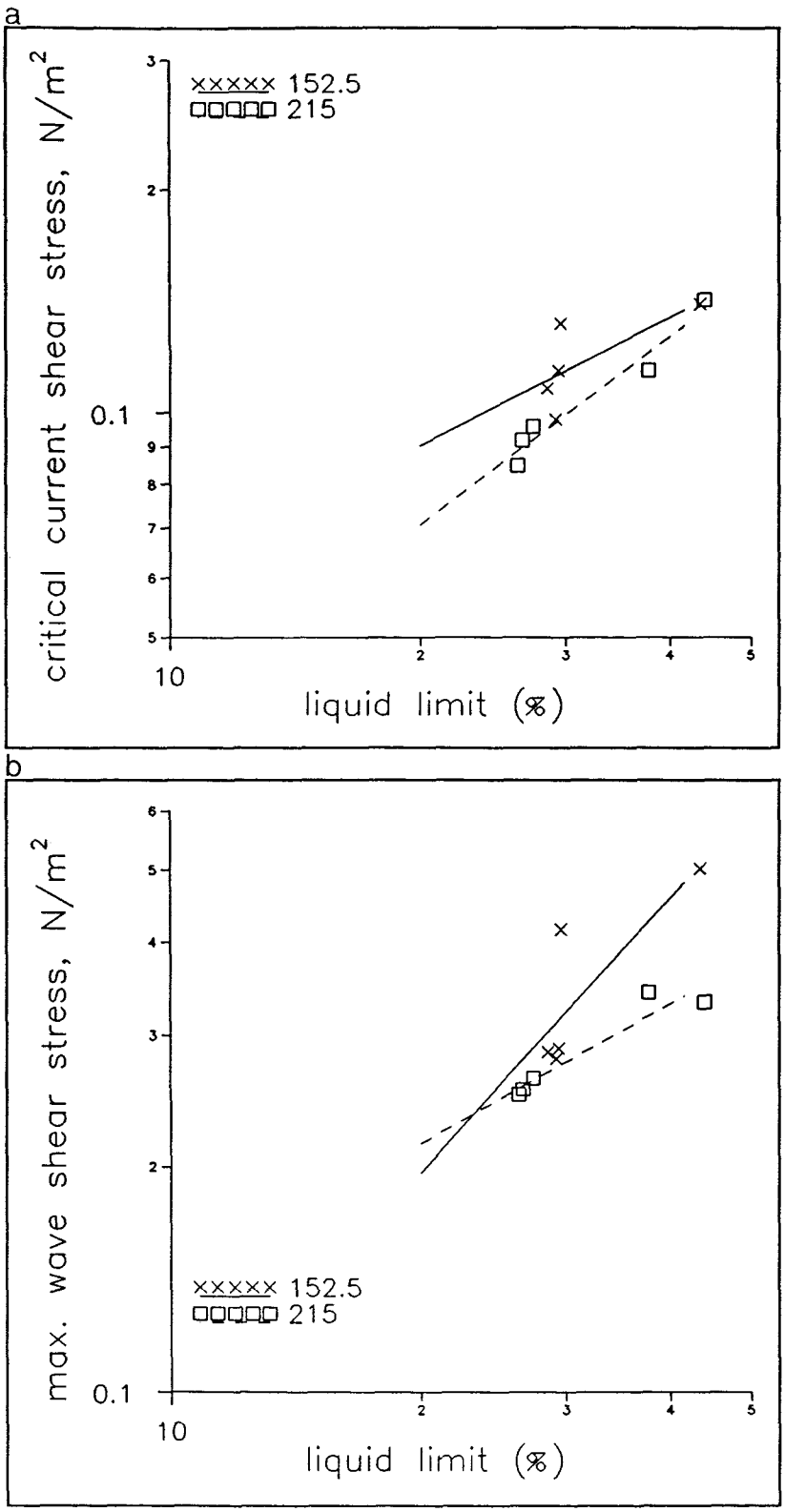

Fig. 9.2. Correlation between (a) critical current-induced shear stresses and (b) maximum critical wave-induced shear stresses (each data point corresponds to the mean critical wave-induced shear stress of the 4 used wave strokes), with the liquid limit of the mixtures. Key: □, mixtures of 215 μm sand; and x, mixtures of 152.5 μm sand.

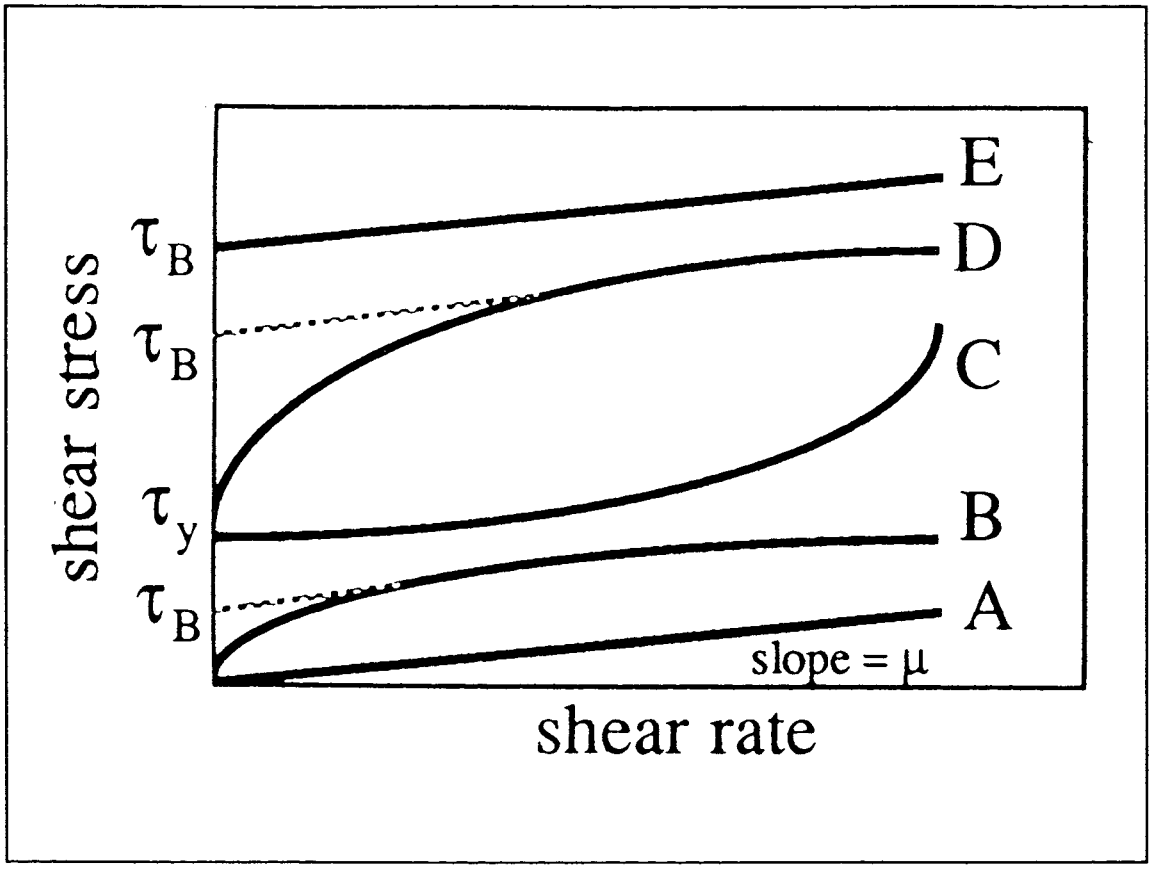

Fig. 9.3. Rheological models for flow behaviour (from Dade & Nowell, 1991).
Key: A—Curve representative of Newtonian viscous flow.
B—Curve which typifies shear-thinning, or pseudoplastic behaviour.
C—Curve representative of shear-thickening, or dilatant behaviour.
D-Curve which typifies a shear-thining material with true yield stress τ_y.
E—Curve which illustrates an ideal Bingham behaviour.

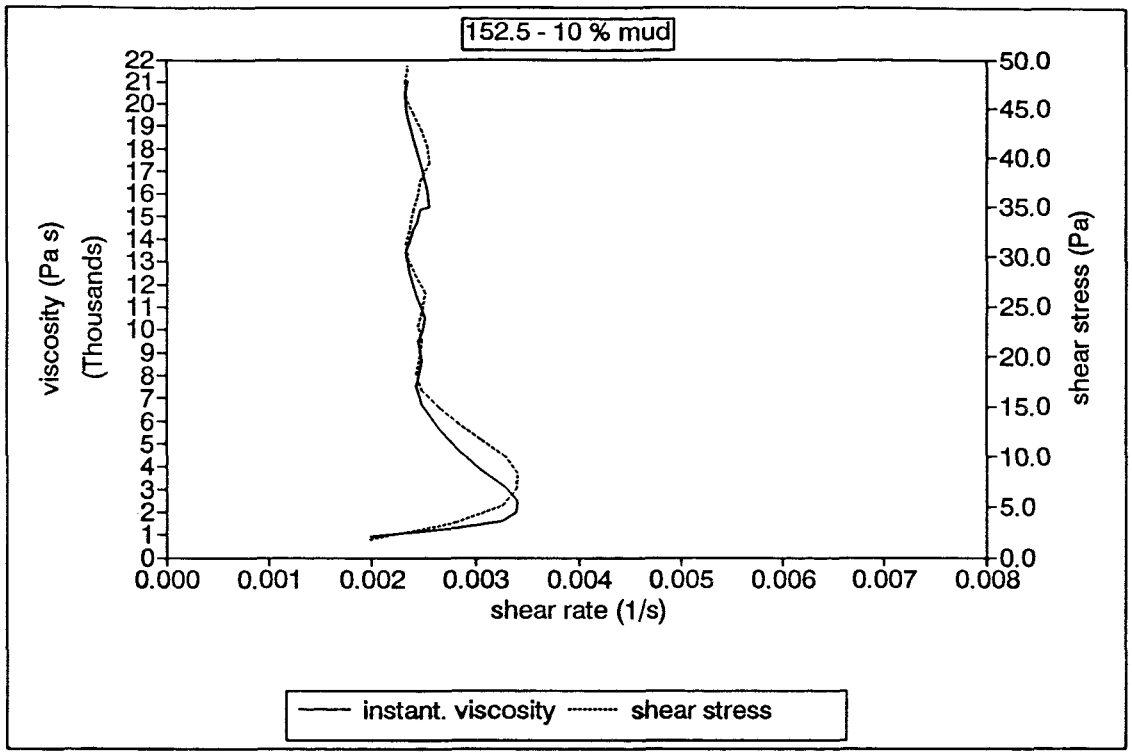

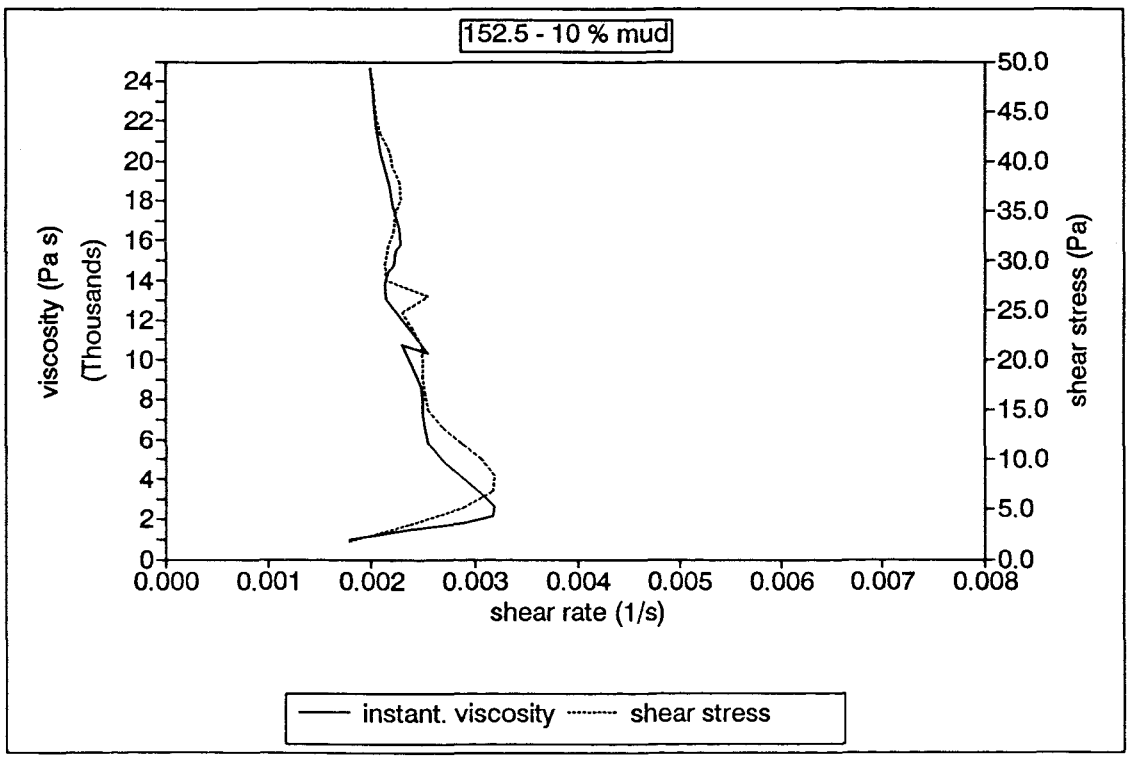

Fig. 9.4. Rheological curves for the 152.5 μm sand admixtures, containing 10% of mud.

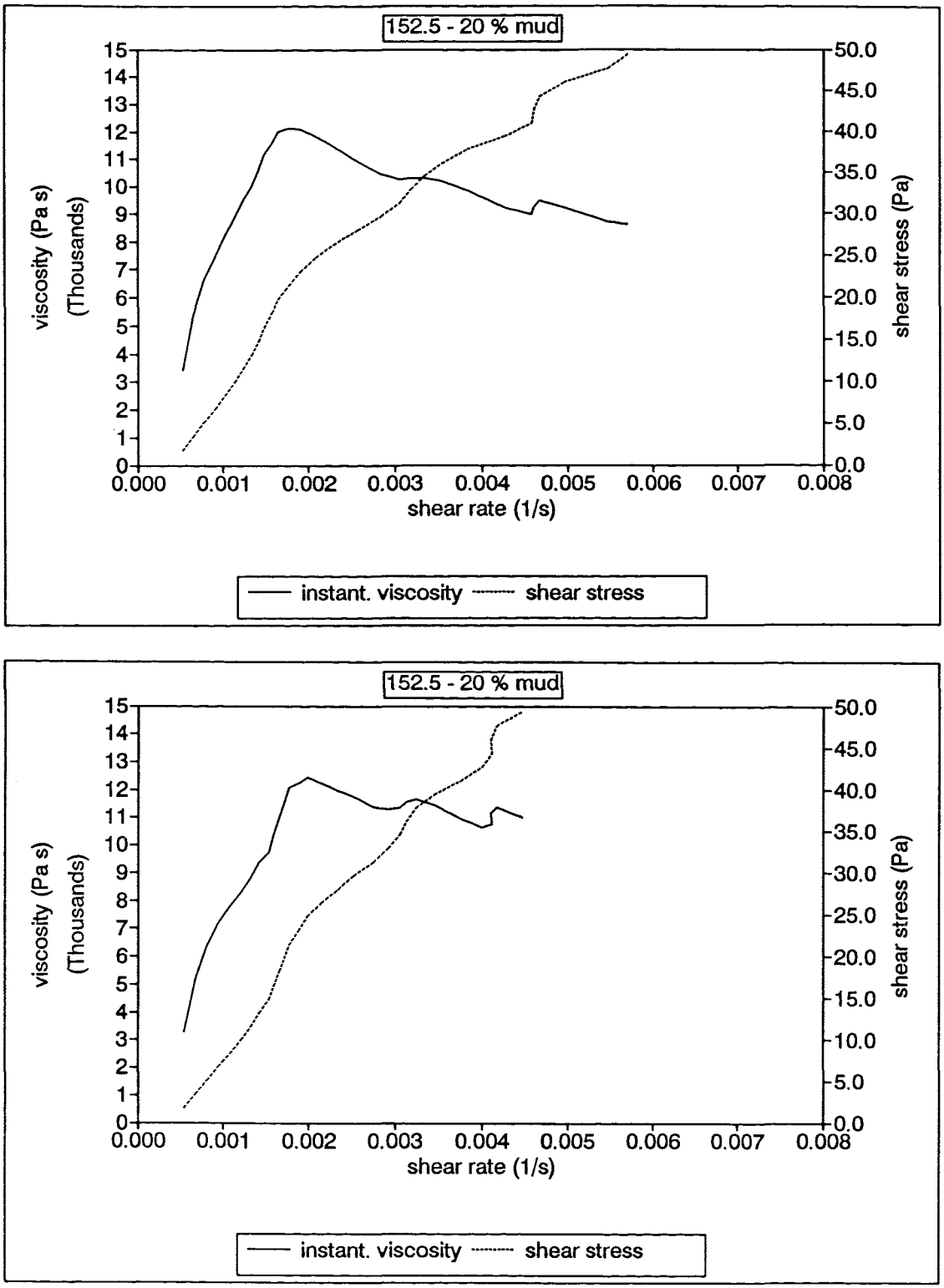

Fig. 9.5. Rheological curves for the 152.5 μm sand admixtures, containing 20% of mud.

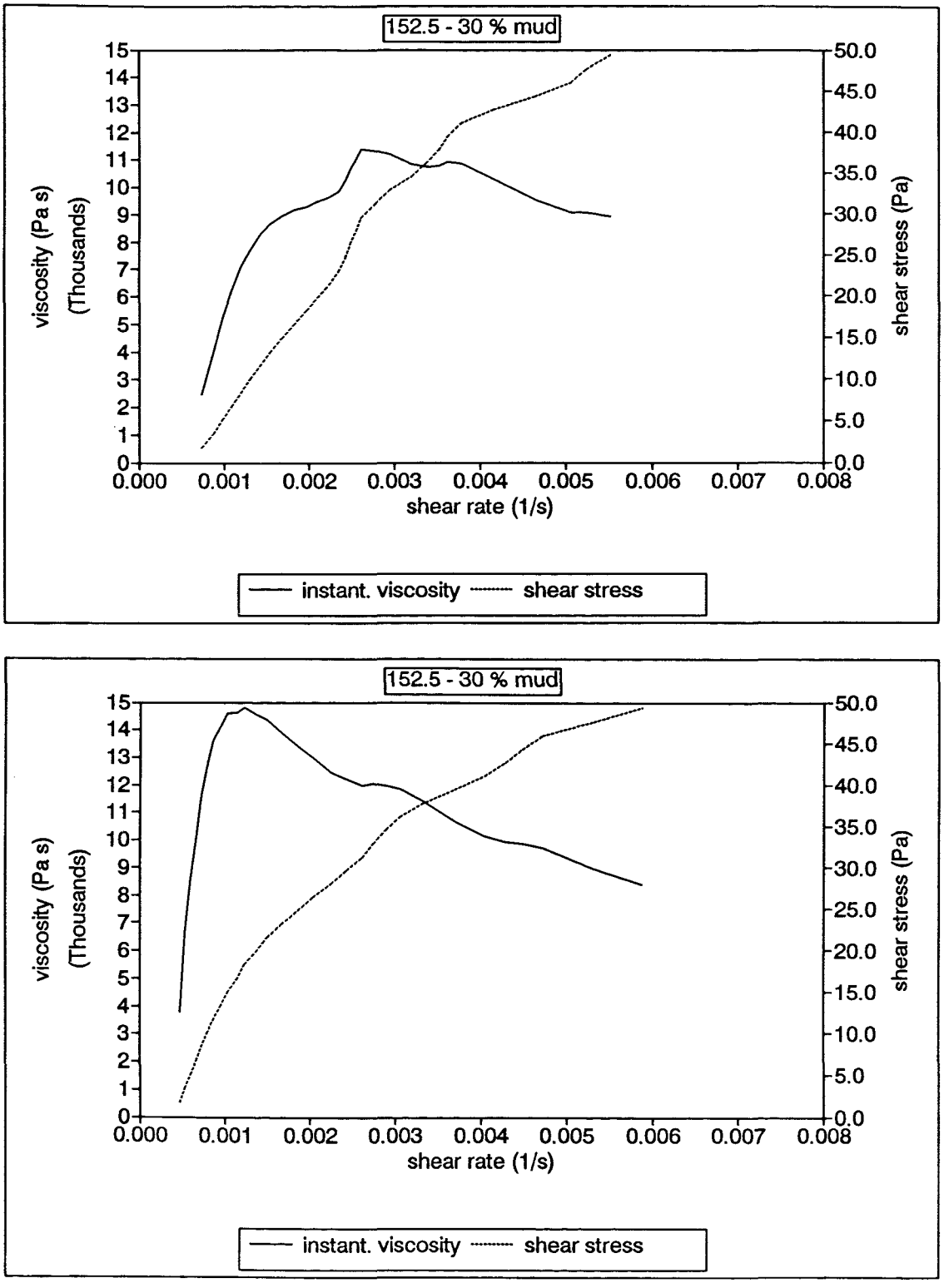

Fig. 9.6. Rheological curves for the 152.5 μm sand admixtures, containing 30% of mud.

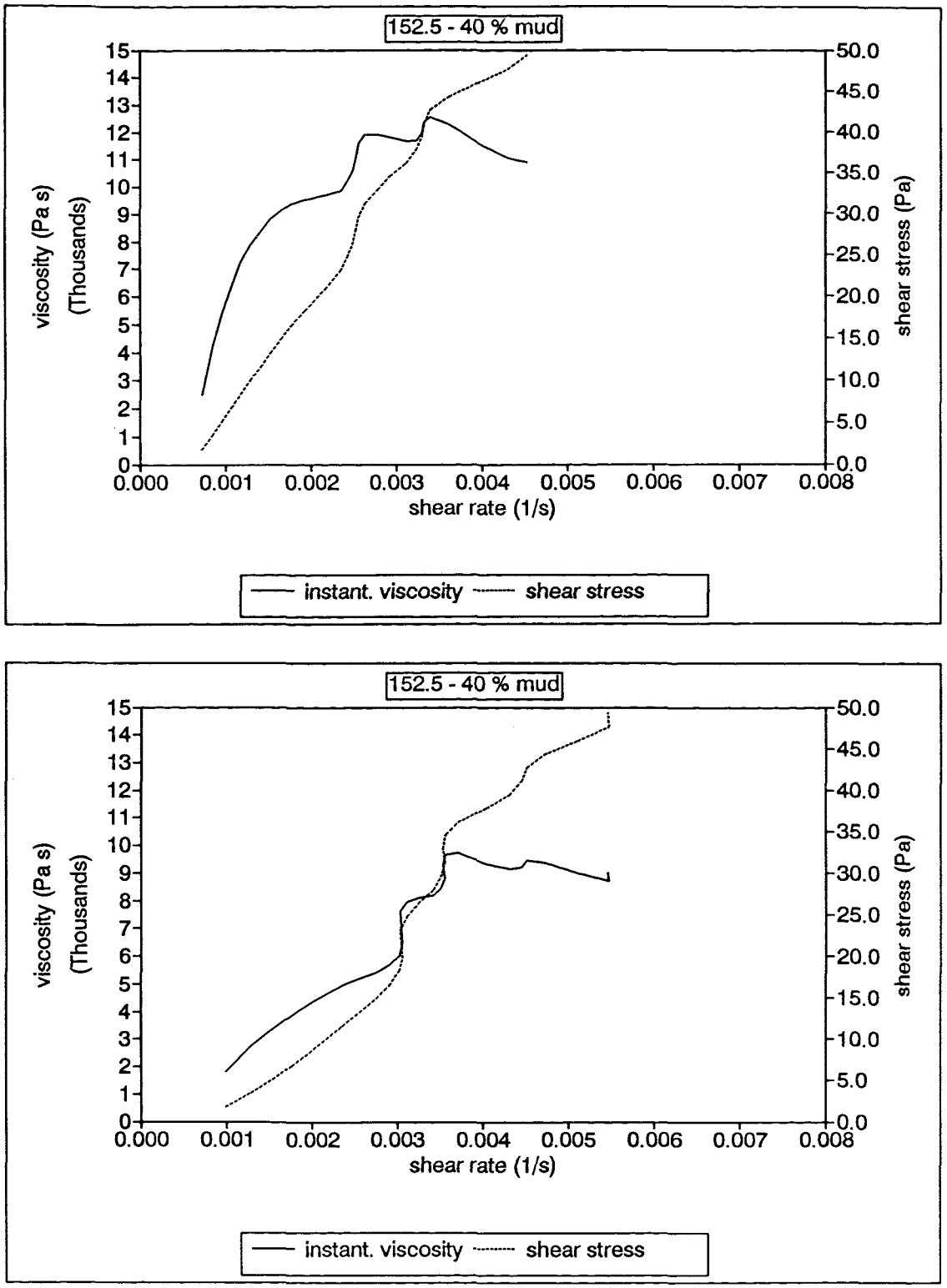

Fig. 9.7. Rheological curves for the 152.5 μm sand admixtures, containing 40% of mud.

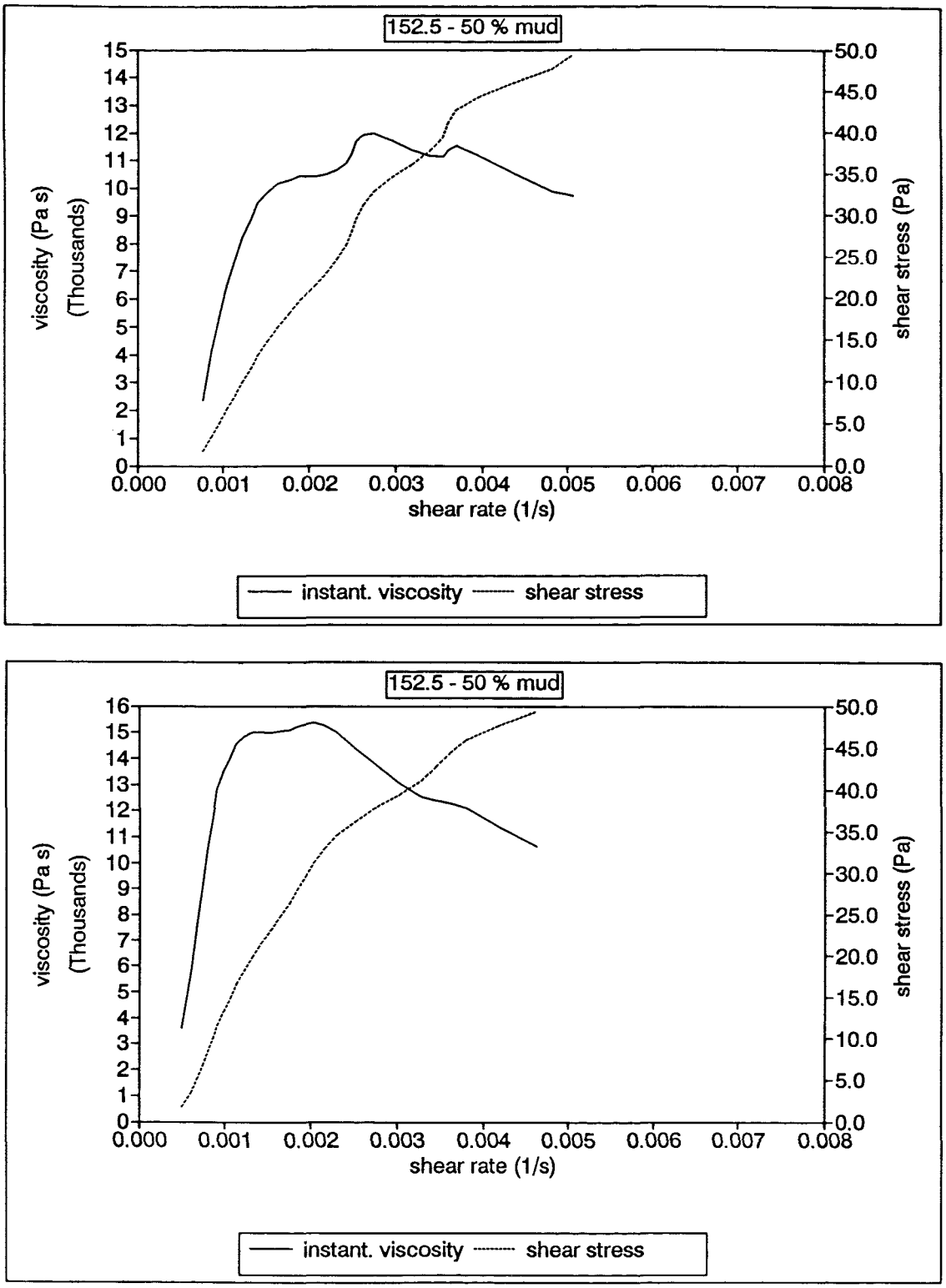

Fig. 9.8. Rheological curves for the 152.5 μm sand admixtures, containing 50% of mud.

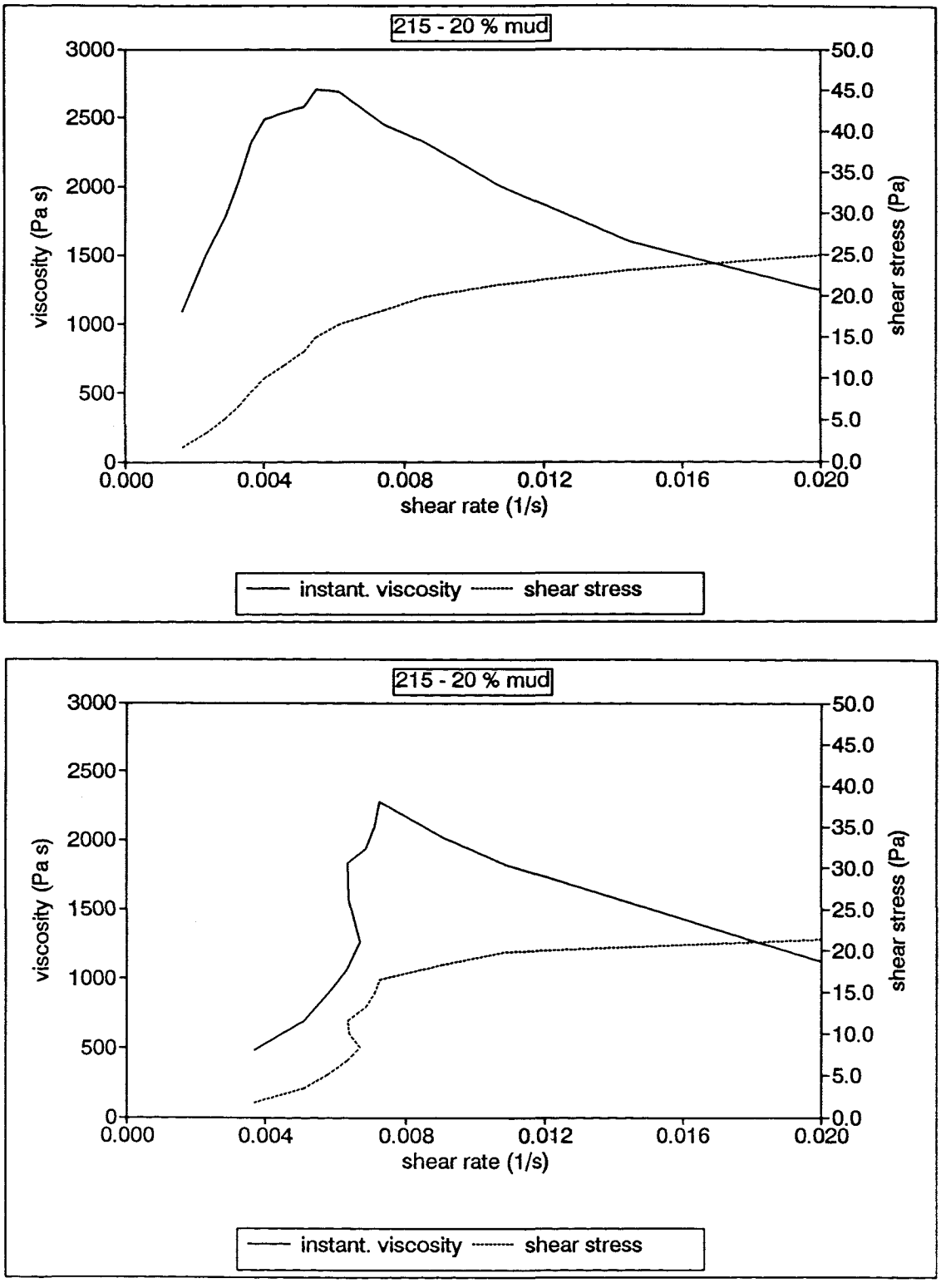

Fig. 9.9. Rheological curves for the 215 μm sand admixtures, containing 20% of mud.

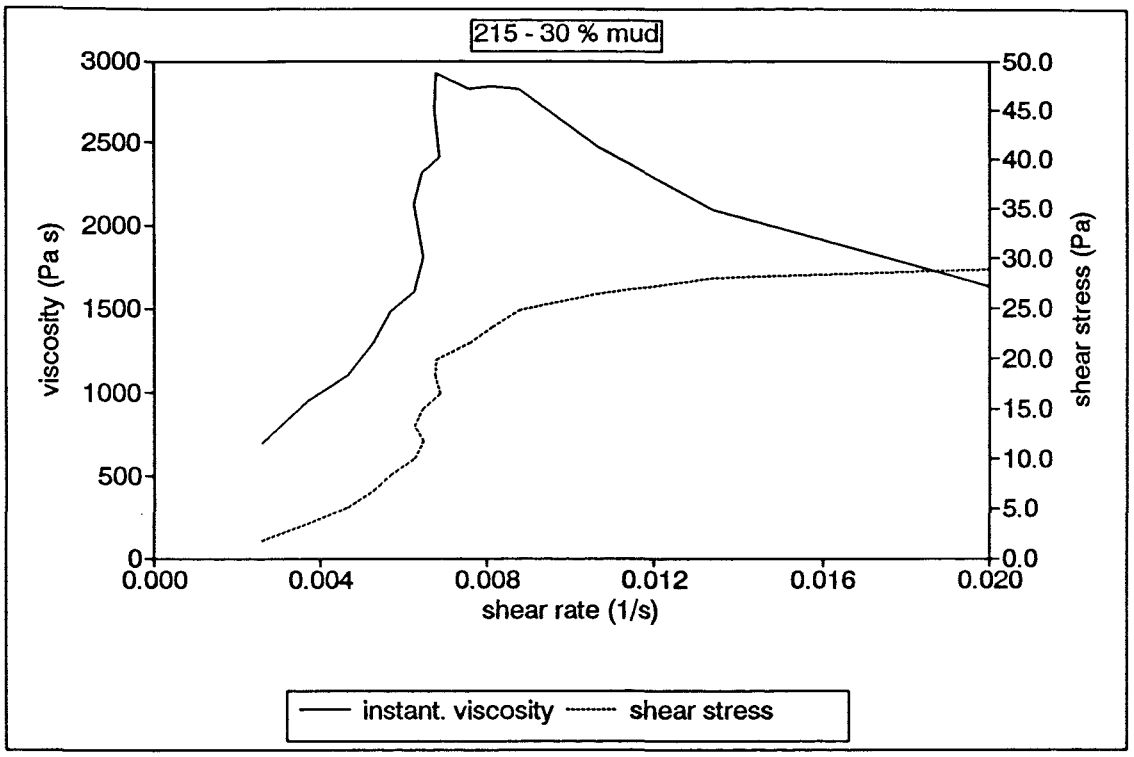

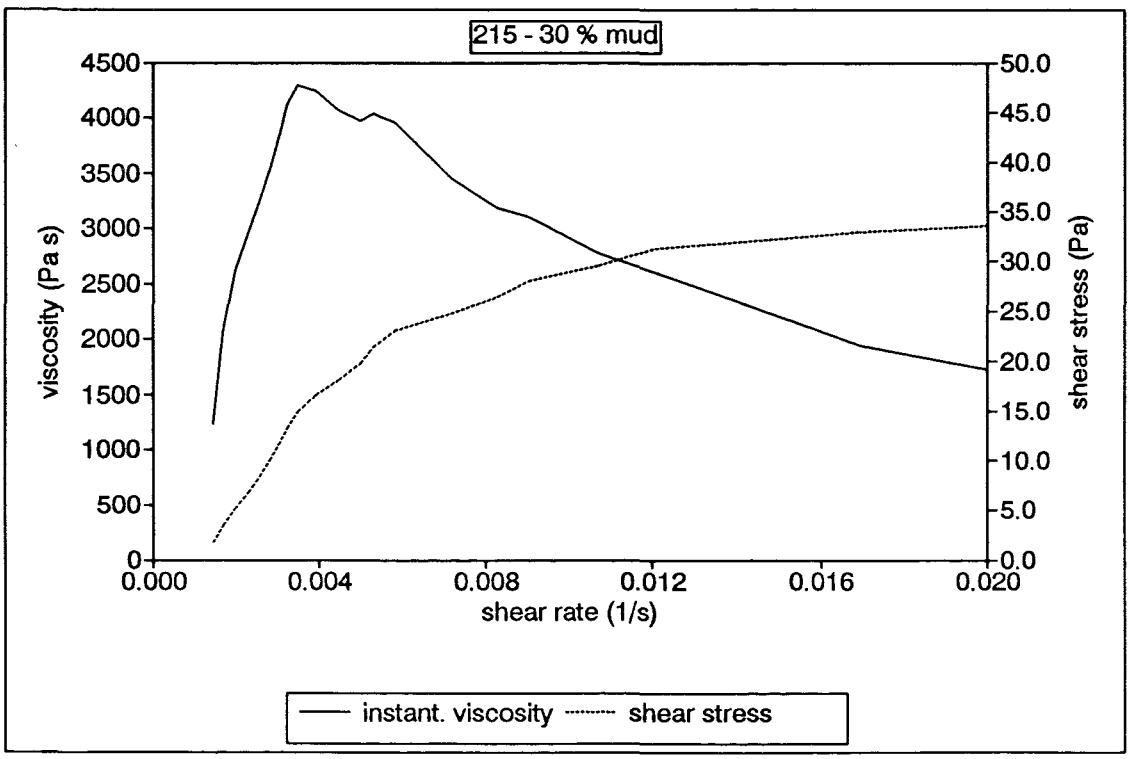

Fig. 9.10. Rheological curves for the 215 μm sand admixtures, containing 30% of mud.

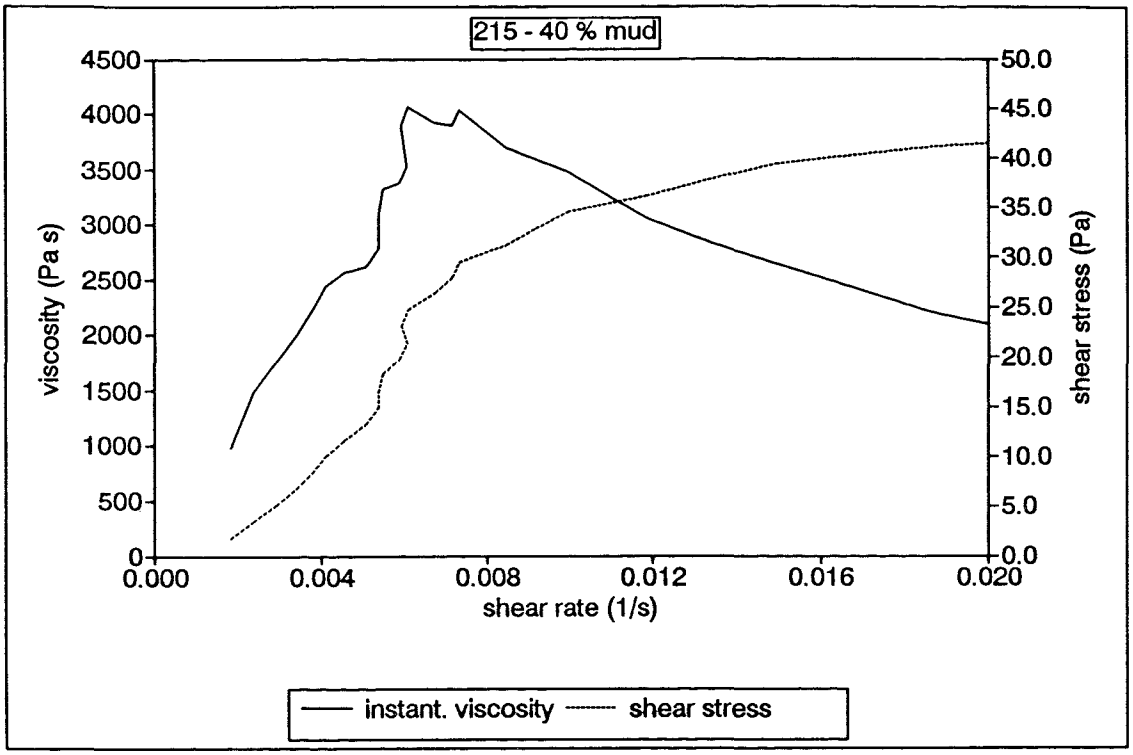

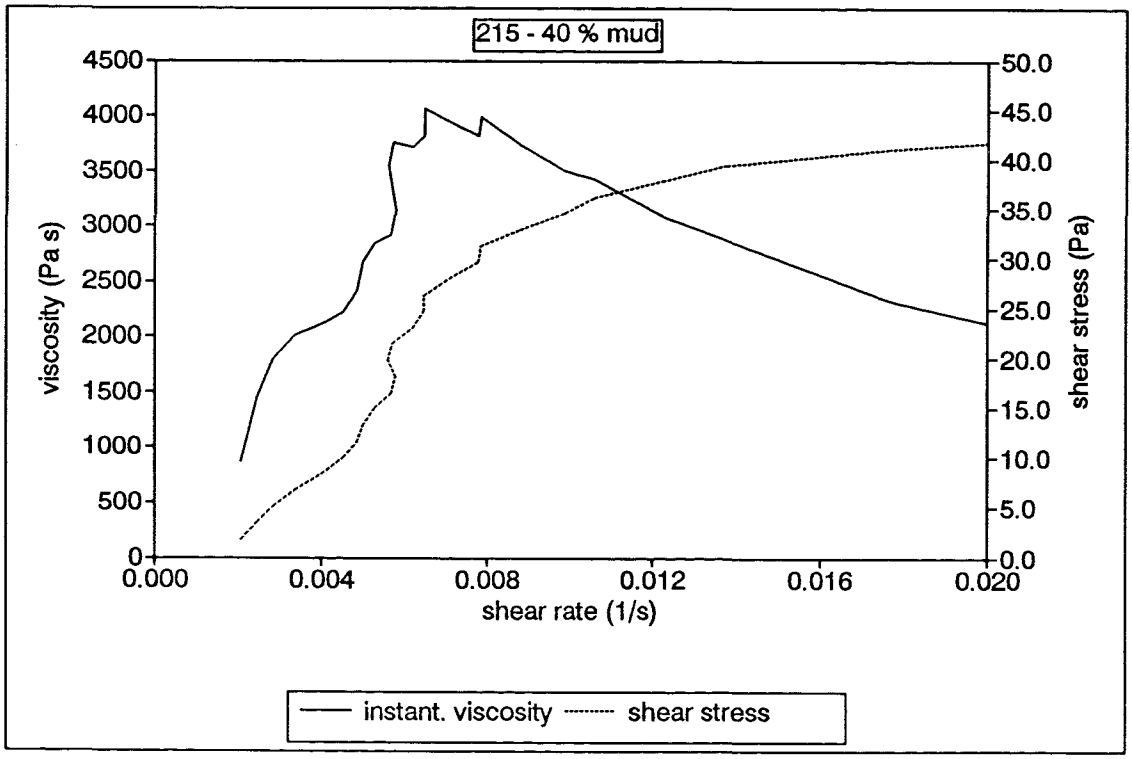

Fig. 9.11. Rheological curves for the 215 μm sand admixtures, containing 40% of mud.

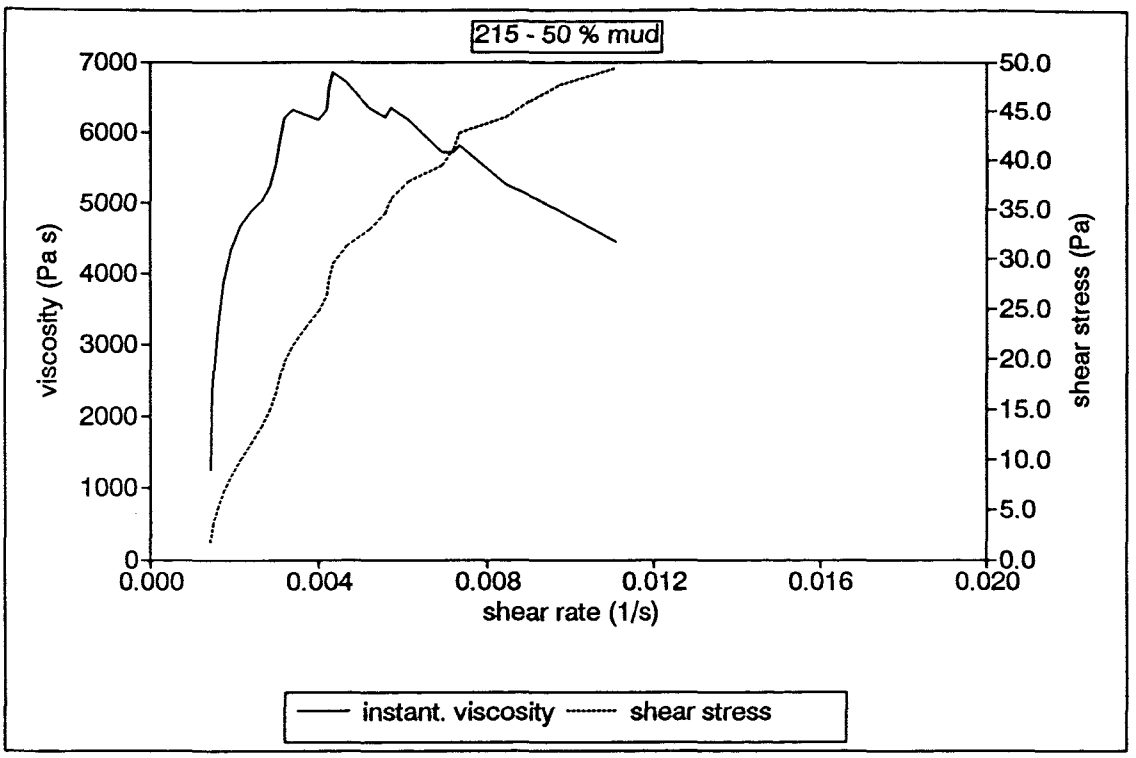

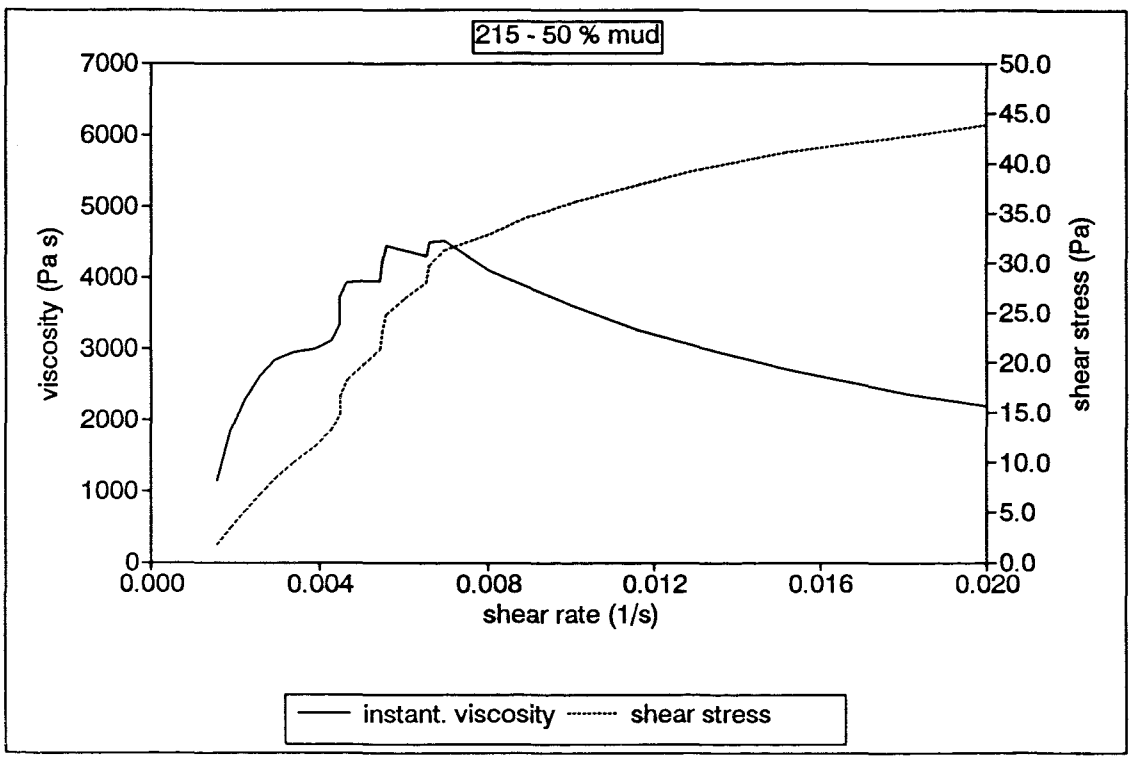

Fig. 9.12. Rheological curves for the 215 μm sand admixtures, containing 50% of mud.

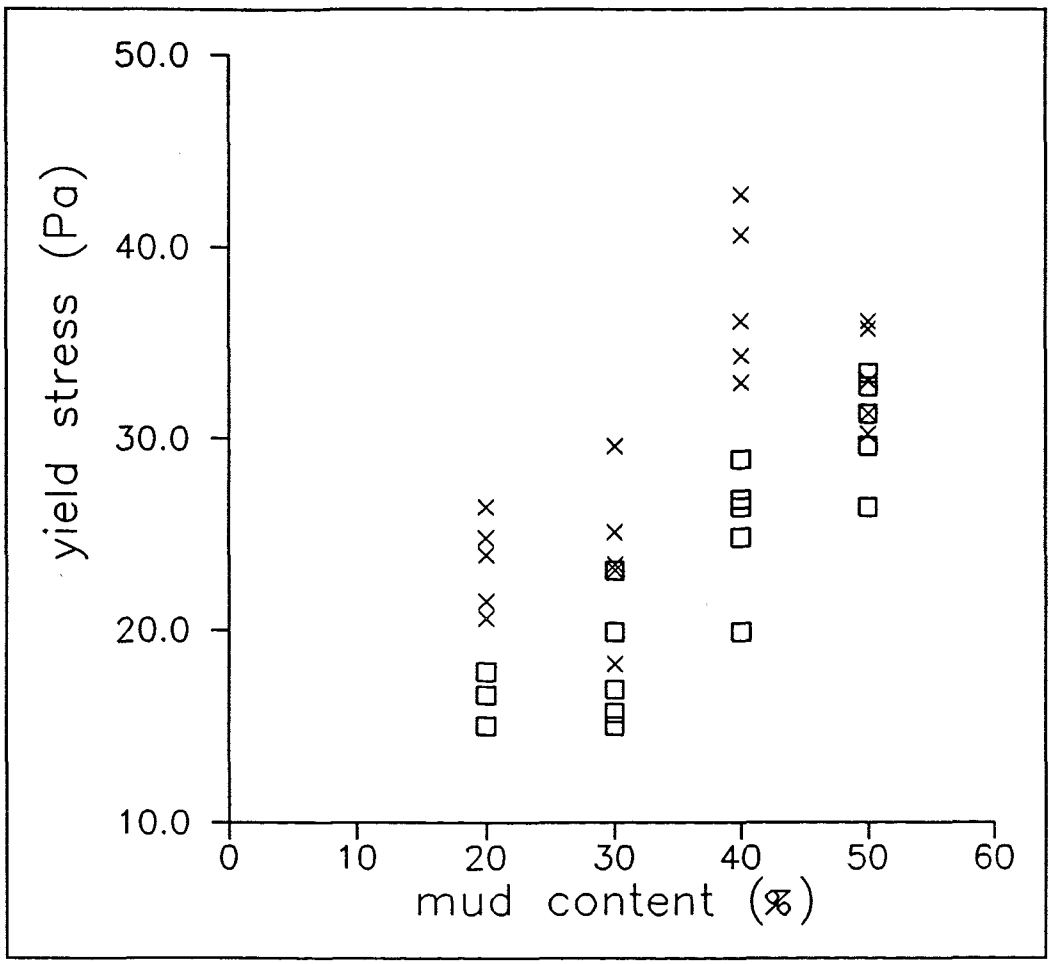

Fig. 9.13. Yield stress variation, with mud content, for sediments investigated for erodibility in the flume. Key: □, mixtures of 215 μm sand; and x, mixtures of 152.5 μm sand.

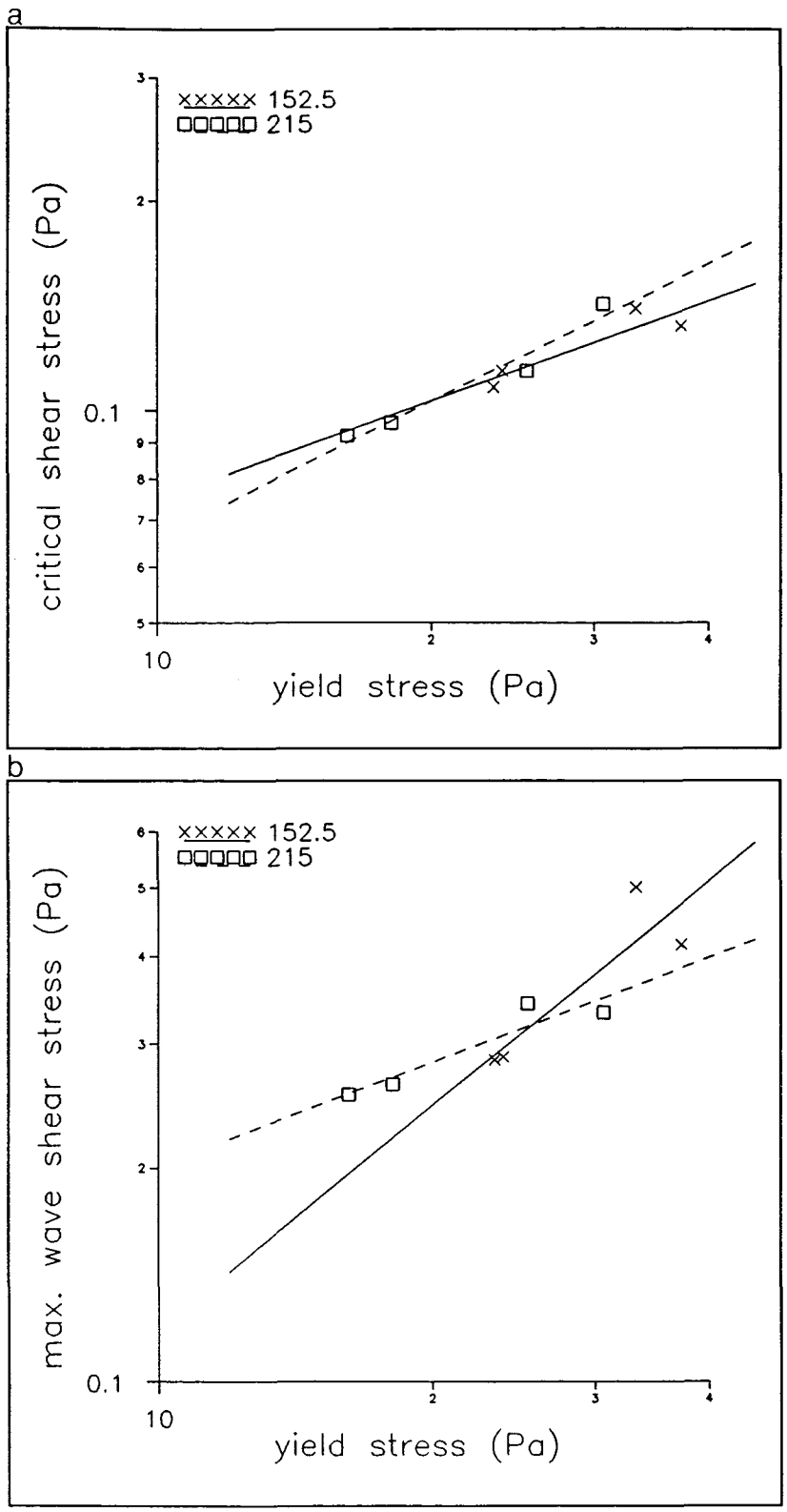

Fig. 9.14. Correlation between (a) critical current-induced shear stresses and (b) maximum critical wave-induced shear stresses with the yield stress of the mixtures. Wave-induced stress represents the mean value of the (4) wave strokes used whilst yield stress represents the mean value of 5 tests. Key: □, mixtures of 215 μm sands; and x, mixtures of 152.5 μm sands.

sand size (μm)	mud content (%)	YIELD STRESS DEFINITION - τ_y (Pa)						
		test 1	test 2	test 3	test 4	test 5	mean value	st. deviation
152.5	20	21.5	24.8	20.6	23.9	26.4	23.4	2.1
	30	29.6	23.1	20.2	23.4	25.1	24.3	3.1
	40	42.7	36.1	32.9	40.6	34.3	37.3	3.7
	50	33.0	31.3	35.7	30.2	36.1	33.3	2.3
215	20	15.0	16.6	15.0	16.6	17.8	16.2	1.1
	30	19.9	15.0	23.1	16.9	15.7	18.1	3.0
	40	24.8	26.4	19.9	28.9	26.8	25.4	3.0
	50	29.6	31.3	26.4	32.7	33.4	30.7	2.5

Table 9.1. Yield stress (τ_y) values obtained from the rheometer tests (for details, see text).

CHAPTER 10

CONCLUSIONS
AND
PROPOSALS FOR FUTURE RESEARCH

10. CONCLUSIONS AND PROPOSALS FOR FUTURE RESEARCH

10.1. CONCLUSIONS

The results obtained during the experiments described should be used with caution, when the shear strength (i.e. threshold of movement or liquid limit or yield stress) and pore water pressure response of natural marine sand-mud deposits have to be investigated. Clay mineral types, Ph and temperature of the eroding (ambient) fluid, the chemical properties of the pore and eroding fluids, internal sediment structure, degree of sediment saturation and biological activity also affect the establishment of the physical characteristics and properties of sediment mixtures. The conclusions which may be drawn from the results of the present investigation are outlined below.

(1) The critical current-induced shear stresses needed to displace fine-grained sand were increased by 2-90% with the addition of clay, although the bulk density of the sediments was reduced. The increase was 40-90% larger for clay quantities in excess of 11-14% (by dry weight).

(2) Sediment deposits subjected to high levels of stress history were more resistant (by a factor of 1.3) to erosion than beds unaffected by such activity. However, this process was more intense (by a factor of 1.7) for the muddiest of the deposits ($M > 40\%$), under the influence of rapid consolidation.

(3) Under oscillatory flow conditions, the critical erosion wave-induced orbital velocity is related linearly to mud contents (M) when the clay fraction is in excess of 11%. For clay contents $\leq 11\%$, the cohesive material does not affect the erodibility of the sediment deposits.

(4) The Komar & Miller (1973) formula which describes the critical erosion conditions for non-cohesive sediments, under the action of waves, can predict sufficiently the erosion behaviour of mixtures with $M \leq 30\%$.

(5) The erodibility of fine-grained sediment beds is more difficult (by a factor of 3) under laminar wave flows, than under turbulent steady currents.

(6) Within a combined flow regime, for specific wave conditions, an increase in clay content causes a linear increase in the erosion threshold speed of the superimposed unidirectional current.

(7) Within a combined flow regime, the wave boundary layer acts as a protective barrier for the sediment bed; this opposes the competence of the overlaying steady current component to erode. Wave boundary layers associated with short period waves (6 s) are more stable than those associated with larger periods (10 s). Thus, approximately 40% higher steady flows are required for the dislodgment of sediment particles.

(8) Under all flow conditions, the mixtures consisting of the larger grain-sized sands demonstrate 15% (in an average) less resistance to erosion.

(9) With $M > 30\%$, the influence of clay on the pore pressure response of the sandy deposits is considerable. The amplitudes of the pore water pressure fluctuations are reduced significantly (maximum reduction of 50-60%), within the upper 20 mm of the sediment bed. Such a reduction is greater for the higher wave frequencies and the larger near-bed wave amplitudes.

(10) Under combined flow conditions, pore pressure

dampening is enforced further by the action of the unidirectional current component.

(11) The pore pressure amplitude is not related to the threshold of movement of the sediments.

(12) The bulk shear strength of the sediments, as represented by their liquid limit, increases abruptly following the 'linear mixture law' as suggested by Tan *et al.* (1994); this occurs when clay content exceeds a limit of 11-14 % (see above).

(13) There is a positive and significant linear correlation between the liquid limit and the critical erosion shear stresses for the 215 μm sand admixtures, obtained under unidirectional and oscillatory flow conditions.

(14) Rheological examination of the sediments showed a increase in the yield stress, with the mud content. Further, significant shear-thinning behaviour, together with a distinct increase (55%) in yield stress, were observed for the muddier mixtures (M > 30%).

(15) Relationships between yield stress and erosion threshold shear stresses, obtained under steady and wave flows, have been derived.

10.2. PROPOSALS FOR FUTURE RESEARCH

10.2.1. Experimental Apparatus Improvements

(a) Pressure sensors

The pressure sensor system has two types of noise associated with it: (i) a variable offset; and (ii) noise

within the signal, caused by the interconnecting equipment i.e. analogue apparatus, power supply, cables, transformers etc.

The transducers have an inherent noise level equivalent to 0.01 cm of pressure head. The accuracy of the final signal is required to be within 0.02 cm of pressure head, if pore pressure measurements at small depths (in a few cm) have to be undertaken.

During the present study the offset varied over several millimetres of pressure head, whilst the final signal noise ranged from 0.04 to 0.06 cm of pressure head. For future measurements both problems should be solved, in order to obtain reliable results.

(b) Video system

The existing video system has a major limitation; this is that, due to the oblique viewing angle, the camera does not provide an accurate definition of the area of interest of the sediment bed. Consequently, the system needs to be improved.

Indeed, it would be relatively easy to mount the camera immediately above the area of interest. Similarly, there are no difficulties in moving the tracking mechanism to above the flume, rather than alongside the channel. A problem arises in viewing the sediment bed through the water surface. However, two solutions present themselves: (a) to construct a simple glass window i.e a 'glass bottomed boat' effect, which may cause problems by having a restricted channel for the water to flow through and lead to an increase in the flow velocity; and (b) the use of a waterproof camera mounted just below the water surface. With either of the solutions, a suitable lens

should be used which allows the full definition of the camera to be concentrated upon the area of interest.

The above modifications are readily achievable.

(c) Filter for reservoir tanks

The sediments investigated in the flume inevitably cause contamination of the flume's water reservoir. Two suggestions may be put forward to improve the situation.

Firstly, the placement of a 63 μm (plankton) net over the outlet to the flume, reaching to the base of the reservoir, to retain any sand-size or larger material. Secondly, the use of a separate pump and filter system to filter continuously the flume water; this will prevent the build-up of the finer-grained material within the recirculating water supply.

Both of the propositions are inexpensive and can be implemented relatively easily.

(d) Wires

The system of wires connecting the crank system to the oscillating plate could, to some advantage, be changed to an alternative material. The existing material consists of stainless steel wire rope. This material is resistant to bending around the relatively small pulley blocks and has considerable mass. The result is that, at low speeds, the oscillating plate 'snatches' due to the energy required to overcome the bearings and the vibration of the long unsupported run of cable along the top of the flume.

The existing wire ropes could be replaced by Kevlar rope;

this is lightweight, strong and very resistant to stretching. Likewise, the long unsupported run could be reduced with a series of supporting pulleys.

This change could be instituted rapidly, at only minimal expense.

(e) The 'standing wave effect'

The resonance phenomena (see Section 7.1.1), between the oscillating plate and the overlying water mass, can sometimes produce standing waves; these could be the source of significant experimental error in the data obtained. Hence, in order that these effects are minimised two solutions may be suggested.

Firstly, the oscillating plate fronts must be reconstructed, resulting in an improved hydrodynamic design offering minimum resistance to the water flow conditions. In addition, the plate thickness should be reduced. Secondly, the tail gate which regulates the height of the water column inside the flume channel, should be replaced by a new one made from porous material. In this way, standing wave energy could be absorbed significantly.

10.2.2. Proposed Experiments

The tests undertaken in the present study were all carried out using mud fractions characterised by certain chemical and physical characteristics and collected from the same field location (Severn Estuary). Therefore, in order for the identified trends to be validated, further experimental work is needed on mixtures containing muds from different locations i.e. river banks, estuaries/intertidal flats, and shallow and deep marine

environments. Further, the sand component used in the mixtures could be of medium or coarse grain size. Finally, emphasis must be place upon the performance of experiments under oscillatory and combined flow conditions, since the present stage of knowledge in this particular area is very limited.

In order to minimise the variables which affect the behaviour of sand-mud mixtures, all the experiments carried out in the present study have been with beds which have been created artificially in the laboratory environment. This approach has resulted in beds incorporating two distinct grain sizes (mud and sand), rather than a broader ranging grain size distribution. Therefore, although great care has been taken to simulate real environmental conditions, this is not always possible. Thus, it is recommended that further measurements are undertaken in the field, in order to investigate the behaviour of sand and mud mixtures in the natural environment.

REFERENCES

REFERENCES

AGNEW, R. (1965) A two layer theory for unsteady flow. *Proc. 2nd Australas. Conf. Hydraul. Fluid Mech.*, **51**, 137-157.

ANDO, K. & YAMAMOTO, T. (1991) Measurements of bond energy of clays and ocean wave attenuation. In: *Microstructures of Fine-Grained Sediments: From Mud to Shale* (Ed. by R.H. Bennett, W.R. Bryant & M.H. Hulbert), Springer, New York, 389-394.

ARULANANDAN, K., LAGANATHAN, P. & KRONE, R.B. (1975) Pore and eroding fluid influences on surface erosion of soil. *Proc. A.S.C.E.*, **101(GTI)**, 51-66.

AXE, P. & COLLINS, M.B. (1993) South coast mobility study: Preliminary report to Hydraulics Research, Wallingford. *Tech. Report SUDO/TEC/93/2C*, University of Southampton.

BAGNOLD, R.A. (1946) Motion of waves in shallow water: Interaction of waves and sand bottoms. *Proc. R. Soc. London*, **A187**, 1-15.

BAKKER, W.T. (1974) Sand concentration in oscillatory flow. *Proc. 14th Conf. Coastal Engng*, A.S.C.E., Copenhagen, 1129-1148.

BEEN, K. & SILLS, G.C. (1985) Self-weight consolidation of soft soils: An experimental and theoretical study. *Geotechnique*, **31**, 519-535.

BIJKER, E.W. (1966) The increase of bed-shear in a current due to wave motion. *Proc. 10th Conf. Coastal Engng*, A.S.C.E., Tokyo, 746-765.

BJERRUM, L. (1973) Geotechnical problems involved in foundations of structures in the North Sea. *Geotechnique*, **23(3)**, 319-358.

BLATT, G., MIDDLETON, G. & MURRAY, R. (1980) *Origin of Sedimentary Rocks*. Prentice-Hall Inc., New Jersey, 782 pp.

BONNEFILE, R.L. & PERNECKER, L. (1966) Le debut d'entrainement des sediments sous l'action de la houle. *Bull. C.E.R.C.*, **15**, 27-32.

BREVIK, I. (1980) Flume experiments on waves and currents: smooth bed. *Coastal Engng*, **4**, 89-110.

B.S. 1377 (1975) *Methods of Testing Soils for Civil Engineering Purposes*. British Standards Inst., London, 143 pp.

CARLING, P.A. (1983) Threshold of coarse sediments transport in broad and narrow natural streams. *Earth Surf. Process. Landforms*, **8**, 1-18.

CARLSON, E.J. & ENGER, P.F. (1963) Studies of tractive forces of cohesive soils in earth canals. *U.S. Bureau Reclamation, Hydraul. Branch Report*, Denver, **504**.

CARSTENS, M.R., NEILSON, F.M. & ALTINBILEU, H.D. (1969) Bed forms generated in the laboratory under an oscillatory flow: Analytical and experimental study. *U.S. Army C.E.R.C., Tech. Memo 28*.

CEBECI, T. (1977) Calculation of unsteady two-dimensional laminar and turbulent boundary layers with fluctuations in external velocity. *Proc. R. Soc. London*, **A355**, 225-238.

CHAN, K.W., BAIRD, M.H.I. & ROUND, G.F. (1972) Behaviour of dense particles in a horizontally oscillating liquid. *Proc. R. Soc. London*, **A330**, 537-559.

CHEPIL, W.S. (1959) Equilibrium of soil grains at the threshold of movement by wind. *Proc. Soil Sci. Soc. Am.*, **23**, 422-438.

CHEPIL, W.S. (1961) The use of spheres to measure lift and drag on wind-eroded soil grains. *Proc. Soil Sci. Soc. Am.*, **25**, 343-345.

CHIOU, W.A., BRYANT, W.R. & BENNETT, R.H. (1991) Clay fabric of gassy submarine sediments. In: *Microstructures of Fine-Grained Sediments: From Mud to Shale* (Ed. by R.H. Bennett, W.R. Bryant & M.H. Hulbert), Springer, New York, 333-352.

CHRISTENSEN, B.A. (1975) On the stochastic nature of scour initiation. *Proc. 15th Congr. I.A.H.R.*, **2**, 65-72.

CHRISTOFFERSEN, J.B. & JONSSON, I.G. (1985) Bed friction and dissipation in a combined current and wave motion. *Ocean Engng*, **12(5)**, 387-423.

CLAUSER, F.H. (1956) *The Turbulent Boundary Layer*. Adv. Appl. Mech., **4**.

COKELET, E.D. (1977) Steep gravity waves in water of arbitrary uniform depth. *Philos. Trans. R. Soc. London*, **A286**, 183-230.

COLEMAN, N.L. (1981) Velocity profiles with suspended sediment. *J. Hydraul. Res.*, **19(3)**, 211-229.

COLLINS, J.I. (1964) Effect of currents on mass transport of progressive water waves. *J. Geophys. Res.*, **69(6)**, 1051-1056.

COLLINS, M.B. & RIGLER, J.K. (1982) The use of settling velocity in defining the initiation of motion of heavy mineral grains under unidirectional flow. *Sedimentology*, **29**, 419-426.

CRABTREE, R.W. (1988) A classification of combined sewer sediment types and characteristics. *Water Res. Centre Pub.*, UK.

DADE, W.B. & NOWELL, A.R.M. (1991) Moving muds in the marine environment. *Proc. COASTAL SEDIMENTS '91*, A.S.C.E., Seattle, 54-71.

DADE, W.B., NOWELL, A.R.M. & JUMARS, P.A. (1992) Predicting erosion resistance of muds. *Marine Geology*, **105**, 285-297.

DAVIES, A.G. & WILKINSON, R.H. (1977) The movement of non-cohesive sediment by surface water waves, Part 1: Literature survey. *Inst. Oceanographic Sci, Report 45.*

DEAN, R.G. (1974) Evaluation and development of water wave theories for engineering application. *C.E.R.C. Spec. Report 1.*

DEAN, R.G. & DALRYMPLE, R.A. (1992) *Water Wave Mechanics for Engineers and Scientists.* Adv. Ser. Ocean Engng, **2.**

DE RAAF, J.F.M. & BOERSMA, J.R. (1971) Tidal deposits and their sedimentary structures (seven examples from western Europe). *Geologie en Mijnbouw*, **50(3)**, 479-504.

DINGLER, J.R. (1975) *Wave Formed Ripples in Nearshore Sands.* Ph.D. Thesis, University of California San Diego.

DUNN, I.S. (1959) Tractive resistance of cohesive channels. *Proc. A.S.C.E.*, **85(SM3)**, 1-24.

DURRIEU DE MADRON, X., NYFFELER, F., GODET, C.H. (1990) Hydrographic structure and nepheloid spatial distribution in the gulf of Lions Continental Margin. *Cont. Shelf Res.*, **10**, 915-931.

DYER, K.R. (1986) *Coastal and Estuarine Sediment Dynamics.* Wiley-Interscience, Chichester, 342 pp.

EAGLESON, P.S. & DEAN, R.G. (1959) Wave-induced motion of bottom sediment particles. *Proc. A.S.C.E., J. Hydraul.*, **85(HY10)**, 53-79.

FAAS, R.W. (1991) Rheological boundaries of mud: Where are the limits? *Geo-marine letters*, **11**, 143-146.

FENTON, J.D. & ABBOTT, J.E. (1977) Initial movement of grains on a stream-bed: the effect of relative protrusion. *Proc. R. Soc. London*, **A352**, 523-537.

FLAXMAN, E.M. (1963) Channel stability in undisturbed cohesive soils. *Proc. A.S.C.E.*, **89(HY2)**, 87-96.

FODA, M.A. & TZANG, S.Y. (1994) Resonant fluidisation of silty soil by water waves. *J. Geophys. Res.*, **99(C10)**, 20463-20475.

FOLK, R.L. (1974) *Petrology of Sedimentary Rocks*. Hemphill, Texas, 188 pp.

GARDNER, W.D. (1989) Periodic resuspension in Baltimore Canyon by focusing of internal waves. *J. Geophys. Res.*, **94**, 18185-18194.

GEORGE, C.B. & SLEATH, J.F.A. (1978) Oscillatory laminar flow above a rough bed. *Proc. 16th Conf. Coastal Engng*, A.S.C.E., Hamburg, 898-910.

GIBBS, H.J. (1962) A study of erosion and tractive force characteristics in relation to soil mechanics properties. *U.S. Bureau Reclamation, Report Em-643*.

GODDET, J. (1960) Etude du debut d'entrainement des materiaux mobiles sous l'action de la houle. *La Houille Blanche*, **15**, 122-135.

GRAF, W.H. & PAZIS, G.C. (1977) Les phenomenes de deposition et d'erosion dans un canal d'alluvionnaire. *J. Hydraul. Res.*, **15**, 151-165.

GRANT, W.D. & MADSEN, O.S. (1979) Combined wave and current interaction with a rough bottom. *J. Geophys. Res.*, **84(C4)**, 1797-1808.

GRASS, A.J (1970) The initial instability of fine sand. *Proc. A.S.C.E.*, **96(HY3)**, 619-632.

GRISSINGER, E.H., LITTLE, W.C. & MURPHEY, J.B. (1981) Erodibility of streambank materials of low cohesion. *Trans. A.S.A.E.*, **24(3)**, 624-630.

GUST, G. (1976) Observations on a turbulent-drag reduction in dilute suspension of clay in sea-water. *J. Fluid Mech.*, **75**, 29-47.

HALLERMEIER, R.J. (1982) Oscillatory bed-load transport: Data review and simple formulation. *Cont. Shelf Res.*, **1(2)**, 159-190.

HAMMOND, T.M. & COLLINS, M.B. (1979) The design and use of an oscillating trolley wave simulator, for installation in unidirectional flow flumes. *Estuarine Coastal Marine Sci.*, **9**, 801-811.

HEATHERSHAW, A.D. (1974) Bursting phenomena in the sea. *Nature*, **248**, 394-395.

HEDGES, T.S. (1986) *Coastal and Offshore Engineering: Wave Theories*. Course Notes, Dept. Civ. Engrs, University of Liverpool.

HINO, M., SAWAMOTO, M. & TAKASU, S. (1976). Experiments on transition to turbulence in an oscillatory pipe flow. *J. Fluid Mech.*, **75**, 193-207.

HINO, M., KASHIWAYANAGI, M., NAKAYAMA, A. & HARA, T. (1983) Experiments on the turbulence statistics and the structure of a reciprocating oscillatory flow. *J. Fluid Mech.*, **131**, 363-400.

HJULSTROM, F. (1935) The morphological activity of rivers as illustrated by River Fyris. *Bull. Geol. Inst. Upsala*, **25**, 221-527.

HORIKAWA, K. & WATANABE, A. (1967) A study on sand movement due to wave action. *Coastal Engng Jpn*, **10**, 39-57.

HSU, J.R.C. & JENG, D.S. (1993) Short-crested wave-induced soil response in a porous seabed of infinite thickness. *J. Numerical Analytical Methods in Geomechanics*, **17**, 553-576.

INMAN, D.L. (1949) Sorting of sediment in light of fluid mechanics. *J. Sedim. Petrol.*, **19**, 125-145.

INST. CIV. ENGRS (1985) *Coastal Engineering Research*. Thomas Telford, London, 123 pp.

ISHIHARA, T. & SAWARAGI, T. (1962) Laboratory studies on sand drift, the critical velocity and the critical water depth for sand movement and the rate of transport under wave action. Fundamental studies on dynamics of sand drifts: Report 3. *Coastal Engng Jpn*, **5**, 59-65.

JOHNS, B. (1975) The form of the velocity profile in a turbulent shear wave boundary layer. *J. Geophys. Res.*, **80(36)**, 5109-5112.

JOHNS, B. (1977) Residual flow and boundary shear stress in the turbulent bottom layer beneath waves. *J. Phys. Oceanogr.*, **7**, 733-738.

JONASZ, M. (1987) Non-spherical sediment particles-comparison of size and volume distribution obtained with an optical and a resistive particle counter. *Marine Geology*, **78**, 137-142.

JONES, R.J., CAMERON, B. & FISHER, J.J. (1993) Analysis of cliff retreat and shoreline erosion: Thompson Island, Massachusetts, U.S.A.. *J. Coastal Res.*, **9(1)**, 87-96.

JONSSON, I.G. (1963) Measurements in the turbulent wave boundary layer. *Proc. 10th Congr. I.A.H.R.*, London, 85-92.

JONSSON, I.G. (1966a) Wave boundary layers and friction factors. *Proc. 10th Conf. Coastal Engng*, A.S.C.E., Tokyo, 127-148.

JONSSON, I.G. (1966b) The friction factor for a current superimposed by waves. *Coastal Engng Hydraul. Lab., Progress Report 11*, University of Denmark.

JONSSON, I.G. (1980) A new approach to oscillatory rough turbulent boundary layers. *Ocean Engng*, **7**, 109-152.

KAJIURA, K. (1968) A model of the bottom boundary layer in water waves. *Bull. Earthquake Res. Inst.*, **46**, 75-123.

KALKANIS, G. (1964) Transportation of bed material due to wave action. *U.S. Army C.E.R.C., Tech. Memo 2*.

KAMPHUIS, J.W. (1975) Friction factors under oscillatory waves. *Proc. A.S.C.E., J. Waterway Harbours Coastal Engng*, **101(WW2)**, 135-144.

KAMPHUIS, J.W. & HALL, K.R. (1983) Cohesive material erosion by unidirectional current. *J. Hydraul. Engng*, **109(1)**, 49-61.

KANDIAH, A., (1974) *Fundamental Aspects of Surface Erosion of Cohesive Soils*. Ph.D. Thesis, University of California.

KATORI, S., SAKAKINAMA, T. & WATANABE, A. (1984) Measurement of sand transport in a cross unidirectional oscillatory flow tank. *Coastal Engng Jpn*, **27**, 193-203.

KEMP, P.H. & SIMONS, R.R. (1982) The interaction between waves and a turbulent current: Waves propagating with the currents. *J. Fluid Mech.*, **116**, 227-250.

KIRBY, R. & PARKER, W.R. (1983) Distribution and behaviour of fine sediment in the Severn Estuary and Inner Bristol Channel, UK. *Can. J. Fish. Aquat. Sci.*, **40**, 83-95.

KIRCHNER, J.W., DIETRICH, W.E., ISEYA, F. & IKEDA, H. (1990) The variability of critical shear stress, friction angle, and grain protrusion in water-worked sediments. *Sedimentology*, **37**, 647-672.

KOMAR, P.D. (1970) The competence of turbidity current flow. *Bull. Geol. Soc. Am.*, **81**, 1555-1562.

KOMAR, P.D. & MILLER, M.C. (1973) The threshold of sediment movement under oscillatory water waves. *J. Sedim. Petrol.*, **43**, 1101-1110.

KOMAR, P.D. & MILLER, M.C. (1974) Sediment threshold under oscillatory waves. *Proc. 14th Conf. Coastal Engng*, A.S.C.E., Copenhagen, 756-775.

KRAMER, H. (1935) Sand mixtures and sand movement in fluvial models. *Trans. A.S.C.E.*, **100**, 798-873.

KRAUS, N.C. & SMITH, J. McKee (1994) Pore pressure and sediment density measurements at SUPERTANK. *U.S. Army C.E.R.C., Tech. Report 94-3.*

KRUIJT, J.A. (1976) On the influence of seepage on incipient motion and sand transport. *River Harbour Lab., Report STF-60/A760464*, Tech. University of Norway.

KURIHARA, M., SHINOHARA, K., TSUBAKI, T. & YOSHIOKA, M. (1956) Sand movement on a sandy beach by wave action. *Proc. 3rd Conf. Coastal Engng Jpn* (in Japanese).

LAMBE, W.T. & WHITMAN, R.V. (1969) *Soil Mechanics*. Wiley-Interscience, New York, 563 pp.

LARRAS, J. (1956) Effects de la houle et du clapotis sur les fonds de sample. *IV J. Hydraul., Report 9*, Paris.

LAVELLE, J.W. & MOIFELD, H.O. (1987) Do critical shear stresses for incipient motion and erosion really exist? *J. Hydraul. Engng*, A.S.C.E., **113(3)**, 370-388.

LEADON, C.J. (1985) The Suwannee River Estuary: Cohesive sedimentation. Presented in *4th Symp. Coastal Management*, Baltimore.

LEE-YOUNG, J.S. & SLEATH, J.F.A. (1988) Initial motion in combined wave and current flows. *Proc. 21st Conf. Coastal Engng*, A.S.C.E., Malaga, 1140-1151.

LENHOFF, L. (1982) Incipient motion of sediment particles. *Proc. 18th Conf. Coastal Engng*, A.S.C.E., Cape Town.

LHERMITTE, P. (1958) Contribution a l'etude de la Gouche limite des houles progressives. *C.O.E.C. Imprimerie Nationde*, Paris, **(136)**.

LHERMITTE, P. (1960) Movements des materiaux de pond sous l'action de la houle. *Proc. A.S.C.E.*, **1**, 211-261.

LI, H. (1954) Stability of oscillatory flow along a wall. *U.S. Army Beach Erosion Board, Tech. Memo 47.*

LI, Z. & KOMAR P.D. (1986) Laboratory measurements of pivoting angles for applications to the selective entrainment of gravel in a current. *Sedimentology*, **33**, 413-423.

LIGHTHILL, M.J. (1954) The response of laminar skin friction and heat transfer to fluctuations in stream velocity. *Proc. R. Soc. London*, **A224**, 1-23.

LINDSAY, P., BALLS, P.W. & WEST, J.R. (1996) Influence of tidal range and river discharge on suspended particulate matter fluxes in the Forth Estuary (Scotland). *Estuarine Coastal Shelf Sci.*, **42**, 63-82.

LYLE, W.M. & SMERDON, E.T. (1965) Relation of compaction and other soil properties to erosion resistance of soils. *Trans. A.S.A.E.*, **8(3)**, 419-422.

MADSEN, O.S. (1974) Stability of sand bed under breaking waves. *Proc. 14th Conf. Coastal Engng*, A.S.C.E., Copenhagen, 776-794.

MADSEN, O.S. & GRANT, W.B. (1976) Sediment transport in the coastal environment. *M.I.T. Ralph M. Parsons Lab., Report 209*.

MADSEN, O.S. (1978) Wave-induced pore pressures and effective stresses in a porous bed. *Geotechnique*, **28(4)**, 377-393.

MALOUTA, D.N., GORSLINE, D.S. & THORNTON, S.E. (1981) Processes and rates of recent (Holocene) basin filling in an active transform margin: Santa Monica Basin, California, Continental Borderland. *J. Sedim. Petrol.*, **51(4)**, 1077-1095.

MANOHAR, M. (1955) Mechanics of bottom sediment movement due to wave action. *U.S. Army Beach Erosion Board, Tech. Memo 75*.

MARTIN, C.S. (1970) Effect of a porous sand bed on incipient sediment motion. *J. Water Resources.*, **6(4)**, 1162-1174.

MARTIN, C.S. & ARAL, M.M. (1971) Seepage forces on interfacial bed particles. *Proc. A.S.C.E., J. Hydraul.*, **97(HY7)**, 1081-1100

MC CAVE, I.N. (1984) Erosion, transport and deposition of fine-grained marine sediments. In: *Fine-grained Sediments: Deep-water Processes and Facies* (Ed. by D.A.V. Stow & D.J.W. Piper), Geol. Soc., Spec. Pub. 15, 35-69.

MEHTA, A.J. (1993) *Nearshore and Estuarine Cohesive Sediment Transport.* A.G.U., Washington D.C., 581 pp.

MEHTA, A.J. & LEE, S.C. (1994) Problems in linking the threshold condition for the transport of cohesionless and cohesive sediment grain. *J. Coastal Res.*, **10(1)**, 170-177.

MERKLI, P. & THOMMAN, H. (1975) Transition to turbulence in oscillating pipe flow. *J. Fluid Mech.*, **68**, 567-575.

MIDDLETON, G.V. & SOUTHARD, J.B. (1984) *Mechanics of Sediment Movement*. Soc. econ. Paleont. Miner., Short Course 3, 401 pp.

MIGNIOT, C. (1968) A study of the physical properties of various forms of very fine sediment and their behaviour under hydrodynamic action. *La Houille Blanche*, **(7)**, 591-620.

MIGNIOT, C. (1977) Action des courants, de la houle et du vent sur les sediments. *La Houille Blanche*, **32(1)**, 9-47.

MIGNIOT, C. (1989) Measurement of mechanical characteristics of muds deposited in navigation channels. *Proc. 18th J. Hydraul., Report 13*.

MILLER, M.C., McCAVE, I.N. & KOMAR, P.D. (1977) Threshold of sediment motion under unidirectional currents. *Sedimentology*, **24**, 507-527.

MIRTSUKHULAVA, T.E. (1966) Erosional stability of cohesive soils. *J. Hydraul. Res.*, **4**, 37-49.

MOHEREK, A.J. (1978) Flume experiments on sand, silt, and clay mixtures from the offshore dredged material disposal site, Galveston, Texas. *Tech. Report D-78-34*, A.M. University of Texas.

MURRAY, J.D. (1965) Viscous damping of gravity waves over a permeable bed. *J. Geophys. Res.*, **70(10)**, 2325-2331.

NAKAMURA, A., ONISHI, R. & MINAMIDE, H. (1973) On the seepage in the sea-bed due to waves. *Proc. 20th Conf. Jpn Soc. Civ. Engrs Coastal Engng*, 421-428 (in Japanese).

NALLURI, C. & ALVAREZ, E.M. (1992) The influence of cohesion on sediment behaviour. *J. Water Sci. Technol.*, **25(8)**, 151-164.

NASH, L. (1987) *Settling Velocity and Threshold Characteristics of Biogenic Sediments*. Ph.D. Thesis, University of Wales.

NATARAJAN, P. (1969) *Sand Movement by Combined Action of Waves and Currents*. Ph.D. Thesis, University of London.

NEIL, C.R. (1967) Mean velocity criterion for scour of coarse uniform bed material. *Proc. 12th Congr. I.A.H.R.*, Fort Collins, **3**, 46-54.

NEIL, C.R. & YALIN, M.S. (1969) Quantitative definition of beginning of bed movement. *Proc. A.S.C.E.*, **95(HY1)**, 585-588.

NIKURADSE, J. (1933) Stromungsgesetze in rauhen Rohren. *V.D.I. Forschungsheft*, **361** (translators: Nat. Advis. Comm. Aeronaut. (1950), *Tech. Memo 1292*).

O'BRIEN, J.S. & JULIEN P.Y. (1988) Laboratory analysis of mudflow properties. *J. Hydraul. Engng*, **114(8)** 877-887.

OFFEN, G.R. & KLINE, S.J. (1975) A proposed model of the bursting process in turbulent boundary layers. *J. Fluid Mech.*, **70**, 209-228.

OLDENZIEL, D.M. & BRINK, W.E. (1974) Influence of suction and blowing on entrainment of sand particles. *Proc. A.S.C.E., J. Hydraul.*, **100(HY7)**, 935-950.

ONISHI, Y., GRABER, H.C. & TRENT, D.S. (1993) Preliminary modelling of wave-enhanced sediment and contaminant transport in New Bedford Harbour. In: *Nearshore and Estuarine Cohesive Sediment Transport* (Ed. by A.J. Mehta), A.G.U., Washington D.C., 541-557.

OTSUBO, K. & MURAOKA, K. (1988) Critical shear stress of cohesive bottom sediments. *J. Hydraul. Engng*, **114(10)**, 1241-1256.

PAINTAL, A.S. (1971) A stochastic model of bed-load transport. *J. Hydraul. Res.*, **9(4)**, 527-554.

PANAGIOTOPOULOS, I., SYLAIOS, G. & COLLINS, M.B. (1994) Threshold studies of gravel size particles under the co-linear combined action of waves and currents. *Sedimentology*, **41(5)**, 951-962.

PEIRCE, T.J., JARMAN, R.T. & TURBILLE, C.M. (1970) An experimental study of silt scouring. *Proc. Inst. Civ. Engrs*, **45**, 231-243.

POSTMA, H. (1967) Sediment transport and sedimentation in the estuarine environment. In: *Estuaries* (Ed. by G.H. Lauff), Am. Assoc. Adv. Sci. Pub., 158-179.

POWERS, M.C. (1953) A new roundness scale for sedimentary particles. *J. Sedim. Petrol.*, **23**, 117-119.

PRANDTL, L. (1952) *Essentials of Fluid Dynamics*. Blackie & Son Ltd, Glasgow.

PREVOST, J.H., EIDE, O. & ANDERSON, K.H. (1975) Discussion of "wave-induced pressures in permeable sea beds" (by Moshagen, H. & Torum, A.). *Proc. A.S.C.E., J. Waterway Harbours Coastal Engng*, **101(WW4)**, 464-465.

PURI, K.K. (1980) Damping of gravity waves over porous beds. *Proc. A.S.C.E., J. Hydraul.*, **106(HY2)**, 303-312.

RAMAPRIAN, B.R. & TU, S-W (1980) An experimental study of oscillatory pipe flow at transitional Reynolds numbers. *J. Fluid Mech.*, **100**, 513-544.

RANCE, P.J. & WARREN, N.F. (1968) The threshold of movement of coarse material in oscillatory flow. *Proc. 11th Conf. Coastal Engng*, A.S.C.E., London, 487-491.

RAO, M.N. (1971) An erosion study of halloysite clay. *Dept. Civ. Engng, Report 75*, University of Auckland.

RATHBUN, R.E. & GUY, H.P. (1967) Measurement of hydraulic and sediment transport variables in a small recirculating flume. *Water Resources Res.*, **3**, 107-122.

RAUDKIVI, A.J. & HUTCHISON, D.L. (1974) Erosion of kaolinite clay by flowing water. *Proc. R. Soc. London*, **A337**, 537-554.

RAUDKIVI, A.J. (1990) *Loose Boundary Hydraulics*, 3rd edn. Pergamon Press, Oxford, 526 pp.

REID, R.O. & KAJIURA, K. (1957) On the damping of gravity waves over a permeable sea bed. *Trans. A.G.U.*, **38(5)**, 662-666.

RUSNAK, G.L. (1957) The orientation of sand grains under conditions of unidirectional fluid flow. *J. Geology*, **65**, 384-409.

SARGUNAM, A., RILEY P., ARULANANDAN, K. & KRONE, R.B. (1973) Physico-chemical factors in erosion of cohesive soils. *Proc. A.S.C.E.*, **99**, 555-558.

SARPKAYA, T. (1966) Experimental determination of the critical Reynolds number for pulsating Poiseuille flow. *Trans. A.S.M.E., J. Basic Engng*, **88**, 589-598.

SATO, S. & KISHI, T. (1954) Shearing force on sea bed and movement of bed material due to wave motion. *J. Res., Public Works Res. Inst.*, **1(3)**, 1-11.

SATO, S., IJIMA, T. & TANAKA, N. (1962) A study of critical depth and mode of sand movement using radioactive glass sand. *Proc. 8th Conf. Coastal Engng*, A.S.C.E., Mexico, 304-323.

SEED, H.B., WOODWARD, R.J.Jr. & LUNDGREN, R. (1964b) Fundamental aspects of the Atterberg limits. *J. Soil Mech., Foundation Div. A.S.C.E.*, **90(SM6)**, 107-131.

SEED, H.B. & RAHMAN, M.S. (1978) Wave-induced pore pressure in relation to ocean floor stability of cohesionless soils. *Marine Geotechnology*, **3(2)**, 123-149.

SHIELDS, A. (1936) Application of similarity principles and turbulence research to bed-load movement. *Preussische Versuchsanstalt Wasserbau Schiffbau*, Berlin, **26** (translators: Ott, W.P. & Van Uchelen, J.C., *W.M. Keck Lab. Hydraul. Water Resources, Report 167*, California Inst. Technol.).

SILVESTER, R. & MOGRIDGE, G.R. (1970) Reach of waves to the bed of the continental shelf. *Proc. 12th Conf. Coastal Engng*, A.S.C.E., Washington, 487-491.

SIVAPULLIAH, P.V. & SRIDHARAN, A. (1985) Liquid limit of soil mixtures. *J. Geotechnical Testing*, **8(3)**, 111-116.

SLEATH, J.F.A. (1970) Wave-induced pressures in beds of sand. *Proc. A.S.C.E., J. Hydraul.*, **96(HY2)**, 367-378.

SLEATH, J.F.A. (1974) Velocities above a rough bed in oscillatory flow. *Proc. A.S.C.E., J. Waterway Harbours Coastal Engng*, **100(WW4)**, 287-304.

SLEATH, J.F.A. (1976) On rolling grain ripples. *J. Hydraul. Res.*, **14(1)**, 69-81.

SLEATH, J.F.A. (1978) Measurements of bed load in oscillatory flow. *Proc. A.S.C.E., J. Waterway Port Coastal Ocean Engng*, **104(WW3)**, 291-307.

SLEATH, J.F.A. (1984) *Sea Bed Mechanics*. John Willey & Sons, New York, 325 pp.

SLEATH, J.F.A. (1988) Transition in oscillatory flow over rough beds. *Proc. A.S.C.E., J. Waterway Port Coastal Ocean Engng*, **114(1)**, 18-34.

SLEATH, J.F.A. (1991) Velocities and shear stresses in wave-current flows. *J. Geophys. Res.*, **96(C8)**, 15237-15244.

SMERDON, E.T. & BEASLEY, R.P. (1961) Critical traction forces in cohesive soils. *Agricultural Engng*, **42**, 26-29.

SMERDON, E.T. (1964) Effect of rainfall on critical tractive forces in channels with shallow flow. *Trans. A.S.A.E.*, **7(3)**, 287-290.

SNEED, E.D. & FOLK, R.L. (1958) Pebbles in the lower Colorado River, Texas, a study in particle morphogenesis. *J. Geology*, **66**, 114-150.

STEPHENSON, G. (1973) *Mathematical Methods for Science Students*, 2nd edn. Longman Scientific & Tech., Essex.

STERNBERG, R.W. (1968) Friction factors in tidal channels with differing bed roughness. *Marine Geology*, **6**, 243-260.

STERNBERG, R.W. (1972) Predicting initial motion and bed-load transport of sediment particles in the shallow marine environment. In: *Shelf Sediment Transport: Process and Pattern* (Ed. by D.J.P. Swift, D.B. Duane & O.H. Pilkey), 61-82.

STONE, S.J. & JAMES, A.E. (1992) Elastic properties of cohesive sediments. Presented in *U.K. OCEANOGRAPHY '92*, University of Liverpool and Proudman Oceanographic Centre.

SUMER, B.M. & OGUZ, B. (1978) Particle motions, near the bottom in turbulent flow in an open channel. *J. Fluid Mech.*, **86**, 109-127.

SUMER, B.M. & DEIGAARD, R. (1981) Particle motions near the bottom in turbulent flow in an open channel. *J. Fluid Mech.*, **109**, 311-337.

SUTHERLAND, A.J. (1967) Proposed mechanism for sediment entrainment by turbulent flows. *J. Geophys. Res.*, **72**, 6183-6194.

SWART, D.H. (1976) Coastal sediment transport: Computation of longshore transport. *Delft Hydraul. Lab., Report Z-968: Part 1.*

TAN, T.S., GOH, T.C., KARUNARATNE, G.P. & LEE, S.L. (1994) Shear strength of very soft clay-sand mixtures. *J. Geotechnical Testing,* **17(1)**, 27-34.

TAYLOR, B.D. & VANONI, V.A. (1972) Temperature effects in low-transport, flat-bed flows. *Proc. A.S.C.E.*, **98(HY8)**, 1427-1445.

TERWINDT, J.H.J. & BEUSERS, H.N.C. (1972) Experiments on the origin of flaser, lenticular and sand-clay alternating bedding. *Sedimentology*, **19**, 85-98.

THOMAS, S.D. & SILLS, G.C. (1994) Wave generated pore pressures in the sea-bed. *Internal Report*, University of Oxford.

TOMLINSON, B.N. (1993) *Erosion Studies of Mixed Sand Beds Under the Combined Action of Waves and Currents*. Ph.D. Thesis, University of Southampton.

TORFS, H. (1994) Erosion of mixed cohesive/non-cohesive sediments in uniform flow. Presented in *4th Inter. Conf. Nearshore Estuarine Cohesive Sediment Transport, INTERCOH '94*, H.R. Wallingford.

TORFS, H., WILLIAMSON, H. & HUYSENTRUYT, H. (1995) Settling and erosion characteristics of mud-sand mixtures. Presented in *Inter. Conf. Coastal Res. Large Scale Experiments, COASTAL DYNAMICS '95.*

TROMANS, P.S. (1978) *Stability and Transition of Periodic Pipe Flows*. Ph.D. Thesis, University of Cambridge.

VAN RIJN, L.C. (1987) The effect of waves on cohesive bed surfaces. *Proc. Coastal Port Engng Developing Countries*, Hydraul. Res. Inst., Nanjing, **2**, 1518-1532.

VANONI, V.A. (1964) Measurements of critical shear stress for entraining fine sediments in a boundary layer. *W.M. Keck Lab. Hydraul. Water Resources, Report KH-R-7*, California Inst. Technol..

VINCENT, G.E. (1957) Contribution to the study of sediment transport on a horizontal bed due to wave action. *Proc. 6th Conf. Coastal Engng*, A.S.C.E., Miami, 326-355.

VON KARMAN, T. (1952) On the foundations of high speed aerodynamics. *Proc. 1st Congr. Appl. Mech.*, A.S.M.E., New York, 673-685.

VOULGARIS, G., WALLBRIDGE, S., TOMLINSON, B.N. & COLLINS, M.B. (1995) Laboratory investigations into wave period effects on sand bed erodibility, under the combined action of waves and currents. *J. Coastal Engng*, **26**, 117-134.

WADELL, H. (1932) Volume, shape and roundness of rock particles. *J. Geology*, **40**, 443-451.

WATERS, G.Z. & RAO, M.V.P. (1971) Hydrodynamic effects of seepage on bed particles. *Proc. A.S.C.E., J. Hydraul.*, **97(HY3)**, 421-439.

WENTWORTH, C.K. (1919) A laboratory and field study of cobble abrasion. *J. Geology*, **27**, 507-521.

WEST, J.R., KNIGHT, D.W. & SHIONO, K. (1984) A note on flow structure in the Great Ouse Estuary. *Estuarine Coastal Shelf Sci.*, **19**, 271-290.

WESTRICH, B. (1989) Modelling of contaminant transport in Rivers with emphasis on the interaction with movable boundaries. In: *Sediment Transport Modelling* (Ed. by S.S.Y. Wang), Hydraul. Div. A.S.C.E., 130-135.

WHITE, S.J. (1970) Plane bed threshold of fine grained sediments. *Nature*, **228(5267)**, 152-153.

WILLETS, B.B. & DROSSOS, M.E. (1975) Local erosion caused by rapid forced infiltration. *Proc. A.S.C.E., J. Hydraul.*, **101(HY12)**, 1477-1488.

WILLIAMS, S.R.J. (1984) *Experimental Studies of Sand Threshold Under Waves and Currents*. Ph.D. Thesis, University College of Wales.

WILLIAMS, P.R. (1992) Comments on *Delft Hydraulics Rheology Report*. Private communication.

WILLIAMSON, H.J. (1991) Tidal transport of mud-sand mixtures: Sediment distributions-A literature review. *H.R. Wallingford, Report SR-286*.

WILLIAMSON, H.J. & OCKENDEN, M.C. (1992) Tidal transport of mud-sand mixtures: Laboratory tests. *H.R. Wallingford, Report SR-257*.

WILLIAMSON, H.J. (1994) Recent field measurements of erosion shear stress using ISIS. Presented in *4th Inter. Conf. Nearshore Estuarine Cohesive Sediment Transport, INTERCOH '94*, H.R. Wallingford.

WIT, P.J. & KRANENBURG, C. (1992) Liquefaction and erosion of China Clay due to waves and current. *Proc. 23rd Conf. Coastal Engng*, A.S.C.E., Venice, 2937-2947.

YAMAMOTO, T.H., KONING, L., SELLMEIJER, H. & VAN HIJUM, E. (1978) On the response of a poro-elastic bed to water waves. *J. Fluid Mech.*, **87**, 193-206.

APPENDIX

WRITER'S SCIENTIFIC PAPER

Panagiotopoulos, I, Sylaios, G, Collins, M.B. (1994) **Threshold studies of gravel size particles under the co-linear combined action of waves and currents** Blackwell Publishing Ltd: 41 (5), 1365-3091 doi: 10.1111/j.1365-3091.1994.tb01434.x